

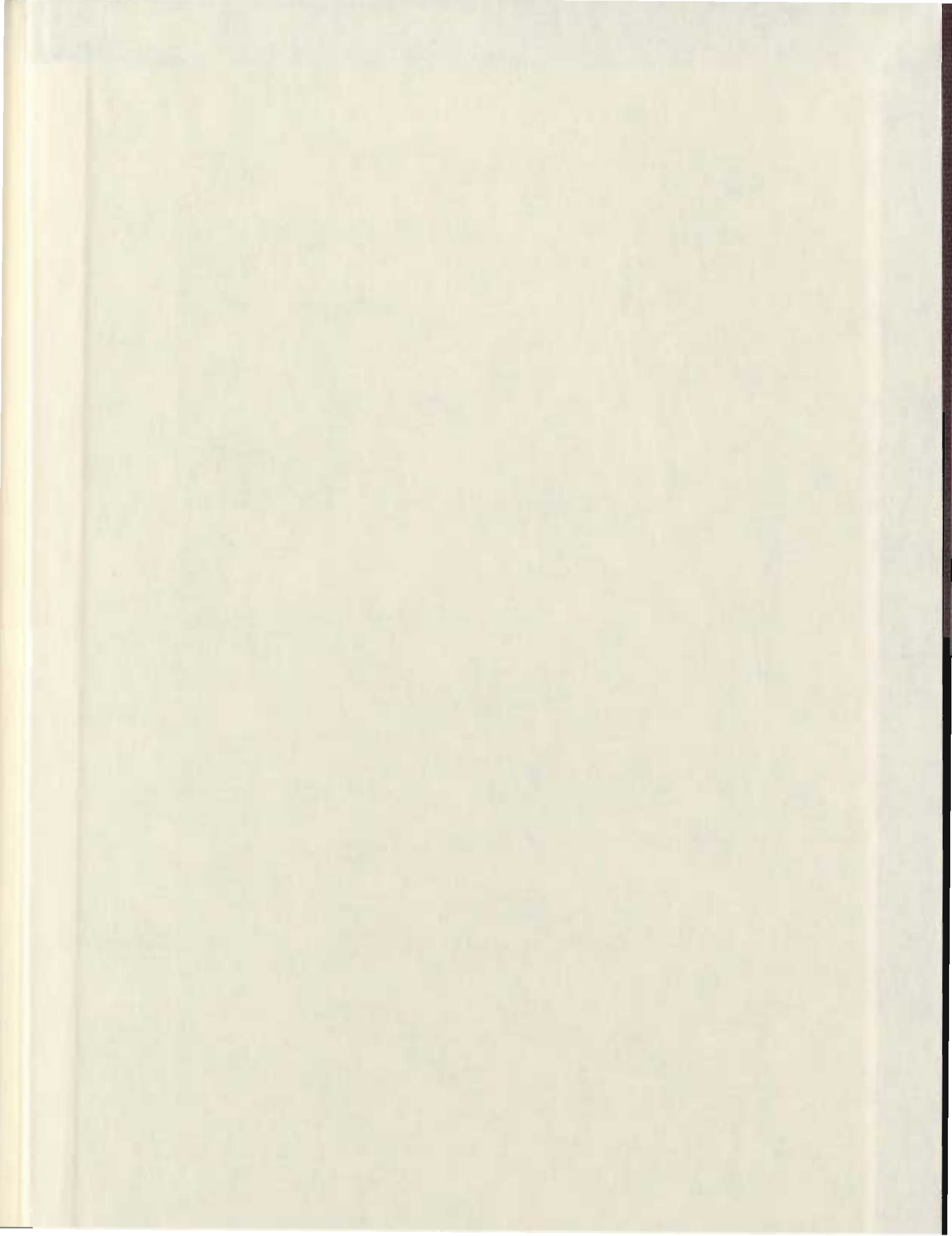
A COMPILED GEOLOGICAL, GEOCHEMICAL, AND  
METALLOGENIC STUDY OF A MAGMATIC  
NICKEL-COPPER SULPHIDE OCCURRENCE AT THE  
CIRQUE PROPERTY, NAIN PLUTONIC SUITE,  
NORTHERN LABRADOR

CENTRE FOR NEWFOUNDLAND STUDIES

**TOTAL OF 10 PAGES ONLY  
MAY BE XEROXED**

(Without Author's Permission)

BERNI LORI DWYER



## INFORMATION TO USERS

This manuscript has been reproduced from the microfilm master. UMI films the text directly from the original or copy submitted. Thus, some thesis and dissertation copies are in typewriter face, while others may be from any type of computer printer.

**The quality of this reproduction is dependent upon the quality of the copy submitted.** Broken or indistinct print, colored or poor quality illustrations and photographs, print bleedthrough, substandard margins, and improper alignment can adversely affect reproduction.

In the unlikely event that the author did not send UMI a complete manuscript and there are missing pages, these will be noted. Also, if unauthorized copyright material had to be removed, a note will indicate the deletion.

Oversize materials (e.g., maps, drawings, charts) are reproduced by sectioning the original, beginning at the upper left-hand corner and continuing from left to right in equal sections with small overlaps.

ProQuest Information and Learning  
300 North Zeeb Road, Ann Arbor, MI 48106-1346 USA  
800-521-0600

UMI<sup>®</sup>





## **NOTE TO USERS**

**Page(s) not included in the original manuscript are unavailable from the author or university. The manuscript was microfilmed as received.**

**244**

**This reproduction is the best copy available.**

**UMI**





National Library  
of Canada

Acquisitions and  
Bibliographic Services

395 Wellington Street  
Ottawa ON K1A 0N4  
Canada

Bibliothèque nationale  
du Canada

Acquisitions et  
services bibliographiques

395, rue Wellington  
Ottawa ON K1A 0N4  
Canada

*Your file Votre référence*

*Our file Notre référence*

The author has granted a non-exclusive licence allowing the National Library of Canada to reproduce, loan, distribute or sell copies of this thesis in microform, paper or electronic formats.

The author retains ownership of the copyright in this thesis. Neither the thesis nor substantial extracts from it may be printed or otherwise reproduced without the author's permission.

L'auteur a accordé une licence non exclusive permettant à la Bibliothèque nationale du Canada de reproduire, prêter, distribuer ou vendre des copies de cette thèse sous la forme de microfiche/film, de reproduction sur papier ou sur format électronique.

L'auteur conserve la propriété du droit d'auteur qui protège cette thèse. Ni la thèse ni des extraits substantiels de celle-ci ne doivent être imprimés ou autrement reproduits sans son autorisation.

0-612-66761-8

A COMPILED GEOLOGICAL,  
GEOCHEMICAL, AND METALLOGENIC STUDY  
OF A  
MAGMATIC NICKEL-COPPER SULPHIDE OCCURRENCE  
AT THE CIRQUE PROPERTY,  
NAIN PLUTONIC SUITE, NORTHERN LABRADOR

by  
Berni Lori Dwyer

A thesis submitted to the  
School of Graduate Studies  
in partial fulfillment of the  
requirements for the degree of  
Master of Science

Department of Earth Sciences/Faculty of Science  
Memorial University of Newfoundland

May, 2001



## ABSTRACT

Located approximately 40 kilometers south of Okak Bay, the Cirque property lies within an area spanning 40 km long by 5-10 km wide that contains several localized, magmatic Ni-Cu sulphide occurrences. With the exception of the OKG prospect located approximately 35 km north of the Cirque prospect, most of the magmatic Ni-Cu sulphide occurrences are hosted within Mesoproterozoic varieties of leucotroctolite, leuconorite, leucogabbro, and anorthosite of the Nain Plutonic Suite.

The Cirque property (LBN, Licence #1764M), so named because the gossan lies within a 1 km wide cirque, consists dominantly of massive and layered anorthosite and lesser amounts of leuconorite/leucogabbro and leucotroctolite. Outcrop exposure has defined the mineralized zone to strike approximately 1 km northwest and dip to the west. Ground and borehole geophysical surveys have defined a corresponding narrow zone (250 to 300 m wide) plunging steeply to the southeast. Six drill holes at the top and two of six drill holes at the base of the cirque have intersected sulphide zones of variable widths and textures. Mineralization consists of massive, net, and disseminated pyrrhotite with minor chalcopyrite. Trace pentlandite occur as fine flame-lamellae within massive pyrrhotite.

Overall, the metal contents in all of the holes are low (average Ni/Cu =  $\leq 1$ , Pd and Pt values <50 ppb). The best intersection is from borehole LBN-4 (390.35m): 0.28% Ni, 0.44% Cu, and 0.12% Co over 5.1 m. Localized, elevated Cu values were intersected in several boreholes but were not extensive; the greatest is 3.9% Cu over 20 cm in a 1.5 cm wide sulphide vein @ 923.92 m in borehole LBN-8. Values from neighbouring properties to the north (Canadian States Resources; Licence #1514M) and west (Noranda Mining and Exploration Ltd.; Licence #915M) are anomalous; highest values from grab samples are 0.36-0.85% Ni and 1.8% Ni, respectively.

Sulphide mineralization at the Cirque gossan consists of thin, irregular lenses and stringers, steeply dipping to the west and east, wrapping around and crosscutting iron stained, unmineralized leucoanorthosite. Fractured and embayed edges of plagioclase crystals by sulphide minerals at the Cirque gossan suggest thermal erosion of a semi-crystallized plagioclase-rich fractionate by a Fe-rich sulphide melt which had mobilized from depth. Although not common, thermal erosion textures have also been reported on the neighbouring Canadian States Resources property (Licence #1514M). This epigenetic-style of magmatic sulphide mineralization is important because, although the host magma for the sulphide mineralization is absent, analyses can still be made based on the geology and geochemistry of the gossan.

Major and trace element geochemistry of the rocks at the Cirque indicate that there are at least two magma sources: one formed anorthosites, leucotroctolite, and leuconorite/leucogabbro with similar REE signatures and positive Eu anomaly and another, richer in incompatible elements with a slight negative Eu anomaly, formed the ferrodiorite dykes which intrude the anorthosites. The parental (or least fractionated) material for the

anorthosites, leucotroctolite, leuconorite/leucogabbro could possibly have a geochemical composition similar to a clinopyroxenite sample located in talus along the cirque wall.

Isotopic data ( $\bar{I}\text{Sr} = 0.704$  to  $0.706$  and  $\epsilon\text{Nd} = -8.76$  to  $-2.72$ , calculated at  $1.39$  Ga, and  $\delta^{34}\text{S}_{\text{CDT}} = 2.5$  to  $3.0\%$ ) indicate that the crustal contaminants of the magma in the Cirque area are the Paleoproterozoic Churchill Province gneiss and the Nain Province gneiss. The Tasiuyak gneiss may also be a possible source, but to a lesser extent. Estimated total crustal contamination is between 20 to 60%.

Sulphide geochemistry of the Cirque area indicate that the Canadian States Resources property, Licence #1514M may have a different source magma than that of the Cirque sulphides, however, the epigenetic-style mineralization on the Noranda "Hilltop" property suggests that the source of the sulphides may be to the west where pyrrhotite-bearing pyroxenite sill and dykes have been observed. Low R factors (25 to 100) and PGE ratios indicate that the initial sulphide melt at the Cirque may have segregated from a metal-poor magma possibly due to a low degree of partial melting and extensive crystal fractionation history. Nonetheless, given that extensive zone of localized anomalous Ni and Cu values, it is still possible that a significant Ni-Cu sulphide occurrence may exist in the surrounding area.

## ACKNOWLEDGMENTS

Dr. Derek Wilton is gratefully acknowledged for his role as supervisor as well as for his encouragement and financial support for the duration of this study. Financial support is also appreciated from the Women's Association of the Mining Industry of Canada (1997-1998) and the Provincial Government Special Scholarship for Students to Pursue Graduate Studies Related to Resource Development (1998-1999, 1999-2000). Cartaway Resources Corporation, particularly Walter Nash, is thanked for giving me the opportunity to work in such a beautiful part of the world and on such an interesting project. Access to core, reports, and other *inhouse* information is gratefully appreciated.

Gratitude is also expressed for the various technical support given throughout this study: from Memorial University - Mike Tubrett, Lakmali Hewa, Maggie Piarianin, Alison Pye, Pam King, Pat Horan, Richard Cox, Rick Soper, and Darren Smith; from the Puttuaalu Lake camp: all those who helped with core sampling; and also Catherine Dwyer and Kyle Tapper.

Additional information was kindly supported by John Archibald from High North Resources, Noranda Mining and Exploration Ltd., Dr. Andy Kerr (Newfoundland and Labrador Department of Mines and Energy), Dr. Derek Wilton, and fellow students: Dr. Steve Piercey, Rod Smith, and John Hinchey. Discussions with Dr Andy Kerr, Bruce Ryan, Frank Puskas, and Tim Beesley are greatly appreciated.

For support and encouragement, special thanks to my friends and fellow students Sherif Abdwallah, Martin Guerrero, Kellie Emon, Steve Schwarz, and Jim Brydie as well as to Maureen Moore, Gerry Ford, and Gerri Starkes at the departmental office who have always been helpful.

Finally, many thanks to my family for their encouragement and support during this study, and to my husband Robert Taylor, a warm 'thank you' for your continuous assistance, support, and encouragement throughout.



## TABLE OF CONTENTS

	Page
Chapter 1 INTRODUCTION	1
1.1 Preamble	1
1.2 Location and access	3
1.3 Physiography	3
1.4 Previous work	8
1.5 Past exploration programs	10
1.6 The Cirque property	15
1.7 Orthomagmatic sulphide deposits	18
1.7.1 The Voisey's Bay deposit	21
1.7.2 Mineralization	23
1.7.3 Present model for the genesis of the Voisey's Bay deposit	28
1.8 Purpose	34
1.9 Scope	35
Chapter 2 REGIONAL AND LOCAL GEOLOGY	37
2.1 The geology of the Torngat Orogen, Churchill Province, and Nain Province	37
2.1.2 The Torngat Orogen	39
2.2 The Nain Plutonic Suite	42
2.2.1 Model for the evolution of massif-type anorthosite and related rocks	47
2.2.2 Jotunite petrogenesis	55
2.3 Local geology	57
2.3.1 Archean rocks	58
2.3.2 Paleoproterozoic rocks	62
2.3.3 Mesoproterozoic rocks - the Nain Plutonic Suite	65
2.4 Grid geology	67
2.4.1 Anorthosite (Unit 1)	74
2.4.1.1 Leucoanorthosite - Giant Propylite (Unit 1a)	74
2.4.1.2 Leucoanorthosite - Buff Brown (Unit 1b)	75
2.4.1.3 Leucoanorthosite - Bleached (Unit 1c)	82
2.4.2 Leucotroctolite-leuconorite-leucogabbro (Unit 2)	89
2.4.3 Ferrodiorite (Unit 3)	94
2.4.4 Pyroxenite (Unit 4)	96
2.4.5 Quartz-potassium feldspar-biotite pegmatite dykes (Unit 5)	102
2.5 Alteration	102
2.6 Structural relationships	105
2.7 Geological interpretations of neighbouring properties	111
2.8 Summary	111



Chapter 3 SULPHIDE MINERALIZATION	115
3.1 Introduction	115
3.2 Geological surveys and interpretations	123
3.2.1 Airborne MAG and HLEM	126
3.2.2 Ground MAG and HLEM	128
3.2.3 Surface PEM	130
3.2.4 Downhole PEM	132
3.3 Mineralization	136
3.3.1 Textures of sulphide mineralization	151
3.3.1.1 Disseminated, net-textured, and massive sulphides	155
3.3.2 Contact relationships	165
3.3.3 Evidence of sulphide mobilization	168
3.4 Mineralization on neighbouring properties	174
3.5 Assay results from the Cirque	184
3.6 Interpretation of sulphide mineralization in the Cirque area	194
Chapter 4 SILICATE GEOCHEMISTRY	199
4.1 Introduction	199
4.2 Silicate geochemistry	201
4.2.1 Magnesian number	206
4.2.2 Discrimination diagrams	207
4.2.3 Bivariate plots of MgO versus major and trace elements	212
4.3 Trace element distribution plots	221
4.3.1 Rare earth element and multi-element geochemistry	222
4.3.2 Multi-element geochemical signatures on the Cirque property	228
4.3.3 Additional trace element data from external sources	233
4.3.4 Comparisons with intrusions from the Voisey's Bay deposit area	237
4.4 Crustal contamination and Sm-Nd and Rb-Sr isotopic systems	245
4.4.1 Results of radiogenic isotope analyzes for the Cirque samples	248
4.5 Summary	268
Chapter 5 SULPHIDE GEOCHEMISTRY	271
5.1 Introduction	271
5.2 Electron microprobe analyses	273
5.3 Sources of sulphur for sulphide mineralization	280
5.3.1 Results of selenium analyses using the electron microprobe technique	280
5.3.2 Sulphur isotope geochemistry	285

5.4 Nickel and copper contents	293
5.5 Platinum Group Element geochemistry	299
5.5.1 PGE content at the Cirque	302
5.5.2 Modelling of Ni, Cu, and PGE	307
5.6 General comparisons with the Voisey's Bay deposit	316
 Chapter 6 DISCUSSION AND CONCLUSION	 320
6.1 Summary	320
6.2 Speculation on the potential for economic magmatic Ni-Cu±PGE sulphides	326
6.3 Conclusion	329
 REFERENCES CITED	 331
 APPENDICES	
A1 Analytical procedures	355
A2.1 Summary of drill hole locations at LBN	367
A2.2 Summary of drill hole logs and assay data	368
A2.3 Additional assay results of selected samples	394
A2.4.1 Scatter plots of Cu% versus Ni% from drill holes	403
A2.4.2 Histograms plots of Ni/Cu for assays from drill holes	406
A2.4.3 Downhole cross sections of mineralized intersections	409
A3.1 Microprobe data -Table of endmember fractions	413
A3.2 Metal contents of sulphide-bearing rocks from the Cirque	414
A3.3 Major and trace element geochemistry from XRF analyses	418
A3.4 Trace element geochemistry (ICP-MS) of sulphide-poor rocks	424
A3.5.1 Electron microprobe analytical results: sulphide samples - Cirque grid	427
A3.5.2 Electron microprobe analytical results: sulphide samples from properties throughout the NPS	430
A3.6 PGE-Au-Ni-Cu data for semi-massive to massive sulphides	433
A3.7 Sulphur isotope data for samples from the Cirque property	434

## **LIST OF FIGURES**

Figure 1.1 Claims map from Black Pine Ltd. (ca. 1995)	2
Figure 1.2 Location map showing Cartaway's LB-N (Cirque) property	4
Figure 1.3 Part of topographic map NTS 14E/1 (Alliger Lake) mapsheet	6
Figure 1.4 Aerial photograph showing the Cirque property	7
Figure 1.5 Claims map (for 1995-1996) showing the LB-N	12
Figure 1.6 Map of Noranda's "Hilltop" property (Licence # 915M)	13
Figure 1.7 Grid map (1: 5,000 scale) of the Cirque grid	17
Figure 1.8 Plot of estimated size and grade	20
Figure 1.9 Geological map of the Voisey's Bay - Anaktalik Bay	22
Figure 1.10 General geology map of the Voisey's Bay deposit	24
Figure 1.11 Schematic cross section of the Voisey's Bay Ni-Cu-Co deposit	25
Figure 1.12a Cross section of the Voisey's Bay Ni-Cu-Co deposit	30
Figure 1.12b Schematic plan view model of the Voisey's Bay deposit	30
Figure 2.1 Lithotectonic terranes of northern Labrador	38
Figure 2.2 Geology of northern Labrador and northern Quebec	41
Figure 2.3 Regional map showing locations of anorthosite	44
Figure 2.4 The Nain Plutonic Suite and other Elsonian plutonic intrusions	45
Figure 2.5 Cross section of the Kiglapait Intrusion	48
Figure 2.6 Schematic model for the evolution of an anorthosite massif	51
Figure 2.7 Compiled regional geology map	59

Figure 2.8 Color-contoured regional aeromagnetic map	61
Figure 2.9 Geological map showing the LBN (Cirque) property	68
Figure 2.10 Geology map (mapped at 1:5,000 scale) of the Cirque grid	70
Figure 2.11 Cross sectional view (looking north) showing the geology	71
Figure 2.12 Classification of anorthositic and related rocks	73
Figure 2.13 Field sketch showing leucogabbro (Unit 2)	113
Figure 3.1a Claims map showing locations of known sulphide occurrences	116
Figure 3.1b Claims map showing location of known sulphide occurrences	117
Figure 3.2 Grid map (1:5,000 scale) showing the gossan locations	122
Figure 3.3 Airborne geophysical (magnetic and electromagnetic)	127
Figure 3.4 Plan view of part of the Cirque grid	129
Figure 3.5 Grid plot of drill hole traces projected to surface	131
Figure 3.6 Plan view of projected borehole PEM conductors	133
Figure 3.7 Cross section of the Cirque, looking north, of drill holes	135
Figure 3.8 Photo compilation and trace of Cirque gossan	137
Figure 3.9 Stereoplot of poles to foliation planes of sulphide lenses	150
Figure 3.10 Cross section of twelve drill holes from the Cirque	169
Figure 3.11 Cross section looking west showing sulphide intersections	170
Figure 3.12a Cross section of twelve drill holes from the Cirque grid	185
Figure 3.12b Cross section of twelve drill holes from the Cirque grid	186
Figure 3.12c Cross sections looking west (along 536100m E)	187



Figure 3.12d Plan view (scale 1:7,500) of twelve drill hole traces (Cu %)	188
Figure 3.12e Plan view (scale 1:7500) of twelve drill hole traces (Ni %)	189
Figure 3.13a Cross sectional view (looking north) along 6323000m N	191
Figure 3.13b Cross section looking west along 536100m E	192
Figure 3.13c Plan view of twelve drill hole traces at the Cirque	193
Figure 4.1 Location map showing the general locations	202
Figure 4.2 An AFM discrimination diagram (wt%) from Irvine and Baragar	209
Figure 4.3 AFM diagrams (Irvine and Baragar 1971) for mafic rocks	210
Figure 4.4 AFM plots from Piercey (1998) of (a) Paleoproterozoic anorthositic	211
Figure 4.5a MgO (wt%) versus major elements for the Cirque rocks	214
Figure 4.5b MgO (wt%) versus trace elements for the Cirque rocks	215
Figure 4.6 Plot of FeO wt% versus $Al_2O_3$ wt% of samples from the Cirque	219
Figure 4.7 $TiO_2$ (wt%) versus (a) $Al_2O_3$ (wt%) and (b) FeO (wt%)	220
Figure 4.8 REE plot for progressive fractionation in the Kiglapait Intrusion	223
Figure 4.9 Rare earth element plots for (a) anorthosite, (b) leucotroctolite	224
Figure 4.10 Multi-element plots showing (a) anorthosite, (b) leucotroctolite	229
Figure 4.11 Comparative multi-trace element plots of average anorthosite	232
Figure 4.12 Multi-element plots of (a) anorthosite, (b) gabbro-norite	234
Figure 4.13 REE plots from Piercey (1998) of subsurface and surface	236
Figure 4.14 Plot of Ce versus Yb (normalized using primitive mantle values)	241
Figure 4.15 Compilation multi-trace element plot of average compositions	244

Figure 4.16 Plot of Th/Nb versus La/Sm of the Cirque rocks	247
Figure 4.17 Fields of $\epsilon\text{Nd}_{(1.30\text{ Ga})}$ of the Cirque rocks	252
Figure 4.18 Plot of age (Ga) versus $\epsilon\text{Nd}$ for Mesoproterozoic NPS intrusions	254
Figure 4.19 Plot of $^{87}\text{Sr}/^{86}\text{Sr}$ initial versus $\epsilon\text{Nd}$ both calculated at 1.3 Ga	257
Figure 4.20 Plot of $^{87}\text{Sr}/^{86}\text{Sr}$ initial versus $\epsilon\text{Nd}$ at 1.32 Ga	259
Figure 4.21 Plot of $f_{\text{Sm/Nd}}$ versus $\epsilon\text{Nd}$ at 1.3 Ga	264
Figure 5.1a Ternary plot of Cu, Ni, and Co (element percent) for Cirque rocks	275
Figure 5.1b Ternary plot of Cu, Ni, and Co (element percent)	275
Figure 5.2 Histogram of $\text{Se/S} \times 10^6$ of pyrrhotite and pyrite	282
Figure 5.3 Histograms of $\text{Se/S} \times 10^6$ of pyrrhotite and chalcopyrite	283
Figure 5.4 Histogram of $\delta^{34}\text{S}$ of chalcopyrite and pyrrhotite	287
Figure 5.5 Plot of average $\delta^{34}\text{S}_{\text{CDT}}$ (per mil) versus $\text{Se/S} \times 10^6$	288
Figure 5.6 Ranges of $\delta^{34}\text{S}_{\text{CDT}}$ values of the Cirque sulphides	290
Figure 5.7 Ranges of $\delta^{34}\text{S}$ values from various zones	292
Figure 5.8 Histograms of Ni/Cu of sulphide-bearing outcrop	295
Figure 5.9 Plot of Ni (wt%) versus Cu (wt%)	296
Figure 5.10 MgO (wt%) versus (a) Ni (ppm), and (b) Cu (ppm)	298
Figure 5.11 Mantle normalized PGE-Au-Ni-Cu patterns	303
Figure 5.12 Metal ratio plots of sulphide-bearing rocks from the Cirque	305
Figure 5.13 Plot of Cu/Pd versus Pd (ppb) of sulphide-bearing rocks	308

Figure 5.14 Plot of calculated R factors for the Cirque sulphides	311
Figure 5.15 Plot of recalculated PGE-Ni-Cu-Au concentrations	314
Figure 5.16 Plot of mantle normalized PGE-Ni-Cu-Au patterns	315

## **LIST OF PLATES**

Plate 2.1 GP anorthosite (Unit 1a) overlying BB anorthosite (Unit 1b)	76
Plate 2.2 GP anorthosite xenolith within BB anorthosite	77
Plate 2.3 Coarse-grained, anhedral, cumulate plagioclase	78
Plate 2.4 GP anorthosite incorporated into finer grained BB anorthosite	79
Plate 2.5 Drill core showing varied modal percentages and textures	80
Plate 2.6 Anorthosite with orthopyroxene megacryst	81
Plate 2.7 Varied occurrences of pyroxene in BB anorthosite	83
Plate 2.8 Igneous layering within BB anorthosite	84
Plate 2.9 Core sections showing large dark plagioclase crystals	85
Plate 2.10 Bleached anorthosite capping a gossan	87
Plate 2.11 Veins of Bleached anorthosite crosscutting GP anorthosite	88
Plate 2.12 Sharp contact between leucoanorthosite to the left and leuconorite	90
Plate 2.13 Variable textures and modal mineralogy of leuconorite/leucogabbro	92
Plate 2.14 Weakly aligned pyroxenes in leuconorite	93
Plate 2.15 Microprobe photograph of cumulate orthopyroxene	95
Plate 2.16 Ferrodiorite with aligned euhedral subophitic plagioclase laths	97
Plate 2.17 Ferrodiorite with clinopyroxene and lesser orthopyroxene	98
Plate 2.18 Pyroxene and magnetite-rich ferrodiorite veins	99
Plate 2.19 Ferrodiorite dyke along the north arm of the Cirque	100
Plate 2.20 Narrow veins of clinopyroxene and oxides	101

Plate 2.21 Quartz-K feldspar-biotite pegmatitic dykes	103
Plate 2.22 Contact between quartz-feldspar-biotite pegmatitic dyke	104
Plate 2.23 Altered anorthosite showing sericite dusting	106
Plate 2.24 Example from core of the most altered anorthosite	107
Plate 2.25 Fine-grained light green alteration of plagioclase	108
Plate 2.26 Top photo shows fine-grained net-textured pyrite	109
Plate 3.1 View of the cirque walls looking to the southwest	138
Plate 3.2 View of Gossan #1 in the cirque from the top of the talus	140
Plate 3.3 Mineralized boulders from the talus near Gossan #2	141
Plate 3.4 Discontinuous stringers and pods of massive sulphides	142
Plate 3.5 Back wall of the cirque showing capped by Bleached anorthosite	143
Plate 3.6 View from the back wall towards the southeast	143
Plate 3.7 Close up views of stringers and patches of sulphide mineralization	146
Plate 3.8 Band of gossan capped by Bleached anorthosite	147
Plate 3.9 Sulphide mineralization consists of pyrrhotite (po) with chalcopyrite	152
Plate 3.10 Core sample showing 3 cm wide massive pyrrhotite	153
Plate 3.11 Pyrite mineralization is dominantly associated with anorthosite	154
Plate 3.12 Magnetite and ilmenite with pyrrhotite	156
Plate 3.13 Massive pyrrhotite with chalcopyrite	156
Plate 3.14 Disseminated pyrrhotite in leucoanorthosite	157
Plate 3.15 Net-textured pyrrhotite with trace chalcopyrite	158

Plate 3.16 “Wormy” net-textured pyrrhotite from LBN-8	160
Plate 3.17 Massive pyrrhotite samples from drill holes LBN-3 and LBN-11	161
Plate 3.18 Massive pyrrhotite with chalcopyrite bleb	162
Plate 3.19 Leucoanorthosite with 2 cm wide chalcopyrite-rich band	163
Plate 3.20 Massive pyrrhotite with minor chalcopyrite	164
Plate 3.21 Contacts of massive sulfide in anorthosite	166
Plate 3.22 Blebs of chalcopyrite are typically located within massive pyrrhotite	166
Plate 3.23 Top photo shows aligned pseudonet-textured pyrrhotite	167
Plate 3.24 Core samples of semi-massive pyrrhotite with xenoliths	172
Plate 3.25 Fractured plagioclase crystals as a result of sulphide injection	173
Plate 3.26 Scalloped grain boundaries of plagioclase	175
Plate 3.27 Large plagioclase crystal with bent twinning	175
Plate 3.28 Injections of pyrrhotite as thin veins cross-cutting cleavage planes	176
Plate 3.29 Intrusions of pyrrhotite into plagioclase crystals	177
Plate 3.30 A magnetite and clinopyroxene-rich sample	180
Plate 3.31 Core sample from the Canadian States Resources property	182
Plate 3.32 Massive sulphide sample from Canadian States Resources	183
Plate 3.33 View of the Cirque gossan (to the southwest)	195

## **LIST OF TABLES**

Table 1.1 Size and grade of selected nickel-copper sulphide deposits	19
Table 3.1 Compilation of available prospecting and drilling results	118
Table 3.2 Summary of geophysical survey results	124
Table 3.3 Summary of 3-D PEM borehole survey results	134
Table 3.4 Compilation of magmatic sulphide occurrences in northern Labrador	178
Table 4.1a Ranges of major element concentrations	204
Table 4.1b Ranges of selected trace element concentrations	205
Table 4.2 Sm-Nd and Rb-Sr isotope data for samples from the Cirque property	249
Table 4.3 Rb-Sr and Sm-Nd isotopic characteristics of the Nain Plutonic Suite	251
Table 4.4 Calculated values of Neodymium Crustal Indices	266
Table 5.1 Calculated concentrations of metal elements in the sulphide liquid	310



## **CHAPTER 1**

### **INTRODUCTION**

#### **1.1 Preamble**

Prior to the discovery of the world class magmatic Ni-Cu-Co deposit at Voisey's Bay in 1993, very little mineral exploration had been undertaken in northern Labrador. Once regarded as "sheer desolation, abysmal and chaotic" (Prichard 1911), geological mapping in northern Labrador by early government geologists and exploration companies was limited. In 1995, amidst the largest staking rush ever in the history of the province, Cartaway Resources Corporation acquired several hundred square kilometres of mineral claims in northern Labrador (Figure 1.1). That same year, Cartaway conducted extensive geological and geophysical surveys on most of those claims.

The Cirque property (also known as LBN; Licence #1764M) is located in northern Labrador, within the large Nain Plutonic Suite anorthosite-granite massif which straddles two Precambrian structural provinces; the Nain and Churchill. Two large gossans (each approximately 200 m wide and 500 m high) were discovered in a small cirque on the northwest corner of the property. The most mineralized grab sample yielded assay values of 0.36% Ni, 0.61% Cu, and 0.12% Co. Neighbouring property owners (*eg.* Noranda, Canadian States Resources, Ace Developments) also discovered gossans with anomalous base metal concentrations. Results from diamond drilling and geophysical surveys at the Cirque area indicated a narrow (200-300 m wide) conductive sulphide zone (pyrrhotite-rich

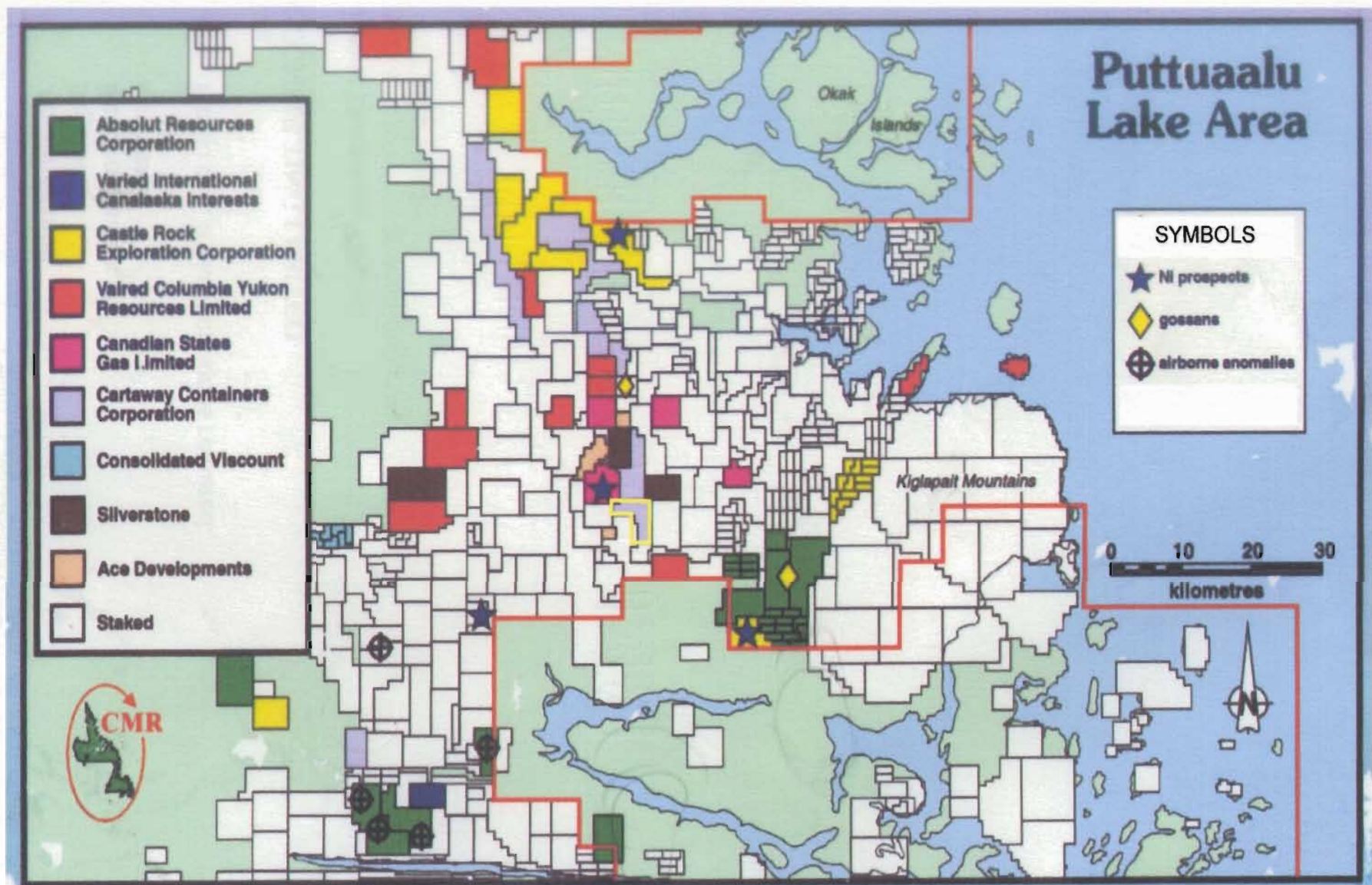


Figure 1.1 Claim map from Black Pine Limited (?) showing the vast number of mineral claims in the south Okak Bay area. Cartaway Resources' LBN or Cirque property is light purple and outlined in bright yellow in the centre of the map.

with minor chalcopyrite) dipping to the east and plunging to the southeast. Sulphide mineralization, although sub-economic at this time, is believed to have formed from orthomagmatic processes, suggesting a potential for a significant (if not economic) deposit similar in genesis to the Voisey's Bay deposit. The significance of such a mineralized occurrence is that it opens up the area south of Okak Bay for further mineral exploration.

## **1.2 Location and access**

The Cirque property (LB-N, Licence # 1764M) consists of 72 mineral claims (1 claim = 0.5 km<sup>2</sup>), 75 km northwest of the town of Nain in northern Labrador (Figure 1.2); it is located on the NTS 14 E/1 Alliger Lake 1:50,000 scale topographic map sheet. The study region is situated at the far northwest corner of the property, spanning an area of approximately 4.5 x 2 km. Regular scheduled flights by Air Labrador between Nain and Goose Bay allow for easy travel to northern Labrador. Northern Lights Air Services (turbo single otter) and Air Schefferville (single otter) provided direct access from Goose Bay and/or Nain to the Cartaway base camp located at the northeast side of Puttuaalu Lake. The study area itself can be reached by helicopter from the camp site which is approximately 17 km north northeast. Technical support for the camp was provided by D&J Construction in Nain and Labrador Expediting Services in Goose Bay.

## **1.3 Physiography**

The study area is mountainous and rugged, underlain by large, steep sided hills that

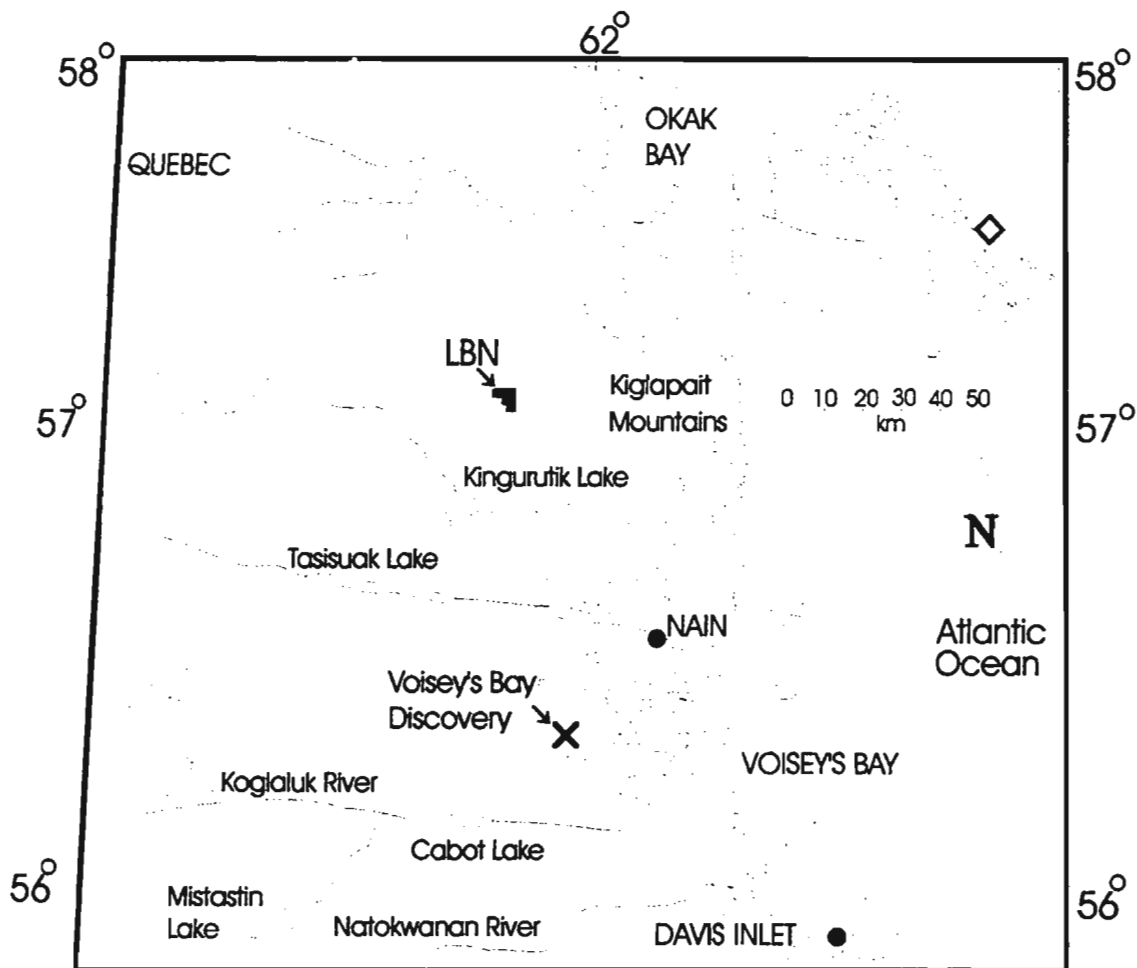


Figure 1.2 Location map showing Cartaway's LBN (Cirque) property, Licence # 1764M in northern Labrador.

were carved during several Pleistocene glacial events (Green 1974). There is a general northeast trend of paleoglacial flow determined from drumlins, eskers, and crag and tail landforms south of Okak Bay (Klassen *et al.* 1992). However, there is little glacial information for the area south of Puttuaalu Lake.

The highest and lowest elevations (above sea-level) in the area are 975.61 m and 213.41 m, respectively (Figure 1.3), for a maximum relief of 762 m. The valleys are broad and flat and contain sand, gravel, and scrub vegetation, with little outcrop. The tops of the hills are barren with felsenmeer and scree, and virtually no vegetation (Figure 1.4). Over 75% of low relief outcrop is covered by a thin layer (<5.0 m thick) of glacial debris. Intense weathering of the area has moved and broken much of the existing outcrop.

The study area has been designated as the “Cirque”, but there are two other neighbouring cirques to the immediate south of the study area. The Cirque itself opens to the east and contains a crescent-shaped pond that dries up in the summer. Two small streams from the Cirque run into the pond and another runs from the pond out of the Cirque to the east. The Cirque floor is small, spanning 0.75 m<sup>2</sup>, yet it is covered by as much as 50 m thickness of glacial gravel and boulders. The steep walls of the Cirque allow for better bedrock observation, but only the lower parts are accessible by first climbing a steep talus slope. The talus slope consists of car-sized boulders all around the sides of the Cirque walls and at times can be very dangerous for climbing. The tight area within the Cirque has hampered the drilling programs and has somewhat limited the location of the drill sites.

In the spring (April-early June) the area is wind swept and snow-covered. Summers

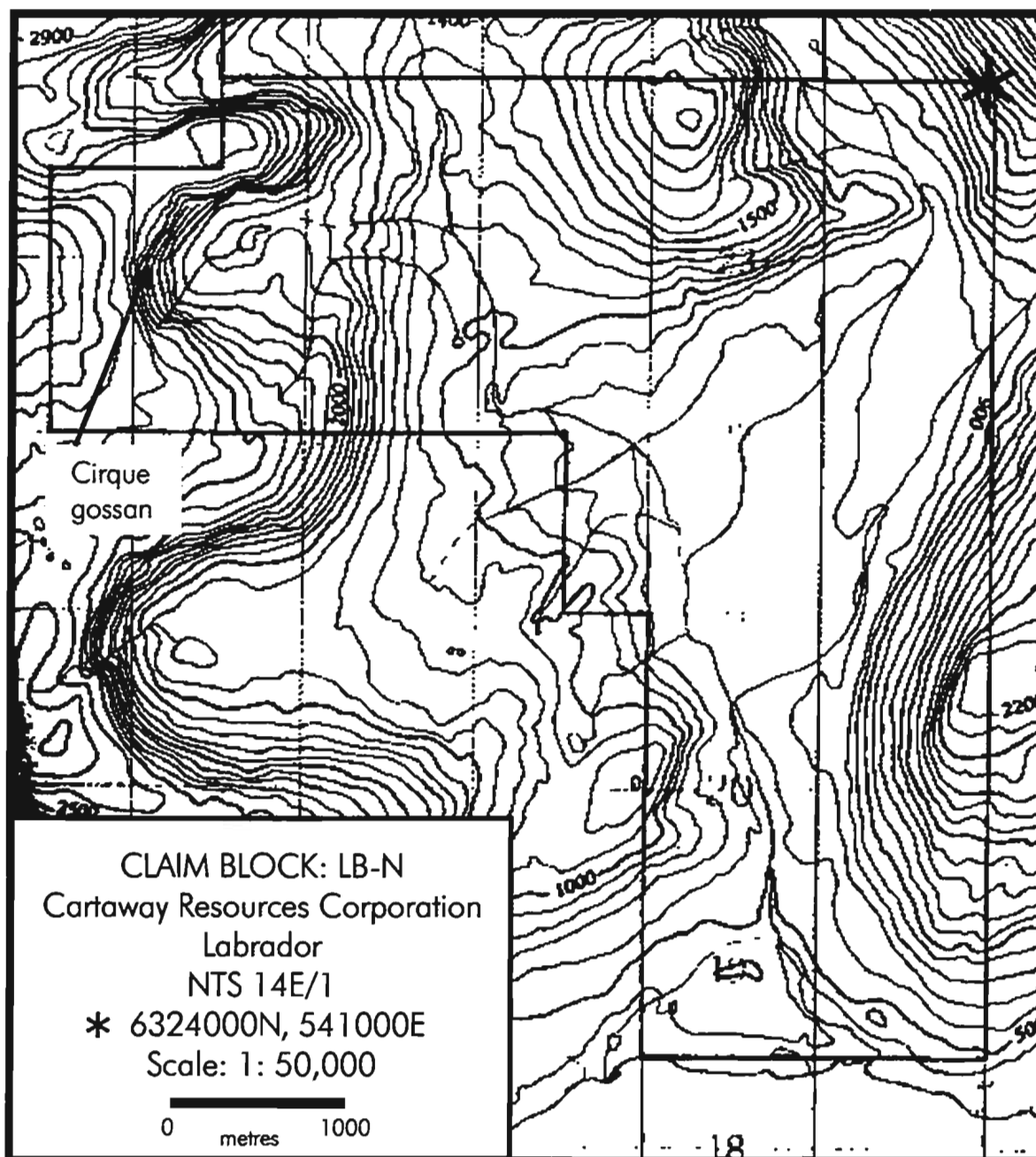


Figure 1.3 Part of a topographic map (NTS 14E/1; Alliger Lake mapsheet) showing Cartaway Resources LB-N (Cirque) property; Licence # 1764M. Elevation contour lines are in feet.



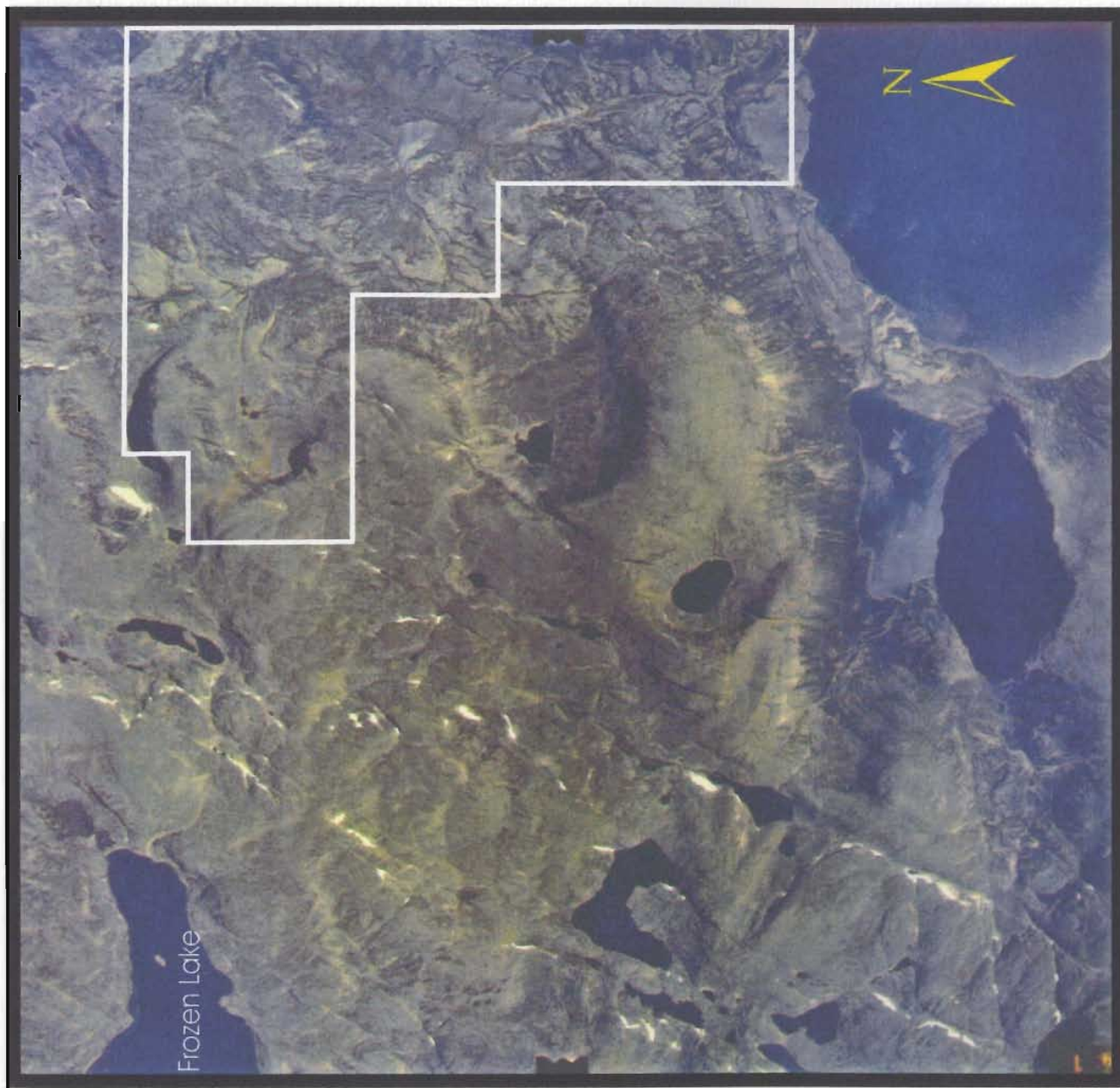


Figure 1.4 Aerial photograph showing the Cirque property; scale 1:40,000.

are short (late June–August) with temperatures as high as 27°C, though some snow patches exist all summer in shady areas. In the fall (September–October), temperatures are cooler with fog and extremely low clouds impeding aircraft flights. Snow begins to fall in early November. The sharp topographic contrast and closed area of the cirque result in intense high winds that make flying dangerous. Early spring and fall are the worst seasons, affecting the drill programs and at times preventing access to the area altogether.

#### **1.4 Previous work**

The area north of Nain was first mapped as far north as Okak Bay and as far west as Tessersoak Lake by E.P. Wheeler II (1942; 1960) in the 1920s. Using dog team and canoe, he mapped the various mafic and felsic units that comprise the Nain Plutonic Suite (NPS) and the surrounding country rocks of the Puttuaalu Lake area. The NPS anorthosite was subdivided into dark facies, pale facies, and buff weathering groups based on the colour of weathered surfaces (Wheeler 1960). Other rock types observed by Wheeler were leucogabbro, adamellite (pyroxene quartz monzonite; Ryan *et al.* 1995) and other granitoids, gneisses, mafic dykes, and pegmatites. Wheeler was one of the first to compare the geological units of northern Labrador with similar rocks in Norway, Quebec, and areas of eastern United States and Quebec (Emslie *et al.* 1994).

In 1977, as part of his Ph.D thesis, Ranson conducted an east-west transect south of Okak Bay with subsequent studies on the mineralogy and geochemistry of the rock units in the NPS, from east of Puttuaalu Lake to the west of Imiakovik Lake, producing the most



detailed map (1:100,000) for the Alliger Lake-Iglusuataliksuak Lake area (Ranson 1976,1981). Using previous data, a 1:250,000 scale compilation map of the area was produced by Taylor (1971). Ryan (1990) revised Taylor's map and revisited the area several times (Ryan 1991; Ryan *et al.* 1995; Ryan 1996; Ryan and Hynes 1996; Ryan *et al.* 1997; Ryan *et al.* 1998). At present, Ryan and others are revising the map of the northern NPS based on geochronology and structural re-interpretations. Kerr (Kerr and Smith 1997; Kerr 1997, 1998) has been visiting the area since 1995, recording rock and sulphide textures in core and outcrop of various properties.

Regional lake sediment and water surveys and airborne geophysical surveys have also been conducted by the Newfoundland Department of Mines and Energy. Lake sediment geochemical data define background nickel and copper values, averaging 19 ppm and 30 ppm, respectively for the Alliger Lake area; the most elevated values were 56 ppm and 90 ppm, respectively (GSC Open File 1210). Airborne geophysical surveys, conducted in 1996 and 1997, outlined a small (approximately  $< 5 \text{ km}^2$ ) high magnetic anomaly, possibly dipping to the west near the Cirque property. There are also two distinct magnetic zones in the area; the magnetic Paleoproterozoic plutons and the low magnetic Mesoproterozoic plutons of the NPS (Ryan *et al.* 1998).

Emslie and Ermanovics (Emslie and Russell 1988; Emslie and Hunt 1990; Emslie and Stirling 1993; Emslie *et al.* 1994; Emslie 1996; Emslie *et al.* 1997; Ermanovics *et al.* 1989) of the Geological Survey of Canada have studied areas within and around the NPS, concentrating mainly on the granitic complexes and Archean gneisses, respectively. Other

areas within the NPS, not necessarily near the study area, have been studied by numerous geologists, making significant contributions to the understanding of the NPS. Many of these studies were of individual intrusions (eg Kiglapait, Newark Island, Barth Island, Hettasch, Jonathon Island; Wiebe 1987; Wiebe 1985; Synder *et al.* 1993; DePaolo 1985; De Waard 1976). Hynes (1997) mapped an area approximately 7 km north of the study area, studying the petrography and geochemistry of layered mafic units within the NPS. Piercey (1998) investigated a series of mineralized pyroxenite dykes on Castle Rock's OKG property south of Okak Bay and 30 km north of the Cirque property.

### **1.5 Past exploration programs**

Because little was understood about the potential of the Nain Plutonic Suite (NPS) to host significant magmatic sulphide deposits, plus the lack of accessibility to the area, little attention was paid to the northern NPS prior to 1995. In anorthosite-adamellite complexes of northern NPS, several occurrences of magnetite, ilmenite, pyrrhotite, molybdenite, beryl, and labradorite have been reported (Green 1974). Douglas (1953) and Morse (1969) also defined local occurrences of magnetite, ilmenite, and pyrrhotite in anorthosite and gabbro but no detailed follow up work was done. In the early 1970s, Kennco prospected the Kiglapait Intrusion in which veins and lenticular pyrite, pyrrhotite, and chalcopyrite mineralization were discovered, however, platinum group minerals were not reported (Wardle 1996). In 1986, Platinum Exploration Canada Inc. evaluated the Kiglapait Intrusion (*op. cit.*). In 1995, on the heels of the Voisey's Bay nickel-copper-cobalt discovery, several

exploration companies staked vast areas within the Nain Plutonic Suite, particularly near the inferred contact between the Nain and Churchill provinces. Various exploration companies have prospected and drilled discontinuous patches of gossan extending for about 25 km north and 5 km south of the Cirque property (Figure 1.5). Noranda Exploration Ltd. held property (Licence #915M) to the immediate west of Cartaway Resources's Cirque (LBN) property and Canadian States Resources, now High North Resources, held property to the north of the Cirque property. A couple of kilometres to the south, Ace Developments held a small mineral block (later owned by Cartaway Resources; Licence #910M), also on a cirque. On these and surrounding properties, combined helicopter-borne magnetic and electromagnetic (EM) surveys were conducted, along with ground geophysics (Pulse EM, MAX-MIN, VLF). On the Noranda and Canadian States properties, diamond drill programs were conducted in 1995 and 1996 based on geophysical results, grid mapping, and prospecting of gossanous zones.

On the Noranda property ("Hilltop"; Licence #915M), several small EM conductors (maximum strike length of 800 m and 25-75 m wide) were identified on several grids (Figure 1.6; Squires *et al.* 1997). All of these conductors occur in interlayered olivine gabbro/norite, and pyroxenite, however, the main rock type is anorthosite. Four of Noranda's six drill holes intersected significant sulphide mineralization, described as sporadic massive and semi-massive zones (dominantly pyrrhotite and minor chalcopyrite) hosted in a discontinuous pyroxene-rich dyke (*op. cit.*). The highest assay values (0.45% Ni, 0.26% Cu, and 0.14% Co over 0.80 m) are subeconomic. Locally, thin (max 20 cm or less)

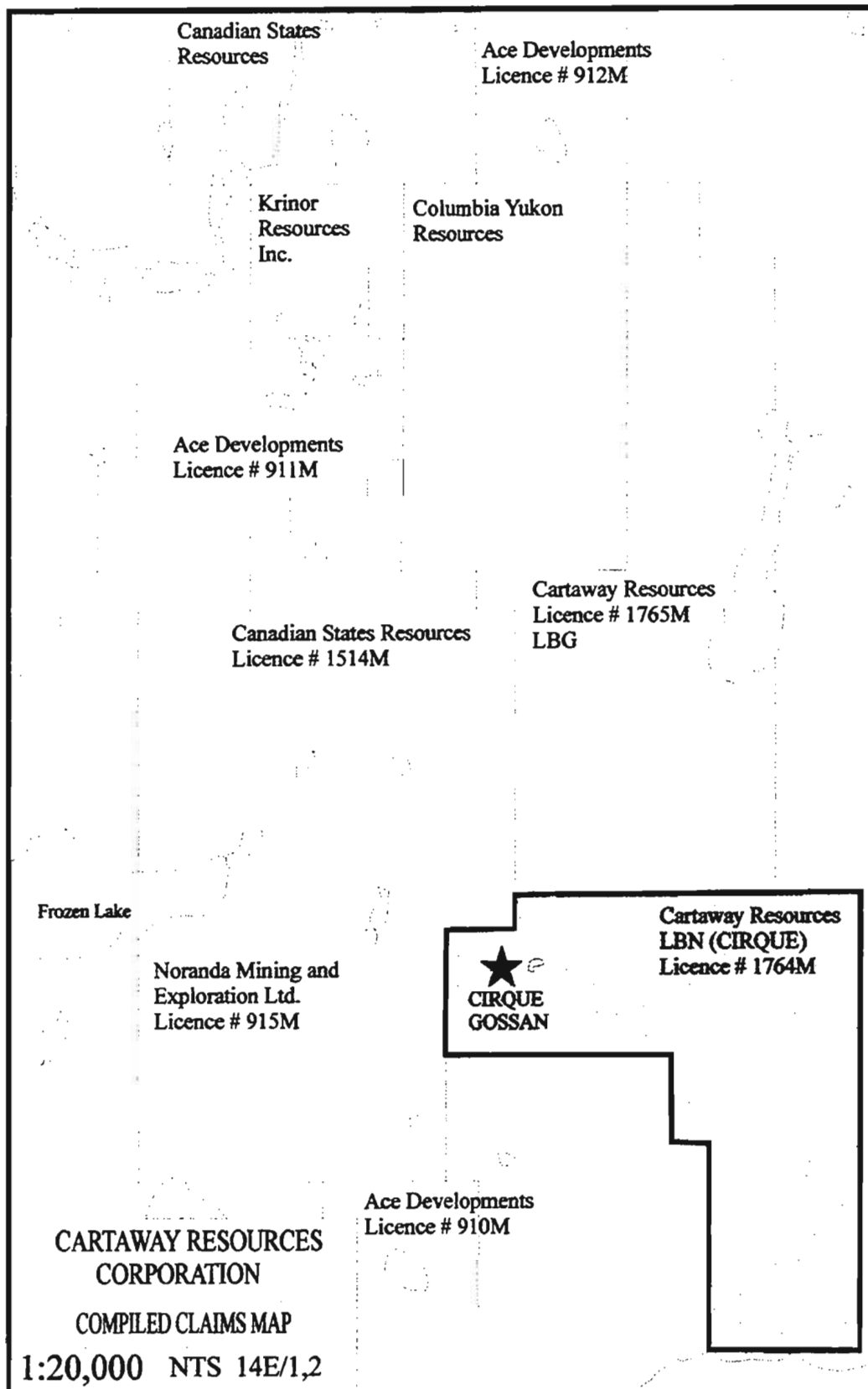


Figure 1.5 Claims map (for 1995 -1996) showing the LBN or Cirque property (Licence # 1764M) property and neighbouring properties; NTS 14E/1,2; scale 1:20,000.

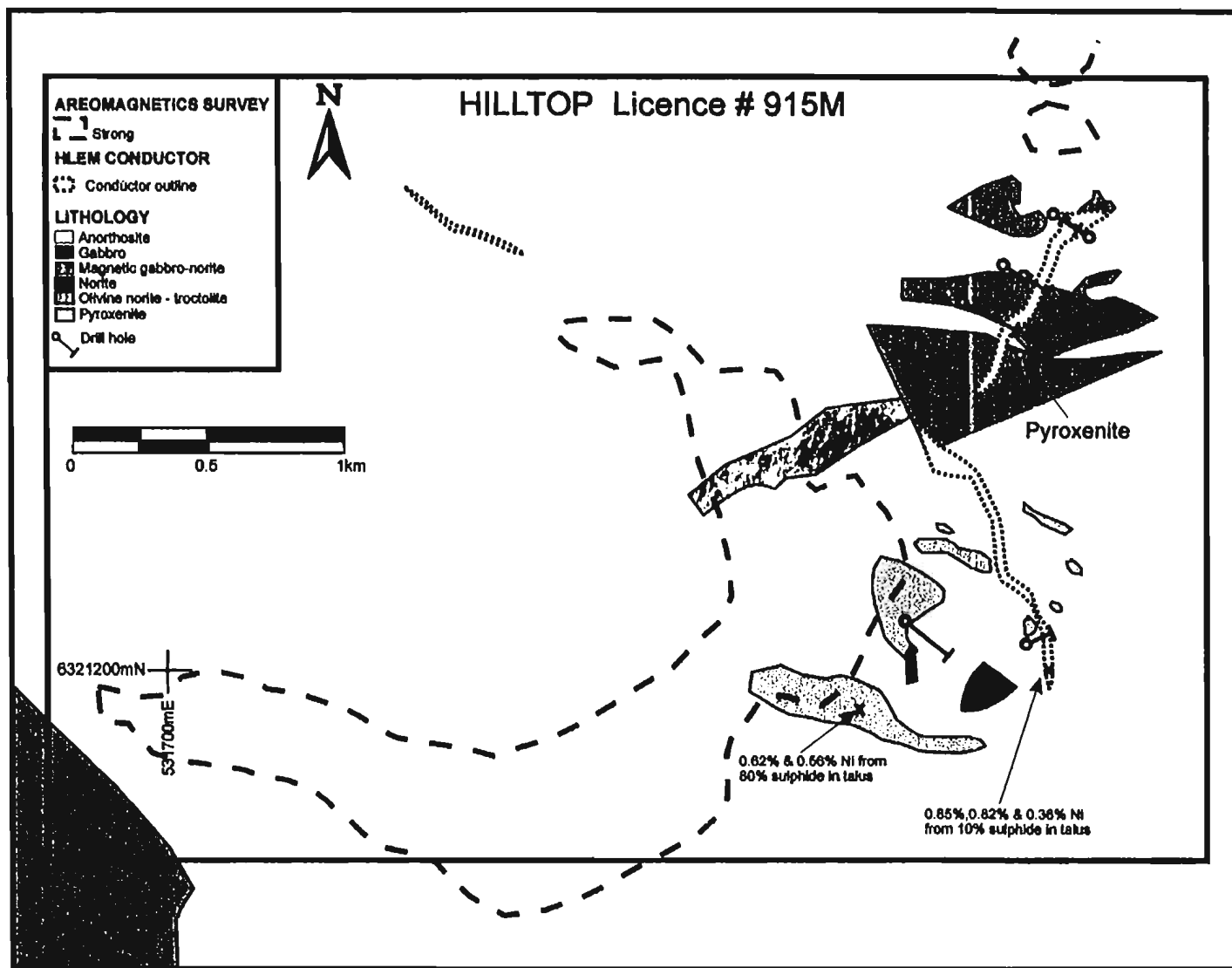


Figure 1.6 Map of Noranda's "Hilltop" property (Licence # 915M) west of the Cirque property showing geology, aeromagnetic signatures, HLEM conductors, and drill hole locations (from Squires et al. 1996).

chalcopyrite-rich zones (maximum 1.76% Cu) were recorded (*op. cit.*). No further work was done on the property in 1997 although it is still retained by Noranda Exploration Ltd.

On the Canadian States property, a gossan, delineated by an airborne magnetic survey, is thought to be a NW extension of the Cirque gossan. Assay values were higher than Noranda's (up to 1.8% Ni, 0.30% Cu, 0.17% Co; Kerr 1998) with the highest nickel value being 2.6%. Most of the sulphide lenses on the surface were leached out and drill holes failed to intersect continuous economic mineralization greater than a few metres. No further work was done after 1996.

To the south, the Ace Developments property contains one of the highest combined lake sediment anomalies in the Nain Plutonic Suite (38-46 ppm Ni, 57 ppm Cu, 35-54 ppm Co; *Anon.* 1996). In 1996, Ace Developments (Licence #912M) discovered eight sulphide showings; four of which were massive and extensive, occurring within olivine gabbro in the south end of the property. The highest grab sample assay was 0.57% Ni, 0.52% Cu, and 0.15% Co. Ground and airborne geophysical surveys were conducted and small anomalies were located, however, low EM responses made the property a low priority. It should be noted that most of the property covers a small steep-walled cirque which may have affected the geophysical results. In 1997, Cartaway geologists did follow up mapping and sampling with modest results.

Exploration has also been ongoing sporadically since 1995 in the surrounding area north and south of the Cirque. Eastfield Resources, Pele Mountain Resources Inc., Krinor Resources, NDT Ventures, Columbia Yukon Resources, Ace Developments, Castle Rock

Exploration Ltd. have all prospected, mapped, and some have drilled massive anorthosite and related mafic rock types from north of Nain to south of Okak Bay. Results have been mainly subeconomic but informative nonetheless. Core samples from Krinor's (joint ventured with Castle Rock) and Columbia Yukon's properties southwest of Puttuala Lake assayed with values as high as 0.5 - 1% Ni and concentrations of >1% Ni were reported from core on the Pele Mountain property northwest of Puttuala Lake. Due to low assays, low commodity prices, and inaccessibility of the area, many companies have since moved out or ceased exploration temporarily. Drilling and mapping results, however, suggest the area may still have the potential for economic magmatic sulphide deposits.

### **1.6 The Cirque property**

The Cirque property (LBN, Licence #1764M) gossan extends discontinuously on surface for ~1 km and is exposed for about 500 m along the cirque wall. Mineralization consists of massive, net, and disseminated pyrrhotite with minor chalcopyrite. One of the highest assays derived from outcrop was 0.36% Ni, 0.61% Cu, and 0.12% Co.

At the Cirque property extensive prospecting, mapping, and geophysical programs were conducted from 1995 to 1997, mostly on the 5.4 km<sup>2</sup> grid. Hundreds of whole rock samples were assayed for nickel, copper, and cobalt and a few for gold, platinum, and palladium. Several samples were also assayed for whole rock geochemistry.

The drilling program initially began in November, 1995. However, intense winds and snowfall stranded the drill crew on the top of the Cirque for two days and severely

damaged their camp and drill rig. In early May 1996, Midwest Drilling restarted and continued until June, drilling six holes at the top of the Cirque. From August to October, 1996 holes 7-10 were drilled on the Cirque floor. In September, 1997, a third program lasted for six weeks and holes 11 and 12 were drilled on the Cirque floor. Over 6875 metres of drill core were obtained. Down hole pulse EM surveys were conducted on only holes 7 to 12, as holes 1-6 were frozen. Sperry Sun measurements of down hole azimuth and dip were taken for several holes. Frozen and plugged holes that were not measured were extrapolated from the surface. Hundreds of core samples were assayed for Ni, Cu, and Co. Magnetic susceptibility readings were taken to distinguish the more magnetic (monoclinic) pyrrhotite from less magnetic (hexagonal) pyrrhotite. Core is presently stored at the Cartaway camp site at the northeast corner of Puttuaalu Lake. Representative samples were kept at the Cartaway office in Pickering, Ontario and at Memorial University in St. John's.

Out of twelve holes drilled on the Cirque property (Figure 1.7), six drill holes at the top of the cirque intersected several massive sulphide zones, while at the base of the cirque, two of six holes intersected massive sulphides. The host to the mineralization is leucoanorthosite. In all the intersections, assays revealed modest values of nickel, copper, and cobalt. Chalcopyrite is observed in massive pyrrhotite along contacts with plagioclase inclusions and anorthosite. Within massive sulphides, chalcopyrite is bleb-like (up to 6 x 0.3 cm) and minor pentlandite lamellae occur within pyrrhotite. On the property, a geophysically defined conductive and magnetic narrow zone associated with the gossan is approximately 250 to 300 m wide and dips steeply southeast.



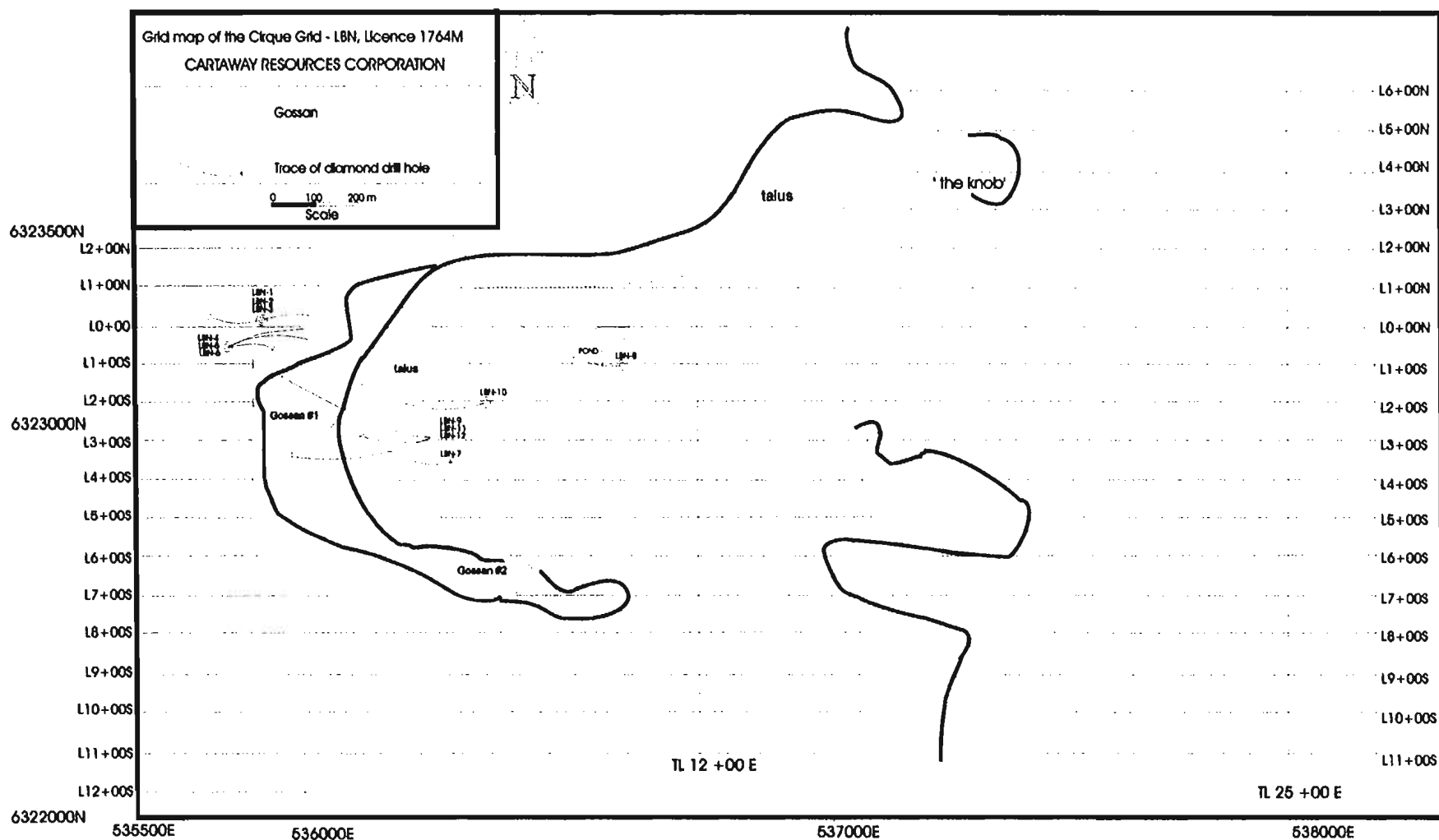


Figure 1.7 Grid map (mapped at 1:5,000 scale) of the Cirque grid (LBN property; Licence # 1764M) held by Cartaway Resources Corporation in 1997, showing surface traces of twelve diamond drill holes and gossan locations.

Other properties owned by Cartaway in the surrounding area (LB-G, CAN12, LB-HJK) have been prospected and mapped with subsequent discoveries of sulphide occurrences in anorthosite and leucogabbro. Drill programs were conducted on all properties with subeconomic results. LB-G has been returned to vendor, but the remaining and additional properties have been retained for further exploration surveys.

Since 1998, Cartaway Resources Corporation no longer exists and the properties are no longer owned by the company.

### **1.7 Orthomagmatic sulphide deposits**

Most economic Ni deposits seem to be related to anorogenic magmatism which occurs during periods of tectonic quiescence. There are several general anorogenic types, ranging from volumetrically large stratiform complexes with high Ni:Cu ratios to small intrusions with generally low Ni and Cu. Table 1.1 (*summarized from Eckstrand 1996*) lists the types of deposits in anorogenic magmatic environments with examples from around the world. Figure 1.8 is a plot of the grades and tonnages of these deposits.

The world's greatest producer of nickel today is a huge sheet-like body in Sudbury that has the world's largest concentration of Ni-Cu sulfides which grade 3.5% Ni and 2% Cu (Naldrett 1994). These deposits have been mined for over 100 years producing approximately two thirds to three quarters of total world nickel production. It is also the second largest Canadian copper producer, and one of two Canadian producers of PGE's and cobalt. The Sudbury deposit is unique because its genesis is believed to have started as a

Table 1.2 Size and grade of selected nickel-copper sulphide deposits (*after* Eckstrand 1996).

No.	Deposit	Age	Size (Mt)	Ni %	Cu %	References
1	Sudbury, ON	Proterozoic	1648	1.2	1.03	Canadian Mines Handbook 91-1; Naldrett 1994
2	Thompson Nickel Belt (INCO), MB	Proterozoic	89	2.5	0.13	INCO Prospectus 1968; Naldrett 1994
3	Raglan deposits (6), Ungava, PQ	Proterozoic	18.5	3.13	0.88	Northern Miner 1992, 11-02
4	Voisey's Bay, NF & LAB*	Proterozoic	124.4	1.66	0.88	Newfoundland Dept. Natural Resources, 1999
5	Noril'sk-Talnakh district, Russia	Triassic	555	2.7	2.07**	DeYoung <i>et al</i> 1985; Naldrett 1994
6	Jinchuan, China	Proterozoic	515	1.06	0.67	Chen & Mingliang 1987; Naldrett 1994
7	Duluth Complex, USA	Proterozoic	4000	0.2	0.66	Listerud & Meineke 1977
8	Kambalda district, Australia	Archean	48	3.6	0.25**	DeYoung <i>et al</i> 1985; Naldrett 1994
9	Agnew, Australia	Archean	46.764	2.08	0.1**	Billington 1984
10	Mt. Keith, Australia	Archean	270	0.6	NA	DeYoung <i>et al</i> 1985

\* not updated    \*\* Cu grade approximate    NA not available

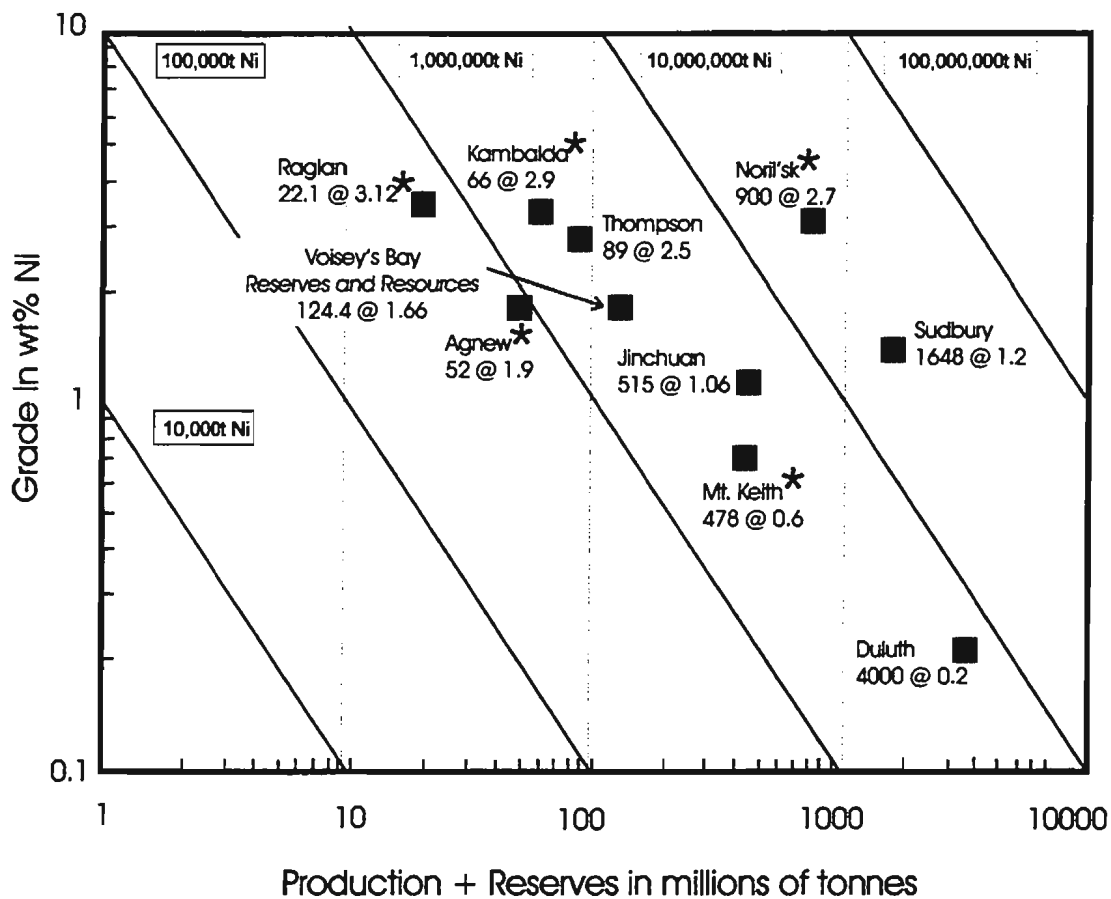


Figure 1.8 Plot of estimated size and grade of selected nickel and copper sulphide deposits (from Li and Naldrett 1999). Value given for each deposit is tonnage @ % Ni. \* Table 1.1 lists different tonnages and Ni grades for some of the deposits due to different sources.

result of a huge meteorite impact, which penetrated the crust and caused huge volumes of mafic magmatism to intrude the impact crater which spans approximately 60 x 27 km (Eckstrand 1996).

#### **1.7.1 The Voisey's Bay deposit**

The Ni-Cu-Co deposit discovered at Voisey's Bay, Labrador is believed to have formed as a result of a series of mafic intrusions into sulphur-rich metasedimentary rocks of the Tasiuyak Gneiss and the enderbitic orthogneiss (Ryan *et al.* 1995; Naldrett *et al.* 1996). The Voisey's Bay sulphides occur within the gabbro and troctolite varieties of the Reid Brook Complex, or RBC (Ryan 1996), which is located in the southeast part of the Nain Plutonic Suite. The RBC consists of granite, anorthosite, gabbro and "leuco" varieties, ferrodiorite, and troctolite (Figure 1.9; Ryan *et al.* 1995; Ryan 2000). Ryan (2000) suggests the abandonment of the term "the Reid Brook intrusion/complex" in light of detailed mapping results by Diamond Fields Resources and Inco Ltd. geologists and geochronological studies (Amelin *et al.* 1997; Li *et al.* 1998; Lightfoot and Naldrett 1999) in the Voisey's Bay deposit area. Two separate troctolitic intrusions, have recently been subdivided from the RBC: (i) olivine-bearing gabbroic and troctolitic rocks of the Voisey's Bay Intrusion (VBI; crystallization age is 1333 Ma; Amelin *et al.* 1999) which hosts major Ni-Cu sulphide deposits (Evans-Lamswood 1999) and (ii) the Mushuau Intrusion (MI) which consists of leucogabbro and melanotroctolites of 1317 to 1313 Ma age (Li *et al.* 2000), a crystallization age approximately 20 Ma years younger than the VBI (*op cit.*). Only a few

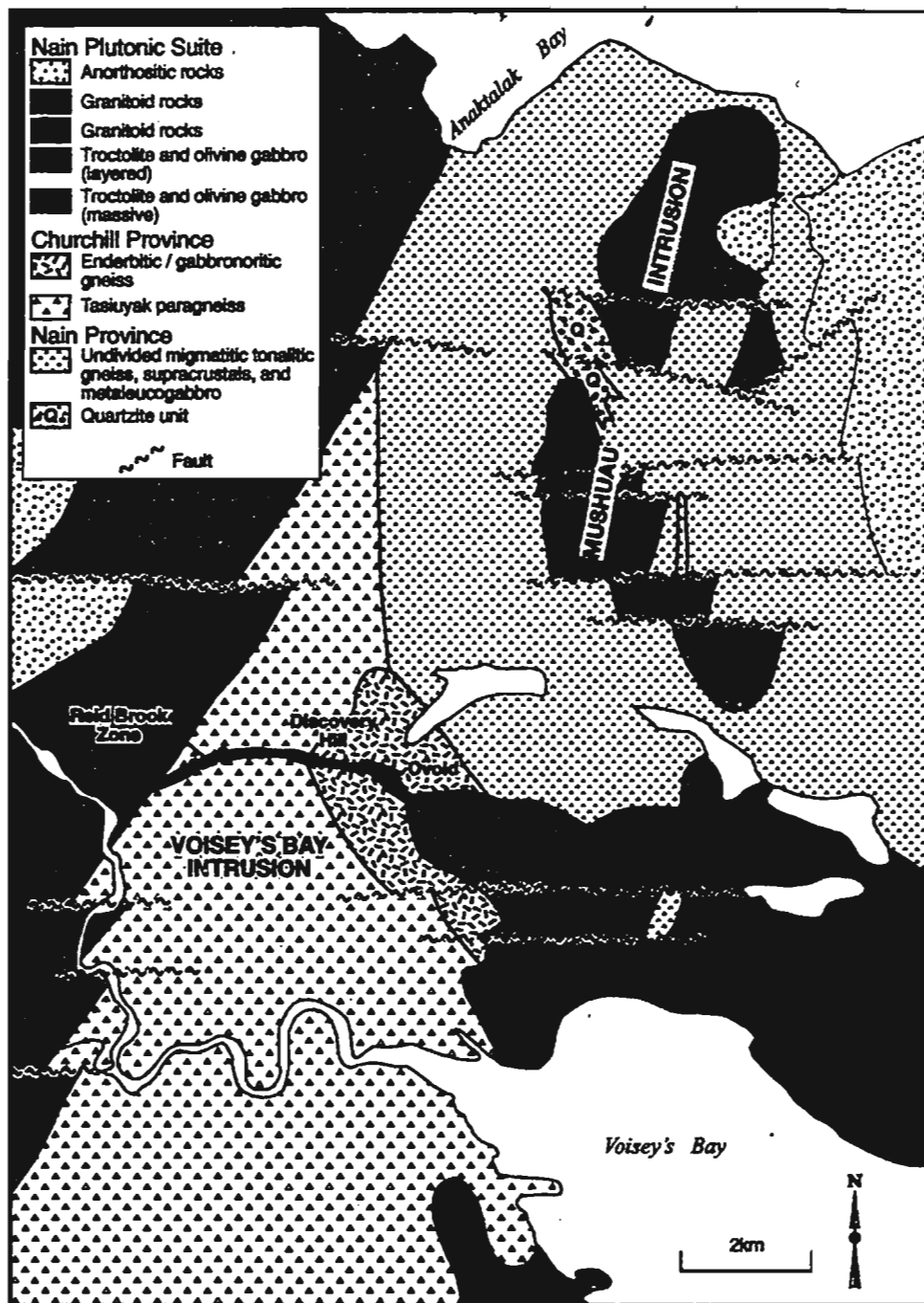


Figure 1.9 Geological map of the Voisey's Bay-Anaktalik Bay area showing the Voisey's Bay deposit (including the Reld Brook zone, the Discovery Hill, the Ovoid, and the Eastern Deeps) located between gneisses of the Archean Nain Province (east) and the Paleoproterozoic Churchill Province (west). This map is from Ryan (2000) who modified it from C. Li of the University of Toronto.

minor Ni-sulphide showings, such as the Sarah showing, have been discovered in the MI.

Intruding the entire area of the VBI are several smaller granitic-syenitic intrusions of the Voisey's Bay granite (1305 Ma; Amelin *et al.* 1999) which are believed to have resulted in contact metamorphic features throughout the VBI (*op cit.*). Geochronological studies of various intrusions throughout the NPS show that the MI is similar in age to several other intrusions, such as the Kiglapait Intrusion (1306 Ma; Morse 1969), and the Newark Island intrusion (1305 Ma; Simmons *et al.* 1986) and that the VBI is the oldest known troctolitic intrusion in the NPS (Li *et al.* 2000).

### 1.7.2 Mineralization

The Voisey's Bay deposit consists of five mineralized zones or smaller deposits: (i) the Ovoid, (ii) the Mini Ovoid, (iii) the Discovery Hill Zone, (iv) the Reid Brook Zone or the Western Deeps, and (v) the Eastern Deeps (Evans-Lamswood 1999; Figures 1.10 and 1.11).

The Ovoid consists of a 500-600 m long by 350 m wide by 100 m deep lens of massive sulphide beneath 10 to 20 m of glacial overburden (Naldrett *et al.* 1996; Naldrett *et al.* 1997; Lightfoot and Naldrett 1999). The host rock grades from dominantly sulphide-free olivine gabbro in the center to varied-textured troctolite (VTT), which contains up to 25 volume % gneiss fragments and patches of sulphides (Li and Naldrett 1999). Ferrodioritic and ferrogabbroic rocks along the margins of the massive sulphides are in contact with enderbitic orthogneiss (Li and Naldrett 1999; Lightfoot and Naldrett 1999). Diamond drill-hole intersections from the Ovoid, as large as 104.3 m of massive sulphides,

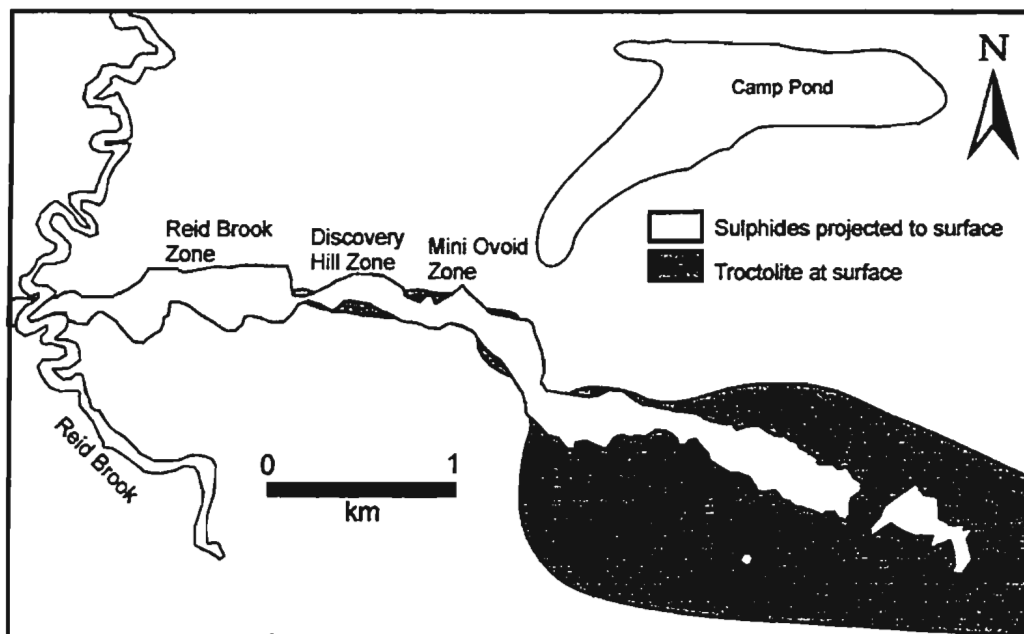


Figure 1.10 General geology map of the Voisey's Bay deposit area showing the surface projection of the Ni-Cu sulphides (from Lightfoot and Naldrett 1999).



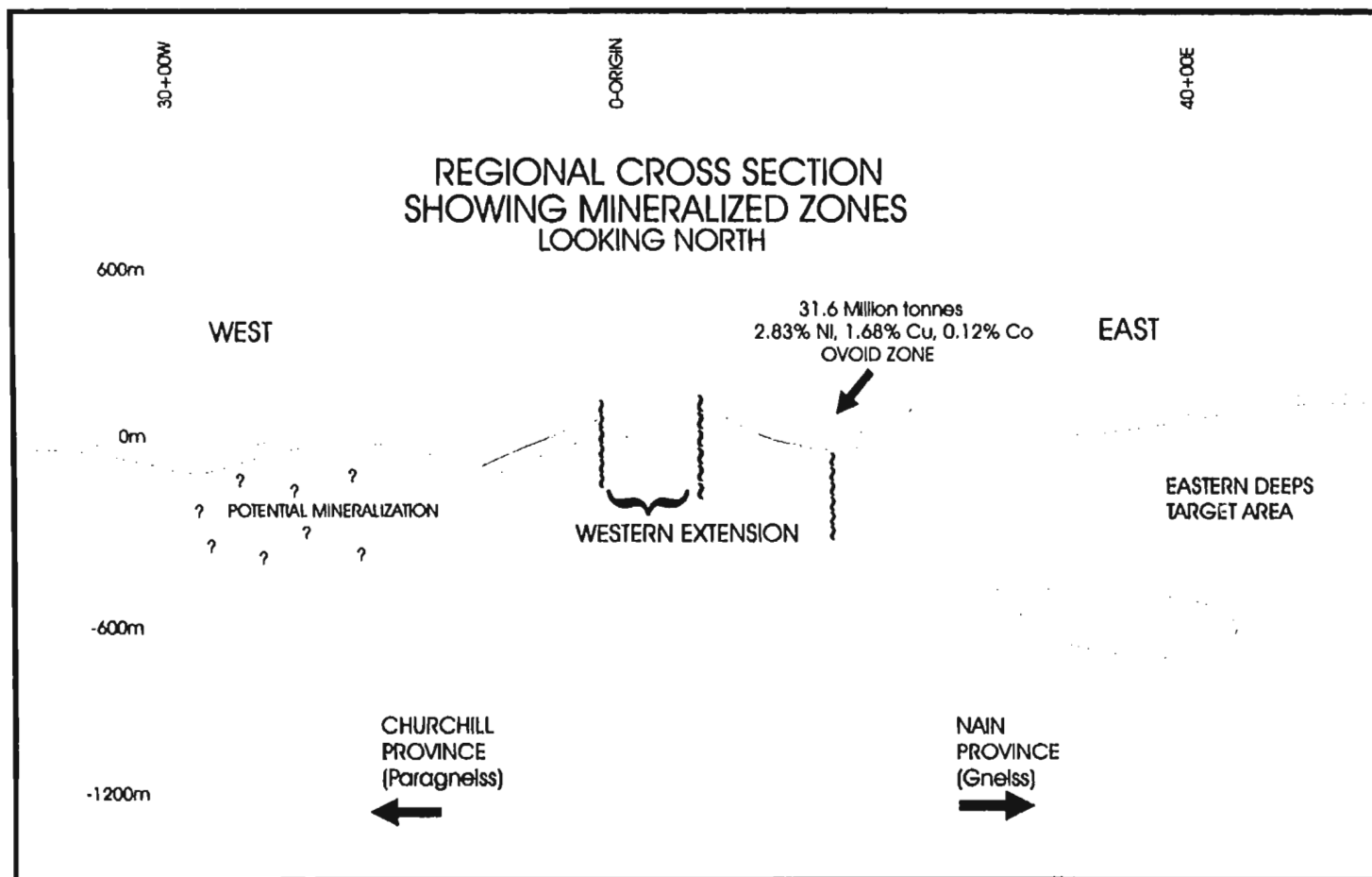


Figure 1.11 Schematic cross section of the Volsey's Bay Ni-Cu-Co deposit showing the Eastern Deeps, Ovoid, and Western Extension (after Naldrett et al. 1996).

are now believed to be the central part of a large wineglass-shaped massive sulphide body overlying a layer of fragments consisting of 25 volume % gneissic basement, troctolite, peridotite, and sulphides known as the Basal Breccia Sequence (BBS; Li and Naldrett 1999). The BBS lies within the sulphide-bearing troctolite which overlies the Archean plagioclase-biotite basement gneisses. The Mini Ovoid represents the western continuation of the Ovoid and consists of massive sulphides within a subvertical troctolitic dyke (Evans-Lamswood 1999).

The Western Extension, lying to the far west of the Ovoid, consists of the Reid Brook Zone (west) and the Discovery Hill Zone (east) and represents the western extension of the troctolite dyke for 3.0 km with a thickness ranging from 30 to 100 m (Naldrett *et al.* 1996; Evans-Lamswood 1999). The Discovery Hill Zone consists of disseminations and veins of semi-massive and massive sulphides in a sub-vertical troctolitic dyke (*op. cit.*). Further to the west, the Reid Brook Zone consists of a steeply dipping troctolitic sheet (45-50°N) which then shallows to 20°N farther to the east. Mineralization consists of lenses of massive and disseminated sulphides underlain by the BBS and overlain by troctolite (Upper Sequence Troctolite; UST) containing disseminated sulphides (Naldrett *et al.* 1996). The percent of sulphides in the troctolite increases with depth from <2% to 45-50% within 10-50 m. At depth, the troctolite known as the “leopard-textured troctolite” (LT), typically contains up to 50% interstitial sulphides and 10 modal % black oikocrysts of augite or olivine enclosing plagioclase within a generally yellow matrix (Li and Naldrett 1999).

The Eastern Deeps lies to the east of the Ovoid and consists of a elongate flat-lying

troctolitic feeder or dyke located distally to the main sub-vertical troctolitic body (Evans-Lamswood 1999). The Eastern Deeps contains disseminated and lenses of massive and semi-massive sulphides (greater than 50 x 10 tons of ore grading 1.36% Ni; Li and Naldrett 1997) within troctolite sandwiched between the basal contact of the Reid Brook Intrusion troctolite with a variable pegmatitic to medium-grained texture (VTT) and the underlying BBS (Naldrett *et al.* 1996; Naldrett *et al.* 1997). The entire zone is overlain by barren intrusive rocks which have insignificant geophysical and geochemical signatures (Kerr 1997). Ferrogabbroic rocks lie along the margin and in contact with the enderbitic orthogneisses, gabbro-noritic gneisses, and quartzofeldspathic migmatites (Lightfoot and Naldrett 1999). The troctolite outcrops on surface and dips uniformly 25°SE and is intruded by syenite and monzonite (Naldrett *et al.* 1996; Li and Naldrett 1999). Typically separating the BBS and the gneissic country rock is a thin layer of sulphide-poor, inclusion-free troctolite (normal troctolite or NT; Li and Naldrett 1997). Depth to the top of the massive sulphide zone is about 600 to 1000 m from surface. The maximum grade of massive sulphide is 1.47% Ni, 0.67% Cu, and 0.07% Co in a 32 m thick zone. Lower grades (0.44% Ni, 0.22% Cu, and 0.02% Co) occur within a 287 m zone of massive sulphides (Diamond Fields Resources Inc., *press release*, November 1995).

Generally, mineralization at Voisey's Bay is most abundant beneath the UST and within the top part of the BBS and sulphides increase in abundance with depth from disseminated to semi-massive (about 50%). Some holes have abrupt intersections of massive sulphide before hitting the lesser mineralized layer of the BBS. In the Ovoid, the

massive sulphides consist of about 75% pyrrhotite (monoclinic and hexagonal), 12% pentlandite, 8% chalcopyrite-cubanite, and 5% magnetite (Naldrett *et al.* 1996).

### **1.7.3 Present model for the genesis of the Voisey's Bay deposit**

The earliest model describing the genesis of the Voisey's Bay sulphide deposit was proposed by Ryan *et al.* (1995) who stated that the first stage in the development of the deposit was the transport of hot, MgO-rich, relatively unfractionated mafic magma from the mantle along or near the suture which separates the sulphur-bearing gneissic rocks of the Nain and Churchill provinces. Since then, there have been many studies done which have further defined the genetic history of sulphide mineralization of the Voisey's Bay deposit [*cf.* Naldrett *et al.* (1996), Evans-Lamswood (1999), Li and Naldrett (1999), Lightfoot and Naldrett (1999), Ryan (2000), Amelin *et al.* (2000), Evans-Lamswood *et al.* (2000), and Li *et al.* (2000)]. Others have applied this model for exploration elsewhere [*cf.* Hoatson *et al.* (1998), who compared the Voisey's Bay deposit with the Sally Malay layered mafic-ultramafic intrusion, in the East Kimberley, Western Australia].

According to the model, mantle-derived basaltic magma ascended through the middle lithospheric crust via east-west lineaments produced during the 1.8 Ga collision of the Churchill and Nain provinces. Basaltic magmatism was also emplaced along deep subvertical faults which had formed as a result of the domal uplift during the 1.3 Ga anorogenic magmatic event which formed the Nain Plutonic Suite (Ryan *et al.* 1995; Evans-Lamswood 1999). Continuous pulses of magma along the suture line and series of faults

(*op. cit.*) allowed for rapid transport of the magma through the crust with little crystal fractionation. Once emplaced in a chamber at shallower depths, possibly within a structural trap (*op. cit.*), the magma slowly cooled resulting in troctolite and olivine-rich gabbro in the center and ferrodiorite and ferrogabbro along the margins and in contact with the gneissic country rock (Ryan *et al.* 1995; Naldrett *et al.* 1996; Evans-Lamswood 1999; Li and Naldrett 1999).

The entire deposit consists of several sulphide bodies which outline the rapid upward transport and deposition of the sulphides through a series of multi-channeled conduits or dykes into existing magma chambers (Evans-Lamswood *et al.* 2000). Naldrett *et al.* (1997), Evans-Lamswood (1999), Li and Naldrett (1999), and Lightfoot and Naldrett (1999) interpret the mineralization of the Voisey's Bay deposit to consist of two magma chambers, one stratigraphically lower than the other, separated by a ~ 1km long conduit. As a result of tectonic displacement along several east-west trending sinistral faults and NW and NE brittle conjugate fault sets (Evans-Lamswood 1999), several "windows" of the deposit formed, enabling better definition of the deposit. Figure 1.12a illustrates the different erosion levels which have either exposed or removed significant overburden in several areas of the deposit. Figure 1.12b is a plan view of the deposit (*from* Lightfoot 1997, 1998; Lightfoot and Naldrett 1999) showing the two magmatic chambers, Eastern Deeps, and the Reid Brook Zone, which are interpreted by Li and Naldrett (1999) to be the upper chamber and the top of the lower chamber, respectively. Evans-Lamswood (1999) interprets the Western Deeps (or Western Sub-Chamber; Lightfoot and Naldrett 1999) to be the lower

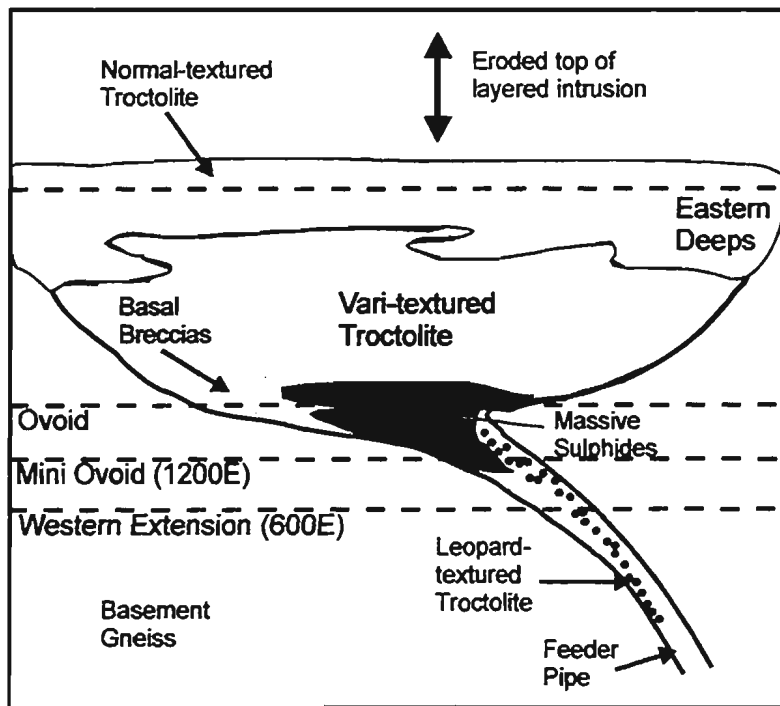


Figure 1.12a Cross section of the Voisey's Bay Ni-Cu-Co deposit showing the Eastern Deeps, the Ovoid, and the Western Extension (from Naldrett et al. 1996; Lightfoot and Naldrett 1999).

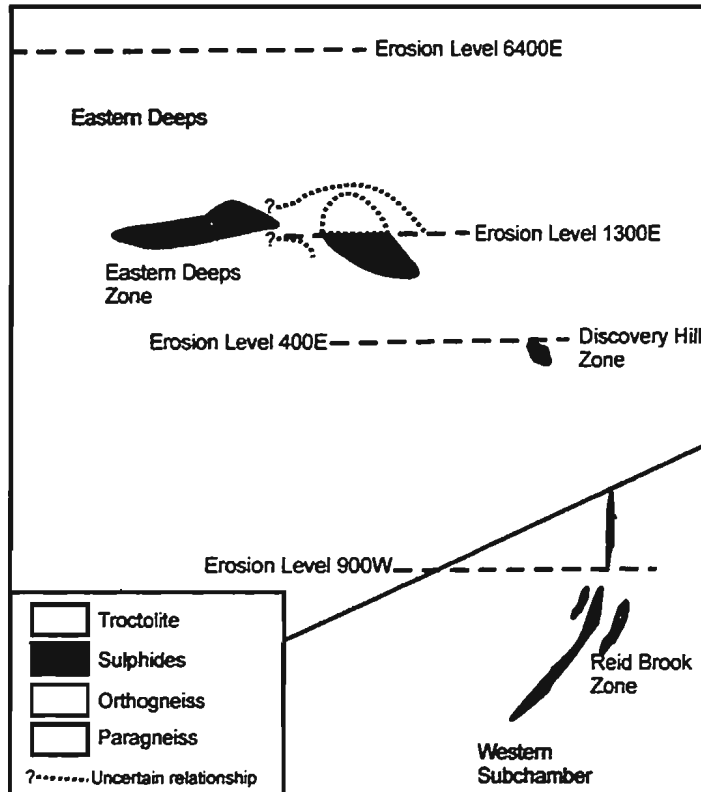


Figure 1.12b Schematic plan view model of the Voisey's Bay deposit showing the conduit, Ovoid, Eastern Deeps, and Western Subchamber at various erosion levels (from Lightfoot 1997; 1998; Lightfoot and Naldrett 1999).

chamber. The Ovoid represents the base of the Eastern Deeps intrusion or the upper chamber (Naldrett *et al.* 1997; Li and Naldrett 1999) and the Mini-Ovoid represents the point at which the feeder connecting the two chambers enters the upper chamber (Lightfoot and Naldrett 1999). The Discovery Hill Zone represents a cross section of the feeder between the two chambers, the Western Extension represents a deeper part of the intrusion, and the Reid Brook Zone represents the top of the lower chamber (Li and Naldrett 1999). Breccia sequences consisting of various Nain and Churchill province gneisses, interstitial sulphides, and troctolitic and ultramafic inclusions occur along the basal contact in every zone indicating a high velocity of mafic magma.

The transfer of hot mafic (and possibly ultramafic) plumes from the mantle resulted in extensive dilatency of the zones of weakness and the formation of the core of a basin-like structure at depth (Evans-Lamswood 1999). The driving force of the upward movement along these conduits was continuous surges of relatively fresh magma from depth; movement continued until the magma slowed down or became trapped (Ryan *et al.* 1995; Evans-Lamswood 1999; Lightfoot and Naldrett 1999; Li and Naldrett 1999). Continued heating of the area led to further dilatency and the formation a graben-like structure, establishing further structural traps for sulphide deposition (Evans-Lamswood 1999). The first chamber for magma pooling was the Western Deeps. The Eastern Deeps, representing a stratigraphically higher chamber, is located at the core of the basin-like structure (*op. cit.*). The Ovoid formed as a result of west-directed extension of the floor of the Eastern Deeps chamber (*op. cit.*).

It is currently thought that sulphides formed after the first 'wave' of mafic magma was emplaced (Ryan *et al.* 1995; Li and Naldrett 1999; Lightfoot and Naldrett 1999; Evans-Lamswood 1999). Evidence of variable Ni contents in olivine within the olivine gabbro and NT, VTT, and BBS in the first large intrusion and the Feeder Troctolite, and the mineralized troctolite and BBS in the conduit, suggest that initial magmatic pulses crystallized Ni-depleted olivines indicating sulphide segregation occurred prior to emplacement at the present level. Subsequent pulses up the feeder were sulphide-unsaturated and crystallized Ni-undepleted olivines (Li and Naldrett 1997). The sulphur content increased due to assimilation of the sulphur-bearing Tasiuyak Gneiss, and to a lesser extent the Archean Nain Province (Emslie *et al.* 1994; Ripley *et al.* 1999). Because sulphide saturation had not been reached prior to, or during, crystal fractionation, olivine scavenged Ni from the magma resulted in the first magma pulses forming forsteritic troctolite and gabbros in the lower chamber (Western Deeps; Evans-Lamswood 1999; Li and Naldrett 1999). Subsequent magma, rich in metals and sulphur, pushed the existing metal-poor magma ahead and upwards through a feeder and into another chamber (Eastern Deeps), approximately 1 km above the first chamber (Li and Naldrett 1999; Evans-Lamswood 1999); the Ovoid was filled with sulphide material as the magma pushed even further to the west. Sulphide saturation is thought to have resulted from the ingestion of significant amounts of sulphur from the surrounding country rock, however, felsification of the magma by incorporation of SiO<sub>2</sub> from the silica-rich gneisses may have also played a role (Ripley 1999; Ripley *et al.* 1999). Sulphide segregation occurred in the Reid Brook subchamber and the



sulphides were then moved upwards through the conduit to the overlying Eastern Deeps subchamber (Li *et al.* 2000).

The velocity of the sulphide-laden magma as it enters the lower chamber was high and so the semi-crystallized Ni-rich olivine-bearing fractionated melts and xenoliths of the gneissic country rock were carried forward and deposited in topographic lows and embayments along the way (Evans-Lamswood 1999; Li and Naldrett 1999; Lightfoot and Naldrett 1999). Sulphides, being denser than the silicate material were deposited first within the feeder connecting the two chambers and near the mouth of the feeder in the top chamber (Ryan *et al.* 1995; Evans-Lamswood 1999; Li and Naldrett 1999; Lightfoot and Naldrett 1999). As with a fast flowing river carrying sediments, the sulphides formed laminar deposits where the velocity of the magma decreased (*op. cit.*). If ever the flow velocity decreased during the mineralization deposition event, the sulphides settled backdown into the feeder at depth to be subsequently pushed upwards with later, fresh, high velocity magma, resulting in mixing of fresh and older magma. Continuous influxes of chalcophile elements most likely contributed to an elevated tenor (Naldrett *et al.* 1996; Evans-Lamswood 1999). Initial magma pulses which entered the Eastern Deeps subchamber formed the Normal troctolite and Varied-textured troctolite (Li *et al.* 2000). Sulphides from these magmas formed the disseminated mineralization and subsequent reactions with fresh magma resulted in greater Ni, Cu, and PGE contents than the earlier massive sulphides in the conduit (*op cit.*).

Subsidence of the magma pulses caused the crustal rock to fracture upon cooling.

Any remaining sulphide liquids were pushed upwards through the choked conduits and inward through the newly formed fractures in the country rock (Evans-Lamswood 1999). The lack of sulphide mineralization north of the Eastern Deeps suggests a pinching of the feeder resulting in the sulphide melt moving laterally along fracture surfaces forming the deposit structure of the Eastern Deeps feeder (*op. cit.*).

## 1.8 Purpose

The main purpose of this project is to study the previously unknown magmatic sulphide occurrence at the Cirque property and to evaluate its economic potential. Considering the attention that the northern NPS has received the last few years, such a comparison will greatly enhance future interpretations of magmatic sulphide mineralization by exploration companies in the northern NPS.

The world class magmatic Ni-Cu-Co±PGE sulphide deposits at Voisey's Bay are located approximately 80 km south of the NPS-hosted gossan at Cartaway's Cirque property. Intersections of the gossan on the Cirque property indicate that the sulphide mineralization is less extensive and contains subeconomic base metal values compared to the Voisey's Bay deposit. There are, however, some significant features in common between the Voisey's Bay deposit and the Cirque mineralization. Both are located within the NPS, and mineralization is hosted in coalesced magmas of anorthosite-norite-gabbro-leucotroctolite lithologies. Both areas are proximal to the northwest-trending cratonic suture separating the Archean Nain Province and the Archean and Paleoproterozoic rocks of

the Churchill Province; this tectonic location is important as a structural weakness for the intrusion of the magmas and also a sulphur source for magmatic sulfide mineralization.

Interpretations of the assay values and textures of the mineralized zones in drill core at the Cirque property suggest that at least a portion of the sulphides within the horizons have been remobilized and that there may be more sulphides at depth, possibly a nickel-rich 'restitute' at lower depths (F.P.F. Resources 1996). It is believed that the separation and accumulation of sulphide minerals in the mafic silicate magma occurred at depth and that mobilization of the sulphides took place after semi- to complete cooling of the parental mafic igneous intrusion. Pervasive erosion of plagioclase crystals and leucoanorthosite inclusions, crystals cross cut by pyrrhotite veins on a macro-scale, and brittle fracturing on a micro-scale support the idea of sulphide remobilization from a magmatic source below.

Presently, the geology of the area south of Okak Bay is being re-interpreted and plutons are being reclassified as either Late or Middle Proterozoic. A detailed examination of the geology and geochemistry of the Cirque will add to these re-interpretations of the northern Nain Plutonic Suite. More importantly, however, the results from this study will greatly contribute to the understanding of the geology and sulphide mineralization of the Cirque gossan and surrounding area.

## **1.9 Scope**

Interpretations of the geology were completed using a 1:5000 scale grid map, twelve diamond drill logs, plus local and regional maps. Samples were collected during grid

mapping and core logging. Holes 1-5, originally logged by a previous geologist with Cartaway Resources, were re-logged by the author for consistent descriptions of the units and mineralization in the twelve holes. Petrographically examined polished thin sections of sulphide-poor and sulphide-bearing rocks, as well as detailed observations of hundreds of selected core samples, illustrate the variety of host rock and sulphide textures present. Whole rock and Ni-Cu-Co and PGE assay data from Cartaway's rock and core samples, plus geochemical data derived from additional rock and core samples collected later by the author were incorporated to produce a large database of trace and major element analyses (XRF and ICP-MS). At Memorial University selected core samples (rock and pulps) and hand samples of both sulphide-poor and sulphide-bearing rocks were assayed for major and trace elements, including Ni, Cu, Co, and PGE. Plagioclase, olivine, orthopyroxene, clinopyroxene, ilmenite, and magnetite were analysed using electron microprobe techniques to determine cumulate geochemistry of the rocks. Pyrrhotite, chalcopyrite, and pentlandite of mineralized samples from the Cirque property and other mineralized gossans throughout the NPS were also analysed using electron microprobe to determine sulphide geochemistry. Sulphur isotope analysis determined the sulphur source for sulphide mineralization and Sm/Nd and Rb/Sr isotope analyses indicated the magma source of the mafic units. In all, this thesis is a thorough investigative approach toward evaluation of a newly discovered sulphide occurrence.

## **CHAPTER 2**

### **REGIONAL AND LOCAL GEOLOGY**

#### **2.1 The geology of the Torngat Orogen, Churchill Province and Nain Province**

The geology of northern Labrador consists of the Nain Province to the east and the Churchill Province (or Trans-Hudson Orogen) to the west (Figure 2.1). The Churchill Province consists of reworked Archean orthogneiss and migmatite units with Paleoproterozoic intrusive and supracrustal rocks. Its inner Archean core is known as the Rae Province (Hoffman 1988; Wardle and Wilton 1995). The Nain Province consists of Early to Late Archean (3.8 - 2.7 Ga; Ryan 1991) tonalitic to granodioritic orthogneiss and lesser granitoid rocks; the metamorphic grade ranges from greenschist to upper amphibolite (Xue 1992). Following a period of extensive mafic dyke intrusion between 2300-2100 Ma (Ryan 1991), the gneisses were eroded and then overlain by Lower Proterozoic supracrustal sequences of the Mugford and Ramah groups (Wilton 1996).

Circa 1.85 billion years ago the Nain Province collided with the Churchill Province, producing the Torngat Orogen. Rivers and Mengel (1994) propose an eastward subduction of the Rae Province, however, Van Kranendonk and Ermanovics (1990) and Bertrand *et al.* (1993) suggest a westward subduction of the Nain Province. The suture between the Nain and Churchill provinces is a linear segment of metamorphosed and deformed flyschoid deposits from both the Rae and Nain provinces (Wardle *et al.* 1995). Dominant structural features imparted by the Torngat Orogeny include fold axes and faults with general

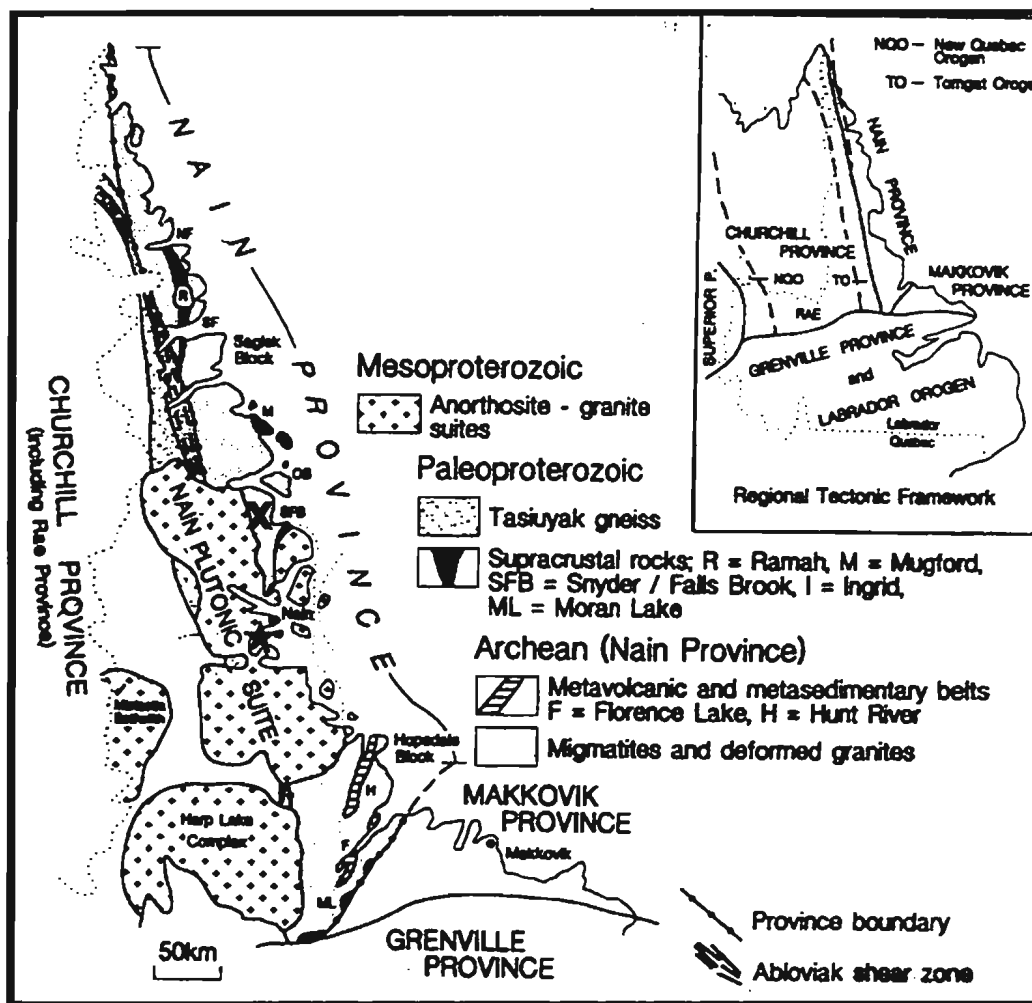


Figure 2.1 Lithotectonic terranes of northern Labrador (from Ryan et al. 1995). The "X" marks the general location of the Cirque property. Star marks the general location of the Voisey's Bay deposit.

north-northeast trending foliations, particularly along the margins of the Nain and Churchill provinces.

Within the Nain Province there are two distinct lithotectonic areas: the Saglek Block and the Hopedale Block, which are separated by Mesoproterozoic plutonic rocks of the Nain Plutonic Suite. The Saglek Block (3.35 - 3.31 Ga; Wilton 1996) comprises the northern part of the Nain Province and consists of high grade gneiss with Archean to Early Proterozoic supracrustal sequences. Variably deformed and metamorphosed Paleoproterozoic anorthosite to ultramafic intrusions are present within the gneiss terranes. The Hopedale Block (3.2 - 3.1 Ga; Wilton 1996) consists dominantly of tonalitic Maggo Gneiss and tholeiitic Weekes Amphibolite with the Hunt River and Florence Lake greenstone belts (Wilton 1996). The tonalitic-trondjemite-granodiorite rocks of the Kanairiktok Intrusive Suite, yielding a U/Pb zircon age of  $2858 \pm 4/-3$  Ma (Loveridge *et al.* 1987), represent the final plutonic activity in the Hopedale Block.

### **2.1.2 The Torngat Orogen**

The Paleoproterozoic Torngat Orogen is a deep seated suture zone dipping steeply to the east separating the generally nonmagnetic Churchill Province to the west from the generally magnetic Nain Province to the east. The Torngat Orogeny marks a period of oblique collision between the Nain and Churchill provinces and subsequent deformation as a result of sinistral shearing and crustal thickening along the collisional zone (1860 - 1740 Ma; Bertrand *et al.* 1993). The Torngat Orogen includes the Torngat Mountain Range and

extends from the northern-most Labrador to approximately 450 km southeast, ranging from 15 to 40 km wide. From west to east, the Torngat Orogen (Figure 2.2) consists of the (i) Lac Lomier Complex, (ii) the Tasuiyak Gneiss Complex, (iii) the Burwell Domain, and (iv) reworked units along the foreland of the Torngat Orogen that lie within the Nain Province (Wardle *et al.* 1995).

The Lac Lomier Complex consists of Archean granitoid gneisses which are adjacent to those of the Rae Province. These gneisses were later deformed along with Early Proterozoic rocks and then intruded by orthopyroxene-bearing tonalite to granodiorite plutons, thought to be coeval with  $1877 \pm 1$  Ma plutons (Bertrand *et al.* 1993) in the Tasuiyak Gneiss Complex.

The Tasuiyak Gneiss Complex is parallel to the suture zone and consists of late Archean - Early Proterozoic accretionary wedge flyschoid material along the eastern margin of the Churchill Province (Scott and Machado 1994a; Wardle *et al.* 1995) that was reworked to form a distinctive, low magnetic, 30 km wide zone of garnet-sillimanite-biotite-graphite quartzofeldspathic gneiss ( U/Pb zircon,  $1877 \pm 1$  Ma; Bertrand *et al.* 1993).

The Abloviak Shear Zone (ASZ), located along the eastern side of the Tasuiyak Gneiss Complex, is a linear zone of highly metamorphosed (granulite grade) and deformed units formed by sinistral shearing along the provinces' margins and oblique tectonic collisional deformation (Wardle *et al.* 1995). The ASZ represents the final emplacement of the Nain and Rae Provinces at 1845 - 1820 Ma (Bertrand *et al.* 1993; van Kranendonk and Wardle 1994, 1997; van Kranendonk 1996) with the last sinistral strike-slip movement



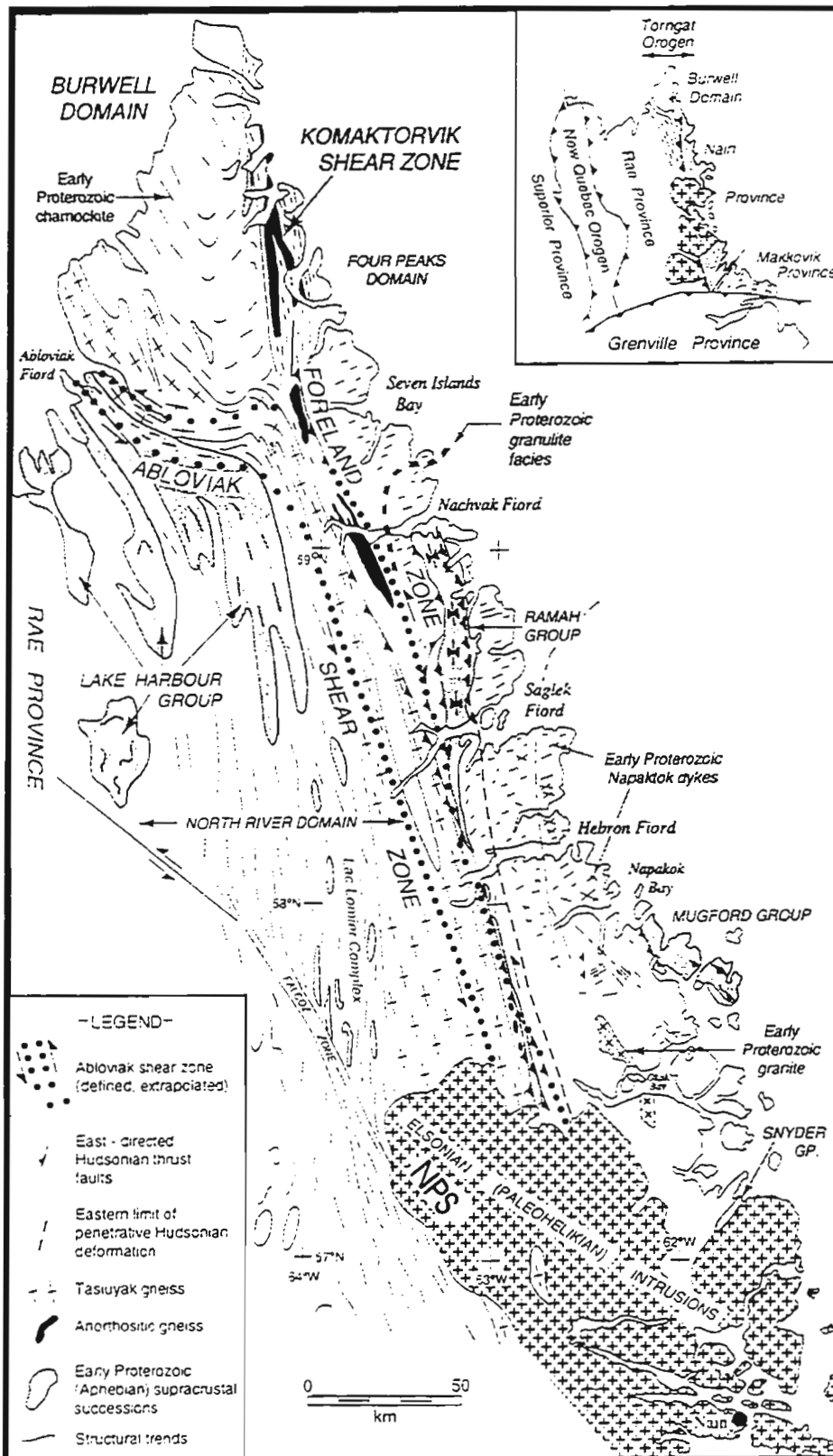


Figure 2.2 Geology of northern Labrador and northern Quebec, showing the distinct terranes of the Torngat Orogen: Lac Lomier; Tasiuyak Gneiss Complex; Burwell Domain; reworked units within the Nain Province (van Kranendonk 1990).

occurring at 1.73 - 1.75 Ga (van Kranendonk 1996).

The Burwell Domain, thought to have originated as the roots of a magmatic arc (Wardle *et al.* 1992), consists predominantly of Early Proterozoic charnockite (orthopyroxene-bearing granite) and amphibolite facies diorites, tonalites and granites which intruded the Tasuiyak Gneiss Complex and contain enclaves of Archean (Campbell 1994) mafic granulite and orthogneiss (Wardle *et al.* 1993). Intrusions of metatonalite (U/Pb zircon age of  $1869 \pm 3/-2$  Ma) and megacrystic granite (minimum U/Pb zircon age of  $1864 \pm 2$  Ma) are present within the Burwell Domain and the Nain Province (Scott and Machado 1994, 1995).

## **2.2 The Nain Plutonic Suite**

Following a period of tectonic quiescence, an extensive Middle Proterozoic episode of repetitive, multi-phase mafic to felsic plutonism (Emslie and Hunt 1990; Ryan 2001) developed parallel to the suture zone *ca.* 1350-1290 Ma (Ryan and Emslie 1994; Ryan *et al.* 1995). Spanning from northern to central Labrador, during a 60 million year period of anorogenic magmatism (Ryan *et al.* 1997), huge volumes of granitoid to mafic magma intruded the Nain-Churchill-Grenville crust above a mantle hotspot to depths of about 6 to 14 km (Berg 1979; Emslie *et al.* 1994) and coalesced to form stitching plutons and large batholiths. Although a plume-related source is the most popular method of magma transport, Amelin *et al.* (2000) suggest lithospheric thinning due to extension along a pre-existing line of weakness may have resulted in magmatic intrusions. The resultant plutons

were generally unaffected by succeeding tectonism, however, uplift and erosion of the Elsonian plutons occurred shortly after emplacement (Emslie 1978). Like the Harp Lake Intrusive Suite, it is thought that the NPS may have been uplifted as a result of crustal thickening from huge volumes of magma emplaced in an extensional environment (Amelin *et al.* 2000). Basaltic dykes, which crosscut all of the granitic and mafic intrusions within the NPS, are thought to be about 50 million years younger than the main NPS magmatic event (Carlson *et al.* 1993), and support the idea of crustal thickening, uplift, and erosion of the intrusions within the NPS (Wiebe 1985; Amelin *et al.* 2000). Field relationships, geochemistry, and isotopic data suggest that the dykes represent the precursor material from which the NPS magmatism was derived (Amelin *et al.* 2000).

Intrusions located south of the Grenville Front, in what is now southern Labrador, were subject to deformation and metamorphism as a result of the Grenvillian and Labradorian orogenies. Overall, this period of plutonism is thought to be a northern extension of the mafic-granitic plutonism which intruded the crust from as far south as the Adirondacks in eastern North America (Xue 1992; Figure 2.3).

As a complete package, the NPS spans an area of over 19,000 km<sup>2</sup> (Emslie *et al.* 1994), from south of Okak Bay to north of the village of Hopedale and from islands off the east coast to about 100 km inland on the west side of the Nain - Churchill suture zone (Figure 2.4). The NPS consists of anorthosite - mangerite (*i.e.* orthopyroxene-bearing monzonite) - charnockite (*i.e.* orthopyroxene-bearing granite) - granite (AMCG) suites whose intrusions were focused along the cratonic suture zone between the Nain and Churchill

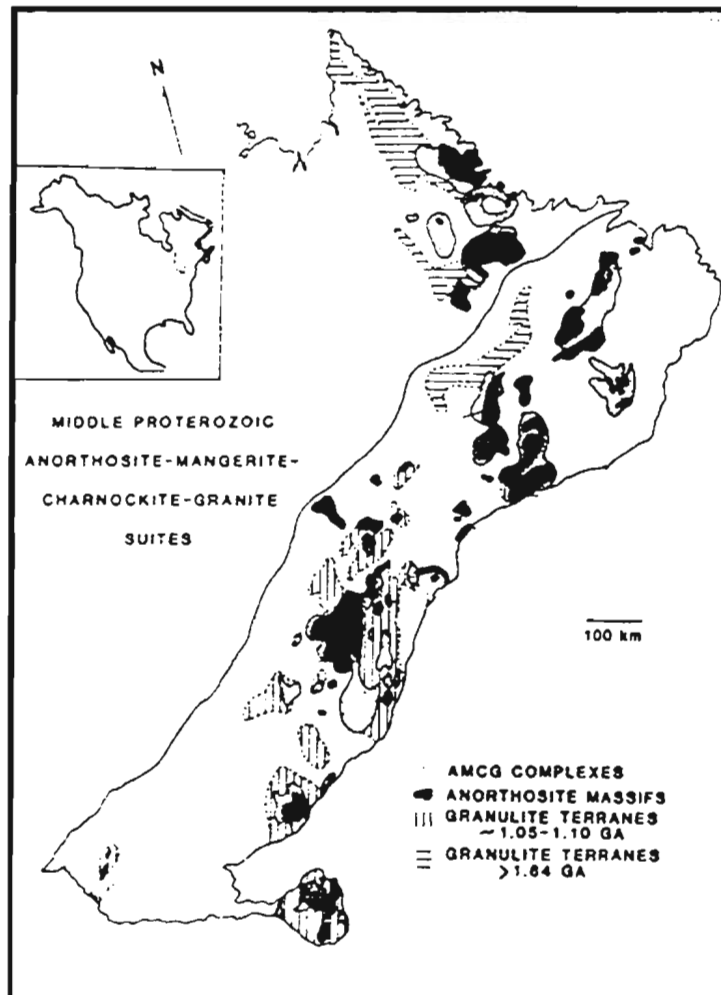


Figure 2.3 Regional map showing locations of anorthosite and related rocks of the AMCG suite (from Emslie and Hunt 1990). Magmatism was very extensive and included several separate intrusions.

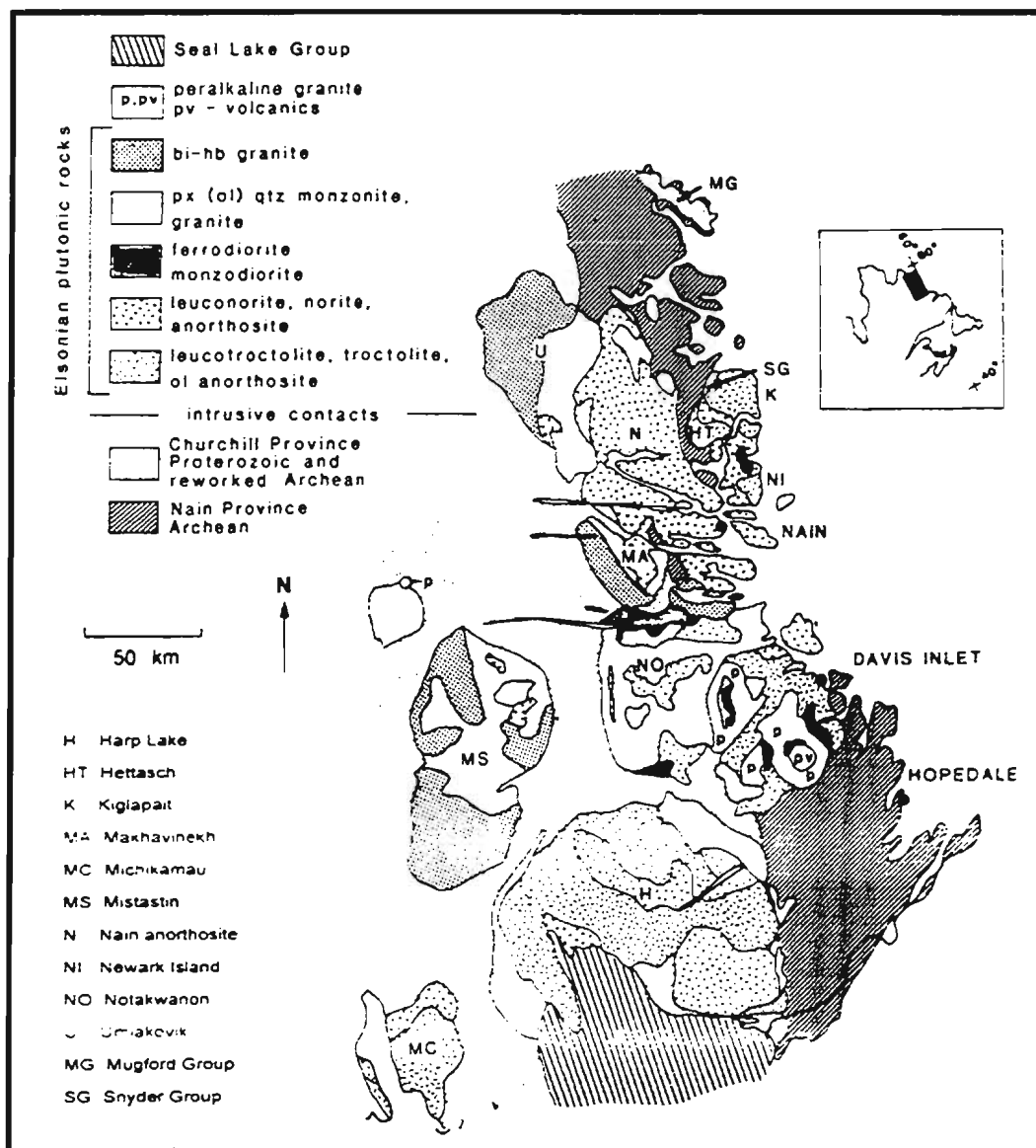


Figure 2.4 The NPS and other Elsonian intrusions in central and northern Labrador (from Emslie et al. 1994). The NPS includes Umiakovic Batholith, Makhavinekh pluton, Notakwanon Batholith, Nain anorthosite, and the Kiglapait, Hettasch, Newark Island intrusions.

provinces. Ryan (1990) subdivided the NPS into four main rock types in order of decreasing volume: (1) anorthosite rocks which include norite, leuconorite, anorthosite, and some gabbroic and troctolitic variants, (2) troctolite rocks which include predominantly troctolite and olivine-bearing gabbroic layered intrusions, (3) iron-rich gabbroic-dioritic rocks and related compositions, and (4) granitic rocks which include granite, monzonite, syenite, and monzondiorite. The mafic units, which are generally interlayered (particularly anorthosite and leucogabbro / leuconorite) with gradual contacts as a result of continuous fractional crystallization and replenishment from the magma source below (Wheeler 1960), consist of coarse-grained, cumulate plagioclase with variable percentages of coarse-grained, cumulate pyroxene (dominantly hypersthene and augite) and with or without significant oxide minerals. Local layering of pyroxene crystals and feldspar laths occurred as a result of crystal settling during fractional crystallization. Mineral foliation, seen locally in pyroxene and plagioclase crystals, may also be due to magmatic squeezing and crystal alignment of a moving magma body at the time of slow crystallization. Aligned minerals in plutonic bodies observed near contacts with the continental crust are thought to have formed as a result of stress and strain during magma emplacement (Ryan 1991).

There are several distinct intrusions within the NPS that have been studied in varying degrees of detail. Each large intrusive body has distinct geochemical and structural features (*e.g.*, geological units, igneous layering, foliations, chilled margins). One in particular is the Kiglapait Intrusion (KI), a lopolith underlying the Kiglapait Mountains northeast of Nain,

which consists of a series of rhythmic and graded layering of troctolite, gabbro, ferrodiorite, monzonite, and syenite plutons (Morse 1979, 1994) that form a huge layered, concave intrusion spanning an area of approximately 560 km<sup>2</sup> by 8 km wide and ~ 9 km thick (Figure 2.5). The KI formed as the result of a single injection of high alumina, low-K tholeiitic magma with little contamination (Morse 1969, 1979a,b; Wardle 1996) and was emplaced at  $1306 \pm 2$  Ma (U-Pb zircon dating by Krogh quoted by Yu and Morse 1992). Morse (1969, 1979a,b) estimates the full crystallization time of the intrusion was about 1 million years. The KI, unique in terms of the NPS as metal-sulphide fractionation and accumulation within the parental magma of a closed system, formed several sulphide layers, one being the “Main Ore Band” (Ryan *et al.* 1995). As such, the KI has been an area of interest for its Platinum Group Element (PGE) potential since 1970s. As early as 1995, it was being explored by Archean Resources Ltd. for Ni-Cu-Co and PGE sulphide mineralization.

### **2.2.1 Model for the evolution of massif-type anorthosite and related rocks**

Massif-type anorthosites typically occur as large (surface areas up to 30,000 km<sup>2</sup>) Mid-Proterozoic (1.7 - 0.9 Ga) batholiths often intruding high grade metamorphic terranes (Ashwal 1993; Taylor *et al.* 1984; Scoates and Mitchell 2000). Their general geochemical natures consist of intermediate plagioclase compositions (An<sub>40-60</sub>), Mg/(Mg+Fe) ratios between 40-50, Rb depletions, very low Rb/Sr ratios, and enrichments in Eu and other rare earth elements (Taylor *et al.* 1984). Radiogenetic isotope data indicate low initial <sup>87</sup>Sr/<sup>86</sup>Sr ratios ranging from 0.7025 to 0.7070 and  $\epsilon$ Nd values varying from enriched (-6) to depleted

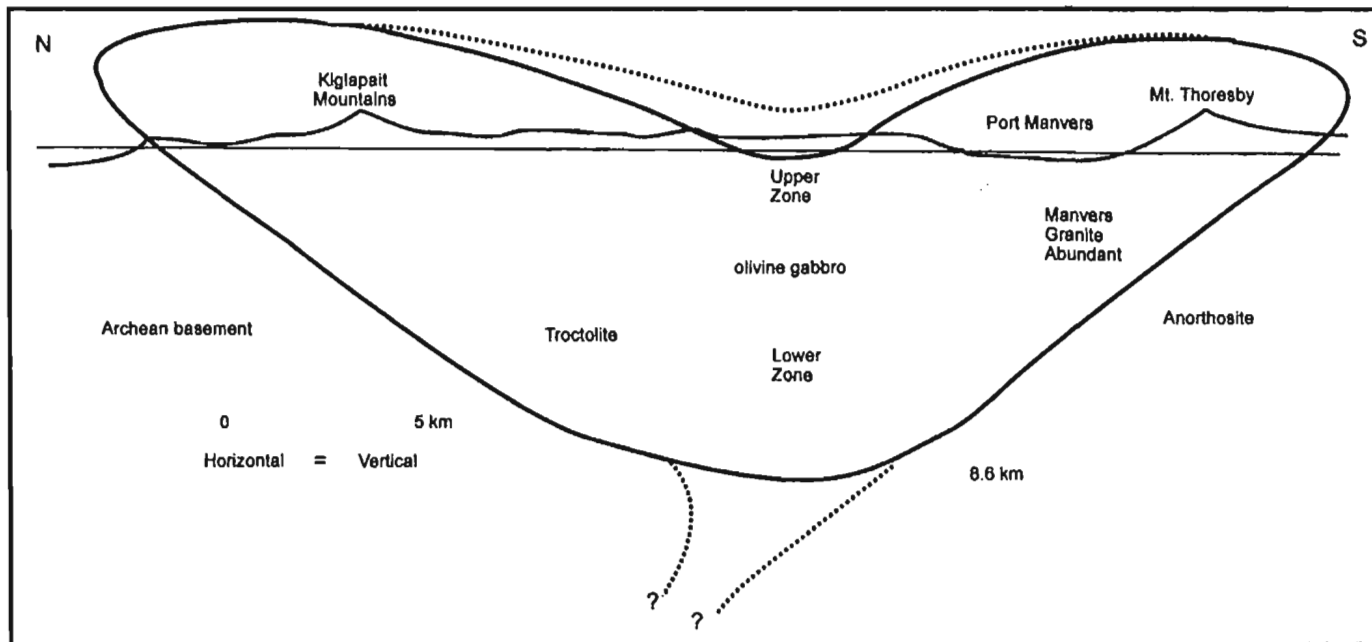


Figure 2.5 Cross-section of the Kiglapait Intrusion (adapted from Morse 1979).



(+4; Taylor *et al.* 1984).

Several models have been proposed over the years to explain the huge volumes of plagioclase-rich melts that these massifs represent; see Ashwal (1993) for a brief summary of some of these ideas. One of the more popular genetic models includes the following generic features: anorogenic emplacement of a mantle plume into the lower crust, fractionation of a parental magma [possibly an Fe-rich tholeiite (Ashwal 1993)], anatexis of the most lower crust leading to residual anorthosite, and emplacement of the anorthosite massifs at intermediate to shallow crustal levels (Emslie *et al.* 1994; Ashwal and Wooden 1983; Taylor *et al.* 1984; Fountain *et al.* 1989). Debate is ongoing over various aspects of this model, such as the depth of emplacement, the significance of lower crustal anatexis, and the possibility that the anorthosite melt evolved from crustally-derived granitoids (Ashwal 1993). Ashwal (1993) claims that the depth of emplacement of the anorthosites was intermediate to shallow citing thermobarometric evidence from contact aureoles which indicates emplacement at depths of 6-14 km for the Nain anorthosites (Berg 1977a,b; 1979) and at temperatures of 1100-1000°C and pressures of 3 kbar [based on pyroxene thermometric studies by Ranson (1986)]. Crystallization conditions of associated monzosyenites of the Laramie anorthosites also indicate emplacement depths of 10-15 km (Fuhrman *et al.* 1988; Kolker and Lindsley 1989; Grant and Frost 1990).

Although there can be considerable variation in composition and texture of the lower crustal rocks (which would affect permeability and heat transfer through crustal material), heat flow of the mantle plume, and contact areas of the mantle material in different

anorogenic settings, the heat source would have to create over 20% silicic anatextic melt in order to produce significant felsic magmas (Fountain *et al.* 1989). Taylor *et al.* (1984) proposed two sources for such heat: (i) radioactive decay of U, K, and Th and (ii) hot mantle-derived material below the crust. Since segregation of the felsic melt from the crust will actually result in a loss of these heat-producing elements from the lower crustal rocks, Taylor *et al.* (1984) conclude that it is not possible for the heat to be maintained for extended periods at the base of the crust. Thus, they proposed that either a mantle “hotspot”, or a line plume, was the heat source for the NPS-style granitic plutons (*op. cit.*). The widespread emplacement of AMCG suites along the eastern side of North America suggests that there was extensive (several hundred million years) mantle plume-lower crust interactions at temperatures exceeding 1300°C (Taylor *et al.* 1984).

Based on radiogenic dating and structural emplacement of plutonic phases, the NPS is believed to have initially intruded to the west and south first and with intrusions moving progressively eastward (Hamilton 1994). According to the latest genetic model (Figure 2.6) proposed by Emslie *et al.* (1994) and Emslie and Hegner (1993), after a period of extensive rifting and crustal thinning, magma from a mantle plume or hotspot accumulated at the base of the crust resulting in crustal anatexis with the subsequent production of felsic melts (Emslie 1978, 1985; Morse 1982; Duchesne 1984). These magmas moved upward, intruding the relatively undepleted continental crust and producing water-undersaturated granitoid melts of charnockitic - mangeritic - adamellitic (*i.e.* quartz monzonite) - granitic compositions. Anatectic granitoid melt formation and its subsequent removal from the base

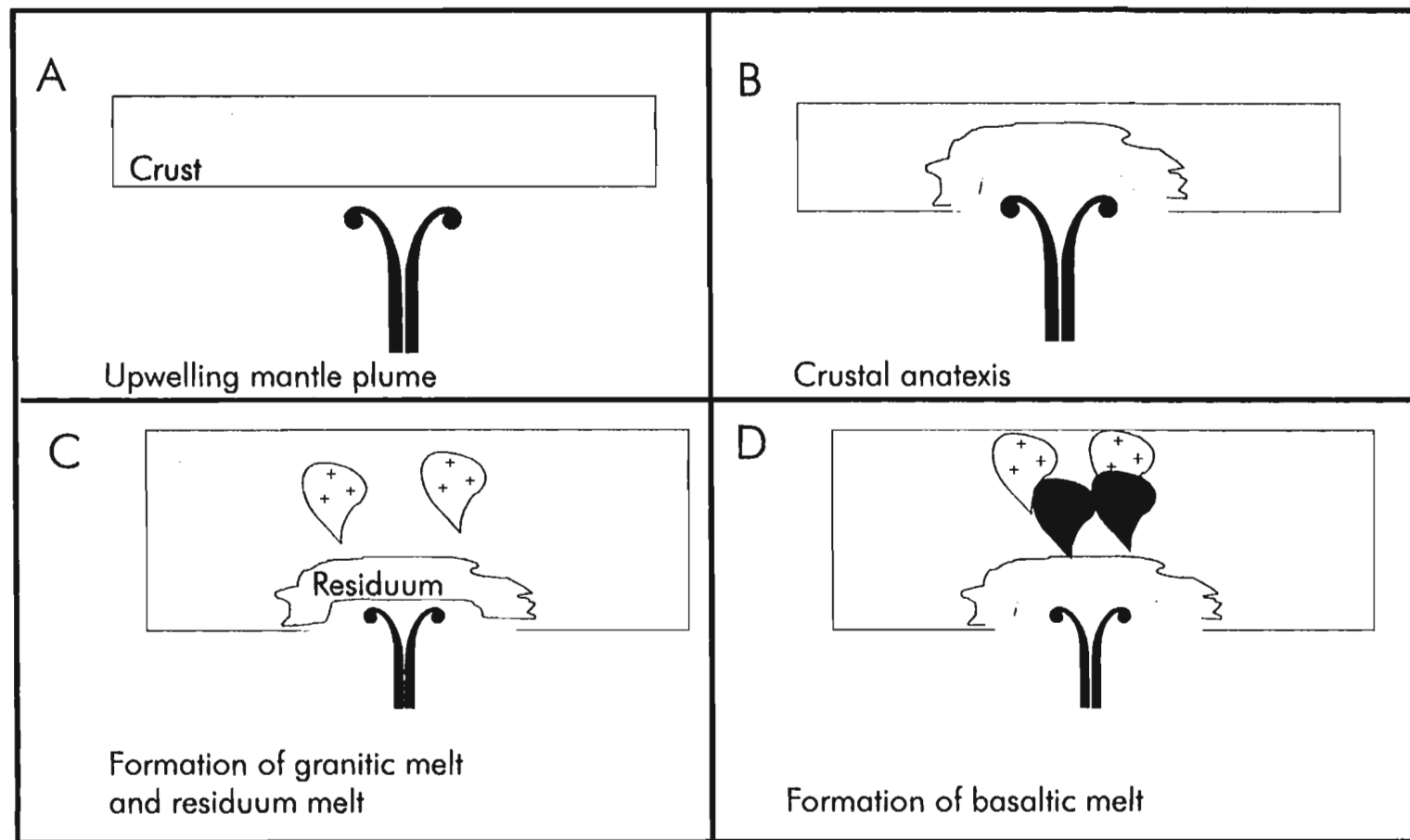


Figure 2.6 Schematic model for the evolution of an anorthosite massif beginning with (a) mantle plume upwelling to the base of the crust, (b) crustal anatexis due to heat from the plume, (c) ascension of felsic melt leaving behind a residuum of crustal melt material, and (d) continued mantle upwelling resulting in the mantle material mixing with the residuum and crust, forming contaminated basaltic magma which rise behind the felsic melts. Subsequent fractional crystallization of the basaltic magma results in the formation of the anorthosites and related mafic rocks.

of the continental crust left behind a dehydrated, plagioclase-pyroxene-enriched granulite residuum which would play an important role as a contaminant to later pulses of uprising mantle magma (Emslie and Hegner 1993; Fountain *et al.* 1989; Emslie *et al.* 1994). The residuum is thought to have been depleted in SiO<sub>2</sub>, Rb, Ba, Zr, Pb, U, REE (particularly LREE) and enriched in those elements compatible with the plagioclase and pyroxene of the residue (Ca, Al, Mg, Sr, Eu, and Ti). The inherently low Rb/Sr ratios in the residuum, therefore, would be reflected in the initial <sup>87</sup>Sr/<sup>86</sup>Sr ratios of the resulting contaminated anorthositic and mafic rocks (Taylor *et al.* 1984).

Evolution of mafic intrusions through assimilation of the partial melt residue, proceeding granulites, and country rock by mantle-derived magma would be very efficient, since the residue would probably be at temperatures in excess of 900°C (Emslie *et al.* 1994). Continuous pulses of mantle-derived basaltic magma maintained the elevated crustal temperatures to granulite grade allowing for mantle-derived, fractionated, plagioclase-pyroxene-rich mafic magmas to accumulate at the base of the crust (Emslie *et al.* 1994). In a thermally maintained environment (*i.e.* elevated temperatures in the surrounding crust and granulite intrusions) with an extended period of contamination and subsequent crystal fractionation of the Al-rich basaltic magma, a large volume of plagioclase-rich anhydrous liquid (*i.e.* anorthosite) would be produced (*op. cit.*). The anorthositic magma (>50% large uniformly sized plagioclase crystals) accumulated and either floated to the top of the magma chamber or remained in place as thick layers of plagioclase-rich melt which thermally insulated the chamber from cooling (Emslie *et al.* 1994; Ashwal 1993; Fram and Longhi

1992). Prolonged crystal fractionation led to progressive crystallization of plagioclase, olivine, and high-Al pyroxene (orthopyroxene>clinopyroxene) along the plagioclase + olivine cotectic and plagioclase + orthopyroxene cotectic, respectively (Emslie *et al.* 1994). The remaining uncrystallized melt (possibly tholeiitic with 17-18 wt%  $\text{Al}_2\text{O}_3$ ) contained elevated Al, Fe/Mg, and REE concentrations (Ashwal 1993). The mafic minerals, being denser than the plagioclase, sank and accumulated over time below the less dense plagioclase crystals, forming ultramafic cumulates as an endmember in the magma mixing process. These ultramafic cumulates are not commonly observed because they are either located at the base of the intrusive suite or they were recycled back to the mantle plume along with crustal contaminants, further altering the geochemistry of subsequent basaltic pulses (Ashwal 1993; Arndt and Goldstein 1989).

The oxygen fugacity changed and the temperature lowered as the melt ascended giving rise to an accumulation of magnetite and ilmenite-rich mafic melts enriched in incompatible elements. These remained at the base of the plagioclase-rich magma or sank to the bottom of the chamber. Ferrodiorite or jotunite rocks, occurring as small dykes or localized intrusions, are the least abundant rock type in the NPS and are thought to be the products of trapped residual liquid (rich in Fe, Ti, P and incompatible elements) within the aluminous melt that was later “squeezed” out into other intrusions as the aluminous magma cooled and pooled at the base of many anorthositic massifs (Emslie *et al.* 1994).

To summarize, geochemical inhomogeneties within the anorthosites and consanquinous mafic rocks are due to numerous factors that would have been introduced

throughout the processes of mantle upwelling, silicic segregation, partial melting and mixing of the basaltic component with the crustal residuum and country rocks. Ferrodioritic or jotunitic rocks were likely derived as the residual liquid of a fractionated mafic magma. Field relationships support this model; as granitoids cap massive anorthosite (with/without leucogabbro-leuconorite-leucotroctolite layering) and ferrodiorite rocks occur as dykes and small intrusions within the anorthosite and related rocks (Ryan *et al.* 1997). Entrained basaltic material which quickly rose along path of previous magma was more primitive due to less time for fractionation and assimilation of the surrounding semi-solidified magmas and country rock. These more primitive magmas crystallized to form the troctolite and related plutons (Ryan 2000). According to this model of plagioclase crystal fractionation at shallow levels in the crust and mafic minerals (olivine and pyroxene, and oxide minerals) at depth and at higher pressure conditions, areas of large extensive anorthosite intrusions near the surface suggests the presence of even larger mafic plutons at depth (Fram and Longhi 1992).

Layering is evident within the NPS suggesting regular episodes of crystal fractionation and magma replenishment. Multiple episodes of magma upwelling, fractionation, and subsequent intrusions of separate melt fractions, which later coalesced, are thought to have occurred over the tens of millions of years during the history of emplacement of the NPS with the period of granitic magmatism occurring twice as long as that of mafic magmatism (Berg *et al.* 1994).

### 2.2.2 Jotunite petrogenesis

Jotunites (~ ferrodiorites) are characteristically enriched in FeO, TiO<sub>2</sub>, P<sub>2</sub>O<sub>5</sub>, SiO<sub>2</sub>, K<sub>2</sub>O, depleted in MgO, Na<sub>2</sub>O, Sc, Cr, Co, Ni, Rb, Th, U and V (Owens *et al.* 1993; Vander Auwera *et al.* 1998) and contain variable, yet high, concentrations of Zn, Ga, Zr, Y, Sr, and REE (Owens *et al.* 1993). Overall, these rocks consist of sodic plagioclase (~An<sub>25</sub>-An<sub>45</sub>) and clinopyroxene and orthopyroxene (~En<sub>60</sub>-En<sub>80</sub>), and variable modal abundances of K-feldspar (mesoperthite) and quartz (*op. cit.*). Studies by Owens *et al.* (1993) of several anorthosite-massifs throughout the Grenville Province in Quebec established at least three main types of jotunites and related rocks: (i) dykes crosscutting massive anorthosite plutons (*eg.* Labrieville region), (ii) intrusions that occur along the margins of massive anorthosite and leucogabbro intrusions (*e.g.*, Morin Complex), and (iii) large intrusions (*e.g.*, St. Urbain region). Actually, each of these locations has more than one type of jotunite occurrence. Geochemical studies of the marginal rocks and dykes by Owens *et al.* (1993) and Vander Auwera *et al.* (1998) suggest that the marginal rocks are more primitive, while the jotunite dykes have highly fractionated REE and trace element patterns. Vander Auwera *et al.* (1998) state that the “primitive” jotunite liquid itself undergoes fractionation to form what is commonly seen as dykes and small intrusions within larger bodies of anorthosite and norite/gabbro variants. Within the Fe-Ti-P-rich melt (or FTP), fractionation, or “liquid line of descent”, continues along the following trend with changing T, P, and *f*O<sub>2</sub> and increasing SiO<sub>2</sub>: jotunite (hypersthene monzodiorite; monzonorite) or ferrodiorite (or ferrogabbro which

is olivine bearing; Mitchell 1991) or oxide-apatite gabbro-norite  $\Rightarrow$  mangerite (hypersthene monzonite) and charnockite (hypersthene granite)  $\Rightarrow$  quartz mangerite and syenite (Dymek 1993; Owens *et al.* 1993; Vander Auwera *et al.* 1998). Final SiO<sub>2</sub>-rich fractionates which are thought to have fractionated plagioclase and pyroxene earlier, are suggested to have formed granitoids in Rogaland, Norway (Vander Auwera *et al.* 1998).

Overall, due to their variable trace element geochemical signatures, the genesis of ferrodiorite-jotunite rocks is still being debated (*cf.* Ashwal 1993; Owens *et al.* 1993; Vander Auwera *et al.* 1998) with a variety of possibilities. For example, they might represent the liquid formed from crustal anatexis (Duchesne *et al.* 1978) or the parental material for andesine anorthosite suites (Duchesne *et al.* 1974; Duchesne and Demaiffe 1978), or transitional rocks between co-magmatic anorthosite and mangerite (Owens *et al.* 1993), or are derived from fractionation of mafic magmas which are not related to the anorthositic suite (Emslie 1985), or are an intermediate liquid between co-magmatic anorthosite and granite (Michot 1960, 1965; Philpotts 1966), or are the result of liquid immiscibility (Philpotts 1978, 1981; Force and Carter 1986).

According to Vander Auwera *et al.* (1998) who studied the jotunitic intrusions within the Rogaland Province, the geochemical differences between the marginal jotunites and the dykes suggest a 'liquid line of descent' from the more primitive marginal jotunites to the more fractionated jotunites (evolved jotunite to mangerite to quartz mangerite and charnockite) and, therefore, the evolution of anorthosites and jotunites are unrelated.



Instead, jotunitites are the precursor to the ferrodiorites, magnerites, and charnockite and thus are genetically separate from anorthosites and leucotroctolite-leuconorite/leucogabbro rocks. Vander Auwera *et al.* (1998) even suggest that the Al-rich basalts, thought by some to be the source for the anorthosites and related mafic rocks (Owens *et al.* 1993; Emslie *et al.* 1994), may be the source for the least fractionated jotunitites and that the anorthosites may actually be derived from subsequent fractionation of the jotunitites. Other workers (*cf.* Mitchell 1991; Demaiffe 1985; Dymek 1993; Owens *et al.* 1993; Mitchell *et al.* 1996) state that fractionation of jotunitites is possible with the liquid line of descent as defined by silica depletion and iron enrichment rather than silica enrichment and iron depletion (Owens *et al.* 1993). However, major and trace element geochemical data indicate that the jotunitites first were derived from fractional crystallization of a mafic magma which initially formed anorthosites, then troctolite and norite-gabbro varieties; jotunitites were the remaining melt. The mere fact that jotunitites and related rocks have intermediate compositions suggests that they may have evolved from a more Al-rich basalt which first fractionated plagioclase, olivine and orthopyroxene, before continuing the jotunitite to syenite “liquid line of descent”.

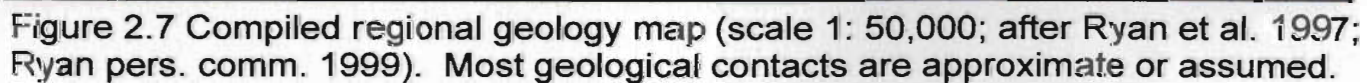
### 2.3 Local geology

The Cirque property is located on the NTS map sheet 14E/1 (Alliger Lake), approximately 75 km northwest of the community of Nain. The area was mapped as early as the 1940's by E.P. Wheeler II and as recently as 1998 by Ryan of the Newfoundland Department of Mines and Energy. Originally the Alliger Lake area was thought to consist

mainly of Mesoproterozoic rocks with Archean rocks to the northeast and minor Paleoproterozoic rocks. Recent geochronological data from Emslie and Loveridge (1992) and Connelly and Ryan (1994), however, indicate that many of the granitic and anorthositic bodies which intrude the Archean gneisses between Okak Bay and Webb's Bay are Paleoproterozoic, suggesting a longer history of magmatic activity in the area. Ryan *et al.* (1997) list three distinct ages for rocks on the 14E/1 map sheet; (1) Archean gneisses, (2) Paleoproterozoic anorthositic and granitoid intrusive rocks, and (3) Mesoproterozoic anorthosites and related rocks. Figure 2.7 is a revised 1:50,000 regional compilation map by Ryan *et al.* (1997; 1998; *pers. comm.* 1999). A recent re-interpretation of the boundary between Paleoproterozoic and Mesoproterozoic intrusive rocks has also changed based on a regional aeromagnetic map (Figure 2.8) that indicates that the northeast corner is underlain by high magnetic Paleoproterozoic deformed anorthositic intrusions and Archean gneisses, whereas in the southwest corner consists of dominantly low magnetic Mesoproterozoic intrusions of anorthosite and mafic varieties (Ryan *et al.* 1998).



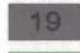
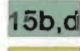
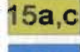

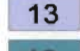
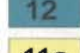


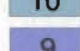
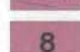
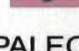
### **2.3.1 Archean rocks**

Archean gneisses of the Nain Province underlie the northeast part of the map sheet. In Figure 2.7, Ryan *et al.* (1997) subdivided the gneisses into four units, ranging from dominantly quartzofeldspathic gneiss in the far northeast corner, to mafic and ultramafic rocks grading up to amphibolite and granulite gneisses in the southeast and northeast corners. Pink to white aplitic granite and migmatized to massive mafic-ultramafic rocks

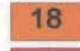

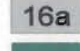
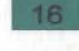


# LEGEND



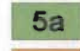


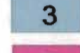

## MESOPROTEROZOIC

-  21 Porphyritic pyroxene diorite
-  20 Olivine gabbro
-  19 Diorite, ferrodiorite
-  15b,d Well-layered gabbro-noritic (dioritic) rocks
-  15a,c Massive leuconoritic to anorthositic rocks
-  14 Massive dark-grey leuconorite
-  13 Grey to brown leuconorite and anorthosite
-  12 Pale-mauve to grey anorthosite
-  11a Pale-grey anorthosite
-  11 Reddish-brown troctolite and leucotroctolite
-  10 Dark grey to buff anorthosite and leuconorite
-  9 Grey to brown norite and anorthosite
-  8a Strongly foliated leuconorite
-  8 Massive coarse-grained leuconorite

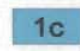
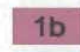
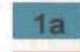
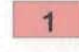
## PALEOPROTEROZOIC (?)

-  18 Clinopyroxene fayalite+/- hornblende monzonite and quartz monzonite diorite\*
-  17 Clinopyroxene fayalite monzonite\*
-  16a Pink to grey anorthosite\*
-  16 Buff (olivine bearing?) leuconorite\*


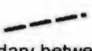


## PALEOPROTEROZOIC

-  7 Mesocratic granulites
-  6 Quartzofeldspathic granulites
-  5a Foliated monzonitic (?) to gabbro-noritic dyke
-  5 Foliated hornblende quartz monzonite
-  4 Undivided leucogabbroic to anorthositic rocks exhibiting variable secondary alteration and deformation
-  3 Brown diorite to ferrodiorite
-  2 Alliger Lake granite

## ARCHEAN

-  1c Complex unit comprising quartzofeldspathic gneiss, meta-anorthosite, pink aplitic granite, and tonalite
-  1b Migmatized to massive mafic and ultramafic rocks
-  1a Leucogabbro and anorthosite gneiss
-  1 Undivided quartzofeldspathic gneiss

## SYMBOLS

-  Mylonitic zone
-  Fault zone (approximate, assumed)
-  Interpreted boundary between Paleoproterozoic and Mesoproterozoic rocks
-  Sulphide showing
  - ① Cartaway's Cirque area
  - ② Canadian States showing
  - ③ Hilltop showing (Noranda Mining and Exploration Ltd.)
  - ④ Krinor Resources/Castle Rock

\* denotes those units re-interpreted by Ryan (pers. comm. 1999) to be Paleoproterozoic rather than Mesoproterozoic. Original unit numbers assigned by Ryan et al. (1997) are kept here for reference with Ryan et al. (1997).



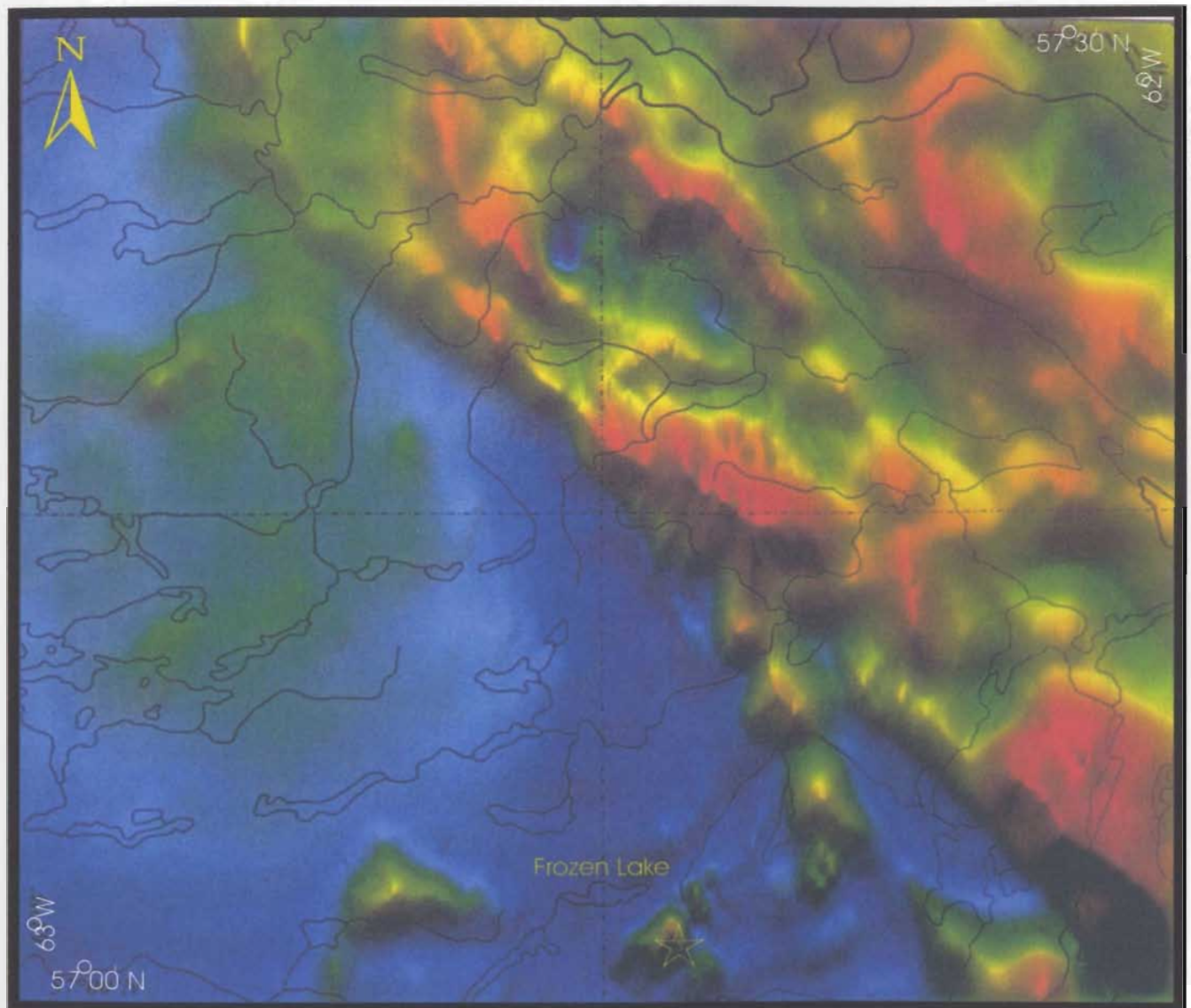


Figure 2.8 Colour contoured (blue = low, red = high) regional aeromagnetic map from Ryan et al. (1997) showing the northeast corner of NTS map area 14E surveyed in 1996 and 1997 (from GSC map 07453G GSC, 1983). The star marks the approximate location of the Cirque gossan.

with variable alteration occur on the west and north sides of Igloodataliksuak Lake, were intruded by Paleoproterozoic leucogabbro to anorthositic units (Unit 4). Metasedimentary rocks are not common but occur northeast of Laura Lake (Hynes 1997) and consist of grey to white quartzite and garnet-sillimanite gneisses. Interlayered with the dominantly undivided quartzofeldspathic gneiss (Unit 1) are rafts of mafic and ultramafic gneisses (Unit 1 a,b,c). These metagabbroic rocks range from metres to hundreds of metres across and occur as fine- to medium-grained layered mafic intrusions deformed with migmatites and gneisses (Hynes 1997). The foliations of the Archean gneisses range from dominantly northeast-trending, steeply dipping to the west to northwest-trending, steeply dipping to the west in the far northeast corner of the map sheet. Variations in foliations are, in part, due to the variable deformation episodes during the Torngat Orogen and in part due to emplacement of subsequent mafic and felsic plutons.

### **2.3.2 Paleoproterozoic rocks**

Previously thought to be Mesoproterozoic, many units within the Alliger Lake map sheet have since been redefined as Paleoproterozoic based on textural (*e.g.*, granulite), structural (*e.g.* pyroxene alignment) and geochronological evidence. Emslie and Loveridge (1992), Ryan (1993), Connelly and Ryan (1994), Ryan *et al.* (1997) have reinterpreted the anorthosite and related mafic units north of Puttuala Lake and have concluded that variably foliated anorthosite and granitoid rocks from Webb's Bay to Okak Bay were deformed during the Torngat Orogen (*cf.* Bertrand *et al.* 1993 and van Kranendonk 1996), thereby

indicating that these rocks are about 800 million years older than the average age of plutons from the Nain Plutonic Suite. Hamilton (1997) and Hamilton *et al.* (1998) estimate that the magmatic event occurred between ca. 2135-2045 Ma in a similar anorogenic environment which produced the NPS (Piercey 1998).

On the regional map in Figure 2.7, the Paleoproterozoic rocks range from felsic to mafic plutons, diorite, ferrodiorites, and anorthosites. Most of the units (2-5a) occur in the centre of the map sheet in a northwest-southeast trend, separating the Archean from the Mesoproterozoic rocks. Here, a mylonitic zone runs for about 5 km in a northwest direction from north of Iglusuataliksuak Lake to north of Miller's Pond where it continues in the same direction as an approximated fault.

The Alliger Lake Granite (Unit 2) intruded the Archean gneiss south of Frank Lake and north of Iglusuataliksuak Lake. It consists of medium-grained, grey to pink to blue quartz, biotite, hornblende-rich granite with local mylonitic zones (Ryan *et al.* 1997). The age of crystallization of the Alliger Lake Granite was classified as Paleoproterozoic based on preliminary results of U-Pb isotopic studies by Emslie and Hamilton (Ryan *pers. comm.* 1997). Southwest of Alliger Lake is a transitional contact, between the granite and variable deformed, altered anorthositic and leucogabbroic rocks (Unit 4) to the west, consisting of a sliver of diorite and ferrodiorite (Unit 3) and described by Ranson (1976) as being fine- to medium-grained with dark brown weathering. The diorite also grades into dark grey gabbro with blue quartz to the west (Ranson 1976; Ryan *et al.* 1997). A small inlier (approximately 0.5 km<sup>2</sup>) of hornblende-quartz monzonite, weathered pink to grey and granite with younger

hornblende (- pyroxene) monzonite (Unit 5), are medium-grained with faintly blue quartz and potassium feldspar augens (1 cm<sup>2</sup>) and are located in the north central part of the map sheet, northeast of Puttuaalu Lake, completely surrounded by Mesoproterozoic monzonitic and dioritic rocks. The metamorphosed monzonites and granites have pink to grey weathered surfaces. Another inlier (approximately 0.31 km<sup>2</sup>), located west of Iglusuataliksuak Lake, consists of granulitic gabbro-noritic and possibly monzonitic dykes (Unit 5a) within the extensive leucogabbroic and anorthositic rocks of Unit 4. Both Unit 5 and 5a are local, non-extensive, moderately to steeply dipping to the northeast and trending generally to the northwest.

Units 6 and 7 are thin slivers located in the far southwest corner of the map sheet. Unit 6 consists of buff weathered quartzofeldspathic granulite gneisses with minor mafic gneisses (Hynes 1997). These rocks are extensively layered and lie between two large Mesoproterozoic anorthositic plutons. Unit 7 consists of weakly layered, red-brown weathered metasedimentary and ultramafic mesocratic granulites (Ryan *et al.* 1997). Gabbroic metaplutonic rocks intruded by pre-metamorphosed and post-metamorphosed dykes of variable composition (diabase, olivine diabase, monzonite, diorite, aplitic to pegmatitic granite) are also of Paleoproterozoic age.

Units 16 to 18 from Ryan *et al.* (1997) have recently been re-interpreted by Ryan (*pers. comm.* 1999) to be Paleoproterozoic. Unit 16 is large pluton of leuconorite ( $\pm$ olivine) with igneous layering dipping to the northeast. Within this body is a smaller intrusion (Unit 16a) of pink to grey anorthosite interpreted by Hynes (1997) to be the core of Unit 16. The



most felsic units on the map sheet, the clinopyroxene fayalite  $\pm$  hornblende monzonite and local monzonite, are Units 17 and 18. Unit 18 is more extensive and occurs in the north and central portions of the map sheet, intruding Archean and Paleoproterozoic rock types. Unit 17 has a much smaller surface exposure and contains no quartz.

### 2.3.3 Mesoproterozoic rocks - the Nain Plutonic Suite

The southwestern portion of the map sheet comprises anorthosite, leuconorite, leucogabbro, and lesser amounts of diorite and monzonite, all belonging to the NPS. In a section across this part of the massif, Ranson (1981) described the anorthosites and leuconorites as being massive, coarse-grained, with overall plagioclase compositions of An<sub>45</sub> - An<sub>52</sub>, and with K<sub>2</sub>O contents between 0.15 to 0.27 wt%. Three dominant facies were identified by Ranson (1981): (1) augite and oxide-bearing anorthosite, (2) oxide-rich anorthosite with abundant magnetite and ilmenite, (3) and leuconorite with inverted pigeonite content greater than orthopyroxene. In the more plagioclase-rich anorthosite intrusions, the presence of large orthopyroxene megacrysts (OPM) suggests that OPM crystallization occurred at high pressure, at depths near the lower crust or upper mantle (Emslie *et al.* 1994; 8-10 kbar, similar to that of the Harp Lake Intrusive Suite (10-12 kbar); Fram and Longhi 1992). Plagioclase $\pm$ OPM-rich liquid later ascended to shallower levels by being incorporated into anorthositic mushes (Emslie 1975). Plagioclase lamellae within the OPM formed as a result of decompression and re-equilibration of the newly emplaced magma. Morse (1975), however, attributes the plagioclase lamellae to plagioclase exsolving

from pyroxene in an alumina-rich magma after Fe-Ti oxides crystallized to form magnetite, thereby releasing SiO<sub>2</sub> to aid in the plagioclase *in-situ* crystallization within the OPM.

The most common rock types are the mafic rocks which occupy approximately one third of the map sheet. Units 8 and 8a consist of leuconorite with variable degrees of foliation that occur in the far southwest corner. Units 9 and 10, also in the same area, are massive anorthosite, norite, and leuconorite. Units 11a to 12 are dominantly massive, pale mauve anorthosite. Wheeler (1960) named these rocks “pale facies” due to the dominance of pale plagioclase and the low content of hypersthene. Both are small intrusions and are truncated by younger, larger plutonic bodies. Two small linear units of reddish brown troctolite and leuconorite (Unit 11) form a discontinuous semi-circle in the map area. One body (Unit 11) completely rims Unit 11a, a pale grey anorthosite. Petrographic results, however, contradict the presence of olivine-bearing rocks, stating that the “olivine” is actually brown orthopyroxene (Squires *et al.* 1997). The larger, more extensive plutonic bodies are massive, locally layered anorthositic, leuconoritic, and leucogabbroic (Unit 13 - 15a, c). The massive leuconoritic and anorthositic rocks of Unit 15a, c and the more layered norite to leucogabbroic-noritic (dioritic) rocks of Units 15b and d, are interlayered, west-northwest dipping intrusions with gradational contacts and cross- and trough-cross layering and imbrication of black plagioclase xenocrysts (Hynes 1997). In the northwest corner, Unit 15 has been truncated by massive, east dipping, buff leucocratic ( $\pm$  olivine) leuconorite which weathers a brownish yellow colour (Hynes 1997) and has been re-interpreted by Ryan (*pers. comm.* 1999) to be possibly Paleoproterozoic. Small, discontinuous ferrodiorite and

diorite dykes occur as linear intrusions throughout the map sheet: north of Iglusuataliksuak Lake, east of the Cirque grid, and west and northwest of Puttuaalu Lake. Overall, most of the Mesoproterozoic ferrodiorite intrusions define a general northwest trend. The rocks are hornblende- and magnetite-rich with a dark brown, crumbled surface.

The youngest intrusions are narrow olivine gabbro and diorite dykes. The gabbro dyke (Unit 20) intersects the Archean gneiss (Unit 1) and Paleoproterozoic Alliger Lake Granite (Unit 2) to the west in a northwest direction. The diorite dyke (Unit 21) is not as extensive and is located southwest of Puttuaalu Lake. It contains porphyritic pyroxene and intrudes the leuconorite rocks of Unit 6.

## **2.4 Grid geology**

Figure 2.9 outlines the geological units underlying the Cartaway property and surrounding properties as defined by the regional geological mapping. Figure 2.10 is the grid map of the Cirque property, mapped by the author on a 1:5,000 scale in 1996. Due to the variable modal abundances and to a lesser extent texture variations, detailed stratigraphic correlations between drill holes are difficult to make, however, general features of the main units can be defined (Figure 2.11).

The immediate Cirque area was the site of extensive Mesoproterozoic plutonism. The rock units consist dominantly of anorthosite (approximately 90% of grid geology), with plagioclase compositions ranging from andesine to labradorite ( $An_{48-55}$ ) with layers of leucogabbro, leuconorite, and leucotroctolite at higher elevations (approximately 8% of grid

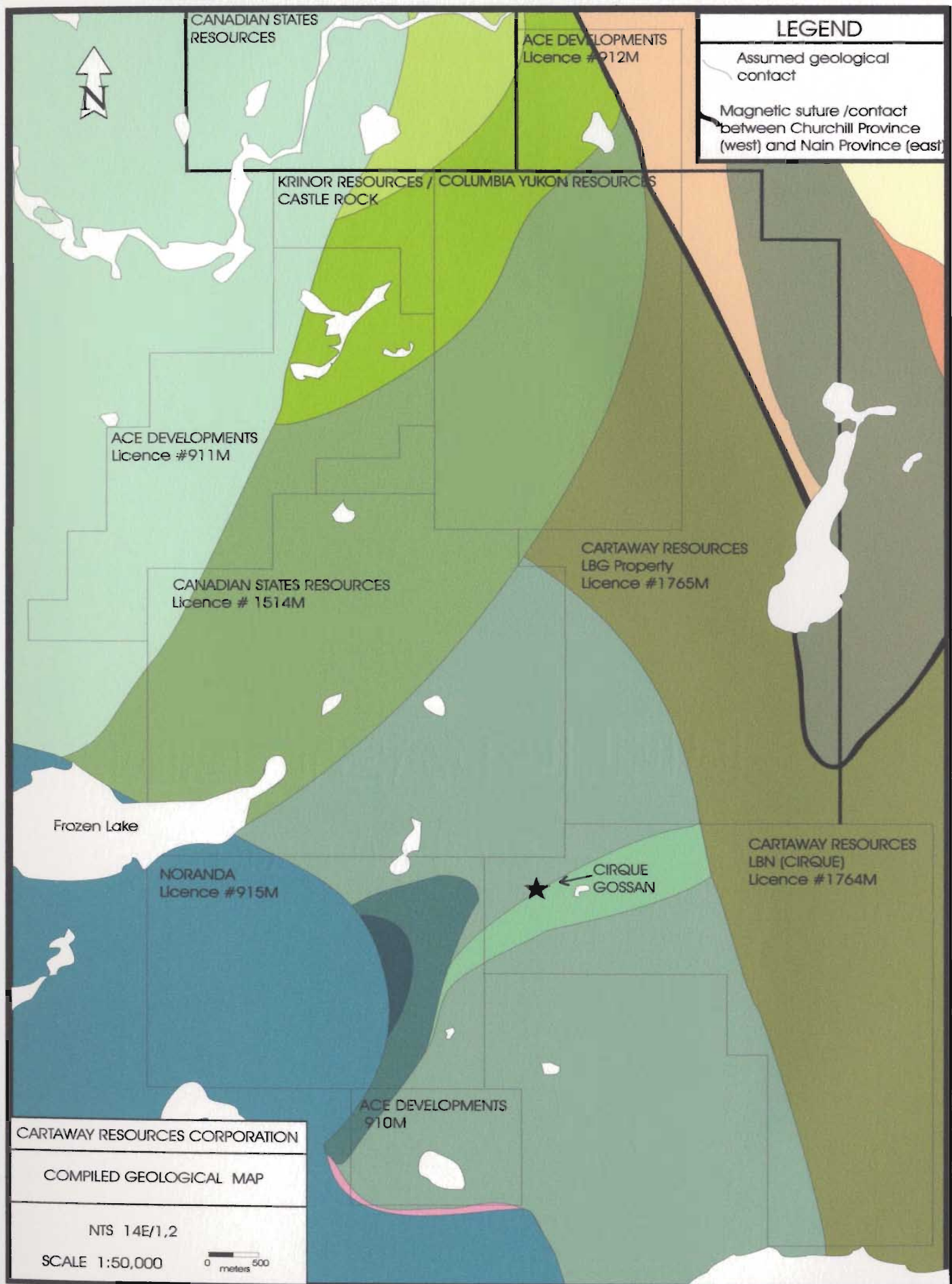


Figure 2.9 Geological map showing the LBN (Cirque) property (Licence #1764M) and neighbouring properties; NTS 14E/1,2; scale 1:50,000 (from Cartaway 1997 adapted from Ryan et al. 1997 and Ryan pers. comm. 1999).

---

## LEGEND

### Mesoproterozoic

	Massive dark grey leuconorite and anorthosite
	Olivine-bearing (?) norite and leuconorite
	Layered gabbro-norite
	Purplish-grey anorthosite to leucotroctolite
	Pale grey to red-brown leuconorite and anorthosite
	Dark grey to buff anorthosite and leuconorite
	Mottled leucotroctolite and troctolite
	Massive grey anorthosite
	Massive grey to pale mauve anorthosite
	Grey to dark brown norite to anorthosite

### Paleoproterozoic ?

	Quartzofeldspathic granulite
	Gabbro to anorthosite with varying degrees of metamorphic and structural overprint
	Buff olivine bearing (?) leuconorite
	Pale grey to red-brown leuconorite and leucoanorthosite
	Hornblende-fayalite monzonite and pyroxene diorite

---

Figure 2.9 Accompanying legend. Units within each age group are not in chronological order.

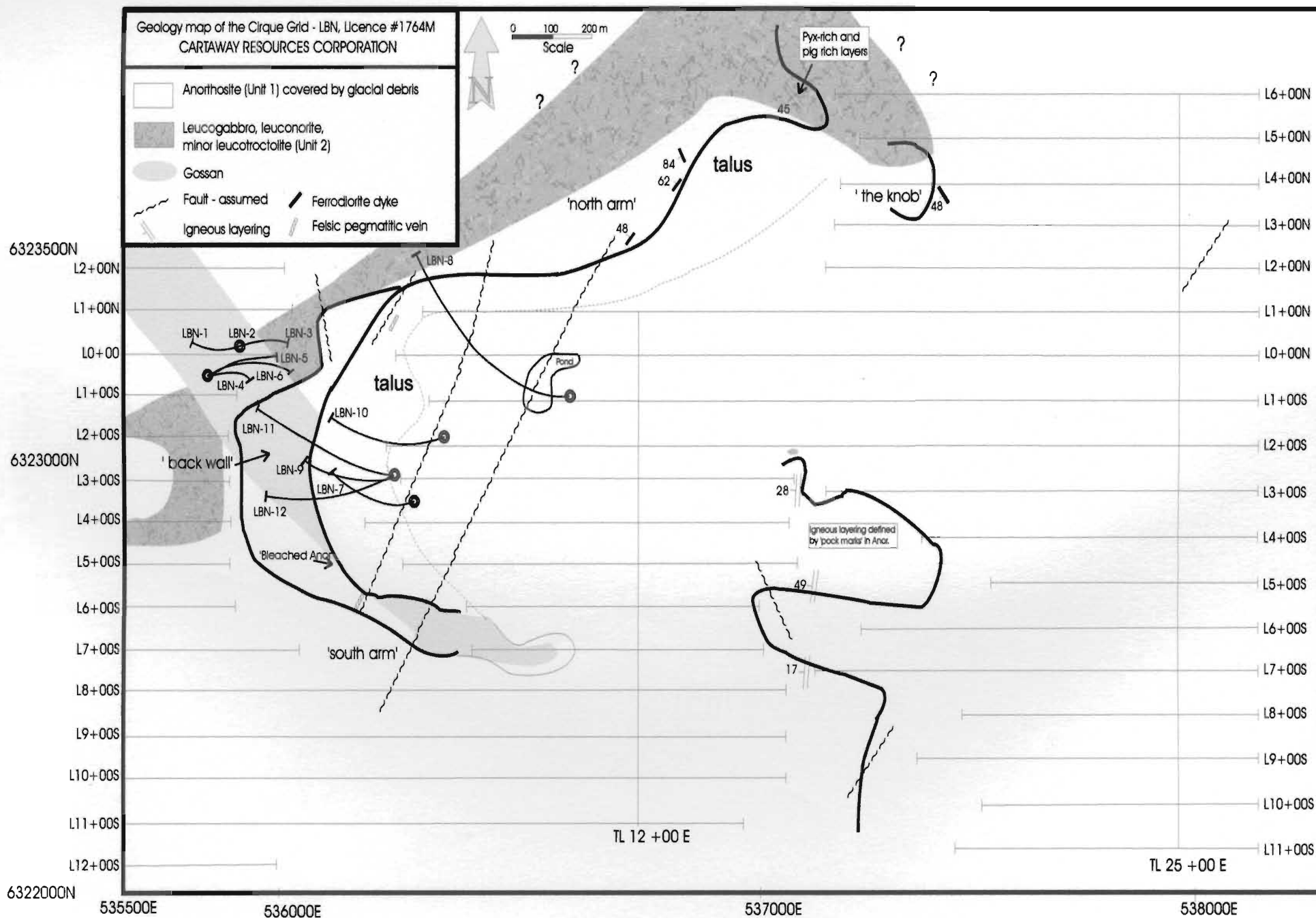


Figure 2.10 Geology map (mapped at 1:5,000 scale) of the Cirque grid (LBN property, Licence #1764M).

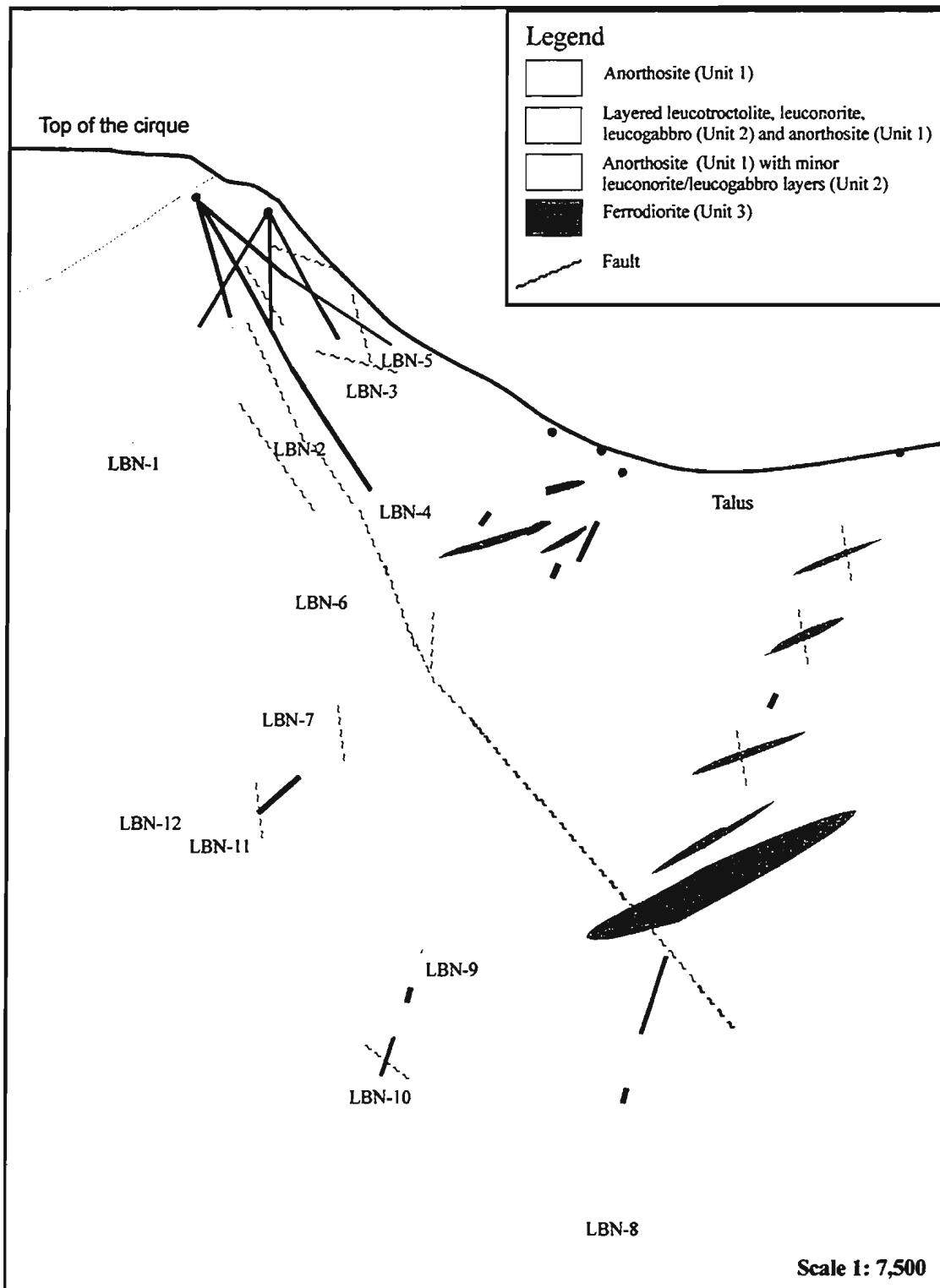


Figure 2.11 Cross sectional view (looking north) showing the geology as interpreted from outcrop and drill core. Sulphide intersections are shown as black bars along drill holes which are projected along 6322600 mN.

geology). Medium-grained, cumulate clinopyroxene, orthopyroxene, and magnetite modally make up about 5 - 20 % of the anorthosite overall, and define three distinct subunits of anorthosite with relatively different magmatic ages.

A thin ferrodiorite dyke intrudes the anorthosite horizontally along the base of the cirque wall but then peters out to the northeast and several more are intersected in a few of the drill holes. In the same location are thin interlayers of plagioclase-rich and pyroxene-rich rock that at first were thought to form a metamorphic fabric but upon closer inspection were revealed to have formed as a result of fractional crystallization within the magma chamber. Localized patches of very coarse to fine-grained pyroxene ( $\pm$  oxide)-rich veins intrude anorthosite throughout the grid.

Granitic pegmatite veins are the youngest magmatic phase and occur parallel to late northeast trending faults cross-cutting massive anorthosite. Overall outcrop exposure is approximately 20 % and is generally limited to the steep cirque walls.

The following is a detailed field and petrographic description of each rock type. Rock units are described according to the I.U.G.S. classification scheme for gabbroic rocks (Figure 2.12) which is based on the modal abundances of plagioclase, pyroxene (orthopyroxene and clinopyroxene) and olivine. Cumulate textures were described using the recommendations of Irvine (1982) and Mathison (1989). At times, where the unit contacts are not sharp, or a large unit contained several layers of different modal abundances, an overall name had been assigned (*e.g.*, leucoanorthosite with several layers with up to 15 % pyroxene was called anorthosite).



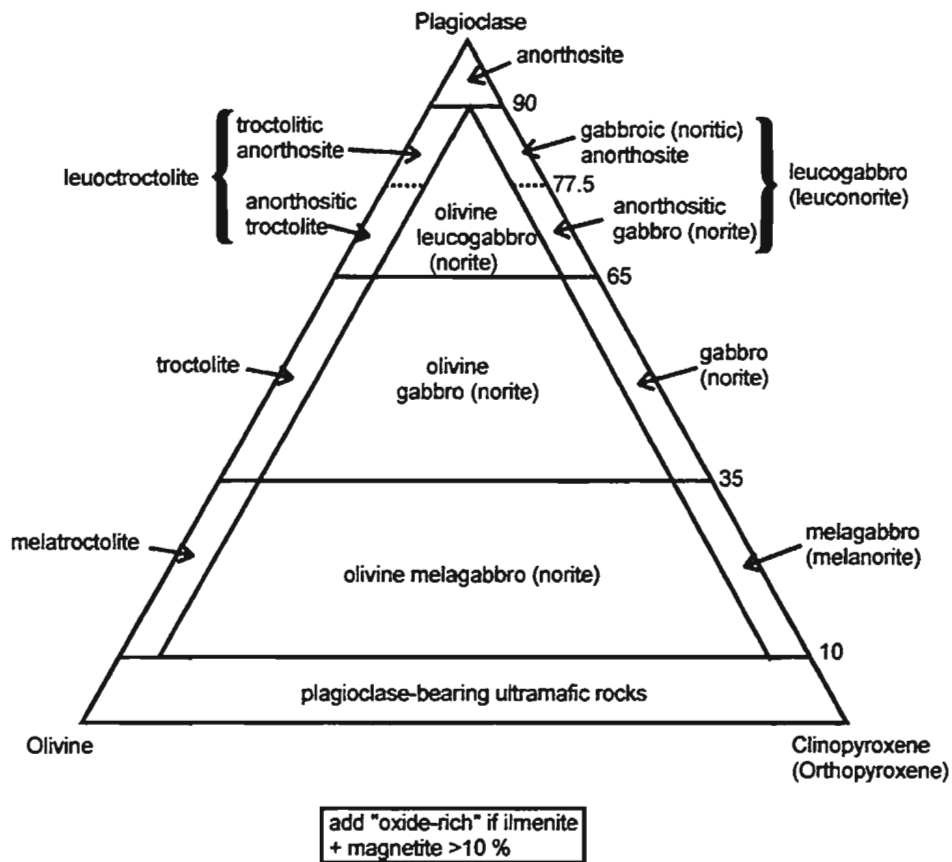


Figure 2.12 Classification of anorthositic rocks and related rocks as recommended by the IUGS Subcommittee on the Systematics of Igneous Rocks (Streckeisen 1976).

### **2.4.1 Anorthosite (Unit 1)**

The geology of the grid consists mainly of massive, coarse-grained adcumulate to mesocumulate monomineralic anorthosite (unshaded in Figure 2.9; much of the area is covered by thin felsenmeer) with varying percentages of mafic minerals (andesine-labradorite:  $An_{48-55}$ ,  $En_{51-54}$ ; see Appendix A3.1). Although it more likely represents several intrusions of anorthositic magma that coalesced to form the massive anorthosite seen in the field area, three distinct types of anorthositic rocks have been observed on the grid and are informally given names for this study as: Giant Porphyry anorthosite, Buff Brown anorthosite, and Bleached anorthosite, each a subunit of Unit 1. Each subunit is identified by mineralogy, colour, and texture; intrusion relationships can be distinguished among these subunits and are discussed below.

#### **2.4.1.1 Leucoanorthosite - Giant Porphyry (Unit 1a)**

The Giant Porphyry (GP) unit consists of very coarse-grained labradorite-rich anorthosite (> 90 %), commonly displaying labrador schiller of green and blue. GP is virtually free of mafic minerals and oxides except for local coarse-grained ( $\leq 1$  cm) clinopyroxene crystals and/or magnetite-ilmenite blebs. Throughout the unit are thin ( $\leq 1$  cm wide) clinopyroxene and/or Fe-Ti oxide veins and within the large plagioclase crystals are tiny needle-like dark coloured minerals, possibly rutile. The GP anorthosite commonly displays a mortar texture with large purple-blue, anhedral to euhedral plagioclase crystals surrounded by coarse-grained (yet finer grained than GP anorthosite), light green or beige

plagioclase groundmass, or locally by fine-grained sulphides or thin micro-veins or pyrite plating. In places where sulphides are present, the crystal edges of plagioclase are frayed or embayed with rusty-colored cracks. The maximum crystal size of the dark blue-purple labradorite is about 10 cm. In diamond drill holes, particularly LBN-11 and LBN-12, brown plagioclase (possibly bytownite) is interlayered with the bright blue-purple labradorite variety; the average layers are a few metres wide.

Sharp contacts, along the base of the north arm, have also been observed indicating a younger anorthosite body (Unit 1b) below the GP (Plate 2.1). In places, especially along the north wall, large rounded xenoliths (spanning 1 - 2 m<sup>2</sup>) of GP are enclosed by the finer grained tan-grey colored anorthosite (BB) as shown in Plates 2.2 and 2.3. Plate 2.4 shows whole pieces of GP broken up and “floating” in Unit 1b, appearing to be incorporated into Unit 1b at the time of the latter’s crystallization.

#### **2.4.1.2 Leucoanorthosite - Buff Brown (Unit 1b)**

The most abundant unit on the grid, Buff Brown (BB), is typically coarse-grained, dull grey-tan and consists of plagioclase, a maximum of 15 % cumulate pyroxene (clino- and/or ortho-) with variable textures (Plate 2.5). Accessory minerals are magnetite (0 - 7 %) and olivine (0 ≤ 1 %). Variable contents of stubby, reddish-brown rutile laths occur within pyroxene porphyry (Plate 2.6). Locally, anhedral to euhedral plagioclase crystals are either randomly oriented or aligned and surrounded by finer grained anhedral plagioclase and

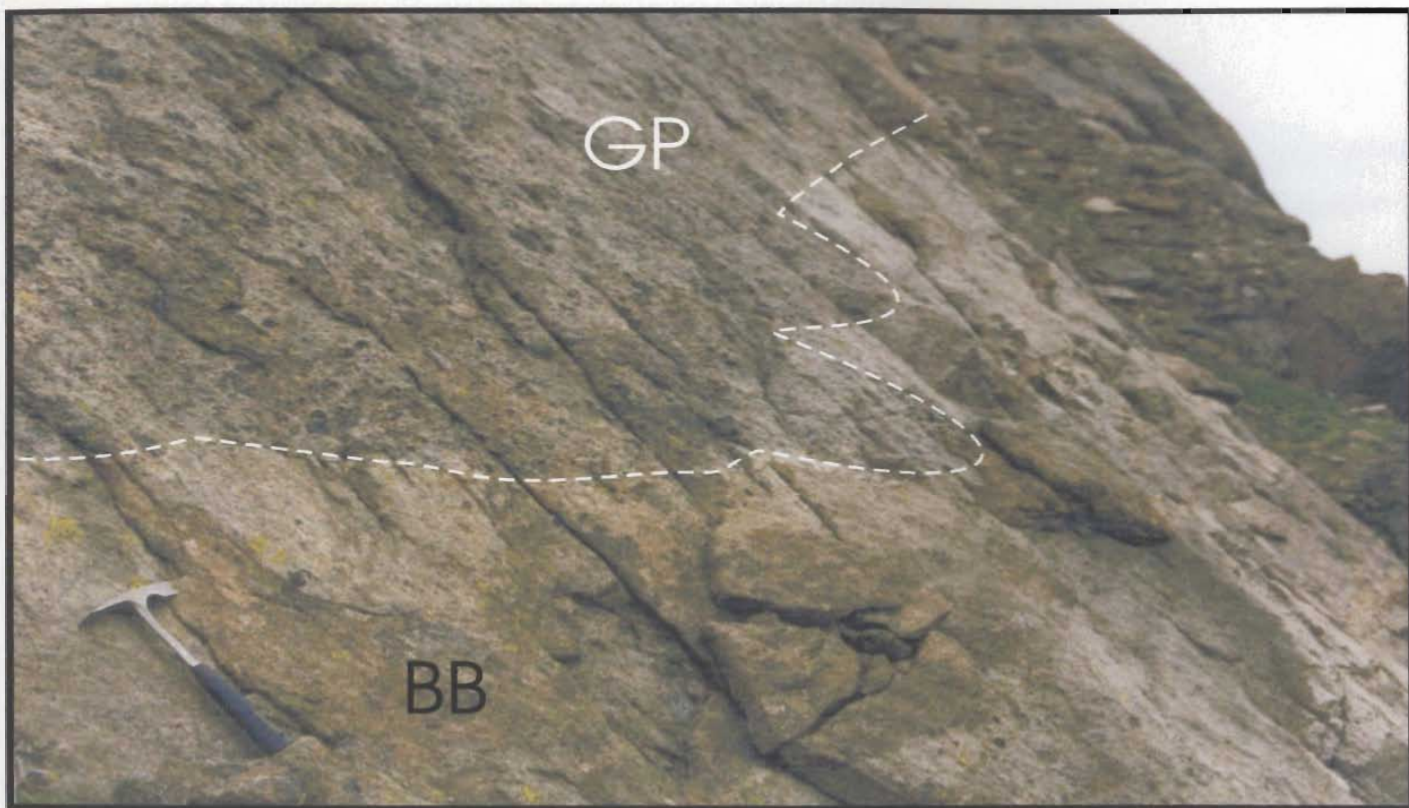


Plate 2.1 GP anorthosite (Unit 1a) overlying BB anorthosite (Unit 1b). Photo was taken along the north arm wall.

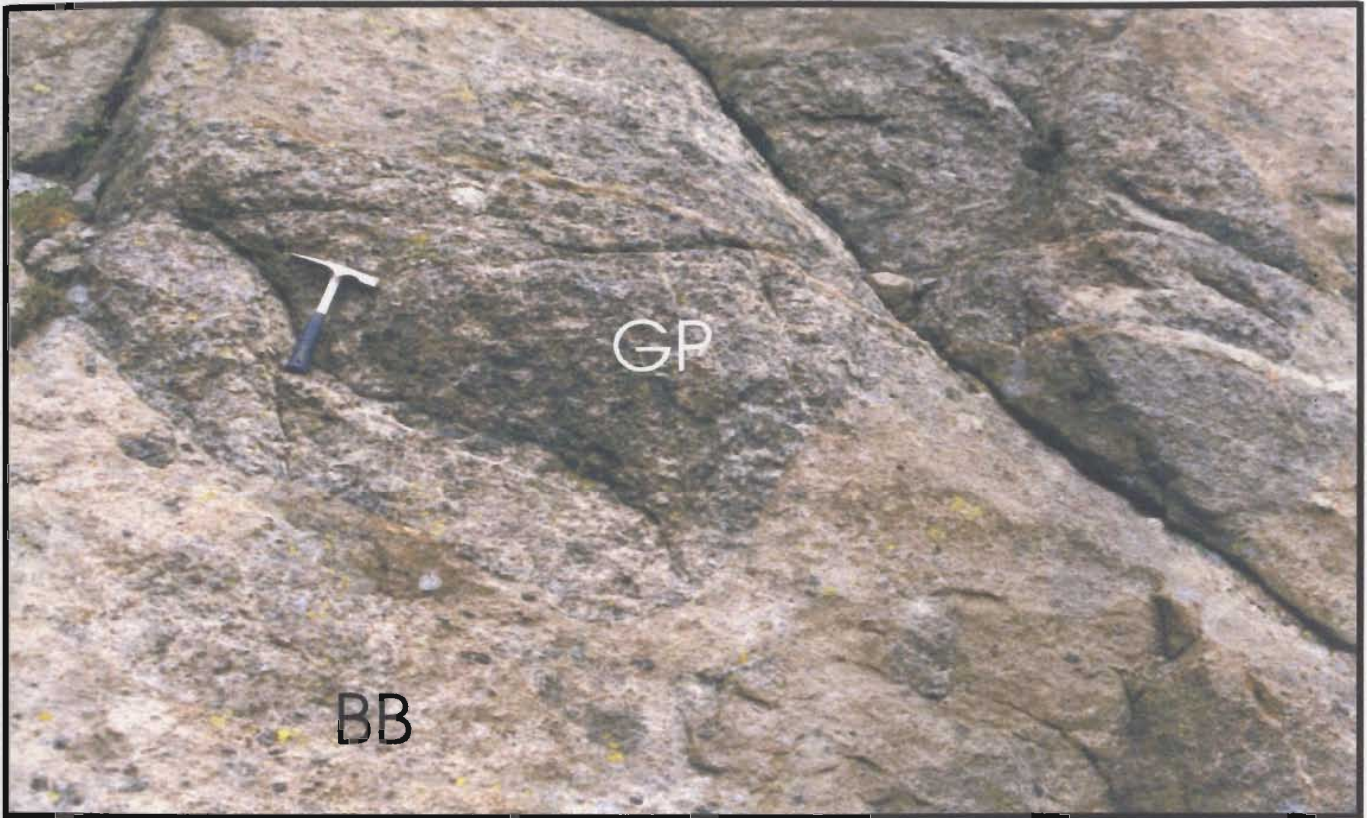


Plate 2.2 GP anorthosite (Unit 1a) xenoliths within BB anorthosite (Unit 1b). Photo was taken along the north arm wall.





Plate 2.3 Coarse-grained, anhedral, cumulate plagioclase intruded by finer grained cumulate plagioclase. Photo was taken in cross polars; field of view is 9 mm (1.5 power). Sample is altered anorthosite (Unit 1 b) near a fault.



Plate 2.4 GP anorthosite (Unit 1a) incorporated into finer grained BB anorthosite (Unit 1b).



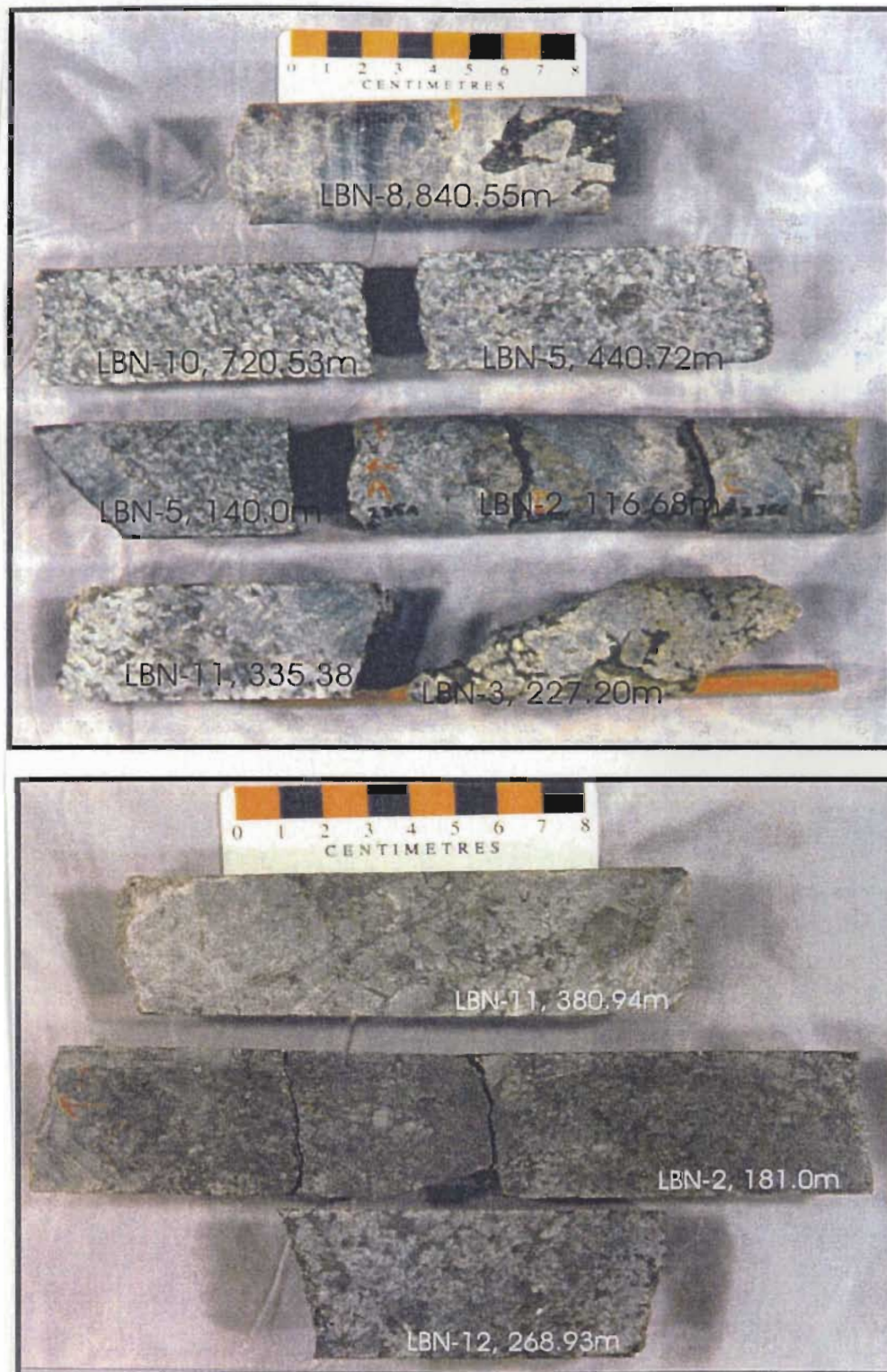


Plate 2.5 Drill core showing varied modal percentages and textures of pyroxene (top photo) and magnetite/ilmenite (bottom photo) in anorthosite. Note how the oxides appear to disaggregate the plagioclase in borehole LBN-11 (380.94 m).



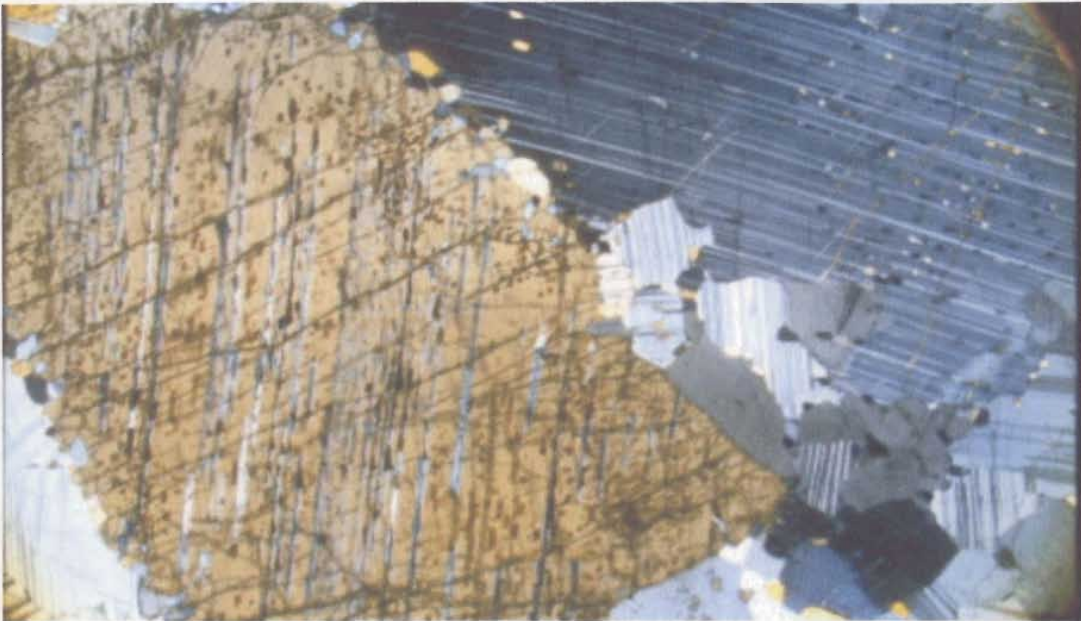


Plate 2.6 Anorthosite (Unit 1b) with orthopyroxene megacryst containing rutile along the cleavage planes and exsolution lamellae. Plagioclase contains minor small pyroxene. Photo was taken in cross polars at 1.5 power (field of view is 9 mm).

cumulate pyroxene, oxides, and to a lesser extent, disseminated pyrrhotite.

Medium to coarse-grained (ranging from <1 cm to ~ 5 cm), anhedral, interstitial pyroxene (dominantly orthopyroxene) generally weathers to tan brown and occurs as irregular patches or locally aligned bands (<1 to 30 cm wide) that often thin out (Plate 2.7). Within the thicker bands are rounded inclusions of anorthosite. Regular layers of pyroxene weather in “pock marks” in the cirque wall in the southwest part of the grid (between L 3 + 00 S to L 6 + 00 S; Plate 2.8). Layering is local and the general trend is north with a moderate dip to the west. Thin veins (1 cm wide) of coarse-grained magnetite and dark green clinopyroxene crosscut the Unit 1 b anorthosite in several areas. These veins are also observed in drill core. As mentioned in the previous section, the BB anorthosite is often seen to have been injected into the GP anorthosite with dark blue to purple (called “black” by Ryan *et al.* 1997), rounded porphyritic laths and irregular crystals (< 1 cm to 10 cm) of plagioclase (GP anorthosite) surrounded by coarse-grained, light brown BB anorthosite (Plate 2.9). Locally the plagioclase crystals are often aligned parallel to the flow direction of the BB anorthosite.

#### **2.4.1.3 Leucoanorthosite - Bleached (Unit 1c)**

Bleached anorthosite occurs strictly as veins or dykes (maximum of 1 m wide, 3 m long) within the GP and BB anorthosite and is mapped on the south arm and in the south corner of the cirque. In outcrop, the Bleached anorthosite is coarse-grained, recrystallized,





Plate 2.7 Varied occurrences of pyroxene in BB anorthosite (Unit 1b) in cirque wall. Top photo shows a local band of randomly oriented pyroxene minerals. Bottom photo shows thin layers of aligned pyroxene minerals.





Plate 2.8 Igneous layering (shown by dashed white line) within BB anorthosite (Unit 1b) defined by weathered out pyroxene-rich layers. Photo was taken along the southeast part of the grid, looking northwest.



Plate 2.9 Core sections showing large dark plagioclase crystals (GP anorthosite, Unit 1a) injected by finer grained, tan plagioclase (BB anorthosite, Unit 1b).

and light-grey with sharp contacts with the BB anorthosite. Along the back wall of the cirque, the Bleached anorthosite lies above a gossanous zone (Plate 2.10), trending to the southeast and dipping between 48°- 68° west. Smaller veins or dykes strike southwest-northwest and are steeply dipping (Plate 2.11). Ryan *et al.* (1997) observed a similar type of anorthosite and interpreted it to be an east-northeast trending “dyke-like body intruding dark grey to buff anorthosite and leuconorite and pale grey anorthosite “ (see Figures 2.6 and 2.8).

In thin section, the bands consist dominantly of coarse-grained, stubby, cumulate, anhedral plagioclase crystals with frayed, irregular grain boundaries, alkali feldspar, and sericite and talc dusting. Minor cumulate pyroxene (1 % or less) is coarse-grained, but finer grained than the plagioclase and appears to have altered to biotite and chlorite. Trace fine-grained to very fine-grained disseminated pyrrhotite, possibly pyrite and/or oxides were also observed. Overall, the texture is grainy or recrystallized with saussuritization alteration. Such a granular, recrystallized nature is thought to be the result of deformation of plagioclase while the magma was completely or partially solidified (Duchesne and Demaiffe 1978).

The distinctly white anorthosite has been observed in other locations near the Cirque property. For instance, to the west an approximately 30 metre wide intersection of “a curious ‘bleaching’ and recrystallization of the anorthosite” has been recorded in two drill holes on the Hilltop property (Squires *et al.* 1997) and north of the Cirque area there are





Plate 2.10 Bleached anorthosite (Unit 1c) capping a gossan along the south wall of the cirque.



Plate 2.11 Veins of Bleached anorthosite (Unit 1c) crosscutting GP anorthosite (Unit 1a) along the south wall of the cirque.



large exotic rafts of white anorthosite locally crosscut older anorthositic rocks at a low angle (Hynes 1997). Ryan *et al.* (1997) also mentions this type of anorthosite located on the Canadian States property, east of Frozen Lake.

The source of these rafts or dykes have not yet been determined, however Ryan *et al.* (1997) suggest that they could be either exotic, older yet cognate, or derived somehow from the massive mauve, grey anorthosite located further to the northeast. Other workers have observed similar dykes of leucoanorthosite (such as St. Urbain and Morin, Quebec; Emslie 1975b), however, few detailed studies have been done (Ashwal 1993). Some earlier suggestions include that perhaps the dykes represent the parental magma of the pluton (Weibe 1979) and they represent plagioclase-rich magmas (Dymek 1980; Gromet and Dymek 1980, 1982). Studies by Fram and Longhi (1992) on fine-grained to porphyritic dykes with plagioclase, olivine, orthopyroxene,  $\pm$  augite suggest that the anorthosite dykes may have crystallized in an open system, as apophysis of the main plutonic body which later intruded anorthositic bodies already emplaced.

#### **2.4.2 Leucotroctolite - leuconorite - leucogabbro (Unit 2)**

Leuconorite and leucogabbro in drill core are dominantly interlayered with leucotroctolite and anorthosite and have sharp to gradual contacts (Plate 2.12). At the top of the cirque, drill core intersected several layers of dominantly leuconorite, leucogabbro, and leucotroctolite. Further to the south at the top of the Cirque, boulders (possibly subcrop) of medium-grained Fe-rich gabbro ( $\sim 15\%$  pyroxene,  $7\%$  magnetite) cover an area of  $\sim 25\text{ m}^2$ .

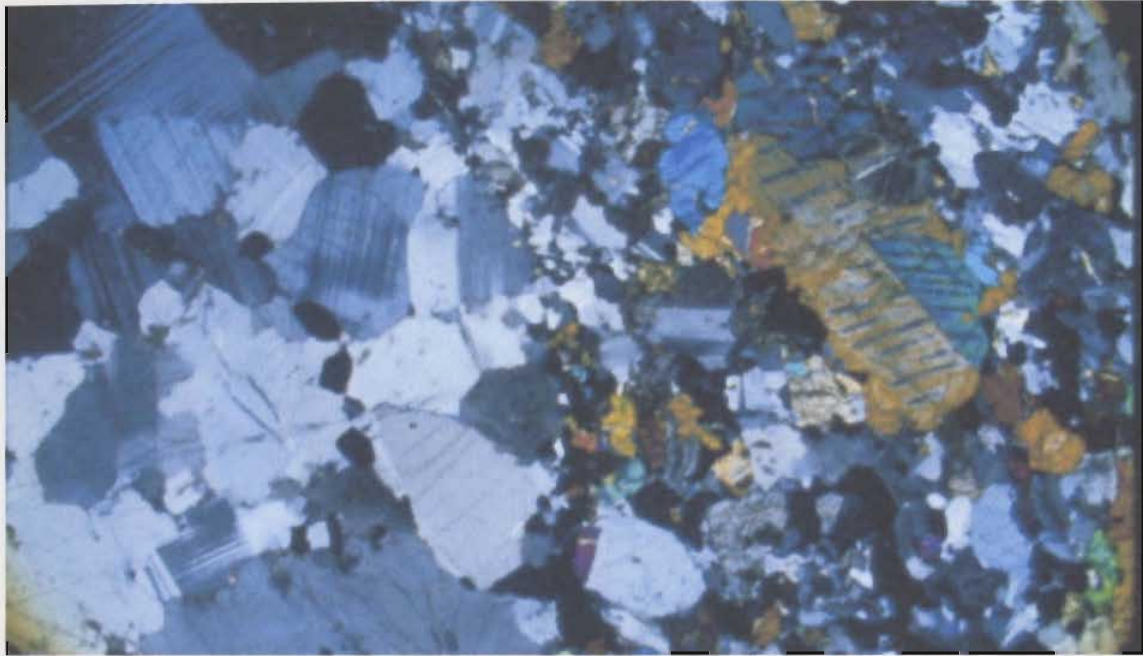


Plate 2.12 Sharp contact between leucoanorthosite (Unit 1b) to the left and leuconorite (Unit 2) to the right. Photo was taken in cross polars; field of view is 9 mm (1.5 power). Sample is LBN-12 (105.47m). Note the weak alignment of pyroxene parallel to contact.

Because of the texture and mineralogical similarities the term leuconorite/leucogabbro is used in this study to define those units that are more orthopyroxene or clinopyroxene-rich. Leuconorite is more common than leucogabbro, however, both units vary in modal percentages of pyroxene, texture, grain size, and degree of mineral alignment. On surface the pyroxene, especially the orthopyroxene, weathers a tan-brown colour. Although inverted pigeonite is the most common pyroxene throughout the Cirque area, both orthopyroxene and clinopyroxene have undergone some degree of unmixing resulting in pyroxene/pyroxene exsolution lamellae (*cf.* Shelley 1993). Leucotroctolite is not a significant occurrence, however, all three pyroxene-olivine rich subunits appear to cap the massive tan anorthosite (BB).

The leuconorite/leucogabbro has a maximum of 70% subhedral to anhedral intergrown, adcumulate plagioclase ( $An_{48}$ ; see Appendix A3.1), 15 - 30% cumulate, anhedral, generally weakly aligned orthopyroxene and clinopyroxene, trace olivine, with minor blebs of magnetite and ilmenite (Plate 2.13). Cumulate olivine is a very minor accessory mineral and pristine olivine was not identified in polished thin section. Plate 2.14 shows localized layers of weakly aligned coarse-grained pyroxene with plagioclase.

Leucotroctolite was identified in fresh drill core but was not observed in outcrop. In this phase, green vitreous olivine ranges from 5 to 20% in a dominantly plagioclase-rich matrix. In drill holes LBN-96-1 to 3, leucotroctolite, leucogabbro, and leuconorite are interlayered for approximately 20 metres with each layer about 1 - 5 m wide and dipping to the west. On the Noranda "Hilltop" property, olivine-rich units were observed by Ryan *et*

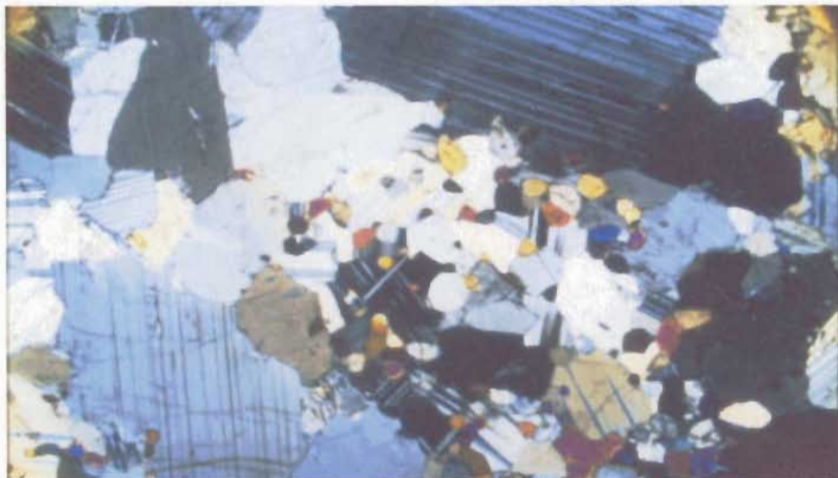
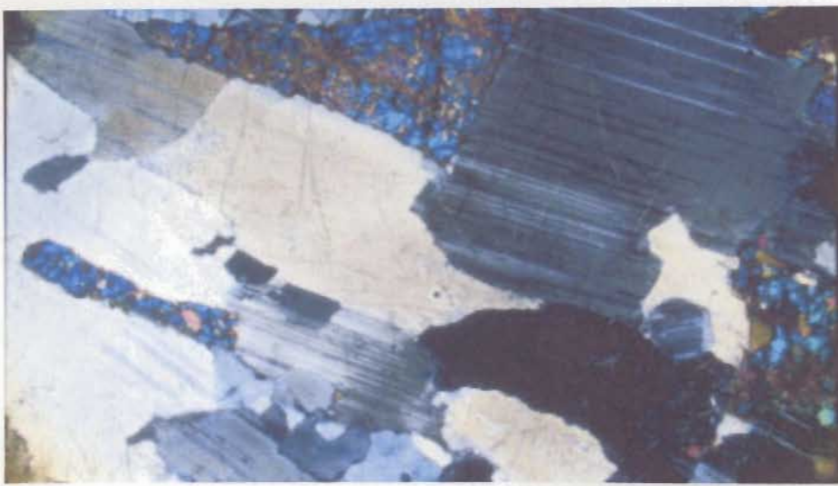


Plate 2.13 Variable textures and modal mineralogy of leuconorite/leucogabbro (Unit 2). Pyroxene ranges from clinopyroxene to orthopyroxene or both and from low modal abundance with interstitial, cumulate texture (top photo), stubby and distributed homogeneously throughout the unit (middle photo) to localized patches of pyroxene (bottom photo). All photos were taken in crossed polars with 1.5 power (field of view 9 mm).





Plate 2.14 Weakly aligned pyroxenes in leuconorite (Unit 2). Photo was taken near the tip of the north arm wall.

*al.* (1997), but were not confirmed by Noranda workers (Squires *et al.* 1997). Kerr (1998) notes relict olivine as green serpentinized clots with oxide inclusions may be present on Noranda's "Hilltop" property. At low pressure (less than 5 kbar) and in relatively dry magmatic conditions, olivine is thought to react with the remaining melt to form orthopyroxene (Kushiro 1969; Giest *et al.* 1990); however, the formation of the orthopyroxene-magnetite symplectic textures observed in some of the olivine minerals (Plate 2.15) are probably the result of weathering or the oxidation of olivine (Shelley 1993).

Medium-grained, homogeneous textured pyroxene-plagioclase dykes crosscutting anorthosite were intersected in several drill holes. These dykes range in width from <50 cm to ~ 2 m, have sharp contacts, and contain insignificant abundances of sulphide minerals. The lack of significant oxide minerals distinguish them from ferrodiorite dykes. Such layers have also been observed on Noranda's "Hilltop" property (Squires *et al.* 1996), the Canadian States Resources property, Licence #1514M (Canadian States Resources *inhouse* data 1995, 1996), and NDT's "Nain Hill" prospect (Hinchey 1999).

### **2.4.3 Ferrodiorite (Unit 3)**

Jotunites, which were discussed earlier, include ferrodiorites, ferrogabbros, gabbroic and dioritic rocks rich in magnetite and ilmenite. One or two dykes, which crosscut anorthosite along the far northern wall of the cirque, consists of equigranular, cumulate, medium- to coarse-grained, anhedral plagioclase (35 - 70 %), pyroxene (En<sub>31</sub>; 15 - 20 % with clinopyroxene > orthopyroxene), and trace apatite. Magnetite and ilmenite (7 - 40 %)

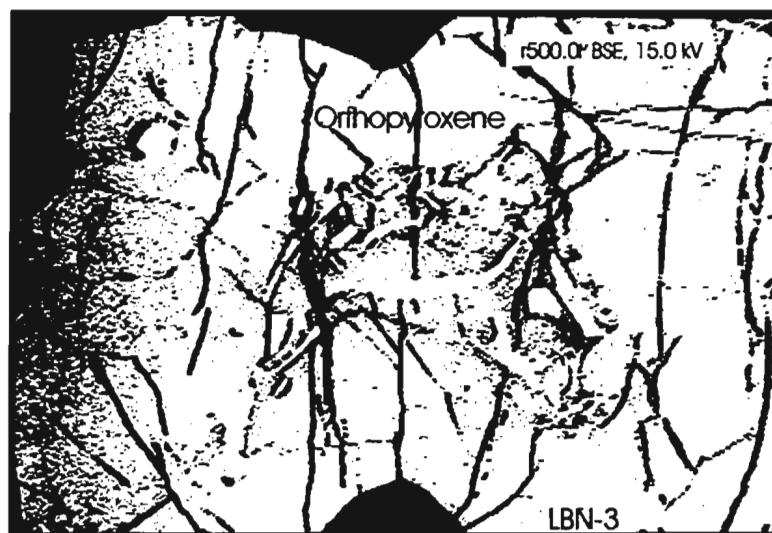


Plate 2.15 Microprobe photograph of cumulate orthopyroxene with a core of magnetite, ilmenite, and possibly olivine lamellae.

form an homogeneous, subophitic to granular texture with aligned minerals (plagioclase porphyry and pyroxene) near and parallel to the contact (Plates 2.16 and 2.17). Minor fine-grained pyrrhotite (maximum 7%) and trace chalcopyrite are evenly disseminated throughout. Alteration minerals include minor biotite and a “dusting” of sericite on the plagioclase and pyroxene minerals.

Along the north arm, near L 1 + 00 N, one or two dykes separate the very coarse-grained blue, grey labradorite-rich leucoanorthosite (GP) below and the coarse-grained tan, brown anorthosite (BB) with dark plagioclase porphyry above (Plate 2.18). At another location along the wall, the coarser grained pyroxene-rich dyke (10 - 25 cm wide) intersects BB anorthosite. Within the dyke are inclusions of BB anorthosite. The dyke continues along the north arm wall to the east where it meets with another (?) ferrodiorite dyke, and then around the point of the north arm where it pinches off (Plate 2.19). The ferrodiorite dyke, approximately 0.8 - 1.5 m wide, striking northeast and dipping to the northwest at 48 degrees, extends for about 100 m where it strikes sharply to the north and dips steeply to the west. The dyke weathers a rusty chocolate brown colour and has sharp contacts with the leucoanorthosite (BB). Another ferrodiorite dyke (6 × 1 m) is located along the ‘knob’ (see Figure 2.10), crosscutting the coarse-grained BB anorthosite at 147/48° W.

#### **2.4.4 Pyroxenite (Unit 4)**

Except for thin 1 cm wide veinlets of coarse-grained clinopyroxene and magnetite crosscutting anorthosite (Plate 2.20), there are only two examples of pyroxene-rich rock.



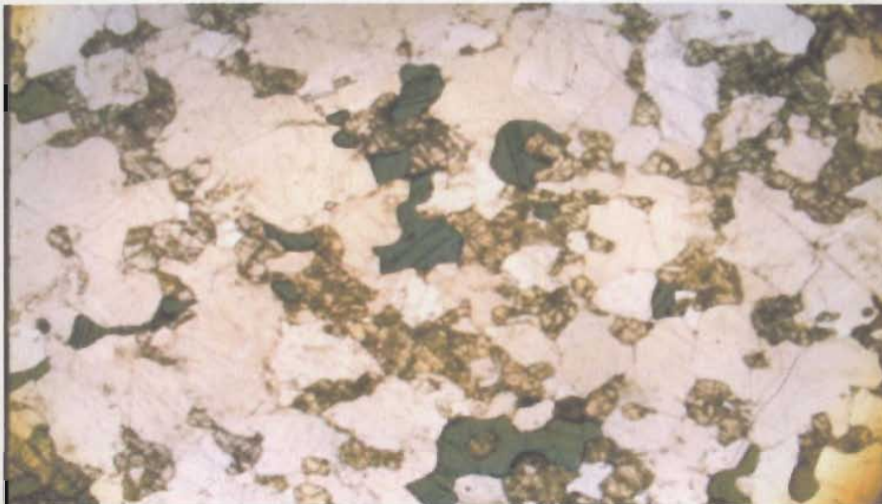


Plate 2.16 Top: Ferrodiorite (Unit 3) with aligned euohedral subophitic plagioclase laths and finer grained stubby clinopyroxene and orthopyroxene, plagioclase, and disseminated oxides. Middle: Ferrodiorite with anhedral, cumulate plagioclase, weakly aligned clinopyroxene (and lesser orthopyroxene), and oxides associated with pyroxene. Bottom: Ferrodiorite with aligned orthopyroxene rimmed with magnetite. Plagioclase is the light grey-white mineral. The ferrodiorite is crosscut by several thin rusty veins reflecting surface weathering. Top photo was taken in crossed polars; bottom two photos were taken in plane of polarized light. All were taken under 1.5 power of magnification (field of view = 9 mm).

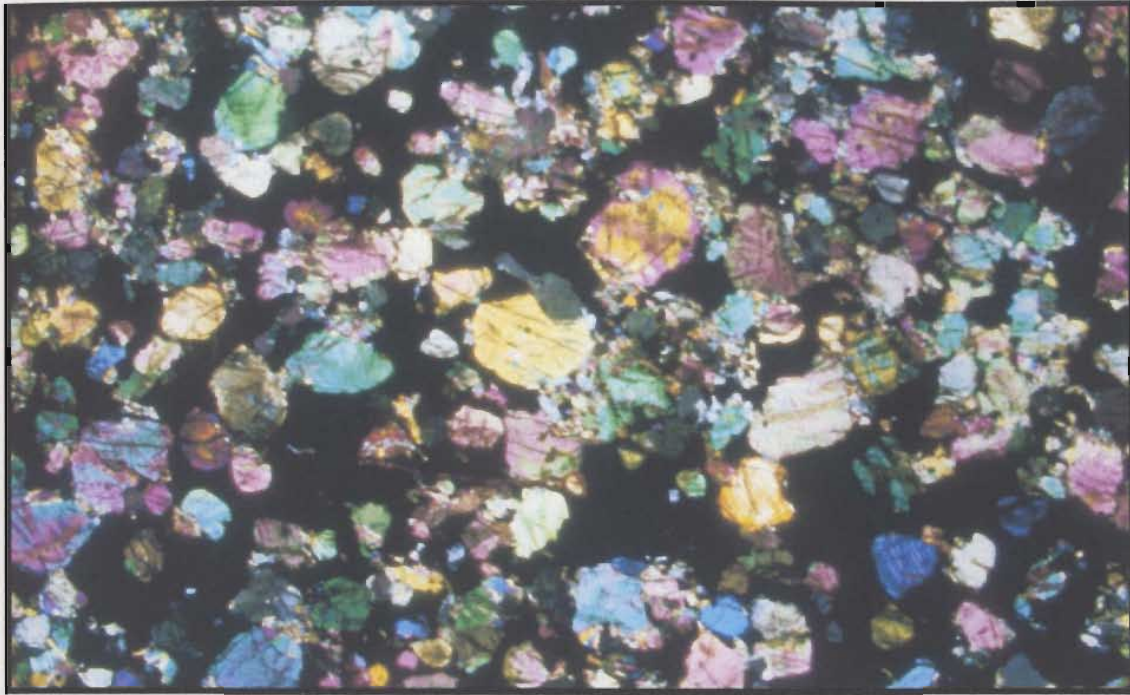


Plate 2.17 Ferrodiorite with clinopyroxene and lesser orthopyroxene surrounded by a network of opaque minerals (sulphides; black). Photo was taken in transmitted light at 1.5 power (field of view = 9mm).



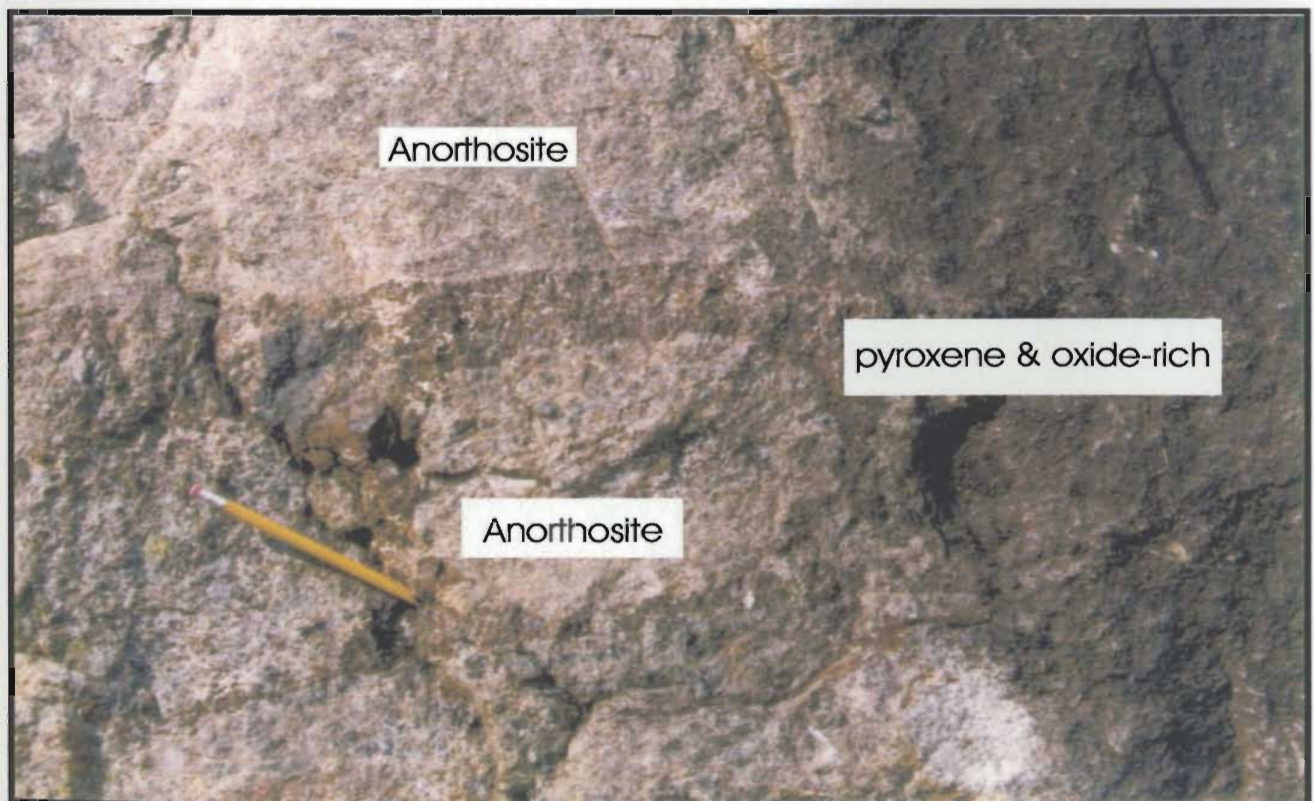
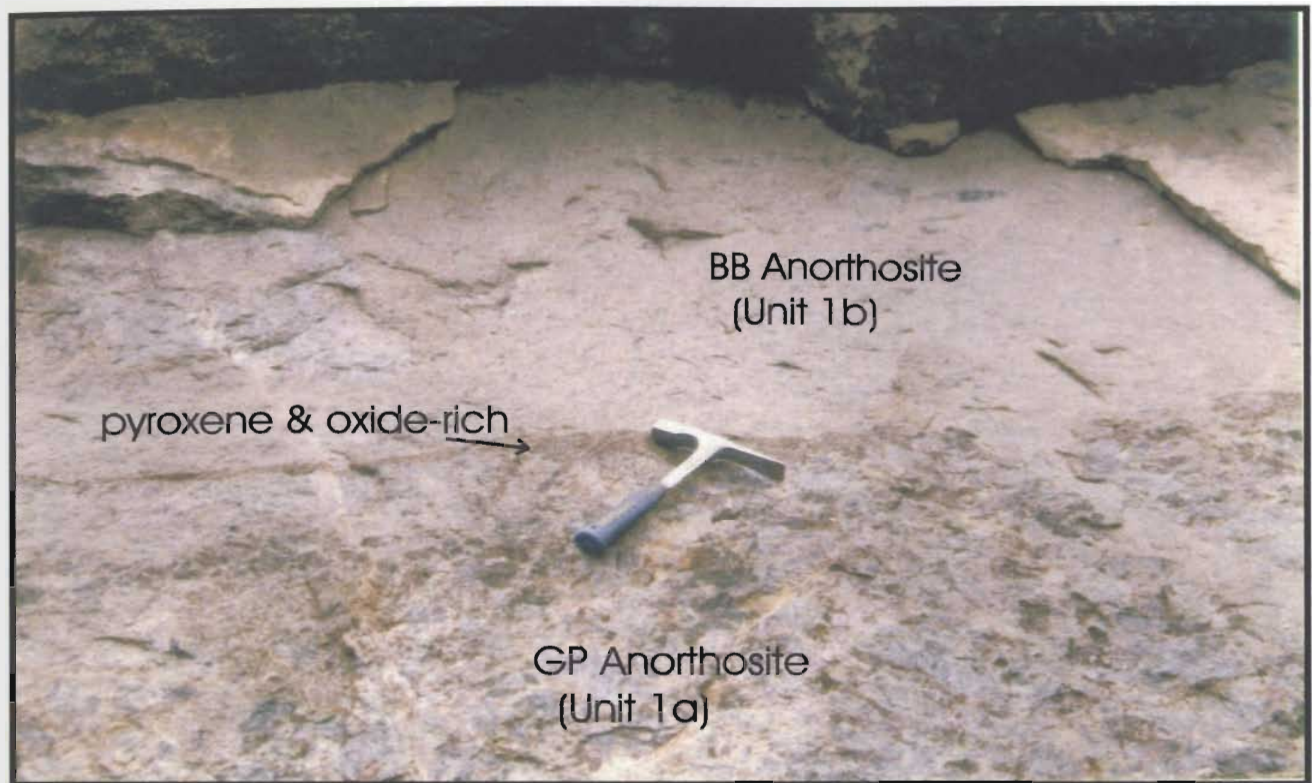


Plate 2.18 Pyroxene and magnetite-rich ferrodiorite veinlets crosscutting anorthosite. Top photo: Veinlet separates BB anorthosite (above) from GP anorthosite (below). Bottom photo: Veinlet has incorporated anorthosite (BB) xenoliths.



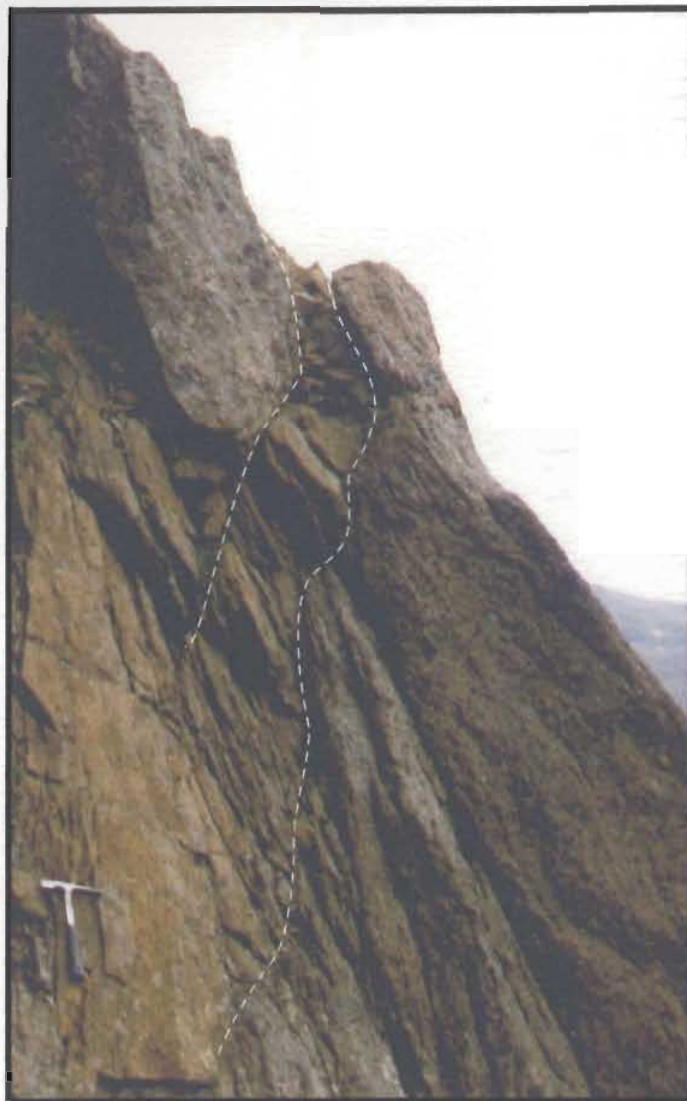


Plate 2.19 Ferrodiorite dyke along the north arm of the crique, crosscutting anorthosite. Photos are of the same dyke. View is to the northeast.

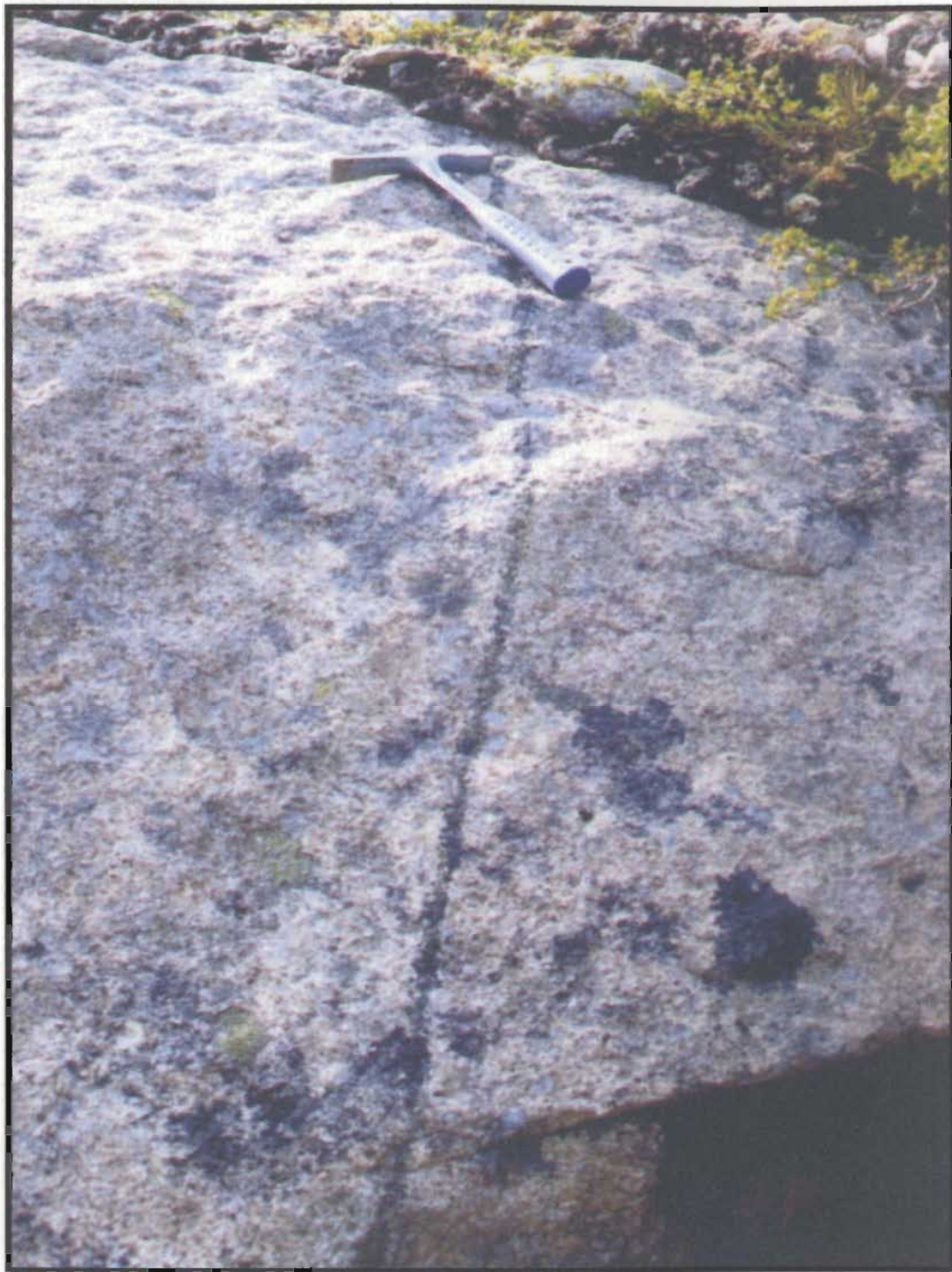


Plate 2.20 Narrow veins (1-2 cm wide) of clinopyroxene and oxides crosscutting leucoanorthosite (Unit 1b).

One sample, consisting of over 90% coarse-grained stubby clinopyroxene with disseminated pyrrhotite, was found in the talus at the base of the back wall of the cirque. The second sample was taken from end of the north arm where pyroxene-rich and plagioclase-rich layers (~ 10 cm and ~ 2 cm wide, respectively) trend approximately northeast. Near these layers is a coarse-grained clinopyroxene-rich and magnetite layer or dyke, approximately 25 cm wide, sandwiched between coarse-grained plagioclase-pyroxene (leuco-) gabbro to the north and anorthosite to the south and trending to the northwest.

#### **2.4.5 Quartz - feldspar - biotite pegmatite dykes (Unit 5)**

Pegmatitic quartz - potassium feldspar - biotite dykes ranging from 20 to 40 cm wide are parallel to the more significant northeast trending, steeply dipping to vertical faults on the Cirque grid. Smaller veins (< 1 to 10 cm wide) crosscut leucoanorthosite along the base of the back wall (Plate 2.21) and also occur above, below, and within fault zones in drill core. In polished thin section, the contacts with the leucoanorthosite (BB) are sharp, with the pyroxene in the BB anorthosite closest to the contacts altered to hornblende and biotite and the plagioclase breaking down to sericite (Plate 2.22).

#### **2.5 Alteration**

In general, the rocks have little or no alteration except along the contacts with the faults and pegmatitic dykes. Sericite, talc, chlorite, serpentine, and minor hornblende and biotite are evidence of minor alteration in anorthosite and associated mafic units. Localized





Plate 2.21 Quartz - K feldspar- biotite pegmatitic dykes (left) and veins (right) crosscutting anorthosite. The dykes in the left photo are located along the base of the back wall of the cirque.

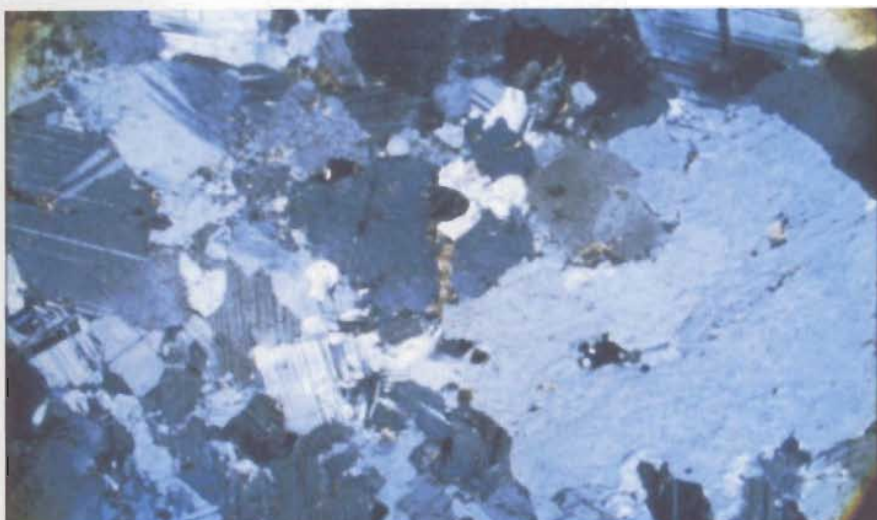


Plate 2.22 Top: Contact between quartz-feldspar-biotite pegmatitic dyke (Unit 4; right) and anorthosite (Unit 1b; left) showing alteration of anorthosite (sericite, hornblende, epidote, biotite, antiperthite and microcline feldspar). Bottom: Pegmatitic dyke showing antiperthite and microcline feldspar. Both photos were taken in plane polarized light at 1.5 power (field of view: 9 mm).



black rims (possibly hornblende) around pyroxene in altered anorthosite were intersected in drill core (Plate 2.23). The fault zones intersected by drill core consist of crumbled core with numerous thin veins and stringers (<1 cm wide) of soft pink talc, quartz, chlorite, and pegmatite (Plate 2.24). Disseminated, blebs, and stringers of pyrite are also found within some of the more extremely altered zones with fault gouge and intense fracturing resulting in some core loss. Also intersected by several drill holes were zones of very fine-grained, green leucoanorthosite indicating saussurization with/without obscure ( $\leq 1$  cm) rounded purple plagioclase porphyry and chloritized pyroxene (Plate 2.25).

In mineralized core intersections, the host anorthosite exhibits a weak sericite alteration to a very fine-grained, granular (sugary textured), light green alteration of intense sericite. Pyrite, occurring as fine disseminations to net-textured clots to “snowflake” texture, is typically present in the more altered, light green zones, usually along the fringes of disseminated and bleb pyrrhotite (Plate 2.26).

## **2.6 Structural relationships**

In cross section ( see Figure 2.11), the cirque consists dominantly of anorthosite with thin layers of leuconorite/leucogabbro and leucotroctolite dipping to the west. In outcrop, there is only minor evidence of igneous layering which is exhibited as: (1) thin (~ 1 cm wide) northwest trending, moderately southwest dipping, plagioclase-rich and clinopyroxene-rich layers (located on the far east end of the north arm) and (2) ~ 10 cm wide layers of medium-grained pyroxene forming hollowed out clots or “pock marks” in anorthosite (located on the

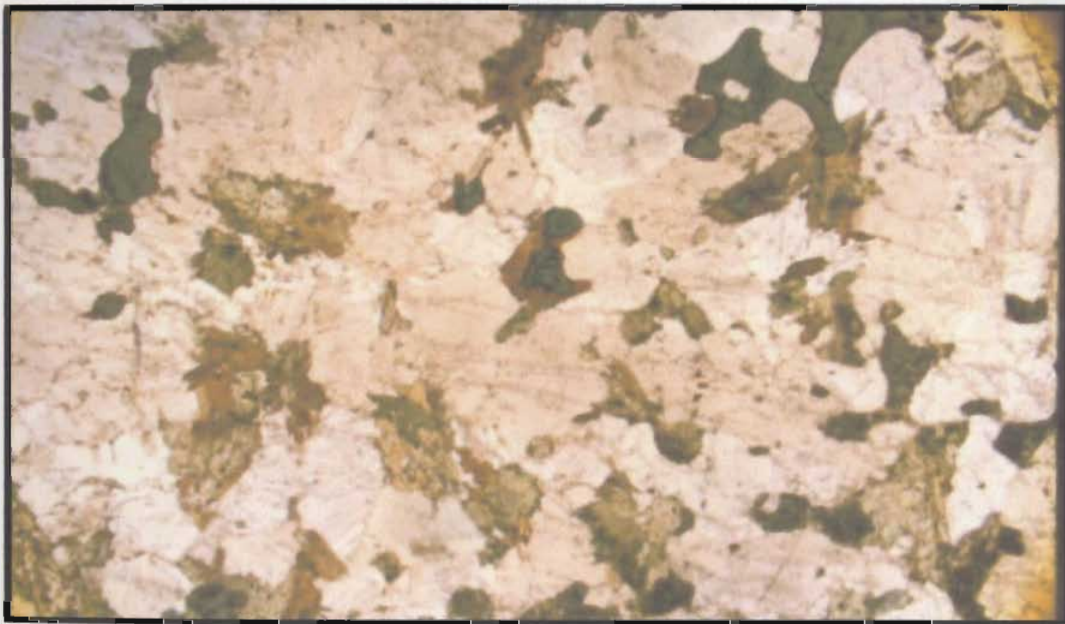
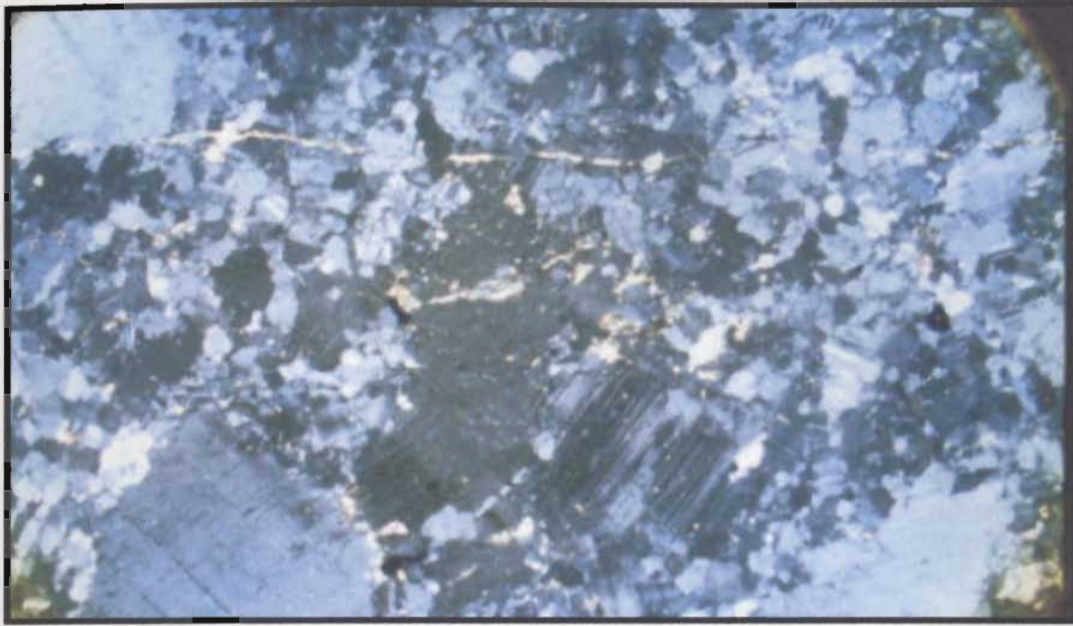


Plate 2.23 Top: Altered anorthosite (Unit 1b) showing sericite dusting, plagioclase recrystallization, and thin veinlets of carbonate. Bottom: Altered anorthosite (Unit 1b) showing cumulate pyroxene altered to hornblende and biotite and sericite dusting on plagioclase. Interstitial oxides are minor. Both samples were taken from outcrop near contact with a pegmatitic dyke. Top photo was taken in crossed polars; bottom photo was taken in plane of polarized light; (1.5 power; field of view = 9 mm).



Plate 2.24 Examples from core of the most altered anorthosite. Samples are taken from various fault zones intersected by drill holes. A: hematite, chlorite, and sericite; B: sericite; C: talc, sericite; D: talc, sericite, chlorite.





Plate 2.25 Fine-grained, light green alteration of plagioclase in leucoanorthosite (drill hole LBN-7, 483.0 m). Several zones of saussuritization and disaggregation of plagioclase were intersected by drill core.

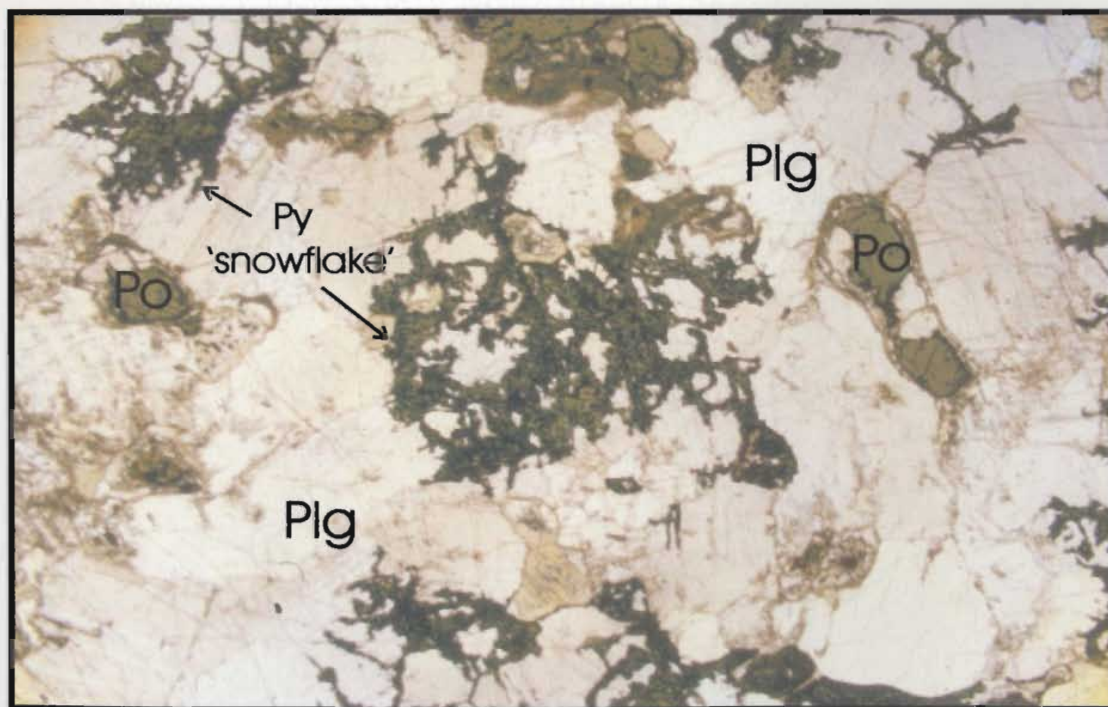
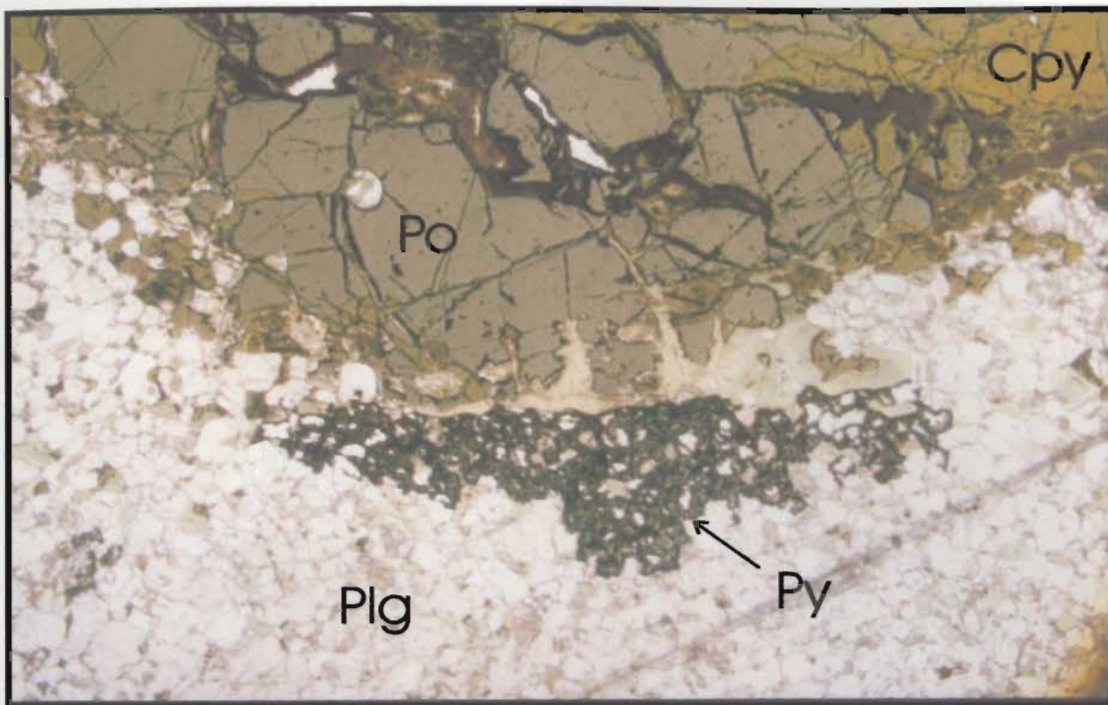


Plate 2.26 Top photo shows fine-grained, net-textured pyrite (py) along pyrrhotite (po) boundaries. Bottom photo shows pyrite clots or "snowflakes" with altered plagioclase (plg) and degraded pyrrhotite. Both photos were taken in reflected light at 1.5 power (field of view = 9 mm). Cpy = chalcopyrite.

southwest part of the grid). Local patches of mafic minerals in the anorthosite, as mentioned earlier, form weak to strong fabrics of foliated pyroxene and oxide minerals. A few large plagioclase phenocrysts are locally aligned as well, indicating some movement within the magma chamber during crystallization or perhaps a magmatic sedimentary process (Irvine 1980).

Bent plagioclase twinning, pyroxene exsolution lamellae, and undulose plagioclase extinction, observed elsewhere in the area (Hynes 1997), are the products of internal movement in a crystal mush during crystallization. Large cracked plagioclase crystals that appear to have disaggregated into smaller anhedral crystals, and anorthosite that is altered a very light green colour with a fine-grained sugary (granular) texture [described as “chill features” by F.P.F Resources (1996)] with or without pyrite, suggest alteration resulted from the injection of a hot fluid body which caused the anorthositic rock to be thermally eroded and incorporated into the intruding body. Pyrrhotite-rich sulphides are the dominant intruding body (discussed in Chapter 2), the second most are the felsic dykes, causing the light green alteration in the anorthosite. Thermal erosion textures will be discussed in greater detail in the next chapter.

Structural lineaments and/or faults throughout the Cirque area are dominantly north-northeast to northeast trending. Vertically to subvertically dipping and northeast dipping faults with associated quartz-potassium feldspar-biotite pegmatite dykes crosscut anorthositic rocks at both corners of the cirque, striking from the north arm to the south arm.

## 2.7 Geological interpretations of neighboring properties

To the west of the Cirque property, the Noranda “Hilltop” property consists of east-southeast striking, west dipping interlayered magnetite-rich norite and anorthosite units intersected by gabbro, norite, and clinopyroxenite dykes (Squires *et al.* 1997). Local field relationships indicate that the magnetite-rich norite intruded the sulfide-bearing anorthosite (*op. cit.*).

To the north, the geology on Canadian States Resources property (Licence #1514M) consists of layering in coarse-grained anorthosite with varieties of norite, leuconorite, gabbro, leucogabbro, and troctolite layering. Fine-grained granitic dykes and fine-grained leucogabbro dykes crosscut the larger mafic bodies (Canadian States Resources *inhouse* data 1995, 1996). Leuconorite, described as having 15 - 20 % magnetite, may possibly be ferrodiorite dykes. Pyroxenite may have been intersected but was not identified by their geologist. The same fine-grained, light green alteration of plagioclase also occurs throughout the anorthosite, as well as the same affects of thermal erosion of plagioclase crystals by injected sulphides (*op. cit.*).

## 2.8 Summary

Xenoliths of Giant Porphyry anorthosite within Buff Brown anorthosite indicate that the oldest anorthosite phase on the Cirque grid was the labradorite-rich GP anorthosite. Although GP anorthosite is dominantly plagioclase-rich, the presence of orthopyroxene megacrysts suggest semi-crystallization at higher pressure (~8-10 kbar) in the lower crust or

upper mantle before being transported as mushes or suspensions to the upper crust (Fram and Longhi 1992). The GP anorthositic mushes may have been carried along by partially crystallized BB anorthositic liquid to shallower depths or were intruded by subsequent BB anorthositic crystal-liquid mushes, or both. Either way, an open system allows for the geochemical homogeneity of the anorthositic plutonism and the presence of deformed and/or suspended crystals (Fram and Longhi 1992). At shallow levels in the crust (~3 kbar), plagioclase crystallization increased, followed by cotectic crystallization of plagioclase and mafic minerals (*op cit.*). Plagioclase-rich liquids of variable composition continued to intrude the existing plutons, as dykes and small intrusives (*op cit.*).

Capping the BB anorthosite are leuconorite/leucogabbro and leucotroctolite. The interlayering of these units with the BB anorthosite at the top of the cirque indicates that the mafic units probably formed coevally with the BB anorthosite through crystal fractionation, however, there is some evidence that at least some of the leucogabbro intruded the BB anorthosite (Figure 2.13).

Ferrodiorite dykes intruded the larger intrusions of anorthosite and mafic bodies. The limited exposure of the pyroxenite unit indicates that it formed coevally with the BB anorthosite, leuconorite/leucogabbro, and leucotroctolite rocks. However, it is possible that the pyroxenite may have also intruded these rocks after anorthosite emplacement. Its exact age with respect to being younger or older than the ferrodiorite rocks is unknown due to lack of field evidence. Subsequent to the emplacement of the BB anorthosite and the coeval “leuco-” varieties, the rocks were crosscut by faults and pegmatitic dykes.



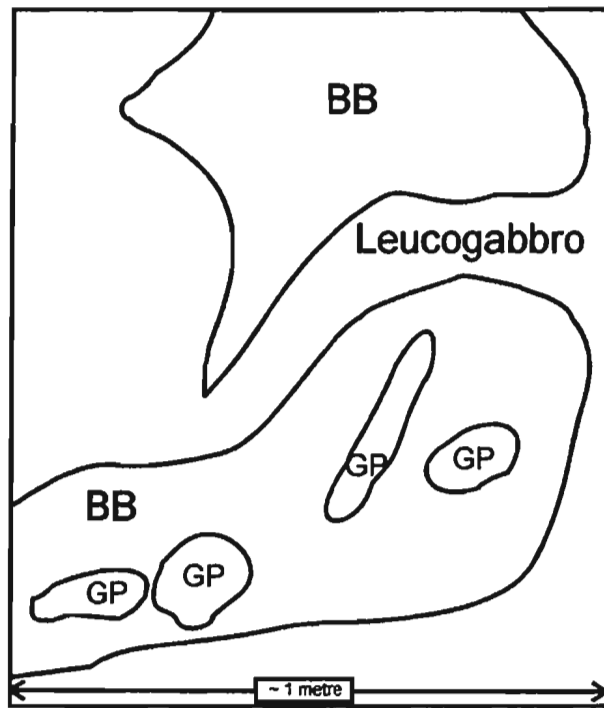


Figure 2.13 Field sketch showing leucogabbro (Unit 2) intruding Buff Brown anorthosite (Unit 1b; BB) which contains Giant Porphyry anorthosite xenoliths (Unit 1a: GP). Outcrop is located at the top of the Cirque near 5+25S, 2+50E.

Mineralization dominantly occurs within the anorthositic rocks even at the top of cirque where anorthosite is interlayered with leuconorite-leucogabbro-leucotroctolite (Unit 2). The relationship between the sulphide mineralization and the geology of the Cirque grid will be discussed in Chapter 3.

## **CHAPTER 3**

### **SULPHIDE MINERALIZATION**

#### **3.1 Introduction**

In the Alliger Lake - Puttuaalu Lake area, extensive geological mapping, geophysical, and drill programs carried out by numerous exploration companies since 1995 have delineated several nickel-copper sulphide occurrences as shown in Figures 3.1a and b. A narrow (5 km wide) north-trending belt of localized sulphide mineralization spans approximately 40 km from the OKG showing (Castle Rock Exploration Limited) north of Umiakoviarusek Lake to a prospect of discontinuous massive pyrrhotite and lesser chalcopyrite on the Cartaway property (Licence #910M; previously held by Ace Developments) approximately 3 km south of the Cirque property. Mineralization ranges from disseminated to semi-massive to massive pyrrhotite with minor chalcopyrite  $\pm$  pentlandite  $\pm$  magnetite and is generally exposed along or in proximity to north to northeast trending lineaments and faults. With the exception of Castle Rock's OKG prospect, where sulphide mineralization is syngenetic within a series of Mesoproterozoic pyroxenite dykes cutting Paleoproterozoic anorthosite (Piercey 1998; Piercey and Wilton 1999), the host rocks in all other occurrences are dominantly massive to layered Mesoproterozoic anorthosites with gabbro/norite varieties. Overall, assay results are subeconomic, however, small intersections of massive sulphides from several properties had Ni and Cu values greater than 1 %. Table 3.1 lists most of the properties in the area with the best reported

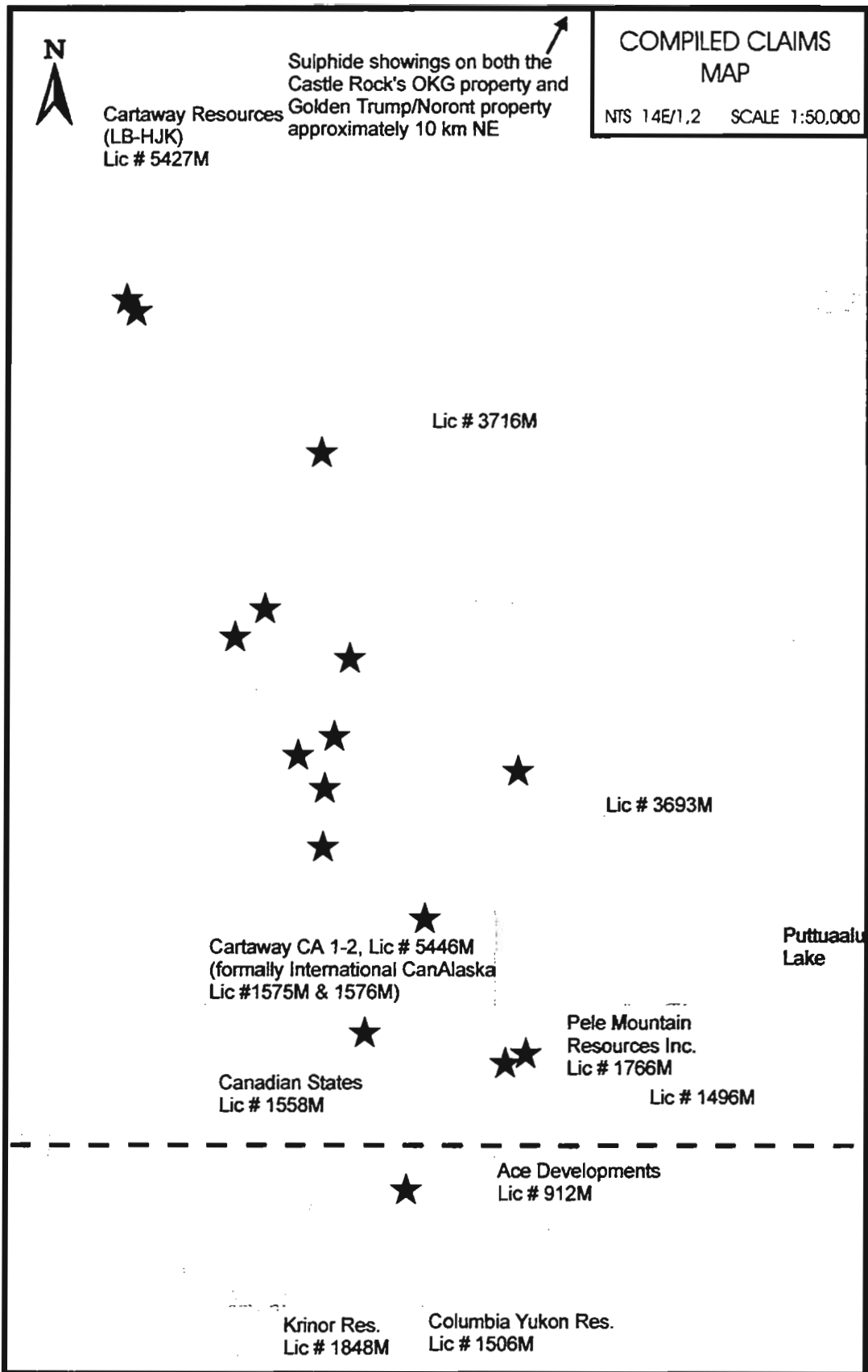


Figure 3.1a Claims map showing locations of known Ni-Cu sulphide occurrences (star) on NTS 14E/1,2. Figure 3.1b continues below dashed line.

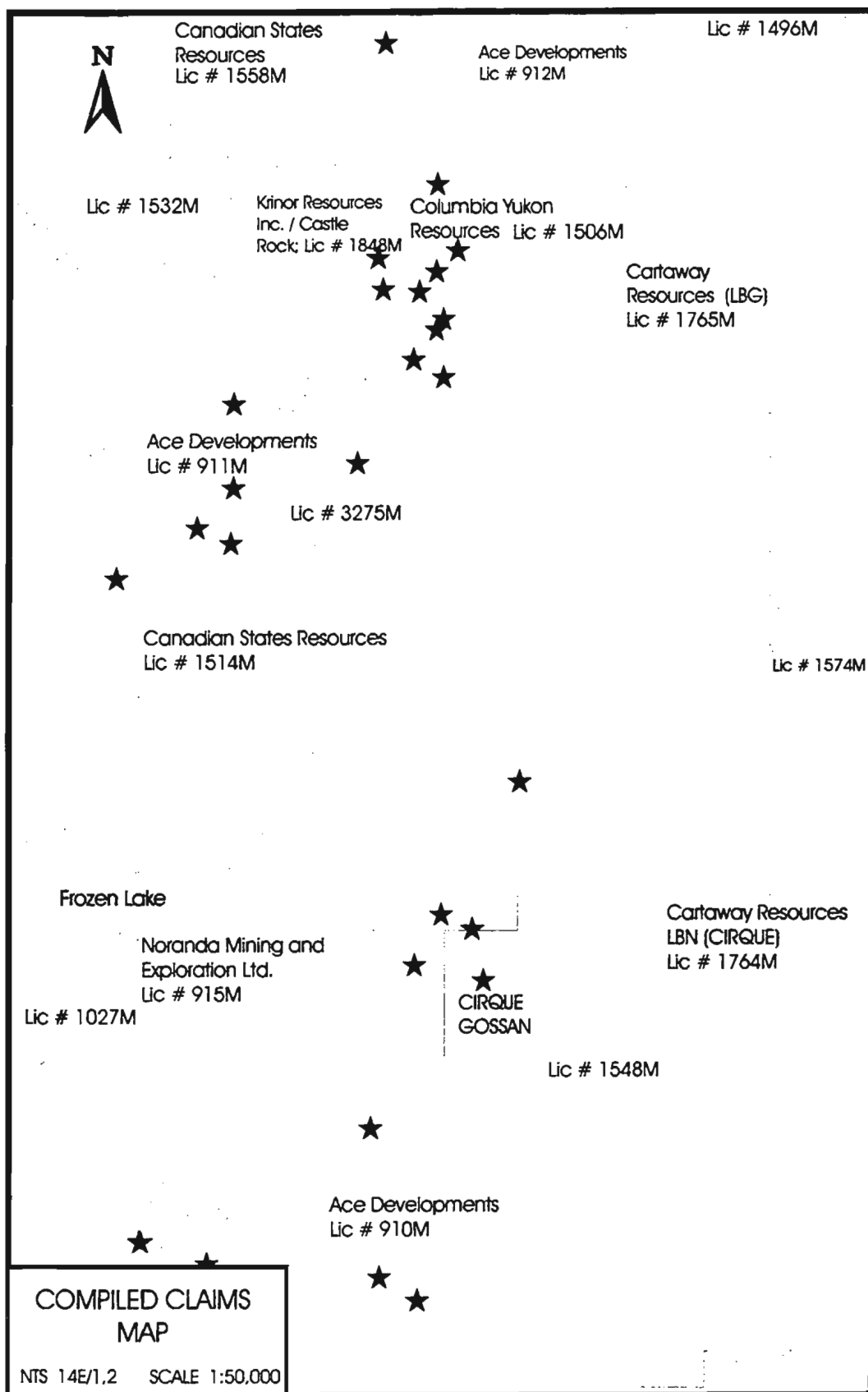


Figure 3.1b Claims map showing locations of known Ni-Cu sulphide mineral occurrences (star) on NTS 14E/1,2.

Table 3.1 Compilation of available prospecting and drilling results from exploration companies who held property in the Puttuala Lake area between 1995-1997. Refer to Figure 3.1a and b for property locations (except for Castle Rock's OKG prospect further north of LB-HJK).

Company	Property, Location	Property Geology	Mineralization	Grades	Source
Ace Developments	Lic # 910M	ol-lgabbro, Inorite, anor, ferro	massive po with minor cpy	Grab: 0.51% Ni, 0.52% Cu, 0.15% Co	Ace Developments / Avalon Mining Ltd. (1996); Cartaway Resources <i>inhouse</i> compilation (1997)
Ace Developments	Lic # 911M	layered norite-Inorite, anor, ol-gabbro dykes, mag-rich diabase dykes (ferro?)	small gossans of diss to mass po with cpy; cpy veins	Grab: 0.57% Ni, 0.60% Cu, 0.14% Co	Ace Developments / Avalon Mining Ltd. (1996); Cartaway Resources <i>inhouse</i> compilation (1997); Kerr and Smith (1997)
Ace Developments	Lic # 912M	anor, Inorite, norite-gabbro layers, ferro, possibly a NW trending pyx dyke	5% po with minor cpy, location unknown	Grab: 279ppm Ni, 867ppm Cu, 106ppm Co	Ace Developments / Avalon Mining Ltd. (1996); Cartaway Resources <i>inhouse</i> compilation (1997)
Canadian States Resources	Lic # 1514M	layered anor and Inorite, fgr mafic rock, dykes of "ferro", mag-rich troc	discontinuous gossans; massive po with minor cpy and pn, mag	Grab: 1.8% Ni, 0.3% Cu, 0.17% Co, 0.93% Cr, 0.23% Zn Core: 1.77%Ni, 0.81% Cu, 0.12% Co over ~10 m	Canadian States Resources (1997); Kerr and Smith (1997); Kerr (1998)
Canadian States Resources	Lic # 1558M	anor, leucogabbro-melanogabbro, troc	trace po, cpy, py to massive po, minor cpy and py	0.46% Ni, 0.29% Cu, 0.14% Co	Canadian States Resources (1997)
Cartaway Resources	Lic # 1764M - LBN, 'Cirque'	anor, ltroc, lgabbro-Inorite, ferro, pyx	diss, net-textured, semi massive to massive po with minor cpy, trace pn	Grab: 0.59% Ni, 0.13% Cu Core: 0.25% Ni, 0.65% Cu, 0.11% Co over 1.1 m	Cartaway Resources (1997); Beesley (1997)
Cartaway Resources	Lic # 1765M - LBG	anor, minor pyroxene-rich layers	minor po, cpy, py	Core: 0.39% Ni, 0.38% Cu, 0.11% Co over 0.43 m	Cartaway Resources (1997); Beesley (1997)
Cartaway Resources	Lic # 5427M - LB-HJK	anor, granite, gneiss, mag-rich troc	diss to massive po with minor cpy	Grab: 0.1-0.5% Ni Core: 0.08% Ni, 0.12% Cu, 0.03% Co	Cartaway Resources (1997)

Cartaway Resources (formally International Canalska Resources)	Lic # 5446M - CA-1 & 2 (formally Lic # 1575M & 1576M)	anor intruded by ol-bearing gabbroic dykes, Inorite, minor ferrodiorite dykes	local zones of diss po, cpy in anor	Grab: 0.97% Ni, 0.47% Cu, 0.08% Co	Hennesy and Mersereau (1996); Cartaway Resources (1997)
Castle Rock Exploration Limited	Lic # 1532M	Paleoproterozoic and Mesoproterozoic anor, ferrogabbro, rare peg dykes	8-10% diss to mass c gr po, minor cpy	Grab: 0.08% Ni, 0.15% Cu	O'Sullivan (1997)
Castle Rock Exploration Limited/United Compass Resources	Lic # 1539M, OKG prospect	Paleoproterozoic Fe-rich monzonites and anor, ltroc plugs, felsite dykes, Mesoproterozoic pyx dykes	stringers of po, cpy, pn; diss to mass dominantly assoc with pyx dykes	Grab: 1.78% Ni, 1.44% Cu, 0.21% Co; Core: 0.88% Ni, 0.56% Cu, 0.05% Co over 7.6m	Kerr and Smith (1997); Piercey (1998); Piercey and Wilton (1999)
Castle Rock Exploration Limited/Krinor Resources Inc.	Lic # 1848M	ol (?) - nor/Inor, anor gabbro/norite	discordant gossans with vein-like sulphides concentrated in layered notite; diss to mass po with cpy	Grab: 1.31% Ni, 0.52% Cu, 0.21% Co; Core: 0.5 - 1.0% Ni	Cartaway Resources <i>inhouse</i> compilation (1997); Kerr and Smith (1997)
Columbia Yukon Res. & Silverstone	Lic # 1506M	layered and massive troc, anor, lgabbro, gabbro, f gr mafic dykes	discordant pods of diss to mass po, py, 1-3%cpy, cpy veins; some po may be hosted in pyx	Grab: 0.77% Ni, 0.59% Cu, 0.16% Co; Core: 0.67% Ni, 0.38% Cu, 0.09% Co over 5.7m; max 1% Ni in core	Coates and Beilhartz (1997); Kerr and Smith (1997)
Donner Minerals (joint venture with several other companies)	South Voisey's Bay Project	Paleoproterozoic biotite-rich metasedimentary gneiss of CP; Mesoproterozoic granite and gabbro of the NPS and HLPS	diss to small zones of mass sulphide; syngenetic po with cpy, minor pn in ol gabbro	Grab: up to 0.45% Ni, 0.52% Cu, 0.04% Co; Core: 1.93% Ni, 1.07%Cu, 0.26%Co over 0.6m; Core: 11.75% Ni, 9.7% Cu, 0.43% Co over 1.1m	Kerr and Smith (1997); Kerr (1998); Kerr (1999); Smith <i>et al.</i> 1999



Golden Trump Resources/ Noront Resources	adjacent to Castle Rock's OKG prospect	not available	not available	Grab: 0.54% Ni, 0.22% Cu, 0.07% Co; Core: 0.82% Ni, 0.48% Co, 0.06% Co over 6.4m	Kerr and Smith (1997)
NDT Ventures/Takla Star Resources	Lic # 756M, Unity claims, Projecty 44; Nain Hill Prospect	variety of foliated Inor, anor, gabbro-norite, Paleoproterozoic (?) granite	diss to massive po with cpy, mag, pn exsolution; diss with minor cpy in a finer grained pyroxene-rich rock which intrudes Inor	Core: 0.51% Ni, 0.37% Cu, 0.04% Co over 6.94m; Core: 1.65% Ni, 0.30% Cu, 0.15% Co over 0.81m	Kerr and Smith (1997); Kerr (1998); Hinchey <i>et al</i> (1999); Hinchey (1999)
Noranda Mining & Exploration Inc.	Lic # 915M, 'Hilltop'	anor, norite, ol-gabbro/norite, troc-ltroc, pyx, f gr melanocratic (py-rich) mafic rock	diss to massive sulphides (po with minor cpy), local thin cpy-rich zone (1.76% Cu); syngenetic sulphides in a "pyx"	Grab: 0.36-0.85% Ni; Core: 0.45% Ni, 1.01% Cu over 20cm, 5.56% Cu over 10cm	Squires <i>et al</i> (1996 - 97); Kerr and Smith (1997)
Pele Mountain Resources Inc.	Lic # 1766M	anor, ol (?) -Inorite, ferro	not available	Core: > 1.0% Ni	Cartaway Resources <i>inhouse</i> compilation (1997); Kerr and Smith (1997)
Staghorn Lake area (several companies)	Several claims including those held by NDT Ventures (Project 10-1)	anor, Inor-nor	discordant pods of mass po with cpy	Grab: 1.86% Ni, 0.95% Cu, 0.165% Co; Core: 0.29% Ni, 0.28% Cu, 0.07% Co over 0.8 m (exact locations are unknown)	Kerr and Smith (1997)

LEGEND: CP = Churchill Province; NPS = Nain Plutonic Suite, HLPS = Harp Lake Plutonic Suite

Rock type: ol = olivine, nor = norite, Inor = leuconorite, ferro = ferrodiorite, anor = anorthosite, pyx = pyroxenite, troc = troctolite, ltroc = leucotroctolite,

peg dykes = pegmatitic dykes, lgabbro = leucogabbro

Sulphide minerals: po = pyrrhotite, cpy = chalcopyrite, py = pyrite, pn = pentlandite

Textures: diss = disseminated, c gr = coarse-grained, f gr = fine-grained

assay values from rock and core samples.

Two prospects ('Nain Hill' and 'South Voisey's Bay Project') located approximately 75 and 175 south, respectively of the Cirque area, are also described for comparison. The Nain Hill prospect (held by NDT Ventures and Takla Star Resources; Project 44) is located 3 km from the town of Nain and consists of disseminated and local zones of massive pyrrhotite and lesser chalcopyrite hosted in dominantly gabbro-noritic rocks of probable Mesoproterozoic age (Hinchey 1999; Hinchey *et al.* 1999). The South Voisey's Bay Project consists of numerous properties held and operated jointly by Donner Resources and several other exploration companies. The group of properties, located approximately 120 km south of Nain, consists of disseminated and small localized zones of semi-massive to massive pyrrhotite and chalcopyrite hosted in olivine gabbro and leucogabbro located at the base of mafic sills (Smith *et al.* 1999). The syngenetic style of mineralization and the presence of contaminated sulphide-bearing olivine-rich mafic rocks are believed to be very similar to those observed at the Voisey's Bay deposit located approximately 80 km to the northeast (*op. cit.*)

As mentioned earlier in Chapter 1, the sulphide occurrence on the Cirque property can be traced on surface for approximately 400 m by ~150 m wide, striking to the northwest onto the Canadian States Resources property, Licence #1514M (Figure 3.2). Numerous grab and core samples were collected during the three year exploration program conducted by Cartaway Resources. For this study, many sulphide-bearing samples were analysed from each drill hole (LBN-96-1 to 10, LBN-97-11 and 12). Holes LBN-97-1 to 5 were relogged

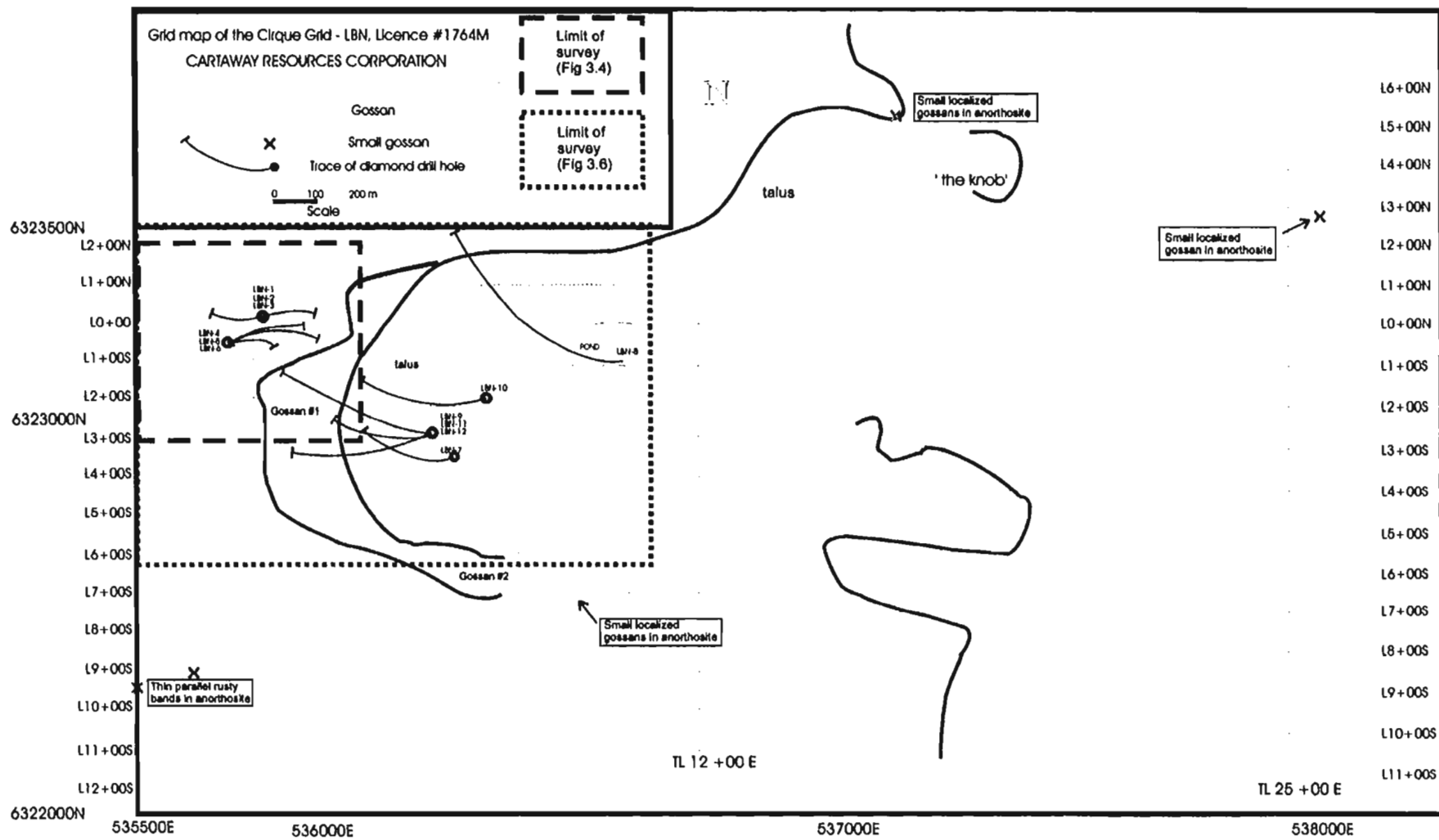


Figure 3.2 Grid map (1:5,000 scale) showing the gossan locations on the Cirque grid. Most of the grid is covered in glacial debris. Refer to figures 3.4 and 3.6 for the results of the geophysical surveys.

and, in places, resampled and the mineralized samples were assayed for Ni, Cu, and Co by Cartaway Resources Corporation; selected samples were also assayed for Pt, Pd, and whole rock analyses (major and trace elements). Most of the outcrop samples collected on the grid and core samples used for this study were assayed using XRF and ICP-MS techniques in the Earth Sciences Department, Memorial University for whole rock analyses. A sulphide-bearing sample was also collected from the neighbouring Noranda and Canadian States properties for comparison. Descriptions of these analytical methods are in Appendix A1 and the results are listed in Appendix A2.2 and A2.3.

This chapter describes the nature and abundance of sulphide mineralization on the Cirque and surrounding properties, with particular attention given to sulphide textures and the 'sulphide - host rock' relationship. Sulphide geochemistry will be discussed in Chapter 5.

### **3.2 Geophysical surveys and interpretations**

Airborne electromagnetic and magnetic surveys over the Cirque property were conducted in 1995 by SIAL Geophysics Ltd. Ground horizontal loop electromagnetic (HLEM) and magnetometer (MAG) surveys were conducted on the Cirque grid in 1995 and 1996 by JVB Ltd and *inhouse* geophysical operators. Ground and borehole pulse electromagnetic (PEM) surveys were conducted in 1996 and 1997 by Crone Geophysics and Exploration Ltd. More complete individual summaries of the HLEM, MAG, and PEM surveys and the general interpretations of each are given below. Table 3.2 provides a brief description of each survey and its results.

Table 3.2 Summary of geophysical survey results for the LBN (Cirque) property.

Company	Survey Date	Method	Results
JVX Geophysics Ltd. (JVX Ltd. 1995)	Sept. 1995	HLEM  MAG	<p>- Strong in-phase and quadrature responses on L2+50E, 1+00S and 0 indicative of a shallow buried conductive body (&lt;50m from the top of the body), possibly dipping to the SE.</p> <p>- Broad, shallow responses on L1+00S at 1+25E, 3+50E, and 4+50E are possibly a series of thin vertical conductors.</p> <p>- Sharp in-phase anomalies throughout the grid may be magnetite-rich overburden and/or terrain variations.</p> <p>Mag 1: coincides with airborne anomaly typical of a mafic intrusion.</p> <p>Mag 2 and 4: NE of Mag 1, appear at the SW and NE edges, respectively of the HLEM zone; possibly related to secondary magnetite mineralization (eg, po) through a fracture or contact.</p> <p>Mag 3: a distinct NNW/SSE trending magnetic high coinciding with the HLEM zone.</p> <p>Mag 5: NE of the HLEM zone; seems to trend towards the SE, extent unknown; several magnetic responses at various locations suggest magnetite-rich overburden.</p>
SIAL Geophysics Ltd.* (Woolham 1995)	Nov. 1995  Nov. 1995	Combined helicopter-borne EM  Combined helicopter-borne MAG	<p>Two conductive bodies: #1 is located ~1.2km NE of the Cirque; #2 occurs on the Cirque grid and is highly conductive, "perhaps a complex structure reflecting a narrow flat lying ribbon-like body"; trending NW.</p> <p>- Generally trending N-S to NNE, four complex magnetic high areas (A,B,C,D), all associated with conductive zones.</p> <p>- On the grid, anomaly D is circular with a negative core, "typical of a mafic intrusive vertical plug-like source exhibiting several phases of intrusion"</p> <p>- Anomaly D coincides with the EM zone #2, crossing at right angles, with the SSE end of the EM zone ending within the magnetic low core.</p>

Company	Survey Date	Method	Results
Crone Geophysics & Exploration Ltd. (Watson 1996)	Nov. 1996	Surface PEM	<ul style="list-style-type: none"> <li>- Anomalies are due to bedrock sources, could not fully define the conductor due to steep hills on the west end of the grid.</li> <li>- Conductor on L0 and L1+00S, &gt;150m below surface.</li> <li>- Conductor(s) on L3+00S, L4+00S, and L5+00S, possibly massive sulphides closer to the surface.</li> <li>- Remainder of surveyed area have variations of weak conducting surface material.</li> </ul>
	Nov. 1996-1997	3-D Borehole PEM	<ul style="list-style-type: none"> <li>- Hole LBN-7 was drilled to test the extent of the mineralization intersected in holes LBN-1 to 5 at the top of the Cirque. Holes LBN-8 to 12 were drilled to intersect geophysical anomalies.</li> <li>- Conductive anomalies located in DDH 7 to 12 are interpreted to be lenses of mineralization of various sizes (eg. Massive to semi-massive) and orientations</li> <li>-Crone (1996) interpret the overall dimensions to be NE trending zone between L4+00S and L2+00N and 4+00E to 8+00E. However, the author of this study suspects the actual strike of the zone to be NW.</li> <li>- Surface conductor was also identified suggesting the target area extends from near surface (150m) to approximately 1100m below surface and perhaps even further.</li> <li>- Surface conductors at ~L6+00E to L8+00E on L0 to L5+00S interpreted to be the expression of downdip extent of conductor intersected by LBN-11 (see Table 3.3).</li> <li>- Broad cross-over anomalies are interpreted to be separate, steeply dipping conductive sulphide bodies within a favorable horizon.</li> </ul>

\* SIAL Geophysics Ltd surveyed LB-N and LB-G properties.

HLEM = Horizontal loop electromagnetic survey, MAG= magnetometer survey,

EM= electromagnetic survey, PEM= pulse electromagnetic survey.

Interpretations of the geophysical data were made incorporating the geology and structure of the area; for instance, high percentages of magnetite and/or ilmenite in the mafic units could result in an over-estimation of magnetic anomalies, that is, possible sulphide occurrences (F.P.F Resources 1996). Also, sharp elevation contrasts can impact on the quality of derived airborne data since the helicopter has to maintain a constant speed and low clearance (60 m), thereby affecting accurate readings of the geophysical equipment.

### **3.2.1 Airborne MAG and HLEM**

Data from the airborne electromagnetic and magnetic surveys (Figure 3.3) have defined a low amplitude “depressed” semi-circular northeast trending zone (maximum of ~450 m x 200 m) which suggests a steeply dipping mafic intrusive and corresponds to the position of the ferrodorite dykes (Unit 3) along the north arm and knob. Also on the grid are three north-northeast striking linear magnetic trends which correspond to the fabric defined by magnetite-rich zones in the rock. The shaded areas mark high amplitude magnetic areas interpreted to be possible mafic intrusive centers (*ie.* magnetite-rich mafic intrusive bodies; Woolham 1995). Assumed faults are based on magnetic trend interruptions and/or discontinuities.

On the grid, the strong northwest trending narrow oval-shaped, flat-lying conductor (~400 m x 100 m) crosses perpendicular to the magnetic low, terminating at the center of the magnetic trend. Interpretation of this conductor is difficult especially when compared to the magnetic low in the area and it indicates a complex structure, however, it does



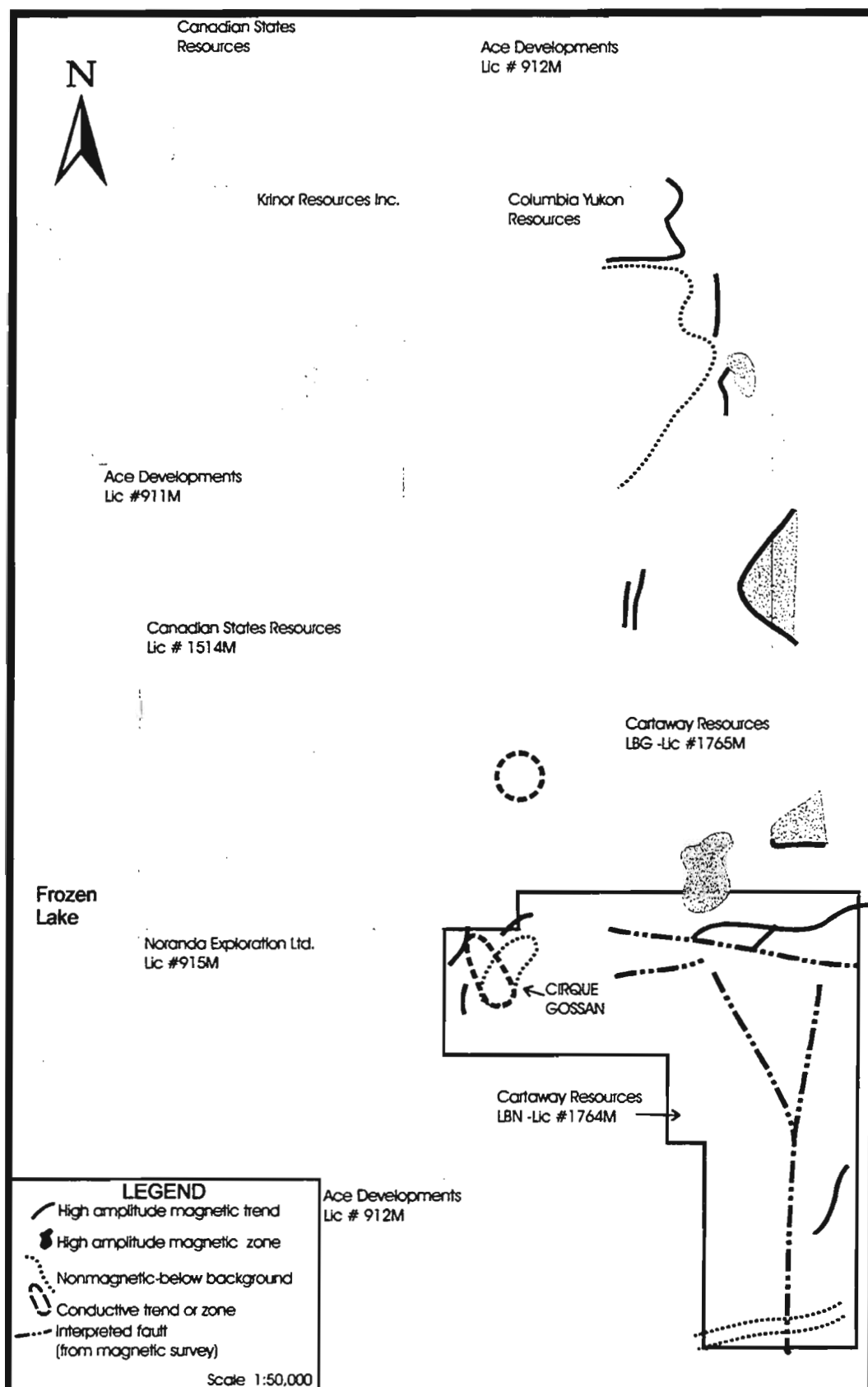


Figure 3.3 Airborne geophysical (magnetic and electromagnetic) compilation map showing the LBN property (Cirque; Lic #1764 M); NTS 14E/1,2 (Woolham 1995).

correspond to the location and trend of the Cirque gossan. It is also possible that readings from this area were affected by sharp elevation contrasts and interpretations should be made with caution. Approximately 1 km to the north, straddling the Canadian States (Licence #1514M) and Cartaway's LB-G property (Licence #1765M), is a second good, flat-lying, but small, conductor. Drilling of this conductor was undertaken by both companies, intersecting only subeconomic sulphide mineralization.

Other anomalous magnetic trends and zones to the north and east on LBN and LBG properties were interpreted to define mineralized areas. Reconnaissance mapping and prospecting on these areas, however, revealed no significant sulphide mineralization. Based on reconnaissance geological mapping, these anomalies seem to correspond generally to the north-northwest trending ferrodiorite unit, defined by Ryan *et al.* (1997) which is similar to Unit 3.

### **3.2.2 Ground MAG and HLEM**

A large, moderately strong, HLEM conductor was defined on the grid in early 1995 (Figure 3.4, refer to Figure 3.2 for location on the grid). It is located near L1+00S, 2+50E, and L0 and is approximately northwest trending, 750 m long and a maximum of 250 m wide, petering out to approximately 50 m wide to the northwest and open to the southeast. It is interpreted to be either a broad flat body, or a thin and vertical one buried at a shallow depth (<50 m) and possibly dipping to the southeast (JVX Ltd. 1995). Another response is also outlined on L1+00S at 3+50E and 4+50E. Extensive glacial cover may mask any conductor

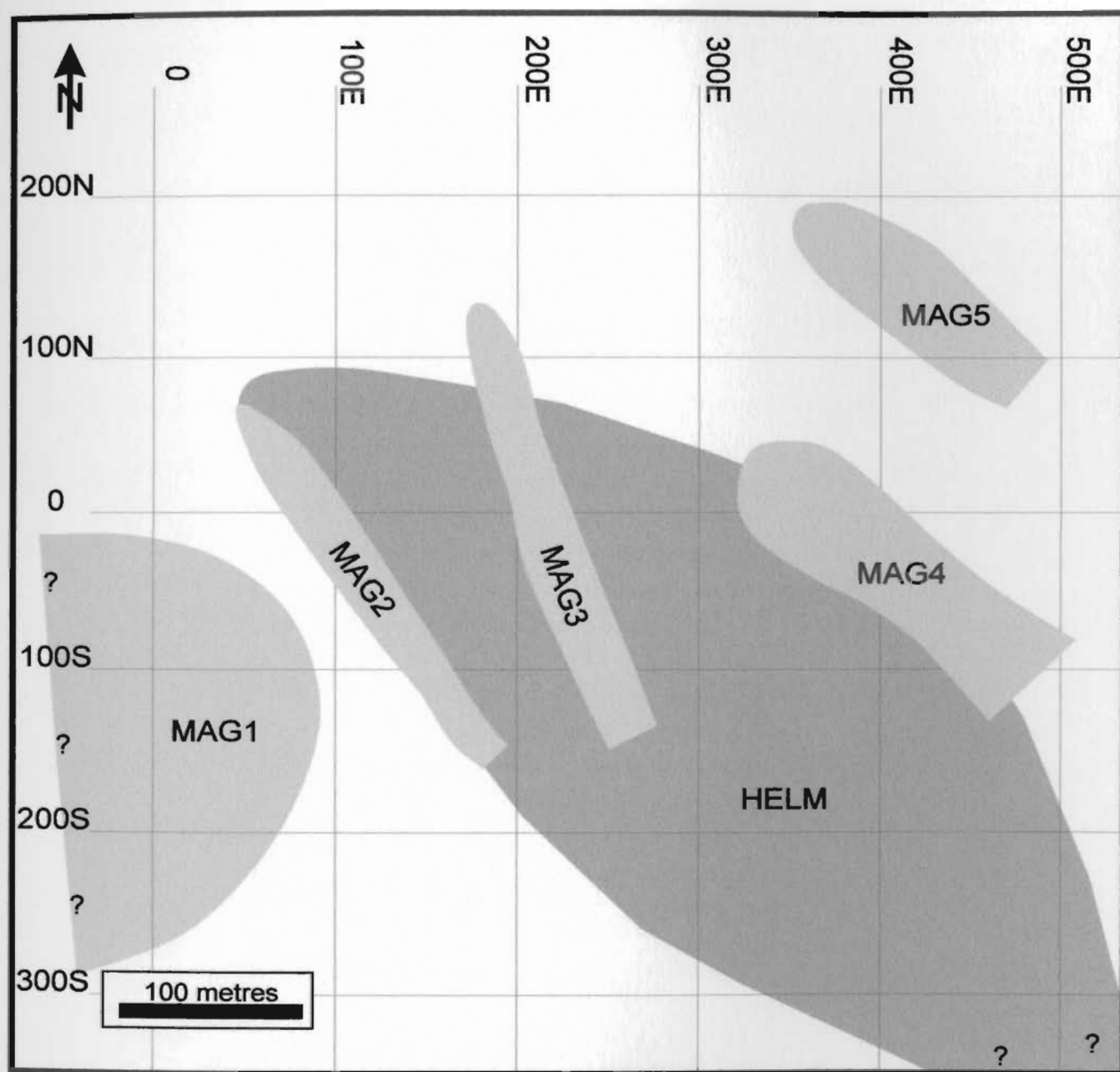


Figure 3.4 Plan view of part of the Cirque grid showing five subsurface magnetic anomalies and one large northwest trending HLEM conductor (JVX Ltd. 1995). Question marks denote the unknown limit of the anomalies.

at the bedrock surface making further conductors difficult to detect.

Initially, five magnetic anomalies were defined. Mag 1 is rounded, spanning nearly 300 m long (between L0 and L3+00S) and 150 m wide (from 1+00E and open to the west, near the property boundary). Mag 1 corresponds to airborne HLEM results and is believed to reflect both boulders and outcrop of magnetite-rich gabbro that have been mapped on top of the Cirque. Mag 2, 3, 4, and 5 are narrow (25-75 m wide) northeast trending anomalies. Mag 2, 3, and 4 correspond to the HLEM conductor and indicate a magnetic conductor, quite possibly one or more sulphide bodies. The magnetic anomalies are about 150-250 m long, and open at the southeast end. Compared to the occurrence of sulphide intersections in drill core (Figure 3.5), the magnetic and HLEM anomalies seem to define the gossan quite accurately. Based on known mineralization on the neighbouring Canadian States property (Licence #1514M) to the north, the northwest end of the magnetic body is also believed to be an extension of the mineralization to the northwest. It is also possible that some of the magnetic anomalies reflect magnetite-rich layers within the anorthosite-leuconorite-leucogabbro units. The large gossan at the Cirque does, however, lie parallel to the delineated anomalies. JVX Ltd. (1995) interpreted most of the magnetic responses to result from "secondary magnetic mineralization through a contact or fracture."

### **3.2.3 Surface PEM**

Surface pulse electromagnetic (PEM) surveys were undertaken from 1996 to 1997. Surveys in 1996 were confined to the bottom of the Cirque, the valley floor and the top

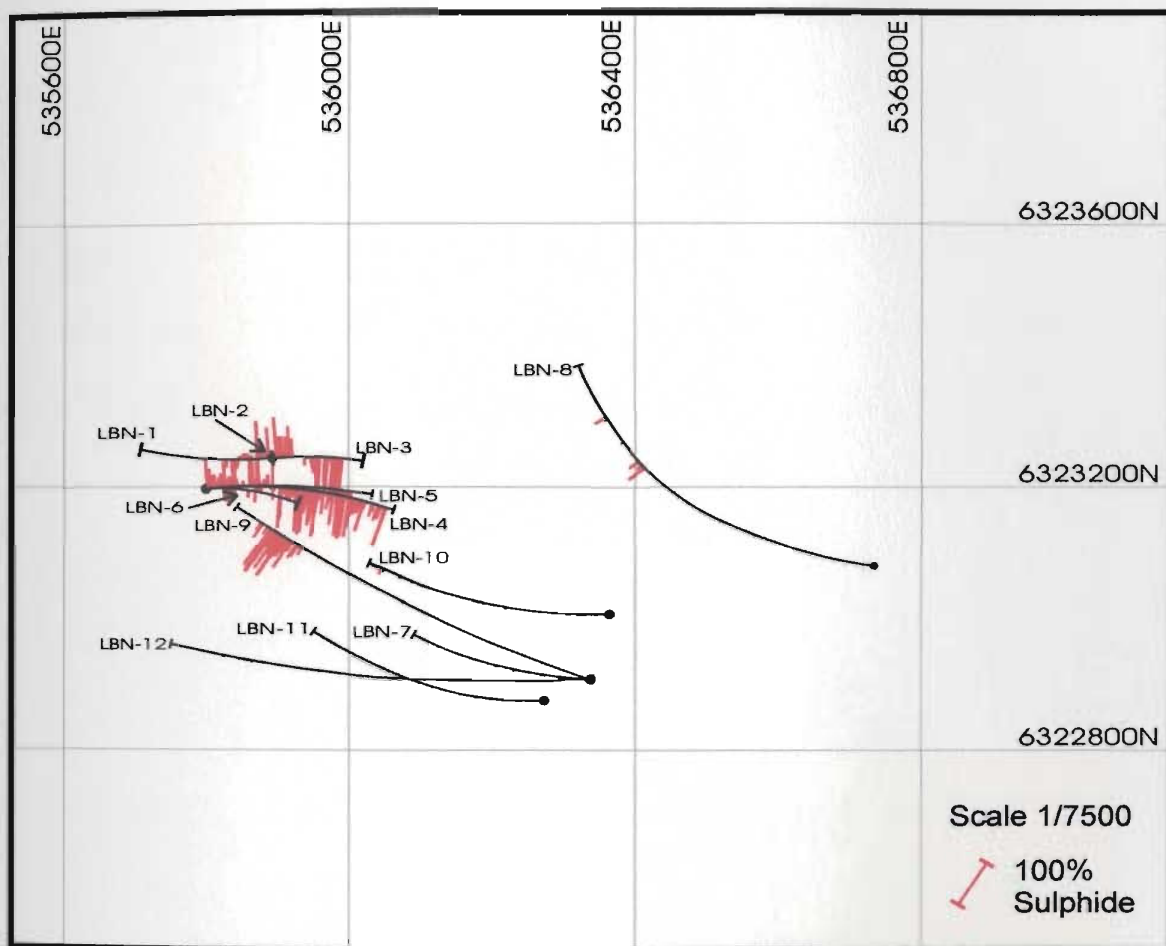


Figure 3.5 Grid plot of twelve drill hole traces projected to surface with histograms of percent sulphide.

lower south arm. In 1997, PEM surveys were conducted at the very top of the Cirque to test the extent of the northwest trend. At present, only data from the 1997 surveys are available and their interpretations are shown in Figure 3.6 in plan view. Both surveys were hampered by weakly conductive glacial cover and extreme topographic variations which prevented readings being collected from many places. HLEM conductors were traced from L0 and L1+00S at a maximum 150 m below the surface to an area from L3+00S to L5+00S closer to the surface. The conductive body is interpreted to be massive sulphide mineralization especially when compared to the drill hole sulphide intersections shown in Figure 3.5. No further significant conductive trends were defined on the surveyed areas.

#### **3.2.4 Downhole PEM**

In the fall of 1996, diamond drill holes LBN-96-7, 8, 9, and 10 were surveyed by down-hole PEM and the results defined several conductive anomalies. These conductors have been interpreted to be mineralized lenses of various sizes and orientations (Figure 3.6). Table 3.3 summarizes the survey results and explains the identified conductors. Figure 3.7 is an interpretative cross sectional view showing the locations of the discontinuous conductive bodies below surface. Each conductor corresponds to sulphide intersections, as small as 10 cm, suggesting that caution should be used when interpreting PEM conductors to define large scale sulphide mineralization. Using down-hole and surface PEM, a northeast trending zone of mineralization, approximately 200 m wide and 600 m long, has been interpreted by Watson (1996) to extend from the near surface (~150 m) to

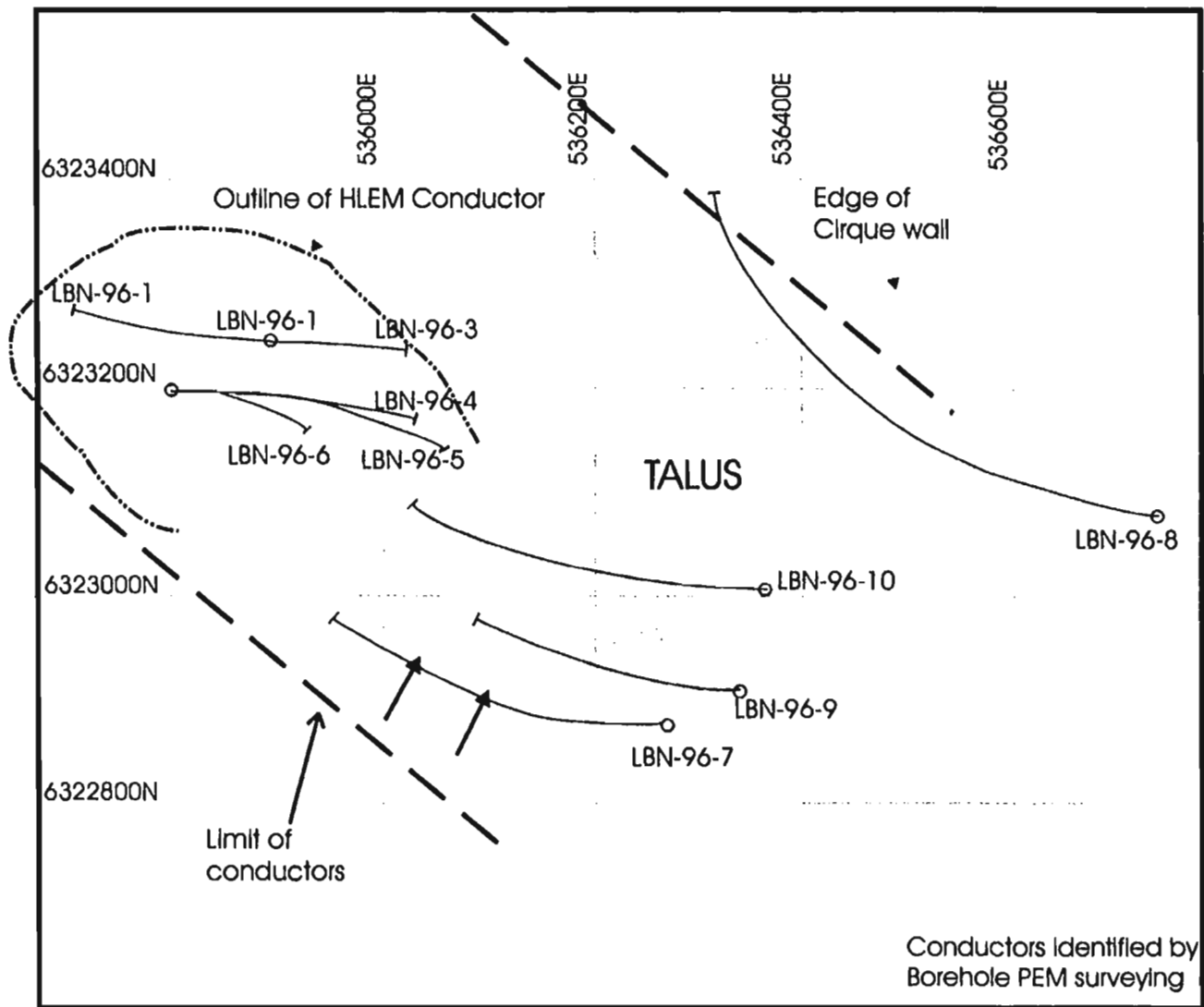


Fig 3.6 Plan view of projected borehole PEM conductors (grey) and surface HLEM conductors (dashed-dot line). Boreholes (LBN 1-6) were not surveyed using PEM.



Table 3.3 Summary of 3-D PEM borehole survey results.

Drill hole	Depth of conductor from surface (metres)	Description
LBN-96-7	90-370	Small conductor north of hole.  Conductor lying south of hole approximately 250 m below surface possibly top of pipe-like structure plunging to the north below the hole
LBN-96-8	580  740  770-840  920  960-EOH	Off in-hole response indicating the hole is near the edge of the conductor, over 200 m to the southwest; could possibly be the northern edge of the conductor in LBN-9 and 10.  Small in-hole response corresponding with a narrow sulphide zone.  High conductive body above hole and centered to the north.  Small in-hole response corresponding to some mineralization in the hole.  Responses indicate a steeply dipping conductor at depth, possibly massive sulphides, lying parallel and south of the hole.
LBN-96-9	160  450-EOH	Small conductor south of the hole, possibly same conductor identified at the top of LBN-7.  Broad off-hole anomaly indicating conductor is lying parallel to the hole; centre of the conductor is north of the hole.
LBN-96-10	-	Hole goes beneath the conductor; centre of the conductor is south of the hole, between holes LBN-9 and 10.
LBN-96-11	610-690	In-holes conductor corresponds to intersected sulphides; centre of conductor is updip and south of the hole; conductor is at least 600 m depth extent with a minimum length of 400 m.

Data obtained from "Geophysical Survey Report for Cartaway Resources, Cirque Property" and subsequent memos written by Watson (1996; 1997) of Crone Geophysics and Exploration Ltd.

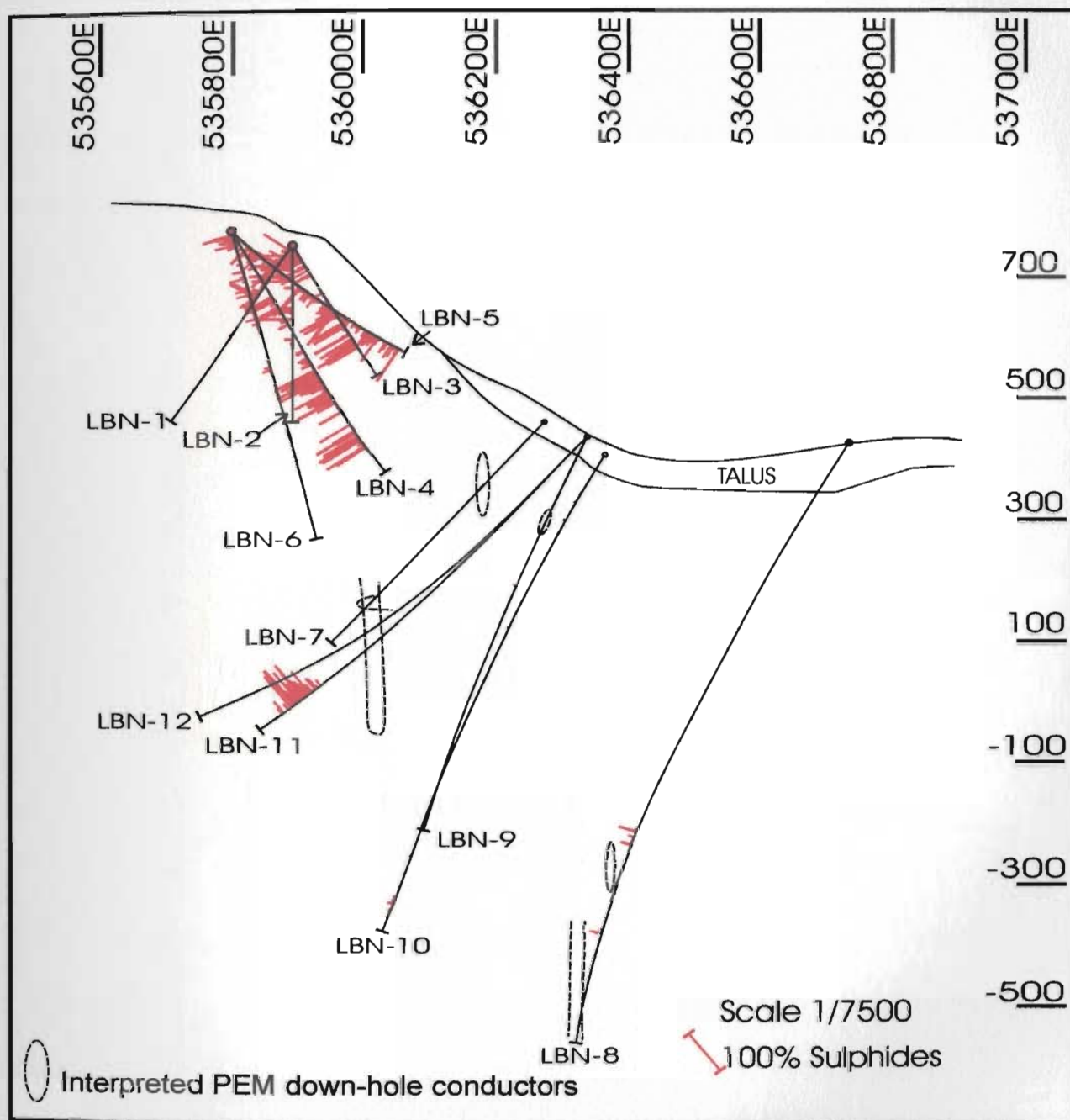


Figure 3.7 Cross section of the Cirque, looking north, of drill holes with sulphide intersections and down-hole PEM conductors projected onto 6323000m N. Depth is in metres. PEM surveys were conducted on boreholes LBN-7 to 11 (Watson 1996, 1997).

approximately 1100 m (greatest depth of drill hole) and span L4+00S and L2+00N and 4+00E to 8+00E. Figure 3.6 shows the plan view interpretation of the PEM data by Crone Geophysics and Exploration Ltd (Watson 1996). Based on the location and trend of the massive sulphide mineralization mapped on the Cirque and intersected in drill core, the plan view projection of the PEM conductor has been re-interpreted to be actually northeast trending and approximately 600 metres wide.

### **3.3 Mineralization**

On the air photo of the Cirque property and surrounding area (Figure 1.3), the gossan on the Cirque grid is very distinct and appears to extend for about 400 metres in a northwest direction onto the neighbouring property (Licence #1514M) held by Canadian States Resources. From the ground, the gossan can be easily traced as a narrow band along the cirque wall, spanning approximately 900 metres across and 400 metres high (Figure 3.8).

For this study, there are two distinct gossans identified along the wall (Plate 3.1). Gossan #1 is located in the centre of the back wall and extends to the top of the cirque, between lines 2+00S and 1+00N. Gossan #1 is the main area of sulphide mineralization and the focus of most of the sampling, geophysical surveys, and all of the drilling. Gossan #2, is located near the south corner, along the south arm and does not outcrop on the top of the cirque. It was sampled extensively; however, its inaccessibility both from the top and the bottom made further surveys impossible.

In the centre of the back wall (Gossan #1), the rusty colour spans the entire height

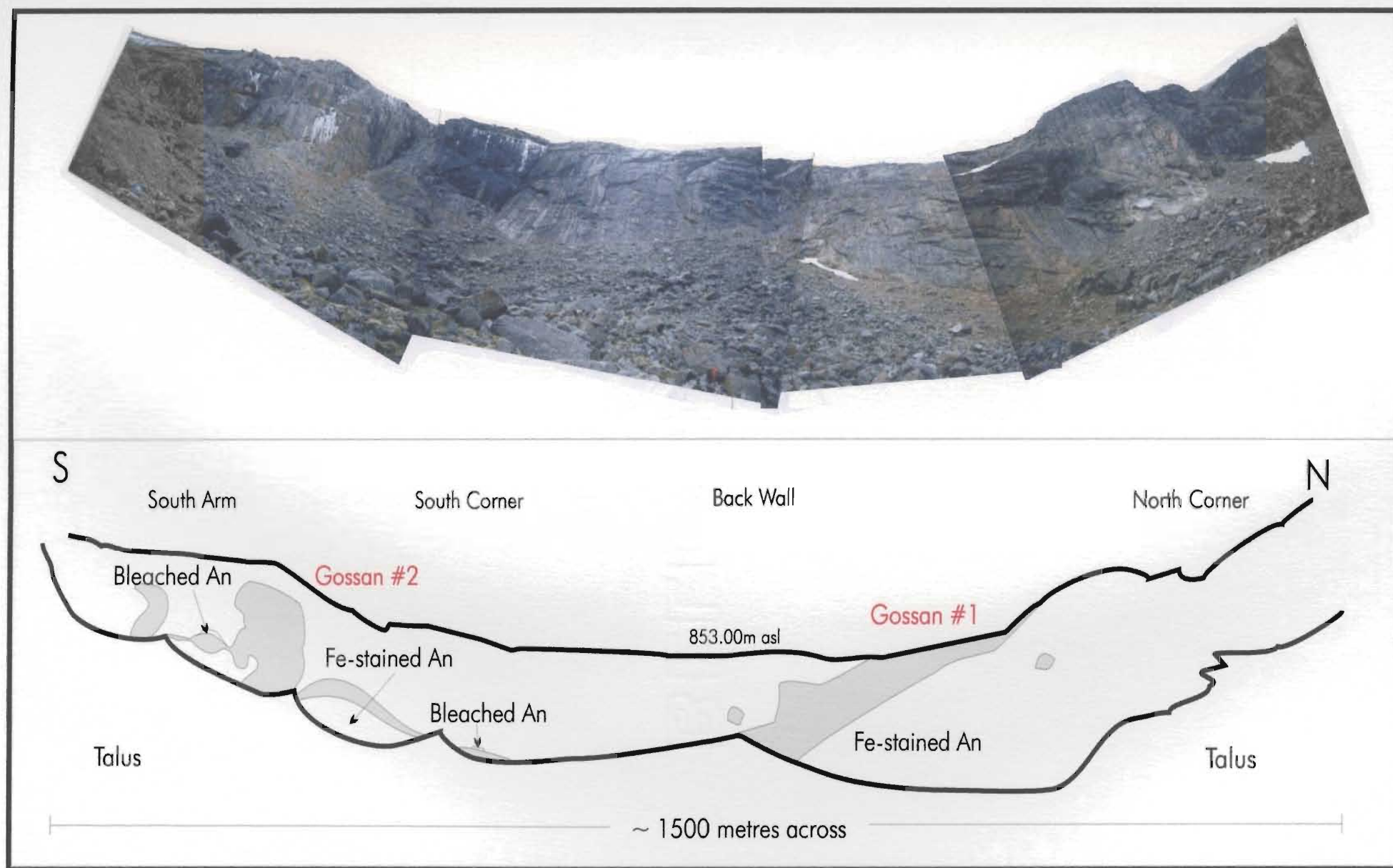


Figure 3.8 Photo compilation (top) and trace of Cirque gossan (grey; bottom) including Gossan #1 and #2 which forms a narrow band along the cirque wall. View is facing west. An = anorthosite.



Plate 3.1 View of the cirque walls looking to the southwest. Note the extent of sulphide mineralization, from Gossan #1 to Gossan #2.

of the wall (400 metres from the top of the talus slope) and 200 metres wide, however, upon closer inspection, the Gossan #1 has a sharp contact with barren anorthosite that has iron oxide surface staining. As shown in Plate 3.2 (viewed to the southwest), Gossan #1 appears to trend to the northwest and dip to the south or southwest.

Generally, both gossans consist of bands (Plates 3.3) and discontinuous pods of massive pyrrhotite (dominantly magnetic) and minor chalcopyrite (average < 1 %). Boulders from the talus and outcrop further up the wall indicate that the host is leucoanorthosite (Unit 1a and Unit 1b) with coarse-grained, dark blue schiller plagioclase and only minor cumulate pyroxene and magnetite. Pentlandite was not observed in outcrop. Where isolated, the mineralized patches are approximately 1 m<sup>2</sup> or less and do not appear to be associated with faults, although overall, sulphide mineralization is located near a northeast trending fault discussed in Chapter 2.

Plate 3.4 shows the mineralization at Gossan #1 approximately one third up the back wall. Massive pyrrhotite with minor chalcopyrite blebs occur as weathered out, dark purple-orange discontinuous irregular pods or lenses which appear to wrap around plagioclase crystals. Rounded inclusions or xenoliths of leucoanorthosite within massive pyrrhotite are stained a rusty colour and can be identified by their lack of crumbly weathering.

Moving away from Gossan #1 to the south, along the base of the wall, the gossan appears to have disappeared but then it crops up before the south corner (Plate 3.5), consisting of <1 % disseminated pyrrhotite and small <10 cm wide discontinuous pods of minor pyrrhotite. Overall, the rusty patch (~35 m long and ~15 m high) appears to be





Plate 3.2 View of Gossan #1 in the cirque wall, from the top of the talus (looking west). Note the sharp contrast between the sulphide mineralization and barren anorthosite which has been stained a rusty colour from the weathered sulphides above.





Plate 3.3 Mineralized boulders from the talus near Gossan #2 showing stringers/bands of disseminated to massive sulphides.

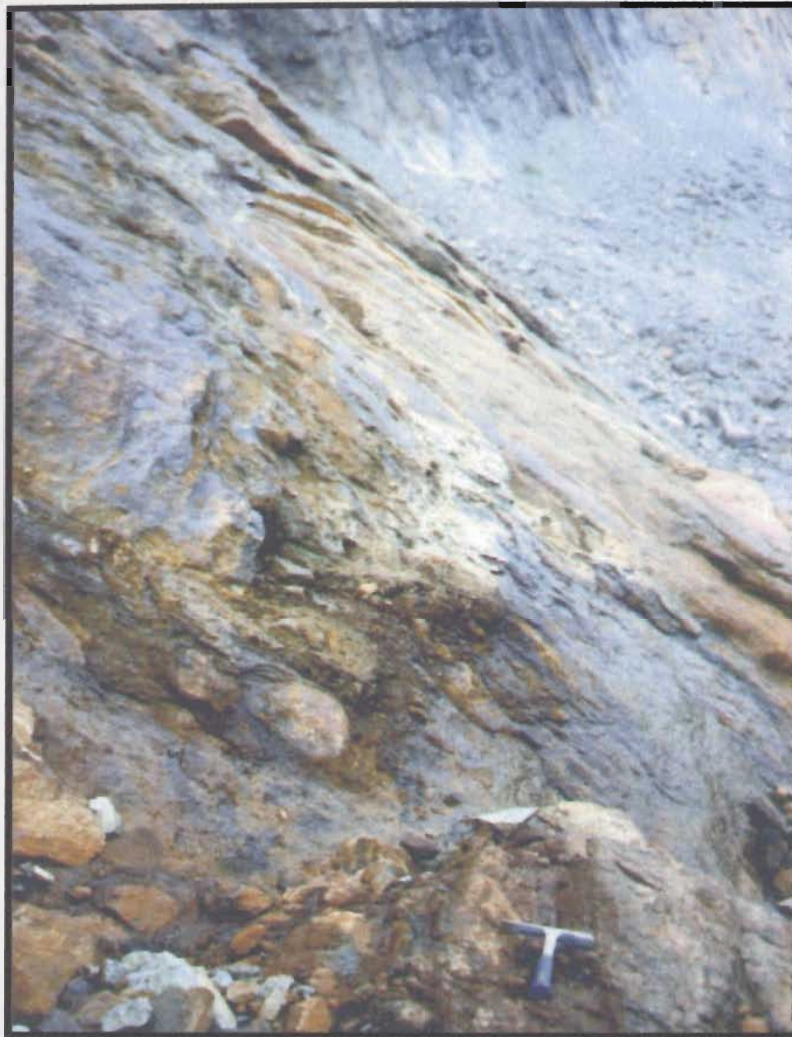


Plate 3.4 Discontinuous stringers and pods of massive sulphides in Gossan #1, looking to the northeast. Note the crumbly massive sulphides wrapping around the barren anorthosite with iron-oxide staining.





Plate 3.5 Back wall of the cirque showing gossan capped by Bleached anorthosite (centre) and a 25 m area of disseminated pyrrhotite in leucoanorthosite (lower left corner); view is to the west.

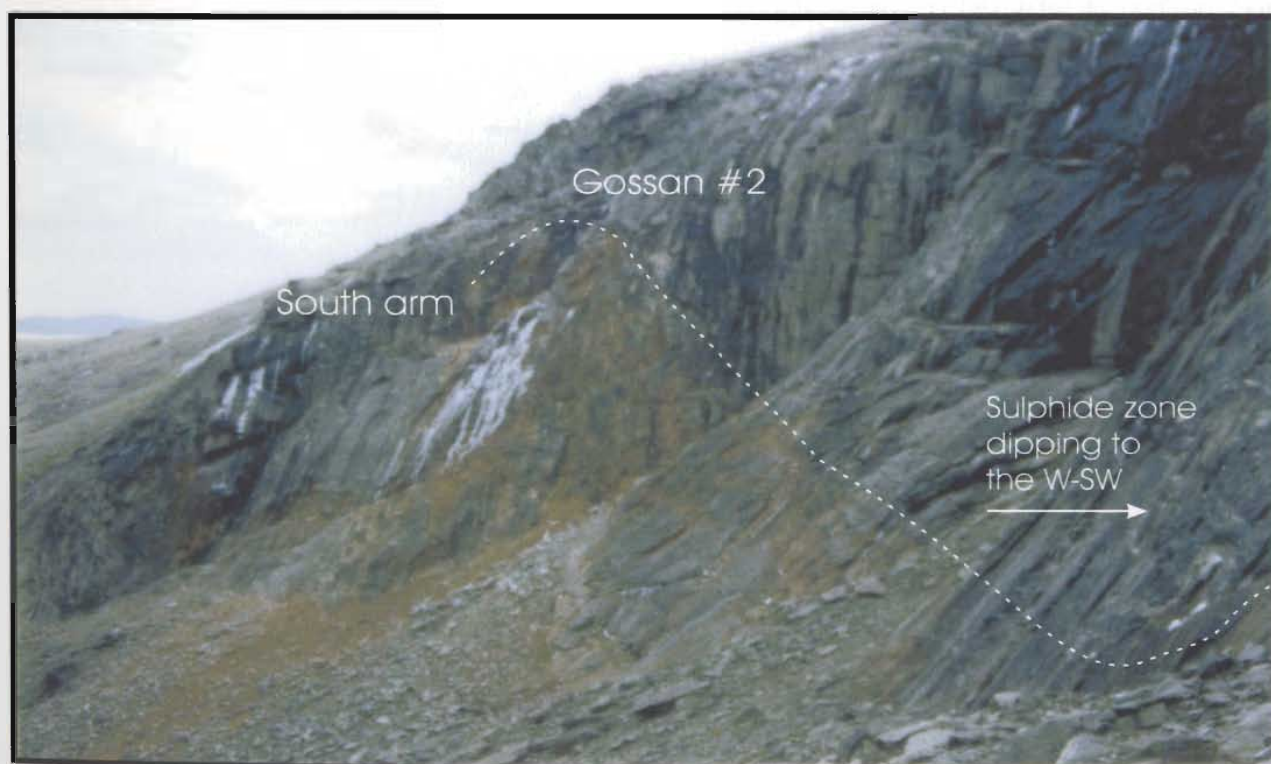


Plate 3.6 View from the back wall of the cirque towards the southeast showing a large (25 m) area of patchy gossan dipping to the west-southwest (foreground) and Gossan #2 (centre).

continuous with Gossan #1 (talus covers much of the lower wall here) and has a sharp contact with a band (approximately 1 m wide) of Bleached anorthosite (Unit 1c) which appears to be trending 334/48°NE. The Bleached anorthosite appears to cap the gossan below, suggesting perhaps a “chill zone” between the sulphides and the barren leucoanorthosite above. Thin (~5 cm wide) rusty bands or veins occur about 4 cm above the Bleached anorthosite, trending 310/68°NE to 315/50°NE. A pyrrhotite band (10 cm wide) trending 345/50°NE, runs beneath the Bleached anorthosite into the gossan and peters out or is cut off. In the same area there is well formed local cleavage trending 332/75°NE. Another pyrrhotite-rich band (10-15 cm wide) directly above this one, is non-linear, intersecting the barren anorthosite. Other thin 3-4 cm wide rusty bands trend 350/38°NE with ~15% net-textured pyrrhotite in coarse-grained anorthosite. In places, the sulphides appear to have remobilized into anorthosite along fractures.

At the south corner, near a fault, mineralization or rusty patches were not observed. However, out of the corner and along the south wall (facing east), about 25 m from the last gossan, is a continuous gossan spanning 30 metres (Plate 3.6) with minor (<1 %) disseminated to local massive pyrrhotite with <1 % chalcopyrite blebs. Closer inspection of this area (refer to Figure 3.8), shows that sulphide mineralization is confined to a narrow southwest dipping layer less than 5 m wide and much of the area is anorthosite with rusty staining and small localized gossans. This rusty weathered area has a sharp contact with the barren leucoanorthosite. Above the barren anorthosite, the anorthosite (BB) is fine-grained, light green colour with sericite alteration and plagioclase recrystallization.

In the same photo (Plate 3.6), just behind this gossanous area [to the east (left) along the south arm in Figure 3.8], is Gossan #2, located in almost the entire height (~400 m) of the wall, approximately 25 m wide and located near or along a northeast trending vertical fault which has left a narrow (~ 25 m wide) notch in the wall (refer to Figure 3.2). The weathered surface of Gossan #2 is similar to that of Gossan #1; purple-orange rusty lenses or irregular veins of dominantly massive, coarse-grained pyrrhotite. The lenses are discontinuous, wrapping around iron stained, unmineralized, dark blue leucoanorthosite (dominantly Unit 1a) as shown in Plate 3.7. Similarly at Gossan #1, a few lenses have been measured trending 109° - 137° and dipping 55° - 60° to the south into the Cirque. Overall, however, when observing the gossans along the south arm (looking southeast as in Plate 3.6), the mineralization seems to be dipping steeply into the Cirque wall, to the southwest. From this view, mineralization appears patchy with a sharp contact with the barren anorthosite above and extends, in places, the full height of the wall.

Moving further east, beyond Gossan #2, rusty weathering extends for approximately 25 m. Plate 3.8 shows mineralization in the area to be band-like (~2 m wide) overlain by a <1 m wide band of Bleached anorthosite (Unit 1c). As before, the gossan consists of a rusty purple-orange weathered surface with minor crumbly, coarse-grained pyrrhotite. Both areas were out of reach for closer observation and sampling.

Further to the east, near L 7+00S and 10+00E along the south arm (left of area shown in Plate 3.8), is an isolated outcrop of leucoanorthosite (Unit 1b) with several rounded patches (<1 m<sup>2</sup>) of iron staining. The patches consist of <1 % disseminated pyrrhotite,



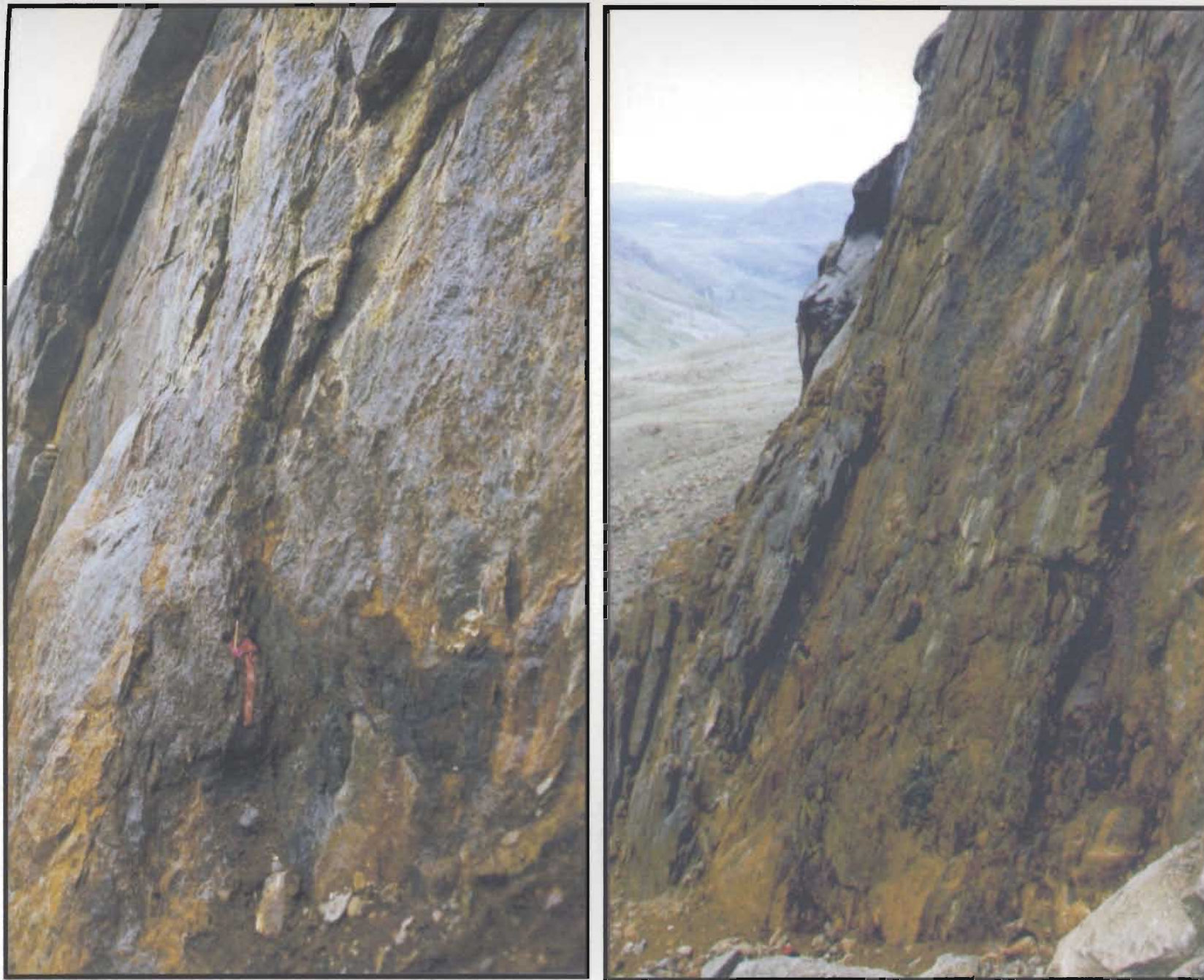


Plate 3.7 Close up views of stringers and patches of sulphide mineralization in Gossan #2 with iron-stained anorthosite xenoliths. Scales are flagging tape and a pencil for the left photo and a red backpack for the right photo. Views are to the east.

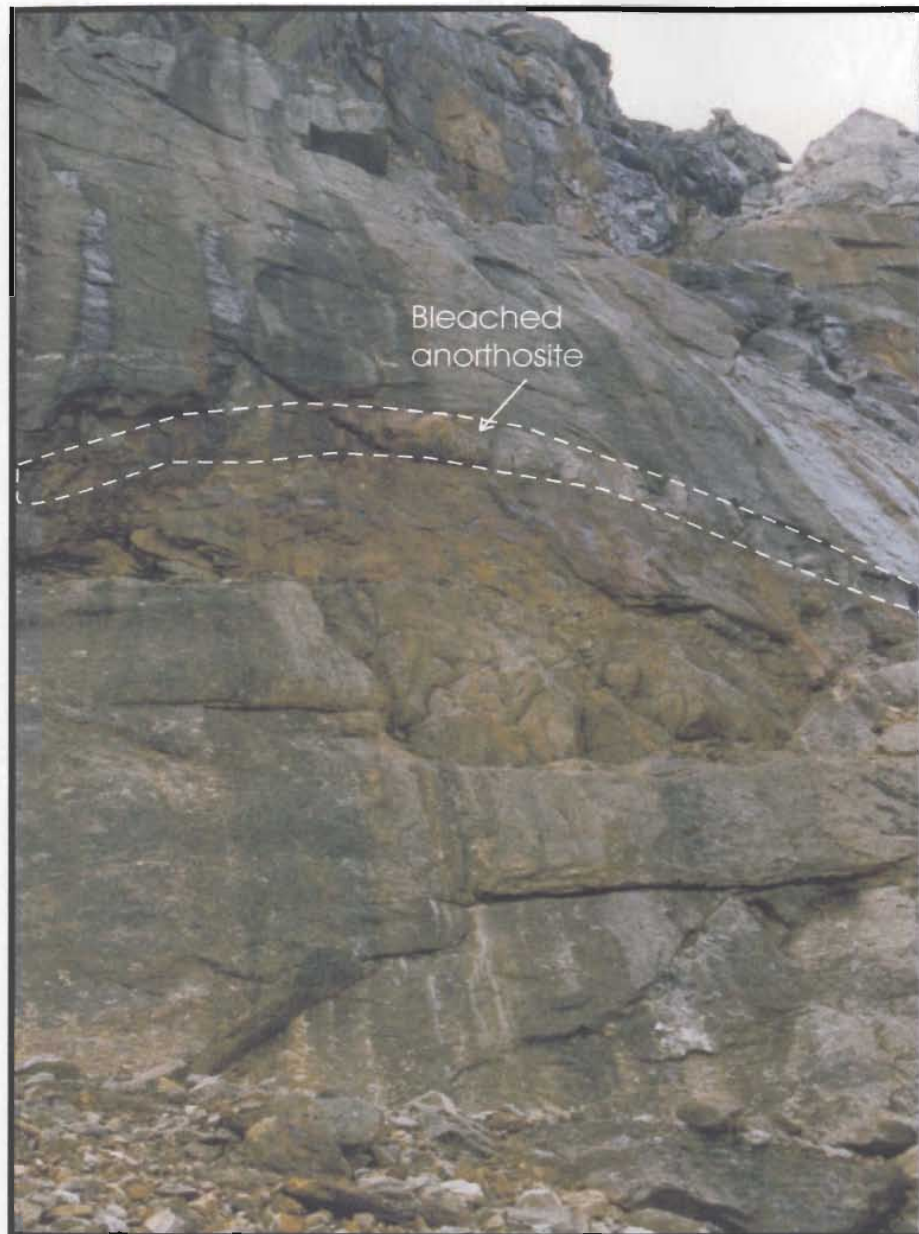


Plate 3.8 Band of gossan capped by Bleached anorthosite and with barren anorthosite above and below. Photo was taken just east of Gossan #2, along the south arm, looking south.



minor chalcopyrite and green, recrystallized anorthosite. Some of the rusty mineralized areas are discontinuous but banded or vein-like (approximately 20 to 25 cm wide and over 50 cm long) and trending between 15° to 50° (and in places 320° which is parallel to the trend of Gossan #1). Samples from this area (LD-96-10 to 18; refer to Appendix A2.3.2) were assayed for Ni, Cu, and Co by Cartaway Resources in 1996 with the greatest values being 0.59% Ni, and 0.51% Cu. Overall, concentrations are not high reflecting low sulphide content (<1 % pyrrhotite, trace chalcopyrite).

There are no other occurrences of significant sulphide mineralization, except for a few localized rounded (1 m<sup>2</sup> wide) patches of rusty weathering (iron staining) developed on anorthosite with minor sulphide mineralization along the east end of the north arm and near L3+00 S, TL25+00 E which consists of elongated (0.5 × 3 m) rusty zone trending 85° and dipping 45°S along 40 cm wide fracture zone at 320°/82°NE. On the top of the cirque, massive sulphides are difficult to trace due to glacial debris, however, towards the northwest corner of the property is a low (<1 m high) ridge with small discontinuous pods of massive, coarse-grained pyrrhotite. Two rusty parallel bands (20 cm wide) trending 150° (dip undeterminable) are located near the western boundary, between L9+00S and L10+00S. Further along to the south, near L9+00S, L1+50S, are small localized patches (8 m by 0.50m wide) of disseminated sulphides (<1 %) in green, altered leucoanorthosite (Unit 1b). As discussed in Chapter 2, <1% fine-grained, disseminated, interstitial pyrrhotite occurs within the ferrodiorite dykes. Figure 3.2 indicates the exact locations of the mineralized areas.

Although the overall trend of the entire Cirque gossan is northwest (~320°) with the

gossan comprising thin veinlets, pods, and stringers with variable strikes and dips (Figure 3.9), most of the individual sulphide veins and stringers which make up Gossan #1 and #2 strike to the northeast and dip both to the northwest and southeast. Some veins and stringers also trend to the northwest and dip to the northeast (as shown in Figure 3.2). Many of the stringers and veins dip steeply to the southeast towards the cirque floor, and further to the east along the south arm are thin veins of iron staining which strike parallel to the overall northwest trend.

Although many sulphide lenses dip to the east, the contacts of sulphide occurrences along the walls of the cirque and on top of the cirque suggest an overall west dipping zone of sulphide lenses. Geophysical survey results indicate a southeast plunging, northwest trending continuation of this zone off the grid. Support is given in Kerr and Smith's (1997) summary of the first six diamond drill holes drilled at the top of the cirque as they state that the west dipping and vertical holes are "barren" and the east dipping holes intersect sulfide mineralization to a maximum depth of 200 m. As a result of this present study of the drill core, the west dipping and vertical holes would not have intersected the zone of mineralization if the zone is located below these holes and dipping to the west.

Kerr and Smith (1997) and a report written by F.P.F Resources (1996) note that Gossan #1 and #2 are displaced and they attribute this to movement of the anorthosite along at least one northeast striking, southeast dipping fault in the back wall of the cirque. The report by F.P.F Resources (1996) states that down-dropping of the area (where the last six holes are collared) along a NNW-SSE trending fault was the result of an extensional event

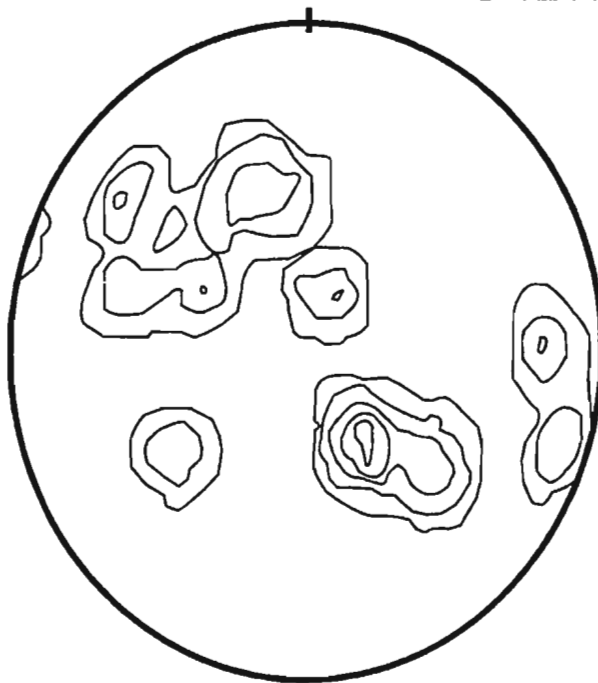


Figure 3.9 Stereoplot of poles to foliations planes of sulphide lenses from Gossan #1 and #2 outcrops. Sulphide mineralization is trending northeast and dipping to the northwest and southeast. Other lenses are also trending to the northwest and dipping to the northeast. Number of measurements = 15.

(from doming? *op. cit.*) that followed the emplacement of the massive anorthosite in the area and that sulphide melt moved along regular fractures which resulted from this distension. Although faults were intersected in drill core and mapped on surface, there was no apparent displacement of the two main gossan zones nor were there any marker horizons with which to measure displacement in the mafic rocks.

### **3.3.1 Textures of sulphide mineralization**

Sulphide intersections in drill core ranged from < 1 mm wide pyrrhotite-rich (and to a lesser extent chalcopyrite-rich) veinlets to 5 m wide massive sulphide zones. As mentioned previously, pyrrhotite is the most common sulphide mineral occurring dominantly within coarse-grained, blue-grey plagioclase-rich leucoanorthosite (BB and GP). Chalcopyrite, pyrite, and pentlandite (Plate 3.9) occur less frequently and are always associated with pyrrhotite; with chalcopyrite and pyrite commonly found along the contact with anorthosite or disseminated with pyrrhotite near contacts of massive pyrrhotite.

Pyrite mineralization dominantly occurs with degraded pyrrhotite in altered anorthosite and is found along cracks within the pyrrhotite grain and/or rimming pyrrhotite suggesting a breakdown of pyrrhotite to pyrite (Plate 3.10, 3.11). Small veinlike clots of pyrite (<0.5 cm, ~ 7% maximum) which look like snowflakes are found in the fine-grained, light green, altered anorthosite which, as mentioned in Chapter 2, lack a primary igneous texture, suggesting that the pyrrhotite in these zones was completely replaced by pyrite. Microveinlets of pyrite crosscut the leucoanorthosite, intersecting some feldspar crystals.

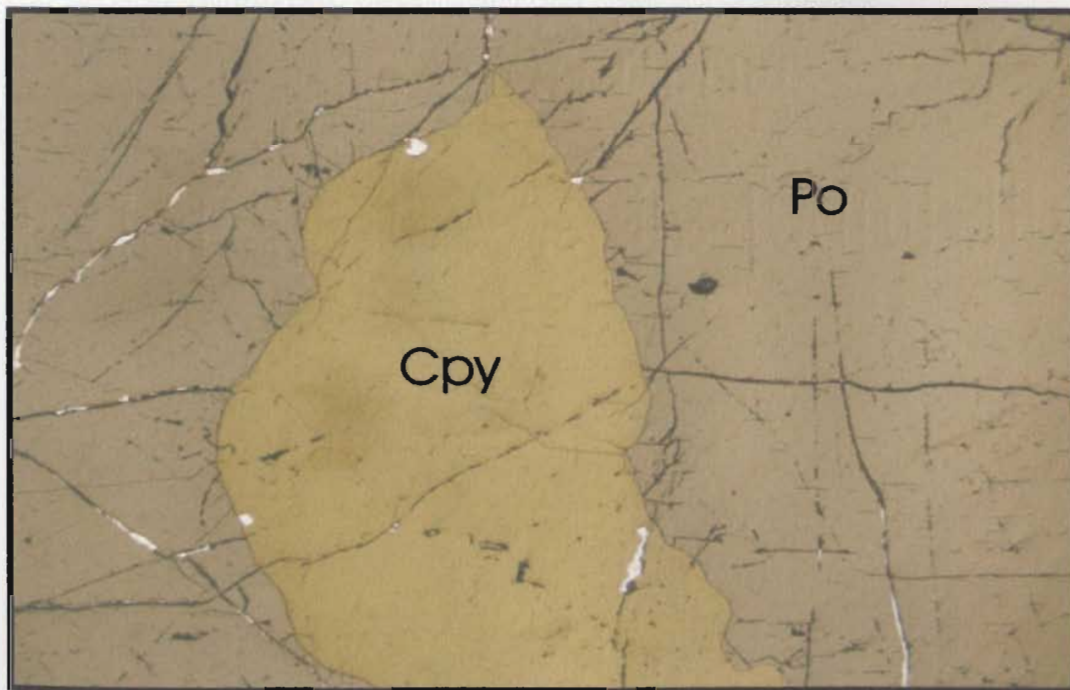
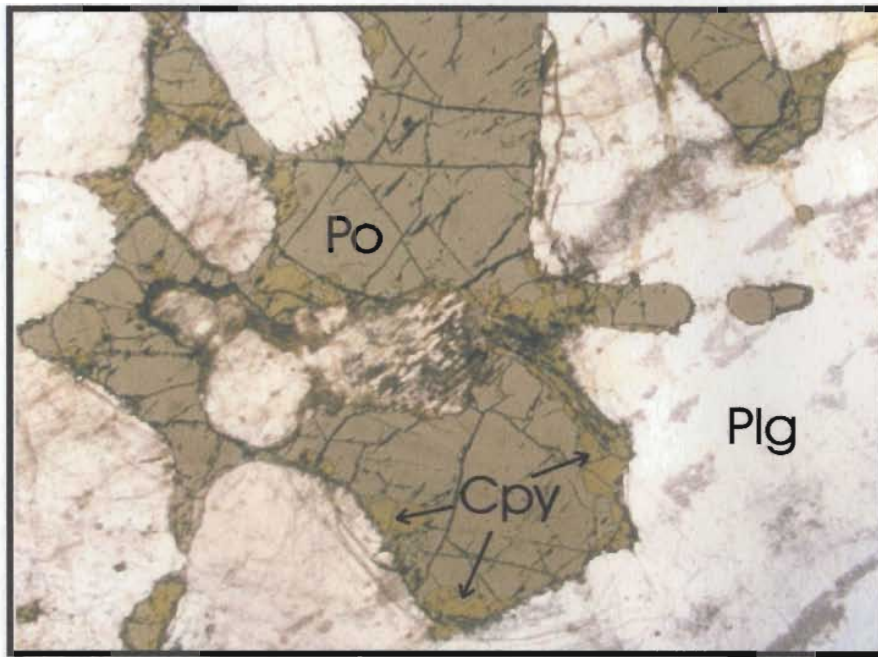


Plate 3.9 Dominantly, sulphide mineralization consists of pyrrhotite (po) with chalcopyrite (cpy). Textures include either irregular blebs (top) or massive (bottom). Both photos are taken in reflected light; top was taken at 1.5 power (field of view = 9 mm) and bottom at 25 power (field of view = 1 mm). Plg = plagioclase.

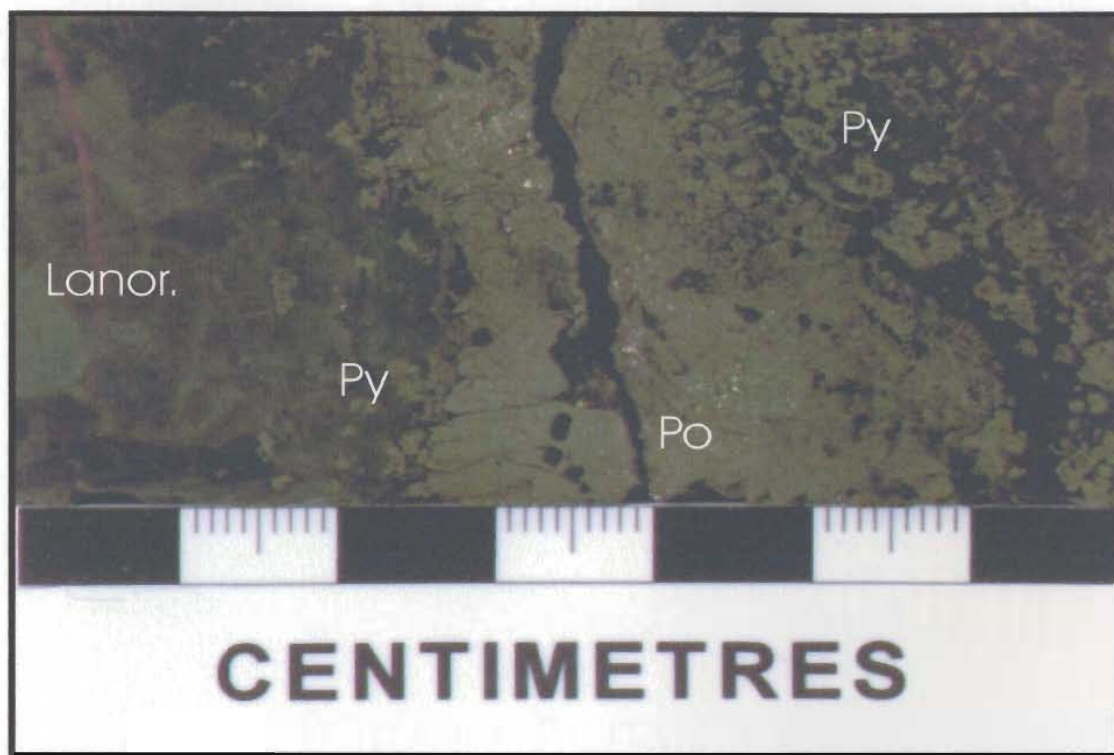


Plate 3.10 Core samples (LBN-4; 348.05 m) showing 3 cm wide massive pyrrhotite (po) intersection rimmed by coarse-grained pyrite (py). Sulphide mineralization occurs within leucoanorthosite (Lanor.).



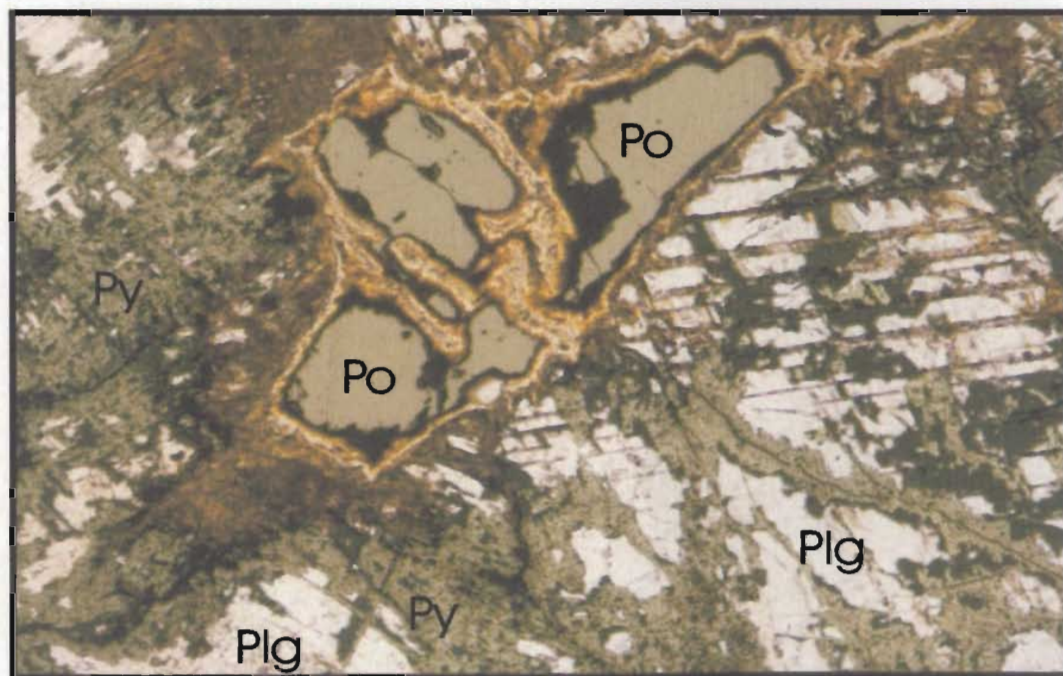
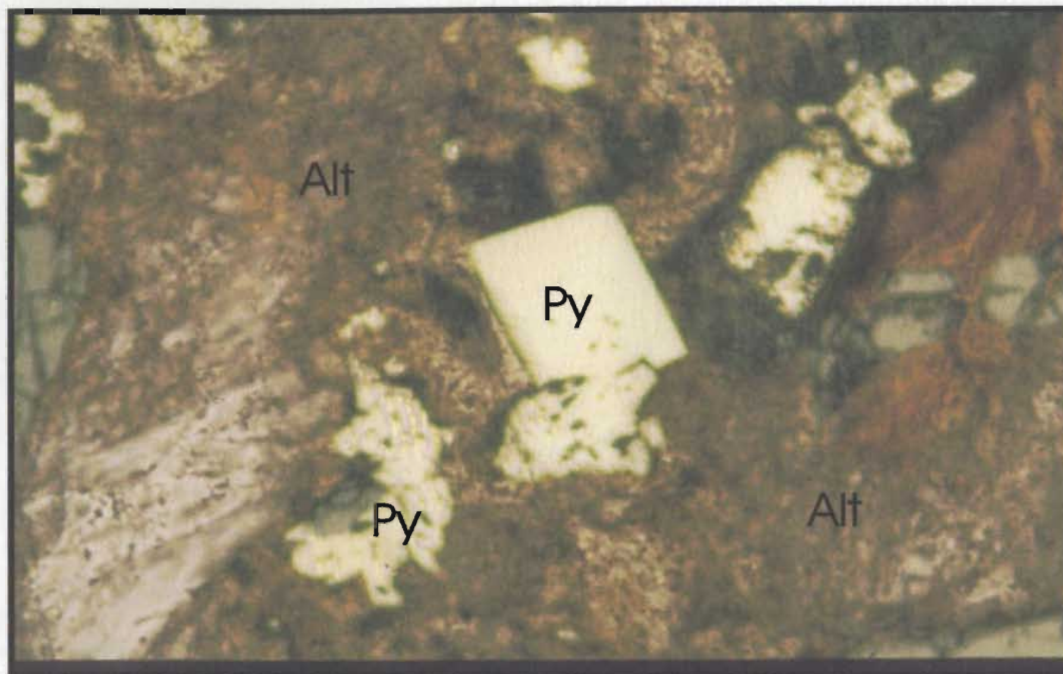


Plate 3.11 Pyrite (py) mineralization is dominantly associated with anorthosite alteration (alt) and occurs as irregular blebs and rare cubes (top). Pyrite is often seen in these altered zones rimming pyrrhotite (po), showing evidence of pyrrhotite breaking down to pyrite (bottom). Both photos were taken in reflected light at 20 power (top photo; field of view = 1 mm) and 10 power (bottom photo; field of view = 2 mm). Plg = plagioclase.



Contacts of pyrrhotite and pyrite mineralization are irregular (30–60° core angle or CA) with the texture ranging from disseminated pyrrhotite to net to disseminated from top to bottom.

Magnetite and ilmenite are not commonly found with sulphide mineralization, but where observed, are irregular blebs near sulphide and pyroxene minerals (Plate 3.12). Pentlandite abundance is low and dominantly occurs as microscopic-scale ‘flame-like’ exsolution lamellae located within pyrrhotite grains (Plate 3.13), indicating low temperature exsolution (~200° - 250°C). Lack of nickel-rich sulphides may mean that Ni may have separated from the iron-rich melt earlier (*cf.* Piercey and Wilton 1999).

Overall, there are three main textures of sulphide mineralization in the anorthosite-hosted gossan at the Cirque property: (i) disseminated, (ii) net to pseudonet-textured, and (iii) semi-massive to massive. The following section describes the three textures as observed in representative core, outcrop samples, and in polished thin sections.

#### **3.3.1.1 Disseminated, net-textured, and massive sulphides**

Separate, non-connecting, interstitial sulphide grains range from trace to 5% fine-grained to 1 mm blebs (Plate 3.14) indicating disseminated pyrrhotite syngenetically crystallized with the silicate magma. Chalcopyrite is fine-grained and occurs dominantly with pyrrhotite, rarely with magnetite, and even less so with pyroxene.

Net-textured pyrrhotite is common in many mineralized areas, occurring as interconnected irregular-shaped sulphide grains that wrap around plagioclase and pyroxene crystals (Plate 3.15). Pseudonet-textured pyrrhotite crystals are elongated and “wormy”,

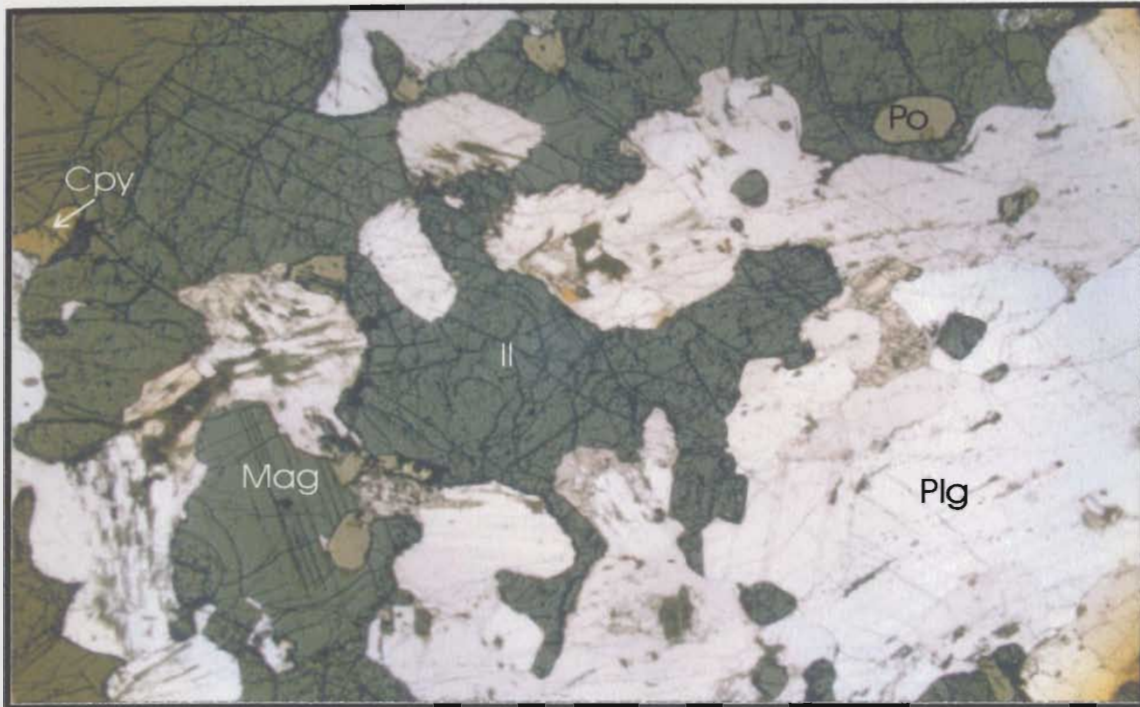


Figure 3.12 Magnetite (Mag) and ilmenite (Il) with pyrrhotite (Po) and chalcopyrite (Cpy) in leucoanorthosite. Photo was taken in reflected light at 2.5 power (field of view = 7 mm). Plg = plagioclase.

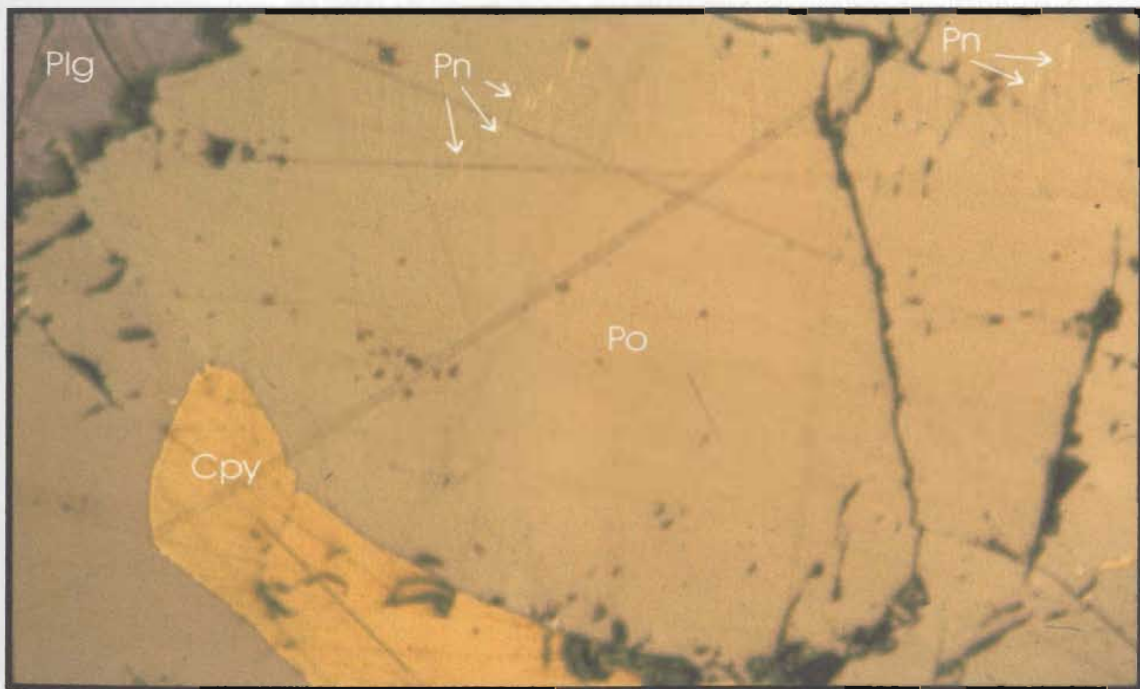


Figure 3.13 Massive pyrrhotite (Po) with chalcopyrite (Cpy) bleb and very small pentlandite (Pn) "flame" lamellae. Photo was taken in reflected light at 10 power (field of view = 2 mm). Plg = plagioclase.

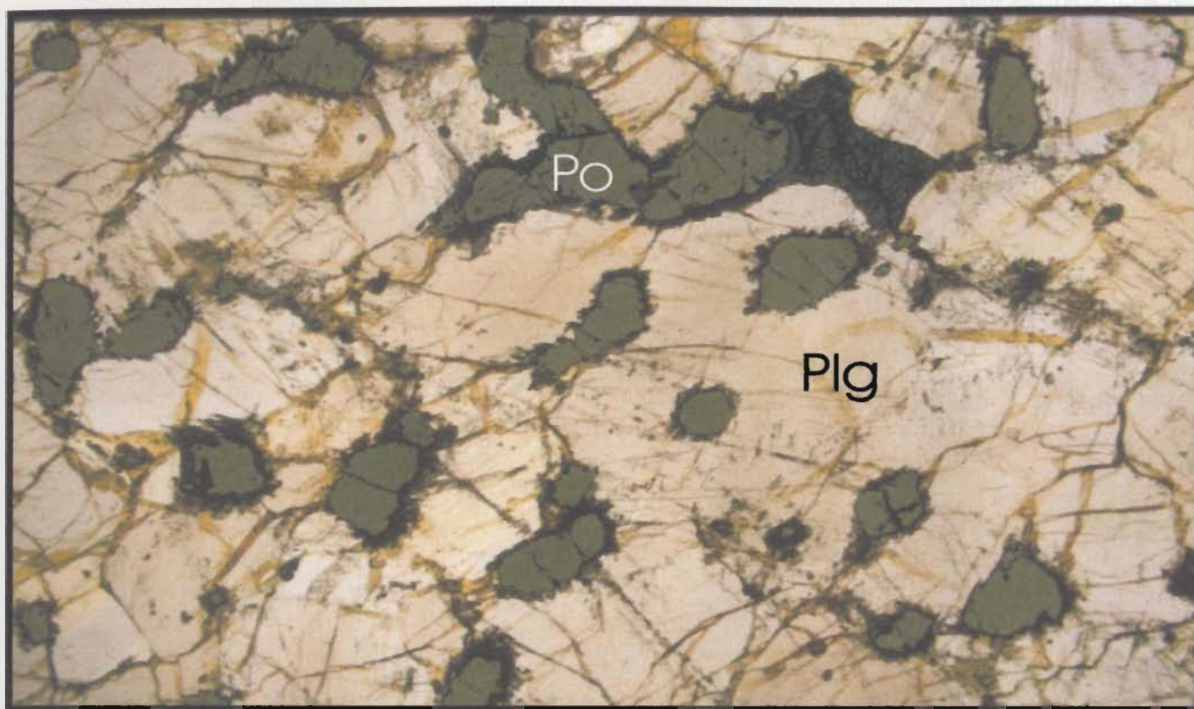


Plate 3.14 Disseminated pyrrhotite (po) in leucoanorthosite. Photo was taken in reflected light at 1.5 power (field of view = 9 mm). Plg = plagioclase



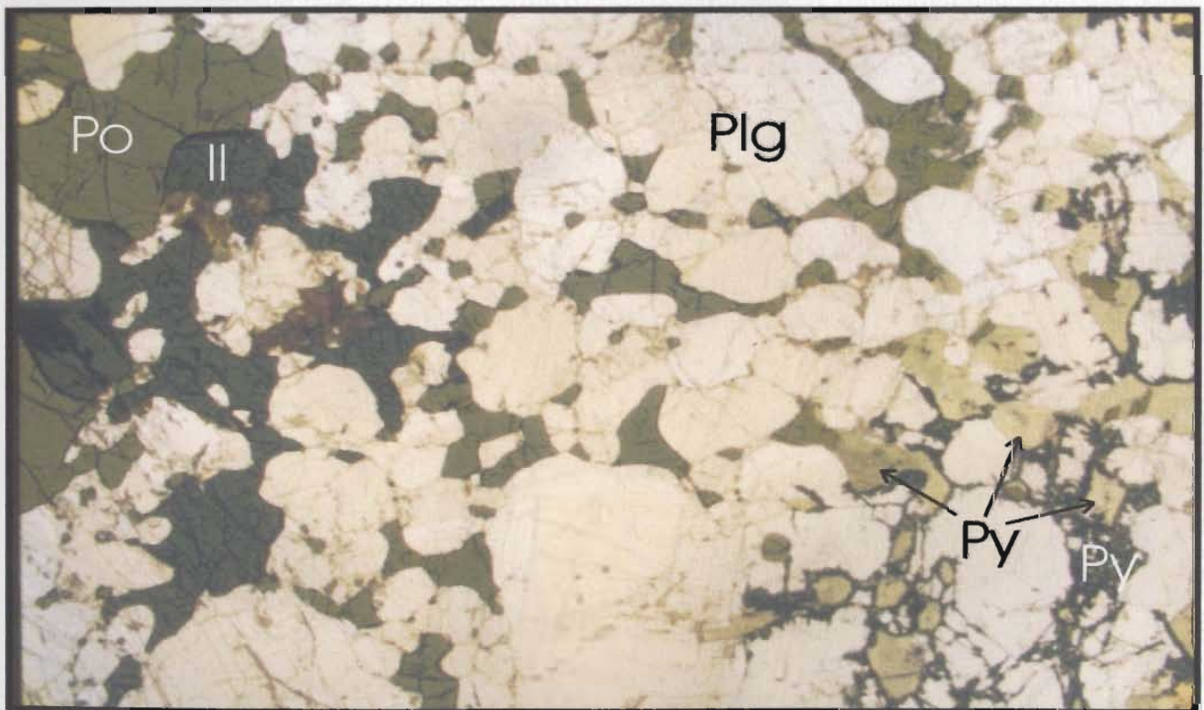
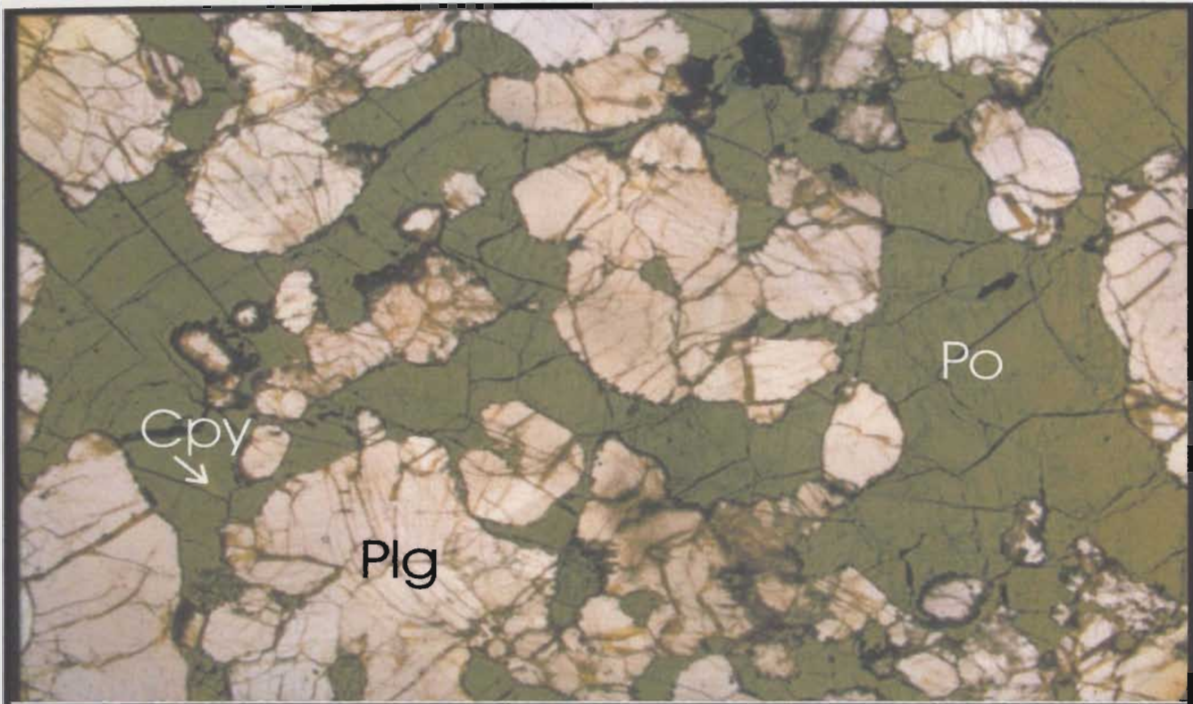


Plate 3.15 Net-textured pyrrhotite (Po) with trace chalcopyrite (Cpy) in leucoanorthosite (top). Pseudonet-textured pyrrhotite with ilmenite (Il) in leucoanorthosite (bottom). The right side of the bottom photo shows pyrite (Py) rimming altered pyrrhotite. Both photos were taken in reflected light at 1.5 power (field of view = 9 mm). Plg = plagioclase.

that is, not entirely connected on the core plane but occur in three dimensions as blebs which have intruded plagioclase crystals. Both net and pseudonet-textured sulphides retain the igneous cumulate texture and the sulphide minerals, dominantly pyrrhotite with <1 % chalcopyrite blebs within the pyrrhotite, usually have no foliation except near contacts with barren anorthosite. The most dominant occurrence of net/pseudonet- textured pyrrhotite is at the outside edges of massive/semi-massive pyrrhotite where the sulphides appear to have percolated around the plagioclase crystal cleavages and in places crosscut the crystal planes by wormlike blebs and very thin (<1mm wide) pyrrhotite, and less commonly chalcopyrite, veinlets (Plate 3.16). Kerr (1998) uses the analogy of a sponge; the plagioclase being the holes in the sponge and surrounded by the sponge itself; the net-textured sulphides wrapping around the plagioclase.

Massive sulphides are dominantly coarse-grained aggregates of pyrrhotite with generally <1% chalcopyrite blebs, very fine-grained pentlandite lamellae, and rare magnetite (Plates 3.17, 3.18). Chalcopyrite blebs range in size from <1 mm to 2 cm and are most often found along contacts with anorthosite; the more elongated chalcopyrite blebs comprise of aggregates aligned parallel or subparallel to the contact. Chalcopyrite is most commonly found in the largest core intersections (eg., 3% chalcopyrite and 90 % pyrrhotite in LBN-4 @ 390.35 - 395.44 m); however, a narrow vein (~1.5 cm wide) of massive chalcopyrite with lesser pyrrhotite and with disseminated pyrrhotite at the contact with anorthosite was intersected in hole LBN-8 (@ 923.92 m) assaying 3.9 % Cu over 20 cm wide sample interval (Plate 3.19). Plagioclase and anorthosite are the dominant inclusions; pyroxene inclusions are rare (Plate 3.20).



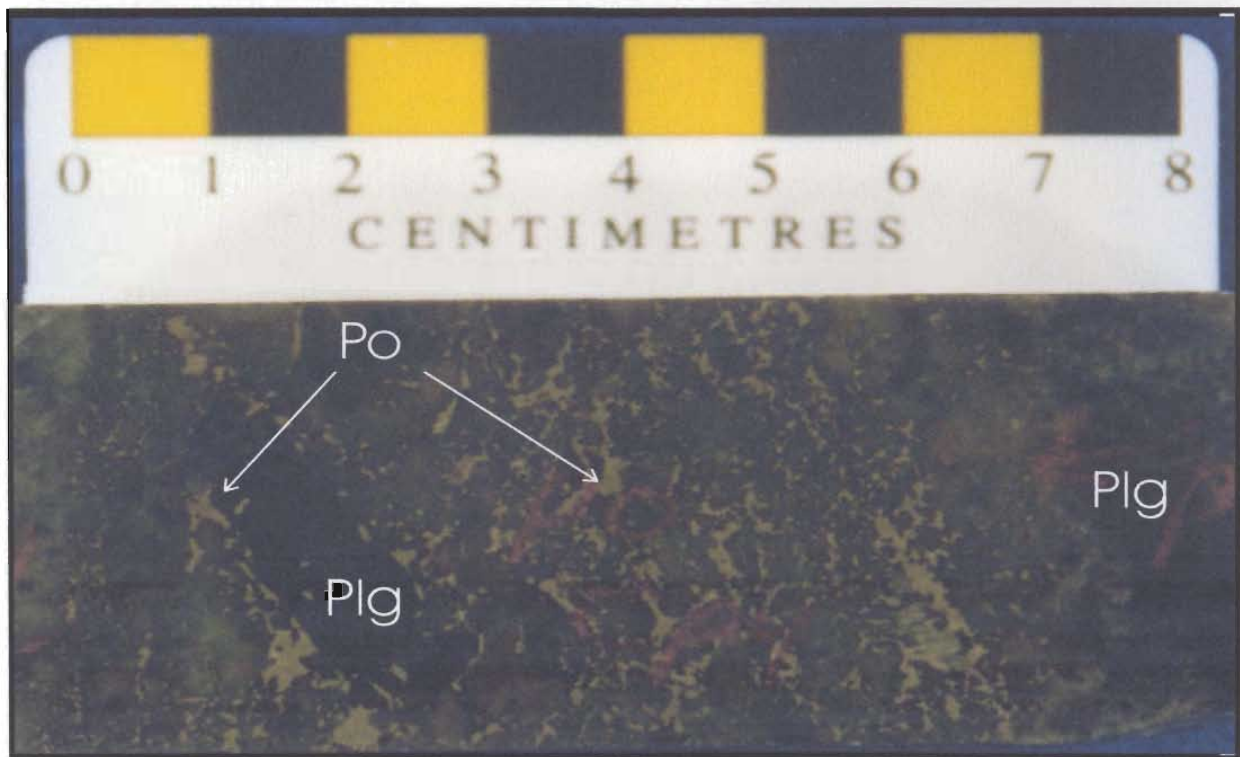
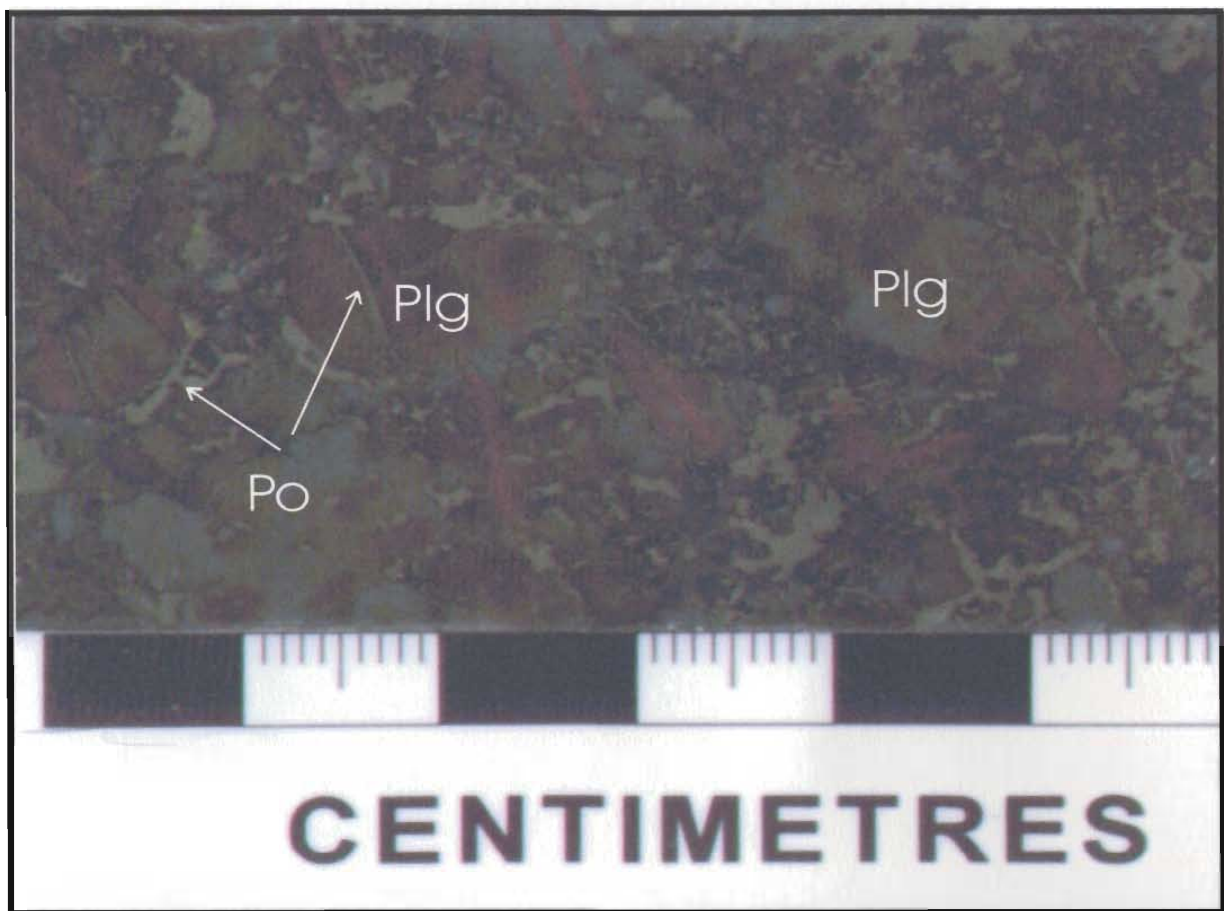


Plate 3.16 "Wormy" net-textured pyrrhotite (po) from LBN-8, 757.7m (top) and LBN-8, 323.82m (bottom). Photos show pyrrhotite wrapping around, and in places invading, plagioclase crystals (plg). Both photos show weak alignment of pyrrhotite grains and veinlets in leucoanorthosite.





Plate 3.17 Massive pyrrhotite (po) samples from drill holes LBN-3, 190.13 m (top) and LBN-11, 656.58 m (bottom) showing chalcopyrite (cpy) blebs and anorthosite/plagioclase inclusions (plg).

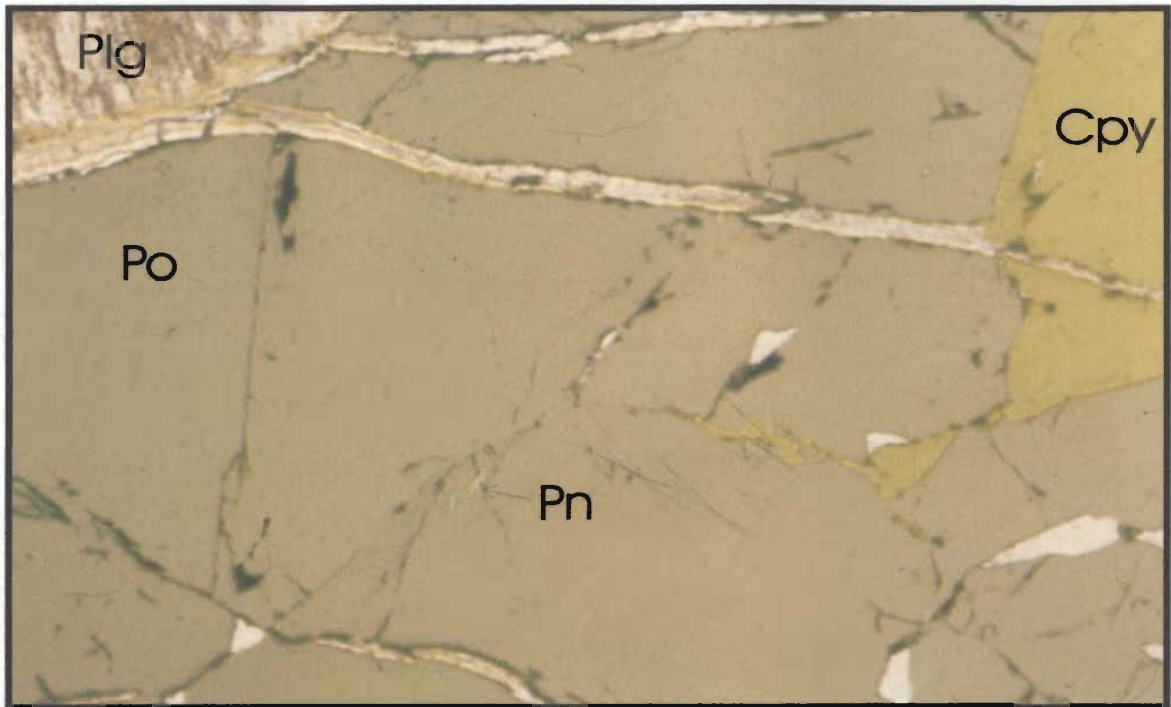


Plate 3.18 Massive pyrrhotite (Po) with chalcopyrite (Cpy) bleb, very fine-grained pentlandite (Pn) "flame" lamellae, and altered plagioclase (plg) inclusion. Photo was taken in reflected light (10 power; field of view = 2 mm).

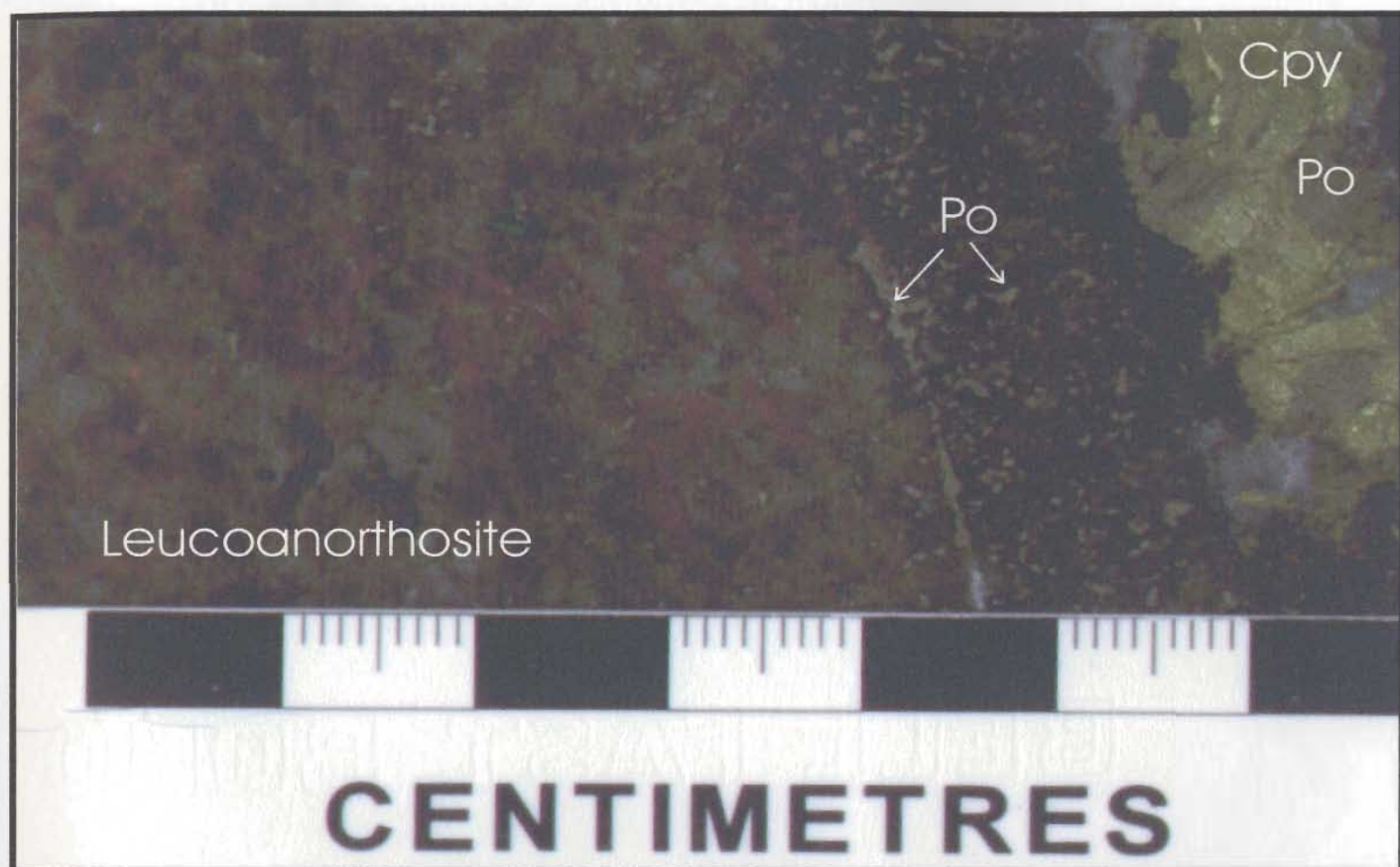


Plate 3.19 Leucoanorthosite with 2 cm wide chalcopyrite (cpy)-rich band (@70 CA) with lesser amounts of pyrrhotite (po) blebs. Disseminated pyrrhotite occurs with chalcopyrite at the contacts with leucoanorthosite. Sample is from LBN-8 at 923.92m.



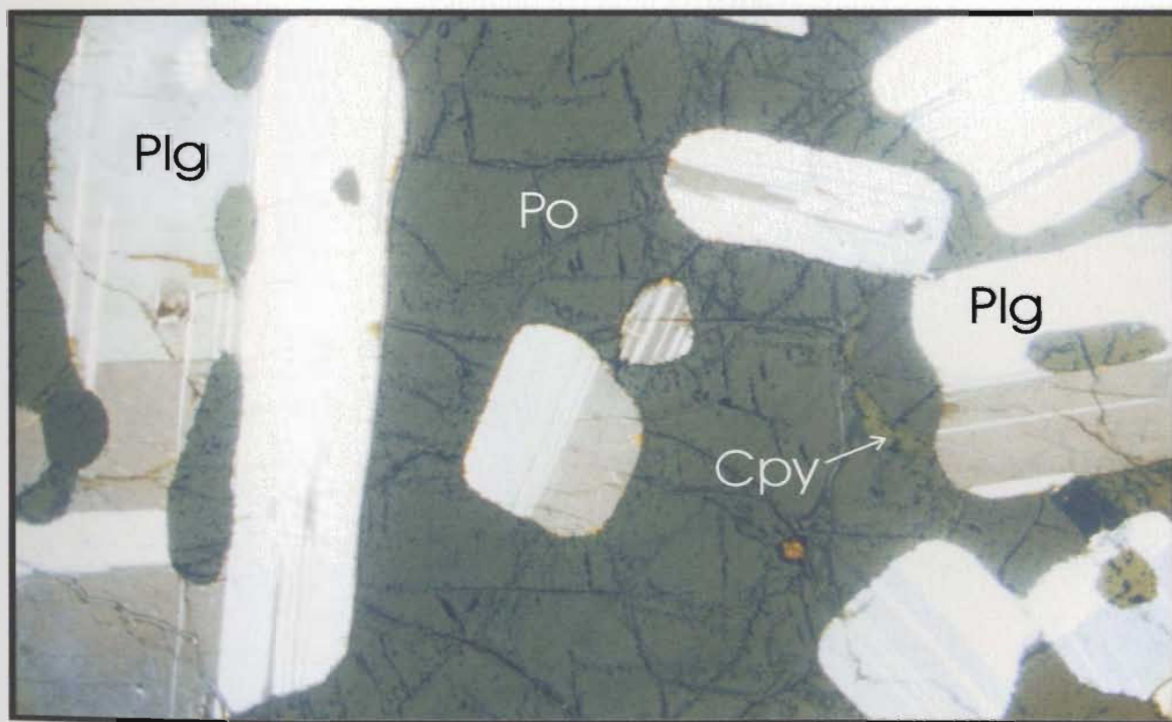
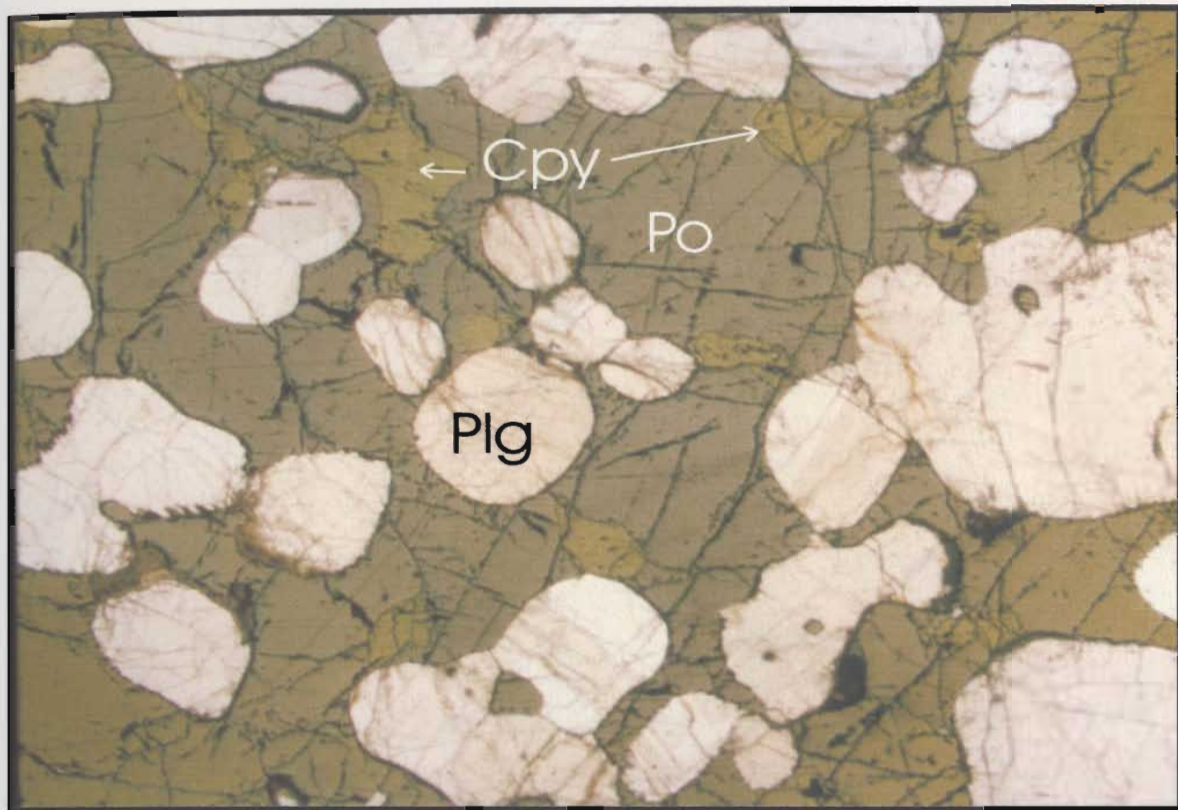


Plate 3.20 Massive pyrrhotite (po) with minor chalcopyrite (cpy) and rounded plagioclase (plg) crystals. The plagioclase inclusions are intruded by sulphides along the grain boundaries and within. The top photo was taken in reflected light under 1.5 power. The bottom photo was taken in transmitted light under 1.5 power. Field of view = 9 mm.

### 3.3.2 Contact relationships

Massive sulphide intersections have variable types of contacts with barren anorthosite; from sharp, abrupt contacts to a range of massive to net-textured to disseminated (as one moves from the interior of the sulphide intersection towards barren anorthosite as seen in Plate 3.21). Any chalcopyrite present commonly occurs within the disseminated and massive pyrrhotite near the contact with leucoanorthosite (Plate 3.22). Often in core, the disseminated texture is found at the upper contact of a massive to semi-massive sulphide band is sharper than at the lower contact which has less disseminated sulphides and less alteration. The F.P.F Resources report (1996) interpreted this as a hanging-wall and footwall, respectively, formed as the sulphides were injected from an unknown depth into a semi-crystallized to fully crystallized anorthositic magma.

In drill core, disseminated pyrrhotite commonly occurs at the outer edge of massive and net-textured pyrrhotite, forming gradual and irregular contacts with the unmineralized, unaltered leucoanorthosite (Plate 3.23). In other places in the core, thin bands or cumulate layers (15 cm wide maximum) of fine- to medium-grained, disseminated-bleb pyrrhotite (15%) with magnetite and pyroxene (<1%), pyrite (<1% to 10%), trace chalcopyrite occur with the leucoanorthosite with abrupt contacts and at angles between 30-50°CA. In drill hole LBN-97-11 at 679.62 m, 10% disseminated-bleb pyrrhotite is aligned at 50 to 90°CA with very trace chalcopyrite and about 5% pyrite in leucoanorthosite with coarse-grained, blue grey porphyry in beige feldspar groundmass. In drill hole LBN-96-3 there is 30°CA alignment of 20% pyrrhotite blebs at 115.40 m in blue grey leucoanorthosite with white



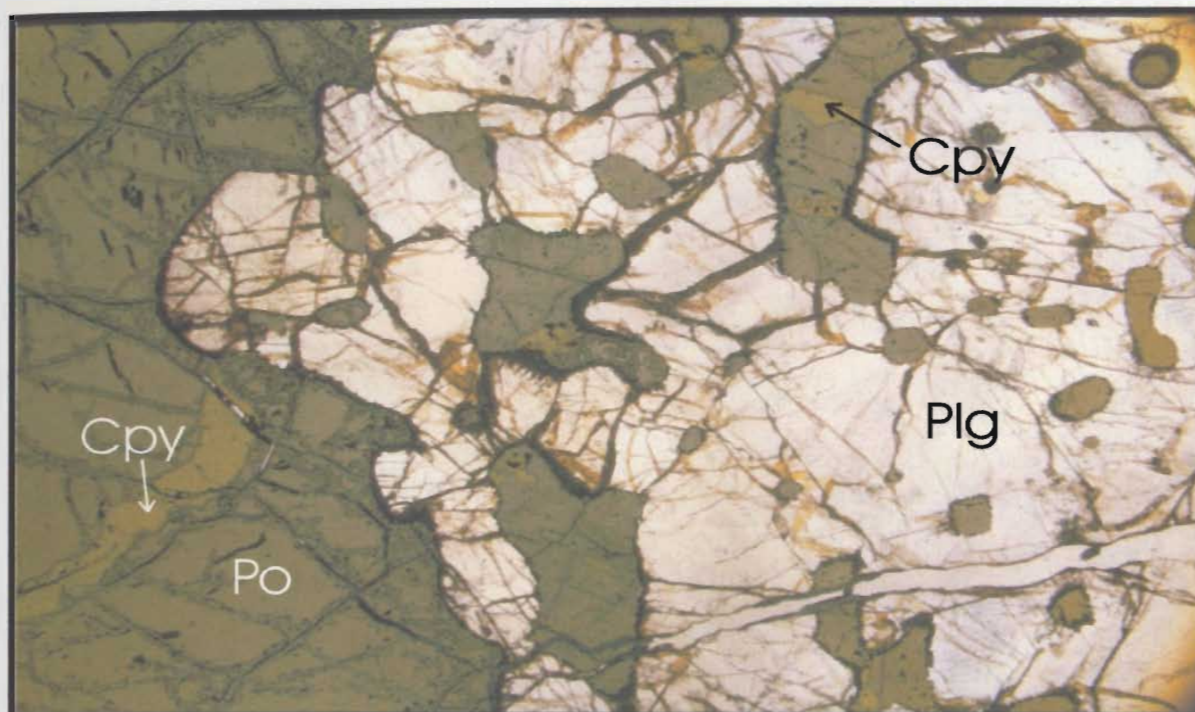


Plate 3.21 Contacts of massive sulphide in anorthosite include a range from massive to net (or pseudonet)-textured to disseminated pyrrhotite (po) with chalcopyrite (cpy) along the sulphide contact. Photo was taken in reflected light under 1.5 power (field of view = 9 mm). Plg = plagioclase.

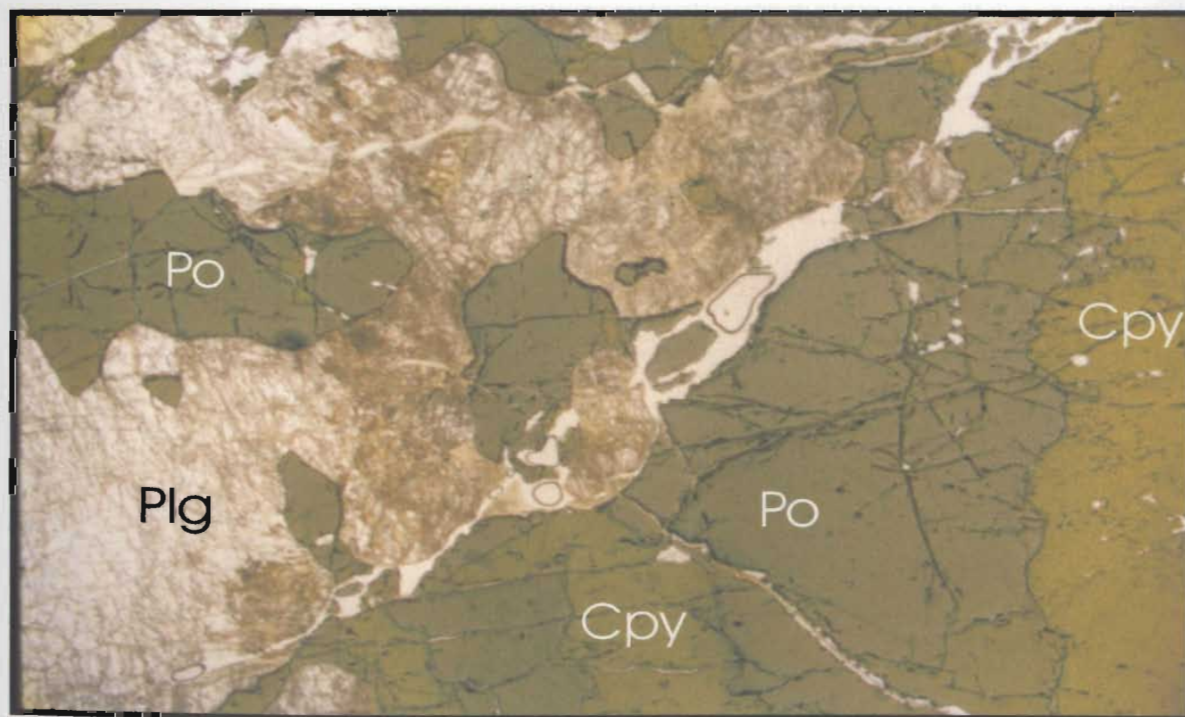


Plate 3.22 Blebs of chalcopyrite (cpy) are often located within massive pyrrhotite (po) at contacts between pyrrhotite and barren anorthosite. Photo was taken in reflected light under 1.5 power (field of view = 9 mm). Plg = plagioclase



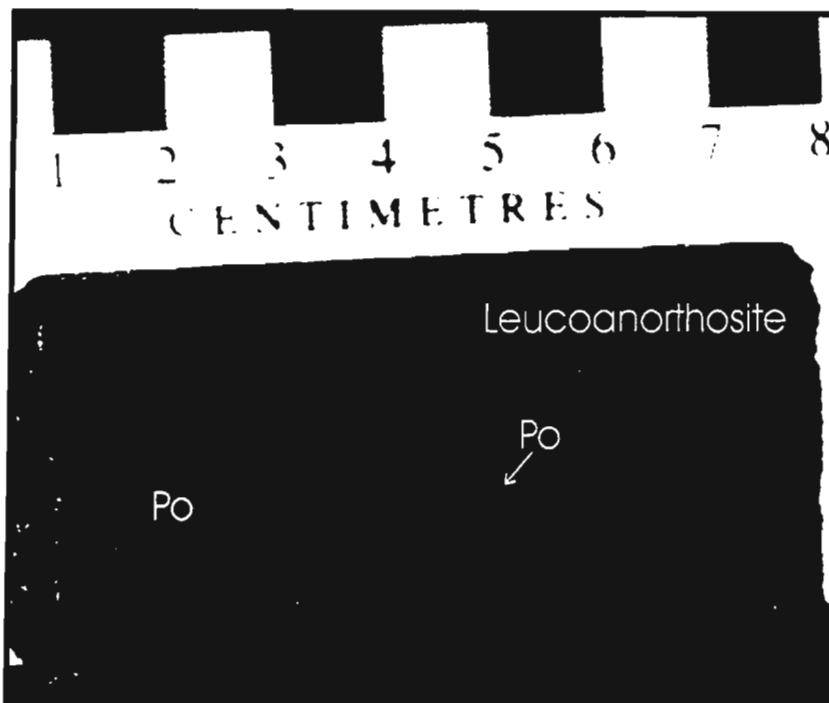
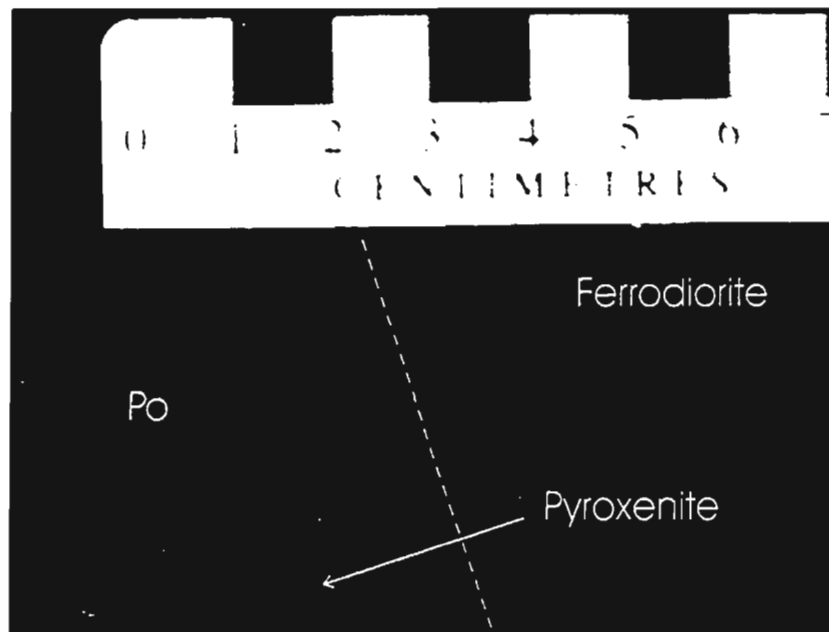


Plate 3.23 Top photo shows aligned pseudonet-textured pyrrhotite (po) band (LBN-8,352.35m) in pyroxenite which is in contact (dashed line) with ferrodiorite. Bottom photo shows semi-massive pyrrhotite with rims of disseminated pyrrhotite in leucoanorthosite (LBN-5, 323.82m; bottom).

groundmass.

Figure 3.10 is a composite cross section of sulphide mineralization with a projected zone of mineralization defined by numerous core angles measurements of sulphide contacts of intersections greater than 10 cm wide from twelve holes that have been projected onto one plane. The cross section, viewed looking north, shows the zone of sulphide mineralization to extend to a depth of 500 m below the cirque floor. Measurements of the orientations of sulphide lenses and stringers in drill core and outcrop show the zone of sulphide mineralization dipping steeply to the east and west, however, outcrop exposure along the back wall (Plate 3.6) shows an overall dip to the west towards the Noranda “Hilltop” property. Figure 3.11, another cross section but viewed looking west, suggests a very narrow (~ 0.3 km wide) zone of mineralization based on sulphide intersections in drill core.

### 3.3.3 Evidence of sulphide mobilization

Sulphide mineralization on surface and in drill core, as previously discussed, consists of veins and discontinuous, irregular pods of disseminated to net-textured to massive sulphides which crosscut barren leucoanorthosite at a range of angles within a narrow zone with minimum alteration, *albeit* light green recrystallized plagioclase, in the anorthosite “host”. Within this zone of mineralization is evidence that most of the sulphides had not crystallized *in situ* in their source magmas, but instead had migrated from the location where they had become immiscible with respect to their parental magma, that is to say, the parent rock is not present in the Cirque area.

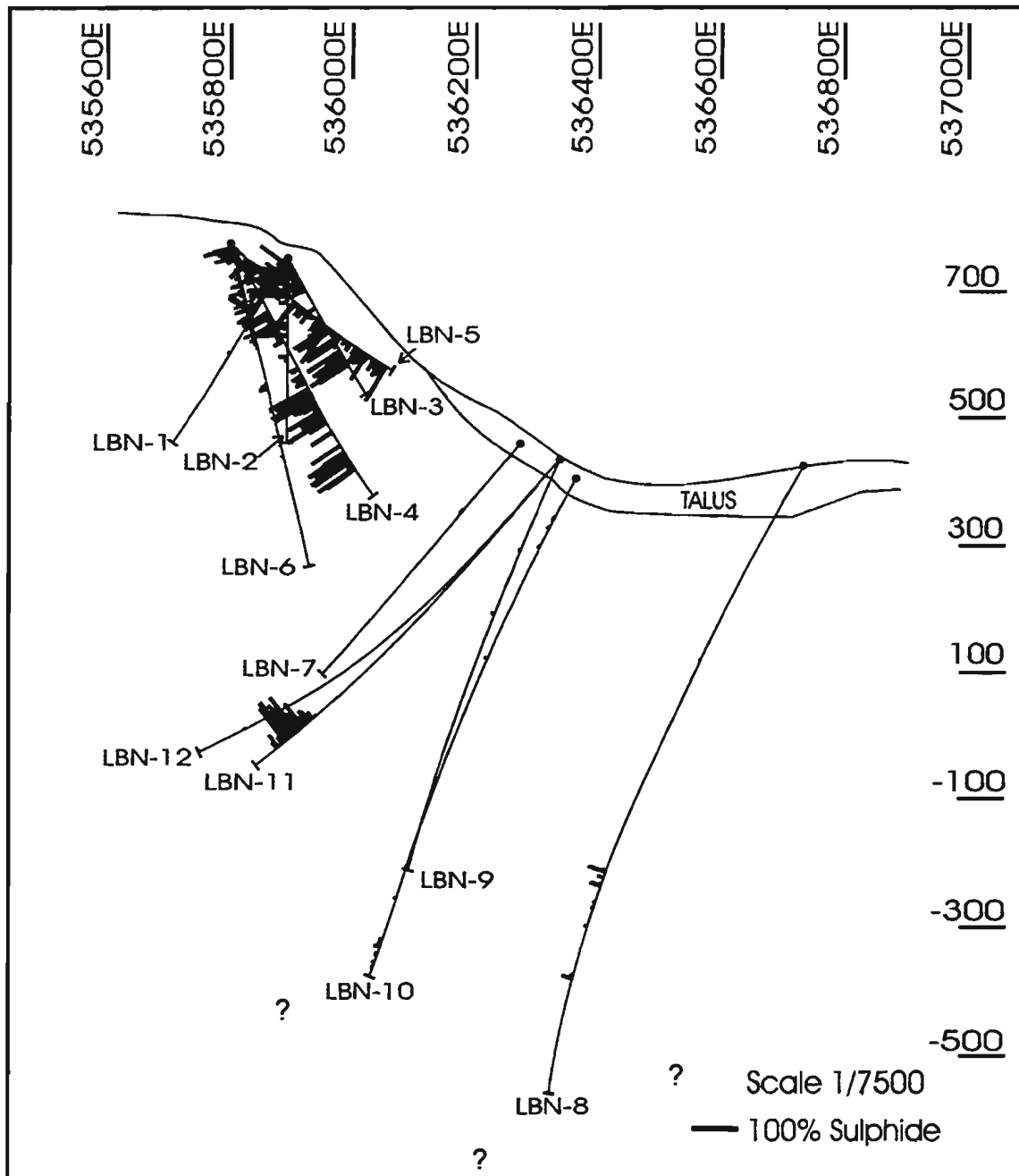


Figure 3.10 Cross section of twelve drill holes from the Cirque, looking north, projected onto 6323000m N showing the zone of sulphide mineralization (grey) as defined by surface mapping and drill hole intersections. Depth is in metres. The entire zone of mineralization consists of irregular and discontinuous pods and veins of disseminated to massive sulphide (pyrrhotite and minor chalcopyrite) within iron-stained unmineralized anorthosite with dominantly low pyroxene and Fe-Ti oxide contents.

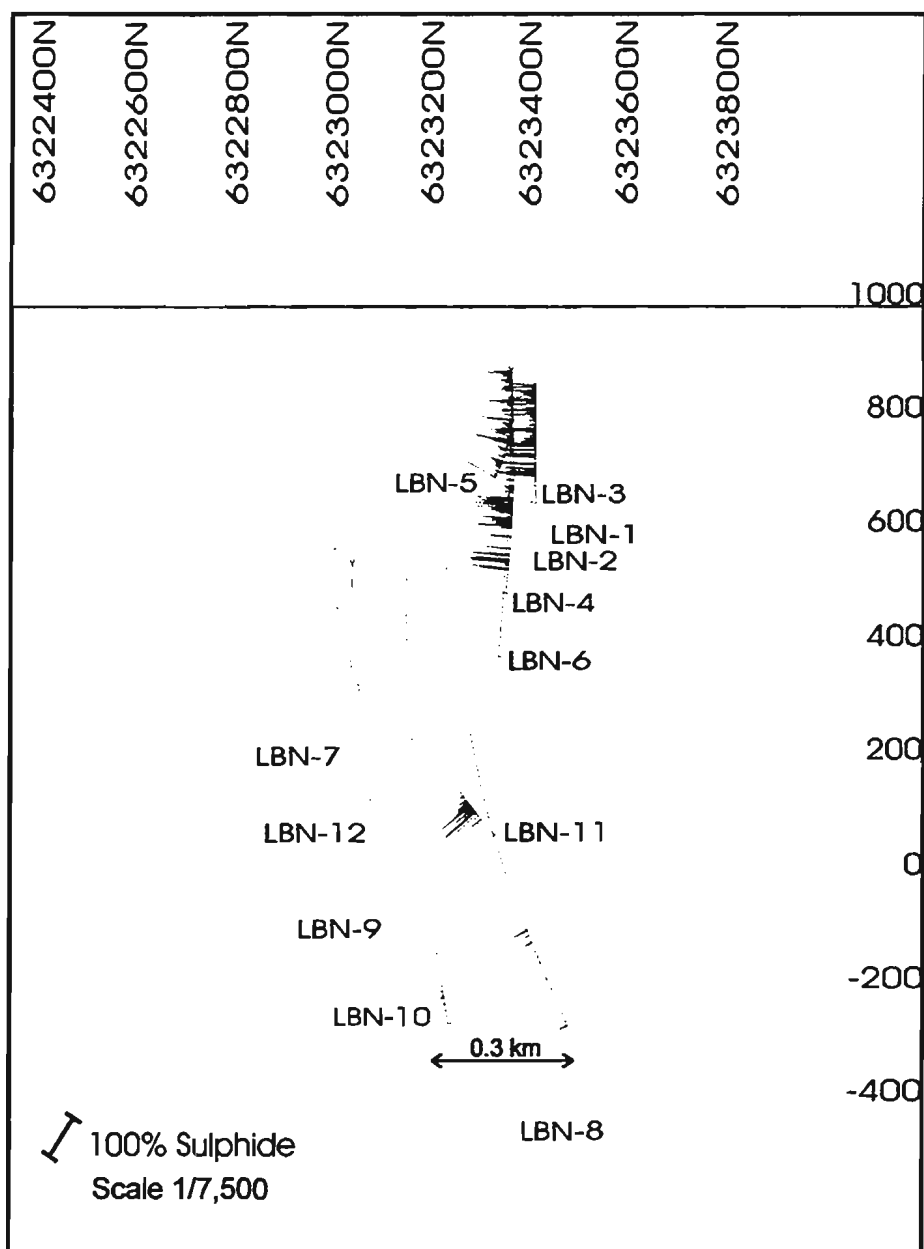


Figure 3.11 Cross section looking west showing sulphide intersections as histograms in drill holes on the Cirque grid projected onto one plane (536100mE). The grey area is the zone of discontinuous disseminated to massive sulphide mineralization interpreted from drill core intersections and surface occurrences. Depth is in metres.

In outcrop and drill core intersections, typical textures suggest thermal erosion in which hot sulphides were injected into a partially crystallized mafic magma resulting in fracturing and disaggregation of the anorthositic rock. Thermal erosion textures have also been noted at the Sally Malay deposit, Western Australia (Hoatson *et al.* 1998), and the Jinchuan deposit (Zongli 1993), however, these textures involve injection of hot mafic magma fracturing and assimilating the cooler country rock as the magma rises.

Drill hole LBN-3 (@ 15.55 m), shown in Plate 3.24 has anorthosite with irregular veins and patches of massive pyrrhotite containing inclusions of anorthosite and plagioclase crystals. Massive pyrrhotite near the contact with anorthosite contains smaller irregular inclusions of anorthosite and plagioclase. The anorthosite inclusions show evidence of being fractured and disaggregated (Plate 3.25) with the inclusions often lying parallel to sub-parallel to the contact with anorthosite indicating the flow direction of the sulphides, similar to that of grains of sand in flowing water. In other intersections, massive sulphides contain anorthosite xenoliths and plagioclase inclusions, particularly elongated inclusions, aligned at measurable angles. As pointed out by Kerr and Smith (1997), “true” net-textured sulphides, which form as a result of crystallization of cumulate silicate minerals moving downward in the magma to settle in the sulphide layer (Naldrett 1973), is not common at the Cirque and most of the net-textured sulphides at the Cirque appear to have formed as a result of disaggregation or brecciation of anorthosite. Although in places net-textured pyrrhotite and minor chalcocopyrite seems to have formed from sulphide immiscibility of the existing mafic magma, net-texture sulphide mineralization dominantly corresponds to the degree of anorthosite erosion by sulphide melt.

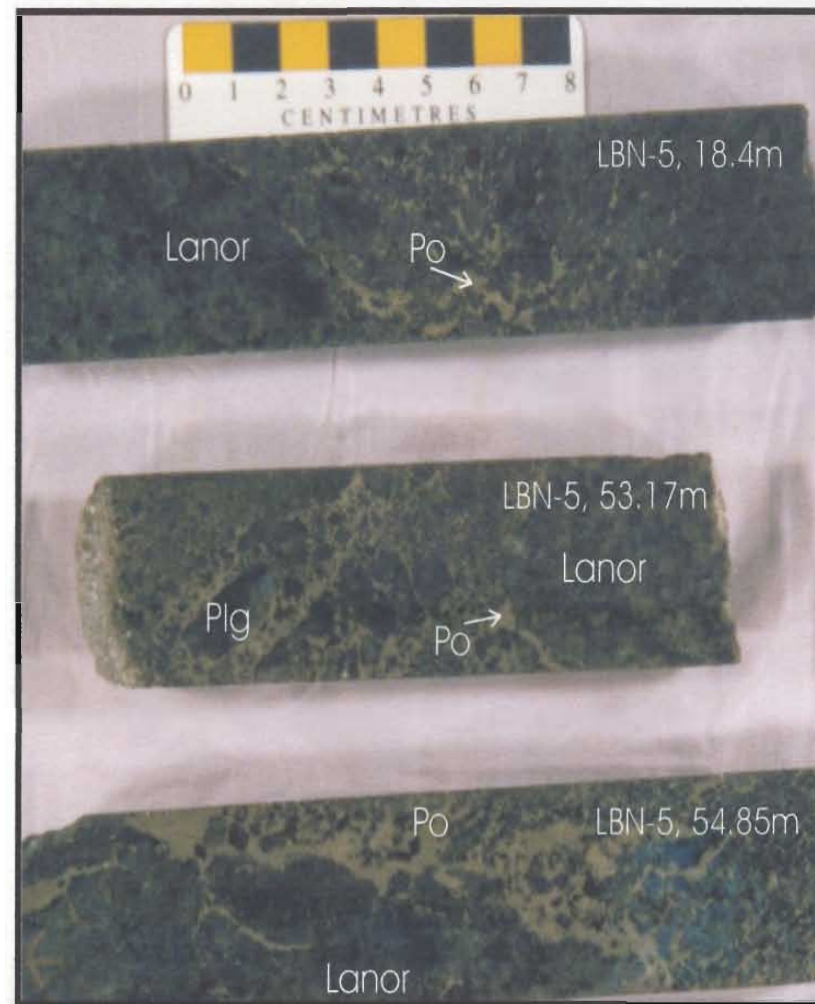
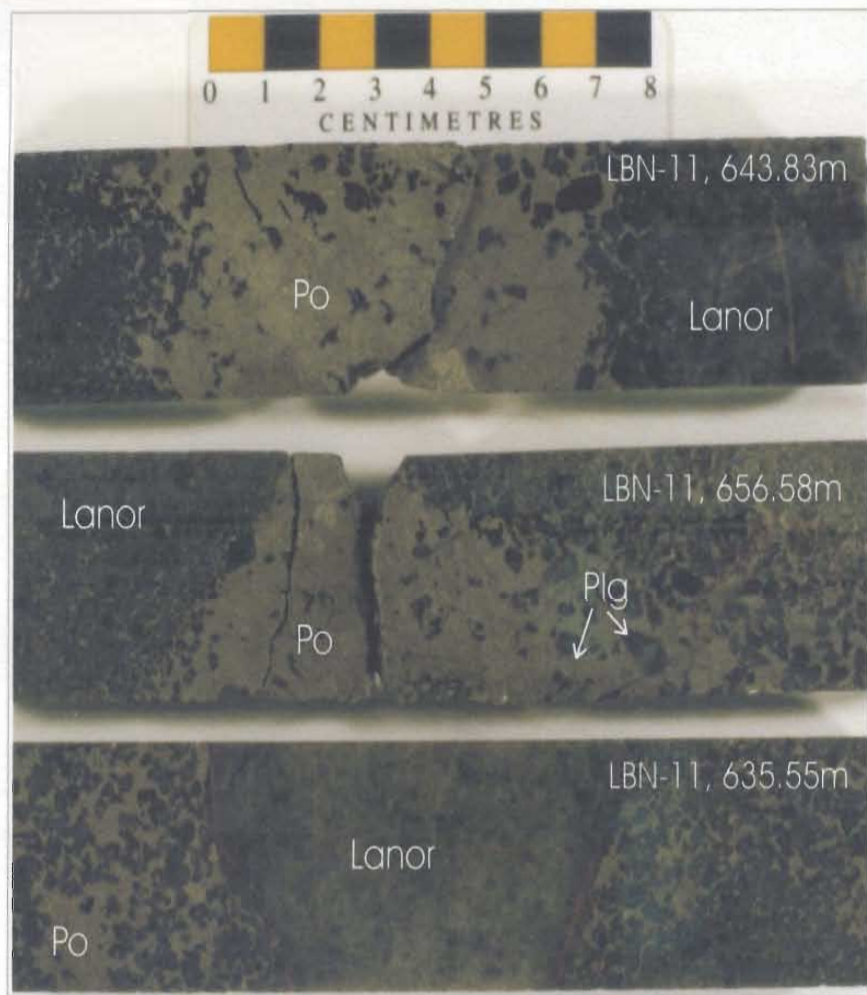


Plate 3.24 Core samples of semi-massive pyrrhotite with xenoliths of disaggregated leucoanorthosite (Lanor) and plagioclase crystals. Samples in both photos show various degrees of sulphide penetration into anorthosite with pyrrhotite (po) wrapping around individual plagioclase (plg) crystals.



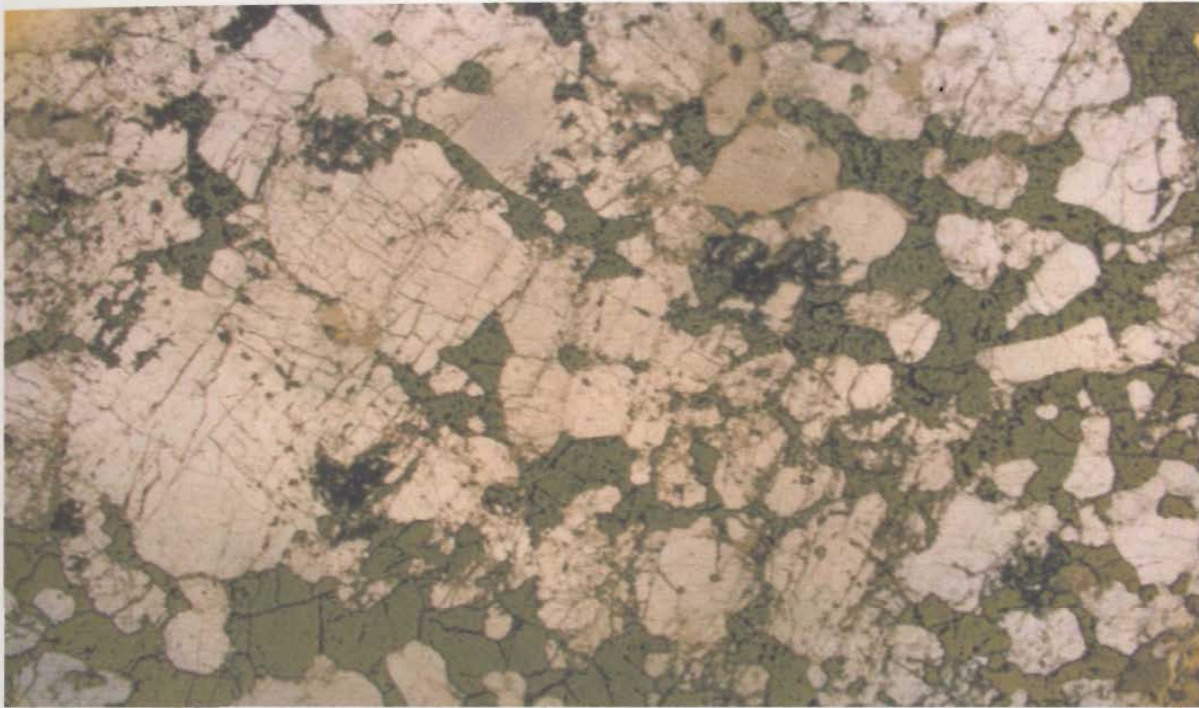


Plate 3.25 Fractured plagioclase crystals as a result of sulphide injection in anorthosite. Photo was taken in reflected light under 1.5 power (field of view 9 mm). Po = pyrrhotite; Plg = plagioclase.

More evidence of thermal erosion is shown by scalloped crystal edges (Plate 3.26) and very thin microfractures of sulphide-rich veinlets crosscutting the crystal or intruding along cleavage planes of plagioclase crystals (Plate 3.27). In zones of massive sulphide mineralization, rounded plagioclase inclusions clearly show signs of erosion by the sulphides; commonly with inclusions of sulphides along fractures and cleavage planes (Plates 3.28, 2.29).

### **3.4 Mineralization on neighbouring properties**

The 'host' rock on the Cirque, leucoanorthosite (Unit 1a and b) with very little pyroxene and no olivine, is one of four types of sulphide host rocks classified by Kerr and Ryan (2000). The other three are 'pyroxenite-hosted', 'ferrodiorite-hosted', and as at the Voisey's Bay deposit, 'gabbro/troctolite-hosted', [Table 3.4; Kerr (1998); Kerr and Ryan (2000)]. Each magma-hosted type will not be discussed in detail here; however, it is noteworthy that such a variety of sulphide occurrences exists. Ferrodiorite dykes along the north arm (Unit 3), as mentioned in Chapter 2, contain minor syngenetic, disseminated pyrrhotite (<10%), however, this does not appear to have the same genesis as the mineralization in the Cirque gossans.

To the west of the Cirque property, Noranda reported localized disseminated to massive pyrrhotite veins and pods with minor chalcopyrite in dominantly leucogabbro - gabbro - norite dykes (?) and anorthosite (Squires *et al.* 1995, 1996; Kerr and Smith 1997;

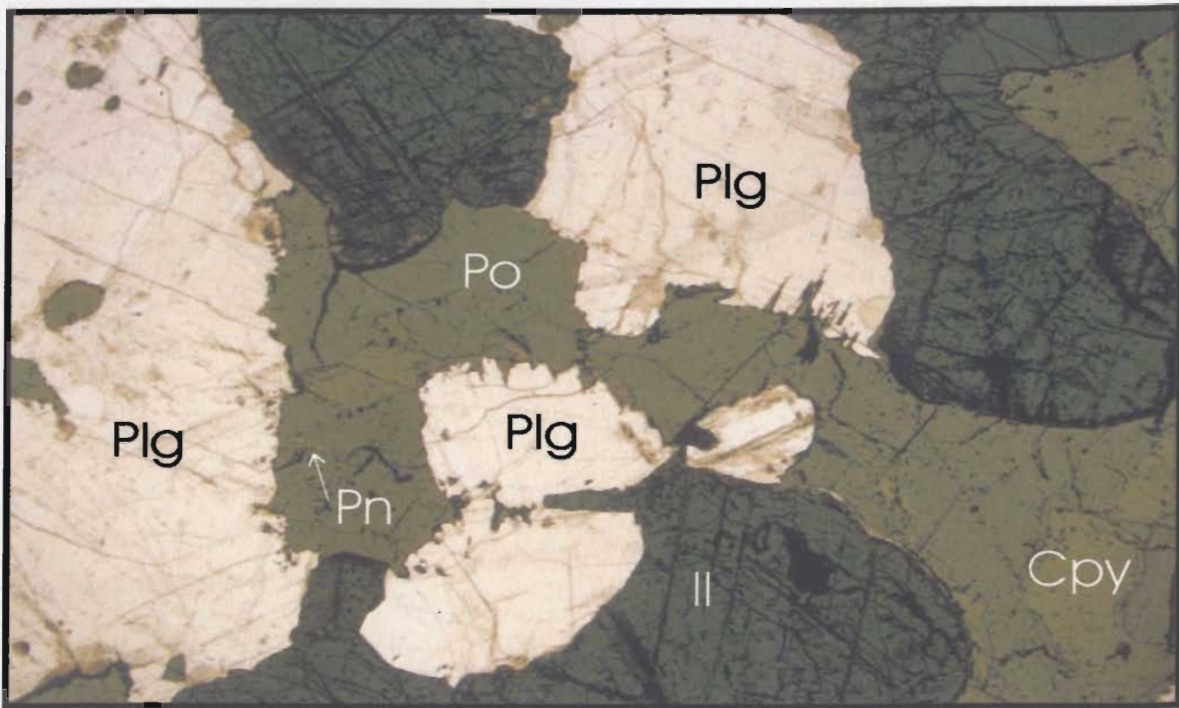


Plate 3.26 Scalloped grain boundaries of plagioclase indicating embayment of sulphides into plagioclase (plg) crystals. Ilmenite (Il) does not appear to be as intrusive. Photo was taken in reflected light under 1.5 power (field of view = 9 mm). Po = pyrrhotite, cpy = chalcopyrite, pn= pentlandite.

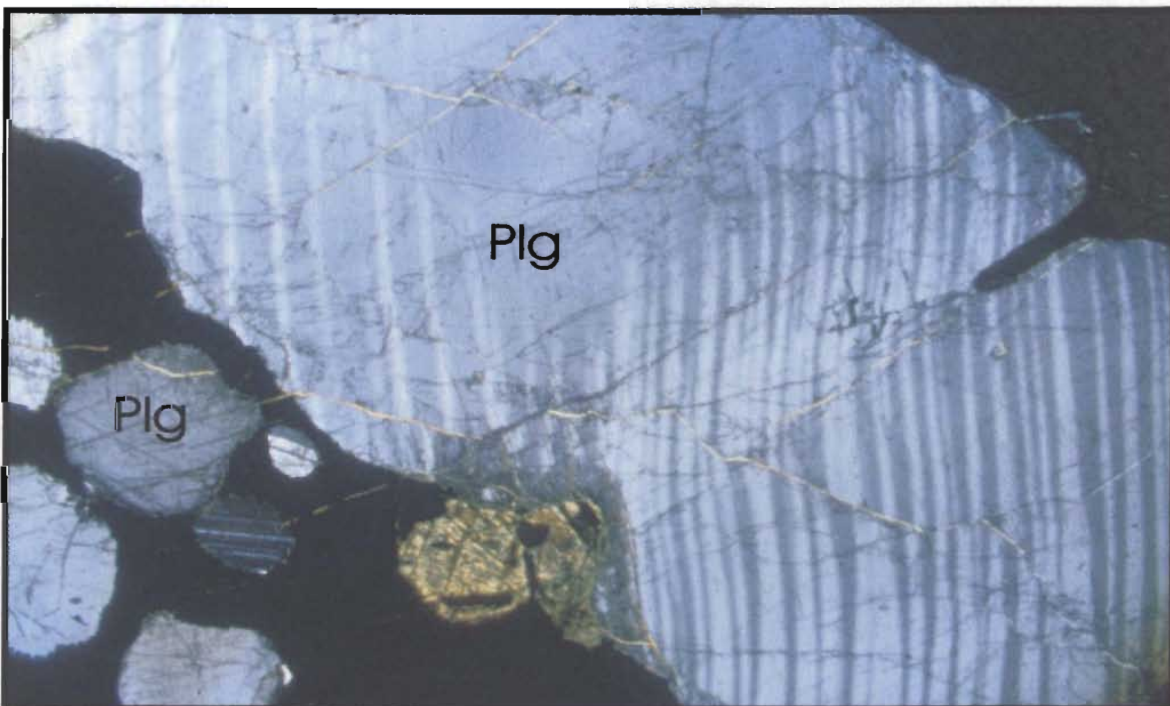


Plate 3.27 Large plagioclase crystal with bent twinning which has been then fractured. Sulphides (black) are shown intruding plagioclase (plg). Photo was taken in transmitted light (crossed polars) under 10 power (field of view = 2 mm).



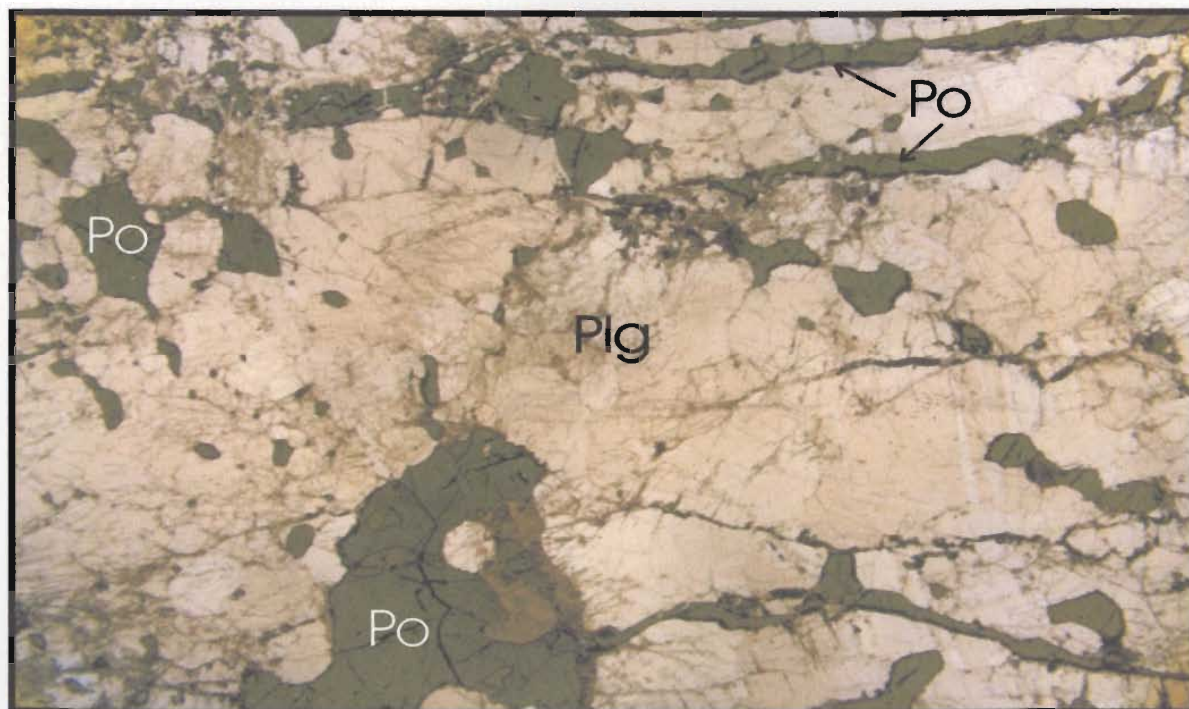
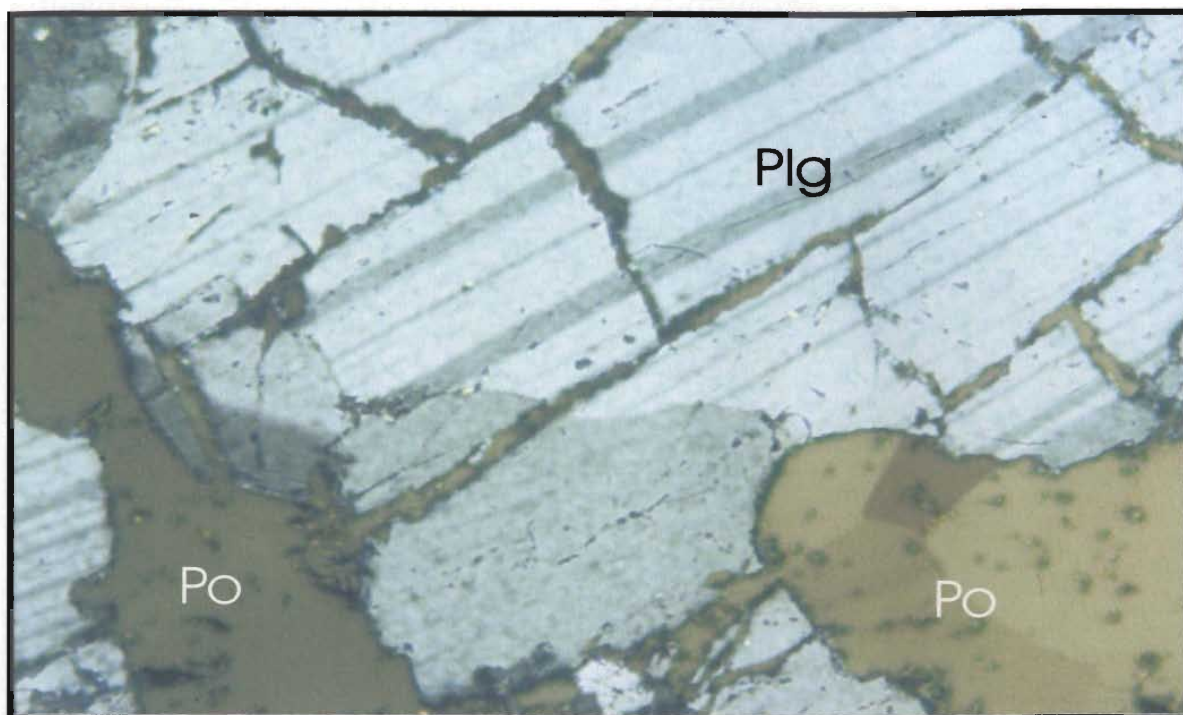


Plate 3.28 Injections of pyrrhotite (po) as thin veins cross-cutting cleavage planes of plagioclase (plg) and as larger irregular blebs (top). Pyrrhotite veins are aligned parallel to sub-parallel in the more altered zones in leucoanorthosite. Both photos were taken in reflected light under 10 power (field of view = 2 mm).

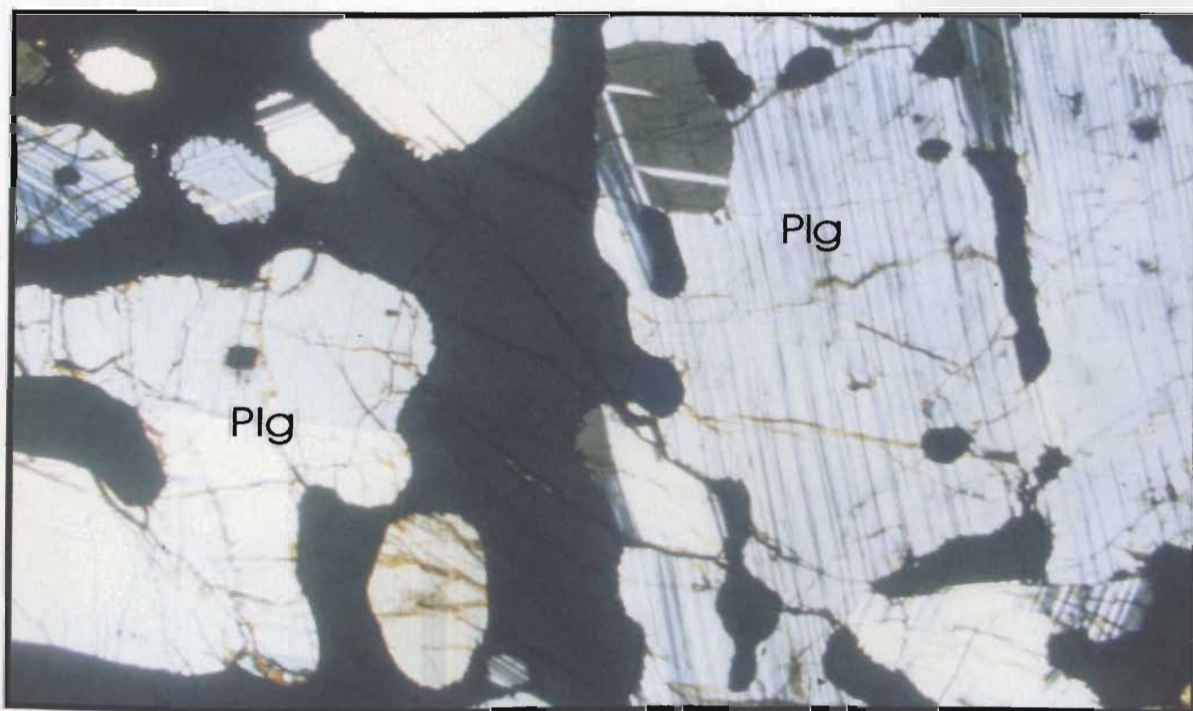
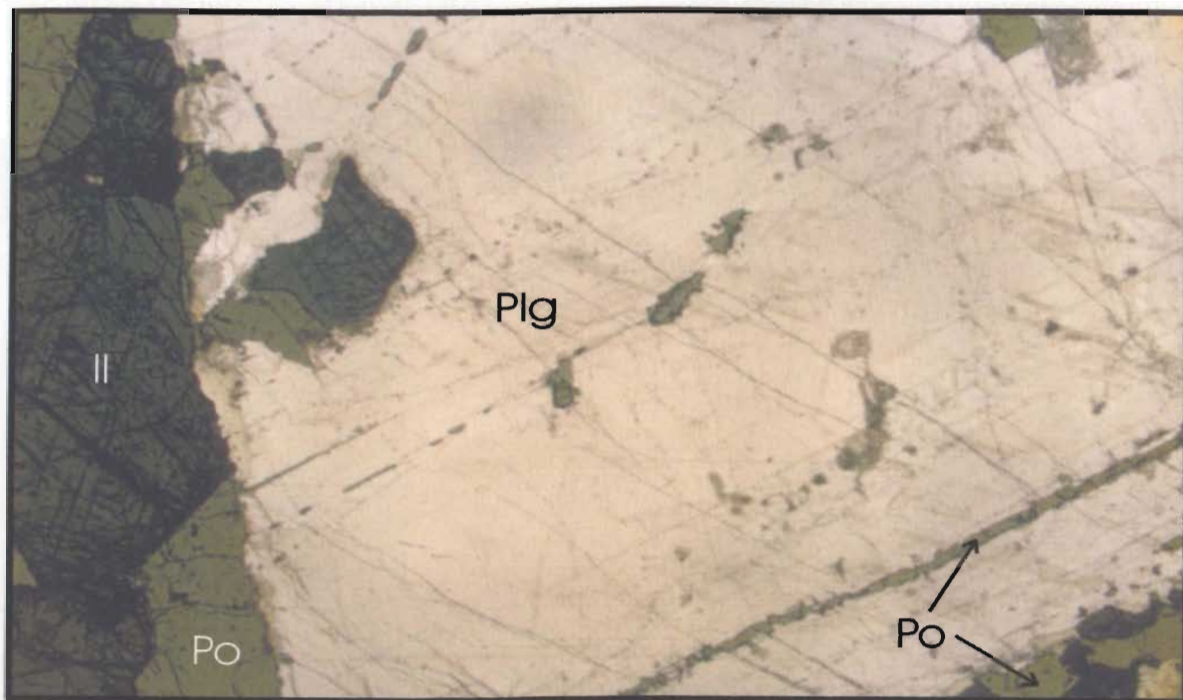


Plate 3.29 Intrusions of pyrrhotite (po) into plagioclase (plg) crystals along cleavage planes (top) and along grain boundaries (bottom). Top photo was taken in reflected light at 1.5 power. Bottom photo was taken in transmitted under 1.5 power. Field of view = 9 mm. Il = ilmenite.



Table 3.4 Compilation of magmatic sulphide occurrences in northern Labrador subdivided by Kerr (1998) and Kerr and Ryan (2000) on the basis of magma host rock. Ni/Cu values are from Kerr and Ryan (2000).

Host type	Description	Mineralization	Syngenetic/ Epigenetic	Ni/Cu ratio (at 100% sulphide)	Examples
Anorthosite	Dominantly anorthosite and leuconorite	Localized zones of disseminated to massive pyrrhotite with lesser chalcopyrite and minor pentlandite; variable magnetite and ilmenite	Epigenetic	Variable but generally >1.5*	Puttuala Lake area [eg Cartaway (Cirque); Canadian States Resources (Lic #1514M); Noranda (Nain Hill)]; Nain area [eg NDT Ventures (Nain Hill)]
Pyroxenite	Orthopyroxene-rich pyroxenite and melanorite (with or without olivine)	Minor disseminated and localized pods of pyrrhotite with lesser chalcopyrite and pentlandite; minor pyrite and magnetite; evidence of gravitational settling of sulphides	Syngenetic	Variable but generally >1.4	Castle Rock (OKG prospect); locations within the Kiglapait Layered Intrusion and in the Igluataaliksuak Lake area
Gabbro-Troctolite	Olivine-gabbro and troctolite spatially associated with orthogneiss and paragneiss of the NP, CP and TG	Localized to significant zones of disseminated to massive pyrrhotite with chalcopyrite, pentlandite and variable magnetite	Syngenetic	Maximum of 4	Voisey's Bay deposit; Donner Minerals (South Voisey's Bay Project); locations within the Kiglapait Layered Intrusion and other layered to semi-layered intrusions
Ferrodiorite	Fe oxide-rich gabbro and diorite dykes	Generally disseminated pyrrhotite, lesser chalcopyrite; overall sulphides are minor	Syngenetic	~0.25	Gallery Resources Ltd. (Umiakovik Lake area), Cartaway (LB-J property)

\* Refer to Appendix A2 for detailed assay results from the Cirque property.

NP = Nain Province, CP = Churchill Province, TG = Tasuikyak Gneiss



refer to Figure 1.6 of this study). Clinopyroxenite and orthopyroxenite with 2 to 10% interstitial pyrrhotite was also found in rubble (Squires *et al.* 1996). In the northeast corner of Licence #915M, Squires *et al.* (1996) reported two veins of coarse-grained pyrrhotite: (i) a 4 m long, 1.3 m (narrowing to 10 cm wide to the south) vein striking to the to the northeast and dipping to the east and (ii) a 4.5 m long, 35 cm to 1.3 m wide vein striking northeast. Much of the mineralization here corresponds to conductors in the area and fine- to medium-grained olivine gabbro and anorthosite (*op. cit.*).

Plate 3.30 shows mineralogy and texture of a cumulate magnetite and pyroxene-rich rock from the Noranda “Hilltop” property with lesser amounts of bleb pyrrhotite and chalcopyrite similar to that found in the ferrodiorite dykes (Unit 3) on the Cirque grid. Kerr and Smith (1997), however, suggest that not all mineralization occurrences in the dykes are syngenetic, but rather that some norite dykes may have actually intersected sulphide-bearing zones in anorthosite. A leucogabbro-gabbro dyke, also on the Noranda property, striking approximately northeast and dipping to the west, contains syngenetic massive sulphides and coarse-grained plagioclase crystals (~ 3 cm - 5 cm) believed to have been entrained in the sulphide melt as it passed through anorthositic rocks before the leucogabbro-gabbro dyke cooled (Squires *pers comm.* 1996). Cross sections of drill holes which intersected disseminated, net-textured, and several metres of massive pyrrhotite with minor chalcopyrite (maximum of 4 cm wide blebs) show the sulphide mineralization to decrease with depth (Squires *et al.* 1996, 1997) and suggest that the surface showing and corresponding magnetic

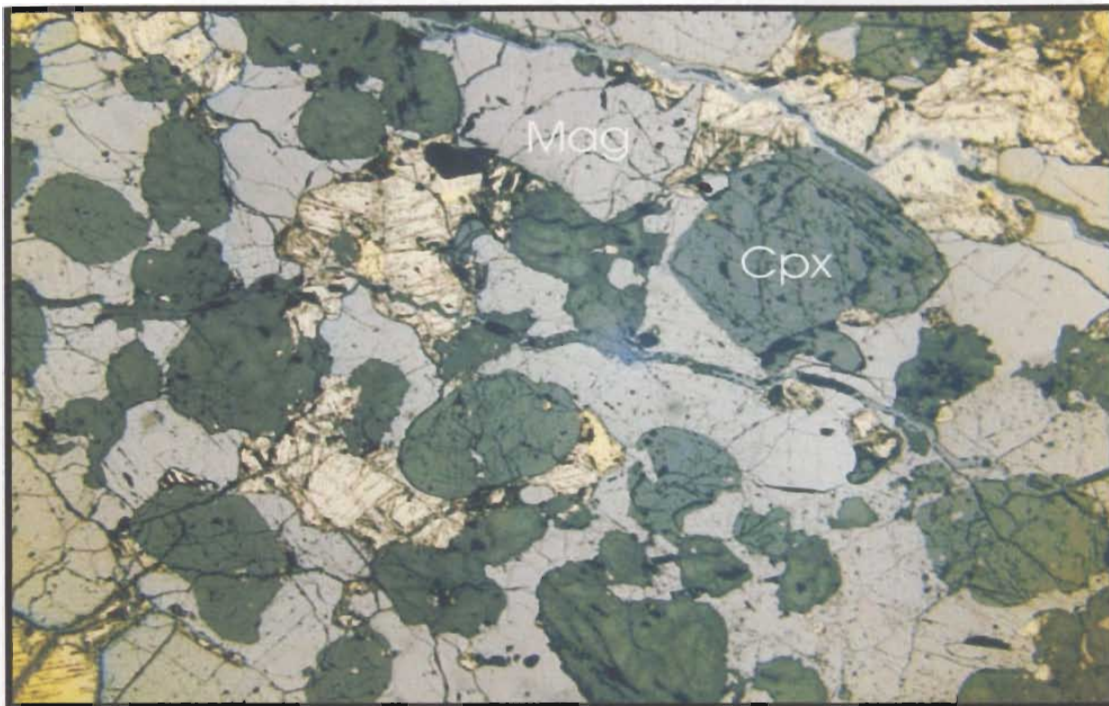


Plate 3.30 A magnetite (mag) and clinopyroxene (cpx)-rich sample from Noranda's "Hilltop" property looks very similar to ferrodiorite dykes from the Cirque (see Plate 3.17). Top photo was taken in reflected light and bottom photo was taken in transmitted light; both under 1.5 power (field of view = 9 mm).

and HLEM conductors are outlining extensive mineralized boulders and the actual mineralized outcrop is much more restricted below surface. Thermal erosion textures in outcrop and drill core are not reported by Noranda, however, Kerr and Smith (1997) did observe evidence of sulphide penetration in largely anorthosite, which in places, are associated with minor green, recrystallized anorthosite.

On the neighbouring property, Canadian States Resources geologists sampled and drilled a gossanous zone on Licence #1514M along strike of the Cirque gossan. Zones E and G are the two main gossans on the property. Zone E is located on the boundary between Cartaway's LBG property (refer to Figure 3.1b) and Zone G is located 1 km along strike of Cartaway's Gossan #1 on the Cirque property.

Zone G consists of massive (Plates 3.31), net-textured, and disseminated pyrrhotite with minor chalcopyrite and pentlandite hosted in leucoanorthosite which displays similar thermal erosion textures and disaggregation of anorthosite by massive sulphides. However, the chalcopyrite, pentlandite, and magnetite abundances are greater than those observed on the Cirque property particularly in massive and disseminated sulphide zones (Kerr and Smith 1997; Canadian States Resources *inhouse* data 1996). Plate 3.32 shows massive pyrrhotite with chalcopyrite rimming plagioclase and anorthosite inclusions and minor pentlandite and magnetite. Like the Cirque sulphides, pyroxene inclusions are generally not present with massive sulphide mineralization and minor alteration, consisting of fine-grained, green recrystallized anorthosite and leuconorite, is spatially associated with sulphide zones (*op. cit.*). Rock types (which consists of interlayered leuconorite and anorthosite with minor

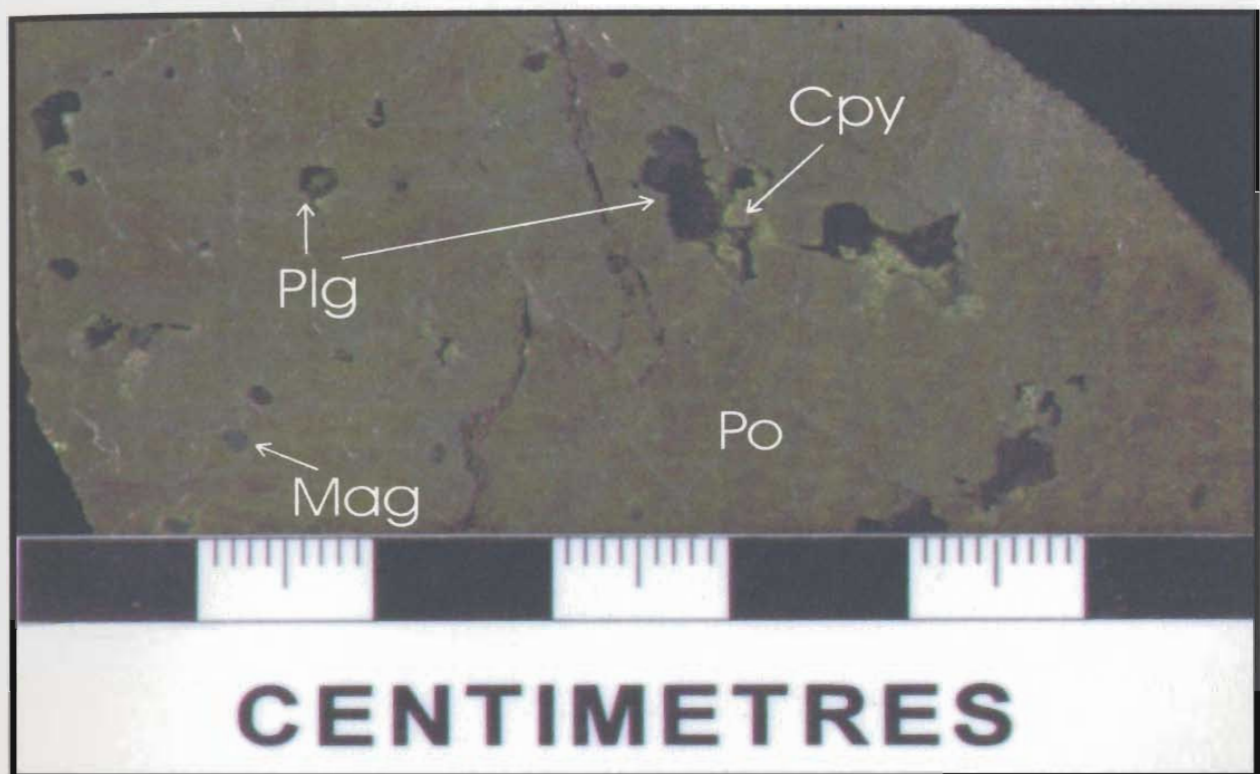


Plate 3.31 Core sample from the Canadian States Resources property (Licence #1514M, G Zone) showing massive pyrrhotite (po) with minor magnetite (mag) and chalcopyrite (cpy) which, in places, rim anorthosite/plagioclase (plg) inclusions.



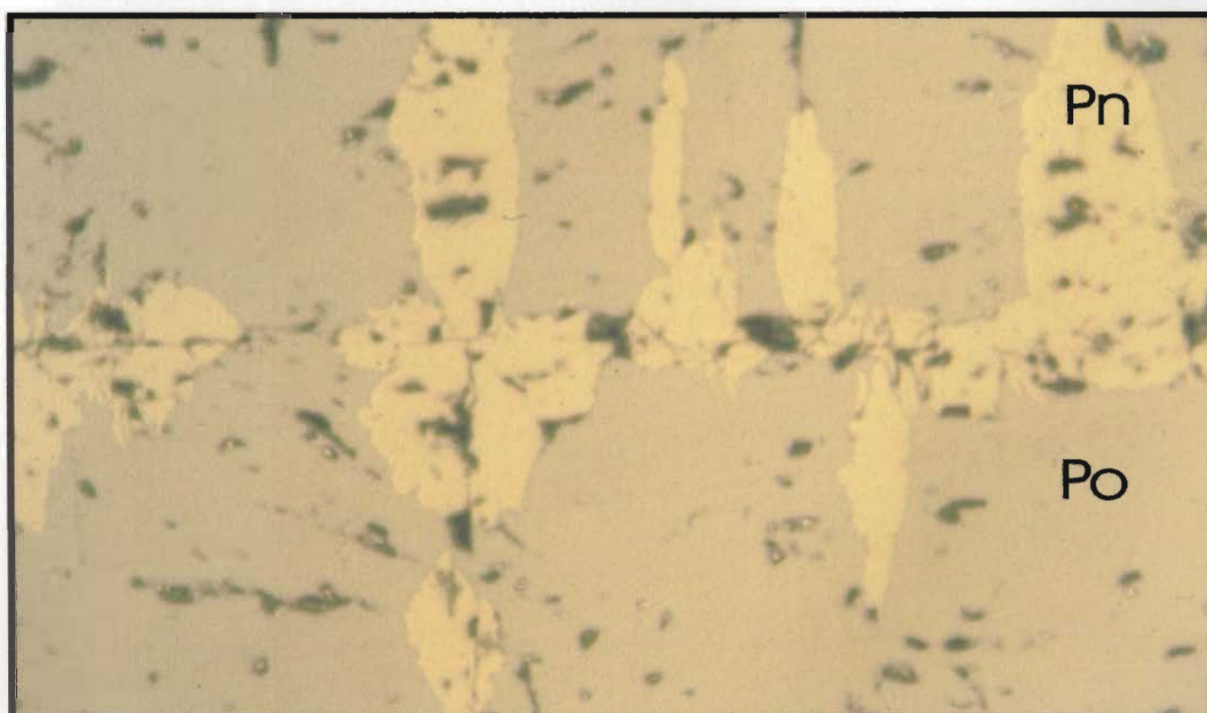
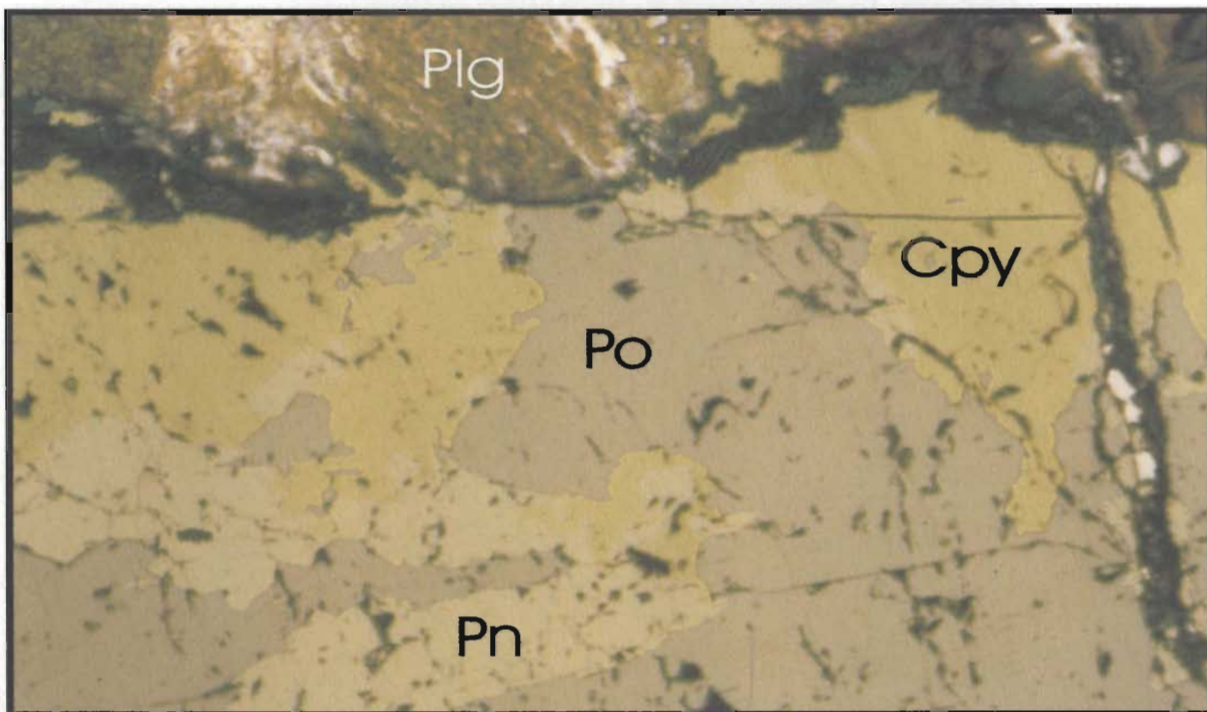


Plate 3.32 Massive sulphide sample from Canadian States Resources property (Lic #1514M). Top photo shows massive pyrrhotite (Po) with chalcopyrite (Cpy), pentlandite (Pn) and altered plagioclase inclusion (Plg). Bottom photo shows massive pyrrhotite with exsolved pentlandite along a fracture. Both photos were taken in reflected light; under 10 power (top; field of view = 2 mm) and 20 power (bottom; field of view = 1 mm).

troctolite and gabbro) and fault zones (with associated alteration and felsic pegmatitic dykes) similar to those intersected at the Cirque property have also been intersected in drill core at both the E and G zones on the Canadian States property (Canadian States Resources *inhouse* data 1996).

### **3.5 Assay results from the Cirque**

Chapter 5 discusses the metal content of the sulphides (from this study) in more detail, however, this section presents the results of outcrop and drill core sampling of sulphide mineralization by Cartaway Resources. Figures 3.12a-e show % Ni and % Cu for each drill hole (except LBN-12). Views are to the north, west and projected to the surface in plan view; depth is in metres. Geochemical data of the surface samples collected by Cartaway in 1995 and assayed by Chauncey Laboratories Ltd in Ontario are listed in Appendix A2.3.1. Appendix A2.3.2 presents surface sample data collected between 1996 to 1997, as part of this study and assayed by Chauncey Laboratories and at Memorial University. Additional data for samples from LBN-1 assayed for major-trace elements by Chauncey Laboratories for Cartaway Resources in 1996 are listed in Appendix A2.3.3.

Overall, the Ni and Cu abundances as listed in appendices A2.3.1 and 2 are low with the maximum Ni and Cu contents being 0.51% and 0.59%, respectively, and the Ni/Cu ratios varying from <1 to >1; the highest Ni/Cu value is 4.54. These values are similar to other areas reported by Kerr and Ryan (2000); for instance, massive sulphide samples from Canadian States Resources (Licence #1514M) and Noranda's 'Hilltop' (Licence #915M)



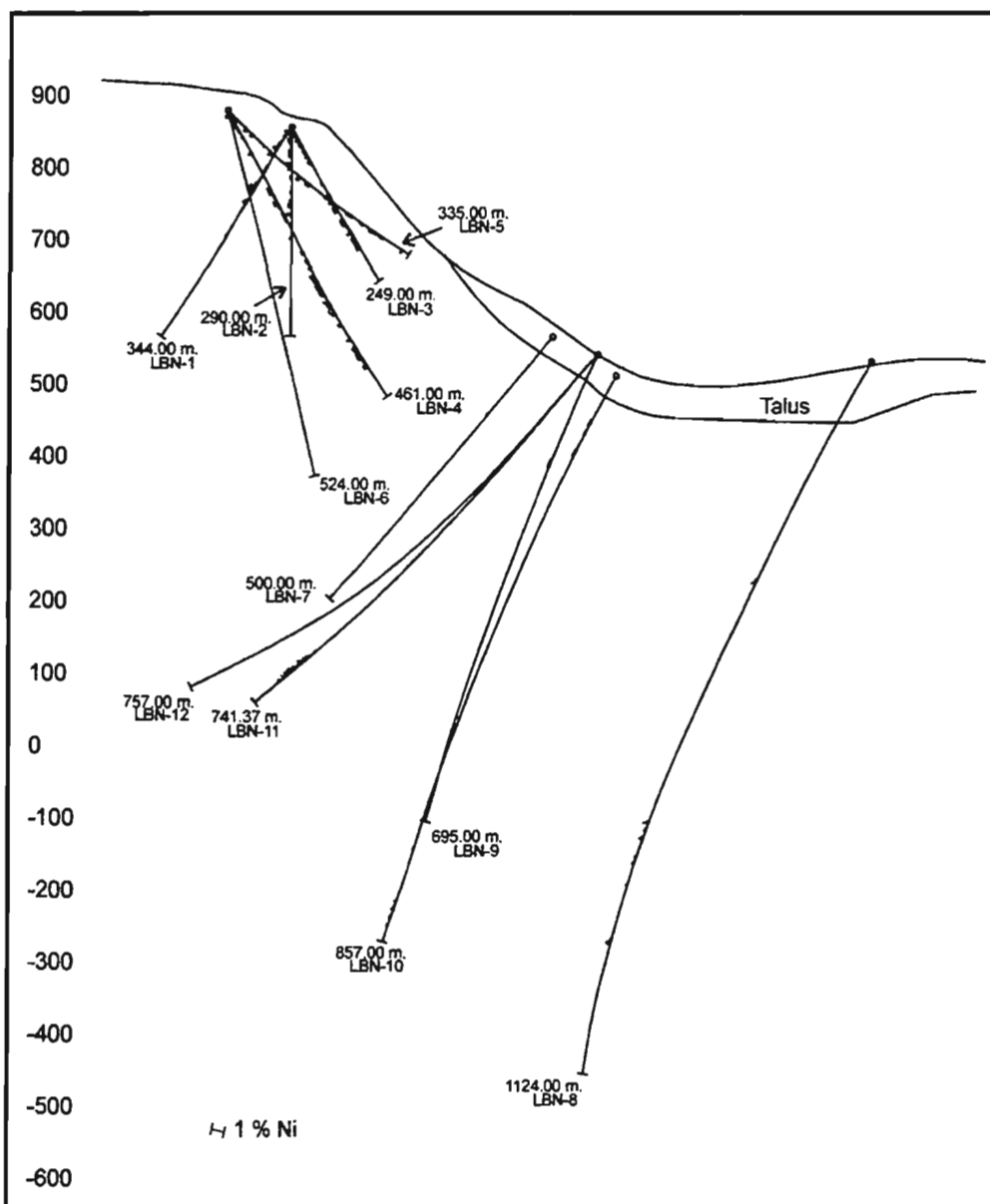


Figure 3.12a Cross section of drill holes from the Cirque grid showing Ni % in sulphide intersections as histograms. View is to the north along section 6323000m N with drill holes projected onto one plane; scale is 1:7,500. Data from LBN-12 are not available at time of study.

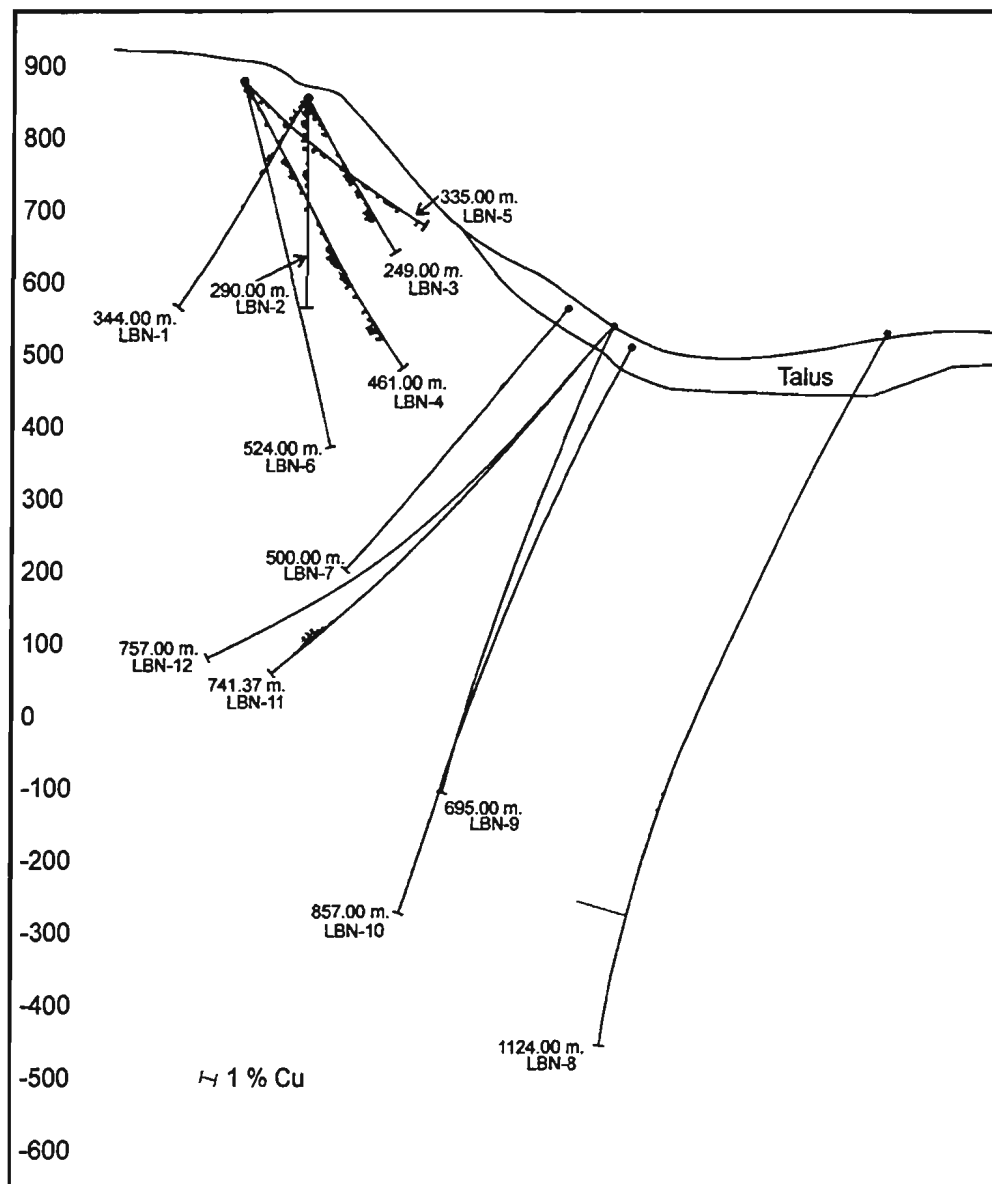


Figure 3.12b Cross section of drill holes from the Cirque grid showing Cu % in sulphide intersections as histograms. View is to the north along section 6323000m N with drill holes projected onto one plane; scale is 1:7,500. Data from LBN-12 are not available at time of study.

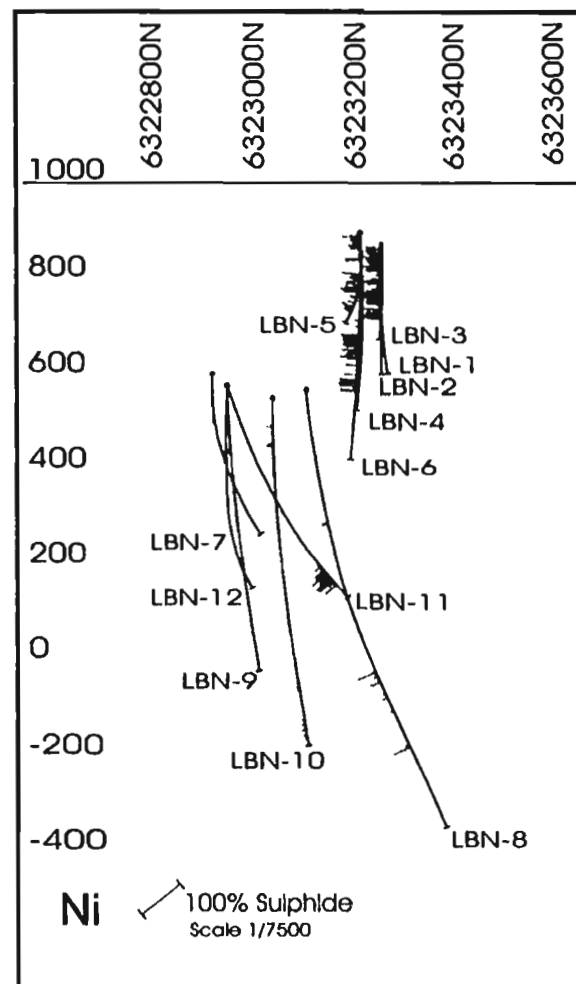
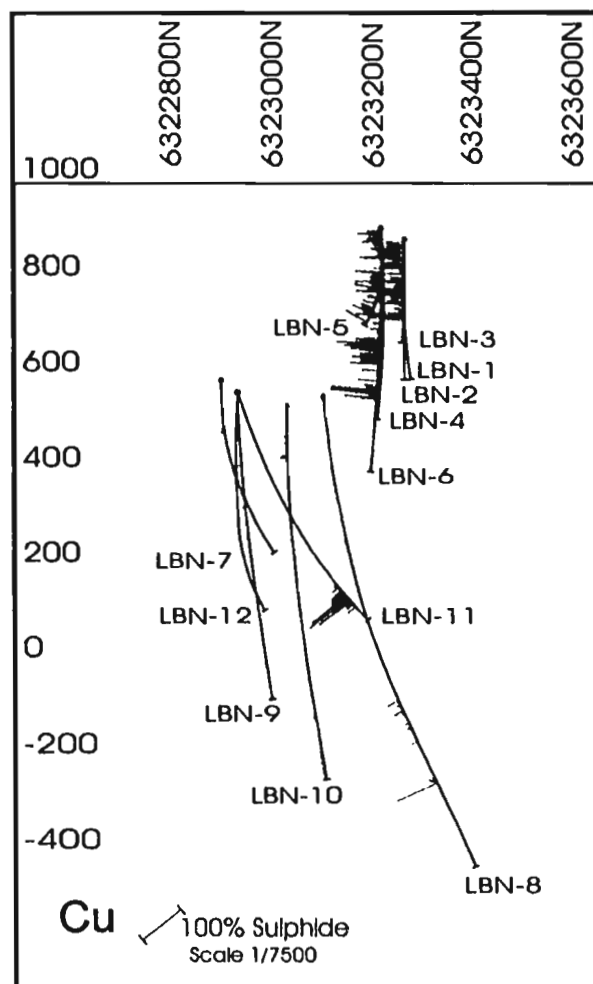


Figure 3.12c Cross sections looking west (along 536100m E) showing weight percent copper and nickel as histograms in sulphide intersections of eleven drill holes. Depth is in metres. Data for LBN-12 are not available.

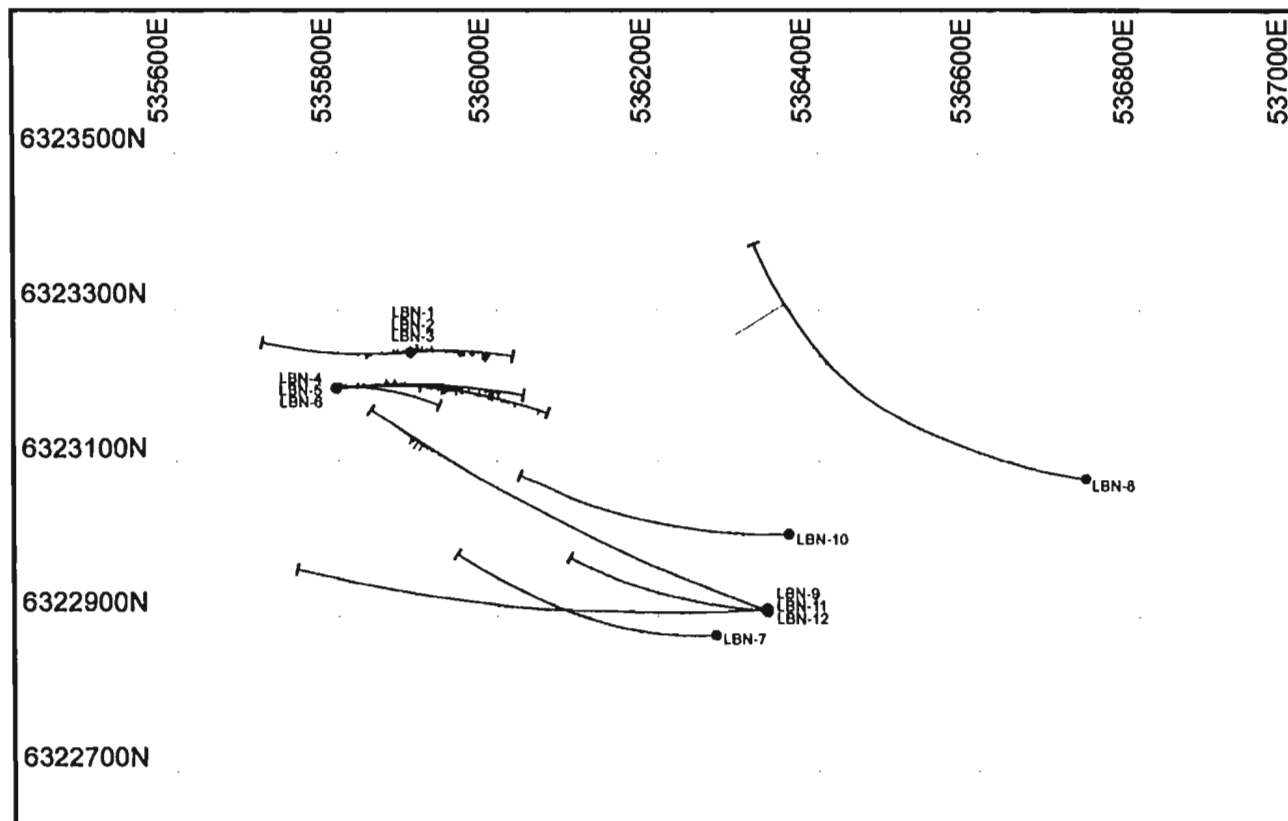


Figure 3.12d Plan view (scale 1:7,500) of eleven drill hole traces from the Cirque grid showing Cu % as histograms. Scale of histogram is 0.25 cm/1%, cutoff at 4 cm. Data for LBN-12 are not available.

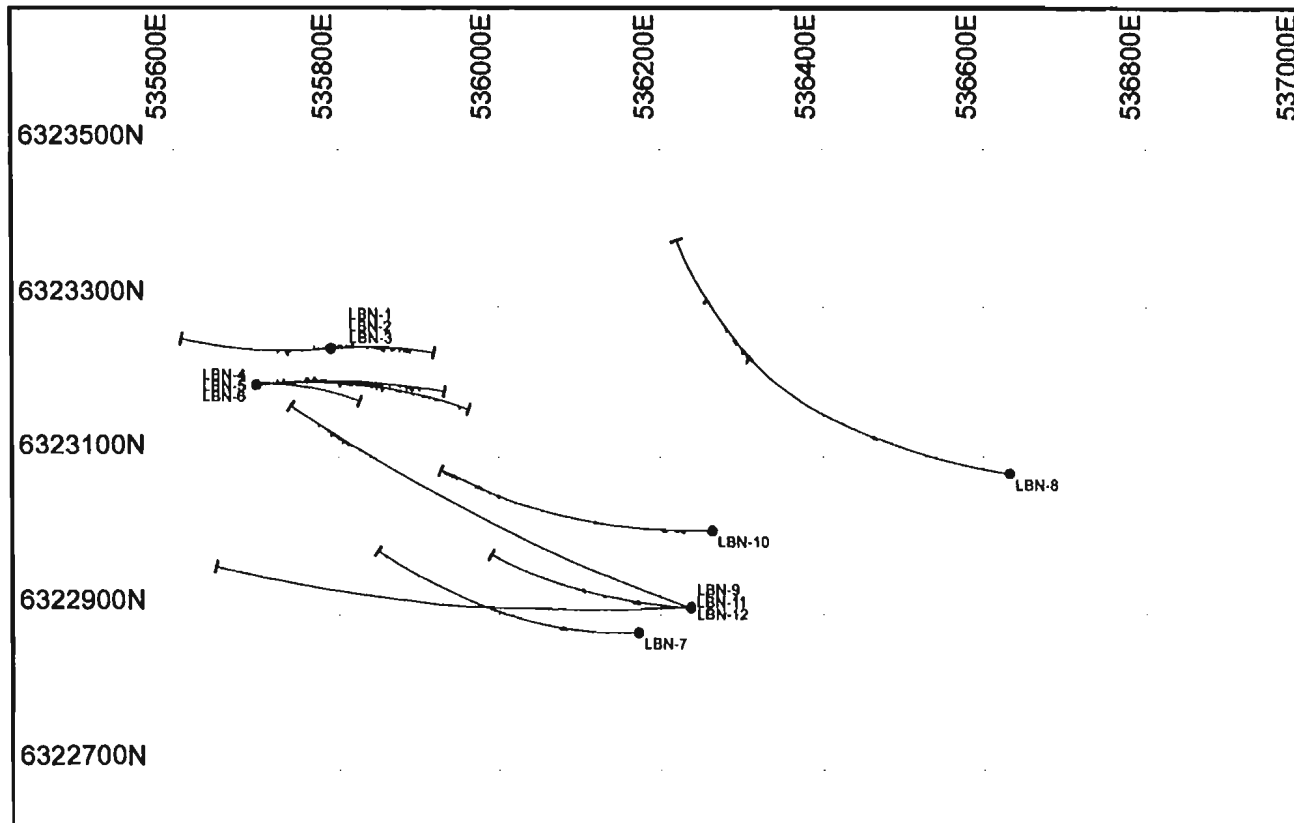


Figure 3.12e Plan view (scale 1:7,500) of eleven drill hole traces from the Cirque grid showing Ni % as histograms. Scale of histogram is 0.25 cm/1%, cutoff at 4 cm. Data for LBN-12 are not available.

properties yielded mean Ni/Cu ratios of 1.79 and 1.49, respectively, however, these values are re-calculated at 100% sulphides.

Assay results of sulphide intersections in drill core are listed in Appendix A2.2 and the average Ni/Cu ratios for each hole are less than two, similar to other Ni/Cu ratios from anorthosite-hosted sulphide occurrences calculated by Kerr and Ryan (*op. cit.*). The intersection with the highest Ni and Cu contents was a very narrow vein (1.5 cm wide) of chalcopyrite and pyrrhotite (20 cm wide sample interval) in drill hole LBN-8 (at 923.92 m) which assayed 0.30% Ni, 3.9% Cu, and 0.14% Co. The best known grade and width combined was in drill hole LBN-4 (at 390.35 m) with 0.28% Ni, 0.44% Cu, and 0.12% Co over 5.1 m (Beesely 1997). High values have also been intersected between 661.0 m and 668.0 m in drill hole LBN-11 of massive and net-textured sulphides (up to 95 % pyrrhotite with <1-1% chalcopyrite). The entire intersection was assayed in sections with the highest Ni and Cu values being 0.54% and 0.18%, respectively, over 0.50 m (75 % sulphides).

Scatter diagrams of core assay Ni and Cu values (Appendix A2.4.1) do not indicate any significant trends or multi-types of mineralization. Except for drill hole LBN-8 and 9 which have sulphide zones with lower Cu and Ni compared to the other holes, Ni and Cu contents seem to homogeneously spread from <0.01 to greater than one percent.

The following three figures (3.13a-c) are compilations of drill hole sulphide intersections with calculated Ni/Cu. Histograms of Ni/Cu for boreholes LBN-1 to 11 are given in Appendix A2.4.2. In each section the ratios do not show any significant variations in Ni or Cu content with depth or to the northwest, but rather reflect the irregularly occurring



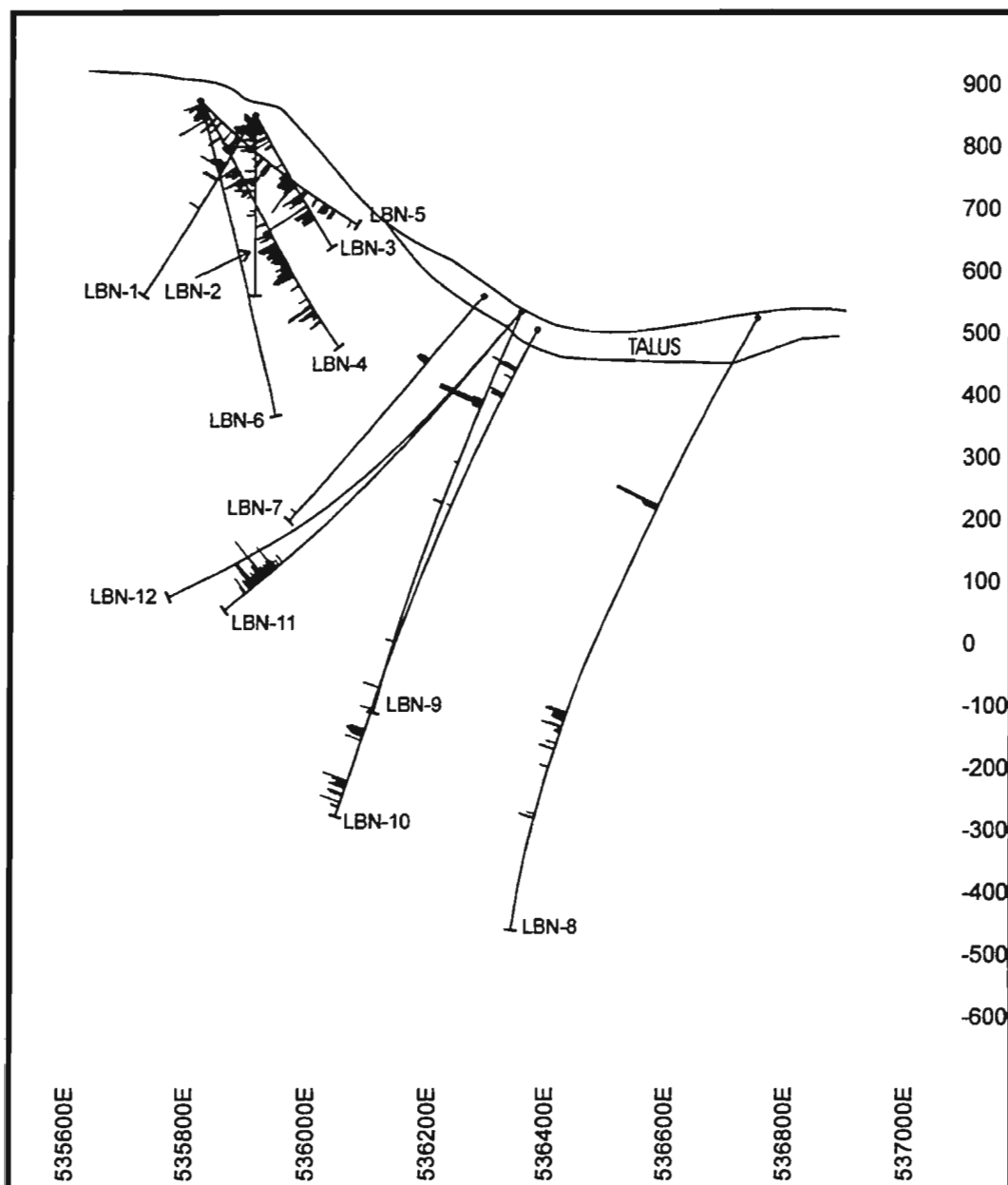


Figure 3.13a Cross sectional view (looking north) along 6323000mN showing histograms of Ni/Cu (histogram scale is 0.25cm/1, truncated at 1 cm). Data from LBN-12 are not available.

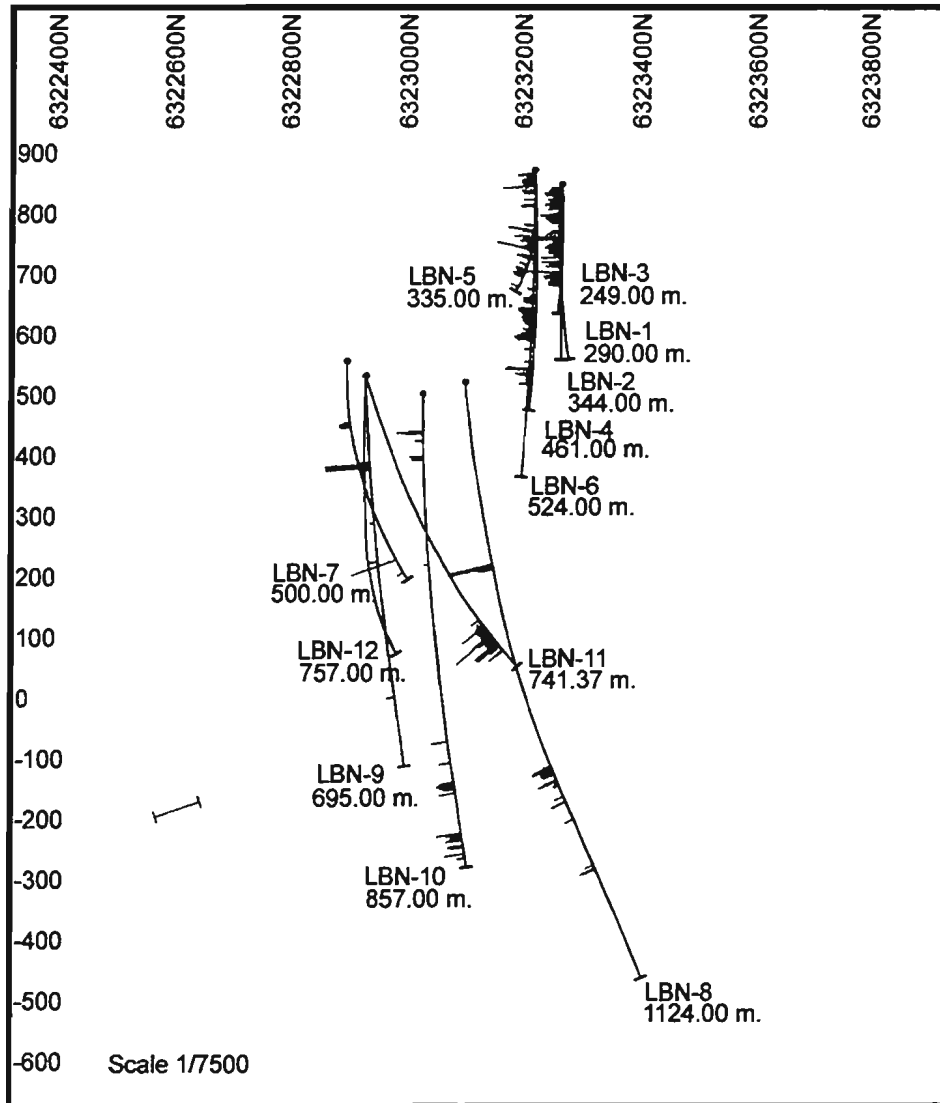


Figure 3.13b Cross sectional view (looking west) along 536100m N of eleven drill holes from the Cirque showing histograms of Ni/Cu (0.25 cm/unit truncated at 4 cm). Data from LBN-12 are not available. Depth is in metres.

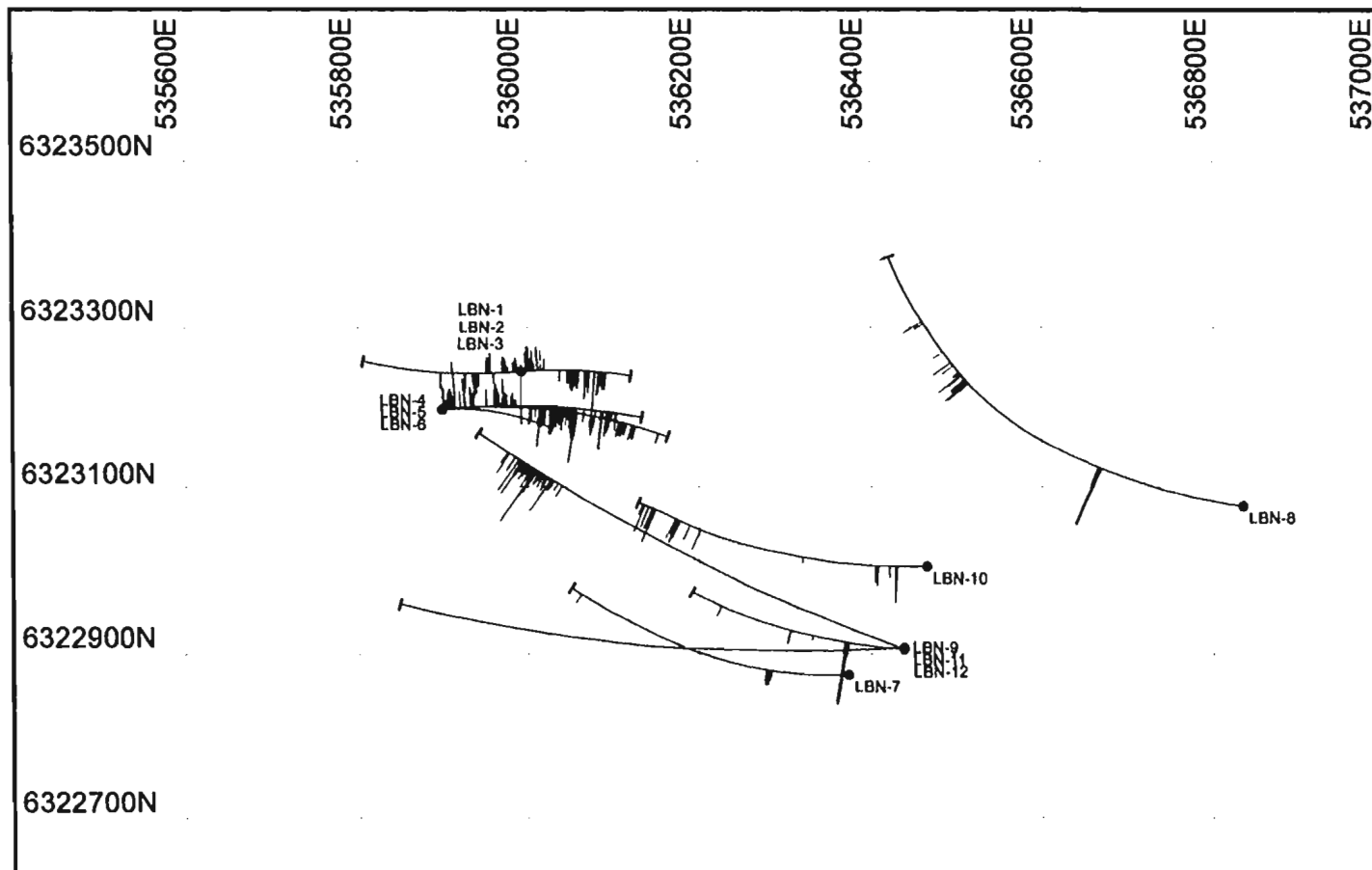


Figure 3.13c Plan view (scale 1:7,500) of eleven drill hole traces from the Cirque grid showing Ni / Cu as histograms. Scale of histogram is 0.25 cm/1%, cutoff at 1.0 cm. Data for LBN-12 are not available.

localized zones of pods and stringers. The 5 m massive sulphide intersection in drill hole LBN-11 and the chalcopyrite-rich vein in drill hole LBN-8, however, do suggest that significant sulphide mineralization may be intersected at depth. The Canadian States sulphide intersections contains significantly more chalcopyrite and nickel (Canadian States Resources *inhouse* data 1996). On the Noranda property (Squires *et al.* 1996, 1997) and other outcrop areas on the Cirque grid, the copper content is locally anomalously higher in veins and as blebs in massive pyrrhotite intersections and areas of disseminated pyrrhotite and chalcopyrite also show anomalously high Cu values. Appendix A2.6 lists the PGE values of core and surface samples assayed at Memorial University using NiS fire assay collection technique followed by the ICP-MS method. Eleven core (drill hole LBN-96-8) samples were analysed in 1996 by Cartaway Resources for Au, Pd, and Pt (whole rock) and the data are presented in Appendix A2.3. All samples had Pd and Pt below detection limit (15 and 30 ppb, respectively). The highest gold value was 35 ppb. Over 30 whole rock samples (drill hole LBN-96-1) have also been analysed by Cartaway Resources in 1996 for multi-trace elements with insignificant results, typically below detection limits.

### **3.6 Interpretation of sulphide mineralization in the Cirque area**

Geophysical results and drill hole intersections suggest that the zone of mineralization is a cylindrically-shaped body of irregular sulphide occurrences steeply plunging to the east. Surface mineralization indicates that this sheet-like body trends to the northwest and mineralization in the cirque wall suggests it to be dipping to the west. Plate 3.33 shows the orientation of the mineralized zone below surface based on contact

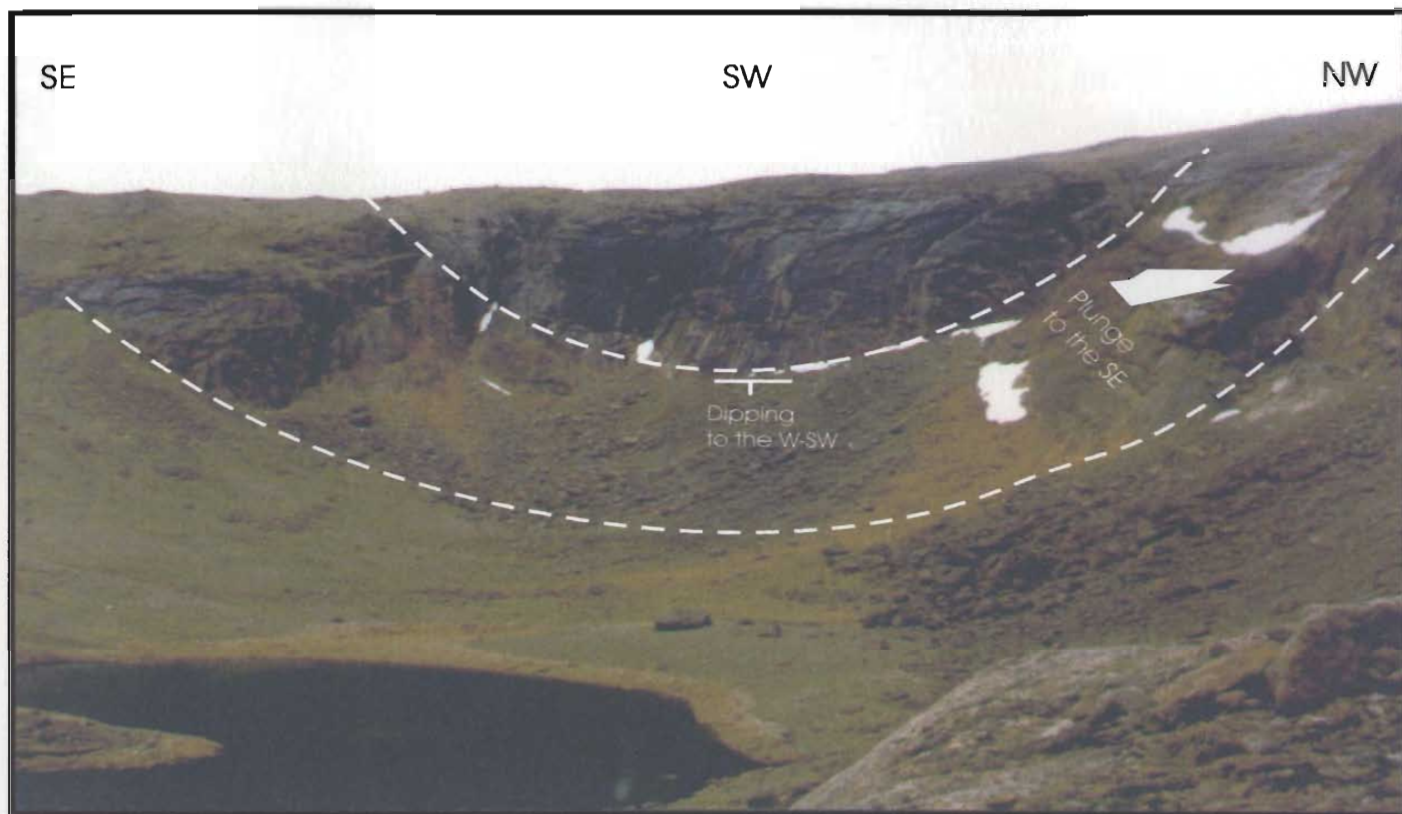


Plate 3.33 View of the Cirque gossan (to the southwest). Dashed white lines are traces of the sulphide mineralization showing it trending to the NW, plunging to the SE, and dipping to the W-SW based on field observations, drill core intersections, and geophysical surveys.

measurements of sulphide lenses and stringers obtained from drill core and outcrop on the Cirque property. From this view, it is clear that the extent of mineralization is not fully defined, particularly below surface, where the sulphides may have originated from an area known to have more mafic rocks (Noranda's Hilltop property; Squires *et al.* 1997).

As discussed earlier, F.P.F Resources (1996) suggested that the sulphides were remobilized along one or more northeast trending faults which formed during a period of Mesoproterozoic NNW-SSE directed crustal extension and rifting, and at the same time, separated to form a Cu-rich melt which moved further upwards and left behind a Ni-rich sulphide melt or "restitute". Although the fault zones have evidence of fluid movement (discussed in Chapter 2) and Gossan #1 and 2 do show a more obscure, wider zone of mineralization in the vicinity of the fault (refer to Figure 3.8), the lack of significant alteration and deformation in the area and the lack of direct sulphide mineralization in or near the fault zones do not support these interpretations of rifting and crustal extension that act as conduits for sulphide movement (F.P.F Resources 1996). This is not to say, however, that this theory is entirely incorrect. The fault zones, and even the northeast trending lineaments, may have acted as conduits at depth and their relationship with sulphide mineralization may not have been clearly observed on the surface. Such turbulent redistribution of sulphide-rich fluids have been reported at Voisey's Bay deposit (Evans-Lamswood 1999; Evans-Lamswood *et al.* 2000), as well at the Sally Malay deposit, Western Australia (Hoatson *et al.* 1998), the Jinchuan deposit (Zongli 1993) and the Sudbury deposit (Naldrett *et al.* 1999). At the Voisey's Bay deposit, a series of rapid injections of metal-



rich, sulphide-bearing mafic magma from an unknown parent magma at depth into existing faults and magma chambers, and not gravity settling, is thought to be the dominant factor of the genesis of the sulphide mineralization (Evans-Lamswood *et al.* 2000). It is possible that the assimilation and brecciation of anorthosite may also support a similar event at the Cirque, just as gneissic breccia within the sulphide-rich conduits is evidence for upwards transport of the sulphide-rich magma at the Voisey's Bay deposit.

The presence of thermally eroded and altered anorthosite indicates that sulphides were injected into a pre-existing anorthositic magma that was either partially or fully crystallized. Movement is best facilitated by a fault or conduit, however, a partially crystallized anorthositic "mush" can also be permeable enough to allow for internal turbulent flow of hot sulphides which assimilated anorthositic xenoliths within the sulphide melt along the way. Localized areas within the anorthosite body may have crystallized enough to result in cracking and brecciation of individual plagioclase crystals. The presence of chalcopyrite along outer contacts of pyrrhotite intersections, as a result of expulsion of Cu from the Fe-rich sulphide phase (Craig and Vaughan 1994) and the lack of a Ni-rich sulphide phase, suggest segregation of the sulphide melt into Cu-rich and Fe-rich phases (F.P.F. Resources 1996; *cf.* Barnes *et al.* 1997) and mobilization of the sulphides from depth (and possibly laterally). Such evidence may indicate the presence of more economic Ni and Cu bearing sulphides at depth near a yet-to-be discovered source magma. Given the interpreted dimensions and orientation of the sulphide mineralized zone at the Cirque property, it seems likely that the source may be located at depth near the conductors at the

Noranda “Hilltop” property to the west. Here, several pyroxenite dykes with pyrrhotite mineralization and subsurface magnetic and conductive anomalies exist in the northeast corner near the boundary with the Cirque property.

Pyroxenite-hosted mineralization on the Noranda property suggests the possibility that later syngenetic magmatic sulphide mineralization formed that was remobilized along the west dipping anorthosite and leuconorite/leucogabbro-leucotroctolitic layers towards the east to precipitate at the Cirque property. Approximately 40 km to the north the OKG prospect on the Castle Rock property, syngenetic, pyroxenite-hosted pyrrhotite mineralization also occurs (Table 3.1 this chapter) with evidence of sulphide mobilization away from the dykes and into the massive anorthosite (Piercey 1998). Kerr (1998) distinguishes the differences of sulphide mobilization on the OKG prospect from that observed on the Cirque property as being due to the relative temperature of the anorthosite at the time of sulphide transport. At the OKG prospect, the Paleoproterozoic anorthosite, being significantly cooler than the hot sulphide melt was more difficult to penetrate, resulting in a limited distance (few centimetres; Piercey and Wilton 2000; Piercey 1998) of sulphide injection (Kerr 1998). The Cirque area, however, with the existing Mesoproterozoic rocks, perhaps still semi-solid, allowed for greater erosion of the plagioclase crystals and thus longer distances for sulphide transfer (*op. cit.*). While the connection between the pyroxenite dykes on the Noranda property is untested at this time, it does allow for possibilities for a potential host of the epigenetic sulphide mineralization in the Cirque area.

## CHAPTER 4

### GEOCHEMISTRY

#### 4.1 Introduction

This chapter presents the results from extensive geochemical analyses conducted on samples from drill core, outcrop, and talus by both the author at Memorial University and Cartaway Resources; numerous samples were analyzed for major and trace elements by several laboratories for Cartaway Resources in 1996 and 1997. The new data on major and trace elements, and rare earth elements (REE) were derived from *X-ray fluorescence* (XRF) and the *inductively coupled plasma - mass spectrometer* (ICP-MS) techniques, respectively at the Department of Earth Sciences, Memorial University. Rb - Sr and Sm - Nd radiogenic isotopes ratios were analyzed at the AURIF labs, Memorial University. All data are listed in Appendix A3 and a description of each analytical method is given in Appendix A1.

Based on petrographic studies, the samples were subdivided into two data sets to distinguish between non-sulphide bearing and sulphide-rich geochemical natures (for instance, to prevent misinterpretations of Fe contents due to the presence of pyrrhotite and pyrite in mineralized samples vs. Fe from pyroxene, fayalite, and magnetite in unmineralized samples). A visual estimate of 5 % sulphide (pyrite, pyrrhotite, and/or chalcopyrite) was the cutoff used to separate the unmineralized (low sulphur) rocks from the mineralized (high sulphur) rocks. Results from the XRF analyses (S, Fe, Ni, and Cu

contents) of the samples reflect this subdivision. A few “non- sulphide bearing” samples have anomalously high Ni and Cu contents relative to the other samples; these samples are included in both datasets.

Additional geochemical data from other properties (Noranda’s “Hilltop”, Canadian States’ Licence #1514M, and Castle Rock’s ‘OKG’ prospect) are presented for comparison. Samples from Kerr (*unpublished data*) were subdivided by him into sets based on percentages of sulphide mineralization. Although not observed by the author, his sulphide-poor samples consist of textural (grain size) and mineralogical varieties of anorthosites, related mafic rocks, pyroxenites, and ferrodiorites similar to the lithologies at the Cirque (Kerr, *pers comm.* 1999). Re-assignment of some samples from Kerr (*unpublished data*) by the author is based on geochemical plots and not petrographic descriptions. Due to the close proximity of the “Hilltop” and Canadian States sample locations, these rocks are believed to have a similar crystallization age as those from the Cirque property (*circa* 1.30 - 1.5 Ga; Emslie 1977; Ashwal and Wooden 1983).

Geochemical plots from the OKG property were derived from Piercey (1998). This prospect, approximately 35 kilometers northeast of the Cirque property, consists of Paleoproterozoic anorthosites, leuconorites, and variably foliated granitoids intruded by Mesoproterozoic pyroxenite dykes ( $\geq 70\%$  orthopyroxene) which host 5-50 % disseminated pyrrhotite (Piercey 1998). Due to the age differences of the host rocks at OKG compared to those at the Cirque, only the Mesoproterozoic pyroxenites are used for comparative study here.

Additional data gathered from various workers in the NPS (Emslie *et al.* 1994; Emslie 1996; Emslie *et al.* 1997) are used in this chapter for comparisons of multi-element and radiogenic isotopic geochemistry. Figure 4.1 is a map showing the general locations of all samples used.

## 4.2 Silicate geochemistry

Due to the cumulate nature of the anorthosite and related rocks, silicate geochemistry is of limited use for determining the geochemical nature of the parental magma. Though fractionation trends can easily be determined using most major and trace elements, Rollinson (1993) and Pearce (1996) caution that geochemical data may reflect elevated compatible element concentrations in rocks with an abundance of phenocrysts. Magma mixing at depth or crustal assimilation of country rock material will also affect geochemical distributions in a rising magma and create even greater divergences from parental magma characteristics. Because cumulate minerals form in an evolving magma with assimilation and crystal fractionation, the geochemical signatures may be misunderstood as reflecting the true melt composition. For instance, Pearce (1996) suggests that since Al generally accumulates in plagioclase, Sc generally accumulates in clinopyroxene, and Ni generally accumulates in olivine (in a sulphur-poor melt), any rocks with >20 wt %  $\text{Al}_2\text{O}_3$  will have significant plagioclase (anorthosite and related mafic rocks), with >50 ppm Sc have significant accumulated clinopyroxene (mafic, pyroxenite, and ferrodiorite rocks), and anorthosite samples with >200 ppm Ni have significant accumulated olivine or Ni-rich

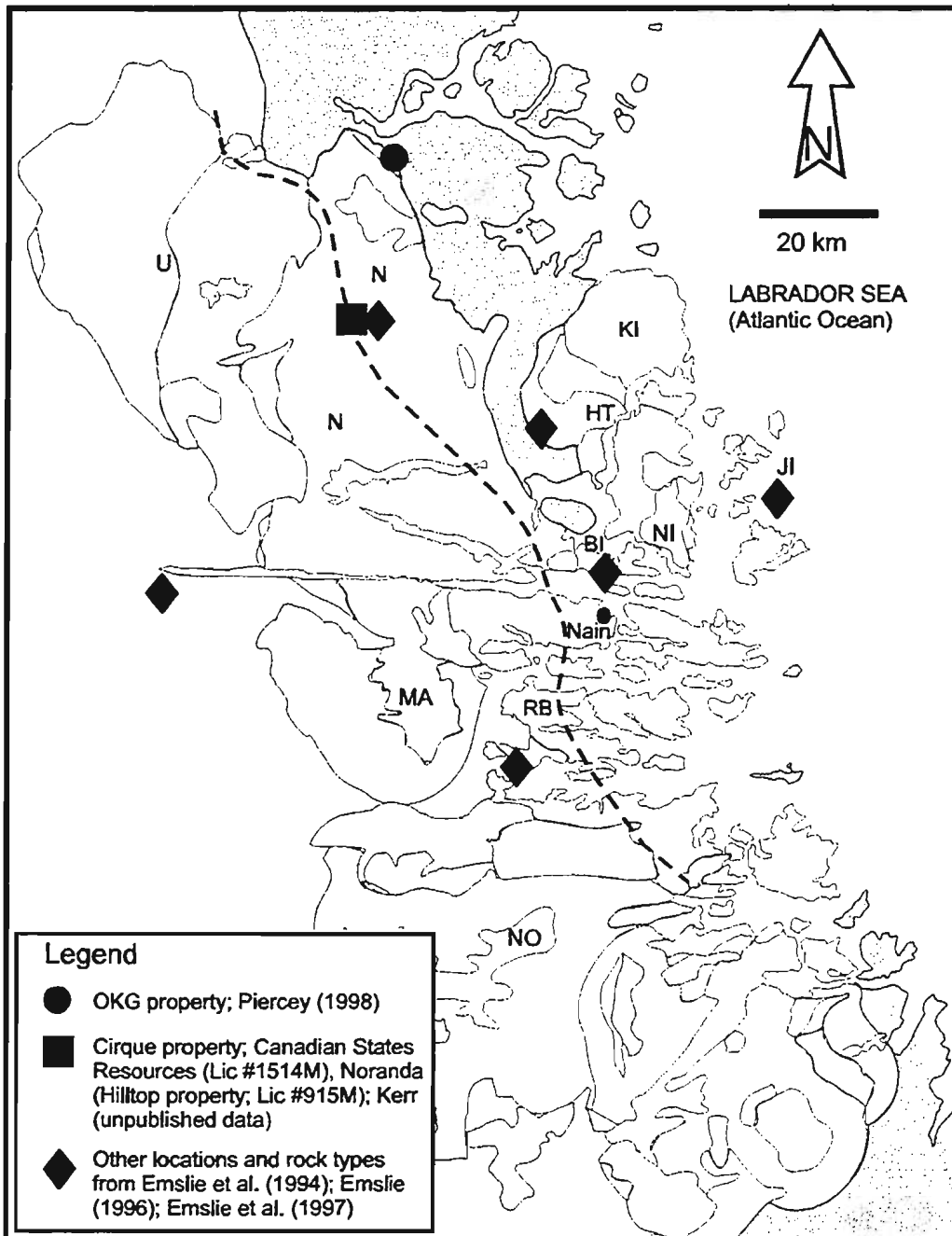


Figure 4.1 Location map showing the general locations of geochemical samples used for comparison with the Cirque rocks. Dashed line is the approximate location of the suture line separating the Nain Province (dark grey) and the Churchill Province (light grey). RB = Reid Brook intrusion, BI = Barth Island intrusion, HT = Hettasch Intrusion, KI = Kiglapait Intrusion, JI = Jonathon Island intrusion. Figure is adapted from Emslie et al. (1994) and Emslie (1996).



sulphide and should not be included with geochemical data used for representation of true melt material but rather as indicators of high abundances of respective cumulate material and pyroxene megacrysts. In the following sections all the geochemical data generated were used to examine the trend of crystal fractionation of the melt and the formation of cumulate minerals; in no way do the data represent true melt compositions.

Tables 4.1a and 4.1b list the concentration ranges for major and selected trace elements in the sulphur-poor rocks as determined by XRF. Rock type designation of the samples was based on modal mineralogy from hand samples and polished thin sections (discussed in Chapter 2). The anorthosites are subdivided into Bleached anorthosite dykes and the anorthosites with <10 % pyroxene; few anorthosites have patchy >10 % pyroxene. Most of the anorthositic samples have <2 % disseminated pyrrhotite, minor chalcopyrite, and the plagioclase crystals are variably altered but not to any great extent overall. The geochemical data support the petrological designations and allow for explanations of any undefinable samples. Overall, the anorthosite samples generally have relatively elevated concentrations of  $\text{Al}_2\text{O}_3$ , Rb, and Sr and the associated mafic rocks have similar geochemical features but with variable  $\text{FeO}^*$ , MgO, CaO, and MnO proportional to modal percentages of pyroxene, and Ti, Fe, V, and Cr proportional to oxide mineralogy. The ferrodiorites generally have the highest concentrations of  $\text{FeO}^*$ ,  $\text{P}_2\text{O}_5$ ,  $\text{TiO}_2$ , V, and Y reflecting elevated abundances of Fe-Ti oxides, apatite, and pyroxene.

Table 4.1a Ranges of major element concentrations (wt %) in sulphide-poor rock types from the Cirque property.

Rock Type	Na <sub>2</sub> O	MgO	Al <sub>2</sub> O <sub>3</sub>	SiO <sub>2</sub>	P <sub>2</sub> O <sub>5</sub>	K <sub>2</sub> O	CaO	TiO <sub>2</sub>	MnO	FeO*	S	[Mg]
Anorthosite (dominantly <10%pyx) n = 42	3.41- 5.67	0.08- 1.93	18.98- 29.50	45.65- 57.48	0.01- 0.46	0.26- 1.26	5.72- 11.96	0-4.01	0.01- 1.79	0.92- 13.58	0.01- 8.08	1.15- 72.20
Noranda anorthosite, n=1	3.52	0.31	26.22	46.50	0.01	0.32	10.63	0.06	0.01	1.25	0.18	30.97
Anorthosite (Bleached) n = 3	4.22- 5.08	0.47- 0.49	27.48- 29.09	53.29- 55.18	0.01- 0.04	0.39- 0.59	9.28- 11.16	0.07- 0.37	0.01- 0.02	1.07- 1.22	0.01- 0.10	38.10- 41.13
Leucotroctolite n = 3	3.33- 3.78	3.99- 5.90	24.66- 22.55	49.43- 48.04	0.06- 0.10	0.39- 0.41	10.27- 9.60	0.41- 0.89	0.09- 0.12	5.58- 7.99	0.03- 0.08	51.54- 52.79
Leuconorite/ Leucogabbro n = 6	3.09- 3.87	3.68- 6.47	19.80- 23.65	46.85- 52.56	0.02- 0.12	0.37- 0.46	7.23- 9.90	0.24- 3.72	0.10- 0.20	6.42- 9.21	0.01- 1.20	45.87- 54.15
Ferrodiorite n = 11	0.35- 3.24	1.65- 6.59	2.28- 20.18	22.04- 47.52	0.14- 3.58	0.01- 0.56	4.47- 12.18	2.69- 10.51	0.14- 0.45	12.51- 42.22	0.01- 4.49	8.96- 34.74
Noranda ferrodiorite, n=1	0.79	2.27	6.59	18.24	0.35	0.14	3.70	8.70	0.19	34.53	3.72	9.05
Pyroxenite n = 2	0.17- 0.26	8.84- 14.69	0.85- 1.68	44.42- 50.23	0.01- 0.05	0.01	7.80- 17.37	0.59- 0.87	0.29- 0.98	12.21- 30.35	0.05- 1.53	30.61- 64.56

Table 4.1b. Range of selected trace element concentrations (ppm) for low-sulphide bearing rocks.

Rock Type	Sc	V	Cr	Ni	Cu	Ga	Rb	Sr	Y	Nb	Ce
Anorthosite (dominantly <10% pyx) n = 42	0-15	0-187	0	0-841	3-1661	22-33	0-6	754-1378	0-7	0-4.6	0-44.41
Noranda anorthosite, n=1	9	bdl		12	16	27	1	1111	0.36	0.27	10.32
Anorthosite (Bleached) n = 3	36599	0	0	0	36608	24-28	0	887-1229	0	0-1.2	4.74-26.12
Leucotroctolite n = 3	36656	33-42	34-41	35-61	36-44	22-24	2	819-889	36559	1.0-1.9	0-1.15
Leuconorite/ Leucogabbro n = 6	36697	43-142	33-108	0-85	36628	19-26	36526	656-884	0	0-4.2	0-28.98
Ferrodiorite n = 11	20-91	103- 1998	0-1449	0-1055	5-2893	18-35	0	42-766	7-75	1.9-19.7	0-137.97
Noranda ferrodiorite, n=1	24	1654	1199	873	2395	29		270	8	16.3	9.69
Pyroxenite n = 2	103-11	64-230	16-464	0-54	21-119	36528	bdl	36768	16-22	0.9-1.2	bdl-33.02

Note: Maximum Ni and Cu values are high due to <1 % fine-grained disseminated pyrrhotite +/- pentlandite  
 Sulphide-poor anorthosite has a maximum of ~ 30 ppm Ni (<1% diss po)  
 bdl = below detection limit

#### 4.2.1 Magnesian number

The MgO contents (in weight percent) of the rock types reflect the various modal percentages of cumulus orthopyroxene and olivine. The *magnesium number* or *magnesium - iron ratio* is calculated as the Mg # or  $[Mg] = (MgO/[MgO+FeO^*]) * 100$  and reflects crystal fractionation in basaltic melts. Generally, rocks with [Mg] values less than 60 are derived from a magma that has undergone fractionation, whereas those with [Mg] values greater than 60 are unfractionated and represent primitive mantle material. Since the Mg and Fe contents are relatively elevated in the initial mafic magma, fractionation of plagioclase to form anorthositic bodies will lead to a low [Mg] and any ferromagnesian crystal formation from the mafic melt should be reflected by a greater lowering of the Mg contents compared to Fe.

Samples from the Cirque property have a wide range of MgO contents (from 0.08 to 14.69 wt%) due to the variable presence of the MgO-rich minerals (Table 4.1a), most specifically orthopyroxene. High iron content, reflected by the presence of oxides in the ferrodiorite dykes, lowers the relative MgO contents in the dykes and results in lower [Mg] values. All rock types, except one of the two pyroxenite samples, have [Mg] values below 60, indicating that they were all derived from a fractionated magma (Table 4.1a).

Although the [Mg] values have a broad range (1.15-72.20), most of the samples are more fractionated than the Bleached anorthosites (38.10-41.13). A [Mg] value for one anorthosite sample is anomalously high (72.20) suggesting a primitive magma source. However, the lack of pyroxene, olivine, and other cumulus minerals suggest that the sample

is actually highly fractionated; it appears that significantly low Fe and Mg contents of this sample incorrectly produce a high [Mg] value. The broad variation of the [Mg] in the anorthositic rocks suggest variability of the anorthositic magma (local pyroxene-rich zones and layers) and different types of anorthosites which intrude each other. Such a suggestion would be supported by the presence of at least three types of anorthositic rocks on the Cirque property (discussed in Chapter 2).

The leuconorite/leucogabbro and leucotroctolitic samples, containing cumulate pyroxene, olivine, and oxide minerals, were likewise derived from a fractionated magma, however, they seem to be the least fractionated with [Mg] values ranging between 45 to 55. The ferrodiorites have lower [Mg] values than the leuconorite/leucogabbro and leucotroctolitic samples, thus indicating a fractionated magma source for the ferrodiorite rocks. One of the two pyroxenite samples (91) appears to be unfractionated with a [Mg] value greater than 60. Petrographically and geochemically, this pyroxenite is different from the other rocks types suggesting either a separate magma source or that the other rock types may be fractionates from a magma with a similar composition to this pyroxenite. As mentioned earlier, however, caution must be made when interpreting the geochemistry of such cumulate-rich rocks.

#### **4.2.2 Discrimination diagrams**

The sulphide-poor mafic rocks, ranging from anorthosite through to ferrodiorite, are dominantly subalkaline with variable percentages of pyroxene, especially orthopyroxene.

Figure 4.2, an AFM plot from Irvine and Baragar (1971), illustrates the different fields for the rock types ranging from MgO-poor anorthositic rocks to the relatively FeO- and MgO-rich leuconoritic-leucogabbroic-leucotroctolitic rocks, and the FeO-rich ferrodioritic rocks. The anorthositic field has a broad range in FeO contents reflecting the variable disseminated pyrrhotite mineralization. Samples with greater abundances of pyroxene and oxides plot further along the MgO and FeO\* sides of the triangle. An anorthosite sample (BWO2) from Noranda's "Hilltop" property is similar to the Cirque anorthosites. The linear trend along the FeO\*- alkali side of the triangle seems to trace, from the bottom to the top, the unmineralized Bleached anorthosites with less pyroxene and up to 2 % disseminated pyrrhotite, through to the more alkaline nature of some anorthosites reflecting their petrology and antiperthitic textures (exsolved alkali feldspars from the Ca-rich feldspars). Since there are only two samples, the pyroxenite field has a dashed outline to indicate that it is not fully defined. The leuconorite/leucogabbro and leucotroctolite samples plot in the calc-alkaline range, whereas the most pyroxene and oxide- rich rocks (pyroxenite and ferrodiorite) and some anorthosites are tholeiitic.

Figures 4.3 and 4.4 are AFM plots of data from Kerr (*unpublished data*) and Piercey (1998), respectively. In each ternary diagram the rock types plot in fields corresponding to those of the Cirque rocks in Figure 4.2. (Some mafic samples from the Canadian States Resources were reassigned to different lithologies from those defined by Kerr based on geochemical data and plot results). One pyroxenite (?) sample from Noranda's "Hilltop" property plotted near the FeO\* apex indicating the gossanous surface described by Kerr



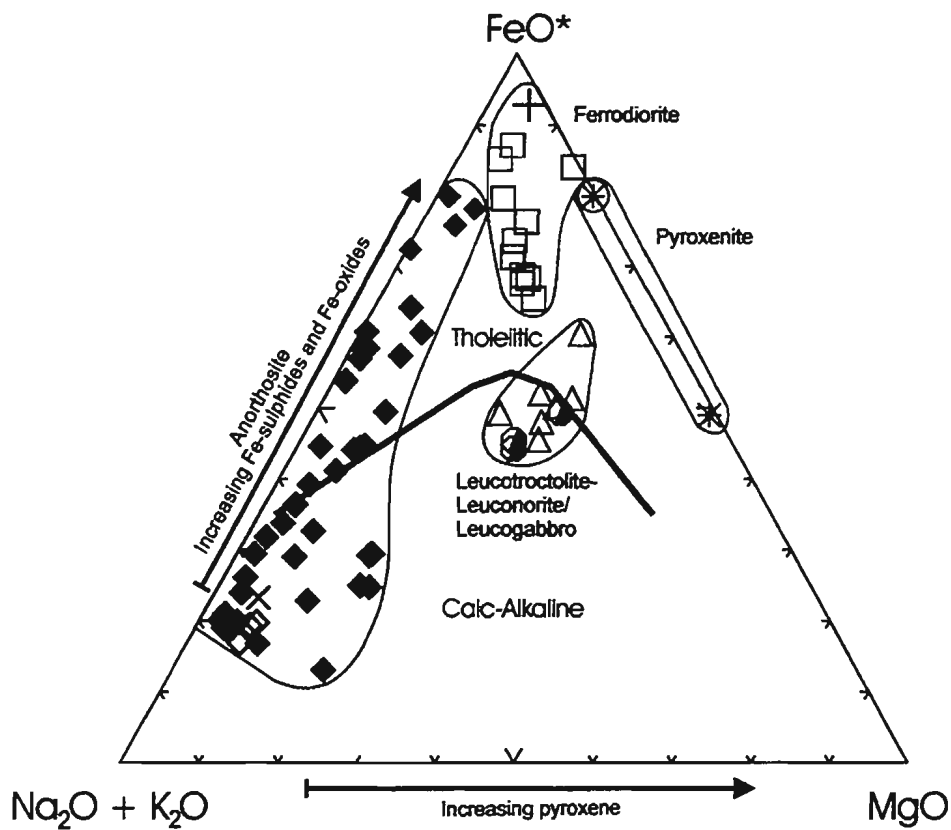


Figure 4.2 An AFM discrimination diagram (wt%) from Irvine and Baragar (1971) showing fields of rock types from the Cirque property. Anorthosite (<10% pyroxene) =  $\diamond$ ; Bleached anorthosite =  $\diamond$ ; leuconorite/leucogabbro =  $\triangle$ ; leucotroctolite =  $\blacktriangle$ ; ferrodiorite =  $\square$ ; pyroxenite: 91 =  $\ast$ , 117 =  $\otimes$ . For comparison, one anorthosite (X) and one ferrodiorite (+) sample from the neighbouring Noranda property are plotted.

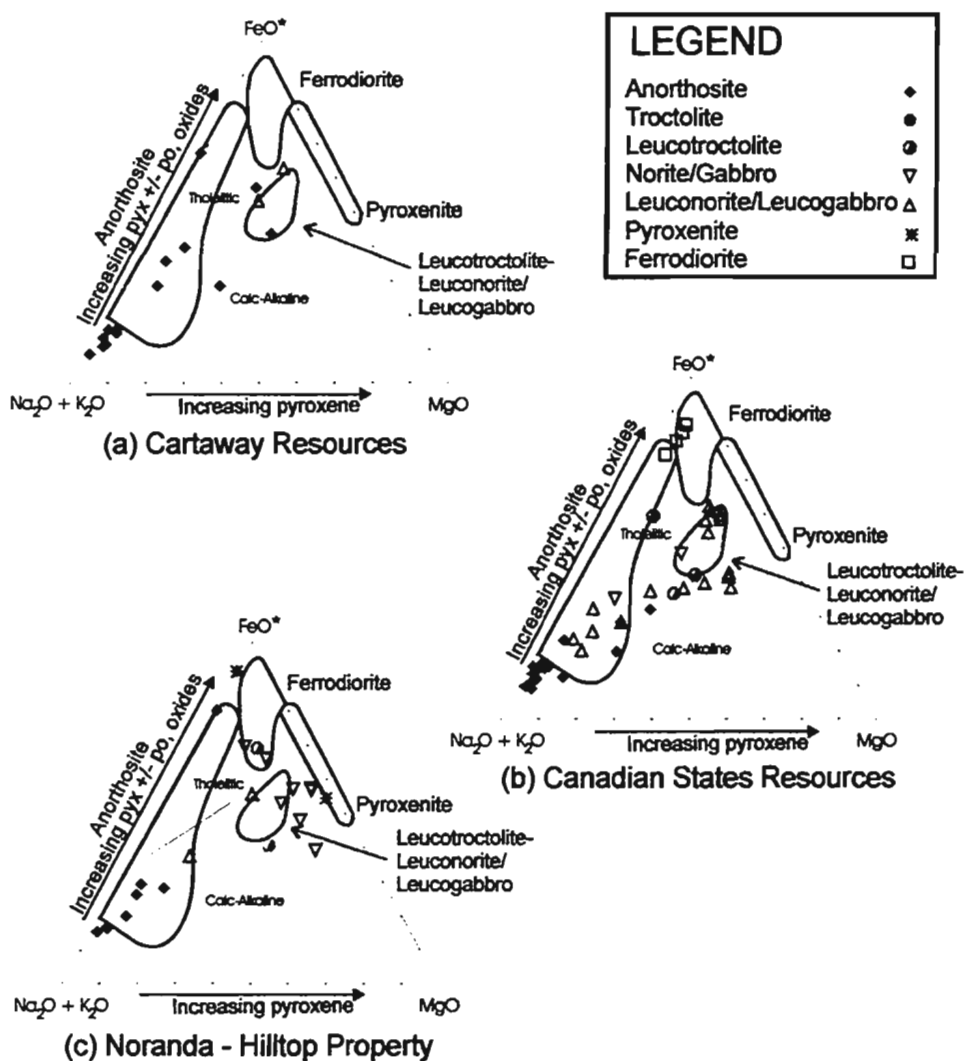


Figure 4.3 AFM diagrams (Irvine and Baragar 1971) for mafic rocks collected by Kerr (unpublished data) from (a) Cartaway Resources, Cirque property, (c) Canadian States Resources - Licence #1514M, (north of the Cirque property), and (c) Noranda's "Hilltop" property - Licence #915M (west of the Cirque property). For comparison, fields of rock units and fractionation trends are from the Cirque samples (this study; Figure 4.2).

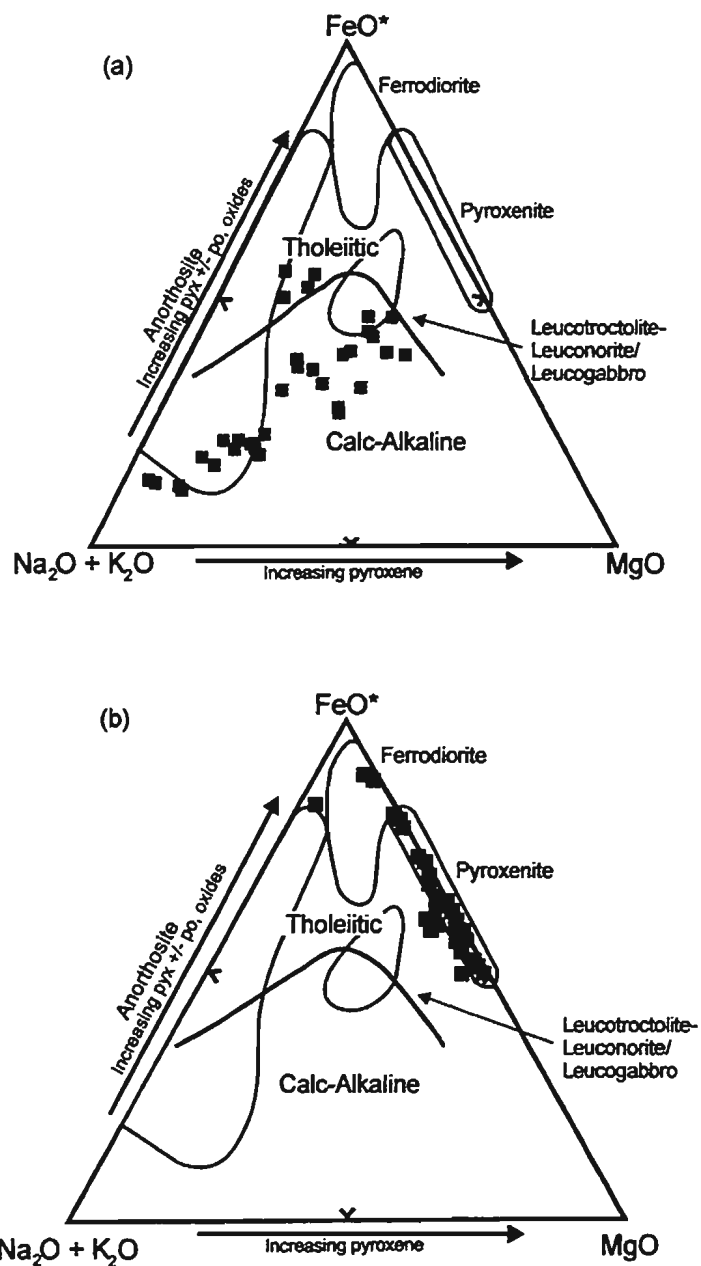


Figure 4.4 AFM plots from Piercey (1998) of (a) Paleoproterozoic anorthositic and Mesoproterozoic pyroxenitic rocks from the OKG property. The grey fields are the units outlined by the Cirque rocks (Figure 4.2). pyx = pyroxene, po = pyrrhotite

(*unpublished data*) and lower concentrations of MgO, Sc, and Zr, relative to the more pyroxene and oxide-rich varieties, suggest a high-Fe anorthosite. The Paleoproterozoic anorthosites from the OKG property (Figure 4.4a) described by Piercey (1998), are more MgO-rich than those of the Cirque property, possibly reflecting a different genetic history. The Mesoproterozoic pyroxenite samples from Piercey (1998), however, show similar geochemistry as that from the Cirque area (Figure 4.4b).

The linear trend of the Cirque samples along the alkali-FeO\* side of the triangle suggests a common geochemical genetic magma which traces the crystal fractionation trend of the aluminous magma. The leucotroctolite and leuconorite / leucogabbro samples are separate and may have originated from either another magma pulse or as an evolved parent from which the anorthosite formed. This plot, however does not provide enough information to extrapolate any further about the origin and evolution of the parental magma. Given the genetic model of the AMCG (Emslie *et al.* 1994; refer to Chapter 1 this study), it is possible that several aluminous magma pulses may be represented by separate clusters of rock types. The geochemistry of each type, however, is uniform (*i.e.* there are not several clusters of any single rock type) and since the genetic model assumes uniform evolution of the AMCG (with varying degrees of contamination), it is assumed that these anorthositic rock types at the Cirque property originate from the same Al-rich magma.

#### **4.2.3 Bivariate plots of MgO versus major and trace elements**

Bivariate plots of MgO contents versus those of other major elements are useful in

determining the effects of crystal fractionation in a mafic magma. More specifically, as a result of crystal fractionation, the Mg-rich solid phases in equilibrium with a mafic melt will change in composition as the concentrations of compatible and incompatible major and trace elements increase or decrease with crystal formation (particularly olivine, plagioclase, orthopyroxene, clinopyroxene, apatite, opaque oxides and sulphides). Figure 4.5 illustrates plots of MgO versus (a) SiO<sub>2</sub> wt%, (b) TiO<sub>2</sub> wt%, (c) Al<sub>2</sub>O<sub>3</sub> wt%, (d) FeO\* wt%, (e) K<sub>2</sub>O wt%, (f) P<sub>2</sub>O<sub>5</sub> wt%, (g) Sc (ppm), (h) Cr (ppm), (i) Sr (ppm), (j) V (ppm), (k) Ni (ppm), and (l) Cu (ppm). Each plot illustrates the trend of crystal fractionation of the more compatible elements of rocks from the Cirque area (including one anorthosite sample and one ferrodiorite sample from the neighbouring Noranda's "Hilltop" property; Licence #915M), with the more incompatible elements being concentrated in the residual liquid. One of the two pyroxenites (91) plots as most closely approximating a parental magma from which leucotroctolite/leucogabbro/leuconorite fractionated. Plagioclase accumulation resulted in anorthosite formation. According to Emslie *et al.* (1994)'s model of AMCG formation, the remaining liquid from the crystallization of anorthositic and mafic rock formed the ferrodiorite rocks.

As discussed in Chapter 2, the Kiglapait Intrusion consists of a large layered single intrusion of high Al and Fe basalt which crystallized to form a Lower Zone of troctolite with cumulate plagioclase and olivine, and an Upper Zone with cumulate layers of augite, titanomagnetite, pyrrhotite, apatite, and ternary feldspar or mesoperthite (Morse 1969; 1981; see Figure 2.5). Since crystallization occurred in a closed system over a period of about one

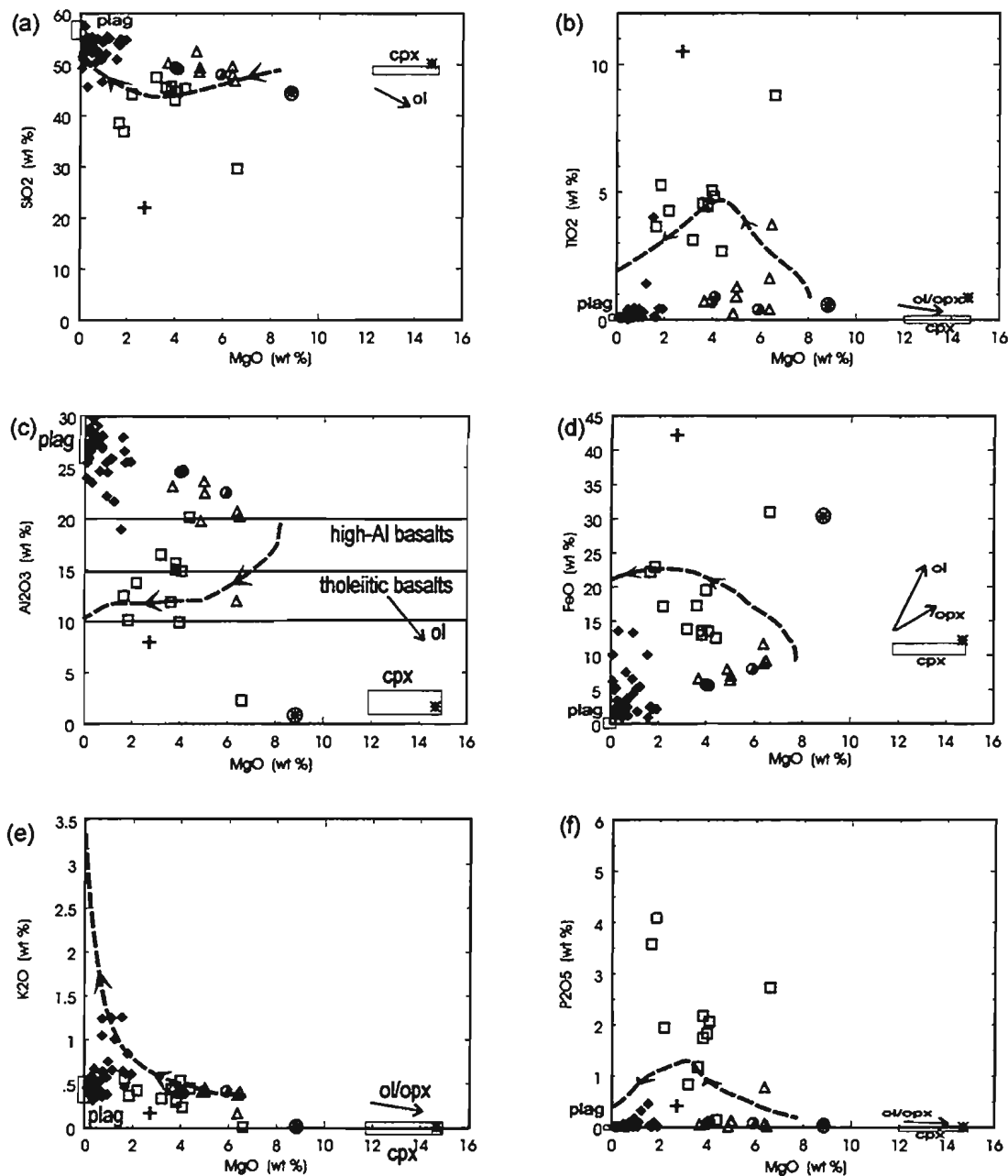


Figure 4.5 MgO (wt%) versus major elements for the Cirque rocks. Anorthosite (<10% pyroxene) = ♦; Bleached anorthosite = ◇; leuconorite/leucogabbro = Δ; leucotroctolite = ⊙; ferrodiorite = □; pyroxenite: 91 = ✱; 117 = ⊗. Noranda samples: anorthosite = ✕; ferrodiorite = +. The dashed line denotes the trend of the closed system fractionation of a troctolitic magma modelled after the Kiglapait Intrusion. The arrows indicate the direction of crystal fractionation during cooling. The general compositional fields of cumulate phases (plagioclase and clinopyroxene) are shown as shaded boxes. Those fields beyond the plot boundaries (olivine and orthopyroxene) are shown with arrows (from Scoates and Mitchell 2000).



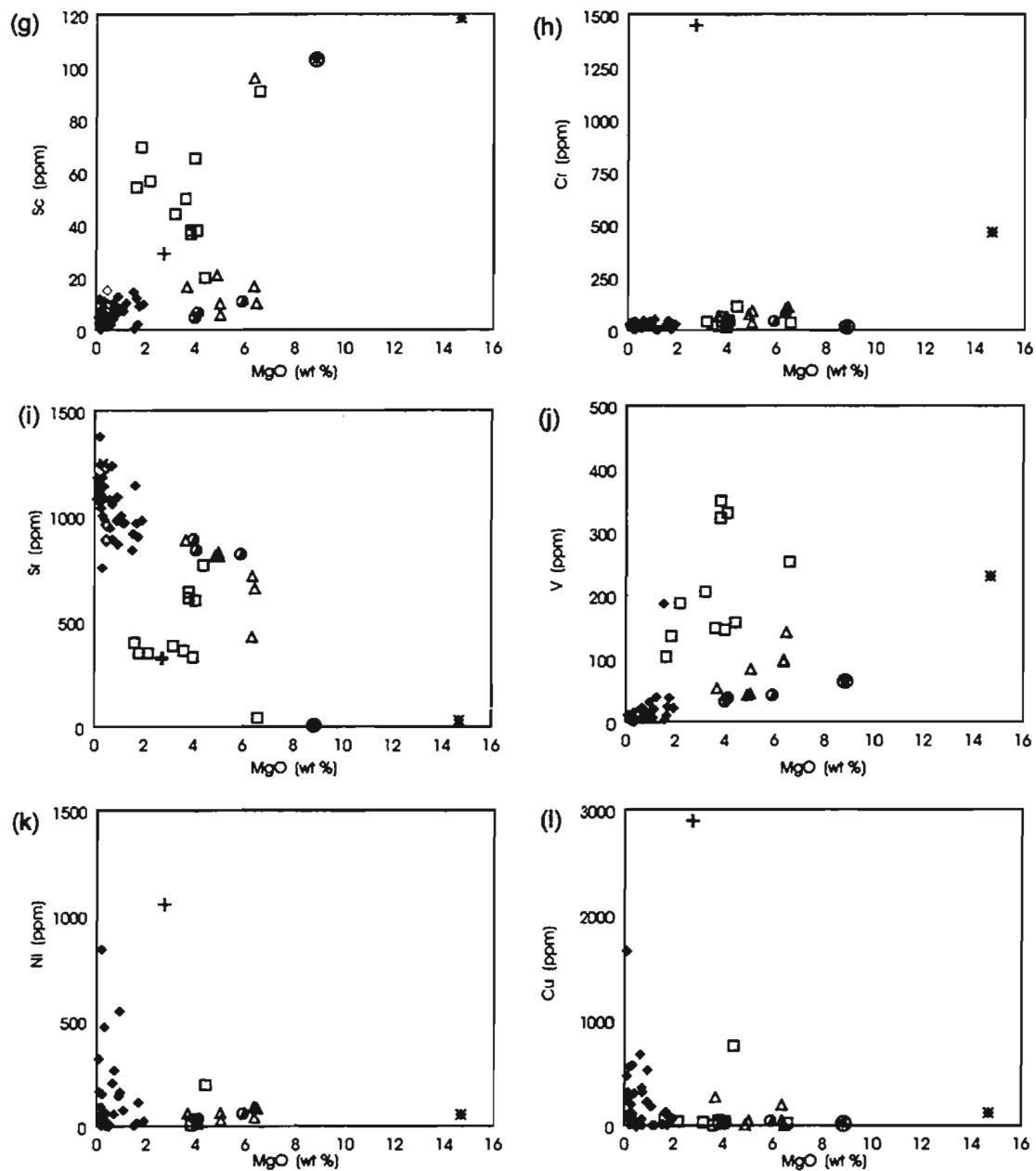


Figure 4.5 MgO (wt%) versus trace elements for the Cirque rocks. Anorthosite (<10% pyroxene) =  $\blacklozenge$ ; Bleached anorthosite =  $\blacklozenge$ ; leuconorite/leucogabbro =  $\Delta$ ; leucotroctolite =  $\bullet$ ; ferrodiorite =  $\square$ ; pyroxenite: 91 =  $\ast$ , 117 =  $\oplus$ . Noranda samples: anorthosite =  $\times$ ; ferrodiorite =  $+$ .

million years, Morse (1981) was able to use major element concentrations to show the crystallization trend of the Kiglapait Intrusion with the major elements increasing or decreasing with respect to decreasing MgO as cumulate olivine, plagioclase, pyroxene, and other minerals crystallized out of the original liquid. In Figure 4.5a to f, the Kiglapait crystallization trends, defined by the dashed line with arrows marking the direction of crystallization from right to left, are also used to compare the crystallization history of the Cirque rocks. Typical compositions of cumulate plagioclase and clinopyroxene are also shown (grey boxes); the straight arrows indicate the direction of crystallization of olivine and orthopyroxene beyond the plot boundaries.

The plots of the Cirque rocks are limited by the lack of material which represents initial magma composition (unlike that of the Kiglapait Intrusion crystallization trend) and the fact that the Cirque area was produced in an open system and thus affected by crustal contamination, magma mixing, and partial melting. In most of the plots, however, the major element fractionation tends to follow (to variable degrees) the crystal fractionation trend of the Kiglapait Intrusion (particularly  $\text{SiO}_2$ ,  $\text{K}_2\text{O}$ ,  $\text{P}_2\text{O}_5$  and  $\text{TiO}_2$ ). The extreme cumulate plagioclase-rich and Fe oxide-rich fractionates which formed the anorthosites and ferrodiorites, respectively tend to have the most variation along the crystallization trends. One pyroxenite sample (91) consistently plots within or near the box marking a clinopyroxene phase indicating the least fractionated material, that is, rock having a chemical composition most like that of the parental material. The second pyroxenite (117) sample appears to plot about halfway along each crystallization trend. This clinopyroxene-

rich layer within an anorthosite body crystallized from the basaltic magma along the crystallization trend as cumulate fractionate. The lack of significant olivine accumulation is reflected by the lack of samples plotting near the olivine phase field (*i.e.* marked by the straight arrow).

The content of MgO wt% ranges from 0 to 15 wt%, indicating the wide range of ferromagnesian minerals from leucoanorthosite to pyroxenite. The silica content of the rocks from the Cirque area range from over 20 wt% to 60 wt% SiO<sub>2</sub> (Figure 4.5a). Concentrations of Al<sub>2</sub>O<sub>3</sub> in a magma are controlled dominantly by plagioclase crystallization (Figure 4.5c). Scoates and Mitchell (2000) defined two types of basalts based on the Al<sub>2</sub>O<sub>3</sub> content; high-Al basalts and tholeiitic basalts. Due to the cumulate nature of anorthosite, these rocks are obviously the richest in Al<sub>2</sub>O<sub>3</sub> and are not included in the basaltic types, however, the other rocks types in the Cirque area dominantly plot just above the high-Al basalts field reflecting the elevated cumulate plagioclase to pyroxene and olivine ratio for the leucotroctolite/leuconorite/leucogabbro rocks. The ferrodiorites, with higher concentrations of oxides and augite, spread evenly between the two fields; some even have as low as ~3 wt% Al<sub>2</sub>O<sub>3</sub>. The rocks with the least amounts of Al<sub>2</sub>O<sub>3</sub> are the pyroxenite samples reflecting the lowest abundances of plagioclase. The total FeO content (Figure 4.5c), which is governed somewhat by the presence of pyroxene (and to a lesser extent in the Cirque rocks, olivine), is greater in the more fractionated mafic melts and the supposed residual liquid (*i.e.* ferrodiorite). Iron oxide and sulphide minerals also contribute to the FeO content. According to the Emslie *et al.*'s (1994) model of AMCG genesis, excess FeO

and incompatible elements, such as  $P_2O_5$  and  $TiO_2$ , are concentrated in the last remaining liquid of the magma chamber, forming ferrodiorite rocks with up to 40 percent magnetite and ilmenite plus relatively higher apatite and mesoperthite contents than the other rock types. According to the model from the Kiglapait Intrusion, Fe enrichment of the liquid magma occurs during the first 96% crystallization, the concentration of  $TiO_2$  peaks at 4.75% with 90% solidified magma, and the liquid becomes saturated in apatite at ~1.3 %  $P_2O_5$ , (Morse 1981), thus the residual rocks would have the highest  $TiO_2$ , FeO,  $P_2O_5$ , and  $K_2O$ , respectively (Figure 4.5b, d, f, and e).

Concentrations of the incompatible elements V and Sc (Figures 4.5g and j) are more abundant in the ferrodiorite and pyroxenite rocks, reflecting the greater concentrations of clinopyroxene relative to the other rock types. Sr follows the same trend as  $Al_2O_3$ , indicating a preference for plagioclase during crystal fractionation (Figure 4.5g). The plots of the compatible Cr, Ni, and Cu versus MgO (Figures 4.5f, i, and j) indicate low contents in the magma precursor and all subsequent rock types. The few elevated Ni and Cu values in anorthositic samples may reflect an influx of metal-rich sulphides from another source as indicated by thermal erosion textures discussed in Chapter 3.

Figures 4.6 and 4.7a and b also illustrate the effects of crystal fractionation within the magma, that is, the accumulation of excess Fe and incompatible Ti in a possible residual liquid as  $Al_2O_3$  and total FeO contents decrease with the formation and subsequent extraction of cumulate plagioclase and ferromagnesian minerals. The parental magma contained relatively low concentrations of  $TiO_2$  and  $Al_2O_3$  compared to all rock types, as

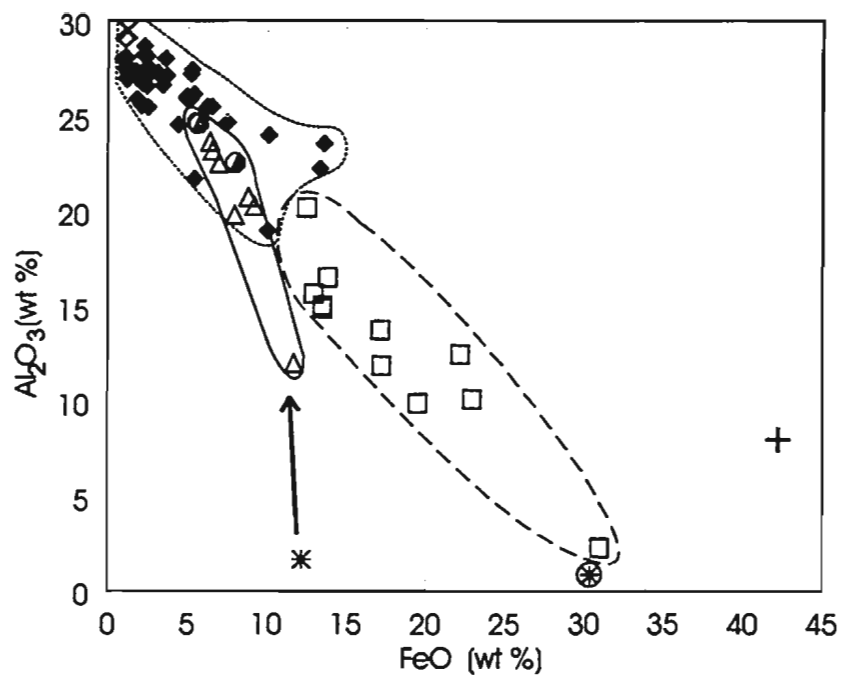


Figure 4.6 Plot of FeO wt% versus  $\text{Al}_2\text{O}_3$  wt% of samples from the Cirque property. Anorthosite (<10% pyroxene) = ◆; Bleached anorthosite = ◇; leuconorite/leucogabbro = △; leucotroctolite = ●; ferrodiorite = □; pyroxenite: 91 = \*, 117 = ⊗. Noranda samples are for comparison: anorthosite = X; ferrodiorite = +. The arrow indicates the general direction of crystal fractionation.

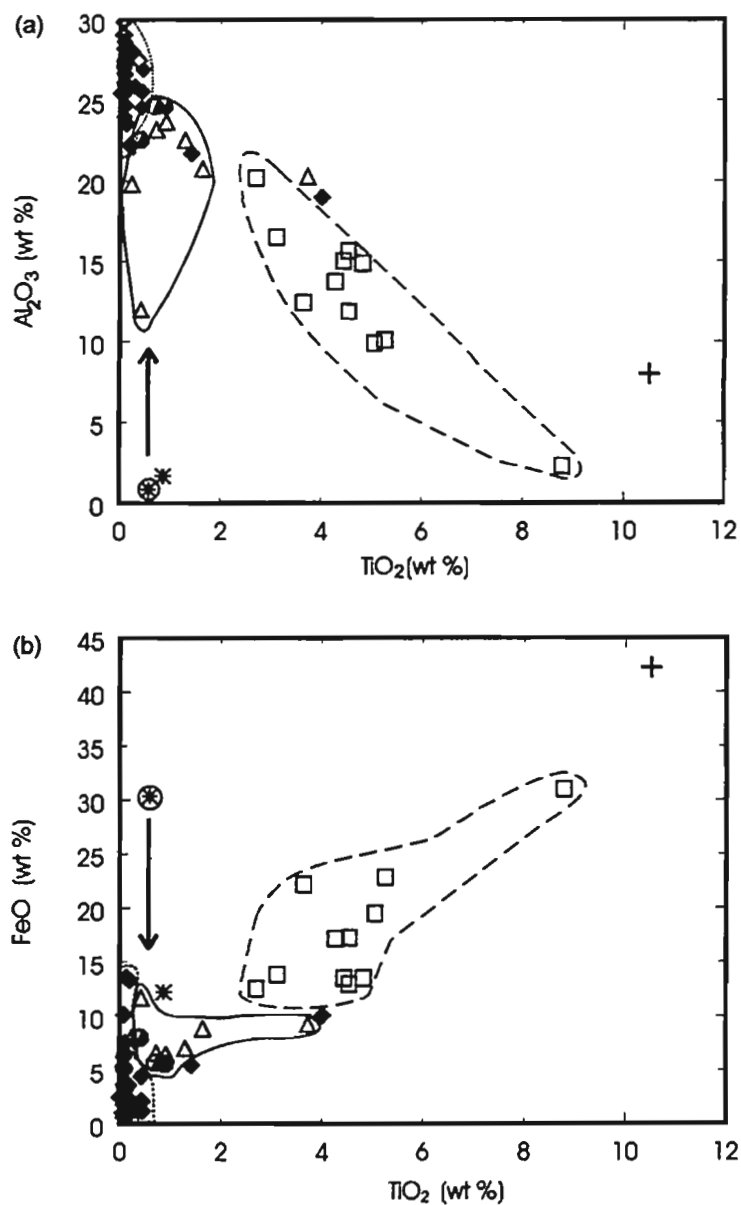


Figure 4.7  $\text{TiO}_2$  (wt%) versus (a)  $\text{Al}_2\text{O}_3$  (wt%) and (b)  $\text{FeO}$  (wt%) showing fields of major rock types from the Cirque property. Anorthosite (<10% pyroxene) =  $\blacklozenge$ ; Bleached anorthosite =  $\diamond$ ; leuconorite/leucogabbro =  $\triangle$ ; leucotroctolite =  $\bullet$ ; ferrodiorite =  $\square$ ; pyroxenite: 91 =  $*$ , 117 =  $\otimes$ . Noranda's samples: anorthosite =  $\times$ ; ferrodiorite =  $+$ . The arrows indicate the general direction of crystal fractionation.



evidenced by the pyroxenite sample 91. The arrows indicate the general direction of crystallization, starting with a composition similar to pyroxenite sample 91, then fractionating to produce leucotroctolite/leuconorite/leucogabbro varieties. Extreme fractionation and accumulation led to the formation of the plagioclase-rich rock (anorthosite varieties) and the other end-member cumulate pyroxenite (117). In Figure 4.7a, each rock type outlined indicates that  $\text{TiO}_2$  (*i.e.* ilmenite) is not common in any of the fractionated rock types except the ferrodiorite rocks (as discussed in Chapter 2) and that the ferrodioritic contains the greatest abundances of  $\text{TiO}_2$  and  $\text{FeO}^*$  and the lowest abundances of  $\text{Al}_2\text{O}_3$ . It is quite possible, therefore, that these ferrodiorite rocks did not originate from the same parental magma as the other rock types.

### 4.3 Trace element distribution plots

Representative anorthosite and mafic rock samples were selected for ICP-MS analyses to produce multi-trace element geochemical plots and examine rare earth element (REE) distributions. Several sulphide-rich samples (dominantly anorthositic ‘hosts’) were also selected and are plotted to compare with barren rocks. The sulphide-poor samples consist of five anorthosites, six mafic rocks (comprising leucotroctolite and leuconorite/leucogabbro), two pyroxenites, and four ferrodiorite rocks samples (including one ferrodiorite sample from the Noranda “Hilltop” property). The anorthosites consist of two Bleached anorthosites (LD-96-7A and LD-96-109), an altered anorthosite with <1% disseminated pyrrhotite and trace disseminated chalcopyrite (LD-96-10), and a core sample from LBN-96-2 (depth 69.3 m) with <10% pyroxene. A fifth anorthositic sample, BW02,

was collected from the Noranda's "Hilltop" property to the west. Out of the six mafic samples, three leucotroctolite samples and one leuconorite sample are all from borehole LBN-2 at depths of 3.43 m, 4.43 m, 6.43 m, and 27.0 m, respectively. The two other mafic samples are a leuconorite, from borehole LBN-5 (@ 11.0 m), and a leucogabbro (LD-96-161) from outcrop. The small amount of leucotroctolite present on the Cirque property prevented the collection of a wide selection of samples. All of the samples of ferrodiorite and one pyroxenite sample (117) from the Cirque property are hand samples collected from the north arm of the cirque wall. The second pyroxenite sample (91) is from talus along the back wall of the cirque, near Gossan #1.

#### **4.3.1 Rare earth element and multi - element geochemistry**

Detailed geochemical research on the Kiglapait Intrusion (Figure 4.8) provides an opportunity to track the crystallization history of an AMCG magmatism, at least in northern Labrador. Because of its unique closed system environment, the trend of crystal fractionation can be traced from troctolite to ferrosyenite (Morse 1985; Scoates and Mitchell 2000) with percent solidification of the magma increasing from 0 to 94% (Morse 1985). The signature of each consecutive fractionated melt is defined by a positive Eu anomaly and increasing concentrations of REE, with the concentrations of the LREE greater than those of the HREE.

The REE signatures for the four rock types in the Cirque area are shown in Figure 4.9. Because the anorthosite is "host" to the sulphide mineralization, its signature (grey

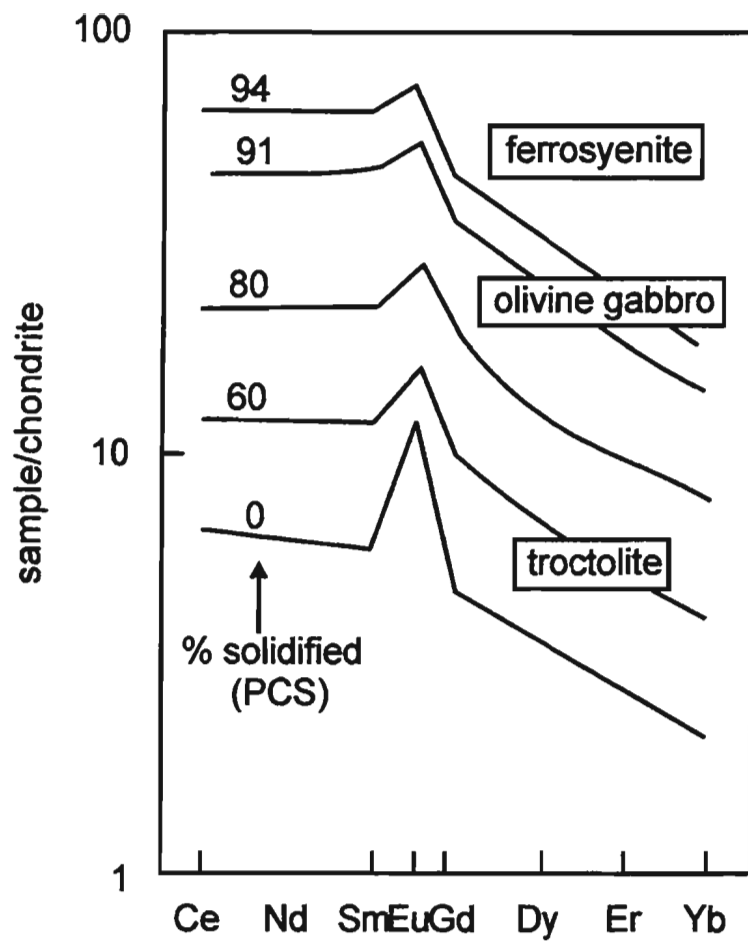


Figure 4.8 REE plot for progressive fractionation in the Kiglapait Intrusion adapted by Scoates and Mitchell (2000) from Morse (1985) using chondrite-normalizing values from Hanson (1980).

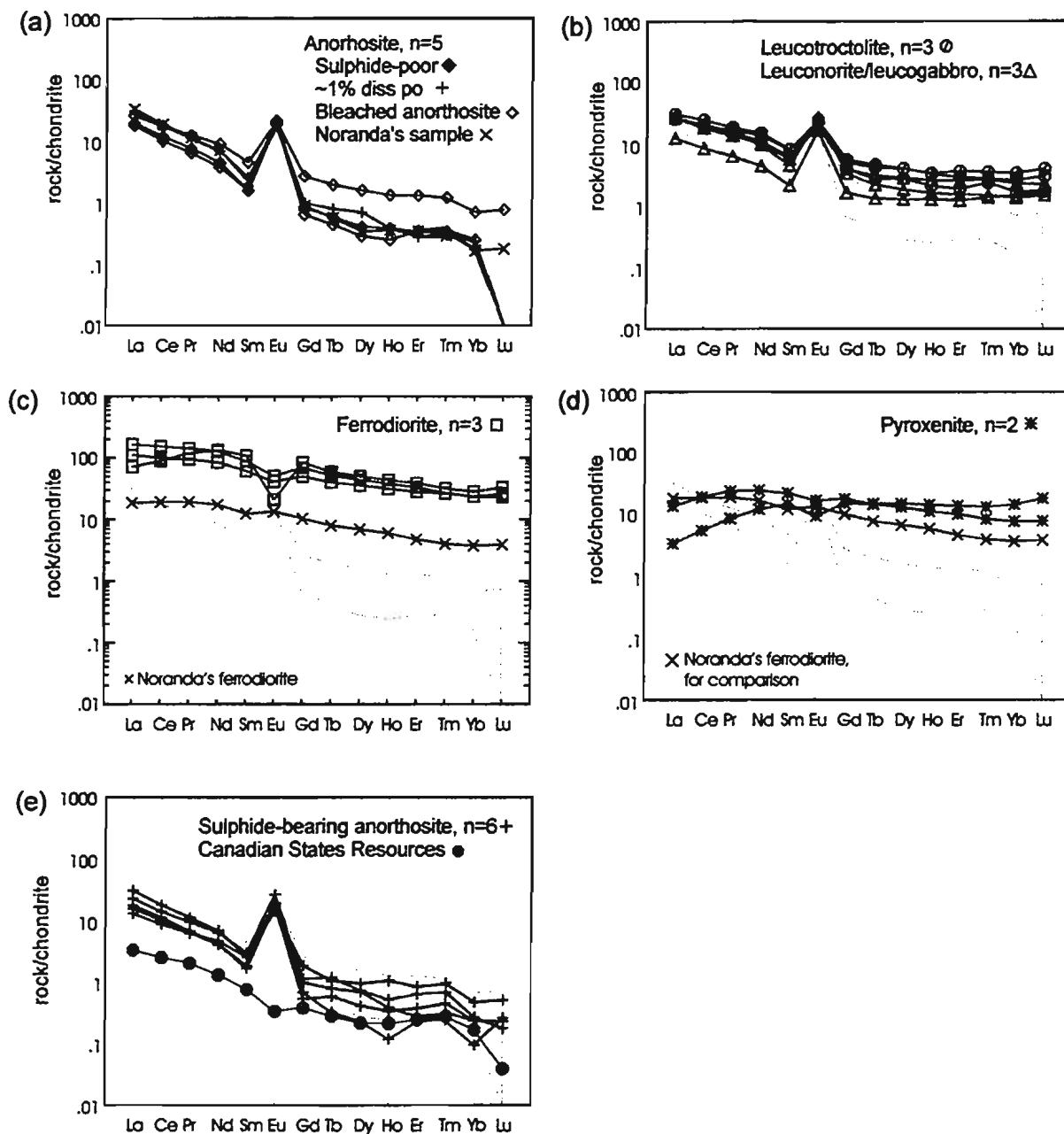


Figure 4.9 Rare earth element plots for (a) anorthosite, (b) leucotroctolite and leuconorite/leucogabbro, (c) ferrodiorite, (d) pyroxenite, and (e) sulphide-bearing anorthosite. All samples are from the Cirque area including two samples (one anorthosite and one ferrodiorite) from the neighbouring Noranda "Hilltop" property. Plots (b) to (e) are compared to the sulphide-poor anorthosites (grey) from (a). The mineralized samples are compared to a massive sulphide sample from the Canadian States Resources property (Licence #1514M). Plots are normalized using chondrite values from Sun and MacDonough (1989).

area) is compared to the other rock types, keeping in mind, however, that anorthosite was not the actual host magma from which the sulphide liquid segregated (as discussed in Chapter 3). The anorthositic rocks have a signature typical of a fractionated magma melt, that is, (i) elevated LREE, indicating fractionation of more compatible phases, (ii) depleted HREE, reflecting lower abundances of ferromagnesian minerals, and (iii) sharp positive Eu anomalies, reflecting a high plagioclase content (Figure 4.9a). The two samples of Bleached anorthosite seem to bracket the other three anorthosite samples especially the HREE, possibly indicating the variable amounts of pyroxene and olivine compared to the regular anorthosites. Leucotroctolite and leuconorite/leucogabbro rocks have similar REE signatures as the anorthosite but with relatively elevated HREE reflecting the greater abundances of cumulate pyroxene and olivine minerals (Figure 4.9b).

The presence of a positive Eu anomaly, consistent in each melt fraction (other than ferrodiorites and pyroxenites), suggests a genetic link of each melt with the same original magma; however Scoates and Mitchell (2000) state that positive Eu anomalies in the signature of each rock type from an AMCG system may be due to the injection and resorption of a plagioclase-rich melt (perhaps as the magma ascended in the crust to lower pressures) or the assimilation of plagioclase-rich mafic granulites from the lower crust. This seems a less likely explanation for the Kiglapait Intrusion which formed under closed system conditions with very little crustal contamination (Scoates and Mitchell 2000), however, it is quite possible that the positive Eu anomalies of the Cirque rocks were formed by any one of these processes, especially since the area south of Okak Bay was a site of extensive open

system plutonism. Given that the presence of plagioclase cumulates, which affects the Eu signature, and that the bivariate plots (Figures 4.5 - 4.7) suggest a single parental magma for the rock types (except the ferrodiorites), it seems likely that the positive Eu anomalies in Figure 4.9) indicate a genetic link between the anorthosite and leucotroctolite/leuconorite/leucogabbro rocks.

The REE signatures for the ferrodiorite rocks are distinctly different from the anorthositic and leucotroctolitic-leuconoritic/leucogabbroic rocks (Figure 4.9c). Of all the rock types from the Cirque grid, the ferrodiorite rocks have the greatest abundance of all the REE (slightly more LREE than HREE) and a moderately negative Eu anomaly. Compared with the REE signatures of the Kiglapait Intrusion in Figure 4.8 which indicate that the ferrosyenites have positive Eu anomalies, suggesting a genetic link with the earlier fractionated melts, the ferrodiorites from the Cirque area appear to be chemically unrelated to the other rocks types. As such they may possibly have originated from a separate high-Al basaltic parental magma or, as suggested for the FTP system by Vander Auwera *et al.* (1998) and Longhi and Vander Auwera (1992), were derived from a primitive mafic magma source, rather than representing the end product or residuum of an anorthositic fractionated magma. An injection of plagioclase-rich melt or crustal material seems unlikely for these ferrodiorites since they also have relatively low abundances of  $\text{Al}_2\text{O}_3$  and Sr reflecting low abundances of plagioclase, thus the ferrodiorites possibly originated from a second magma, separate from the one from which the anorthosites and leucotroctolite and leuconorite/leucogabbro rocks crystallized. Emslie *et al.* (1994), however, state that a



genetic link between consecutive fractionating melts are better shown by decreasing Sr concentrations, rather than similar Eu concentrations (that is, positive or negative anomalies) which are offset by co-crystallizing mafic minerals. Decreasing Sr concentrations indicate a magma which has had significant removal of Sr over time as a result of significant crystallization of cumulate plagioclase (Emslie *et al.* 1994; Vander Auwera *et al.* 1998).

The least fractionated melt appears to be the pyroxenite rocks with a more primitive REE signature, unlike that of the anorthosite rocks (Figure 4.9d). With overall concentrations of LREE less than those of the HREE and the presence of a slightly negative Eu anomaly, these two pyroxenite samples seem to indicate a more primitive magma source separate from that which formed the anorthosites and the leucotroctolite and leuconorite/leucogabbro rocks.

For comparison, a magnetite-rich sample from Noranda's "Hilltop" property is plotted and although its modal composition (50% magnetite, 15% clinopyroxene, 20% plagioclase, trace biotite, 15% pyrrhotite and trace chalcopyrite) and bivariate major and trace element plots (Figure 4.6) suggest the sample to be a ferrodiorite, its geochemical signature resembles that of a pyroxenite sample (Figure 4.9c). Its features include a slightly positive Eu anomaly, weakly elevated LREE concentrations compared to the HREE concentrations, and the overall lower REE concentrations than the ferrodiorites, defining this sample to have derived from an enriched mantle source, perhaps the same source which produced the anorthosites and leucotroctolites and leuconorites/leucogabbros, yet with less contamination from the crustal rocks. The negative Eu anomalies (of various degrees) in

the ferrodiorites and pyroxenites signatures do not seem to suggest a genetic link to the Noranda magnetite-rich sample.

In Figure 4.9e, the chondrite normalized REE fields for the sulphide-bearing anorthosite overlap those of the unmineralized anorthosites. The overall lower REE abundances are probably due to the relatively greater amounts of iron sulphides (*i.e.* the REE contents are diluted). In comparison, the massive sulphide sample from the Canadian States property (Licence #1514M) lacks a positive Eu anomaly and has relatively lower LREE concentrations than the sulphide-poor and sulphide-bearing anorthosites, possibly suggesting that the sulphide melt was in equilibrium with a different mafic magma than the Cirque anorthosites. Given that this is the only sample from the Canadian States property analysed for this study, caution must be made at this point, especially since thermal erosion textures have also been observed in the gossanous areas on the Canadian States property (refer to Chapter 3), and except for <5% rounded plagioclase and magnetite inclusions, this sample does not contain any evidence of a magma host rock.

#### **4.3.2 Multi-element geochemical signatures on the Cirque property**

Extended REE or multi-element plots are also informative for defining crustal contamination and magma mixing. Plots of the different rock types from the Cirque area are shown in Figure 4.10 with values normalized to primitive mantle values from Sun and MacDonough (1989). Overall, elevated concentrations of Sr, Pb, and K for most of the rock types from the Cirque area suggest significant country rock contamination, possibly gneisses

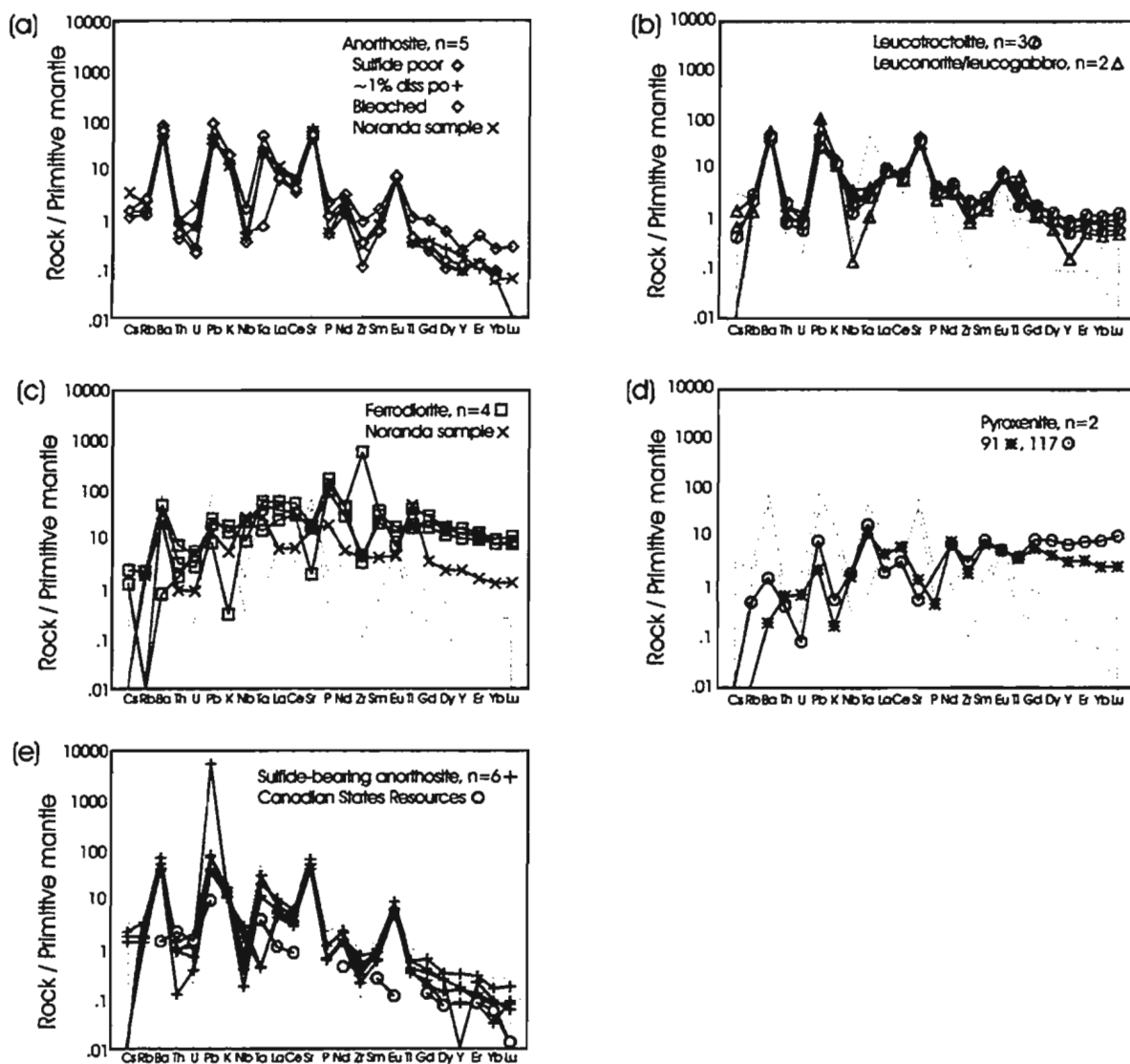


Figure 4.10 Multi-element plots showing (a) anorthosite, (b) leucotroctolite and leuconorite/leucogabbro, (c) ferrodiorite, (d) pyroxenite, and (e) sulphide-bearing anorthosite from the Cirque area. All rock types are compared to the anorthosite field (grey) in (a). The mineralized samples are compared to a massive sulphide sample from the Canadian States Resources property (Licence #1514M). All plots are normalized to primitive mantle values from Sun and MacDonough (1989).

from either the Nain or Churchill provinces, or both (Emslie *et al.* 1994). The anorthosite rocks from the Cirque have depletions of Rb, Th, U, Nb, Nd, Sm and enrichments of Ba, K, Zr, and Ti. Positive Sr and Eu anomalies indicate the dominant plagioclase composition (Figure 4.10a). The leucotroctolite and leuconorite/leucogabbro field (Figure 4.10b) shows similar depletions and enrichments compared to the anorthosite field (grey), plus greater abundances of the HREE due to greater contents of pyroxene and oxide minerals. The ferrodiorite dykes have variable abundances of Ba, K, Pb, and Zr (yet greater than those of anorthosite and even leucotroctolite and leuconorite/leucogabbro), suggesting variable degrees of feldspar crystallization and accumulation of incompatible elements through increased fractional crystallization of all cumulate minerals (Figure 4.10c). Overall, the different multi-element signatures support the suggestion that the anorthosites, leucotroctolite, and leuconorite/leucogabbro share a common parental magma, perhaps, separate from the precursor which formed the ferrodiorite rocks.

The two pyroxenite samples have a wide range of crustal indicator elements (Ba, Th, U, K, and Nb (Figure 4.10d), although lower concentrations than in the anorthosite, leucotroctolite and leuconorite/leucogabbro of Figures 4.10a and b, perhaps reflecting a lesser degree of crustal contamination. The greater HREE concentrations, also seen in Figure 4.9c, most likely reflect the greater modal abundance of clinopyroxene. Since there are only two samples of pyroxenite, limited interpretations can be made regarding the relationship between the other rock types. Nonetheless, the pyroxenite geochemistry may be significant because, as mentioned in Chapter 2, Noranda Ltd. geologists recorded

disseminated to massive sulphide mineralization in drill core (HT-96-3), outcrop, and talus syngenetically hosted by gabbro/clinopyroxenite “dyking” (approximately less than 15 metres wide intersections in drill core) through unmineralized anorthosite (Squires *et al.* 1997).

As shown in Figure 4.9e, the sulphide-bearing anorthosites are geochemically the same as the unmineralized anorthosites from the Cirque since the sulphide-bearing anorthosites share the same field area as the sulphide-poor anorthosites, except for slightly lower Th concentrations and one sample has a significantly elevated Pb concentration (grey; Figure 4.10e). The massive sulphide sample from the Canadian States property has the lowest overall abundances of trace elements (Figure 4.10e), except for Th and its geochemical signature does not seem to correlate with the mineralized anorthosites from the Cirque. Evidence of epigenetic sulphide mineralization on the Canadian States property (*eg.* thermal erosion textures in massive anorthosite) also supports the theory of extensive sulphide mobilization from an undetermined host magma.

Comparative plots of the Cirque rock types (averaged) normalized to the mineralized anorthosites from the Cirque and the massive sulphide sample from the Canadian States property are shown in Figure 4.11a and b. In Figure 4.11a, the plot of unmineralized anorthosite, leucotroctolite/leuconorite/leucogabbro, and pyroxenite are as expected: distinct with increasing concentrations from anorthosite to mafic rocks as a result of crystal fractionation previously discussed. The ferrodiorite rocks plot similarly but with greater concentrations of trace elements. Except for a very low Pb concentration in all of the

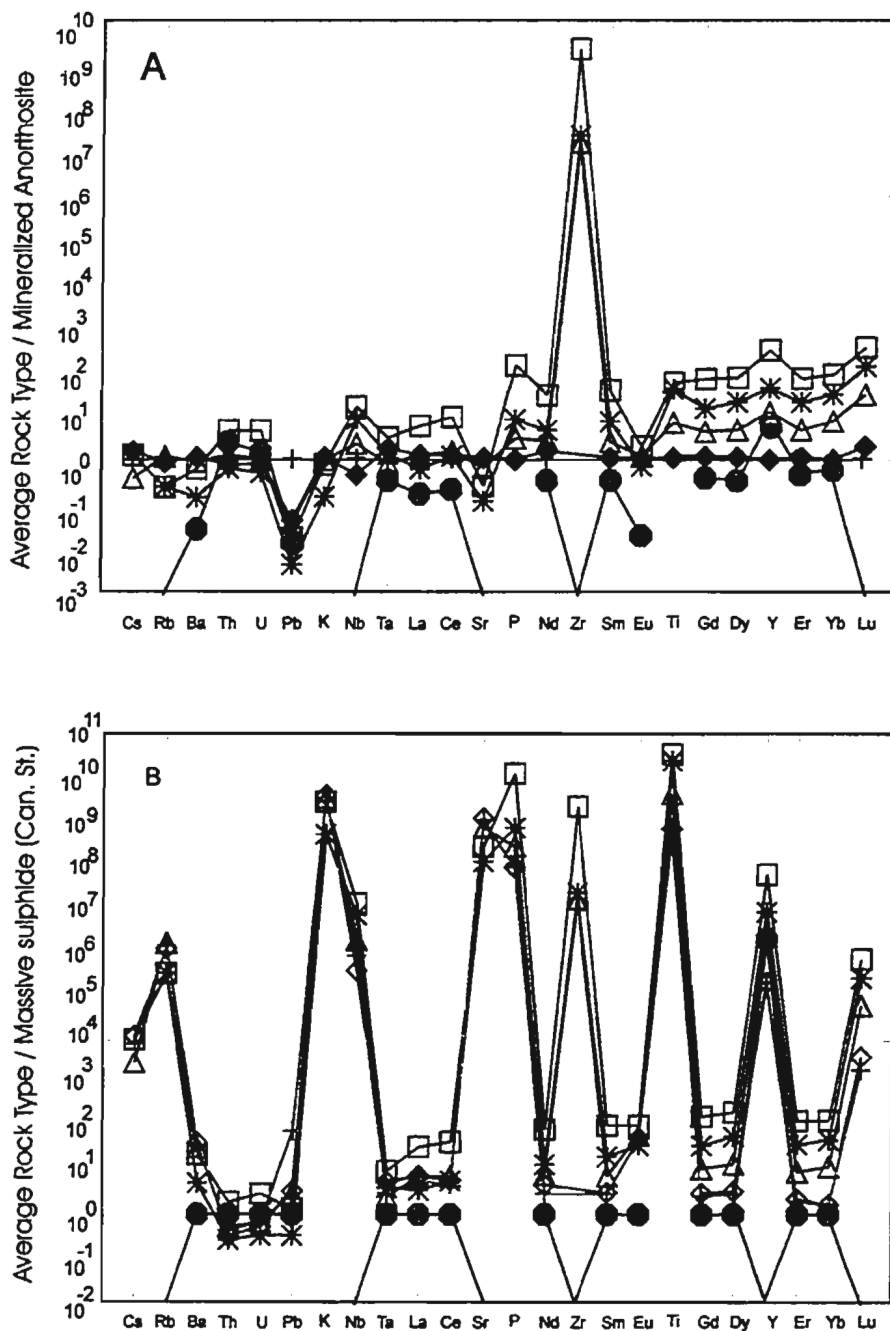


Figure 4.11 Comparative multi-trace element plots of average anorthosite (◆), leucotroctolite and leuconorite/leucogabbro (△), ferrodiorite (□), and pyroxenite (※) against (A) mineralized anorthosite from the Cirque (+) and (B) a massive sulphide sample from the neighbouring Canadian States Resources property (●).

unmineralized rock types, the unmineralized anorthosites and the sulphide-bearing anorthosites are geochemically similar. In Figure 4.11b, the pyroxenite rock type has the lowest concentrations of Th+U+Pb, suggesting the least crustal contamination. In both plots, the Canadian States massive sulphide sample has the overall lowest concentrations of multi-trace elements than any of the rock types from the Cirque, including the mineralized anorthosite, suggesting a deviation from a separate magma source.

#### **4.3.3 Additional trace element data from external sources**

For comparison, trace element plots of compiled data from various intrusions in the NPS (Emslie *et al.* 1994; Emslie 1996; Emslie *et al.* 1997) are presented in Figure 4.12 a to c, respectively, showing the geochemical REE and multi-trace element signatures elsewhere in the Nain Plutonic Suite. Refer to Figure 4.1 for sample locations. Overall, anorthosites, leucotroctolite-leuconorite/leucogabbro, and ferrodiorites from the Cirque property (grey fields) have similar geochemical signatures as the same rock types elsewhere in the NPS, although the samples from Emslie *et al.* (1994), Emslie (1996), and Emslie *et al.* (1997) have greater variations or range of concentrations for any particular element. This is most likely due to the greater number of samples in the datasets and the unique geochemistry of each sample throughout the NPS. Overall, the similar geochemical signatures for the same rock types suggest that throughout the NPS the trend of crystal fractionation is the same. Variations in the concentrations of Ba, K, Nb, Zr, and especially Rb correspond to variable amounts of crustal material assimilated during emplacement.



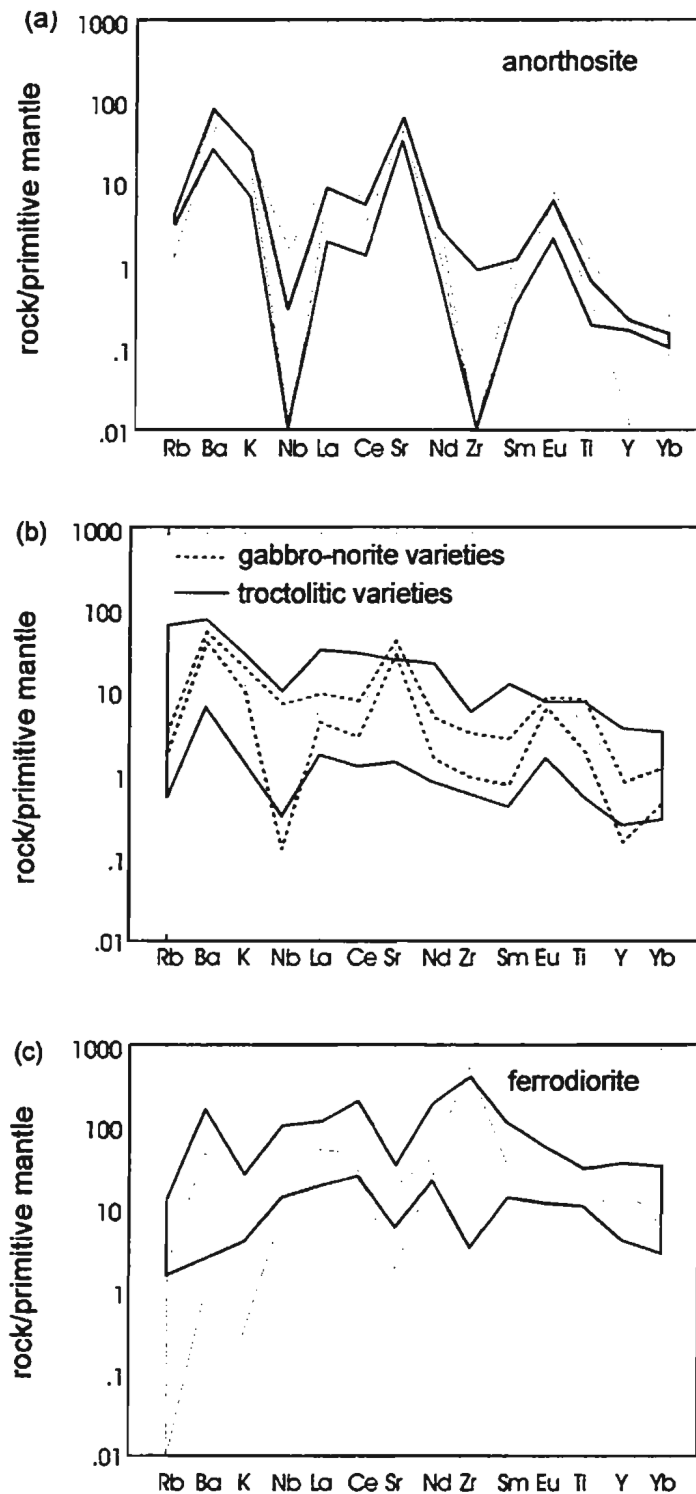


Figure 4.12 Multi-element plots of (a) anorthosite, (b) gabbro-norite and troctolite varieties, and (c) ferrodiorite throughout the NPS (from Emslie et al. 1994; Emslie 1996; and Emslie et al. 1997). The grey fields are plots of similar rock types from the Cirque grid. Plots are normalized using values from Sun and MacDonough (1989).

The two pyroxenite samples from the Cirque property lie in the same geochemical fields of subsurface (*i.e.* drill hole OKG-96-09) and surface pyroxenite dyke samples from the OKG property approximately 35 km north of the Cirque property (Figure 4.13). Pyroxenites from the area are petrographically similar, that is, coarse-grained, cumulate clinopyroxene and orthopyroxene-rich with variable amounts of interstitial plagioclase, olivine, and syngenetic sulphides (Piercey 1998). Unlike the Cirque pyroxenites, however, the OKG pyroxenites intrude Paleoproterozoic anorthosites and are syngenetic hosts to discontinuous zones of disseminated to massive sulphides (*op. cit.*). The surface pyroxenites have depletions of LREE relative to HREE (general elevated concentrations from left to right) and generally flat to negative Eu anomalies (Piercey 1998).

The subsurface pyroxenites have overall higher LREE concentrations compared to the surface pyroxenites, negative to slightly positive Eu anomalies, and generally similar concentrations of HREE (*op. cit.*). Although the overall REE signatures for the subsurface and surface pyroxenite dykes are different, Piercey (1998) concludes that both types were derived from the same depleted mantle source and that a consistent negative Th anomaly in both pyroxenites and the surrounding granitoid and anorthositic rocks suggests a common source of crustal contamination from the Nain Province. The only difference between the two types of pyroxenite dykes is that the subsurface pyroxenite dykes contain more crustal contaminants (*op. cit.*).

Although the Cirque pyroxenites lie within the OKG subsurface pyroxenite field with concentrations of LREE greater than HREE and a negative Eu anomaly, the overall

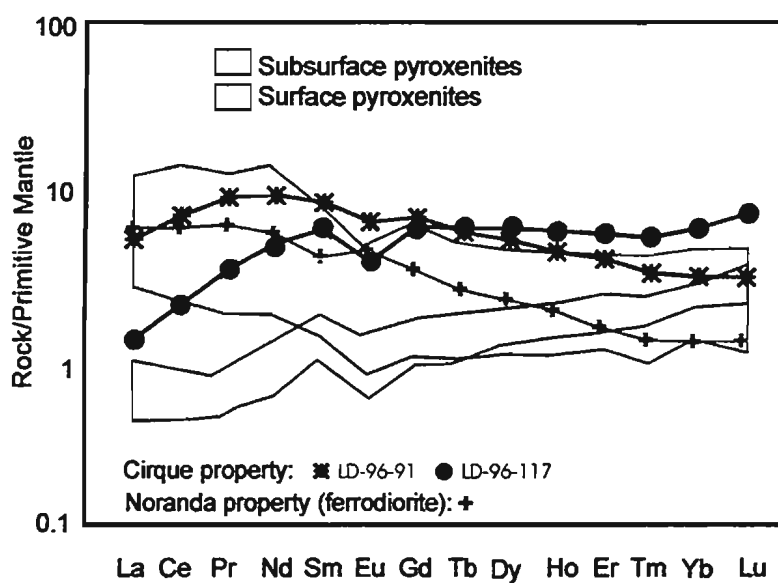


Figure 4.13 REE plot from Piercey (1998) of subsurface and surface pyroxenites from the OKG Castle Rock property and two pyroxenite samples from the Cirque. A magnetite-rich sample (ferrodiorite from the Noranda property), plots in the same field as the OKG subsurface pyroxenites. Both data sources [Cirque and Piercey (1998)] are normalized using primitive mantle values from Hofmann (1988).

shape of the signatures are more like that of the surface pyroxenites with LREE increasing from left to right (that is, lower La and Ce concentrations relative to the other LREE) and a slightly negative Eu anomaly.

For comparison, the “ferrodiorite” sample from Noranda’s “Hilltop” property plots in the same field as the subsurface pyroxenite dykes with slightly positive Eu anomaly and a gradual decrease of REE concentrations from the LREE to the HREE. The low concentrations of HREE relative to the Cirque pyroxenites most likely reflect the lower modal abundances of clinopyroxene. Interestingly, in the AFM discrimination diagram, the same Noranda sample plots with the cluster of the OKG pyroxenites (compare Figure 4.2 and Figure 4.5), suggesting a geochemical overlap of this sample and ferrodiorites from the Cirque area and the OKG pyroxenites. Interpretation of these three samples, with respect to Figure 4.13, suggests that the magma(s) which produced them underwent some degree of crustal contamination and similar Th depletions in each of the Cirque rock types (see Figure 4.11) may also indicate a common crustal contamination, of varying degrees, from the Nain Province.

#### **4.3.4 Comparisons with intrusions from the Voisey’s Bay deposit area**

The sulphide-rich samples range from disseminated to massive sulphide at the Cirque, along with a core sample from the Canadian States property (Licence #1514M), and they plot consistently as anorthosite with positive Eu anomalies. Since most of the sulphide mineralization is found within leucoanorthosite (Chapter 3), this is not surprising. However,

thermal erosion textures suggest that the Cirque anorthosite does not represent the original magma from which the sulphides segregated and so their trace element plots cannot be considered to reflect the geochemistry of the parental magma.

Recent studies of the geology, geochemistry, and geochronology of the rocks within and around the Voisey's Bay deposit by field geologists from Diamond Fields Resources and Inco Ltd. as well as by Amelin *et al.* (1997) and Li *et al.* (1998) have defined two separate intrusions: the Mushuau Intrusion and the Voisey's Bay Intrusion. The two intrusions have been described in more detail in Chapter 1, however, they are briefly discussed below.

The Voisey's Bay Intrusion (VBI) comprises troctolitic rocks (1334 Ma) in the southern part of the Voisey's Bay deposit (Ryan 2000) and are host to the known major Ni-Cu sulphide deposits such as Discovery Hill, the Ovoid, and the Eastern Deeps. Intrusions of *ca.* 1307 Ma granite and hornblende-fayalite-clinopyroxene quartz monzonite have resulted in contact metamorphism of the troctolite (Ryan 2000). The Mushuau Intrusion (MI) is located in the northern part of the deposit and consists of layered melatroctolite along the margins, leucotroctolite towards the centre, and olivine gabbro in the core (Li *et al.* 2000). Smaller, later intrusions of troctolite had crosscut the MI and, in places, resulted in brecciated textures (*op cit.*). The age of the MI ranges from *ca.* 1317 Ma for the layered intrusions and 1313 to 1312 Ma for the massive intrusions (Ryan 2000). So far, only minor magmatic sulphide occurrences have been discovered within the MI (*e.g.*, the Sarah prospect; Li *et al.* 2000).

The significance of the two distinct troctolite intrusions are associated with the origin

and age of each intrusion. The MI is thought to have a more evolved genetic history than the VBI, with greater degree of contamination, different crustal contaminants, and a more fractionated magma source (Li *et al.* 2000; Amelin *et al.* 2000). Thus, an understanding of the differences between the two intrusions may be insightful for interpreting the magmatic evolution of the Cirque area.

Contributing studies by Amelin *et al.* (2000), Li *et al.* (2000), Lightfoot and Naldrett (1999), and Li and Naldrett (1999), Ryan (2000), and Ripley *et al.* (2000), define the most recent model for the Voisey's Bay deposit as involving two separate intrusive events. Overall, major and trace element geochemistry of the Voisey's Bay deposit indicate that the VBI intrusions was derived from a mantle source (Lightfoot and Naldrett 1999; Amelin *et al.* 2000) or plume head (Amelin *et al.* 2000). Ascension to mid-crustal levels resulted in contamination by enderbitic gneiss and Tasiuyak paragneiss (Lightfoot and Naldrett 1999) and Nain Province gneiss (Amelin *et al.* 2000). Amelin *et al.* (2000) estimate the amount of contamination of the Voisey's Bay Intrusion by the Nain Province and Tasiuyak gneiss to have been 10 % and 8-13 %, respectively. The Mushuau Intrusion may have formed from the same mantle-derived magma, but with approximately 15 to 35% contamination of Nain Province gneiss (*op. cit.*).

Amelin *et al.* (2000) state that earlier basaltic magmas ascended and assimilated less crustal material than subsequent magmatic pulses due to the greater contrast in temperatures between the magma and an area of continental crust which had not been intruded by hot granitic restites thought to be the first to form during NPS magmatism. This means that the

older primary melt which formed the Voisey's Bay Intrusion was emplaced at shallow crustal levels quickly with less time for crystal fractionation of the silicate magma, sulphide segregation, and assimilation of the gneissic country rocks. Once the crustal rocks became relatively warmer as a result of magmatic activity, the gneisses of the surrounding Nain and Churchill provinces were more easily incorporated into the magma. The chemistry of the MI precursor reflects the additional crustal material and increased fractionation.

Geochemistry is a effective way of distinguishing the crystal fractionation and contamination histories of the two intrusions, for instance, the VBI has depleted HREE relative to the MI (Lightfoot and Naldrett 1999; Li *et al.* 2000). The plot of Ce versus Yb (Figure 4.14), both normalized to primitive values from Sun and MacDonough (1989), is adapted from Lightfoot and Naldrett (1999) and Li *et al.* (2000) and shows distinct fields of the two intrusions plus the field of conduit rocks. At this point, without full understanding of the genetic history of the Cirque area, comparisons with rocks from the older VBI are preliminary and should be made with caution. Nonetheless, the Cirque rocks are also plotted in Figure 4.14.

A majority of the Cirque samples, particularly the sulphide-poor and sulphide-rich anorthosites (including one anorthosite and one ferrodiorite sample from the Noranda's "Hilltop" property and a massive sulphide sample from the Canadian States Resources property, Licence #1514M), have very low abundances of normalized Yb and Ce suggesting a low degree of crustal contamination (Smith *pers comm.* 2001). However, the samples cluster tightly together and trend into the leucotroctolite samples from the Cirque and seem



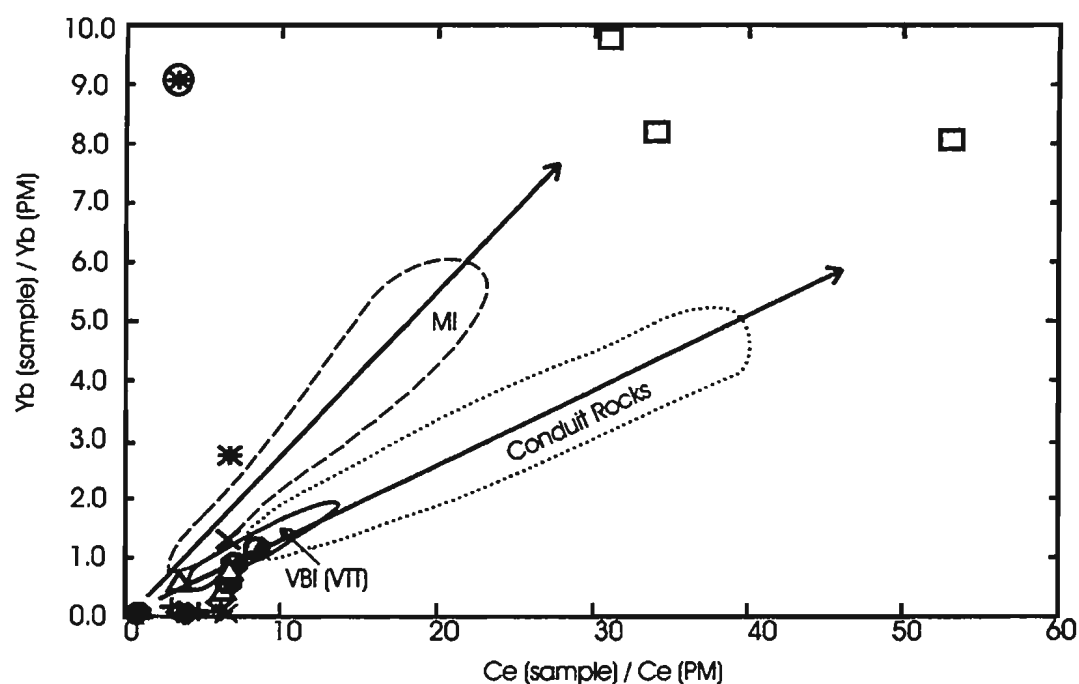


Figure 4.14 Plot of Ce versus Yb [both normalized using primitive mantle values from Sun and MacDonough (1989)] of the Cirque rocks. Plot is adapted from Lightfoot and Naldrett (1989) and Li et al. (2000) with fields from the Voisey's Bay deposit: VBI (VTI)= Voisey's Bay Intrusion (Varied-Textured Troctolite); MI = Mushuau Intrusion; and Conduit rocks. The Cirque rocks include anorthosite (◆), Bleached anorthosite (◇), Leucotroctolite (●), Leuconorite/Leucogabbro (△), pyroxenite (91 ✱; 117 ✱), ferrodiorite (□), sulphide-bearing anorthosite (+). One anorthosite (×) and one ferrodiorite (×) are from Noranda's "Hilltop" property. One massive sulphide sample (●) is from the Canadian States Resources property, Licence #1514M.

to form a line parallel to that of the MI field. Most of the Cirque samples partially lie in and within the VBI field defined by geochemical analyses by Li *et al.* (2000), suggesting similar trace element geochemistry.

The ferrodiorites plot well beyond rocks from both the Cirque and the Voisey's Bay deposit, reflecting either a high degree of crystal fractionation or crustal contamination (or both). Either way, the ferrodiorites appear to be genetically unrelated to the other rocks from the Cirque.

The two pyroxenite samples are within the range of  $Ce/Ce_N$  values of the other Cirque rock types (excluding the ferrodiorites) suggesting a similar crystal fractionation history, however, the  $Yb/Yb_N$  values are much higher. Since crustal contamination increases to the right (Smith *pers comm.* 2001), then the pyroxenites are shown to have the least amount of crustal contamination. One pyroxenite sample (91) plots near the field of the MI, while the second pyroxenite sample (117), *ie.* the fractionate from the anorthosite magma, plots with extremely low Ce-high Yb showing no association with the MI and VBI fields (as earlier trace elements and multi-element signatures indicate). The separate plot of the pyroxenite sample (91) near the MI field may support the idea of a different precursor for the pyroxenite as suggested for the MI and VBI (Lightfoot and Naldrett 1999). Assuming the arrows on the plot from Li *et al.* (2000) indicate the trend of crystal fractionation, however, the pyroxenites samples should not reflect such a high degree of crystal fractionation compared to the other more obviously fractionated rocks from the Cirque. Either the pyroxenite (particularly 91) does not represent a precursor-like material for the

Cirque rocks, as suggested earlier, or the pyroxenite rock is derived from a separate magma source altogether.

Figure 4.15 is a compilation from Li *et al.* (2000) of average multi-trace element data conduit rocks, mineralized and unmineralized and variable types of troctolites from the Voisey's Bay Intrusion and variable types of troctolite from the Mushuau Intrusion, normalized to primitive mantle values from Sun and MacDonough (1989). Overall, the concentrations of all the trace elements in the rocks of the Voisey's Bay deposit are greater than those of the Cirque rocks. Similarities between these rocks types and unmineralized leucotroctolite and leuconorite/leucogabbro rocks and sulphide-bearing anorthosites from the Cirque include elevated concentrations of Ba, Rb, Pb, K, and overall LREE>HREE and depletions of Th+U and negative Nb+Ta anomalies. The anorthosite, leucotroctolite and leuconorite/leucogabbro rocks from the Cirque have similar, *albiet* more pronounced trace element depletions and enrichments than the Voisey's Bay rocks, particularly the Mushuau Intrusion, however, the Cirque rocks have low Cs, Nb, Ta, Y abundances unlike that of the MI or VBI rocks indicating a different genetic or contamination history.

An anomalously positive Ti and negative Zr value for the 'variable' troctolite Mushuau Intrusion most likely reflects, respectively, the variable oxide content and degree of crustal contamination of the Mushuau Intrusion. Generally, the geochemical signatures of each rock type of the VBI and the MI indicate the geochemical similarities of the different intrusions and the small variations of input from crustal material, which according to Li *et al.* (2000), involve the Tasiuyak paragneiss in the Reid Brook zone, enderbitic orthogneiss

## **NOTE TO USERS**

**Page(s) not included in the original manuscript are unavailable from the author or university. The manuscript was microfilmed as received.**

**244**

**This reproduction is the best copy available.**

**UMI**

in the Discovery Hill zone, Ovoid, Mini-Ovoid, and Eastern Deeps (eastern part). They conclude, however, that minor differences of geochemistry of these average rocks of the MI (such as, overall lower concentrations of trace elements in the MI compared to the VBI) do not indicate any genetic relationship with the host rocks of the Voisey's Bay deposit (Li *et al.* 2000).

#### **4.4 Crustal contamination and Sm-Nd and Rb-Sr isotopic systems**

Some of the best evidence supporting the genetic model for anorthosite massifs discussed in Chapter 2 include Sm-Nd and Rb-Sr isotopic data. Processes such as fractional crystallization, magma mixing, partial melting, and contamination alter the geochemical features of an intruding magma body. Because radioactive Rb preferentially partitions into the crust, over time there would be an increase in radiogenic  $^{87}\text{Sr}$  in the crust with respect to a mantle reservoir. Radioactive  $^{147}\text{Sm}$ , on the other hand, partitions preferentially into the mantle, thus radiogenic  $^{143}\text{Nd}$  would increase in the mantle vs. the crust. Overall, Sm-Nd isotopic systems are more reliable than Rb-Sr isotopic systems since the Rb/Sr ratios are generally very low in anorthosites ( $<0.01$ ; Ashwal 1993). Also, the Rb-Sr isotopic systems are more readily affected by metamorphism (Ashwal and Wooden 1985; Ashwal 1993), magma mixing, and crustal contamination (Emslie *et al.* 1994; Taylor *et al.* 1984).

According to Amelin *et al.* (2000), the parental magmas of the VBI were not significantly contaminated by either the Nain nor Churchill provinces during ascent into the lower crust. The MI, however, like many other intrusions throughout the NPS, was probably

extensively contaminated by rocks from the Nain Province and Churchill Province, including the Tasiuyak gneiss (Lambert *et al.* 2000; Ripley *et al.* 2000) and enderbitic gneiss of the Churchill Province (Amelin *et al.* 2000) as it was emplaced at shallow levels in the crust (Amelin *et al.* 2000). Contamination of the parental magmas of the VBI in the upper crust by the Tasiuyak Gneiss is estimated to be approximately 8-13 % (Amelin *et al.* 2000). The MI is estimated to have about 15-35 % contaminants, dominantly from Archean rocks equivalent to the Nain Province (*op. cit.*).

Figure 4.16 shows that overall, rocks from the Voisey's Bay Intrusion lie along a trend between uncontaminated picritic basalts (Lightfoot and Hawksworth 1997), primitive mantle (Sun and MacDonough 1989), and enderbitic orthogneiss (figure is adapted from Lightfoot and Naldrett 1999; Li *et al.* 2000). Breccia fragments and conduit rocks (not shown) have elevated Th/Nb ratios and lie along the trajectories of contaminated tholeiites and within the field of the Tasiuyak paragneiss. Troctolites from the MI plot strictly within the field defined by mafic orthogneiss and do not have high Th/Nb values which suggest less contamination compared to the VBI.

All of the rock types from the Cirque area lie along the same trend as those from the VBI and MI troctolites suggesting a similar genetic history, however, low Th/Nb ratios reflect the lack of conduit rocks and breccia fragments as observed in the VBI. The two pyroxenites (91 and 117) one ferrodiorite (?) lie near the field of uncontaminated picritic basalt (and primitive mantle *from* Sun and MacDonough 1989). Along the fractionation trend defined by rocks from the Voisey's Bay deposit, Th/Nb ratios of the Cirque rocks are

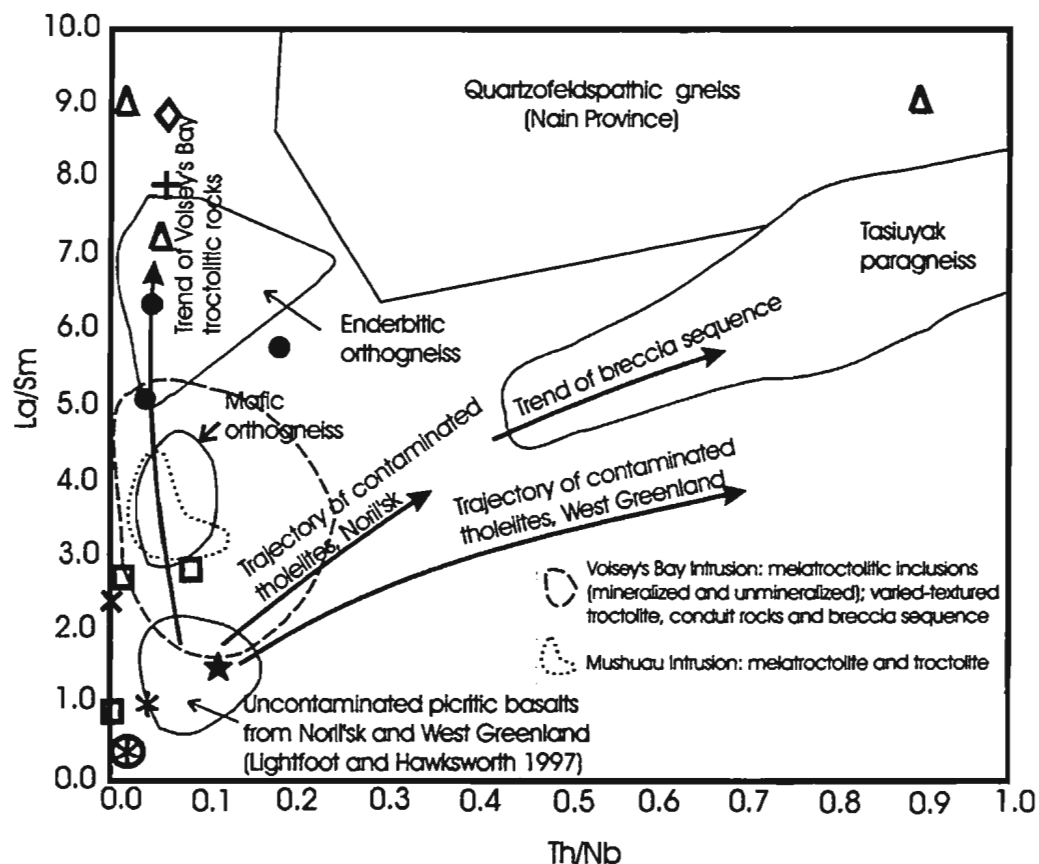


Figure 4.16 Plot of Th/Nb versus La/Sm of the Cirque rocks compared with rocks from the Voisey's Bay and Mushuau intrusions. Plot is adapted from Lightfoot and Naldrett (1999) and Li et al. (2000) who use uncontaminated picritic basalts from Noril'sk and West Greenland (Lightfoot and Hawksworth 1997) and primitive mantle values (★; Sun and MacDonough 1989) as precursor material. Trends of contamination by various crustal material are also plotted. The Cirque rocks consist of Bleached anorthosite (◆); leuconorite/leucogabbro (△), leucotroctolite (●), ferrodiorite (□), pyroxenite (samples 91\* and 117⊗), sulphide-bearing anorthosite (+). A ferrodiorite sample (×) from the Noranda's "Hilltop" property (Lic. #915M) is also included.



low (except for one leuconorite/leucogabbro sample), but have increasing La/Sm ratios (from leucotroctolites to leucoanorthosites to leuconorite/leucogabbro). These samples include Bleached anorthosite and one sulphide-bearing anorthosite. Ferrodiorites from the Cirque have low Th/Nb and La/Sm ratios indicating that, overall, the magma from which the Cirque rocks crystallized had relatively less crustal contamination than those from the VBI.

Most of the sulphide-bearing anorthosites have low Th/Nb ratios, but very high La/Sm ratios (as high as 20; not shown in Figure 4.16), possibly indicating a separate magma source, as previously suggested, with a higher degree of contamination from the Nain Province and enderbitic gneiss of the Churchill Province, but virtually no contamination from the Tasiuyak paragneiss.

#### **4.4.1 Results of radiogenic isotope analyses for the Cirque samples**

In order to evaluate the genetic history of the anorthosite and related rocks at the Cirque, Sm-Nd and Rb-Sr isotope ratios were measured in a suite of samples. The set consists of Bleached anorthosite, anorthosite (pyroxene-rich) - leucogabbro, norite, leucotroctolite, pyroxenite, and a felsic dyke. Using a crystallization age of 1.30 Ga (DePaolo 1985; Emslie *et al.* 1994), the results are listed in Table 4.2. The equations and constants used in the calculations are given in Appendix A1 along with a description of the analytical procedures.

Table 4.2 Sm-Nd and Rb-Sr isotope data (measured and calculated) for samples from the Cirque property. The crystallization age used in the calculations is 1.3Ga (Einslie *et al.* 1994). Refer to Appendix A1 for equations and constants used.

Sample name	536775	536778	25928	25933	LD-96-161	LD-96-91	LD-96-7A	LD-96-107
Rock type	Leucotroctolite	Leucotroctolite	Norite	Norite	Anorthosite/Leucogabbro	Pyroxenite	Bleached anorthosite	Felsic Dyke
Rb (ppm)	1.12	1.41	1.66	6.19	1.51	bdl	1.89	29.15
Sr (ppm)	730.83	774.28	819.2	619.07	651.75	bdl	864.93	322.74
Sr/Nd	85.68	161.31	52.11	93.09	60.35	na	457.63	11.07
<sup>87</sup> Sr/ <sup>86</sup> Sr	0.704	0.704	0.705	0.706	0.705	0.705	0.705	0.711
<sup>87</sup> Rb/ <sup>86</sup> Sr	0.004	0.005	0	0.028	0.007	na	0.006	0.243
( <sup>87</sup> Sr/ <sup>86</sup> Sr) <sub>1.3Ga</sub> or (ISr)	0.704	0.704	0.705	0.706	0.705	na	0.705	0.706
Sm (ppm)	1.44	0.85	2.62	0.99	1.88	0.93	1.09	13.8
Nd (ppm)	8.53	4.8	15.72	6.65	10.8	6.03	7.43	110.71
Sm/Nd	0.169	0.177	0.167	0.149	0.174	0.154	0.147	0.125
<sup>143</sup> Nd/ <sup>144</sup> Nd	0.512	0.512	0.511	0.511	0.512	0.512	0.511	0.511
<sup>147</sup> Sm/ <sup>144</sup> Nd	0.104	0.11	0.103	0.092	0.107	0.095	0.091	0.08
$\epsilon_{Nd}$ (age = 1.3 Ga)	-4.91	-2.72	-8.76	-8.51	-4.51	+1.96	-8.27	-19.46
$\epsilon_{Nd}$ (age = 0)	-20.33	-17.21	-24.4	-25.89	-19.35	-14.92	-25.91	-38.88
T <sub>DM</sub> (Ga)	1.02	0.85	1.29	1.28	0.99	0.6	1.26	1.9
f Sm/Nd	-0.47	-0.44	-0.48	-0.53	-0.45	-0.52	-0.54	-0.59

Note : bdl = below detection limit; na = not available

Overall, the Cirque mafic samples agree with  $[\text{}^{87}\text{Sr}/\text{}^{86}\text{Sr}]_i$  or  $\text{ISr}$  and  $\epsilon\text{Nd}$  values (at 1.3 Ga) calculated for the main mafic rock types elsewhere in the NPS (Table 4.3; *from* Piercey *pers. comm.* 1997). The  $\text{ISr}$  values of the mafic Cirque samples (that is, anorthosite, leucogabbro, and norite varieties) range from 0.704 to 0.706, slightly higher than those from the Voisey's Bay Intrusion (0.703 to 0.704) and the Mushuau Intrusion (0.703 to 0.705) which were calculated by Amelin *et al.* (2000) at 1.32 Ga. The mafic Cirque samples have much lower  $\epsilon\text{Nd}$  values (ranging from -8.76 to -2.72), than those from the VBI, however, they do lie within the range of  $\epsilon\text{Nd}$  values from the MI (Table 4.3; Figure 4.17). The  $\epsilon\text{Nd}$  value for the pyroxenite sample is +1.96, however, Rb and Sr concentrations could not be measured due to lack of plagioclase, thus, the  $\text{ISr}$  value cannot be calculated. The isotopic data for felsic dyke, which intrudes the anorthosites, are  $\epsilon\text{Nd} = -19.46$  and  $\text{ISr} = 0.706$ .

In comparison, based on radiogenetic studies by Amelin *et al.* (2000), gneissic rocks from the  $\epsilon\text{Nd}$  values (at 1.32 Ga) range from -18 to -12 from the Nain Province, -10 to -8 for the Tasiuyak paragneiss, and -5.69 to -2.82 for the enderbitic orthogneiss (both of the Churchill Province). Values of  $\text{ISr}$  for these gneissic rocks calculated by Amelin *et al.* (2000) are: 0.704 to 0.709 (Nain Province), 0.712 to 0.717 (Tasiuyak paragneiss, and 0.704 (enderbitic orthogneiss). Overlapping  $\epsilon\text{Nd}$  values of the Cirque rocks (Figure 4.17) suggest that the dominant source of crustal contamination is the Churchill Province (both the

Table 4.3 Rb-Sr and Sm-Nd isotopic characteristics of the Nain Plutonic Suite

Rock Type	Location	Age	ISr	εNd
Anorthosite	Nain Plutonic Suite	1300Ma	0.703 to 0.706	-3 <sub>2</sub> -13.9
Ferrodiorite	Nain Plutonic Suite	1300Ma	0.706 to 0.709	-8.1 <sub>2</sub> -11.7
Granitoid	Nain Plutonic Suite	1300Ma	0.706 to 0.708	-8.7 <sub>2</sub> -14.1
Troctolite	Kiglapait Intrusion	1305Ma	0.704 (LZ) 0.707 (UZ)	-1.6 (LZ) <sub>2</sub> -5.6 (UZ)
Granitoid	Wheeler Mountain	2125Ma	0.736 to 0.741	-7.7 <sub>2</sub> -8.1
	Mountain Islands	1775Ma	0.710 to 0.714	-7.5 <sub>2</sub> -9.2
	Umiakovik Intrusion	1320Ma	0.709 to 0.706	-7.7 <sub>2</sub> -11.0
	Voisey's Bay syenite*	1320Ma	0.706	-28
Troctolite, Gabbro	Voisey's Bay Intrusion*	1320Ma	0.703 to 0.704	-1 to -2
	Mushuau Intrusion*	1320Ma	0.703 to 0.705	-3 to -10
Gneiss	Nain Province*	1320Ma	0.704 to 0.709	-12 to -18
	Tasiuyak paragneiss*	1320Ma	0.712 to 0.717	-8 to -10
	Enderbiditic orthogneiss*	1320Ma	0.704	-2.82 to -5.69

from *Piercey pers comm.* (1997); \* from *Amelin et al.* (2000)

LZ = Lower Zone; UZ = Upper Zone

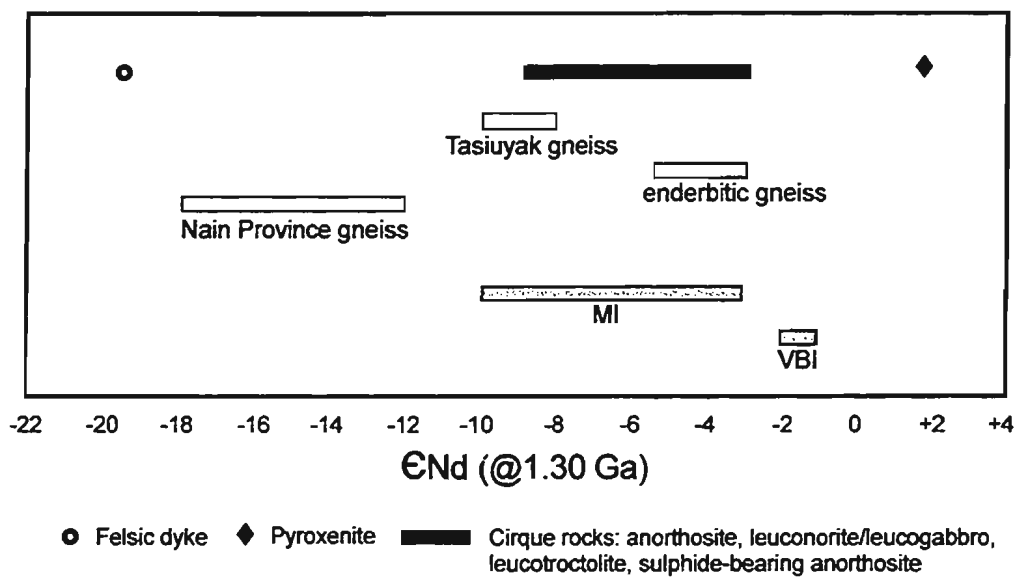
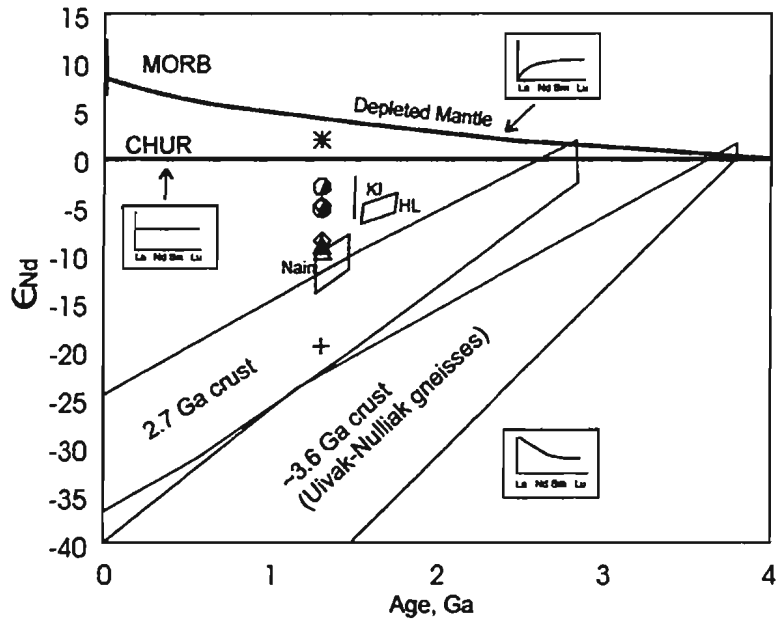


Figure 4.17 Fields of  $\epsilon_{\text{Nd}}$  (@1.30 Ga) of the Cirque rocks. Data from the Nain Province gneiss, Tasiuyak gneiss, and enderbitic gneiss of the Churchill Province are from Amelin et al. (2000). Data from Amelin et al. (2000) of the Voisey's Bay Intrusion (VBI) and Mushuau Intrusion (MI) are included for comparison (grey).

Tasiuyak gneiss and enderbitic gneiss), however, the  $I_{Sr}$  values of the Cirque rocks are much lower than those from the Tasiuyak gneiss and agree with values from the enderbitic gneiss and the Nain Province gneiss. Thus, crustal contamination from both provinces was likely. The felsic dyke from the Cirque, which has a  $I_{Sr}$  value within the range of the Nain Province gneiss, indicates a highly contaminated, fractionated magma.

Figure 4.18 is adapted from Ashwal and Wooden (1985) and Ashwal (1993) and indicates narrow fields for Proterozoic massif-type anorthosites plotted as age versus  $\epsilon Nd$  values. The chondritic evolution line (CHUR) defines the chondritic source for anorthositic massifs. Samples which plot above this line indicate that they were derived from a depleted mantle. Below this line, the source is an enriched mantle with crustal material. Typical REE signatures of each source rock are given for comparison.

The majority of the mafic rocks from the Cirque plot below the CHUR line near most of the mafic intrusions of the NPS, such as the Kiglapait Intrusion. Most samples plot above the field defined by the 2.7 Ga old crust (*eg.* Nain Province; Ashwal and Wooden 1985; Ashwal 1993). Variations around the fields of separate intrusions in Figure 4.18 may reflect inhomogeneous crustal assimilation. The felsic pegmatitic dyke indicates a strong crustal influence, not surprising if the genetic model suggesting crustal anatexis as the source of felsic material is correct. The pyroxenite sample (91) plots above and very close to the chondritic line, supporting the geochemical supposition that it represents the least fractionated source of all the Cirque rock types.



KJ = Kiglapait Intrusion; HP = Harp Lake Intrusion; Nain = Nain Plutonic Suite (exact location not specified; Ashwal 1993); MORB = range of modern MORB (from BSVP 1981).

Figure 4.18 Plot of age (Ga) versus  $\epsilon_{Nd}$  for Mesoproterozoic NPS intrusions. Cirque anorthosites and related rocks are plotted separately: Anorthosite/leucogabbro =  $\diamond$ ; Bleached anorthosite =  $\diamond$ ; Norite =  $\Delta$ ; Leucotroctolite =  $\circ$ ; Pyroxenite =  $*$ ; Felsic dyke =  $+$ . CHUR = chondritic evolution line. Depleted mantle line is from DePaolo (1981). Field showing evolution of the 2.7 Ga crust is from Wooden (unpublished data). Field showing evolution of ~3.6 Ga gneisses is from Collerson et al. (1983). All data excluding that from the Cirque property are adapted from Ashwal and Wooden (1985) and Ashwal (1993).



Crustal contamination has long been accepted as the major contributor affecting the geochemistry and evolution of anorthositic massifs in northern Labrador (*cf.* Ashwal 1993; Emslie *et al.* 1994; Ripley *et al.* 1999; Li and Naldrett 1999; Lightfoot and Naldrett 1999; Amelin *et al.* 2000). Unlike rocks at the Voisey's Bay deposit where partially digested gneissic breccia has helped to identify the type of main crustal contaminant as being the Tasiuyak gneiss (Amelin *et al.* 2000; Li and Naldrett 2000), the Cirque area is not in close proximity to gneissic rocks, nor are any gneissic fragments observed within the mafic intrusions. Nonetheless, given that the magmatic event which produced the NPS involved extensive intrusions into the continental crust on both sides of the suture line, it is assumed that the mafic intrusions at the Cirque were involved with some degree of mixing with the country rock. What has been undetermined thus far are the sources and degrees of crustal contamination of the mafic intrusions during emplacement in the Cirque area. Deep crustal contamination versus a source at shallow levels are difficult to discern at this point, however,  $^{87}\text{Sr}/^{86}\text{Sr}$  values of the Cirque rocks agree with those of Taylor *et al.* (1984) who state that the broad range shows the trend of mantle-derived, uncontaminated magma (low  $^{87}\text{Sr}/^{86}\text{Sr}$  values) with increasing contamination by metasedimentary country rocks or fluids that have passed through them (higher  $^{87}\text{Sr}/^{86}\text{Sr}$  values). The low Rb contents in all but one of the mafic varieties from the Cirque (<2 ppm; Table 4.2) suggest minimal crustal contamination (*i.e.* low Rb/Sr ratios; Taylor *et al.* 1984) possibly caused by dilution from a large intrusive event in the northern NPS or inhomogeneous mixing of the crustal material. Overall, the norite

sample (25433) has relatively higher Rb concentrations (>5 ppm), reflecting possibly greater crustal influences (Morse and Hamilton 1990; Ashwal and Wooden 1985). Rubidium and Sr contents of the felsic dyke, as expected, indicate its source having the greatest crustal contaminants.

Given that the location of the Cirque property is along or near the extrapolated suture line joining the Nain Province and the Churchill Province, it is possible that crustal contaminants may have been derived from either or both provinces, however, according to a plot of  $ISr_{(1.3\text{ Ga})}$  versus  $\epsilon Nd_{(1.3\text{ Ga})}$  (Figure 4.19), it seems that the Churchill province gneiss is the dominant source of contamination for the Voisey's Bay deposit and the Cirque rocks. Figure 4.19, adapted from Emslie *et al.* (1994) and Amelin *et al.* (2000), show the Cirque rocks as having overall  $\epsilon Nd_{(1.3\text{ Ga})}$  values > -10, and plot in two separate clusters: (1) three samples, which include two leucotroctolites and one pyroxene-rich anorthosite/leucogabbro, plot near the field defined as gneissic inclusions in breccias and enderbitic gneiss by Amelin *et al.* (2000) and (2) three samples, which include two norites and one Bleached anorthosite, plot closer to the field defined as the Nain Province gneiss by Amelin *et al.* (2000). The felsic dyke sample plots on the far "east" side of the suture line within the Nain Province field, suggesting crustal contamination from the Nain Province.

Voisey's Bay troctolitic rocks from Amelin *et al.* (2000), calculated at 1.32 Ga also plot distinctly within this figure. Rocks from the Voisey's Bay Intrusion plot near the fields of enderbitic gneiss and gneissic inclusions in breccia, on the western side of the suture line,

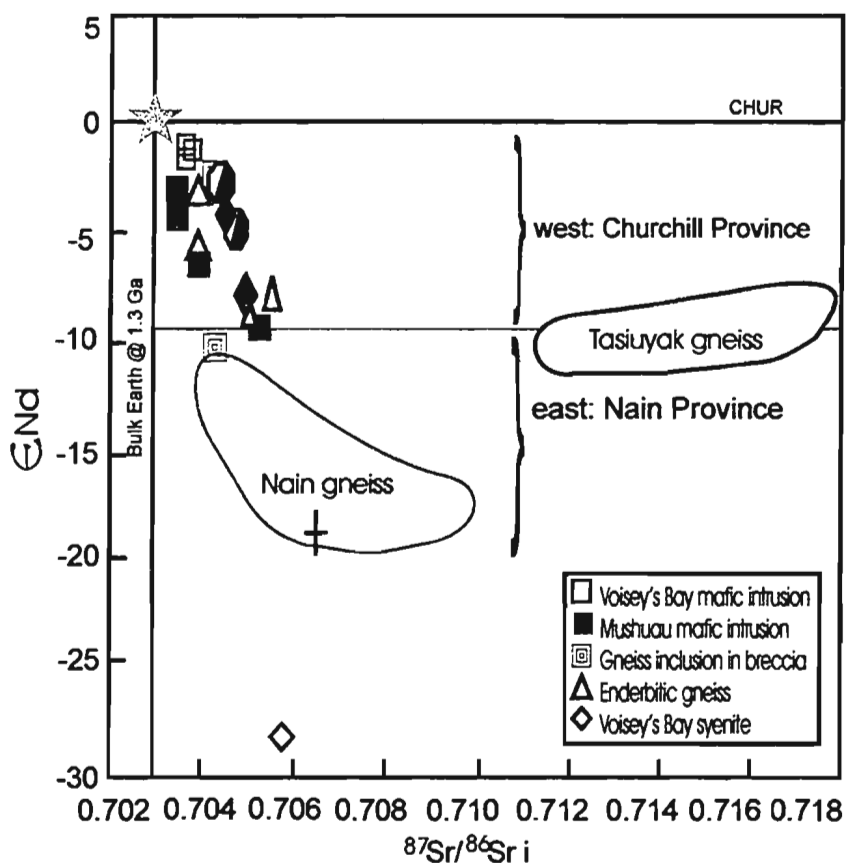


Figure 4.19 Plot of  $^{87}\text{Sr}/^{86}\text{Sr}$  initial versus  $\epsilon_{\text{Nd}}$ , both at 1.3 Ga for the Cirque anorthosites and related rocks. The west and east sides of the Nain and Churchill province suture have been divided according to values by Emslie et al. (1994). Rocks from the Cirque consist of: Anorthosite-Leucogabbro =  $\blacklozenge$ ; Bleached anorthosite =  $\blacklozenge$ ; Norite =  $\triangle$ ; Leucotroctolite =  $\circ$ ; Felsic dyke =  $+$ . CHUR = chondritic evolution line. Bulk Silicate Earth =  $\star$ . Plot of  $\epsilon_{\text{Nd}}(1.32)$  versus  $^{87}\text{Sr}/^{86}\text{Sr}$  initial (1.32) of various rocks (grey) from the Voisey's Bay and Mushuau intrusions and the surrounding country rocks is from Amelin et al. 2000.

close to the first Cirque cluster. Rocks from the Mushuau Intrusion plot similarly to the Cirque rocks, that is, near the field of enderbitic gneiss as well as closer to the eastern side of the suture line. One sample of an inclusion of gneissic breccia plots on the eastern side of the suture line, possibly derived from the Nain Province.

Mixing lines were used by Amelin *et al.* (2000) on a plot of  $^{87}\text{Sr}/^{86}\text{Sr}_{(t@1.32\text{Ga})}$  versus  $\epsilon\text{Nd}_{(t@1.32\text{Ga})}$  to interpret the dominant source of contamination and the degree of contamination in terms of percentages for the Mushuau and Voisey's Bay intrusions. Figure 4.20, adapted from Amelin *et al.* (2000), has several mixing lines with the primary melt (star) being 1.28 Ga low-P Nain dykes. Because the Cirque rocks have  $\epsilon\text{Nd}$  values much lower than those of the VBI, only data from the MI (Amelin *et al.* 2000) are used. Wiebe (1985), who studied numerous dykes throughout Labrador, defined two subtypes of what are known as the Nain dykes (LP and HP), both which are Mesoproterozoic and crosscut all rock types within the NPS. Both types are alkaline to transitional basaltic dykes with abundance plagioclase, olivine, and clinopyroxene (*op cit.*). The LP (low P) Nain dykes are dominantly 10-15 m wide, vertically dipping, and have a east-northeast trend (Wiebe 1985; Gower *et al.* 1990). The HP (high P) Nain dykes are generally <1 to 10 m wide and strike between northwest in the south to north-northeast in the north, forming an arcuate pattern (Wiebe 1985; Gower *et al.* 1990). Although crosscutting relationships have never been observed in the field, the two subtypes of dykes are thought have different emplacement ages (Wiebe 1985). Minima ages determined by K-Ar whole rock methods are  $977\pm44$  Ma for

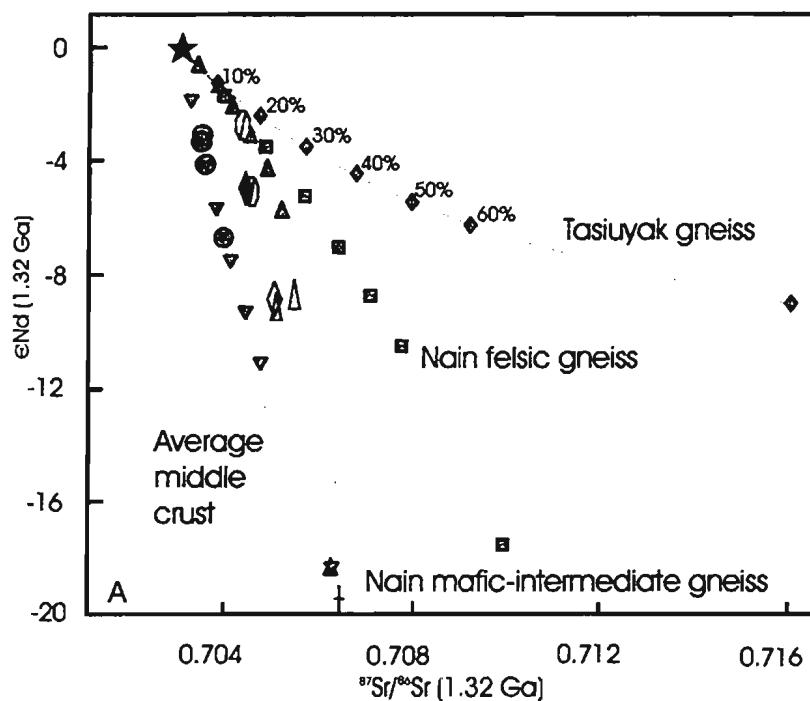


Figure 4.20 Plot of  $^{87}\text{Sr}/^{86}\text{Sr}$  initial versus  $\epsilon_{\text{Nd}}$  at 1.32 Ga of rocks from the Mushuau Intrusion rocks (MI; ●) along mixing lines of mantle endmember (primary melt ★; similar to the Nain basaltic dykes) and possible contaminants: Tasiuyak gneiss (◆); Nain felsic gneiss (■); Nain mafic-intermediate gneiss (▲); and average middle crust (▼). Percent crustal contamination is plotted in increments of 10% from primary melt (100% or no contamination) to increasing contamination along the mixing lines as shown. Plot is adapted from Amelin et al. (2000). Additional samples from the Cirque are plotted for comparison with the MI along the mixing lines, but isotopic data were calculated using 1.30 Ga for the crystallization age. Cirque rocks: Anorthosite-Leucogabbro = ◆; Bleached anorthosite = ◇; Norite = ▲; Leucotroctolite = ◊; Felsic dyke = †.

the LP dykes and  $1042 \pm 54$  Ma for the HP dykes (Wiebe 1985), however, two dates of  $1276 \pm 23$  Ma (Rb-Sr) and  $1385 \pm 143$  Ma (Sm-Nd), respectively, have also been determined (Gower *et al.* 1990 who cite Wiebe *pers comm.* 1989).

Early studies of the Kiglapait Intrusion concluded that the  $\epsilon_{\text{Nd}} (@ 1.3 \text{ Ga})$  value is -3.0 (DePaolo 1985; Emslie *et al.* 1994); however, Amelin *et al.* (2000) state that the more acceptable mantle endmember of the NPS should be the oldest and more primitive mafic intrusions in the area, the *ca.* 1.28 Ga LP Nain basaltic dykes (described by Wiebe 1985) which have isotopic compositions of  $\epsilon_{\text{Nd}} = 0.1$  to  $-0.9$  and  $\text{I}_{\text{Sr}} = 0.7028$  to  $0.7031$  (calculated at 1.32 Ga; Carlson *et al.* 1993). Thus, the geochemical composition of the LP dykes (*e.g.*, MgO = 7.3 to 5.3 wt%) can also be used as estimates of the geochemical composition of the earliest mantle-derived basaltic magmas of the NPS (Amelin *et al.* 2000). For isotopic studies of the Voisey's Bay Intrusion, Amelin *et al.* (2000) interpreted the isotopic data from the LP Nain basaltic dykes to be the mantle component in the Nain Plutonic Suite with  $\epsilon_{\text{Nd}} (@ 1.32 \text{ Ga}) = 0$  and  $\text{I}_{\text{Sr}} (@ 1.32 \text{ Ga}) = 0.70294$  which are also the same values of the assumed Bulk Earth. Amelin *et al.* (2000) does not imply, however, that the mantle source was not partially melted or contaminated by crustal rocks prior to the formation of the Voisey's Bay Intrusion. Bulk Earth isotopic values were used in the study by Amelin *et al.* (2000) due to earlier interpretations (*cf.* Pace and Bell 1989; Shirey 1994) which show that the Bulk Earth may be the mantle source for basaltic intrusions and those of Schärer (1991) who states that Mesoproterozoic magmatism in eastern and northern

Labrador was derived from a mantle source with near Bulk Earth isotopic values. Studies of the basaltic dykes north and along the Grenville Front by Wiebe (1985) and Schärer (1991) suggest a single mantle source for the widespread magmatism which formed the NPS, or at least more than one source with similar chemical and isotopic characteristics. Thus, it is assumed in this study that isotopic values of the mantle component (MC) for the Voisey's Bay Intrusion may be similar to that for the Cirque intrusions and so MC = 0 is also acceptable.

Li *et al.* (2000) suggest that a picrite or high-Mg basalt parental melt is the mantle endmember and so for isotopic studies of the VBI and MI, Amelin *et al.* (2000) considered the isotopic characteristics of parental basalts from which low and high Ti continental flood basalt with 15 wt % MgO (Arndt *et al.* 1993; Lightfoot *et al.* 1993; Wooden *et al.* 1993) are derived. Using  $\epsilon_{\text{Nd}}(@1.32 \text{ Ga}) = 4$  and  $\text{ISr}_{(@1.32\text{Ga})} = 0.70235$  of the mantle-derived basaltic melt, Amelin *et al.* (2000) state that these values are within the range defined by a depleted mantle source (according to Zartman and Haines 1988) and Bulk Earth (at 1.32 Ga) and are acceptable for a source from an evolving plume (Stein and Hofmann 1994). The source material for the Cirque rocks may not have been a picrite or high-Mg basalt due to their low MgO contents (<7 wt% MgO; excluding pyroxenite rocks), however, due to their highly fractionated nature such a parental source may still be possible.

All of the Cirque rocks in Figure 4.20 plot as a range below the Nain basaltic dykes interpreted to be the mantle-derived endmember between the mixing line defining the average middle crust (Amelin *et al.* 2000 used Nd and Sr concentrations from Rudnick and Fountain 1995) and those of the Nain mafic-intermediate gneiss. Estimated percentages of



contamination ranges from 35 % to ~60 % for Nain mafic-intermediate gneiss and 20 % to 50 % for average middle crust. Such a mixture of contaminants, as well as the presence of clusters of Cirque rocks in Figure 4.20, suggest inhomogeneous assimilation of country rock material within the Cirque area. In comparison, the dominant crustal contaminants is 8-13 % Tasiuyak gneiss for the VBI and 15-35 % of the average middle crust (possibly Nain Province gneiss) for the MI (Amelin *et al.* 2000). Thus, it seems that the Cirque rocks have crustal contamination history more similar to the MI than the VBI.

The age of the source or time at which the mafic melt was formed from a depleted mantle reservoir is called the 'depleted mantle model age' or  $T_{DM}$  (DePaolo 1988); refer to Appendix A1 for the equation used for its calculation. Values of  $T_{DM}$  are most useful if the age difference between the magmatic intrusion and the crustal rocks is 500 Ma or greater (Patchett 1989; Piercey 1998). Model ages calculated relative to CHUR ( $T_{CHUR}$ ) were used by earlier workers; however, since many felsic and mafic intrusions emplaced within crustal rocks have originated from non-CHUR sources,  $T_{DM}$  have become more acceptable (DePaolo 1981; Piercey 1998). For the same reason,  $T_{DM}$  is used for this study and the values are listed in Table 4.2.

Although the calculated  $T_{DM}$  values for the mafic rocks from the Cirque are not precise, they suggest that the crustal residence time for the depleted mantle was short since the ages are very close to that of crystallization (refer to Table 4.2) and so mantle-derived magma had little time to assimilate a sufficient amount of crustal rocks and thereby significantly alter the Sr/Rb ratio. The felsic dyke has the highest  $T_{DM}$  value (1.90 Ga) suggesting a greater contribution of crustal rocks. These conclusions, however, are based

on the assumption that the mantle reservoir did not mix with other isotopically different reservoirs, but instead involved a closed system (Piercey 1998). Contrary to this, is the broad range of  $\epsilon_{\text{Nd}}(t=1.3 \text{ Ga})$  which suggests variable crustal contamination or a more open system; hence the calculated  $T_{\text{DM}}$  values should not be interpreted on their own.

The fractionation factor ( $f_{\text{Sm/Nd}}$ ), which indicates the amount of fractionation of Sm and Nd, reflects the amount of crustal contamination of the basaltic magma. According to DePaolo (1988), the CHUR value is  $f_{\text{Sm/Nd}} = 0$ , the depleted mantle is  $f_{\text{Sm/Nd}} > 0$  with Sm enrichment (therefore greater  $^{143}\text{Nd}$  compared to CHUR), and mafic material with crustal components have  $f_{\text{Sm/Nd}} < 0$  with Sm depletions (therefore less  $^{143}\text{Nd}$  compared to CHUR). A typical continental crust has  $f_{\text{Sm/Nd}} \approx -0.4$  (DePaolo 1988; Piercey 1998). The fractionation factor is defined by the degree of partial melting of a mafic intrusion, that is, the Sm/Nd ratio increases with continuous partial melting and fractionation of a closed system (DePaolo 1988; Piercey 1998). The equation used for calculating the fractionation factor is given in Appendix A1 and the results are given in Table 4.2.

Generally, the Cirque anorthosite and mafic samples have a narrow range of fractionation factors (between -0.54 to -0.44) corresponding to a mantle-derived magma with crustal contamination (Figure 4.21). The pyroxenite sample plots above the CHUR line, but has a fractionation factor within this range (-0.52) suggesting some history of crustal contamination and fractionation of its parental magma. The felsic dyke shows the

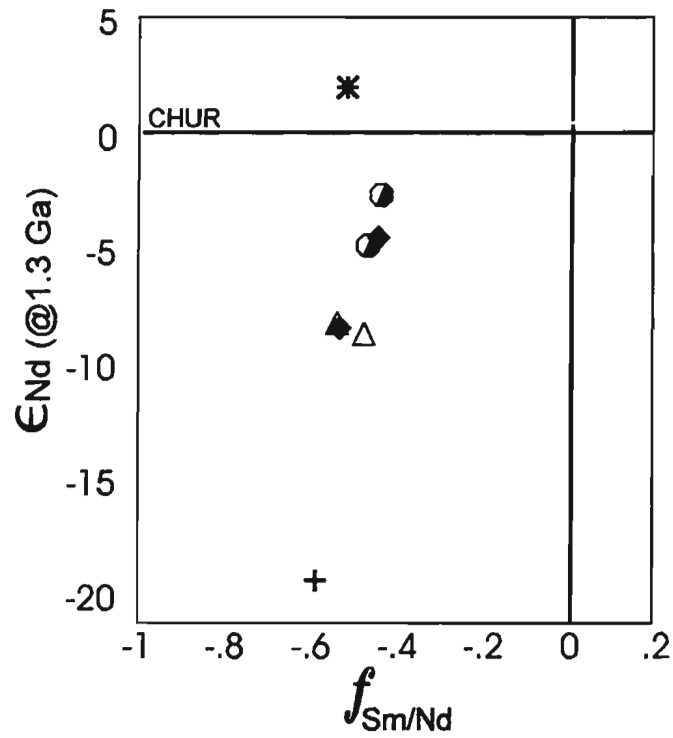


Figure 4.21 Plot of  $f_{\text{Sm/Nd}}$  versus  $\epsilon_{\text{Nd}}$  at 1.3 Ga for selected samples from the Cirque property. Anorthosite/leucogabbro =  $\blacklozenge$ ; Bleached anorthosite =  $\blacklozenge$ ; Norite =  $\circ$ ; Leucotroctolite =  $\blacktriangle$ ; Pyroxenite =  $\ast$ ; Felsic dyke =  $+$ .

highest degree of crustal contamination (-0.59) which is not surprising, for the most fractionated of all the rock types in the area.

Another method of interpreting  $\epsilon\text{Nd}$  values and the relationship of magmatic and crustal components is the 'neodymium crustal index' or NCI (DePaolo *et al.* 1992; Piercey 1998). The equation for determining the NCI is given in Appendix A1. DePaolo *et al.* (1992) use two constants involving the mantle contribution [MC = mantle component;  $\epsilon\text{Nd}_{(t=1.3\text{ Ga})} = -3.0$ ] and the crustal contribution [CC = crustal component]. For the NPS, the CC is  $\epsilon\text{Nd}_{(t=1.3\text{ Ga})} = -21.9$  for the Nain Province, -14.6 for the Churchill Province (Emslie *et al.* 1994), and -9.3 for the Tasiuyak gneiss (Piercey 1998). Emslie *et al.* 1994 calculated NCI values using the above values and  $\text{MC}_{1.30\text{Ga}} = -3.0$  based on the interpretation that the mantle source is similar to that of the Kiglapait Intrusion (DePaolo 1985) which formed in a closed system and olivine-bearing (Reid Brook Intrusion) and mafic rocks of the NPS (Hamilton and Shirey 1992; Hamilton 1993). An alternate MC value of 0, as suggested by Amelin *et al.* (2000) based on his interpretation of the LP Nain basaltic dykes (see above), is also used for comparison with the Voisey's Bay deposit area.

Table 4.4 lists the NCI values calculated using MC = -3.0 from Emslie *et al.* (1994) and MC = 0 (Amelin *et al.* 2000). Used by Emslie *et al.* (1994) to determine the level of contribution of crustal material during magmatic activity, they first assumed that for their study areas, the Nain Province was the major contributor of crustal contaminants. Because the results from this study do not clearly define the major crustal contributor as being either

Table 4.4 Calculated values of Neodymium Crustal Indices (NCI) for the Cirque rocks.

	Leucotroctolite 536775	Norite 25928	Norite 25933	Anorthosite/ Leucogabbro LD-96-161	Bleached Anorthosite LD-96-7A
NCI <sup>1</sup> , CC=NP	0.1	0.3	0.29	0.08	0.28
NCI <sup>1</sup> , CC=CP	0.16	0.5	0.48	0.13	0.45
NCI <sup>1</sup> , CC=TG	0.3	0.91	0.87	0.24	0.84
NCI <sup>2</sup> , CC=NP	0.22	0.4	0.39	0.21	0.38
NCI <sup>2</sup> , CC=CP	0.34	0.6	0.58	0.31	0.57
NCI <sup>2</sup> , CC=TG	0.52	0.94	0.92	0.48	0.89

NCI<sup>1</sup> = NCI values using MC = -3.0 (Emslie *et al.* 1994) and age of 1.30Ga;

NCI<sup>2</sup> = NCI values using MC = 0 (Amelin *et al.* 2000) and age of 1.32Ga

CC = Crustal component; MC = Mantle component; NP = Nain Province;

CP = Churchill Province; TG = Tasiuyak Gneiss

$\epsilon\text{Nd}$  values of CP (-14.6) and NP (-21.9) are from Emslie *et al.* (1994).

$\epsilon\text{Nd}$  value of TG (-9.3) is from Thériault and Ermanovics (1997) and Wilton (*unpublished data*).

the Churchill, Nain provinces, the Tasiuyak gneiss, nor enderbitic gneiss, the NCI values were calculated using CC values for all three crustal sources. The results are given in Table 4.4. The majority of the NCI values consist of mafic varieties ranging from 0 to 0.4 for the Nain Province, 0 to 0.5 for the Churchill Province, 0 to 0.9 for the Tasiuyak gneiss. Pyroxenite has negative NCI values and geologically unfeasible (*i.e.* less than zero crustal contamination of precursor to the mafic rocks from the Cirque). The felsic dyke has highest NCI values (*i.e.*, greater than 100% crustal contamination) and also not geologically feasible. Calculations of NCI values using the enderbitic gneiss as the crustal component ( $CC = -4.01$  averaged from three values from Amelin *et al.* 2000) yielded unacceptable values ( $<0$  and  $>1$ ) and were not used for this study.

Overall, the NCI values suggest that if the Tasiuyak gneiss was the dominant contaminant in the Cirque area than nearly 100% assimilation would have occurred. This amount is not acceptable given that fact that other contaminants were also involved during the extensive magmatic event. Hence, the most reasonable contaminants are the Nain Province and Churchill Province rocks. This agrees with radiogenitic data presented earlier. Using the mantle component as -3.0, the degrees of crustal contamination range from 10 to 30 % for the Nain Province and 13 to 50 % for the Churchill Province. The degrees of contamination are 22 to 40 % for the Nain Province and 31 to 60 % for the Churchill Province if the NCI is calculated using a mantle component of 0. Both ranges are similar, however, because magmatism in the Cirque area is unlikely to have formed in a closed environment,  $\epsilon Nd = 0$  for the LP basaltic dykes ( $MC=0$ ) is preferred. Thus, the calculated

ranges of percent contamination for the Nain and Churchill provinces support the radiogenetic data shown earlier (especially Figure 4.20) and, similar to the model proposed for the Mushuau Intrusion, show contamination from lithologies in both provinces.

#### 4.5 Summary

Although determination of the geochemistry of the parent magma is impossible due to the cumulate nature of the rocks at the Cirque, [Mg] values, and major and trace element geochemistry, define a tholeiitic precursor (with geochemistry similar to the two pyroxenite samples) which fractionated olivine and pyroxene minerals to form separate melts of anorthosite and mafic varieties. The long history of magmatism (that may include more than one magma source) includes crystal fractionation, partial melting, and assimilation of country rocks and has resulted in separate melts intruding each other, as seen on the Cirque grid with three different anorthosite units and layers of leucotroctolite and leuconorite/leucogabbro. The remaining melt, having undergone extreme fractionation and now rich in incompatible elements and excess major elements such as Ti and Fe, settled at the bottom of the magma chamber.

Ashwal (1993) and Ashwal and Wooden (1985) propose that the source of most anorthosite massifs worldwide are either enriched mantle or depleted mantle with crustal contamination. Studies by Heath and Fairbairn (1968) on Rb-Sr isotopic systems of anorthosites from 15 different massifs concluded that the anorthosite intrusions were derived from mafic magmas from the upper mantle or lower crust. Current studies by



Amelin *et al.* (2000) support this statement. According to Emslie *et al.* (1994), however, the presence of large volumes of anorthosite magma (plagioclase and trapped liquid) is best explained by crustal contamination of primitive mantle material. Ashwal and Wooden (1983a,b; 1985) proposed that positive  $\epsilon_{Nd}$  values of many anorthosite massifs indicate LREE depleted sources relative to chondrite material, thus excluding the role of crustal contamination since crustal rocks are typically LREE enriched. Ashwal (1993) favors a depleted mantle source similar to those for mid-ocean ridge basalts, however, he does not entirely discredit evidence which suggests crustal influence for the genesis of some anorthosite massifs.

Although gneissic units have not been observed on the Cirque property nor have been intersected by drill holes, preceding trace element and radiogenic geochemistry support the theory of contamination. A moderate degree of assimilation is expected due to the large volume of anorthosite magma involved and the long period of emplacement. The greatest amount of assimilation would generally be after the initial intrusion of the anorthositic magma into the crust, when the crust has been warmed somewhat by the hot magma below and the contamination is concentrated along the contact of an intruding pluton with the crust; the amount of assimilated material decreases away from the contact towards the centre of the massif. This may best explain the significant degrees of contamination from the Churchill and Nain provinces (total amount of contaminants between 20 and 60 %), resulting in a wide, yet acceptable range of  $\epsilon_{Nd}$  while still having a restrictive initial  $^{87}Sr/^{86}Sr$  values.

As mentioned in the previously (Section 4.3.4), Amelin *et al.* (2000) attribute the differences between the two intrusions of the Voisey's Bay deposit to the fact that the earliest mafic intrusions (which formed the VBI) were the least fractionated and were emplaced at shallow levels in the crust, thus resulting in less assimilated crustal material of the parental magma. Later intrusions are thought to have been larger and incorporated more crustal material and granitoid restites (formed at the beginning of the emplacement of the NPS), thus becoming more fractionated and contaminated. Amelin *et al.* (2000) believe that larger, younger intrusive event formed the MI. Based on the geochemistry and radiogenetic data from this study, it seems that the magmatic history, including the sources and degree of crustal contamination, in the Cirque area is more similar to that which formed the MI than the VBI.

Understanding the host rocks of the sulphides at the Cirque is not straight forward since evidence of significant syngenetic mineralization has not been observed on surface nor intercepted by drill holes. Comparisons with unmineralized rock types in other locations in the NPS have shown them to have the same general geochemical features. Unfortunately, such comparisons for understanding the genesis of sulphide melt in the parental magma are limited since the anorthosites at the Cirque and possibly surrounding area are not the source of the immiscible sulphides. Trace element geochemistry of the massive sulphide sample from the neighbouring Canadian States Resources property does suggest a "yet-to-be-discovered" mafic unit which may be the host for syngenetic mineralization in the Cirque area.

## CHAPTER 5

### SULPHIDE GEOCHEMISTRY

#### 5.1 Introduction

Magmatic Ni-Cu±PGE sulphide ores form due to the accumulation of immiscible sulphide-oxide droplets from a sulphur-saturated mafic or ultramafic silicate melt just before, during, or just after, emplacement in the crust at temperatures  $\geq 900^{\circ}\text{C}$  (Craig and Vaughan 1994). The immiscibility or segregation of sulphides from a silicate magma is caused by sulphide saturation in the magma and the preferential partitioning of Cu, Ni, and PGE metals into the sulphide liquid compared to the silicate magma. The two most common causes of sulphide saturation are (i) excess silica which decreases the sulphur capacity in the magma (Naldrett 1996) or (ii) excess sulphur (Naldrett 1997); both silica and sulphur are abundant in many gneisses and sedimentary country rocks. As more metals are partitioned or “scavenged” from the silicate magma by the sulphide droplets, the segregated sulphide melt becomes progressively enriched in these metals and subsequent accumulation of the sulphide melt in topographic lows in the magma chamber further increases the size and grade of the ore (Barnes *et al.* 1997a). Cooling of the sulphide pool results in sulphide melt fractionation through the sequential formation of sulphide minerals (pyrrhotite, chalcopyrite, pentlandite, cubanite). Often in orthomagmatic sulphide deposits, copper-rich veins crosscut “country rocks” (in the Cirque property this means anorthosite) and metal zonations in Fe-rich massive sulphides are indicated by slightly increased Cu contents

defined by irregular blebs and disseminations of chalcopyrite concentrated along the massive pyrrhotite zones.

To understand the evolution of the sulphide melt and to determine the potential of the Cirque area to host an economic Ni-Cu±PGE magmatic sulphide occurrence, this chapter presents the results of geochemical and stable isotopic analyses of sulphide-rich core and outcrop samples; that is, those samples with >5 % visually estimated sulphide minerals. Tracing the genetic history of sulphide mineralization in the Cirque area is difficult without a full understanding of the magma from which the sulphides segregated. As mobilized sulphides, the metal compositions in the Cirque mineralization may not reflect the original sulphide melt that was in equilibrium with the silicate magma upon sulphide saturation. Nonetheless, the data presented in this chapter represent a segregated sulphide melt mobilized from an unknown host magma at depth.

Concentrations of Ni and Cu were measured at Memorial University in over 100 core and outcrop samples (pyrrhotite, chalcopyrite, pentlandite, and pyrite) with various textures. The Ni, Cu, and Co contents analysed for Cartaway Resources between 1996-1997 in holes LBN-1 to 11 are also included here, however wt% S was not measured (Appendix A2). Sulphide geochemistry from microprobe analyses of pyrrhotite and chalcopyrite minerals, includes data for samples kindly provided by workers from the Voisey's Bay deposit (Voisey's Bay Nickel Ltd.), the "Nain Hill" prospect (NDT Ventures Ltd.), the South Voisey's Bay area (Donner Minerals), and the OKG prospect (Castle Rock Exploration Ltd.). Sulphur isotope analyses were conducted to determine the source of the

sulphur in the sulphides. This chapter also includes the results of PGE analyses for samples from several drill holes. Refer to Appendix A2 and A3 for results of the various analyses described above and Appendix A1 for descriptions of each analytical method.

## **5.2 Electron microprobe analyses**

Microprobe analyses of Ni, Fe, Co, Cu, S, and Se were derived from disseminated to massive sulphides, consisting of (1) coarse-grained pyrrhotite, (2) irregular, isolated grains of chalcopyrite located along and near the outer contacts of massive pyrrhotite, (3) fine-grained pentlandite exsolution lamellae with pyrrhotite grains, and (4) fine-grained pyrite (in places as rims around pyrrhotite grains). The methodology and standards are discussed in Appendix A1 and the data are listed as element percent in Appendix A3.5. The analyses confirm that the sulphide mineralogy consists of (in order of decreasing abundance) pyrrhotite, chalcopyrite, and pentlandite. Minor Cu sulphides (possibly cubanite) were also detected. Pyrite was analysed; however, in this study, pyrite is not the product of magmatic sulfide processes, but rather oxidation weathering of pyrrhotite.

Several samples, also selected from other sulphide occurrences within the NPS; including “Hilltop” property (Noranda), Licence #1514M (Canadian States Resources), OKG prospect (Castle Rock), “Nain Hill” prospect (NDT Ventures), the Voisey’s Bay deposit, and South Voisey’s Bay Project (Donner Minerals), which all have the same sulphide mineralogy but with variable modal abundances. In all of these other properties, magnetite was visually more abundant in the sulphide intersections than at the Cirque,

indicating that they were derived from less reduced systems.

Two samples of pyrrhotite, collected from massive sulphide zones at the Cirque, were analysed using X-ray diffraction (XRD) to determine if the pyrrhotite was monoclinic or hexagonal (see Appendix A1 for a description of the method). Overall, core intersections of massive pyrrhotite (with very little to nil magnetite) were magnetic, varying from weak to strong, suggesting a monoclinic structure. Results of the XRD study, however, were not conclusive, and indicated a mixture of both hexagonal and monoclinic pyrrhotite structures. This is unlike pyrrhotite at the Voisey's Bay deposit and the Pants Lake Intrusion Suite (South Voisey's Bay Project) which are dominantly hexagonal with variable abundances of troilite (FeS) as exsolution lamellae (Naldrett *et al.* 2000b). Troilite in pyrrhotite was not identified in the Cirque sulphides.

Pyrrhotite grains from the Cirque contain 0.32%<sub>avg</sub> Ni, 60.20 %<sub>avg</sub> Fe, and 40.93 %<sub>avg</sub> S. Chalcopyrite grains contain an average 32.77% Cu and 31.04 % Fe. The average Ni and Fe contents in pentlandite are 29.42 % and 26.61%, respectively. The average Co content is significantly higher in pentlandite grains (11.27 %) than in either pyrrhotite or chalcopyrite. Pyrite grains have very low Ni, Cu, and Co contents. Pyrrhotite generally has relatively low Cu and Ni contents in solid solution, depending upon the rate or extent of diffusion of copper-rich and nickel-rich sulphides from the *mss* (Craig and Vaughan 1995). Overall, pyrrhotite from disseminated to massive sulphides at the Cirque in both outcrop and drill hole intersections, and trace disseminated sulphides in the pyroxenite talus sample (91), have low Cu and variable Ni contents (Figure 5.1a). Metal contents in the disseminated and

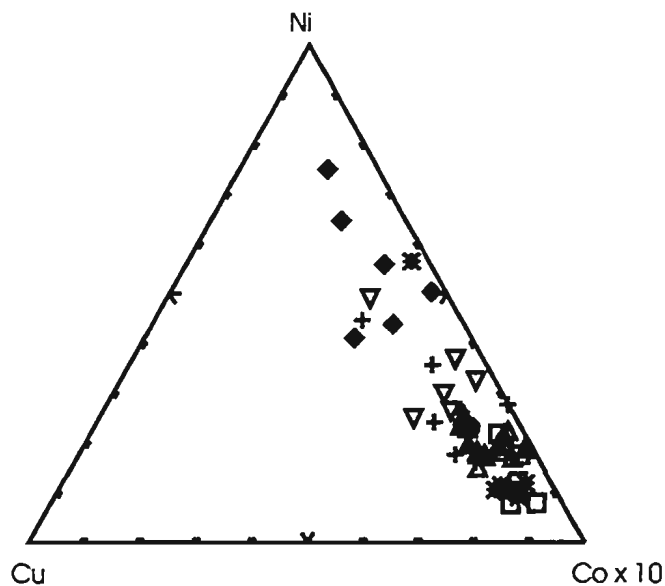


Figure 5.1a Ternary plot of Cu, Ni, and Co (element percent) determined from electron microprobe analyses of pyrrhotite from the Cirque property. Circle = LBN-2, square = LBN-3, triangle = LBN-4, diamond = LBN-8, asterisk = disseminated pyrrhotite in pyroxenite (talus), cross = disseminated pyrrhotite from anorthosite (outcrop). Open symbols = disseminated; filled = massive sulphides; inverted triangle = pyrite from altered anorthosite (LBN-4).

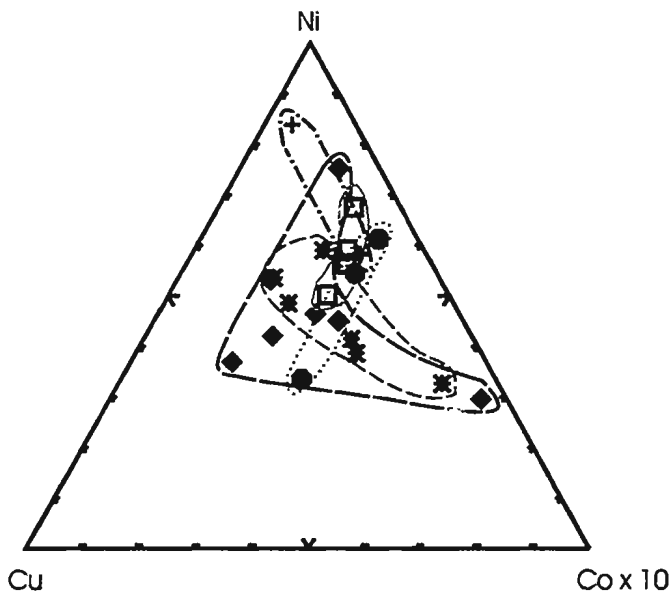


Figure 5.1b Ternary plot of Cu, Ni, and Co (element percent) determined from electron microprobe analyses of pyrrhotite from other sulphide occurrences in the NPS. Hilltop - Noranda = \*; OKG - Castle Rock = □; Licence #1514M - Canadian States Resources = ●; Nain Hill - NDT Ventures = ◆; South Voisey's Bay Project - Donner/Teck = +. Pyrrhotite from the Voisey's Bay deposit (INCO) are not plotted because Co concentrations were below detection limit.



massive pyrrhotite do not vary much, that is, the Ni and Cu contents are distributed evenly in the sulphide melt, however, a few massive pyrrhotite samples from drill hole LBN-8 do have higher Ni contents. This borehole is located further east of the other holes and may indicate that Ni-rich sulphides are increasing in this direction.

In comparison, the average Ni and S contents in pyrrhotite from the different prospects outside the Cirque property consist of 0.12 and 0.39 % Ni and 37.91 and 38.96 % S (Voisey's Bay; two locations) to 0.59 % Ni and 38.82 % S (South Voisey's Bay Project), 0.26 % Ni and 39.14 % S ("Nain Hill"), 0.50 % Ni and 40.20 % S (OKG prospect), 0.22 % Ni and 38.82 % S ("Hilltop" property), and 0.27 % Ni and 41.15 % S (Canadian States Resources property, Licence #1514M). Average Cu and Fe contents in chalcopyrite consist of 32.95 % Cu and 30.56 % Fe ("Hilltop"), 33.62 % Cu and 31.35 % Fe (Canadian States Resources property; Licence #1514M), 31.04 % Cu and 33.32 % Fe ("Nain Hill"), 31.43 and 33.03 % Cu and 32.51 and 30.75 % Fe (Voisey's Bay deposit; two locations), and 33.00 % Cu and 30.90 % Fe (South Voisey's Bay Project), respectively. In both pyrrhotite and chalcopyrite, average Co contents are low (<0.03%), but are as high as 4.66 % in pentlandite from "Nain Hill". Average Ni and Fe contents in pentlandite are higher than those from the Cirque, ranging from 30.99 % ("Nain Hill") to 33.69 % (Voisey's Bay) and 30.17 % (Canadian States Resources property; Licence #1514M) to 34.22 % (Voisey's Bay), respectively.

Although pyrrhotite sulphur contents (disseminated to massive textures) for samples from other properties are similar to those from the Cirque property, the ranges of Ni and Cu

contents are variable and for some, are distinct for a particular occurrence. In a ternary plot (Figure 5.1b) the South Voisey's Bay Project (Donner Minerals) and "Nain Hill" prospect (NDT Ventures) have the highest Ni contents in pyrrhotite. The highest Cu contents were from the "Nain Hill" prospect, "Hilltop" property (Noranda, Licence #915M), sulphides from the Canadian States Resources (Licence #1514M). Samples from the Voisey's Bay deposit were not plotted because Co concentrations were below detection limit. The "Nain Hill" deposit contains the most variable metal contents, overlapping metal contents from the Voisey's Bay deposit and "Hilltop".

Naldrett *et al.* (2000b) conducted microprobe analyses on pyrrhotite, chalcopyrite, and pentlandite (plus other less abundant sulphide minerals) in samples from the Voisey's Bay deposit, Pants Lake area, and Sudbury. Compared to the Cirque sulphides, sulphides from each of these other occurrences had higher average % Ni and S contents in the pyrrhotite grains, slightly lower Fe %, and higher Cu % in the chalcopyrite grains. Electron microprobe studies of pyrrhotite grains from several mineralized zones in the Voisey's Bay deposit and the Pants Lake Intrusive Suite have defined two main mineralized environments (Naldrett *et al.* 2000b). The Pants Lake Intrusive Suite and the Ovoid of the Voisey's Bay deposit have greater abundances of exsolved troilite, ulvospinel and magnetite in pyrrhotite grains than the Eastern Deeps zone (*op cit.*). Overall, the metal/sulphur ratios in pyrrhotite are greater in the Ovoid (and the Pants Intrusive Suite) than in the Eastern Deeps (*op cit*) with Ni and Cu percentages higher and sulphide minerals occurring as larger grain aggregates of pentlandite and chalcopyrite (and lesser cubanite), respectively (*op cit.*).

Hexagonal pyrrhotite with coexisting troilite has average Ni contents between 0.15 % (Reid Brook zone) to 0.22 % (Discovery Hill zone). Ni contents for the same type of sulphide mineralization is 0.12 % at Pants Lake (Naldrett *et al.* 2000b). The Eastern Deeps, however, consists dominantly of monoclinic pyrrhotite containing significantly less troilite and magnetite or ulvöspinel and has greater Ni contents (0.36 %). Copper-sulphides are less abundant and generally occur along the grain boundaries of pyrrhotite. Pentlandite occurs as fine-grained flame lamellae. In troilite-poor pyrrhotite intersections in the Reid Brook zone, the Ni content is 0.26 % (*op. cit.*). For comparison, pyrrhotite grains from the Cirque gossan contain approximately 0.17 % Ni (average,  $n = 11$ ).

Generally, upon segregation from a mafic or ultramafic magma, the composition of the sulphide fraction consists of dominantly S, Fe, Ni, Cu, and trace amounts of Co, Pd, Pt, Rh, Ir, Ru, Os, and Au (Ebel and Naldrett 1996). As the sulphide melt cools from 1200°C to 100°C, it follows definable crystallization trends. According to Naldrett (1969) who conducted experiments on iron sulphide melts, at  $1190^{\circ}\text{C} \pm 1^{\circ}\text{C}$ , pyrrhotite ( $\text{Fe}_{0.917}\text{S}$ ) separates from the magma as an immiscible melt co-existing with silicate vapour and liquid. The pressures for these experiments were not clearly defined, but ranged between 2–4 kbar (Naldrett 1969). In the three phase Fe-S-O system, crystallization occurs at  $988^{\circ}\text{C}$  on the metal-rich side and at  $1083^{\circ}\text{C}$  on the sulphur-rich side. In the Fe-O part of the system, magnetite is the dominant crystallizing oxide mineral, forming euhedral to subhedral grains. Above  $900^{\circ}\text{C}$ , it is in solid solution with hematite. A monosulfide solid solution or *mss* (Fe-S-rich) phase forms at about this temperature with high Cu and Ni concentrations. Upon

cooling to 400 - 500°C, a Cu-rich phase, called the *iss* or intermediate solid solution can fractionate from the sulphide melt. In the Fe-Ni-S system at 600°C, the *mss* can contain a maximum of 1 wt % Cu. By 300°C, most of the Cu has been removed from the *mss*, but some still continue to be expelled from the *mss* at temperatures as low as 100°C. Pentlandite crystallizes at about 400°C or lower, when the *mss* reaches the bulk composition of the ore. Initially, pentlandite forms lamellae in the *mss*, but from 400°C to 100°C, with the formation of the Cu-rich *iss* phase, pentlandite forms chain-like veinlets interstitial to the *mss* grains as observed in the Voisey's Bay deposit. Below 100°C, the diffusion rates of pentlandite are greatly reduced and only pentlandite-rich lamellae or "flames" (as seen in the Cirque sulphides) are formed.

Naldrett *et al.* (2000b) attribute the coarse-grained aggregates of pentlandite in the Ovoid to higher metal/sulphur ratios and greater rates of Ni diffusion from the sulphide melt than those of the Eastern Deeps zone which has only thin lamellae flames of pentlandite. A higher initial metal/sulphur ratio means that the amount of Ni present in the *mss* sulphide melt is relatively high as it will diffuse from the sulphide melt in greater amounts at higher temperatures (*op cit.*) and at higher diffusion rates (Kelly and Vaughan 1983). With so much exsolved from the Fe-rich sulphide melt, the Ni-rich phase often accumulates to form larger masses which later cool to form coarse-grained aggregates of pentlandite (*op cit.*). The presence of chalcopyrite further enhances Ni-sulphide crystallization at higher temperatures allowing for more pentlandite to form (Hill 1984). A low metal/sulphur ratio may explain the formation of the pentlandite lamellae observed in the Cirque sulphides which have

relatively lower abundances of Cu-sulphides. The presence of pentlandite lamellae in the pyrrhotite grains may mean that sulphide fractionation had already occurred at depth and that the Ni and Cu sulphides had segregated from the melt, generating the Fe-rich component observed at the Cirque.

### **5.3 Sources of sulphur for sulphide mineralization**

Aside from the visual observation of country rock xenoliths in sulphide-bearing mafic intrusions (as observed at the Voisey's Bay deposit), sulphur isotopic systems are useful in determining if sulphur-rich country rocks had been assimilated into a mafic magma. The Sm-Nd and Rb-Sr isotopic data reported in Chapter 4 indicate that crustal contamination from either or both the Nain and Churchill provinces is permissible for the Cirque rocks. For this reason, more detailed work on identification of the sulphur source is required.

#### **5.3.1 Results of selenium analyses using the electron microprobe technique**

Selenium often substitutes for sulphur under reduced conditions (Yamamoto *et al.* 1968). Since  $H_2Se$  could possibly be the dominant Se source in a fluid derived from a dehydrated metasedimentary rock, as suggested for the Duluth Complex in Minnesota (Ripley 1990), Se was also analyzed in pyrrhotite, chalcopyrite, pentlandite, and pyrite using the electron microprobe. Concentrations of Se were very low in sulphide minerals from all occurrences, ranging from 0.00 to 0.02 (and in many samples, Se concentrations were below

the detection limit of ~0.017 wt%). The results are listed in Appendix A3.3 along with those from other sulphide occurrences including the Voisey's Bay deposit.

Figure 5.2 is a histogram of the  $\text{Se/S} \times 10^6$  concentrations in pyrrhotite, chalcopyrite, pentlandite, and pyrite from the Cirque sulphides showing a broad range of values (50-500), but with the majority of data between 50 and 350 (average 77.25<sub>pyrrhotite</sub>, 107.28<sub>chalcopyrite</sub>, 105.75<sub>pentlandite</sub>, and 77.76<sub>pyrite</sub>). Values of  $\text{Se/S} \times 10^6$  for other sulphide occurrences are similar (Figure 5.3); the "Hilltop" property, Canadian States Resources property, Licence #1514M, OKG prospect, "Nain Hill" prospect, the Voisey's Bay deposit, and the South Voisey's Bay Project. The most comparable  $\text{Se/S} \times 10^6$  ranges are from those occurrences closer to the Cirque prospect (Licence #1514M, "Hilltop", and OKG prospect) suggesting that more immediate prospects to the Cirque gossan have either less Se substitution or higher S contents. The Voisey's Bay deposit has a broader range of  $\text{Se/S} \times 10^6$  values, but still similar to the Cirque. Overall, S contents in pyrrhotite, chalcopyrite, and pentlandite are slightly higher for the Cirque sulphides and neighbouring prospects than the occurrences further south ("Nain Hill", Voisey's Bay, and South Voisey's Bay Project). Interpretations of Se/S ratios are limited because of the low concentrations of Se detected by the microprobe technique, thus conclusions cannot be made to further compare the various sulphide occurrences used in this study.

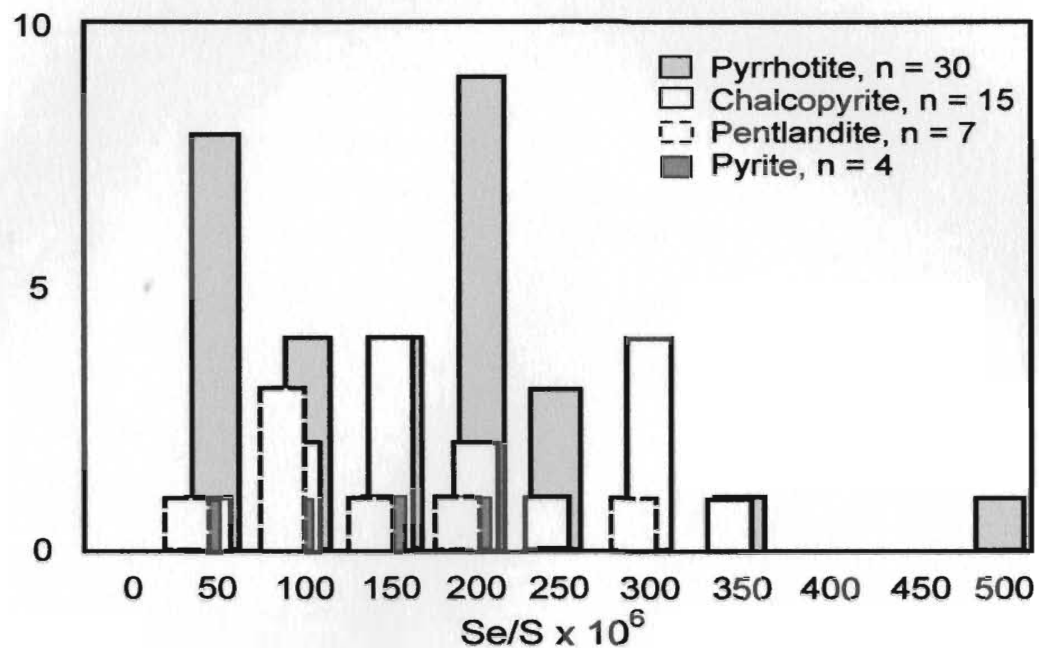


Figure 5.2 Histogram of  $\text{Se/S} \times 10^6$  of pyrrhotite, chalcopyrite, pentlandite, and pyrite from the Cirque grid (core and outcrop samples). Se and S values were measured using the electron microprobe. The range of  $\text{Se/S} \times 10^6$  values are similar for all sulphide minerals.



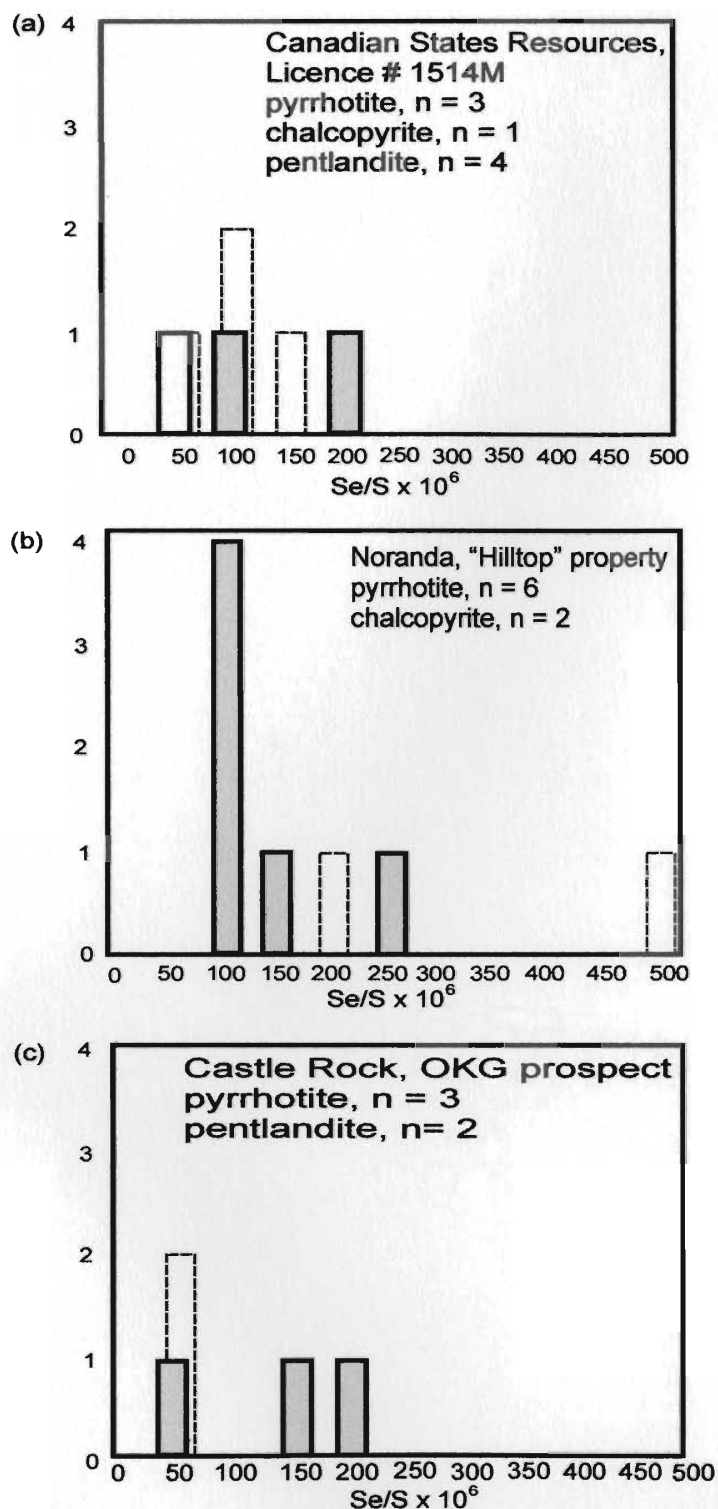
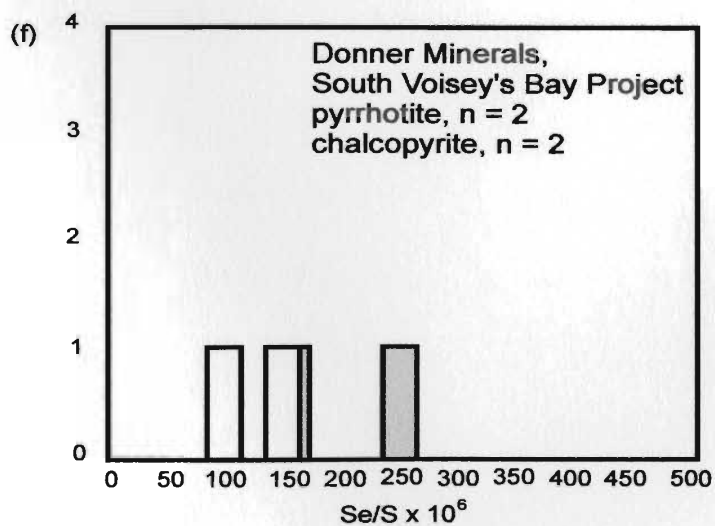
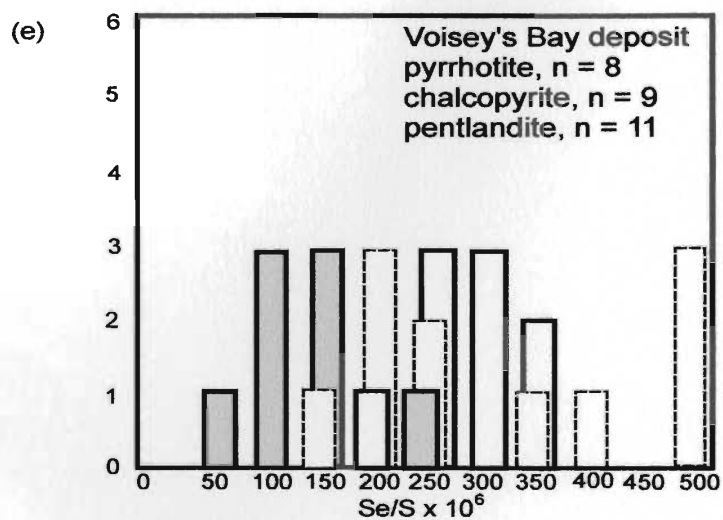
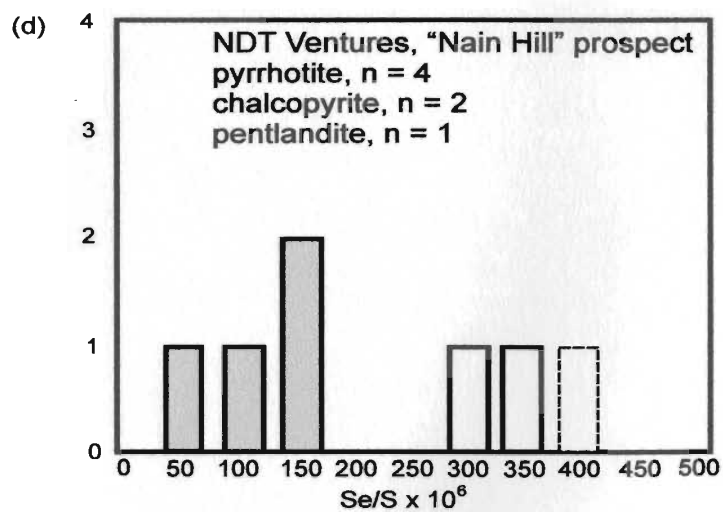


Figure 5.3 Histograms of  $\text{Se/S} \times 10^6$  of pyrrhotite (grey), chalcopyrite (white), and pentlandite (dashed) from (a) Canadian States Resources, Licence #1514M, (b) Noranda, "Hilltop" property, (c) Castle Rock, OKG prospect, (d) NDT Ventures, "Nain Hill" prospect, (e) Voisey's Bay deposit, and (f) Donner Minerals, South Voisey's Bay Project. Sulphur and Se values were measured from massive and semi-massive sulphide samples using the electron microprobe.



### 5.3.2 Sulphur isotope geochemistry

In this study, fifteen sulphide separates (pyrrhotite and chalcopyrite), including two duplicates were derived from eleven massive and semi-massive sulphide core and surface samples from the Cirque (including one massive sulphide sample from the Canadian States property, Licence #1514M). The majority of the sulphide minerals are pyrrhotite; the rest are chalcopyrite. Values of  $\delta^{34}\text{S}$  are calculated using the following equation:

$$\delta^{34}\text{S} = [({}^{34}\text{S}/{}^{32}\text{S})_{\text{sample}} - ({}^{34}\text{S}/{}^{32}\text{S})_{\text{standard}}] / ({}^{34}\text{S}/{}^{32}\text{S})_{\text{standard}} * 1000 \quad \text{Equation 5.1}$$

with  ${}^{34}\text{S}/{}^{32}\text{S}_{\text{standard}} = 0.0450045$  as the value of the troilite (Henderson 1990; Rollinson 1993). Since it is assumed that the composition of mantle material is similar to that of troilite (FeS) of iron meteorites, the most common standard used is the Cañon Diablo Troilite (CDT) and units are expressed as per mil or ‰ (Krauskopf 1979). The heavier sulphur isotope ( ${}^{34}\text{S}$ ), measured in various rock types, is compared to the lighter sulphur isotope ( ${}^{32}\text{S}$ ) and values are given as  $\delta^{34}\text{S}$  (Henderson 1990). The results are given in Appendix A3.4 and the methodology and standards used are discussed in Appendix A1.

Two common S sources are (i) primitive mantle-derived sulphur from uncontaminated mafic and ultramafic bodies ( $\sim 0 \pm 3$  ‰), and (ii) seawater ( $\sim 20$  ‰) which indicates that the sulphur was derived from seawater or marine evaporites (Henderson 1990; Ripley 1999). Any variations in values from known magmatic sources occur because of

sulphur isotopic fractionation by oxidation/reduction within magmatic melts and/or contamination of sulphur from the surrounding country rocks (Rollinson 1993; Ripley 1999).

Figure 5.4 is a histogram of  $\delta^{34}\text{S}$  illustrating that the samples from the Cirque area range from 2.49 ‰ to 3.05 ‰ within the magmatic  $\delta^{34}\text{S}$  field, however, as the radiogenic isotope results suggest in Chapter 4, the slight positive shift may also indicate that contamination from the surrounding continental crust is likely.

Although there is no common dataset with analyses for both S isotope ratios and Se contents, Figure 5.5 is a plot of average  $\delta^{34}\text{S}$  (2.75 ‰) vs  $\text{Se/S} \times 10^6$  from two different datasets of sulphide-rich rocks from the Cirque. Generally,  $\text{Se/S} \times 10^6$  ratios of magmatic sulphides have a wide range due to the variable Se contents in the parental silicate magma and the variable R factors during sulphide segregation which control the Se contents (Maier and Barnes 1999). Most magmatic ores have Se/S ratios ranging from  $50 \times 10^6$  to  $930 \times 10^6$ , however, the accepted range defined for mantle-derived sulphur is  $230 \times 10^6$  to  $350 \times 10^6$  (Eckstrand and Hubert 1987). Because Se is less mobile than S during low temperature alteration, Se/S ratios less than  $230 \times 10^6$  indicate that additional sulphur has been added to the magmatic sulphide melt (*op. cit.*).

The resulting plot (Figure 5.5) indicates that sulphur was derived from a mixture of mantle and crustal components with 82 % of the Se/S ratios below  $230 \times 10^6$ , suggesting that sulphur was dominantly externally derived from a sedimentary source. Such an interpretation agrees with sulphur isotope and radiogenic isotope data. The values higher

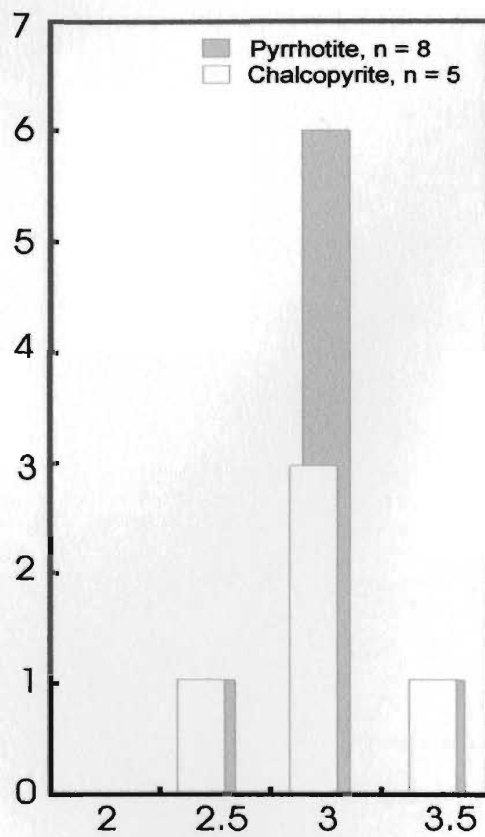


Figure 5.4 Histogram of  $\delta^{34}\text{S}$  of chalcopyrite and pyrrhotite from the Cirque grid (core and outcrop samples).

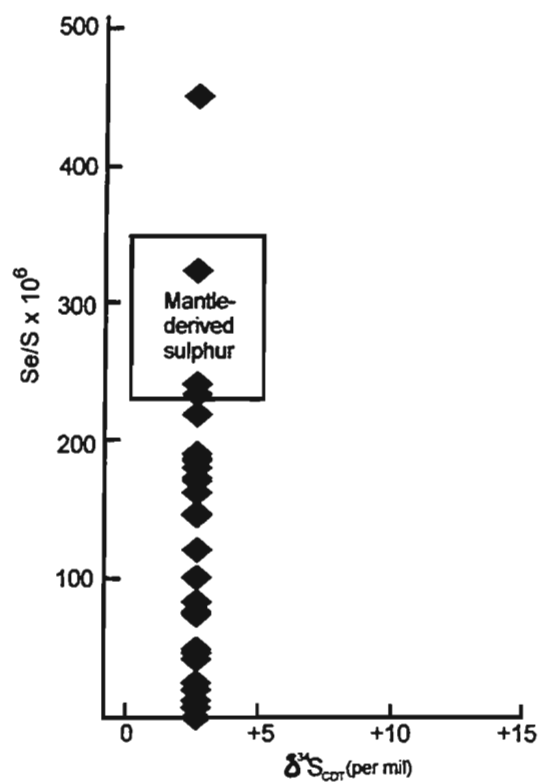


Figure 5.5 Plot of average  $\delta^{34}\text{S}_{\text{CDT}}$  (per mil) versus  $\text{Se/S} \times 10^6$  for the Cirque sulphides. Two datasets, one of  $\delta^{34}\text{S}_{\text{CDT}}$  (per mil) and one of  $\text{Se/S} \times 10^6$  suggest that the mantle derived magma has been contaminated by crustal rocks. Plot is adapted from Eckstrand et al. (1989).

than  $230 \times 10^6$  correspond to the samples having low modal abundances of sulphides (*i.e.* disseminated sulphides).

Average  $\delta^{34}\text{S}$  values for the continental crust are +7.0 ‰ (Chaussidon *et al.* 1989).

Values of  $\delta^{34}\text{S}$  for gneissic rocks from the Nain Province range from 0.2 to 3.3 per mil (Ripley *et al.* 1997). Sulphur from pyrrhotite within the Tasiuyak gneiss has  $\delta^{34}\text{S}$  values of -0.9 to -17.0 per mil with sulphur contents between 0.05 to 0.54 wt% S (Ripley *et al.* 1997; Ripley *et al.* 1999) and even broader ranges of  $\delta^{34}\text{S}$  values from Wilton (*unpublished data*). Paragneissic and orthogneissic rocks of the Churchill Province have  $\delta^{34}\text{S}$  values ranging from < -10 to < +15 per mil (Wilton *unpublished data*). Enderbitic gneiss from the Churchill Province has sulphur contents of <0.03 wt% S and  $\delta^{34}\text{S}$  values between -4.6 to +3.3‰ (Ripley *et al.* 1999).

Se/S analysis of sulphides from LBN-2 to 4 by F.P.F. Resources (1996) indicate a primary mantle-derived sulphur source for the Cirque sulphides rather than “*in situ*” contamination by country rock (*op cit.*). In this present study, however, the broad range of  $\text{Se/S} \times 10^6$  seems to suggest a crustal source of sulphur. The sulphur isotopes from the Cirque lie within the broad range of  $\delta^{34}\text{S}$  values defined by the Churchill Province gneisses, however, this range is broad and not very definitive. The  $\delta^{34}\text{S}$  values also lie within the more narrow range defined by enderbitic gneisses (of the Churchill province) indicating the main source should lie west of the suture line (Figure 5.6). According to Figure 5.6, a slight



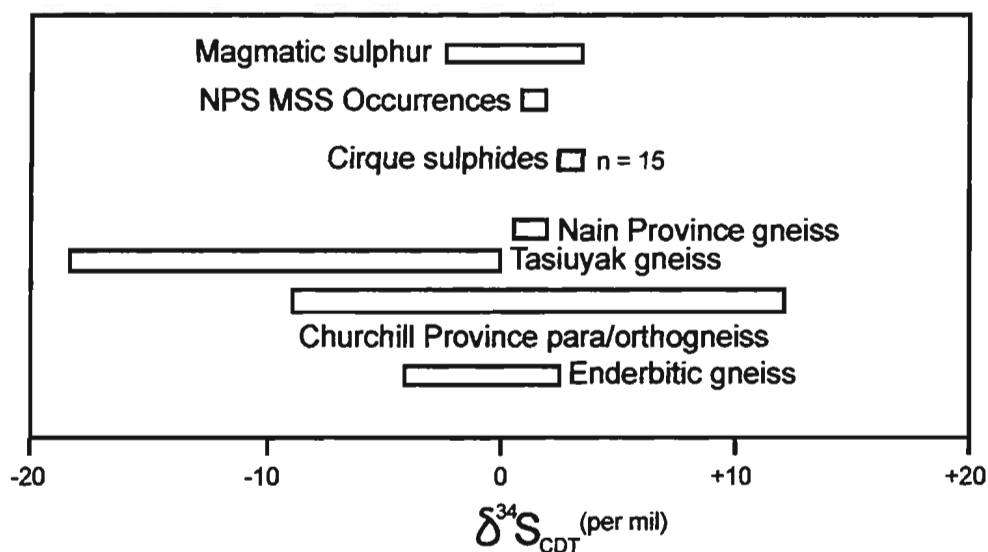


Figure 5.6 Ranges of  $\delta^{34}\text{S}_{\text{CDT}}$  values of the Cirque sulphides (grey). Values of magmatic sulphur, sulphide occurrences throughout the NPS and gneisses from the Nain Province, Tasiuyak rocks, and Churchill Province are plotted to show the most probable source of sulphur for the Cirque sulphide minerals.  $\delta^{34}\text{S}_{\text{CDT}}$  ranges for the Churchill Province, and NPS MSS Occurrences are from Wilton (unpublished data) Those from Tasiuyak gneiss, enderbritic gneiss, and the Nain Province are from Ripley (1997) and Ripley et al. (1999).

overlap with the Nain Province may also be possible, but less significant, however, significant contamination from the Tasiuyak gneiss is not likely. If the Tasiuyak gneiss was the dominant crustal contaminant, then the  $\delta^{34}\text{S}$  values in the orthomagmatic sulphides would be less than 0 ‰. Results of radiogenic isotope data from the Cirque property (see Chapter 4) support this mixture of crustal contamination.

At the Voisey's Bay deposit, Ripley *et al.* (1999) measured the  $\delta^{34}\text{S}$  values in several of the mineralized zones (Figure 5.7) and attributed the assimilation of the silica-rich (and/or S-rich) rocks from the Tasiuyak gneiss as the major contributor to sulphide saturation in the magma which hosted the Voisey's Bay deposit. Sulphides in the Eastern Deeps have  $\delta^{34}\text{S}$  values ranging from -0.5 to +1.8 ‰ in Normal-textured Troctolites and from -2.4 to 1.5 ‰ in the Varied-textured Troctolite and Basal Breccia Sequence. Massive sulphides in the different zones have varied  $\delta^{34}\text{S}$  values: -2.1 to 0 ‰ in the Ovoid zone, -1.8 to -0.1 ‰ in the Discovery Hill zone, and -4.1 to -1.1‰ in the Reid Brook zone. Disseminated sulphides from the Mushuau Intrusion have positive  $\delta^{34}\text{S}$  values (+0.8 to +1.7‰), similar to those from Normal-textured Troctolite in the Eastern Deeps zone (*op cit.*). Overall, the  $\delta^{34}\text{S}$  values are still below those from the Cirque area and only samples from the Eastern Deeps have values above 0 ‰. Because Archean rocks can have  $\delta^{34}\text{S}$  values within the range of pristine mantle values due to low sulphate concentrations in the Archean oceans and/or because of the lack of sulphate-reducing bacteria (Ripley 1999), overlaps in the  $\delta^{34}\text{S}$  fields

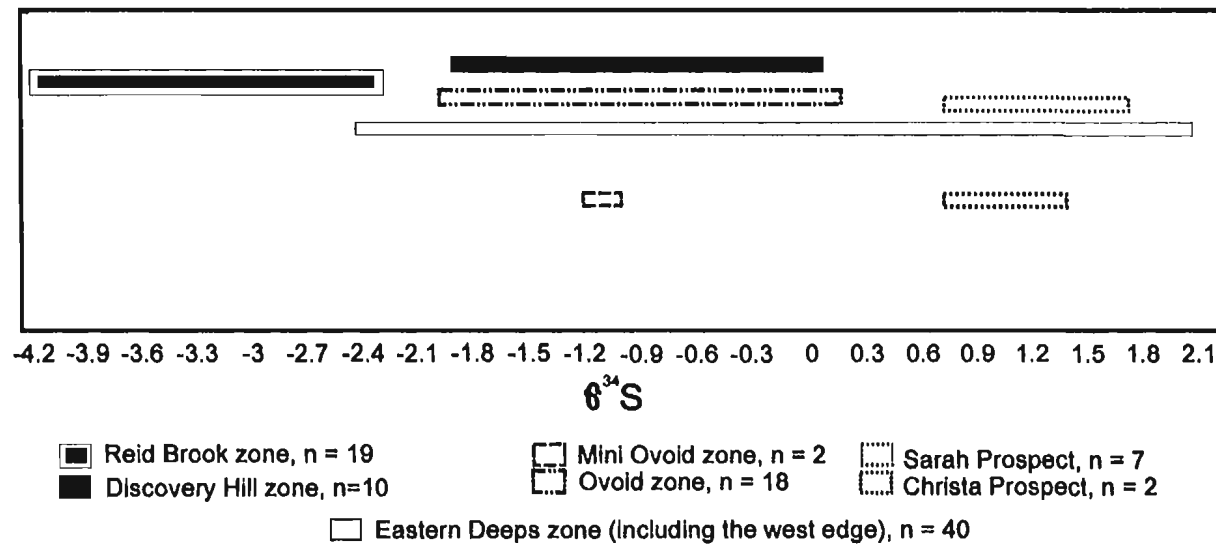


Figure 5.7 Ranges of  $\delta^{34}\text{S}$  values from the various zones of sulphide mineralization within the Voisey's Bay deposit (from Ripley et al. 1999).

for the magmatic source and the Nain and Churchill Provinces make it more difficult to define the actual source of the sulphur for the Cirque sulphides (Ripley 1986; Figure 5.7). It is possible, however, due to the narrow range and uniformity of the  $\delta^{34}\text{S}$  values from the Cirque area that contamination was derived dominantly from the Churchill Province which has isotopically heavier sulphur than the Nain Province (Ripley 1999). Contamination from the Nain Province is also possible considering the location of the Cirque area near the suture line between both provinces (refer to Figure 2.1). This is supported by radiogenic data from Chapter 4 which indicate the Churchill Province, and a lesser extent, the Nain Province as possible contaminants.

#### **5.4 Nickel and copper contents**

In addition to the extensive Ni, Cu, and Co analytical data from drill core and grab samples derived by Cartaway Resources between 1995-1997 (see Chapter 3 and Appendix A2.2 and A2.3), numerous sulphide samples (drill core and outcrop) from the Cirque were also analysed at Memorial University for Ni and Cu using the XRF method; the results are listed in Appendix A3.2. Weak disseminations to patches of massive pyrrhotite with 1 % maximum chalcopyrite in dominantly anorthosite (< 10% pyroxene) were sampled in drill holes LBN-2 to 5. One pyroxenite (91) and two ferrodiorite samples were also analysed, although they have <1% to trace disseminated pyrrhotite. One anorthosite sample and one ferrodiorite sample from the Noranda Hilltop property were also analysed.

The sulphide core intersections assayed by Cartaway between 1996-1997 have already been discussed in Chapter 3 with histograms of Ni/Cu in drill holes LBN-1 to 11 given in Appendix A2.4.1. Cross sections of these drill hole sulphide intersections with Cu (wt%), Ni (wt%) and Ni/Cu versus depth constitute Appendix A3.4.3. Overall, there is no significant change in Cu or Ni contents nor Ni/Cu ratios with depth, however, locally there are slight increasing trends of these metals with depth (for example, in LBN-4) and localized zones of elevated Ni/Cu with depth, as high as 9 in LBN-8 (350.19 m) and 23.33 in LBN-9 (166.35m).

The highest Ni and Cu contents for sulphide-bearing samples analysed for this study (Appendix A3.5) are 0.30 wt% and 0.62 wt% (core) and 0.59 wt% Ni and 1.37 wt% Cu (outcrop), respectively. Ni/Cu ratios range from 0 to 2.48 (core) and 0 to 4.65 (outcrop; Figure 5.8). Ratios of Ni/Cu from the Canadian States Resources prospect (Licence #1514M) are similar (from 0.6 to ~3; Kerr *unpublished data*). Nickel and Cu contents, recalculated to 100% sulphides, range from 0 to 1.36 wt % (core), 0 to 2.38 wt% (outcrop) and 0.15 to 1.57 wt% (core), 0.09 to 2.25 wt% (outcrop), respectively (Figure 5.9). Interestingly, the lowest and the highest recalculated Ni concentrations came from ferrodiorite rocks with minor disseminated pyrrhotite. Overall, the sulphur contents for most of the Cirque core and outcrop samples is <10 wt% S with the highest Ni and Cu values proportional to the greatest sulphur contents (more massive sulphide intersections) and the disseminated sulphides do not have the greatest abundances of Ni and Cu. Recalculated Ni and Cu from the Voisey's Bay deposit from Naldrett *et al.* (2000) have much higher Ni and

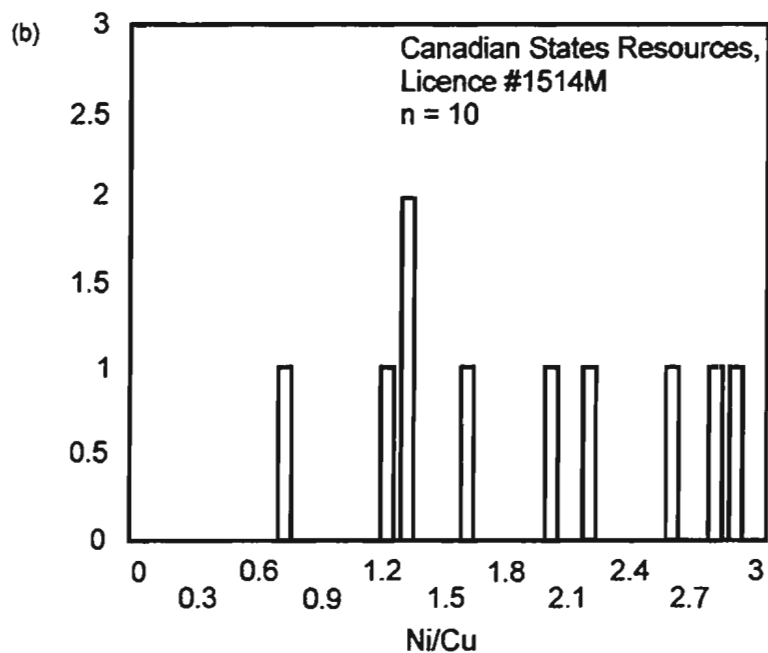
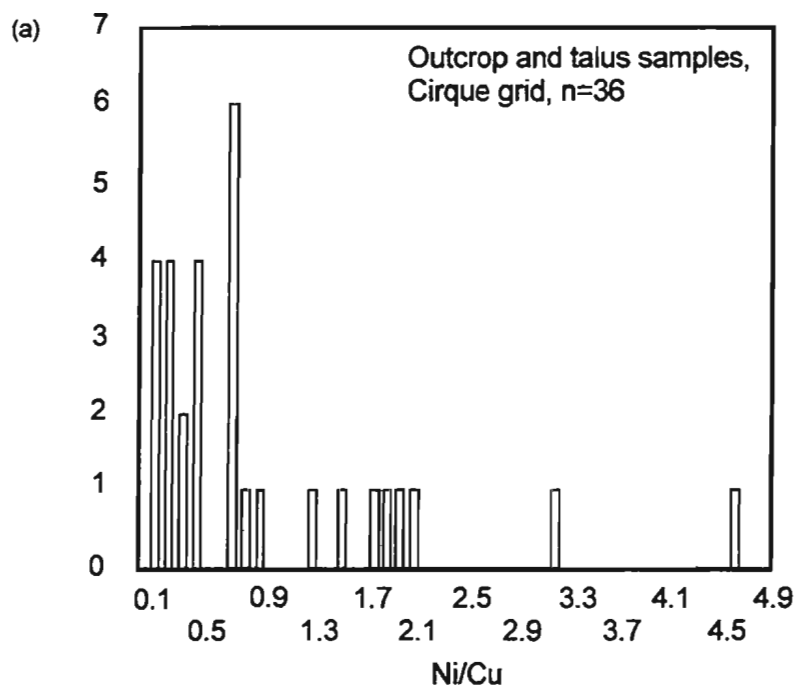


Figure 5.8 Histograms of Ni/Cu of sulphide-bearing outcrop and talus samples from (a) the Cirque grid (plus one ferrodiorite and one anorthosite from the Noranda "Hilltop" prospect) and (b) Canadian States Resources, Licence #1514M (core samples). Geochemical data for (b) are from Kerr (unpublished data).

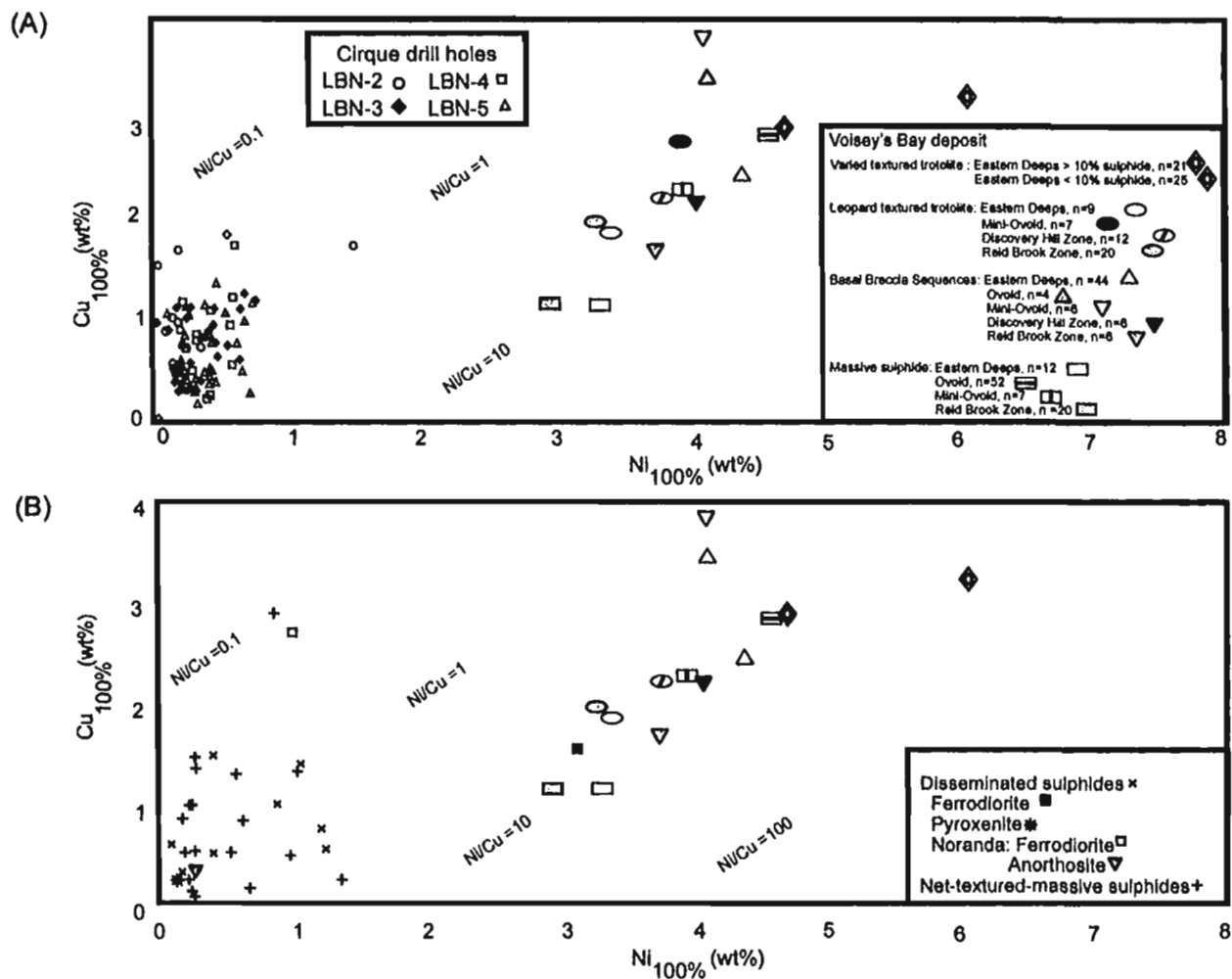


Figure 5.9 Plot of Ni (wt%) versus Cu (wt%), both recalculated as 100% sulphides of (a) core and (b) outcrop samples from the Cirque area. Two outcrop samples from the Noranda "Hilltop" property. Values were calculated using whole rock XRF analyses. Average Ni and Cu contents (recalculated from 100% sulphides) from various mineralized zones in the Volsey's Bay deposit (from Naldrett et al. 2000) are plotted for comparison (grey symbols with the legend in (a) are used in both plots).

Cu values and Ni/Cu ratios are 10 or greater. Thus, in the Varied-textured Troctolite, Basal Breccia Sequence, and even the massive sulphide intersections, the metal contents are much higher than could be expected from the unknown magma from which the Cirque sulphides segregated.

The lack of host magma at the Cirque prevents a more complete interpretation of the sulphide formation, however, Figure 5.10a and b suggest that crystal fractionation within the parental silicate magma occurred prior to sulphide segregation, causing Ni and Cu concentrations to be low in the sulphide segregate. Nickel and Cu can have similar partition coefficients in a sulphide-rich mafic magma, however, Ni has a greater partition coefficient for ferromagnesian silicate minerals (Barnes *et al.* 1997a). Negative correlation of Ni (wt %) and MgO (wt %) in Figure 5.10, however, suggests that the Ni in sulphide-rich rocks at the Cirque is closely associated with olivine crystal fractionation. Cu (wt %) shows a similar yet broader relationship, however, the Cu content is much lower with respect to sulphur content because of lower partition coefficients of Cu in the mafic magma. Increasing values of Cu/(Cu + Ni) values with decreasing MgO contents of the Cirque rocks in Figure 5.10c suggest that the initial host magma may have fractionated Ni into olivine and pyroxene prior to sulphide segregation, thus lowering the metal content in subsequent sulphide melts (Rajamani and Naldrett 1978; Scoates and Mitchell 2000).

Other deposits in Figure 5.10c lie along a line which indicate increasing Cu/(Cu + Ni) with decreasing MgO (wt %) contents (that is, with increasing crystal fractionation). With an average Cu/(Cu + Ni) value of ~0.35 and a MgO content in the silicate melt about 8 wt %,



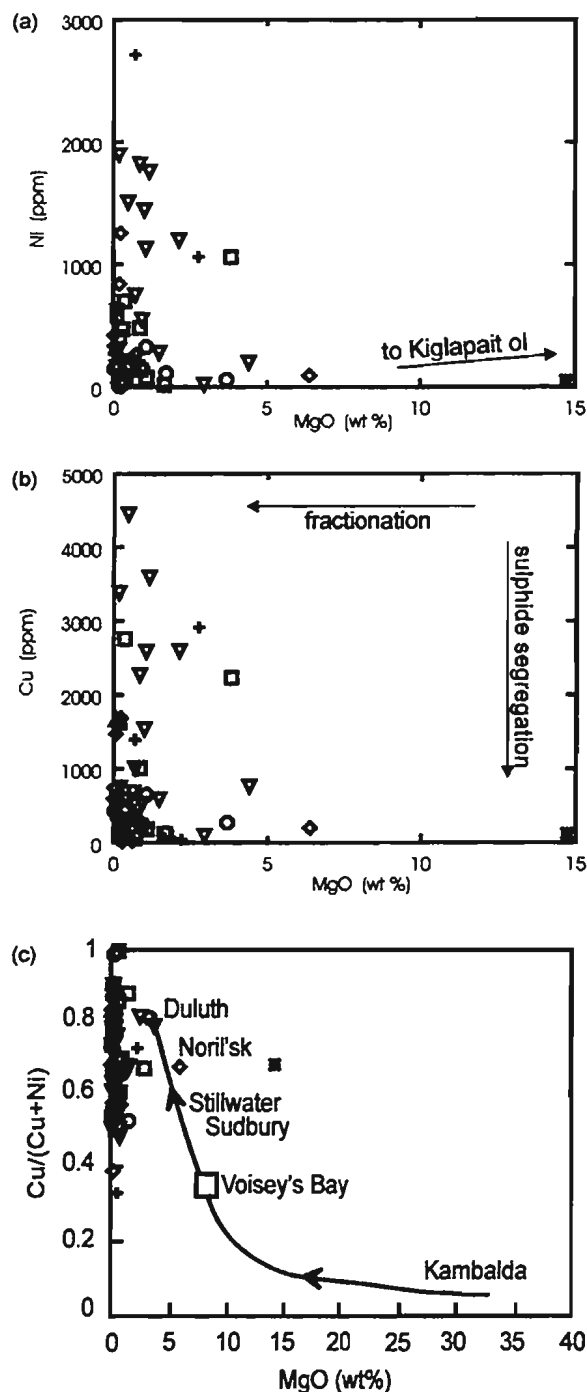


Figure 5.10 MgO wt% versus (a) Ni (ppm), (b) Cu (ppm), and (c) Cu / (Cu+Ni). Plots (a) and (b) show variable concentrations of Ni and Cu, respectively in sulphides segregated from a fractionated mafic magma. Crystal fractionation from a silicate magma depletes the magma in Ni and is indicated by high values of Cu/ (Cu + Ni) with decreasing MgO (wt %) as shown in (c). Drill core: LBN-2 =  $\circ$ ; LBN-3 =  $\square$ ; LBN-4 =  $\triangle$ ; LBN-5 =  $\nabla$ . Outcrop: disseminated to net-textured sulphides =  $\diamond$ ; massive sulphides =  $\blacklozenge$ ; ferrodiorite with disseminated pyrrhotite =  $+$ ; pyroxenite with disseminated pyrrhotite (91) =  $\blacksquare$ ; Low sulphide-bearing rocks from "Hilltop" (Noranda) =  $\times$ . Data are from XRF whole rock analyses of sulphide-bearing rocks from the Cirque. Plots are adapted from Scoates and Mitchell (2000).

Scoates and Mitchell (2000) reason that the host magma at Voisey's Bay is geochemically similar to other intrusions within the NPS (such as the Kiglapait Intrusion, the Hettasch, and Jonathon marginal rocks), as well as mafic dykes from the Laramie anorthosite complex, however, the Voisey's Bay deposit, having average grades of 1.59 wt % Ni and 0.85 wt % Cu (Scoates and Mitchell 2000), is hosted by a troctolitic intrusion that is less fractionated than the interpreted parental magma at the Cirque.

### **5.5 Platinum Group Element geochemistry**

As discussed in Chapter 3, Cartaway Resources assayed several samples for Pt, Pd, and Au from LBN-96-1, 2, and 4. The results are listed in Appendix A2.3.3. All samples yielded Pt and Pd values below detection limit (<30 ppb). One sample from LBN-2 yielded 64 ppb Pt and 8 ppb Pd according to the report by F.P.F Resources (1996). Gold contents were background with a few anomalies and a maximum gold value of 252 ppb (LBN-4; F.P.F Resources 1996). Other than minor sampling, Platinum Group Elements (PGE) were not an exploration target; however, PGE can be useful in determining the fractionation behaviour of a sulphide melt, thus allowing a better understanding of the evolution of sulphur saturation and sulphide mineralization and evaluating its economic potential for PGE, Ni, and Cu.

Abundances of PGE, compared with those of Ni and Cu in mafic and ultramafic rocks are affected by partial melting, crystallization of olivine and chromite, evolution of sulphides, and mobilization of the sulphide melt (Barnes 1990). The amount of partial

melting required to dissolve all sulphides and PGEs present in the source rock depends upon their abundances and the solubility of sulphur in the source magma (Leshner and Stone 1996). Incomplete partial melting will result in a significant amount of residuum being retained in the mantle source and any sulphide derived from the subsequent magma will be depleted in PGE and Ni (Barnes *et al.* 1997a). If the degree of partial melting is high enough to consume all of the source sulphides, then the magma will have an elevated abundance of PGEs. A magma with a high degree of partial melting has Cu and Pd concentrations about four times greater than that of the mantle (*i.e.* 112 ppm Cu and 16 ppb Pd; Barnes *et al.* 1997a). Morgan and Baedeker (1983) state that a relatively high degree of partial melting, about 25 %, is needed to dissolve all the sulphides in a mantle source.

Plume-rift environments allow for a large volume of sulphur laden mantle partial melt material to ascend quickly and reduce the amount of time the magma is in contact with the surrounding country rock (Barnes *et al.* 1997a; Campbell and Griffiths 1990). Upon reaching the crust, such a primitive mantle will experience relatively lower pressure and temperature, and because it is still hotter than the surrounding country rock, large blocks of country rocks will be continually assimilated and mixed with the magma. Assimilating country rock, rich in sulphur (Leshner and Campbell 1993) and/or SiO<sub>2</sub> (Naldrett 1996), or S-rich volatiles from the country rock (Ripley and Alawi 1988), can cause sulphide saturation within the magma and result in sulphide segregation. Timing of sulphide saturation is very important in the formation of an economic deposit. If sulphur saturation and subsequent segregation of the sulphide melt occur prematurely, sulphides rich in Ni, Cu, and PGM will settle in the conduits of the upwelling magma and be emplaced at great depths

(Barnes *et al.* 1997a). Subsequent sulphide segregation will result in a PGE-Ni-Cu-poor sulphide that has mobilized to shallower depths, often in the country wallrock (*op cit.*). If sulphur saturation is attained after magma emplacement when olivine and chromite are fractionating, then there will be less PGE and Ni available for the production of the sulphide minerals as they will have already crystallized out of the magma.

Continuous injections of “fresh” mafic and/or ultramafic magma with various degrees of sulphide solubilities will cause the conditions of the magmatic system to be continuously changing. However, once reaching sulphide saturation, either by assimilation of silica-rich country rock and/or reaching sufficient high sulphur contents in the magma, sulphur scavenges the metals present in the silicate melt. As sulphides form and segregate from the silicate-rich melt, the concentrations of the metals decrease in the silicate magma. Partition coefficients for Ni-Cu-PGE into the sulphide melt are predictable with ranges of 100 to 500 for Ni, 200-2000 for Cu, and  $10^3$  to  $10^6$  for the PGE in sulphide-rich rocks (Naldrett 1982; Barnes *et al.* 1997a). In the sulphide melt, chalcophile elements (Fe, Co, Rh, Ru, Ir, Os, and Ni) favor or partition strongly into the Fe-sulphide melt (mss) and become depleted in Cu, Pt, Pd, and Au relative to the Cu-sulphide melt (Barnes *et al.* 1997b). The more compatible elements Ni, Os, Ir, Ru are fractionated into olivine and chromite preferentially over Pt, Pd, Au, and Cu. Subsequent fractionation of the sulphide melt can result in an Ir-PGE sulphide component (rich in Ir, Os, and Ru) and a Pd-PGE sulphide component (rich in Rh, Pt, Pd, and Au). The Ni content for both components are about the same (Barnes *et al.* 1997a, b).

### 5.5.1 PGE content at the Cirque

Because orthomagmatic sulphides are ultimately derived from the mantle, Barnes *et al.* (1988) suggest normalizing PGE contents in samples to average mantle values rather than chondritic values. Thus, Barnes *et al.*'s (1988) mantle values were used to produce PGE variation patterns for fourteen samples from the Cirque (plus one from the Canadian States property; Licence #1514M). The majority of the samples were of massive to semi-massive sulphides in anorthosite (talus, outcrop, and drill holes samples); two ferrodiorite samples with disseminated sulphides are included for comparison. Analyses for Ni, Cu, PGE, and Au were carried out using the Ni-S bead ICP-MS technique (Jackson *et al.* 1990). A full description of the method and the standards used are given in Appendix A1 and the results are listed in Appendix A3.6.

The PGE concentrations are rather low ( $< 100$  ppb) in the Cirque sulphides with  $Pt_{avg} = 10.10$  ppb and  $Pd_{avg} = 35.71$  ppb. The overall patterns in Figure 5.11 have positive slopes with moderate negative Pt anomalies indicative of a fractionated magma in which the concentrations of the more compatible elements Ni, Os, Ir, and Ru, are lower than the parental magma as they had partitioned into previously crystallized olivine and chromite (Barnes *et al.* 1988). The two ferrodiorite outcrop samples, containing minor disseminated pyrrhotite, have the lowest concentrations of PGE, Ni, Cu, and Au; the iridium content for one of the samples (46) is below detection limit. Besides having the lowest Ni contents, the two ferrodiorite samples do not have the positive slopes of the sulphide-rich anorthosite samples, possibly because of the low sulphide content and the fact that these rocks

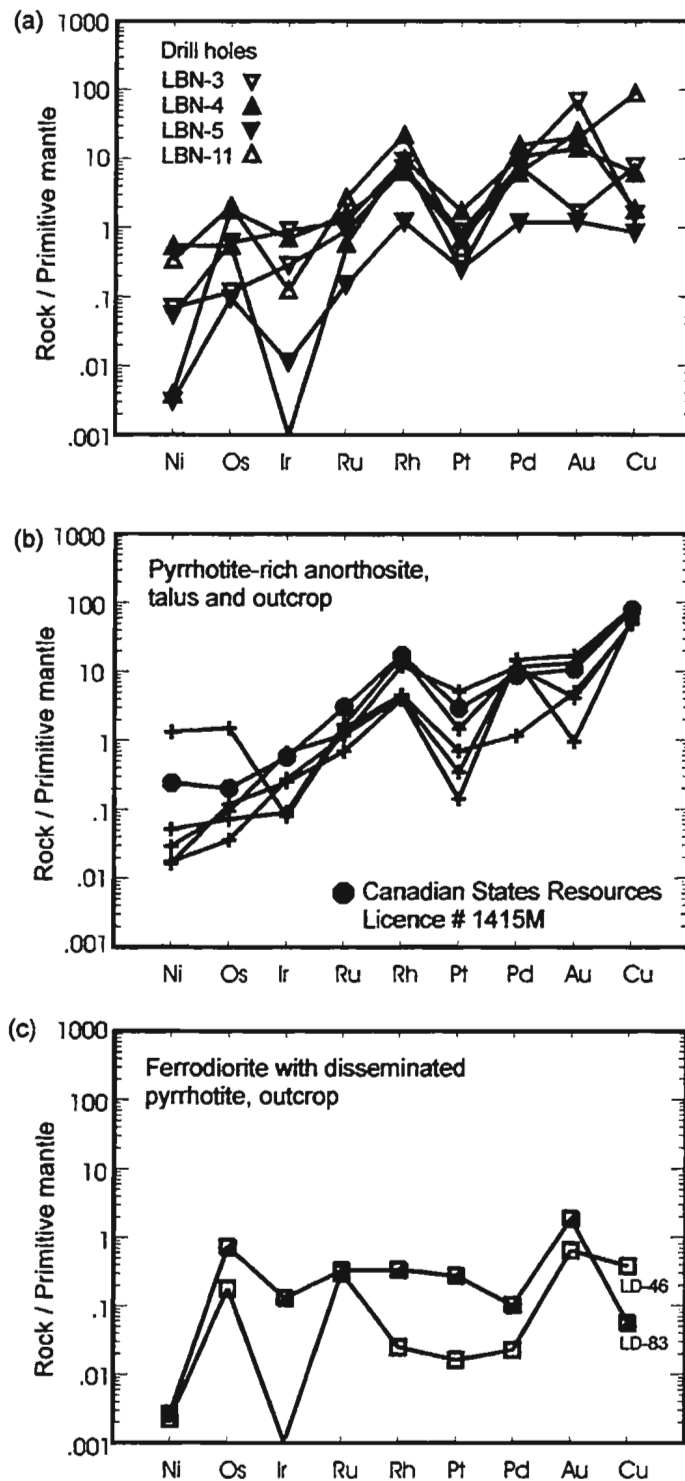


Figure 5.11 Mantle-normalized PGE-Au-Ni-Cu patterns of sulphide-bearing samples from the Cirque: (a) pyrrhotite-rich anorthosite from drill core and (b) outcrop, and (c) ferrodiorite with minor disseminated pyrrhotite from outcrop. Sample set includes a massive sulphide sample from the Canadian States Resources property. All data are normalized using mantle values from Barnes et al. (1988).

crystallized from the most fractionated component of the silicate magma. The lack of a steep pattern, however, may also suggest a separate, less fractionated source magma which originally had low PGE-Ni-Cu-Au contents.

PGE metal ratios can be used to determine the effects of crystal fractionation in olivine and chromite and the segregation of the sulphide melt (Barnes *et al.* 1988; Barnes 1990). Comparisons are made using the least compatible elements, such as Cu, Pt, or Pd against the most compatible elements, such as Ni, Os, Ir, or Ru. Because the partition coefficients of the PGE are much greater than those of Ni and Cu and because Os, Ir, Ru, and Ni are readily removed from the magma by crystal fractionation of olivine and chromite, Barnes (1990) and Barnes *et al.* (1988) limit the use of the ratios, *eg.* Pd/Ir versus Ni/Cu or Ni/Pd versus Cu/Ir.

The range of Pd/Ir ratios from sulphide-bearing anorthosite at the Cirque (including one massive sulphide from the neighbouring Canadian States property) is 8.84 to 127.18 (average = 46.54). The range of Ni/Cu values is 0.01 to 6.19 (average = 1.15) suggesting that fractionation of the PGE was more pronounced than Ni and Cu. One ferrodiorite sample from the Cirque, with disseminated pyrrhotite, has comparatively low Pd/Ir and Ni/Cu ratios (0.78 and 3.33, respectively) reflecting the sulphides originated from a fractionated magma. Figure 5.12a and b define the fields of several deposit types; most of them show clearly the fractionation trend from primitive mantle to flood basalts. Barnes *et al.* (1988) defined these fields based on existing data from numerous deposits around the world, however, they admit that the limits of some of these fields are not fully defined. Overall, the Cirque rocks do not plot in any particular field (spanning high-MgO basalts, layered intrusions, to flood basalts),

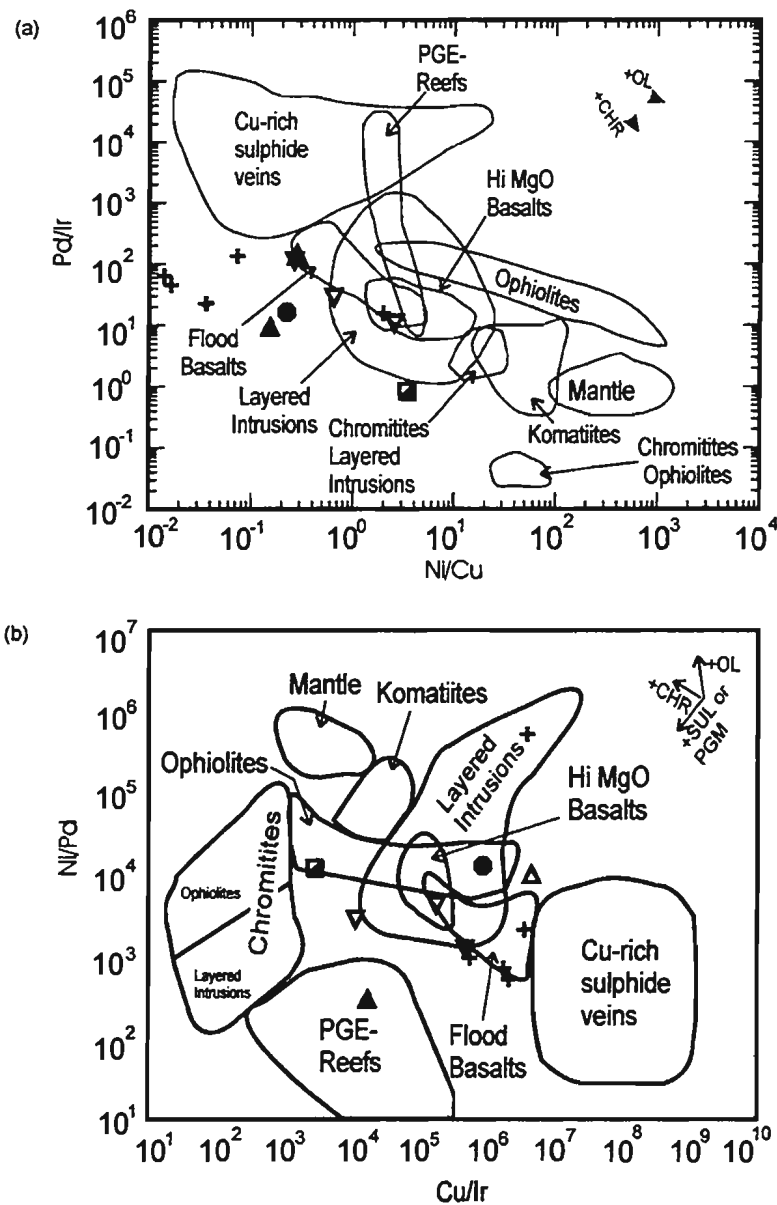


Figure 5.12 Metal ratio plots of sulphide-bearing rocks from the Cirque (a) Ni/Cu versus Pd/Ir and (b) Cu/Ir versus Ni/Pd for sulphide-rich anorthosite outcrop and talus samples (+) and ferrodiorite outcrop sample LD-83 (▢) and drill hole samples of bleb to massive sulphides from LBN-3 (▽), LBN-4 (▲), LBN-5 (▼), and LBN-11 (△). One massive sulphide sample from the Canadian States property, Licence #1514M (●) is also plotted. Fields of deposit type are from Barnes et al. (1988).



but rather broadly lie along a trend parallel to that of olivine crystallization. This suggests an evolved magma where compatible elements (Ni and Ir) had preferentially partitioned into olivine whereas the relatively more incompatible metals (Cu and Pd) remained in the magma.

In Figures 5.12a and b (Ni/Cu versus Pd/Ir and Cu/Ir versus Ni/Pd, respectively) the Cirque samples plot loosely along the olivine (and to a lesser extent, chromite) fractionation vectors, however, they do not lie largely within the high-MgO intrusion field suggesting a low potential for PGE sulphide mineralization (*op cit.*). According to Sharpe (1982), Wilson (1982), Longhi *et al.* (1993), and Davies and Tredoux (1985), all known layered intrusions containing PGE deposits were derived from mafic magmas with 12-18 wt% MgO. Overall, the rocks at the Cirque have MgO contents < 7 wt%, indicating a highly fractionated magma source. Even the least fractionated rock types (pyroxenite and leuconorite/leucogabbro-leucotroctolite varieties) have less than 12 wt% MgO (see Chapter 4), supporting a low probability of the magma (from which the Cirque rocks were fractionated) having significant PGE contents. The ferrodiorite sample, however, plots the closest to the mantle field, suggesting that this rock crystallized from a more enriched magma source compared to the other rock types in the Cirque area, further supporting the possibility of a separate magma source at depth as discussed in Chapter 4.

Sulphide-bearing rocks with Cu/Pd ratios greater than mantle values, indicate a large volume of sulphide melt (*i.e.* low R factor) segregated from the magma close to the source. Palladium, having a higher partition coefficient for sulphides than Cu, fractionated earlier,

thus depleting the remaining magma (Barnes *et al.* 1988; Peach *et al.* 1990; Barnes *et al.* 1997a). The remaining magma, having relatively more abundant Cu than the segregated sulphide melt, later formed another sulphide melt upon reaching sulphide saturation a second time (Peach *et al.* 1990; Thériault *et al.* 1997; Barnes and Maier 1999). The plot of Cu/Pd versus Pd (Figure 5.13) supports the idea of a low PGE-bearing sulphide. Due to low Pd contents, the sulphide-bearing anorthosite rocks plot near the mantle source or in the depleted field suggesting that the more compatible Pd fractionated from the magma earlier relative to Cu, possibly at great depths (Peach *et al.* 1990).

According to Figure 5.13, one ferrodiorite sample crystallized from a depleted source and one from a source similar to mantle composition, both having the lowest Cu/Pd and Pd values. This is an important feature of the Cirque ferrodiorites since they suggest that there might be two sources of magmas; one which formed the mafic and anorthositic rocks and another, more fractionated source, rather than the residuum melt from a fractionated mafic magma. This suggests greater partitioning of Pd (that is, more fractionation of the source magma) or perhaps, the ferrodiorites samples are merely reflecting the <1% sulphide contents of the rock type.

### **5.5.2 Modelling of Ni, Cu, and PGE**

A method for evaluating the economic potential of a particular magmatic sulphide occurrence or deposit is to determine the concentrations of metals ( $C_L$ ) in the silicate magma that were in equilibrium with the sulphide melt (Barnes *et al.* 1997a; Thériault *et al.* 1997).

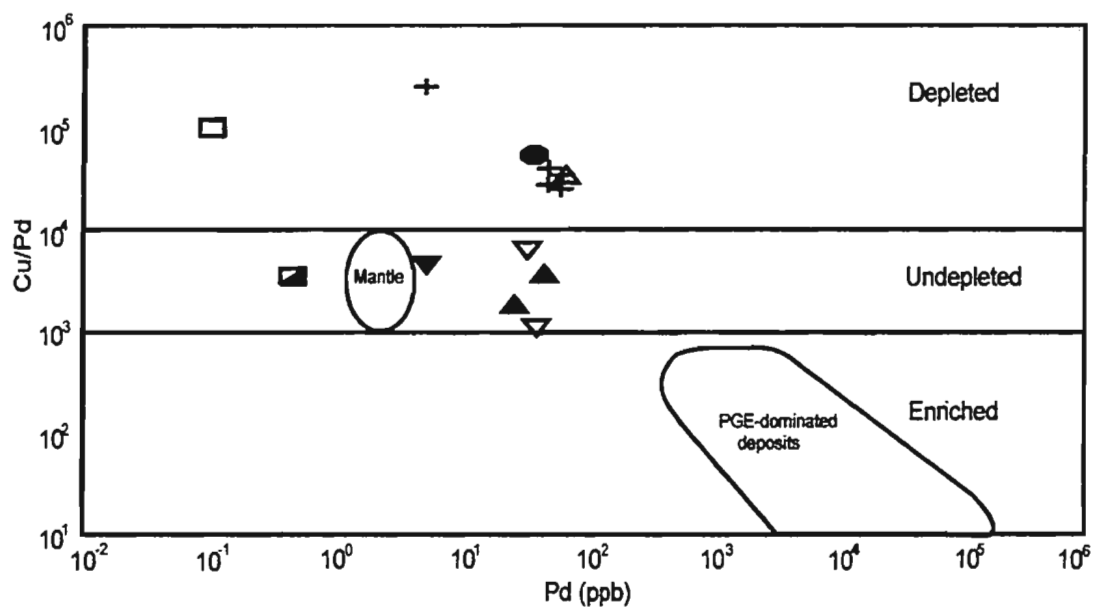


Figure 5.13 Plot of Cu/Pd versus Pd (ppb) of sulphide-bearing rocks from the Cirque: anorthosite outcrop and talus (+), two ferrodiorite samples (46 □; 83 ■), and drill holes (LBN-3 ▽; LBN-4 ▲; LBN-5 ▼, LBN-11 △). A massive sulphide sample from the Canadian States property, Lic #1514M (●) is also plotted. Plot is adapted from Barnes et al.(1993) and Barnes et al. (1997).

Using partition coefficients (D) of PGE (Os, Ir, Ru, Rh, Pt, Pd), Au, Ni and Cu from Barnes *et al.* (1997a) and selected R factor values (25, 50, 100, 1000, 10,000) the following equilibrium fractionation equation from Campbell and Naldrett (1979) was used:

$$C_c = C_L D(R+1) / (R+D) \quad \text{Equation 5.2}$$

where  $C_c$  is the concentration of a metal in the sulphide liquid and the R factor is defined as the ratio of the silicate magma to the sulphide melt (Barnes *et al.* 1997a).

For this study, the concentration of the metal in the starting sulphide melt is not known for the Cirque sulphides,  $C_c$  values from the Duluth Complex from Barnes *et al.* (1997a) are used since they have comparable sulphide mineralization and host rock (Table 5.1). The Duluth Complex consists of several disseminated high sulphide-low Ni-Cu-PGE deposits hosted in dominantly Middle Proterozoic troctolite and noritic varieties which intruded meta-sedimentary units (Barnes *et al.* 1997a, b; Thériault *et al.* 1997). The dominant sulphide minerals are pyrrhotite, chalcopyrite, pentlandite, and cubanite with minor arsenide minerals and a trace PGE bearing mineral called froodite (Thériault *et al.* 1997).

The sulphides at the Cirque have low R factors (25, 50, 100) according to the best fit of the Cirque PGE-Ni-Cu-Au patterns (Figure 5.14). Nickel and Cu concentrations in the Cirque sulphides are somewhat lower than that of the calculated concentrations, possibly due to the fact that Ni and Cu have much lower partition coefficients in a sulphide melt than

Table 5.1 Calculated concentrations of metal elements in the sulphide liquid (Cc) using R factors = 25, 50, 100, 1000, and 10,000 in Equation 5.1. Partition coefficients (D) and element concentrations in silicate magma (CL) are those of the Duluth Complex from Barnes et al. (1997a).

Element	D	CL	R = 25	R = 50	R = 100	R = 1000	R = 10,000
Ni %	500	0.018	0.45	0.83	1.52	6.01	8.57
Os	100,000	0.04	1.04	2.04	4.04	39.64	363.67
Ir	100,000	0.04	1.04	2.04	4.04	39.64	363.67
Ru	100,000	0.1	2.60	5.10	10.09	99.11	909.18
Rh	100,000	0.2	5.20	10.19	20.18	198.22	1818.36
Pt	100,000	3	77.98	152.92	302.70	2973.27	27275.45
Pd	100,000	3	77.98	152.92	302.70	2973.27	27275.45
Au	4,000	1	25.84	50.37	98.54	800.80	2857.43
Cu %	1,500	0.01	0.26	0.49	0.96	6.01	13.04

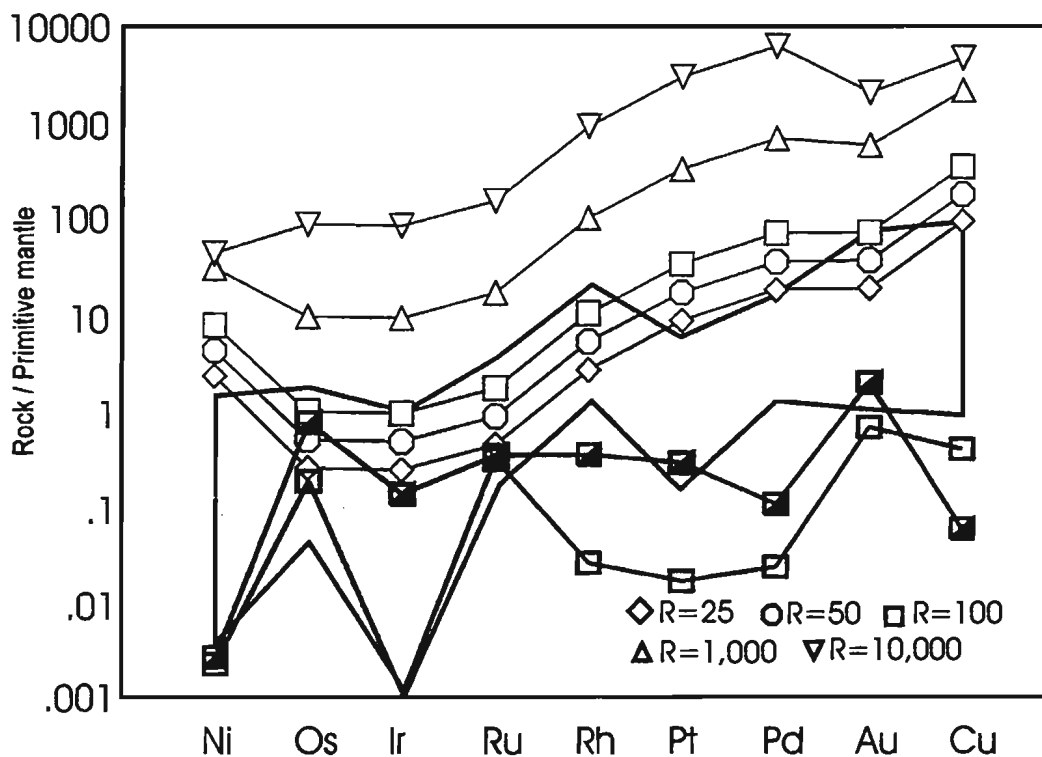


Figure 5.14 Plot of calculated R Factors for the Cirque sulphides using data from the Duluth Complex (Barnes et al. 1997a; refer to Table 5.1 for data used). For comparison, the grey field defines the PGE signatures of sulphide-bearing anorthosites from the Cirque (core, outcrop, and talus including one core sample of massive sulphide from the Canadian States Resources property, Licence #1514M). Two ferrodiorite samples (LD-46  $\square$  and LD-83  $\blacksquare$ ) with minor disseminated pyrrhotite were added for comparison. All data were normalized using primitive mantle values from Barnes et al. (1988).

PGE and Au, or according to Barnes *et al.*'s (1997b) suggestion for low metal contents in sulphides at Duluth, the metals in the Cirque sulphides could have been redistributed during its movement away from the source magma. Low R factor estimations for the Cirque sulphides mean that the amount of metals available at the time of sulphide saturation was low, thus the probability of the sulphides containing sufficient metals upon the time of segregation to form high Ni, Cu and PGE grades is low.

Piercey (1998) used the same values from Barnes *et al.* (1997a) to determine the composition of the initial sulphide melt that was in equilibrium with the silicate melt ( $C_C$ ) for pyroxenite dykes having disseminated and massive sulphides at the OKG property. Although Ni, Cu, PGE, and Au concentrations were generally greater than those from the Cirque property; the R factors for the OKG property mineralization were also estimated to be low (<50 to 500) with better fits for Ni, Os, Ir, Ru, Au, and Cu (Piercey 1998). Piercey (1998) attributed poor agreements of Rh, Pt, and Pd with several possibilities: (i) dilution of Rh and Pd concentrations by the negative Pt anomaly, (ii) incorrect initial composition of the silicate magma, or (iii) incorrect partition coefficients. Such explanations can also be attributed to the inconsistencies of Ni, Cu and to a lesser extent, Pt and Pd at the Cirque, however, it is also possible that the mobilized sulphide melt at the Cirque originated from the Fe-*mss* melt which fractionated from either (i) a PGE-Cu ( $\pm$  Ni)-rich sulphide liquid segregated early from the magma and exists at depth or (ii) an initial PGE-Cu ( $\pm$  Ni)-poor sulphide liquid.

Using metal concentrations from the samples ( $C_L$ ) assayed at Memorial University

and R factors of 25, 50, 100, the metal concentrations in the sulphide melt ( $C_c$ ) were recalculated (Figure 5.15). The calculated metal concentrations in the sulphide melt are higher than those of the silicate liquid considering the “host” rock which represents the silicate liquid consists dominantly of plagioclase cumulates and more importantly, does not represent the actual source magma. With each R factor, the PGE-Ni-Cu-Au patterns have positive slopes with the same depleted Ir, Pt, and Ni for anorthosite and the same lower concentrations in ferrodiorite. Such similarities suggest that the original source magma may have had low concentrations of a PGE-Ni-Cu-Au prior the present emplacement of the sulphides within the anorthosite intrusion.

Using these R factors then,  $C_c$  values were calculated using the concentrations of the metals in known rocks from the Voisey’s Bay deposit. Averaged metal contents (recalculated to 100% sulphides) from Naldrett *et al.* (2000) were further averaged to make four groups: VVTAVG2, LLTAVG4, BBSAVG5, and MSAVG4 which are sulphide-bearing samples from the Varied-textured troctolites, Leopard-textured troctolites, Basal Breccia Sequence, and massive sulphides, respectively. Samples from the Eastern Deeps, Mini-Ovoid, Ovoid, Discovery Hill zone, Reid Brook zone had been analysed by Naldrett *et al.* (2000) and were used in this study to compare the possibility of the host rock at Voisey’s Bay deposit being the same (or similar) to that of the Cirque area. Figure 5.16 shows that for the three different R factors (25, 50, 100), the concentrations of the metals in the four different groups from the Voisey’s Bay deposit are much higher than those from the Cirque. Thus, it is very likely that the host magma for the Cirque sulphides is geochemically



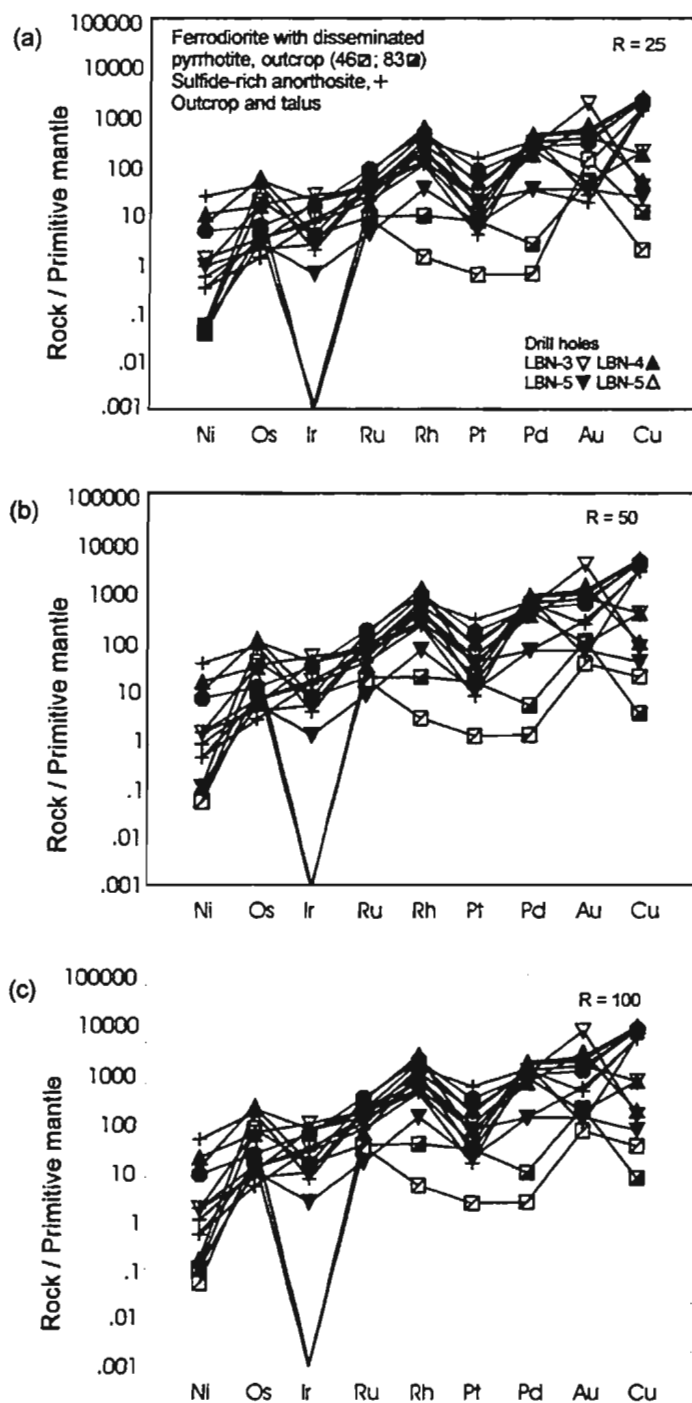


Figure 5.15 Plot of recalculated PGE-Ni-Cu-Au concentrations in the sulphide melt (Cc) of Cirque rocks (plus one massive sulphide sample from the Canadian States Resources property, Licence #1514M ●) using element concentrations from the rocks (CL) and R factors of 25, 50, and 100. Data are normalized using mantle values from Barnes et al. (1988).

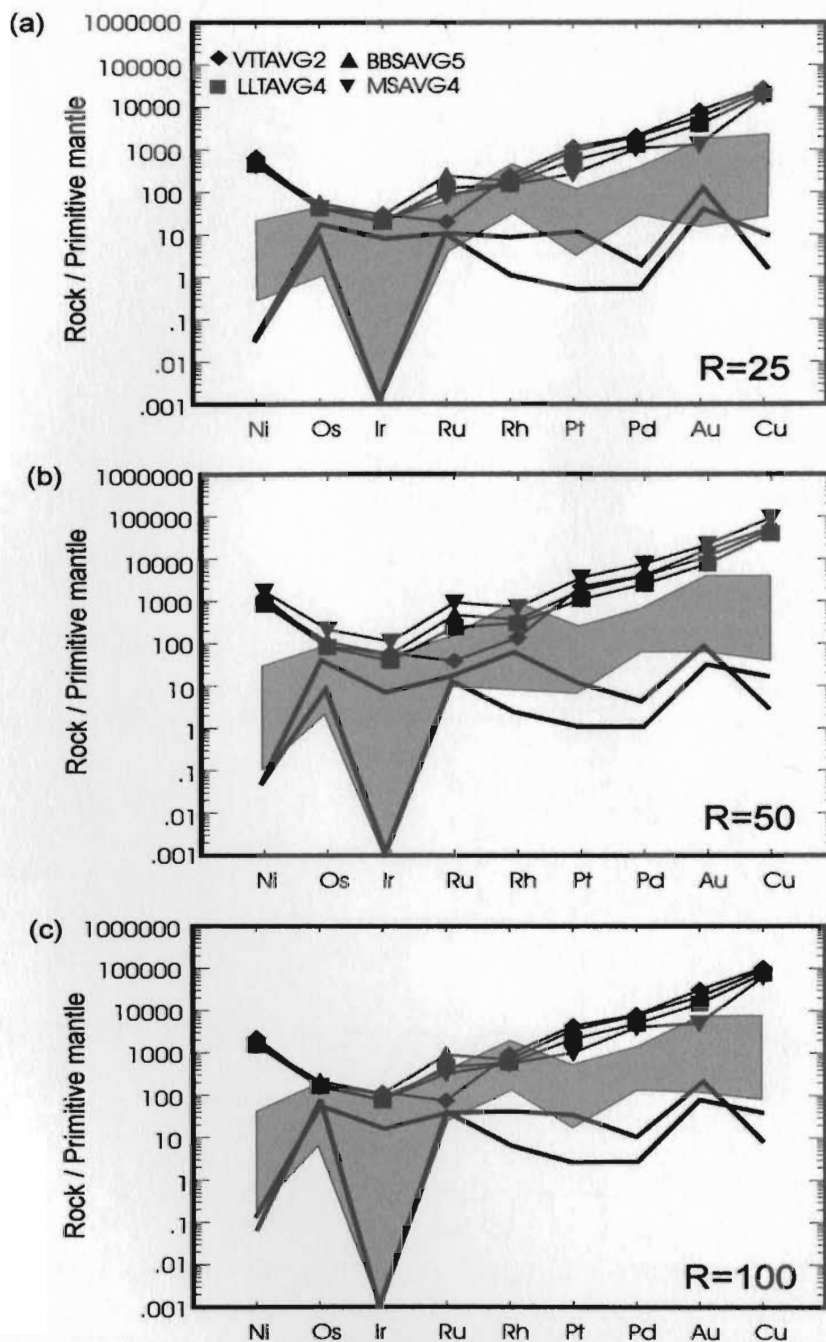


Figure 5.16 Mantle-normalized PGE-Au-Ni-Cu patterns of sulphide-bearing samples four different averaged rock types from the Voisey's Bay deposit. Concentrations of the metals in the silicate liquid ( $C_L$ ) are calculated using three different R factors: (a) 25, (b) 50, and (c) 100. Averaged values (recalculated to 100% sulphides) from Naldrett et al. (2000) are used as the concentrations of the metals in the sulphide liquid ( $C_C$ ) and the partition coefficients (D) are those given by Barnes et al. (1997a). VTTAVG2 consists of Varied-textured troctolite from the Eastern Deeps. LTTAVG4 consists of Leopard-textured troctolite from the Eastern Deeps, Mini-Ovoid, Discovery Hill zone, and Reid Brook zone. BBSAVG5 consists of Basal Breccia Sequence from the Eastern Deeps, Ovoid, Mini-Ovoid, Discovery Hill zone, and Reid Brook zone. MSAVG4 consists of massive sulphides from the Eastern Deeps, Ovoid, Mini-Ovoid, and Reid Brook zone. Plots are compared to samples from the Cirque with corresponding R factors: pyrrhotite-rich anorthosite from drill core and outcrop, plus one massive sulphide sample (core) from the Canadian States Resources property; Lic #1514M (grey) and ferrodiorite with minor disseminated pyrrhotite from outcrop (samples 46 and 83; thick line). All data are normalized using mantle values from Barnes et al. (1988).

different from that of the Voisey's Bay deposit and contained much lower metal concentrations.

### **5.6 General comparison with the Voisey's Bay deposit**

The sulphide deposits at Voisey's Bay consists of massive, coarse-grained aggregates of hexagonal pyrrhotite with and without exsolved troilite, pentlandite, chalcopyrite, and variable abundances of cubanite and magnetite (Naldrett *et al.* 2000b). Troilite occurs in the Reid Brook, Discovery Hill and Ovoid zones with the occurrence of pentlandite dependent on the presence of troilite; occurring as coarse grains in pyrrhotite wherever troilite is found as lamellae within massive pyrrhotite and as finer grains, thus defining differences of several zones of sulphide mineralization, particularly the Eastern Deeps. Naldrett *et al.* (2000b) summarized the differences between the Eastern Deeps and two other zones (Ovoid and Mini-Ovoid) in terms of sulphide mineralization. The Eastern Deeps zone contains considerably less magnetite and troilite than the Ovoid and Mini-Ovoid zones; pentlandite is present as smaller grains along the margins of massive intersections of hexagonal pyrrhotite and as fine lamellae within pyrrhotite grains (*op cit.*). Pyrrhotite grains, analyzed by Naldrett *et al.* (2000b), show the relationship between the presence of troilite and Ni contents. Hexagonal pyrrhotite with coexisting troilite has average Ni contents between 0.15 at.% (Reid Brook zone) to 0.22 at. % (Discovery Hill zone). Ni contents for the same type of sulphide mineralization is 0.12 at. % at Pants Lake. The Eastern Deeps zone, which lack significant troilite in hexagonal pyrrhotite grains, have

greater Ni contents (0.36 at. %). In troilite-poor pyrrhotite intersections in the Reid Brook zone, the Ni content is 0.26 at. % (Naldrett *et al.* 2000b).

Naldrett *et al.* (2000b) explain these differences in pentlandite occurrences and Ni contents in pyrrhotite as being due to inhomogeneous assimilation of Tasiuyak gneiss on a local scale and variably distributed graphite throughout the gneiss, resulting in areas within the magma chamber being more reduced than others. This interpretation is used by Naldrett *et al.* (2000b) to explain why the sulphides of the Eastern Deeps have lower metal/sulphur ratios than those of the Ovoid and Mini-Ovoid. Such an explanation of low metal/sulphur ratio may also be applicable to the sulphides at the Cirque. Like the Eastern Deeps zone, the Cirque sulphides are pyrrhotite-rich with pentlandite occurring as fine exsolution lamellae within pyrrhotite.

At the Cirque, copper, Ni, and PGE concentrations are low ( $\text{Ni/Cu} < 1$ ) in the pyrrhotite-dominated sulphides. The presence of such a large amount of pyrrhotite indicates a high sulphur capacity in the initial mafic magma with the majority of the sulphur most likely coming from the surrounding gneiss country rocks from the Churchill province (possibly enderbitic gneiss) and the Nain Province, as indicated by S isotope analyses. These results support the radiogenic isotopic geochemistry presented in Chapter 4, however, the Tasiuyak gneiss does not seem a possible sulphur source due to  $\delta^{34}\text{S}$  values between 2.5 and 3 per mil. Upon reaching sulphide saturation, sulphides became enriched in Cu, Ni, and PGE and subsequently separated from the silicate magma to form a sulphide phase.

The excess pyrrhotite suggests the sulphides mobilized from an Fe-rich melt and redistribution of the metals during mobilization along the faults resulted in the small amount of fractionated Cu-rich sulphides in the Fe-monosulphide solid solution moving outward and settling along the rim of the massive and semi-massive pyrrhotite (Barnes *et al.* 1997b). Interpretations by F.P.F. Resources (1996), based on visual and geochemical studies, suggest that Cu increases away from the pyrrhotite-dominated sulphides as it moved toward the periphery of the main sulphide body, leaving behind a Ni-rich “restitute” at depth. In core and outcrop samples, copper concentrations are greater than Ni, supporting the idea of a Cu-rich sulphide melt, however, Ni concentrations in core do not increase overall with depth. Nonetheless, excess pyrrhotite indicates the sulphides may have originated from a Fe-rich melt and redistributed the remaining Cu present in the Fe-*mss* during mobilization along the faults to settle along the rim of the massive and semi-massive pyrrhotite. If this is true then this means that the sulphides on the Cirque property have low tenor and are unlikely to be economic. Due to the highly evolved nature of the magma, much of the compatible elements (for example, Ni and Ir) have fractionated early during olivine ( $\pm$  chromite) crystallization. Relatively low Pd/Ir and Cu/Ir ratios and high Ni/Cu and Ni/Pd ratios also suggest a low degree of partial melting which would mean much of the PGE remained in the mantle initially (Barnes *et al.* 1997a). Fractionated Cu-rich (and Ni-rich) sulphides, if they exist, which segregated from the initial sulphide melt, have yet to be intersected. Possible locations for the metal-rich sulphide phase are: (i) partially melted and incorporated back into the mantle, (ii) at depth near its source magma, or (iii) mobilized away from the source

to be emplaced either still at depth below the surface or move upwards by expulsions from crystallizing magmas or along faults to crystallize at a shallow depth. Either way, the Ni and Cu contents at the Cirque are only slightly elevated at depth (even if locally) and the potential for PGE-rich sulphides at depth is low.

## **CHAPTER 6**

### **DISCUSSION AND CONCLUSION**

#### **6.1 Summary**

The Cirque gossan (LBN property, Licence #1764M) is one of many localized magmatic Ni-Cu sulphide occurrences located south of Okak Bay hosted within massive and layered intrusions of anorthosite, gabbro, norite, troctolite (plus 'leuco' varieties of each) of the Mid-Proterozoic Nain Plutonic Suite. These occurrences are typically exposed near or along north to northeast trending lineaments and faults and seem to be located within a zone approximately 40 km long (north-south) and 5-10 km wide (east-west). The Cirque gossan, approximately 250 to 300 m wide and striking nearly 1 km to the northwest, is clearly visible along a steep-sided cirque and can be traced onto the neighbouring Canadian States Resources property (Licence #1514M) to the northwest. Adjacent to the western boundary is the Noranda "Hilltop" property (Licence #915M) which also reported several sulphide zones in outcrop and rubble. Borehole and ground geophysical surveys have defined the Cirque gossan as consisting of several isolated conductors which, together, plunge steeply to the southeast. Outcrop exposure along the cirque wall suggest that the mineralized zone also dips to the west.

The following points summarize the results of this study of the Cirque area.

- (1) The magmatic history of the Cirque area involves crystal fractionation (especially

of plagioclase, pyroxene, and minor olivine) in a mantle-derived tholeiitic magma which eventually formed varieties of troctolite, norite, and gabbro. Huge accumulations of relatively less dense plagioclase cumulates produced massive intrusions of anorthosite, with variable abundances of the mafic minerals, at the top of the magma chamber.

The Cirque property consists dominantly of anorthosite, more specifically, three anorthosite intrusion types. The oldest anorthosite body (GP) is very coarse-grained, labradorite-rich, pyroxene-poor with a few large orthopyroxene crystals. This anorthosite was intruded by a coarse-grained anorthosite (BB) with variable abundances of cumulate orthopyroxene, clinopyroxene, magnetite, and ilmenite. A third body of anorthosite is described as 'Bleached' because of its white colour, recrystallized texture, and lack of mafic minerals. Bleached anorthosite is observed as thin dykes crosscutting the younger anorthosite bodies and, at two locations, lying immediately above the Cirque gossan. Its relationship with the sulphide mineralization is unknown. It may be coincidental or it may be a zone of alteration of the anorthosite (which clearly has been intruded by the sulphides).

At the top of the Cirque are west to southwest dipping layers of leucotroctolite and leuconorite/leucogabbro with variable and localized patches of olivine and orthopyroxene/clinopyroxene, respectively. These layers, although located in zones of sulphide mineralization, do not host any significant amounts of sulphides. Major and trace element geochemical data indicate that the anorthosite and mafic layers are genetically related and formed from crystal fractionation and accumulation of silicate minerals.

North-northeast trending faults, some with pegmatitic K-feldspar-quartz-biotite-rich



veins and dykes, crosscut the Cirque area after emplacement of the mafic magmas.

Two types of clinopyroxenite have been located on the cirque grid. One (91), from talus along the cirque wall, is geochemically a product of a less fractionated magma source - possibly precursor material for the other rock types at the Cirque or perhaps crystallized from a separate mafic magma. The second clinopyroxenite sample (117) was collected from a localized area of thinly layered (~1cm wide) clinopyroxene-rich and plagioclase-rich cumulate layers within massive pyroxene-rich anorthosite. Such an occurrence obviously formed as a result of gradual crystal fractionation of plagioclase and pyroxene within a cooling magma.

Crosscutting the anorthosites (BB and GP) along the north arm in northeast and northwest directions are ~1-1.5 m wide ferrodiorite dykes which have significant magnetite and ≤ 1% disseminated pyrrhotite. The ferrodiorites have the highest concentrations of  $\text{TiO}_2$ ,  $\text{FeO}^*$ ,  $\text{P}_2\text{O}_5$ , and incompatible trace elements suggesting that the ferrodiorite dykes crystallized from a residual melt of a fractionating basaltic magma. However, a slight negative Eu anomaly, unlike that of the anorthosite and related mafic rocks, suggests that they may have formed from a separate magma than that from which the anorthosite and mafic rocks fractionated.

(2) The location of the Cirque gossan is relatively close to the inferred boundary which separates the Paleoproterozoic Churchill Province (west) from the Archean Nain Province (east). Both provinces contain variable abundances of sulphur and silica-bearing

metasedimentary rocks. Ranges of  $\text{ISr}$  (0.704 to 0.706),  $\epsilon\text{Nd}$  (-8.76 to -2.72),  $\delta^{34}\text{S}_{\text{CDT}}$  (2.5 to 3.0 ‰) for anorthosite and mafic rocks suggest that the magma was derived from an enriched mantle-derived source and that a sulphide melt formed as a result of sulphur saturation from additional S (and possibly  $\text{SiO}_2$ ) derived from the Churchill Province, including enderbite gneiss, which it intrudes. Other possible sources of crustal contamination are the Nain Province and to a lesser extent the Tasiuyak gneiss. The total estimated value of crustal rock contamination (Nain and Churchill provinces) in the Cirque area is between 20 to 60%.

(3) Overall, the metal contents in sulphides at Cirque and some of the surrounding properties are low, however, there are several properties which have reported anomalous metal concentrations. The highest Ni and Cu contents (from outcrop) are 0.51% and 0.59%, respectively. Typical Ni/Cu ratios  $\leq$  1-2 but are as high as 4.54. In borehole intersections, the best grade and width combined is 0.28% Ni, 0.44% Cu, and 0.12% Co over 5.1 m from LBN-4 (390.35 m). Localized grades of narrow mineralized zones are as high 0.30% Ni, 3.9% Cu, 0.14% Co (over 20 cm) from a 1.5 cm wide pyrrhotite and chalcopyrite-rich vein which intrudes sulphide-poor anorthosite in LBN-8 (@ 923.92 m).

PGE contents are uneconomic (typical Pt and Pd concentrations are <50 ppb each). Relatively low Pd/Ir, Cu/Ir, and high Ni/Pd, Ni/Cu, and Cu/Pd ratios indicate a low degree of partial melting of the mantle material and low metal/sulphur ratios, resulting in a PGE-

depleted fractionated magma. Low R factors (25-100) also indicate a low metal content, particularly PGEs, of the host magma prior to sulphide crystallization, probably as a result of early olivine and chromite crystallization in the parental magma.

(4) The sulphides in the Cirque gossan occur within anorthosite with variable abundances of pyroxene and oxide minerals and very little olivine. This suggests that (a) the host magma is too fractionated to have any potential from which a metal-rich sulphide melt can crystallize or (b) this is not the host rock. Thermal erosion textures and disaggregation of plagioclase crystals from sulphide-bearing anorthositic rocks in the Cirque property suggest an epigenetic style of mineralization in which sulphides in the Cirque gossan had been emplaced in a plagioclase-rich crystal-liquid mush. As with most sulphides that have moved away from the host magma, segregation of the sulphide melt fraction resulted in a Cu-rich phase having been mobilized from the remaining Fe-rich phase. It is probably this Fe-rich component which now represents Cirque gossan, however, as noted above this does not mean that an original metal-rich sulphide melt ever existed. Without full geochemical analyses of the original host magma only speculations can be made here.

(5) Geophysical interpretations suggest that several separate, steeply dipping sulphide zones exist from close to the surface to as deep as 1100 m and that some of these sulphide zones steepen sharply with depth and have been interpreted to be related to fractures or a contact (JVX Ltd. 1995). Coarse-grained sulphides, seen in outcrop wrapping irregularly and discontinuously around unmineralized anorthosite, do not appear to be

directly related to the northeast trending, vertically dipping fault crosscutting the cirque, however, such transport may have occurred at depth.

(6) A possible source of the sulphides may be located at depth west of the Cirque gossan, on Noranda's "Hilltop" property (Licence #915M). Surface exposure of pyrrhotite-bearing pyroxenite dykes on the northeast corner of the property, although unconfirmed by the author, seem to correlate to a syngenetic-style of sulphide mineralization in clinopyroxenite dykes also observed by Piercey (1998) at the OKG prospect. Pyrrhotite from the OKG prospect moved only a few centimeters from the dykes into the older and cooler anorthosites (Kerr 1998; Piercey 1998; Piercey and Wilton 2000). If the same hypothesis is applied to mineralization in the Cirque area, then greater mobilization could have been aided by incomplete crystallization of the anorthosite.

(7) Trace element geochemistry of the sulphide-bearing anorthosites indicates that the anorthosites and mafic rocks are genetically related to the anorthosites which "host" the sulphides at the Cirque gossan. Comparisons with a massive sulphide sample from the neighbouring Canadian States Resources property (Licence #1514M), however preliminary, seem to indicate that sulphide mineralization is not similar to that of the Cirque gossan. Although similar thermal erosion textures have been observed on this property, an epigenetic style of sulphide mineralization has also been reported on the Canadian States Resources property. Thus, a separate sulphide source may also exist in the area.

(8) The presence of disseminated pyrrhotite within ferrodiorite dykes on the Cirque grid indicate the occurrence of syngenetic-style of sulphide mineralization and supports the idea of a second sulphide source. The dykes, which have major and trace element geochemical signatures which suggest a different magma source, crosscut the massive anorthosite that “hosts” the sulphides of the Cirque gossan. Either the ferrodiorite dykes are carrying sulphides from the same sulphide source at depth or the disseminated sulphides in the ferrodiorite dykes were formed from a separate source, possibly that from which the sulphides on the Canadian States Resources property (Licence #1514M) segregated.

## **6.2 Speculation on the potential for economic magmatic Ni-Cu±PGE sulphides**

Since the discovery in 1993 of the Voisey’s Bay deposit approximately 80 km south, numerous studies have been conducted on the geology, isotopic signatures, and metallogenesis for the deposit resulting in a genetic model involving a unique “plumbing system” where the metals are enriched and the sulphides are segregated at shallow levels in the continental crust (Li and Naldrett 2000; Evans-Lamswood 1999). Another feature of this deposit is that the VBI is much older than that of any other intrusion (1.333 Ga; Li *et al.* 2000) within the NPS, indicating a different geochemical composition of the parental magma, history of crustal contamination and crystal fractionation all of which have significant influences in the formation of the sulphide deposit which it now hosts.

Although comparisons between the Voisey’s Bay deposit and the Cirque Ni-Cu sulphide occurrence are limited, several common features are evident. Important differences

between the two areas of mineralization, however, still indicate that the sulphide potential in the Cirque occurrence is low. The following are the main comparisons between the two areas:

1. Although the significance of different types of crustal contaminants is not well understood, troctolitic rocks of the Voisey's Bay Intrusion were only moderately (8-13%) contaminated, dominantly by the Tasiuyak gneiss and to a lesser extent by enderbitic gneiss of the Churchill Province (Amelin *et al.* 2000; Li *et al.* 2000). The Mushuau Intrusion (MI), which has  $\epsilon\text{Nd}$  (1.3 Ga) values similar to those from the Cirque, has a greater degree of contamination (15-35%), dominantly by the Nain Province gneiss (Amelin *et al.* 2000). Other contaminants in the MI are likely derived from the Churchill Province and include the enderbitic gneiss and the Tasiuyak gneiss (Amelin *et al.* 2000).
2. The Voisey's Bay deposit is hosted within layered and massive troctolite with and without troctolitic and gneissic breccia (Ryan 2000; Li *et al.* 2000; Lightfoot and Naldrett 1999). The lack of a less fractionated mafic (or ultramafic) magma and gneissic breccia at the Cirque gossan is significant as it suggests a geochemically different genetic history from that of the Voisey's Bay deposit. Multi-trace element signatures are generally similar for the two locations, however, overall

concentrations are greater for the Voisey's Bay deposit area and suggest less fractionated rock types, thus greater potential for metal-rich sulphide fractionates.

3. Sulphide minerals within the Voisey's Bay deposit consists of dominantly pyrrhotite, chalcopyrite, and pentlandite; magnetite and troilite contents are variable in the different Voisey's Bay deposits. Ni and Cu values are much higher than those from the Cirque, however, the MI, which is located just north of the Voisey's Bay deposit, hosts only a few sulphide occurrences with insignificant Ni and Cu contents. The MI has sulphide geochemistry similar to that of the Cirque, that is, pyrrhotite-rich with minor chalcopyrite and flame lamellae of pentlandite.
4. The formation of the Voisey's Bay deposit is interpreted to result from a sulphide melt being pushed upwards by pulses of metal-rich silicate magmas into a sulphur-rich country rock. Upgrading of the Ni and Cu contents of the sulphides was due to continuous influxes of metal-enriched magma (Ryan *et al.* 1995; Li *et al.* 2000; Lightfoot and Naldrett 1999) and embayments along the country rock wall which allowed for sufficient sulphide accumulation to form the deposits (Evans-Lamswood 1999). What seems to make the genetic model of the Voisey's Bay deposit so unique is that the basaltic magma, located at the upper mantle-lower crustal region, was not sufficiently contaminated nor fractionated during its emplacement within upper crustal levels, thus sulphide saturation was delayed until metal contents were high

enough and the segregated sulphides were shallow enough to form what are now known as the separate deposits at Voisey's Bay (Amelin *et al.* 2000; Li *et al.* 2000).

5. Sulphide mineralization within the MI involved a greater degree of crustal contamination and a longer history of crystal fractionation, thus reducing the metal content of the magma before the magma and its immiscible sulphide melt reached shallower levels in the crust (Li *et al.* 2000). In comparison, rocks from the Cirque area also contain a high amount of crustal contaminants and the sulphides from the may have had low metals contents initially due to incomplete partial melting of the mantle-derived material and/or prolonged crystal fractionation of ferromagnesian minerals at depth which may have depleted the metals prior to sulphide saturation.

### **6.3 Conclusion**

The results of this study suggests that sulphide mineralization in the Cirque gossan contains low Ni, Cu, and PGE concentrations. The major differences between the Voisey's Bay deposit and the Cirque gossan seems to be the timing of sulphur saturation and the method of sulphide emplacement. Based on the epigenetic style of mineralization and geochemical data, which indicate that the host magma at depth may not have had the potential to initially host a sulphide melt with high tenor, it seems unlikely that an economic magmatic Ni-Cu sulphide occurrence may exist in the Cirque area. Nonetheless, the presence of Ni- and Cu- rich assays in the area surrounding the Cirque gossan suggests that



the source of metal-rich sulphides may be located at depth on the neighbouring Noranda's "Hilltop" property where pyrrhotite and minor chalcopyrite mineralization is hosted within olivine norite/gabbro and pyroxenite (Squires *et al.* 1996, 1997). Similar mineralization has been found on the OKG prospect, approximately 35 km north of the Cirque property. If syngenetic mineralization is actually hosted within magmas of these compositions, and the sulphides were mobilized away from its host magmas into the surrounding semi-crystallized magma, then perhaps there is a possibility that such a magma exists at depth on the Cirque property or in the area.

Preliminary interpretations of the crystallization ages of the Voisey's Bay deposit and South Voisey's Bay area suggest that the relatively older intrusions of the NPS have greater potential to host economic magmatic Ni-Cu sulphide mineralization, however, this has not yet been proven. To do so, would mean an extensive investigation of the metallogeny and geochemistry of known sulphide occurrences throughout the NPS.

## REFERENCES CITED

- 1986. Regional lake sediment and water geochemical reconnaissance data, Labrador. Geological Survey of Canada, Newfoundland and Labrador Department of Mines and Energy, Open File 1210, GS# LAB/0695, 100 pages.
- Anonymous.** 1996. *Partial report on the results of prospecting and mapping of several properties in northern Nain Plutonic Suite by Ace Developments.*
- Amelin, Y., Li, C., Naldrett, A.J.** 1997. Multistage evolution of the Voisey's Bay Complex, Labrador, Canada, revealed by U-Pb systematics of zircon, baddeleyite, and apatite. American Geophysical Union (AGU) Fall Meeting.
- Amelin, Y., Li, C., and Naldrett, A.J.** 1999. Geochronology of the Voisey's Bay complex, Labrador, Canada, by precise U-Pb dating of coexisting baddeleyite, zircon, and apatite. *Lithos.* 47, pages 33-51.
- Amelin, Y, Li, C, Valeyev, O, and Naldrett, A.J.** 2000. Nd-Pb-Sr isotope systematics of crustal assimilation in the Voisey's Bay and Mushuau intrusions, Labrador, Canada. *Economic Geology.* 95, pages 815-830.
- Arndt, N.T. and Goldstein, S.L.** 1989. An open boundary between lower continental crust and mantle; its role in crust formation and crustal recycling. *Tectonophysics.* 161, No. 3-4, pages 201-212.
- Arndt, N.T., Czamanske, G.K., Wooden, J.L., and Fedorenko, V.A.** 1993. Mantle and crustal contributions to continental flood basalt volcanism. *Tectonophysics.* 223, pages 39-52.
- Ashwal, L.D.** 1993. Anorthositic. Springer-Verlag. Berlin, 422 pages.
- Ashwal, L.D. and Wooden, J.L.** 1983. Isotopic evidence from the eastern Canadian shield for geochemical discontinuity in the Proterozoic mantle. *Nature.* 306. No. 15, pages 679-680.
- Ashwal, L.D. and Wooden, J.L.** 1983. Isotope geochemistry of the Proterozoic anorthositic from the Grenville and Nain provinces; mantle sources and tectonic implications. EOS, Transactions, American Geophysical Union. 64. No 18, page 331.
- Ashwal, L.D. and Wooden, J.L.** 1985. Sm-Nd isotopic studies of Proterozoic anorthositic: Systematics and implications. *In* The deep Proterozoic crust in the North Atlantic provinces. D. Reidel Publishing Company, pages 61-73.

- Barnes, S-J.**, 1990. The use of metal ratios in prospecting for platinum-group element deposits in mafic and ultramafic intrusions. *Journal of Geochemical Exploration*. 37, pages 91-99.
- Barnes, S-J. and Maier, W.D.** 1999. The fractionation of Ni, Cu, and the noble metals in silicate and sulphide liquids. *In* Dynamic processes in magmatic ore deposits and their application in mineral exploration. Keays, R.R., Leshar, C.M., Lightfoot, P.C., and Farrow, C.E.G. *eds.* Geological Association of Canada, Short Course Notes. 13, pages 69-106.
- Barnes, S-J., Boyd, R., Korneliussen, A., Nilsson, L.P., Often, M., Pedersen, R.B., and Robins, B.** 1988. The use of mantle normalization and metal ratios in discriminating between the effects of partial melting, crystal fractionation and sulphide segregation of platinum-group elements, gold, nickel and copper: examples from Norway. *In* Geoplatinum 87. Prichard, H.M., Potts, P.J., Bowles, J.F.W., and Cribb, S. *eds.* Elsevier, Amsterdam, pages 113-143.
- Barnes, S-J., Couture, J.F., Sawyer, E.W., and Bouchaib, C.** 1993. Nickel-copper occurrences in the Belleterre-Angliers Belt of the Pontiac Subprovince and the use of Cu-Pd ratios in interplating platinum group element distributions. *Economic Geology*. 88. No. 6, pages 1402-1418.
- Barnes, S-J., Makovicky, E., Makovicky, M., Rose-Hansen J., and Karup-Moller S.** 1997b. Partition coefficients for Ni, Cu, Pd, Pt, Rh, and Ir between monosulfide solid saturation and sulfide liquid and the formation of compositionally zoned Ni-Cu sulfide bodies by fractional crystallization of sulfide liquid. *Canadian Journal of Earth Sciences*. 34, pages 366-374.
- Barnes, S-J., Zientek, M.L., and Severson, M.J.** 1997a. Ni, Cu, and Au and platinum-group element contents of sulphides associated with intraplate magmatism: a synthesis. *Canadian Journal of Earth Sciences*. 34, pages 337-351.
- Beesley, T.** 1996. Geological, prospecting, and ground geophysics report, Licence #1764M, 1765M (LB-N, Cirque Lake; LB-G, Ridge Anomaly), NTS 14E/01. Assessment report for Cartaway Resources Corporation to the Newfoundland Department of Mines and Energy, Mineral Lands Division, 23 pages.
- Beesely, T.J.** 1997. Geological and prospecting report, Licence # 1576 and 1575M (Can-1 and Can-2), NTS 14E/1. Assessment report for Cartaway Resources Corporation to the Newfoundland Department of Mines and Energy, Mineral Lands Division, 17 pages.

- Beesley, T.** 1997. Report on geological mapping and prospecting and a diamond drilling program, Licence # 1764M (LB-N), NTS 14E/1. Assessment report for Cartaway Resources Corporation to the Newfoundland Department of Mines and Energy, Mineral Lands Division.
- Berg, J.H.** 1977a, Dry granulite mineral assemblages in the contact aureoles of the Nain Complex, Labrador. *Contributions to Mineralogy and Petrology*. 64, pages 33-52.
- Berg, J.H.** 1977b. Regional geobarometry in the contact aureoles of the anorthosite Nain complex, Labrador. *Journal of Petrology*. 18, pages 399-430.
- Berg, J.H.** 1979. Physical constraints and tectonic setting of the Nain Complex. Geological Association of Canada - Mineralogical Association of Canada. Program with Abstracts. 4, page 39.
- Berg, J.H., Emslie, R.F., Hamilton, M.A., Morse, S.A., Ryan, A.B., and Wiebe, R.A.** 1994. Anorthositic, granitoid and related rocks of the Nain Plutonic Suite. Field excursion of the Nain area, August 4-10, 1994. International Geological Correlation Programme; IGCP Projects #290 and #315, 69 pages.
- Bertrand, J.-M., Roddick, J.C., van Kranendonk, M.J., and Ermanovics, L.** 1993. U-Pb geochronology of deformation and metamorphism across a central transect of the Early Proterozoic Torngat Orogen, North River map area, Labrador. *Canadian Journal of Earth Sciences*. 30, pages 1470-1489.
- Campbell, L.M.** 1994. Preliminary results from an Sm-Nd isotopic study of Proterozoic crustal formation and accretion in the Torngat Orogen, northern Labrador. In 1993 Report of Eastern Canadian Shield Onshore-Offshore Transect (ESCOOT) Transect Meeting. Wardle, R.J. and Hall, J. eds. LITHOPROBE Report No. 34, pages 100-107.
- Campbell, L.H. and Griffiths, R.W.** 1990. Implications of mantle plume structures for the evolution of flood basalts. *Earth and Planetary Science Letters*. 99, pages 79-93.
- Campbell, L.H. and Naldrett, A.J.** 1979. The influence of silicate : sulfide ratios on the geochemistry of magmatic sulfides. *Economic Geology*. 74, pages 1503-1505.
- Canadian States Resources.** 1996. Inhouse geology and drilling results for Licences #1514M and #1558M, northern Labrador.

- Carlson, R.W., Weibe, R.A., and Kalamarides, R.L.** 1993. Isotopic study of basaltic dikes in the Nain Plutonic Suite: evidence for enriched mantle sources. *Canadian Journal of Earth Sciences*. 30. No. 6, pages 1141-1146.
- Chaussidon, M., Albarè, F., and Sheppard, S.M.F.** 1989. Sulphur isotope variations in the mantle from ion microprobe analyses of micro-sulphide inclusions. *Earth and Planetary Science Letters*. 92, pages 144-156.
- Coates, H.J. and Beilhartz, D.** 1997. Second year assessment report on diamond drilling exploration for licence 1506M in claims in the Puttuala Brook area, eastern Labrador for Columbia Yukon Resources Limited, 14E/01 (October 1996). Newfoundland and Labrador Department of Natural Resources. Open File 14E/01/0147.
- Collerson, K.D.** 1983. The Archean gneiss complex of northern Labrador. 2. Mineral ages, secondary isochrons, and diffusion of strontium during polymetamorphism of the Uivak gneiss. *Canadian Journal of Earth Sciences*. 20, pages 707-718.
- Cook, H.E., Johnson, P.D., Matti, J.C., and Zemmels, L.** 1975. IV: Methods of sample preparation and X-ray diffraction data analyses, X-ray mineralogy laboratory deep sea project, University of California, Riverside. Institute of Geophysics and Planetary Physics, University of California, Riverside, Contribution No. 74-5, pages 999-1007.
- Connelly, J.N. and Ryan, B.** 1994. Late Archean and Proterozoic events in the central Nain craton. In Report of Eastern Canadian Shield Onshore-Offshore Transect (ESCOOT) Transect Meeting. Wardle, R.J. and Hall, J. eds. LITHOPROBE Report No. 36, pages 53-61.
- Craig, J.R. and Vaughan, D.J.** 1994. Ore microscopy and ore petrography. Second edition. John Wiley and Sons Inc. New York. 434 pages.
- Davies, G. and Tredoux, M.** 1985. The platinum-group element and gold contents of the marginal rocks and sills of the Bushveld Complex. *Economic Geology*. 80, pages 838-848.
- Deer, W.A., Howie, R.A., and Zussman, J.** 1992. An introduction to the rock forming minerals. Second edition. Longman Scientific and Technical, New York, 528 pages.
- Demaiffe, D. and Michot, J.** 1985. Isotope geochronology of the Proterozoic crustal segment of southern Norway: a review. In The deep Proterozoic crust in the North Atlantic provinces. Tobi, A.C., and Touret, J.L.R. (eds.), D. Reidel Publishing Company. Boston, pages 411-433.

- DePaolo, D.J.** 1981. Neodymium isotopes in the Colorado Front Range and crust-mantle evolution in the Proterozoic. *Nature*. 291, pages 193-196.
- DePaolo, D.J.** 1985. Isotopic studies in mafic magma chambers: 1. The Kiglapait Intrusion, Labrador. *Journal of Petrology*. 26, pages 925-951.
- DePaolo, D. J.** 1988. Neodymium Isotope Geochemistry: An Introduction. Springer-Verlag. Berlin, 187 pages.
- DePaolo, D.J., Perry, F.V., and Baldrige, W.S.** 1992. Crustal versus mantle sources of granitic magmas: two-parameter model based on Nd isotopic studies: Geological Society of America. Special Paper. 272, pages 439-446.
- DePaolo, D.J. and Wasserburg, G.J.** 1976. Nd isotopic variations and petrogenetic models. *Geophysical Research Letters*. 3, No 5, pages 249-252.
- De Waard, D.** 1976. Anorthosite-adamellite-troctolite layering in the Barth Island structure of the Nain complex, Labrador. *Lithos*. 9, pages 293-308.
- Diamond Fields Resources Inc.** 1995. *Press release*. November.
- Douglas, G.V.** 1953. Notes on localities visited on the Labrador coast in 1946 and 1947. Geological Survey of Canada. Paper 53-1, 67 pages.
- Duchesne, J-C.** 1984. Massif anorthosites: another partisan review. *In* Feldspars and feldspathoids. Brown, W.L. ed. D. Reidel Publishing Company, Holland, pages 411-433.
- Duchesne, J.C. and Demaiffe, D.** 1978. Trace elements and anorthosite genesis. *Earth and Planetary Science Letters*. 38, pages 249-272.
- Duchesne, J.C., Roelandts, L., Demaiffe, D., Hertogen, J., Gijbels, R., and de Winter, J.** 1974. Rare-earth data on monzonitic rocks related to anorthosites and their bearing on the nature of the parental magma of the anorthositic series. *Earth and Planetary Science Letters*. 24, pages 325-335.
- Dymek, R.F.** 1980. Petrographic relationships between andesine anorthosite dikes and labradorite anorthosite wall rock on Mont Du Lac Des Cygnes, St. Urbain anorthosite massif, Quebec. *In* Geological Society of America. 93<sup>rd</sup> annual meeting, Abstract with programs. 12. No. 7, page 419.

- Dymek, R.F.** 1993. Early crustal evolution; insights obtained from the compositions of Archean (meta)sedimentary rocks. *In* Geological Society of America, north-central section, 27<sup>th</sup> annual meeting, Program with Abstracts. 25. No. 3, pages 17-18.
- Ebel, D.S. and Naldrett, A.J.** 1996. Fractional crystallization of sulphide ore liquids at high temperature. *Economic Geology*. 91. 607-621.
- Eckstrand, O.R.** 1996. Nickel-copper sulphide. *In* Geology of Canadian Mineral Deposit Types. Eckstrand, O.R., W.D. Sinclair, and Thorpe, R.I *eds.* Geological Survey of Canada, Geology of Canada. No. 8, pages 584-605.
- Eckstrand, O.R., Grinenko, L.N., Krouse, H.R., Paktunc, A.D., Schwann, P.L., and Scoates, R.F.J.** 1989. Preliminary data on sulphur isotopes and Se/S ratios, and the source of sulphur in magmatic sulphides from the Fox River Sill, Molson Dykes and Thompson nickel deposits, northern Manitoba. *Current Research*. Part C. Geological Survey of Canada. Paper 89-1C, pages 235-242.
- Eckstrand, O.R. and Hulbert, L.J.** 1987. Selenium and the source of sulphur in magmatic nickel and platinum deposits. *In* Geological Association of Canada, Mineralogical Association of Canada, Canadian Geophysical Union, 1987 joint annual meeting, Program with Abstracts. 12, page 40.
- Emslie, R.F.** 1975. Pyroxene megacrysts from anorthositic rocks : new clues to the source and evolution of the parent magmas. *Canadian Mineralogist*. 13, pages 138-145.
- Emslie, R.F.** 1978. Elsonian magmatism in Labrador: age, characteristics and tectonic setting. *Canadian Journal of Earth Sciences*. 15, pages 438-453.
- Emslie, R.F.** 1985. Proterozoic anorthosite massifs. *In* The Deep Proterozoic Crust in the North Atlantic Provinces. A.C. Tobi and J.L.R. Touret, *eds.* D. Reidel Publishing Company, pages 39-60.
- Emslie, R.F.** 1996. Troctolitic rocks of the Reid Brook intrusion, Nain Plutonic Suite, Voisey Bay area, Labrador. *Current Research*. 1996-C. Geological Survey of Canada, pages 183-196.
- Emslie, R.F., Ermanovics, I.F., and Ryan, A.B.** 1997. Geology of the northern Nain Plutonic Suite and its envelope rocks, Labrador. *Current Research*. 1997-C. Geological Survey of Canada, pages 223-234.
- Emslie, R.F., Hamilton, M.A., and Thériault, R.J.** 1994. Petrogenesis of a Mid-Proterozoic anorthositic-mangerite-charnockite-granite (AMCG) complex: isotopic and chemical evidence from the Nain Plutonic Suite. *The Journal of Geology*. 102, pages 539-558.

- Emslie, R.F. and Hegner, E.** 1993. Reconnaissance isotopic geochemistry of anorthosite-mangerite-charnockite-granite (AMCG) complexes, Grenville Province, Canada. *Chemical Geology*. 106, pages 279-298.
- Emslie, R.F. and Hunt, P.A.** 1990. Ages and petrogenetic significance of igneous mangerite-charnockite suites associated with anorthosites, Grenville Province. *Journal of Geology*. 98, pages 213-231.
- Emslie, R.F. and Loveridge, W.D.** 1992. Fluorite bearing early and middle Proterozoic granites, Okak Bay area, Labrador: geochronology, geochemistry and petrogenesis. *Lithos*. 28, pages 87-109.
- Emslie, R.F. and Russell, W.J.** 1988. Umiakovic Lake batholith and other felsic intrusions, Okak Bay area, Labrador. *Current Research*. Part C, Geological Survey of Canada, Paper 88-1C, pages 27-32.
- Emslie, R.F. and Stirling, J.A.R.** 1993. Rapakivi and related granitoids of the Nain Plutonic Suite: geochemistry, mineral assemblages and fluid equilibria. *Canadian Mineralogist*. 31, pages 821-847.
- Ermanovics, I.F., Van Kranendonk, M., Corriveau, L., Mengel, F., Bridgwater, D., and Sherlock, R.** 1989. The boundary zone of the Nain-Churchill provinces in the North River-Nutak map areas, Labrador. *Current Research*, Part C, Geological Survey of Canada. Paper 89-1C, pages 385-394.
- Evans-Lamswoods, D.** 1999. Physical and geometric controls on the distribution of magmatic and sulphide-bearing phases within the Voisey's Bay Ni-Cu-Co deposit, Voisey's Bay, Labrador. Memorial University of Newfoundland. Unpublished Masters thesis, 253 pages.
- F.P.F. Resources.** 1996. Report on geological, geochemical reassessment, Cirque property (LB-N), Okak Bay area, northern Labrador for Cartaway Resources Corporation. *Inhouse report by F.P.F. Resources Inc.*, 88 pages.
- Farrow, C.** 1997. Most recent geochronological results from Memorial University of Newfoundland. INCO, Field exploration office, Copper Cliff. *memorandum*.
- Force, E.R. and Carter, B.A.** 1986. Liquid immiscibility proposed for nelsonitic components of the anorthositic-syenite-gabbro complex, San Gabriel Mountains, California. *In Geological Society of America, 99<sup>th</sup> annual meeting. Abstracts with Programs*. 18. No. 6, page 604.



- Fountain, J.C., Hodge, D.S., and Shaw, R.P.** 1989. Melt segregation in anatectic granites: a thermo-mechanical model. *Journal of Volcanology and Geothermal Research*. 39. No. 4, pages 279-296.
- Fram, M.S. and Longhi, J.** 1992. Phase equilibria of dikes associated with Proterozoic anorthosite complexes. *American Mineralogist*. 77, pages 605-616.
- Fuhrman, M.L., Frost, B.R., and Lindsley, D.H.** 1988. Crystallization conditions of the Sybille monzosyenite, Laramie anorthosite complex, Wyoming. *Journal of Petrology*. 29, pages 699-729.
- Giest, D.J., Frost, C.D., and Kolker, A.** 1990. Sr and Nd isotopic constraints on the origin of the Laramie Anorthosite Complex, Wyoming. *American Mineralogist*. 75, pages 13-20.
- Gower, C. F., Rivers, T., and Brewer, T.S.** 1990. Middle Proterozoic mafic magmatism in Labrador, eastern Canada. In *Mid-Proterozoic Laurentia-Baltica*. Gower, C.F., Rivers, T., and Ryan, B, eds. Geological Association of Canada, Special Paper 38, pages 485-506.
- Grant, J.A. and Frost, B.R.** 1990. Contact metamorphism and partial melting of pelitic rocks in the aureole of the Laramie anorthosite complex, Morton Pass, Wyoming. *American Journal of Science*. 290. No. 4, pages 425-472.
- Green, B.A.** 1974. An outline of the geology of Labrador. Information Circular No. 15. Department of Mines and Energy. Mineral Development Division. Government of Newfoundland and Labrador, 64 pages.
- Gromet, L.P. and Dymek, R.F.** 1980. Evidence for at least two geochemically distinct anorthosite types in the St. Urbain anorthosite massif, Quebec. In *Geological Society of America, 93<sup>rd</sup> annual meeting, Abstracts with Programs*. 12. No. 7, page 438.
- Gromet, L.P. and Dymek, R.F.** 1982. Petrological and geochemical characterization of the St. Urbain anorthosite massif, Quebec; summary of initial results. In *Magmatic processes of early planetary crusts; magma oceans and stratiform layered intrusions*. Walker, D. and McCallum, I.S. (eds.). LPI Technical Report. 82-01, pages 72-74.
- Hamilton, M.A.** 1994. Review of isotopic data for the Nain Plutonic Suite. In *Anorthositic, granitoid and related rocks of the Nain Plutonic Suite, Guidebook to a Field Excursion to the Nain area, August 4-10, 1994*. International Geological Correlation Programme Projects #290 and #315, pages 15-19.

- Hamilton, M.A.** 1997. New U-Pb geochronological results from the Mesoproterozoic Nain Plutonic Suite, Labrador, and implications for the origin and emplacement of massif anorthosites and related rocks. COPENA conference, Abstracts and proceedings, Trondheim, Norway, 2 pages.
- Hamilton, M.A. and Shirey, S.B.** 1992. Nd and Sr isotopic variations in anorthositic rocks of the Nain Plutonic Suite, Labrador. EOS, Transactions, American Geophysical Union. 73. No 14. Supplement, page 355.
- Hamilton, M.A., Emslie, R.F., and Ryan, B.** 1998. U-Pb evidence for Paleoproterozoic anorthositic and granitoid magmatism predating the emplacement of the Mesoproterozoic Nain Plutonic Suite, Labrador. GAC/MAC Annual Meeting, Quebec City, Abstract.
- Hanson, G.N.** 1980. Rare earth elements in petrogenetic studies of igneous systems. *Annual Review of Earth and Planetary Sciences*. 8, pages 371-406.
- Heath, S.A. and Fairbairn, H.W.** 1968.  $\text{Sr}^{87}/\text{Sr}^{86}$  ratios in anorthosites and some associated rocks. In *Origin of anorthosite and related rocks*. Isachsen, Y.W. (ed.). New York Museum and Science Service. Memoir 18, pages 99-110. 1969.
- Henderson, P.** 1990. Inorganic geochemistry. Pergamon Press. Oxford. 353 pages.
- Hennessy, J. and Mersereau, T.** 1996. Geological, geophysical and geochemical report on the 1995 exploration programme, claim groups 1575M and 1576M, Northeast Exploration Services Ltd., April 1996. Newfoundland and Labrador Department of Natural Resources. Open File 14E/01/0111.
- Hill, R.E.T.** 1984. Experimental study of phase relations at 600°C in a portion of the Fe-Ni-Cu-S system and its application to natural sulphide assemblages. In *Sulfide deposits in mafic and ultramafic rocks*. Buchanan, D.L. and Jones, M.J. eds. Special Publication of the Institute of Mining and Metallurgy, pages 14-21.
- Hinchey, J.G.** 1999. Magmatic sulphide-oxide mineralization in the Nain area, northern Labrador: a petrological and geochemical study. Memorial University of Newfoundland. Unpublished Honors Dissertation, 131 pages.
- Hinchey, J., Kerr, A., and Wilton, D.H.C.** 1999. Magmatic sulphide-oxide mineralization in the Nain Hill area (NTS 14C/12), northern Labrador. *Current Research*, Newfoundland Department of Mines and Energy. Geological Survey, Report 99-1, pages 183-194.

- Hoatson, D.M., Sproule, R.A., and Lambert, D.D.** 1997. Are there Voisey's Bay-type Ni-Cu-Co sulphide deposits in the East Kimberley of Western Australia? AGSO Research Newsletter, Australian Geological Survey Organisation. No 27, pages 17-19.
- Hoffman, P.F.** 1988. United plates of America, the birth of a craton: Early Proterozoic assembly and growth of Laurentia. *Annual Reviews in Earth and Planetary Science*. 16, pages 543-603.
- Hofmann, A.W.** 1988. Chemical differentiation of the earth: the relationship between mantle, continental crust, and oceanic crust. *Earth and Planetary Science Letters*. 90, pages 297-314.
- Hynes, A.P.** 1997. A petrographic and pyroxene mineral chemistry study of a layered intrusion of the Nain Plutonic Suite, northern Labrador. Memorial University of Newfoundland. Unpublished Honors Dissertation, 55 pages.
- Irvine, T.N.** 1982. Terminology for layered intrusions. *Journal of Petrology*. 23. Part 2, pages 127-162.
- Irvine, T.N. and Baragar, W.R.A.** 1971. A guide to the chemical classification of the common volcanic rocks. *Canadian Journal of Earth Sciences*. 8, pages 523-548.
- Jackson, S.E., Fryer, B.J., Gosse, W., Healey, D.C., Longerich, H.P., and Strong, D.F.** 1990. Determination of the precious metals in geological materials by inductively coupled plasma-mass spectrometry (ICP-MS) with nickel sulphide fire-assay collection and tellurium coprecipitation. *Chemical Geology*. 83, pages 119-132.
- Jenner, G.A., Longerich, H.P., Jackson, S.E., and Fryer, B.J.** 1990. ICP-MS - a powerful tool for high-precision trace-element analysis in Earth sciences: evidence from analysis of selected U.S.G.S reference samples. *Chemical Geology*. 83, pages 133-148.
- Jones, R.A.** 1975. Harp Lake intrusion, central Labrador. *Inhouse* progress report for Kennco Explorations, (Canada) Limited. January, 51 pages.
- JVX Ltd.** 1995. A report on horizontal loop electromagnetic and magnetometer surveys conducted on the Cirque grid, claim block LB-N (Licence 1764M), Voisey's Bay area, Labrador. *Inhouse* report for Cartaway Container Corporation, 12 pages.
- Kelly, D.P. and Vaughan, D.J.** 1983. Pyrrhotite-pentlandite ore textures : a mechanistic approach. *Mineral Magazine*. 47, pages 453-463.

- Kerr, A.** 1998. Petrology of magmatic sulphide mineralization in northern Labrador: preliminary results. *Current Research*. Newfoundland Department of Mines and Energy, Geological Survey, Report 98-1, pages 53-75.
- Kerr, A.** 1997. A discussion of controls on magmatic base-metal mineralization, with application to northern Labrador. *Current Research*. Newfoundland Department of Mines and Energy, Geological Survey, Report 97-1, pages 57-71.
- Kerr, A.** 1999. Mafic rocks of the Pants Lake intrusion and related Ni-Cu-Co mineralization in north-central Labrador. *Current Research*. Newfoundland Department of Mines and Energy, Geological Survey, Report 99-1, pages 215-253.
- Kerr, A. and Ryan, B.** 1998. Anorthosites and Ni-Cu mineralization north of Voisey's bay, Labrador: spatially married but genetically divorced. *Geological Society of America. Abstract*. 30. No 7. 20 pages.
- Kerr, A. and Ryan, B.** 2000. Threading the eye of the needle: lessons from the search for another Voisey's Bay in Labrador, Canada. *Economic Geology*. 95. 4, pages 725-748.
- Kerr, A. and Smith, J.L.** 1997. The search for magmatic Ni-Cu-Co mineralization in northern Labrador: A summary of active exploration programs. *Current Research*. Newfoundland Department of Mines and Energy, Geological Survey, Report 97-1, pages 73-91.
- Kerr, A., MacDonald, H.E., and Naldrett, N.J.** 2001. Geochemistry of the Pants Lake Intrusion, Labrador: implications for future mineral exploration. *Current Research*. Newfoundland Department of Mines and Energy, Geological Survey, Report 2001-1, pages 191-228.
- Klassen, R.A., Paradis, S., Bolduc, A.M., and Thomas, R.D.** 1992. Glacial landforms and deposits, Labrador, Newfoundland and eastern Quebec; *Geological Survey of Canada*, map 1814A, scale 1:1,000,000.
- Kolker, A. and Lindsley, D.H.** 1989. Geochemical evolution of the Maloin Ranch pluton, Laramie Anorthosite Complex, Wyoming: petrology and mixing relations. *American Mineralogist*. 74, pages 307-324.
- Krauskopf, K.B.** 1979. Introduction to geochemistry. McGraw-Hill Book Company. New York. Second edition. 617 pages.
- Kushiro, I.** 1969. The system forsterite-diopside-silica with and without water at high pressures. *American Journal of Science*. 267-A, pages 269-294.

- Lambert, D.D., Frick, R., Foster, J.G., Li, C., Naldrett, A.J.** 2000. Re-Os isotope systematics of the Voisey's Bay Ni-Cu-Co magmatic sulfide system, Labrador, Canada: II. Implications for parental magma chemistry, ore genesis, and metal redistribution. *Economic Geology*. 95. No. 4, pages 867-888.
- Leshner, C.M. and Campbell, L.H.** 1993. Geochemical and fluid dynamic controls on the composition of komatiite-hosted nickel sulfide ores in Western Australia. *Economic Geology*. 88, pages 804-816.
- Leshner, C.M. and Stone, W.E.** 1996. Exploration geochemistry in komatiites. In *Igneous trace element geochemistry applications in massive sulfide exploration*. Wyman, D.A. ed. Geological Association of Canada, Short Course Notes. 12, pages 153-204.
- Li, C., Amelin, Y., and Naldrett, A.J.** 1998. U-Pb geochronology of the Mushua troctolite complex at Voisey's Bay, northern Labrador, Canada. Geological Society of America. Annual meeting. Abstract.
- Li, C., Lightfoot, P.C., Amelin, Y., and Naldrett, A.J.** 2000. Contrasting petrological and geochemical relationships in the Voisey's Bay and Mushuau intrusions, Labrador, Canada: implications for ore-genesis. *Economic Geology*. 95, pages 771-799.
- Li, C. and Naldrett, A.J.** 1997. The Voisey's Bay Ni-Cu-Co deposit, Labrador, Canada: Variations of olivine composition related to multiple magma injections and sulfide segregation. In *Mineral Deposits: Research and exploration - Where do they meet?* Papunen, H. ed. Proceedings of the Fourth Biennial SGA Meeting, Turku/Finland, pages 461-462.
- Li, C. and Naldrett, A.J.** 1999. Geology and petrology of the Voisey's Bay intrusion: reaction of olivine with sulfide and silicate liquids. *Lithos*. 47, pages 1-31.
- Li, C., Naldrett, A.J., Coats, C.J.A., and Johannessen, P.** 1992. Platinum, palladium, gold and copper-rich stringers at the Strathcona Mine, Sudbury: their enrichment by fractionation of a sulfide liquid. *Economic Geology*. 87. Pages 1584-1598.
- Lightfoot, P.C.** 1997. Geological and geochemical relationships in the Reid Brook Intrusive Complex, Labrador : implications for the origin of the Voisey's Bay magmatic Ni-Cu-Co ores. *EOS, Transactions, American Geophysical Union*. Abstract. Vol. 78. No 46. Supplement, 810 pages.
- Lightfoot, P.C.** 1998. Geological and geochemical relationships in the Reid Brook Intrusive Complex, Labrador: exploration strategies for magmatic Ni-Cu-Co ores at Voisey's Bay. INCO, Field exploration office, Copper Cliff, Pathways '98.

- Lightfoot, P.C. and Hawkesworth, C.J.** 1997. Flood basalts and magmatic Ni, Cu, and PGE sulphide mineralization; comparative geochemistry of the Noril'sk (Siberian Traps) and West Greenland sequences. *Geophysical Monograph* 100, American Geophysical Union, pages 357-380.
- Lightfoot, P.C., Hawkesworth, C.J., Hergt, J., Naldrett, A.J., Gorbachev, N.S., Fedorenko, V.A., and Doherty, W.** 1993. Remobilization of continental lithosphere by mantle plumes: major, trace element, and Sr-, Nd-, and Pb-isotope evidence for picritic and tholeiitic lavas of the Noril'sk district, Siberian trap, Russia. *Contributions to Mineral Petrology*. 114, pages 171-188.
- Lightfoot, P.C. and Naldrett, A.J.** 1999. Geological and geochemical relationships in the Voisey's Bay Intrusion, Nain Plutonic Suite, Labrador, Canada. *In* Dynamic processes in magmatic ore deposits and their application in mineral exploration, Keays, R.R., Leshner, C.M., Lightfoot, P.C., and Farrow, C.E.G. eds. Geological Association of Canada, Short Course. 13, pages 1-30.
- Longerich, H.P.** 1995. Analysis of pressed pellets of geological samples using wavelength-dispersive X-ray fluorescence spectrometry. *X-Ray Spectrometry*. 24, pages 123-136.
- Longerich, H.P., Jenner, G.A., Fryer, B.J., and Jackson, S.E.** 1990. Inductively coupled plasma-mass spectrometric analysis of geochemical samples: a critical evaluation based on case studies. *Chemical Geology*. 83, pages 105-118.
- Longhi, J. and Vander Auwera, J.** 1993. The monzonorite-anorthosite correction: the petrogenesis of terrestrial KREEP. *In* Abstracts of papers submitted to the Twenty-fourth Lunar and Planetary Science conference. 24, pages 897-898.
- Longhi, J., Fram, M.S., Vander Auwera, J., and Monteth, J.N.** 1993. Pressure effects, kinetics, and rheology of anorthositic and related magmas. *American Mineralogist*. 78, pages 1016-1030.
- Loveridge, W.D., Ermanovics, L.F., and Sullivan, R.W.** 1987. U-Pb ages on zircon from the Maggo Gneiss, the Kanairiktok Plutonic Suite and the Island Harbour Plutonic Suite, coastal Labrador, Newfoundland. *In* Radiogenic age and isotopic studies. Report 1, Geological Survey of Canada, Paper 87-2, pages 59-85.
- Maier, W.D. and Barnes, S.-J.** 1999. The origin of Cu sulfide deposits in the Curaçá Valley, Bahai, Brazil: evidence from Cu, Ni, Se, and platinum-group element concentrations. *Economic Geology*. 94, No. 2, pages 165-183.
- Mathison, C. L.** 1989. Petrological encoding of cumulates. *Trans. Institution of Mining and Metallurgy*. Section B: Applied Earth Sci. 98. Jan-Apr, pages B18 - B23.

- Michot, P.** 1960. La géologie de la catazone: le problème des anorthosites, the palingenèse basique et la tectonique catazonale dans le Rogaland méridional (Norvège méridionale). *Norges Geologisk Undersøkelse*. 212, pages 1-54.
- Michot, P.** 1965. Le magma plagioclasiq. *Geol. Rundschau*. 54, pages 956-976.
- Mitchell, J.N., Scoates, J.S., Kolker, A., and Ghazi, A.M.** 1991. REE geochemistry of ferrodiorites and ferrogabbros in the Laramie anorthosite complex, Wyoming. AGU-MSA 1991 Spring meeting, EOS Transactions, American Geophysical Union. 71. No. 17, page 305.
- Mitchell, J.N., Scoates, J.S., Frost, C.D., and Kolker, A.** 1996. The geochemical evolution of anorthosite residual magmas in the Laramie Anorthosite Complex, Wyoming. *Journal of Petrology*. 37, pages 637-660.
- Morgan, J.W. and Baedeker, P.A.** 1983. Elemental composition of sulfide particles from an ultramafic xenolith and the siderophile element content of the upper mantle. Proceedings, 14<sup>th</sup> Lunar and Planetary Science Conference. 2, pages 513-514.
- Morse, S.A.** 1969. Layered intrusions and anorthosite genesis. In: Origin of Anorthosite and related rocks. Isachsen, Y.W., ed. New York State Museum Science Service, Memoir 18, Albany, New York, pages 175-187.
- Morse, S.A.** 1969. The Kiglapait Layered Intrusion, Labrador. Geological Society of America. Memoir. 112, 204 pages.
- Morse, S.A.** 1975. Plagioclase lamellae in hypersthene, Tikkoatokak Bay, Labrador. *Earth and Planetary Science Letters*. 26, pages 331-336.
- Morse, S.A.** 1979. Kiglapait geochemistry I: systematics, sampling, and density. *Journal of Petrology*. 20, pages 555-590.
- Morse, S.A.** 1981. Kiglapait geochemistry IV: the major elements. *Geochimica et Cosmochimica Acta*. 45, pages 461-479.
- Morse, S.A.** 1982. A partisan review of Proterozoic anorthosites. *American Mineralogist*. 65, pages 1087-1100.
- Morse, S.A.** 1985. Nain geochemistry reviewed: anorthosite parent liquids and contamination problems. *Geological Society of America*. Abstract. 17, page 669.

- Morse, S.A. and Hamilton, M.A.** 1990. The problem of unsupported radiogenic strontium in the Nain anorthosites, Labrador. *In* Mid-Proterozoic Laurentia-Baltica. Gower, C.F., Rivers, T., and Ryan, B. *eds.* Geological Association of Canada. Special Paper 38, pages 373-385.
- Naldrett, A.J.** 1969. A portion of the Fe-S-O system and its application to sulfide ore magmas. *Journal of Petrology*. 10, pages 171-201.
- Naldrett, A.J.** 1973. Nickel sulphide deposit - their classification and genesis with special emphasis on deposits of volcanic association. Transactions of the Canadian Institute of Mining and Metallurgy. 76, pages 183-201.
- Naldrett, A.J.** 1984. Summary, discussion, and synthesis. *In* The geology and ore deposits of the Sudbury structure. Pye, E.G., Naldrett, A.J., and Giblin, P.E. *eds.* Ontario Geological Survey, Special volume, No. 1, pages 533-570.
- Naldrett, A.J. (compiler).** 1996. Magmatic sulfide deposits: theory, reality, and exploration. Ore Deposits Workshop 1996. University of Toronto.
- Naldrett, A.J.** 1997. Key factors in the genesis of Noril'sk, Sudbury, Jinchuan, Voisey's Bay and other world-class Ni-Cu-PGE deposits: implications for exploration. *Australian Journal of Earth Sciences*. 44. No 3, pages 283-315.
- Naldrett, A.J., Asif, M., and Krstic, S.** 2000a. The composition of mineralization at the Voisey's Bay Ni-Cu sulfide deposit, with special reference to platinum-group elements. *Economic Geology*. 95, pages 845-865.
- Naldrett, A.J., Asif, M., Schandl, E., Searcy, T., Morrison, G.G., Binney, W.P., and Moore, C.** 1999. Platinum-group elements in the Sudbury ores: significance with respect to the origin of different ore zones and to the exploration for footwall ore bodies. *Economic Geology*. 94, pages 185-210.
- Naldrett, A.J., Keats, H., Sparkes, K., and Moore, R.** 1996. Geology of the Voisey's Bay Ni-Cu-Co deposit, Labrador, Canada. *Exploration Mining Geology*. 5, pages 169-179.
- Naldrett, A.J., Li, C., Krstic, S., and Amelin, Y.** 1997. Geology and genesis of the Voisey's Bay Ni-Cu-Co deposit, Labrador, Canada. *EOS, Transactions, American Geophysical Union. Abstract. Vol. 78. No 46. Supplement*, 810 pages.



- Naldrett, A.J., Singh, J., Krstic, S., and Li, C.** 2000b. The mineralogy of the Voisey's Bay Ni-Cu-Co deposit, northern Labrador, Canada: Influence of oxidation state on textures and mineral compositions. *Economic Geology*. 95, pages 889-900.
- O' Sullivan, J.** 1997. Castle Rock Exploration Corporation, second year assessment report on prospecting carried out July 1996, Licence 1532M - OKK Block. Newfoundland and Labrador Department of Mines and Energy. Open File 14E/0093.
- Owens, B.E., Rockow, M.W., and Dymek, R.F.** 1993. Jotunites from the Grenville Province, Quebec: petrological characteristics and implications for massif anorthosite petrogenesis. *Lithos*. 30, pages 57-80.
- Pace, J.B. and Bell, K.** 1989. Non-depleted sub-continental mantle beneath the Superior province of the Canadian Shield: Nd-Sr isotopic and trace element evidence from Midcontinent rift basalts. *Geochimica et Cosmochimica Acta*. 53, pages 2023-2035.
- Patchett, P.J.** 1989. Radiogenic isotope geochemistry of rare earth elements. *Reviews in Mineralogy*. 21, pages 25-44.
- Peach, C.L., Mathez, E.A., and Keays, R.R.** 1990. Sulphide melt-silicate melt distribution coefficients for the noble metals and other chalcophile metals as deduced from MORB: implications for partial melting. *Geochimica et Cosmochimica Acta*. 54, pages 3379-3389.
- Pearce, J.A.** 1996. A user's guide to basalt discrimination diagrams. In Trace element geochemistry of volcanic rocks: applications for massive sulphide exploration. Wyman, D.A. ed. Geological Association of Canada. Short Course Notes. 12, pages 79-113.
- Philpotts, A.R.** 1966. Origin of anorthosite-mangerite rocks of southern Quebec. *Journal of Petrology*. 7, pages 1-64.
- Philpotts, A.R.** 1978. Liquid immiscibility in anorthosite-quartz mangerite series. Geological Society of America. 91<sup>st</sup> Joint annual meeting. Abstracts with programs. 10, No. 7, pages 471-472.
- Philpotts, A.R.** 1981. A model for the generation of massif-type anorthosites. *Canadian Mineralogist*. 19, pages 233-253.
- Piercey, S.J.** 1998. An integrated study of magmatism, magmatic Ni-Cu sulphide mineralization and metallogeny in the Umiavik Lake region, Labrador, Canada. Memorial University of Newfoundland. Unpublished Masters thesis, 440 pages.

- Piercey, S.J. and Wilton, D.H.C.** 1999. Geochemical and radiogenic isotope (Sr-Nd) characteristics of Paleoproterozoic anorthositic and granitoid rocks in the Umiakoviarsuk Lake region, Labrador, Canada. *Canadian Journal of Earth Sciences*. 32. No 12, pages 1957-1972.
- Piercey, S.J. and Wilton, D.H.C.** 1999. Sulphide petrology and mineralization of the OKG Ni-Cu-Co sulphide prospect, Umiakoviarsuk, Lake region, Labrador. *Current Research*, Newfoundland Department of Mines and Energy, Geological Survey. Report 99-1, pages 297-310.
- Potts, P.J.** 1987. A handbook of silicate rock analysis. Blackie Academic and Professional. London, 622 pages.
- Prichard, H.H.** 1911. Through trackless Labrador. Sturges and Walton, New York, 244 pages.
- Rajamani, V. and Naldrett, A.J.** 1978. Partitioning of Fe, Co, Ni, and Cu between sulphide liquid and basaltic melts and the composition of Ni-Cu sulphide deposits. *Economic Geology*. 73, pages 82-93.
- Ranson, W.A.** 1976. Geology of the Ighlokhsoakhtaliksoakh Lake area. In The Nain anorthosite project, Labrador: Field report 1975. Morse, S.A. ed. Department of Geology, University of Massachusetts, Contribution 26, pages 35-45.
- Ranson, W.A.** 1981. Anorthosites of diverse magma types in the Puttmaaluk Lake area, Nain complex, Labrador. *Canadian Journal of Earth Science*. 18, pages 26-41.
- Ranson, W.A.** 1976. Complex exsolution in inverted pigeonite; exsolution mechanisms and temperatures of crystallization and exsolution. *American Mineralogist*. 71. No 11-12, pages 1322-1336.
- Ripley, E.M.** 1986. Application of stable isotopic studies to problems of magmatic sulfide ore genesis with special reference to the Duluth Complex, Minnesota. In Geology and metallogeny of copper deposits. Friedrich, G., Genkin, A.D., Naldrett, A.J., Ridge, J.D., Sillito, R.H., and Vokes, F.M. eds. Berlin, Springer-Verlag, pages 25-42.
- Ripley, E.M.** 1990. Se/S ratios of the Virginia Formation and Cu-Ni sulfide mineralization in the Babbitt area, Duluth Complex, Minnesota. *Economic Geology*. 85, pages 1935-1940.

- Ripley, E.M.** 1999. Systematics of sulphur and oxygen isotopes in mafic igneous rocks and related Cu-Ni-PGE mineralization. *In* Dynamic processes in magmatic ore deposits and their application in mineral exploration, Keays, R.R., Lesher, C.M., Lightfoot, P.C. and Farrow, C.E.G.. eds. Geological Association of Canada, Short Course Notes. 13, pages 133-158.
- Ripley, E.M. and Alawi, J.A.** 1988. Petrogenesis of pelitic xenoliths at the Babbitt Cu-Ni deposit, Duluth Complex, Minnesota, U.S.A. *Lithos.* 21, pages 143-159.
- Ripley, E.M., Park, Y-R., Li, C., and Naldrett, A.J.** 1997. Sulfur and oxygen isotopic studies of the Voisey's Bay Ni-Cu-Co deposit, Labrador, Canada. American Geophysical Union (AGU), 1997 Fall Meeting, Supplement to EOS, Transactions, 78, No. 46., November 18, 1997, page F810.
- Ripley, E.M., Park, Y-R., Li, C., and Naldrett, A.J.** 1999. Sulfur and oxygen isotopic evidence of country rock contamination in the Voisey's Bay Ni-Cu-Co deposit, Labrador, Canada. *Lithos.* 47, pages 53-68.
- Ripley, E.M., Park, Y-R., Li, C., and Naldrett, A.J.** 2000. Oxygen isotope studies of the Voisey's Bay Ni-Cu-Co deposit, Labrador, Canada. *Economic Geology.* 95. No 4, pages 831-844.
- Rivers, T. and Mengel, F.** 1994. A cross-section of the Abloviak Shear Zone at Saglek Fiord and a preliminary tectonic model for Torngat Orogen. *In* Eastern Canadian Shield Onshore-Offshore Transect (ECSOOT), Report of Transect Meeting (December 10-11, 1993). Wardle, R.J. and Hall, J, eds. University of British Columbia, LITHOPROBE Secretariat, Report 36, pages 171-184.
- Rollinson, H.R.** 1993. Using geochemical data: evaluation, presentation, interpretation. Longman Group UK Limited. Singapore, 352 pages.
- Rudnick, R.L. and Fountain, D.M.** 1995. Nature and composition of the continental crust: a lower crustal perspective. *Review of Geophysics.* 33, pages 267-309.
- Ryan, B.** 1990. Geological map of the Nain Plutonic Suite and surrounding rocks (Nain-Nutak, NTS 14SW). Newfoundland Department of Mines and Energy, Geological Survey Branch. Map 90-44., scale 1:500,000.
- Ryan, B.** 1991. New perspectives on the Nain Plutonic Suite and its country rocks. *Current Research*, Newfoundland Department of Mines and Energy, Geological Survey Branch. Report 91-1, pages 231-255.

- Ryan, B.** 1996. Commentary of the location of the Nain-Churchill boundary in the Nain area. *Current Research*, Newfoundland Department of Natural Resources, Geological Survey. Report 96-1, pages 109-129.
- Ryan, B.** 1997. The Mesoproterozoic Nain Plutonic Suite in Eastern Canada, and the setting of the Voisey's Bay Ni-Cu-Co sulphide deposit. *Geoscience Canada*. 24. No 4, pages 173-186.
- Ryan, B.** 2000. Geological investigations in the type locality of the Nain Plutonic Suite (NTS 14C/12). *Current Research*, Newfoundland Department of Mines and Energy, Geological Survey. Report 2000-1, pages 251-277.
- Ryan, B.** 2000. The Nain-Churchill boundary and the Nain Plutonic Suite: a regional perspective on the geologic setting of the Voisey's Bay Ni-Cu-Co deposit. *Economic Geology*. 95. No.4 , pages 703-724.
- Ryan, B.** 2001. A provisional subdivision of the Nain Plutonic Suite in its type-area, Nain, Labrador (NTS map area 14C/12). *Current Research*. Newfoundland Department of Mines and Energy, Geological Survey, Report 2001-1, pages 127-157.
- Ryan, B. and Emslie, R.F.** 1994. Pre-Elsonian mafic magmatism in the Nain igneous complex, Labrador: the Bridges layered intrusion-comment. *Precambrian Research*. 68, pages 179-181.
- Ryan, B. and Hynes, A.** 1996. Geology of the Alliger Lake area (NTS 14E/1). Newfoundland Department of Mines and Energy, Report of Activities, pages 65-67.
- Ryan, B., Hynes, A., and Ermanovics, L.** 1997. Geology of the Nain Plutonic Suite and its country-rock envelope, Alliger Lake area (NTS14E/1), Labrador. *Current Research*, Newfoundland Department of Mines and Energy, Geological Survey. Report 97-1, pages 29-47.
- Ryan, B., Philips, E., Shwetz, J., and Machado, G.** 1998. A tale of more than ten plutons [Geology of the region between Okak Bay and Staghorn Lake, Labrador (Parts of NTS maps 14E/2,7,8)]. *Current Research*, Newfoundland Department of Mines and Energy, Geological Survey. Report 98-1, pages 143-171.
- Ryan, B., Wardle, R., Gower, C., and Nunn, G.** 1995. Nickel-copper-sulphide mineralization in Labrador: The Voisey Bay discovery and its exploration implications. *Current Research*. Report 95-1. Newfoundland Department of Natural Resources, Geological Survey, pages 177-204.

- Schärer, U.** 1991. Rapid continental crust formation at 1.7 Ga from a reservoir with chondritic isotopic signatures, eastern Labrador. *Earth and Planetary Science Letters*. 102, pages 110-133.
- Scoates, J.S and Mitchell, J.N.** 2000. The evolution of troctolitic and high Al basaltic magmas in Proterozoic anorthosite plutonic suites and implications for the Voisey's Bay massive Ni-Cu sulfide deposit. *Economic Geology*. 95, pages 677-701.
- Scott, D.J. and Machado, N.** 1994a. U-Pb geochronology of the northern Torngat Orogen: results from work in 1993. Lithoprobe Eastern Canadian Shield Onshore-Offshore Transect (ECSOOT) Transect. Report of 1993 Transect Meeting. Wardle, R.J. and Hall, J. (compilers). LITHOPROBE Report 36, pages 141-155.
- Scott, D.J. and Machado, N.** 1995. U-Pb geochronology of the northern Torngat Orogen, Labrador, Canada: a record of Paleoproterozoic magmatism and deformation. *Precambrian Research*. 70. No. 3-4, pages 169-190.
- Shirey, S.B.** 1994. Evolution of the Earth's mantle; perspective from the Re-Os isotopic system. *Mineralogical Magazine*. 58A, L-Z, pages 833-834.
- Simmons, K.R., Synder, G.A., Simmons, E.C., Kalamarides, R.L., Weibe, R.A.** 1986. Pb, Sr, and O isotopic data for rocks from the Nain anorthositic complex, Labrador. Abstract with programs, Geological Society of America. 20, No. 7, page 118.
- Sharpe, M.R.** 1982. Noble metals in the margin rocks of the Bushveld Complex. *Economic Geology*, 77, pages 1286-1295.
- Shelley, D.,** 1993. Igneous and metamorphic rocks under the microscope. Chapman and Hall. New York, 445 pages.
- Smith, R.L., Wilton, D.H.C., Sparkes, K., and Dunning, G.R.** 1999. Magmatic Ni-Cu-Co sulphide mineralization in the Pants Lake Intrusion, South Voisey's Bay Project, Labrador. Geological Association of Canada-Mineralogical Association of Canada. Joint Annual Meeting, Sudbury. Abstract. 24, page 119.
- Squires, G, Mitton, B., and Kendle, F.** 1997. Second year assessment report (geology, geochemistry, geophysics, drilling) on Licence 915M, Cu, Ni, Co exploration in the areas between Hebron Fiord and Shapio Lake, Labrador. Noranda Mining and Exploration Inc.

- Squires, G., Mitton, B., Kendle, F., and Schwarz, S.** 1996. First year assessment report (geology, geochemistry, geophysics) on Licence 915M, Cu, Ni, Co exploration between Hebron Fiord and Shapio Lake, Labrador. Noranda Mining and Exploration Inc.
- Stein, M. and Hofmann, A.W.** 1994. Mantle plumes and episodic crustal growth. *Nature*. 372, pages 63-68.
- Streckeisen, A.** 1976. To each plutonic rock its proper name. *Earth Science Review*. 12, pages 1 - 33.
- Sun, S.-s. and MacDonough, W.F.** 1989. Chemical and isotopic systematics of oceanic basalts: implications for mantle composition and process. *In* Magmatism in the Ocean Basins, Geological Society Special Publication. 42, pages 313-345.
- Synder, D., Carmichael, I.S.E., and Wiebe, R.A.** 1993. Experimental study of liquid evolution in an Fe-rich, layered mafic intrusion: constraints of Fe-Ti oxide precipitation on the T-  $fO_2$  and T-  $p$  paths of tholeiitic magmas. *Contributions to Mineralogy and Petrology*. 113, pages 73-86.
- Taylor, F.C.** 1971. A revision of Precambrian structural provinces in northeastern Quebec and northern Labrador. *Canadian Journal of Earth Sciences*. 8, pages 579-584.
- Taylor, S.R., Campbell, I.H., McCulloch, M.T., and McLennan, S.M.** 1984. A lower crustal origin for massif type anorthosites. *Nature*. 311, pages 372-374.
- Thériault, R.D., Barnes, S.-J., and Severson, M. J.** 1997. The influence of country-rock assimilation and silicate to sulfide ratios (R factor) on the genesis of the Dunka Road Cu-Ni-platinum-group element deposit, Duluth Complex Minnesota. *Canadian Journal of Earth Sciences*. 34, pages 375-389.
- Thériault, R.J. and Ermanovics, I.** 1997. Sm-Nd isotopic and geochemical characterisation of the Paleoproterozoic Torngat Orogen, Labrador, Canada. *Precambrian Research*. 81, pages 15-35.
- Van Kranendonk, M.J.** 1996. Tectonic evolution of the Paleoproterozoic Torngat Orogen: evidence from pressure-temperature-time-deformation paths in the North River area. *Tectonics*. 15, pages 843-869.
- Van Kranendonk, M.J. and Ermanovics, I.** 1990. Structural evolution of the Hudsonian Torngat Orogen in the North River map area, Labrador: evidence for east-west transpressive collision of Nain and Rae continental blocks. *Geoscience Canada*. 17, pages 283-288.

- Van Kranendonk, M.J. and Wardle, R.J.** 1994. Geological synthesis and musings on possible subduction-accretion models in the formation of the northern Torngat Orogen. Eastern Canadian Shield Onshore-Offshore Transect (ECSOOT) Transect Meeting, LITHOPROBE Report 36, pages 32-80.
- Van Kranendonk, M.J. and Wardle, R.J.** 1997. Crustal-scale flexural slip folding during late tectonic amplification of an orogenic boundary perturbation in the Paleoproterozoic Torngat Orogen, northeastern Canada. *Canadian Journal of Earth Sciences*. 34, pages 1545-1565.
- Vander Auwera, J., Longhi, J., and Duchesne, J-C.** 1998. A liquid line of descent of the jotunite (hypersthene monzondiorite) suite. *Journal of Petrology*. 39. No. 8, pages 439-468.
- Wardle, R.J.** 1996. Platinum-group-element potential in Labrador. *Current Research*, Report 87-1, Newfoundland Department of Mines and Energy, Mineral Development Division, Report 87-1, pages 211-223.
- Wardle, R.J. and Wilton, D.H.C.** 1995. The Nain Province. *In* The geology and mineral deposits of Labrador: a guide for the exploration geologist (*compiled by* R.J. Wardle). Newfoundland Department of Natural Resources - Center for Earth Resources Research Report, pages 14-24.
- Wardle, R.J., Swinden, S., and James, D.T.** 1995. The southeast and Churchill province. Labrador '95: The geology and mineral deposits of Labrador, a guide for the exploration geologist. Wardle, R.J. (*compiler*). Workshop handout. Newfoundland Department of Natural Resources, Geological Survey, pages 26-35.
- Wardle, R., van Kranendonk, M., Mengel, F., and Scott, D.** 1992. Geological mapping in the Torngat Orogen, northernmost Labrador: Preliminary results. *Current Research*. Newfoundland Department of Mines and Energy, Geological Survey Branch, Report 92-1, pages 413-429.
- Wardle, R.J., van Kranendonk, M.J., Mengel, F., Scott, D.J., Schwarz, S., and Ryan, B.** 1993. Geological mapping in the Torngat Orogen, northernmost Labrador: Report 2.. *Current Research*. Newfoundland Department of Mines and Energy, Geological Survey Branch, Report 93-1, pages 77-95.
- Watson, D.** 1996. Geophysical survey report for Cartaway Resources, Cirque property by Crone Geophysics and Exploration Ltd. *Inhouse* report.

- Wheeler II, E.P.** 1942. Anorthosite and related rocks about Nain, Labrador. *Journal of Geology*. 50, pages 611-642.
- Wheeler 2<sup>nd</sup>, E.P.** 1960. Anorthosite-adamellite complex of Nain, Labrador. *Bulletin of the Geological Society of America*. 71, pages 1755-1762.
- Wiebe, R.A.** 1979. Fractionation and liquid immiscibility in an anorthositic pluton of the Nain Complex, Labrador. *Journal of Petrology*. 20. Part 2, pages 239-269.
- Wiebe, R.A.** 1985. Proterozoic basalt dikes in the Nain anorthosite complex, Labrador. *Canadian Journal of Earth Science*. 22, pages 1149-1157.
- Wiebe, R.A.** 1987. Evidence for stratification of basic, silicic, and hybrid magmas in the Newark Island layered intrusion, Nain, Labrador. *Geology*. 15, pages 349-352.
- Wilson, A.H.** 1982. The geology of the Great 'Dyke', Zimbabwe: the ultramafic rocks. *Journal of Petrology*. 23, pages 240-292.
- Wilton, D.H.C.** 1996. Metallogenic overview of the Nain Province, northern Labrador. *CIM Bulletin*. 89, No. 997, pages 43-52.
- Wooden, J.L., Czamanske, G.K., Fedorenko, V.A., Arndt, N.T., Chauvel, C., Bouse, R.M., King, B-S.W., Knight, R.J., and Siems, D.F.** 1993. Isotopic and trace element constraints on mantle and crustal contributions to characterization of Siberian continental flood basalts, Noril'sk area, Siberia. *Geochimica et Cosmochimica Acta*. 57, pages 3677-3704.
- Woolham, R.W.** 1995. Report submitted for assessment credits for a combined helicopter-borne magnetic and electromagnetic survey, claim blocks LB-G, LB-H, LB-J, LB-K, LB-N, Hunter/Cirque properties, Labrador for Cartaway Container Corporation. *Inhouse report*, 18 pages.
- Xue, S.** 1992. Chemical characteristics of the Nain anorthosites and their parent magmas. University of Massachusetts, unpublished Ph.D thesis, 409 pages.
- Yamamoto, M., Ogushi, N., and Sakai, H.** 1968. Distribution of sulfur isotopes, selenium, and cobalt in the Yanahara ore deposits, Okayama-Ken, Japan. *Geochemical Journal*. 2, pages 137-156.
- Yu, Y. and Morse, S.A.** 1994. Chemical characteristics of plagioclase and pyroxene megacrysts and their significance to the petrogenesis of the Nain anorthosites. *Geochimica et Cosmochimica Acta*. 58. No. 20, pages 4317-4331.



- Zartman, R.E. and Haines, S.M.** 1988. The plumbotectonic model for Pb isotopic systematics among terrestrial reservoirs - a case for bidirectional transport. *Geochimica et Cosmochimica Acta*. 52, pages 1327-1339.
- Zongli, T.** 1993. Genetic model of the Jinchuan nickel-copper deposit. *In* Mineral Deposit Modelling. Kirkham, R.V., Sinclair, W.D., Thorpe, R.I., and Duke, J.M., eds. Geological Association of Canada, Special Paper 40, pages 389-401.

## **Appendix A1 ANALYTICAL PROCEDURES**

### **Procedure for Ni, Cu, Co assays at Chauncey Assay Laboratories Ltd., Ontario**

The following is a description of the method used at the Chauncey Assay Laboratories Ltd. for assays of drill core and rocks for Ni, Cu, and Cu :

Each sample was first crushed in a jaw crusher, then in a cone crusher (if the sample was damp, it was dried before crushing). The crushed material was divided roughly in half using a riffler. One half was retained as a reject and the second half was pulverized to ~100 mesh. If the crushed sample was very small, the whole sample was pulverized. The pulverized sample was thoroughly mixed and 0.5 gram was placed into a teflon beaker and 2ml HCl and 2ml HF were added. The beaker was placed on a hotplate until the sample material was dried. When ready, 5 ml HCl and 2 ml HNO<sub>3</sub> were added and the sample was left for 30 minutes until the pulverized sample was dissolved; after which, the total volume was brought to 50ml with the addition of 5% HNO<sub>3</sub> solution. The sample was then analysed for Cu, Ni, and Co using the Inductively Coupled Plasma (ICP) method. The final reported values were calculated using the ICP measurement of each metal multiplied by a factor which is based on the weight and volume.

**The following analytical methods were conducted at the Earth Sciences Department of Memorial University of Newfoundland between 1996-1998.**

#### **Crushing and pulverization of core and rock samples**

Each sample was first cut or broken into fist sized samples for easy handling. Each sample was then crushed using a steel jaw crusher and then pulverized to a fine powder (mesh size 200) using a tungsten carbide puck and bowl. Each sample was placed in a small plastic vial and carefully labeled. Between samples, the jaw crusher and tungsten puck were cleaned and wiped with ethanol to remove any traces of the previous sample and to prevent any contamination of the next sample. Samples were separated into mineralized (sulphide-rich) and non-mineralized to avoid any contamination of sulphides into non-mineralized samples. Silica sand was used to clean the tungsten puck between samples, especially if the samples were sulphide-rich and more difficult to clean. Contamination, however small, was still possible from the metal jaw crusher and tungsten carbide puck and bowl.

#### **XRF Pressed Pellet**

Using the same procedures described by Longerich (1995), pressed pellet was made by first adding 5.0g of rock powder sample with 0.70g of BRP-5933 Bakelite phenolic resin in a 100ml glass jar. Two 0.5 inch stainless steel balls are also added to allow for through mixing. The jar is then capped and the contents are mixed with two ball bearings on rollers for 10 minutes. After mixing, the balls are removed and the powder mixture is placed into

a Herzog pellet press and compressed into a disc shape (29 mm diameter) for 10 seconds using 20 tonnes of pressure. The disc was then heated on an aluminum tray at 200°C for 15 minutes, then cooled and properly labeled.

A batch of discs are then loaded for automated analyses using a Fisons/ARL model 8420+ sequential wavelength-dispersive X-Ray spectrometer. The elements measured are: Na<sub>2</sub>O, MgO, Al<sub>2</sub>O<sub>3</sub>, SiO<sub>2</sub>, P<sub>2</sub>O<sub>5</sub>, S, Cl, K<sub>2</sub>O, CaO, Sc, TiO<sub>2</sub>, V, Cr, MnO, Fe<sub>2</sub>O<sub>3</sub>, Ni, Cu, Zn, Ga, As, Rb, Sr, Y, Zr, Nb, Ba, Ce, Pb, Th, and U. The standards used in the procedure are BHVO-1 (USGS reference standard for basalt), DTS-1 (USGS reference standard for diorite), SY-2 and SY-3 (syenite from the Canadian Certified Reference Materials Project), and PACS-1 (reference material from the National Research Council of Canada). Refer to Potts *et al.* (1992), Jenner *et al.* (1990), and Longerich *et al.* (1990) for the values of these reference materials. Assay data are compiled using *inhouse* computer software and listed in LOTUS spreadsheet format. The limits of detection for pressed pellets are as given by Longerich (1995): 0.6-0.7 ppm for Rb, Y, and Nb to a maximum of 100 ppm for Na<sub>2</sub>O and MgO.

### **Inductively Coupled Plasma - Mass Spectrometry (ICP-MS)**

Using a SCIEX ELAN (Perkin-Elmer) model 250 inductively coupled plasma - mass spectrometer and the HF-HNO<sub>3</sub> standard addition method at Memorial University, the following trace elements were analyzed: <sup>167</sup>Er, <sup>169</sup>Tm, <sup>173</sup>Yb, <sup>175</sup>Lu, <sup>177</sup>Hf, <sup>181</sup>Ta, <sup>203</sup>Tl, <sup>206</sup>Pb, <sup>207</sup>Pb, <sup>208</sup>Pb, <sup>209</sup>Bi, <sup>232</sup>Th, <sup>238</sup>U, <sup>7</sup>Li, <sup>85</sup>Rb, <sup>86</sup>Sr, <sup>89</sup>Y, <sup>90</sup>Zr, <sup>93</sup>Nb, <sup>95</sup>Mo, <sup>133</sup>Cs, <sup>137</sup>Ba, <sup>139</sup>La, <sup>140</sup>Ce,

$^{141}\text{Pr}$ ,  $^{145}\text{Nd}$ ,  $^{147}\text{Sm}$ ,  $^{151}\text{Eu}$ ,  $^{157}\text{Gd}$ ,  $^{159}\text{Tb}$ ,  $^{160}\text{Gd}$ ,  $^{163}\text{Dy}$ ,  $^{165}\text{Ho}$ .  $^{254}(\text{UO})$  was collected to monitor oxide formation.

The sample preparation procedure is the same as that described by Jenner *et al.* (1990). Each sample aliquot (0.1 g) is dissolved using HF/HNO<sub>3</sub> (+ boric and oxalic acids) in a Teflon bomb. Samples which were incompletely digested were treated with HCl/HNO<sub>3</sub>. The more insoluble minerals (graphite, chromite, ilmenite, and other oxides), if present, were filtered prior to analyses. The solution was left to evaporate and the sample was dissolved again using HNO<sub>3</sub> and then evaporated again. Once dried, 2-3 ml of 8N HNO<sub>3</sub> was added and transferred to a 125 ml bottle and diluted with water to a total volume of 90 g. Reagent blanks were prepared in two-bottle Teflon stills and then distilled with either quartz-distilled or high-quality Millipore-prepared water.

Data reduction was completed using spreadsheet software and *inhouse* written macros. Samples and standards were background corrected using the mean of all calibration blanks for each particular ICP-MS run (Diegor 1999). One complete run of samples consists of 27 samples including reference materials, reagent blanks, and duplicates.

Results are reported as ppm data with limits of detection quoted as 3 standard deviations of mean background as measured in the blanks (Jenner *et al.* 1990). Individual element detection limits are listed in Jenner *et al.* (1990). As a quality control check, geological reference materials [BR-688-30 (basalt) and MRG-1-30 (gabbro)] were run as unknowns. Most of the elements analyzed were in agreement with the most probable values cited for BR-688-39 and MRG-1-30 material; concentrations close to the detection limits

were less precise and accurate than those of the higher concentrations (Jenner *et al.* 1990). Reagent materials were analysed in each run to check possible reagent contamination. Internal spiked standards were used to correct for instrument drift and matrix effects. Duplicate unknown samples were measured to check for technique reproducibility.

Anomalously high  $^{169}\text{Tm}$  values in the anorthositic samples LD-96-10, LD-96-109, and BW02 are a result of analytical errors associated with low count rates for the thulium being artificially increased by the oxidation of europium oxide; ( $^{153}\text{Eu} + ^{16}\text{O}$ ) forms  $^{169}\text{Tm}$ . Such interferences are possible where LREE concentrations are significantly greater than HREE concentrations. This is confirmed by the fact that all three anomalous  $\text{Tm}^{3+}$  values were analysed during the same run which had a high oxide formation rate. These anomalous values thus were not used for geochemical interpretations.

#### **ICP-MS and Ni-S Fire Assay (PGE Analyses)**

The Ni-S Fire Assay technique described is the first step in analyses of Ni, Cu, Ru, Rh, Pd, Re, Os, Ir, Pt, and Au. First a clay crucible, containing a mixture of 10.0 g of the sample and the following weighed components: 13.3 g  $\text{Na}_2\text{B}_4\text{O}_7$  (borax), 6.7 g sodium carbonate, 3.3 g Ni, 2.0 g S, 4.0 g silica, is heated until the mixture has fused 1050°C for 1.25 hours. Those samples with concentrations of Ni or S > 1% the Ni and S are first reduced in the fusion method. The crucible are then left to cool to room temperature. Next, the crucible is broken with a hammer to release the fused bead. The bead is weighed and dissolved on a hot plate in a 1000 ml beaker using 200-300 ml concentrated HCl. The beaker is heated to

350°C until dissolution occurs. A black precious metal-rich sulphide precipitate is commonly formed.

This solution is allowed to cool completely and then diluted using an equal volume of NanoPure water. The resulting solution is heated on a hotplate while 3.5 ml Te solution and 15 ml freshly  $\text{SnCl}_2$  (stannous chloride) solution is added. The solution is boiled for 30 minutes to coagulate the precipitate. The solution is cooled until warm, then filtered through a Millipore filter system (Whatman-um cellulose nitrate membrane filter paper) to separate the precipitate.

Between each precipitate filtration, the micro-film system is cleaned by placing it in a heated aqua regia solution of 3 parts concentrated HCl and 1 part  $\text{HNO}_3$ ). The system is then rinsed with NanoPure water and the contents are removed from the flask.

Next, 5 ml of  $\text{HNO}_3$ , 5 ml of concentrated HCl are placed in a tube and warmed until the residue is completely dissolved. The tubes are cooled and washed with NanoPure water. The solution is transferred to an acid washed 125 ml container and flushed with more NanoPure water until the weight is 100 g. Finally, one gram of the sample solution is weighed into test tubes and 9 g of the  $\text{HNO}_3$ -HCl acid mixture is added and the weight recorded. The resulting sample mixture is then analysed for PGE (Ni, Cu, Ru, Rh, Pd, Re, Os, Ir, Pt, and Au) using the ICP-MS technique described above. For quality control, the reference standards used are Sarm7-4 and Sarm7-5.

### **Electron Microprobe**

Sulphide and silicate minerals were analysed using an automated CAMECA SX50 3 WD (wavelength dispersive) spectrometer electron microprobe with LINK ED (energy dispersive) spectrometer. Analyses were conducted using the program SPECTA on an exl (Link) computer. Data were reduced by a ZAF correction scheme.

Routine silicate analyses were done using 15kV accelerating voltage and a beam current of 20nA, a 1 micron diameter beam, and a count time of 100 s. The elements measured were Na, Mg, Al, Si, K, Ca, Ti, Mn, Fe, Cr, and V, mainly in olivine, plagioclase, and pyroxene (clinopyroxene and orthopyroxene). The standards used were Bushveld chromite (USGS; USNM 117075), wollastonite (USGS), Natural Bridges Diopside (USNM 11733), Johnstan Hypersthene (USNM 746), San Carlos Hornblende, and Marjalahti olivine.

Fe, Ni, S, Co, Cu, and Se were measured in grains of pyrrhotite, chalcopyrite, pentlandite, and pyrite using 20kV accelerating voltage, a beam current of 30nA, and a beam diameter of 5 microns. For ED, the count times were 150 s for Fe, S, and Cu, 140s for Ni, and 6300 s for Se. For WD, the count times were 70 s for Ni and Co, and 150 s for Se. The standards used were pyrrhotite,  $\text{Co}_3\text{S}_4$ , NiS, Se, CuS, cubanite, and chalcopyrite.

### **X-Ray Diffraction**

A small piece of sulphide from hand picked massive pyrrhotite was ground in ethanol into a powder using a mortar and pestle. The powder was then smeared onto a glass plate and let dry. After drying, the sample was analysed using Rigaku™ RU-200 x-ray diffractometer



(40 kV and 150nA). The spectra were evaluated using the software program MDI JADE to determine whether the pyrrhotite was monoclinic or hexagonal. Sample selection and preparation (preferred orientation, distribution on the slide) may have contributed to difficulty in determining which type of pyrrhotite is present (Cook *et al.* 1975).

### **Rb-Sr and Sm-Nd isotope analyses**

The following descriptions of the procedures for Rb-Sr and Sm-Nd analyses are from an *inhouse* report by Horan (1998) of the Earth Sciences Department, Memorial University of Newfoundland. For each of the ten powdered samples, 0.00001 g is weighed and dissolved using 1 ml of 8N Nitric acid and 2 ml HF. Dissolution takes place over 2 to 7 days and during this time each sample is checked for the presence of white fluoride precipitates which can form in samples with high Al or Mg contents. If precipitate is present, then the sample is re-dissolved using the same acids.

Once fully dissolved, each sample is then divided into isotopic concentration and isotopic dilution fractions. The isotopic dilution fraction is mixed with a weighed amount of ORNL 150Nd-147Sm mixed spike based on the known whole rock Nd concentration which was measured using the ICP-MS. Rb and Sr spiking was also done using corresponding concentrations of previously measured Sr whole rock concentrations determined by ICP-MS.

For Rb/Sr and REE initial separations, each sample was then loaded onto EICHROM TRU-Spec resin which separates the REE's from Rb and Sr. The Rb and Sr separates are

collected using 2B 3N Nitric acid and the TEE's are collected afterwards using 2B (double Teflon bottle distilled) water. All fractions collected are dried. The Rb/Sr fractions are loaded onto the EICHRON SR-Spec resin which removes all trace elements except Sr. Rb is collected using 2B Nitric acid and Sr is collected using 2B water. The REE fractions are placed in Teflon columns which separate the Nd and Sm.

Now, the fractions are ready for the TI-mass spectrometer. If an isotopic dilution Rb/Sr analysis is required then the Rb fraction is loaded on an outgassed Re cathodeon single bead for analysis using the VG MM30B TI-MS. Using a single peak jumping routine, the Rb fraction is analysed and the  $^{87}/^{86}\text{Rb}$  ratio is collected using either the Daly or Faraday detectors. The Sr fraction is loaded on outgassed Re double filaments for analysis using the Finnigan MAT 262V TI-MS. The isotopic composition  $^{87}/^{86}\text{Sr}$  fraction is then analysed using a static (that is simultaneous) faraday multicollector routine. The isotopic dilution Sr fraction is analysed using a static faraday multicollector routine and both ratios  $^{84}/^{86}$  and  $^{87}/^{86}$  are collected. Each routine analyses for 5 blocks of data with each block containing 20 scans, with on line drift and mass fractionation correction and statistical analysis. The  $^{87}\text{Sr}/^{86}\text{Sr}$  errors, based on mass spectrometer measurements, are reported at the 95% confidence level (2 sigma). Using Lotus 123 97, the  $^{87}\text{Sr}/^{86}\text{Sr}$  ratios are calculated with data reduction software created at Memorial University and the calculations are based on measured  $^{87}\text{Rb}/^{85}\text{Rb}$  and  $^{84}\text{Sr}/^{86}\text{Sr}$  spiked ratios. The  $^{87}\text{Rb}/^{85}\text{Rb}$  reported errors, which are absolute 2 sigma, are quadratically added using the 2 sigma errors for  $^{87}\text{Rb}/^{85}\text{Rb}$  and  $^{84}\text{Sr}/^{86}\text{Sr}$  measured isotopic ratios.

The isotopic concentrations and isotopic dilution fractions are pipetted onto Teflon columns using 2 x 0.15N HCl. The first of the LREE are removed using 2 x 0.15N HCl. The isotopic concentration and isotopic dilution Nd fractions are collected using 2x 0.17N HCl. The isotopic dilution Sm fraction is collected using 2 x 0.50N HCl. Two drops of 1N phosphoric acid are added to each of the three collected fractions which are then dried so that one drop remains of each fraction.

The isotopic concentration and isotopic dilution Nd and Sm fractions are now ready for mass spectrometry analysis. They are first loaded on outgassed Re double filaments for the Finnigan MAT 262V TI-MS and then analyzed using faraday multicollector routines. The static faraday multicollector routine collects 5 blocks (20 scans/block) with on line rift and mass fractionation correction and statistical analysis. The  $^{143}\text{Nd}/^{144}\text{Nd}$  errors, based on mass spectrometry measurements, are reported at the 95% confidence level (2 sigma). Using LOTUS 123 97, the  $^{147}\text{Sm}/^{144}\text{Nd}$  ratios are calculated with data reduction software created at Memorial University. These calculations are based on measured  $^{147}\text{Sm}/^{149}\text{Sm}$  and  $^{150}\text{Nd}/^{144}\text{Nd}$  spiked ratios. The  $^{147}\text{Sm}/^{144}\text{Nd}$  reported errors are absolute 2 sigma and are quadratically added using the 2 sigma errors for  $^{147}\text{Sm}/^{149}\text{Sm}$  and  $^{150}\text{Nd}/^{144}\text{Nd}$  measured isotopic ratios.

The following are the equations used to calculate the values in Table 4.2 and Table 4.4 from Rollinson (1993):

$$(^{87}\text{Sr}/^{86}\text{Sr})_i \text{ or } \text{ISr} = ^{87}\text{Sr}/^{86}\text{Sr}_{\text{msd}} - [(^{87}\text{Rb}/^{86}\text{Sr}_{\text{msd}}) \times (e^{\lambda t} - 1)]$$

where time,  $t = 1.30 \times 10^9$  years and the decay constant,  $\lambda = 1.42 \times 10^{-11}$

$$\epsilon_{Nd} = [(^{143}Nd/^{144}Nd_{rock, t} / ^{143}Nd/^{144}Nd_{CHUR, t}) - 1] \times 10^4$$

where  $t = 0$  and  $1.30$  Ga

$$\text{where } ^{143}Nd/^{144}Nd_{CHUR, t} = ^{143}Nd/^{144}Nd_{CHUR, today} - [^{147}Sm/^{144}Nd_{CHUR, today} \times (e^{\lambda t} - 1)] = 0.510959$$

$$\text{where } ^{143}Nd/^{144}Nd_{rock, t} = ^{143}Nd/^{144}Nd_{msd} - [^{147}Sm/^{144}Nd_{msd} \times (e^{\lambda t} - 1)]$$

$$\text{where } (e^{\lambda t} - 1) = 0.008538 \text{ with } \lambda = 6.54 \times 10^{-12}$$

$$T_{DM} = 1/\lambda \ln[(^{143}Nd/^{144}Nd_{msd} - ^{143}Nd/^{144}Nd_{DM, today}) / (^{147}Sm/^{144}Nd_{msd} - ^{147}Sm/^{144}Nd_{DM, today}) + 1]$$

$$\text{where } ^{143}Nd/^{144}Nd_{DM, today} = 0.51235, ^{147}Sm/^{144}Nd_{DM, today} = 0.214$$

$$\text{and the decay constant, } \lambda = 6.54 \times 10^{-12}$$

$$f_{Sm/Nd} = [^{147}Sm/^{144}Nd_{msd} / ^{147}Sm/^{144}Nd_{CHUR, today}] - 1$$

$$\text{where } ^{147}Sm/^{144}Nd_{CHUR, today} = 0.1967$$

$$\text{Neodymium crustal index, NCI} = [\epsilon_{Nd}(\text{rock}) - \epsilon_{Nd}(\text{MC})] / [\epsilon_{Nd}(\text{CC}) - \epsilon_{Nd}(\text{MC})]$$

where MC = mantle component [-3.0 from Emslie *et al.* (1994) and 0 from Amelin *et al.* (2000)]; CC = crustal component [Nain Province = -21.9, Churchill Province = -14.6 from Emslie *et al.* (1994); Enderbittic gneiss = -4.01 from Amelin *et al.* (2000); Tasiuyak gneiss = -9.3 from Thériault and Ermanovics (1997) and Wilton (*unpublished data*).

### Sulphur isotope analysis

Each of the fifteen samples of sulphides, consisting of pyrrhotite and chalcopyrite, were visually checked for purity using a stereoscope and hand picked from crushed massive sulphide samples. Each sample was then ground using a mortar and pestle and weighed; 0.135mg of pyrrhotite and 0.145 mg chalcopyrite. Each weighed sample was then placed in

individual foil cups (approximately 0.5 cm wide) with 0.1 mg  $V_2O_5$  and sealed by folding the capsule with tweezers.

The capsules were individually heated to 1800°C at which point the foil disintegrated and  $SO_2$  gas was released. The sulphur isotope ratios were then analysed using the Carlo-Erba NA1500 Elemental Analyser (EA). The standards used are NBS-123 and MUN-py.

Appendix 2.1 Summary of drill hole locations at LBN (Cirque) property.

Hole	Grid Co-ordinates	Eastings, Northings	Elevation (m)	Dip (degrees)	Azimuth (degrees)	Depth (m)
LBN-1	0+51S, 3+42E	535892.70, 6323243.80	870.5	-50	265	344
LBN-2	0+51S, 3+42E	535892.70, 6323243.80	870.5	-90	0	290
LBN-3	0+51S, 3+42E	535892.70, 6323243.80	870.5	-61	86	249
LBN-4	1+00S, 2+50E	535800.30, 6323197.40	894.3	-60	85	461
LBN-5	1+00S, 2+50E	535800.30, 6323197.40	894.3	-45	85	335
LBN-6	1+00S, 2+50E	535800.30, 6323197.40	894.3	-75	85	524
LBN-7	3+75S, 7+05E	536272.78, 6322875.53	579.1	-49	270	500
LBN-8	1+00S, 12+00E	536733.00, 6323079.58	544.6	-61	274	1124
LBN-9	2+95S, 8+20E	536337.55, 6322908.94	554.51	-65	273	695
LBN-10	2+00S, 8+92E	536364.12, 6323006.39	525	-61	270	857
LBN-11	2+95S, 8+20E	536337.55, 6322908.94	554.5	-45	290	741.37
LBN-12	2+95S, 8+20E	536337.87, 6322908.69	554.51	-45	268	757

Total holes: 12

Total depth: 6877.37 metres

Total assays: 1022

**APPENDIX A2.2** Summary of drill hole logs and assay data from the Cirque grid (1996-1997) LBN property held by Cartaway Resources Corporation. For this study, assay data are incomplete and not available (N.A) for holes LBN-11 and 12.

**Hole No:** LBN-1      **Date:** Apr 30-May 5, 1996      **Grid:** 0+51 S, 3+42 E

**SUMMARY LITHO LOG**

**From    To    Lithological Unit**

0.00	3.50	Overburden
3.50	9.17	L.ANOR
9.17	9.52	MS-po
9.52	15.70	L.ANOR
15.70	15.90	NET po-25%
15.90	16.30	L.ANOR
16.30	16.62	NET po- 25%
16.62	16.70	L.ANOR
16.70	28.30	L.TROC
28.30	36.64	L.ANOR-net-diss po
36.64	37.44	MS-po, 1% cpy
37.44	65.00	L.ANOR with patches of opx
65.00	81.20	ANOR with 5% net po, <1%cpy
81.20	85.55	ANOR
85.55	88.83	L.GAB (10%pyx)
88.83	99.13	L.ANOR
99.13	100.23	MS-70% po, <1%cpy
100.23	103.95	LANOR
103.95	104.25	MS-80% po, <1%cpy
104.25	110.00	LANOR with minimum <1% po
110.00	110.95	LANOR-GP
110.95	114.98	LANOR
114.98	115.98	LANOR-5% net po
115.98	118.68	LANOR
118.68	133.10	ANOR (patchy pyx, po)
133.10	164.14	ANOR w green alteration, calcite, po
164.14	173.73	BROWN LANOR
173.73	174.67	BLUE LANOR
174.67	175.35	ANOR (10% pyx)-7%net/bleb po, 1%cpy
175.35	184.75	LANOR with 5-15%pyx, green alteration
184.75	193.74	BROWN LANOR - with green altered LANOR-BB
193.74	193.84	BAND of 25% net po, 1%cpy, 7%mag
193.84	213.15	ANOR-5-7% cpx ,3%mag
213.15	214.25	LANOR
214.25	227.73	LANOR-GP- green-brown-white alteration
227.73	227.98	"BLEACHED"LANOR
227.98	236.90	ANOR
236.90	239.80	M.ANOR-15% cpx (patchy), diss po
239.80	257.55	ANOR- patchy cpx, mag
257.55	276.03	M.ANOR-15-20% cpx, mag, opx
276.03	278.00	L.ANOR-<5%cpx, mag;1%diss po

**SUMMARY LITHO LOG LBN-1****From To Lithological Unit**

278.00 281.69 LNOR-20%opx, 4%mag  
 281.69 290.11 ANOR-large plagioclase porphyry, alteration  
 290.11 337.03 ANOR-7-10%cpX, mag;<1% diss po  
 337.03 343.00 LANOR, 2-3%very c gr cpx  
 343.00 344.00 EOH

**ASSAY LOG**

From	To	Width	Sample #	Co %	Cu %	Ni %	% Sulphide	Cu/Ni	Ni/Cu
8.10	9.10	1.00	536690	0.006	0.022	0.015	2	1.467	0.682
9.10	9.70	0.60	536691	0.112	0.238	0.210	60	1.133	0.882
9.70	10.70	1.00	536692	0.006	0.008	0.006	1	1.333	0.750
12.35	12.70	0.35	536693	0.025	0.068	0.044	5	1.545	0.647
12.70	13.33	0.63	536694	0.005	0.009	0.006	1	1.500	0.667
13.33	14.00	0.67	536695	0.011	0.032	0.020	5	1.600	0.625
15.60	16.60	1.00	536696	0.049	0.137	0.084	10	1.631	0.613
26.35	26.50	0.15	536697	0.057	0.286	0.095	30	3.011	0.332
30.50	31.28	0.78	536698	0.015	0.032	0.024	5	1.333	0.750
32.00	33.00	1.00	536699	0.038	0.109	0.066	10	1.652	0.606
33.00	34.24	1.24	536700	0.036	0.065	0.060	10	1.083	0.923
36.40	37.40	1.00	536701	0.104	0.264	0.264	75	1.000	1.000
37.40	38.40	1.00	536702	0.017	0.065	0.035	5	1.857	0.538
38.40	39.50	1.10	536703	0.020	0.053	0.037	5	1.432	0.698
65.00	66.00	1.00	536704	0.028	0.080	0.056	5	1.429	0.700
66.00	67.00	1.00	536705	0.001	0.007	0.009	10	0.778	1.286
67.00	68.00	1.00	536706	0.023	0.052	0.045	10	1.156	0.865
72.63	73.63	1.00	536707	0.025	0.049	0.049	10	1.000	1.000
73.63	74.00	0.37	536708	0.017	0.050	0.040	10	1.250	0.800
74.00	75.00	1.00	536709	0.007	0.020	0.016	5	1.250	0.800
75.00	76.00	1.00	536710	0.013	0.037	0.028	10	1.321	0.757
92.50	93.33	0.83	536711	0.054	0.157	0.128	15	1.227	0.815
97.40	98.00	0.60	536712	0.066	0.131	0.160	20	0.819	1.221
99.10	100.30	1.20	536713	0.113	0.281	0.375	60	0.749	1.335
102.95	103.45	0.50	536714	0.103	0.131	0.291	60	0.450	2.221
103.45	104.30	0.85	536715	0.006	0.008	0.005	2	1.600	0.625
104.30	105.55	1.25	536716	0.067	0.334	0.177	20	1.887	0.530
105.55	106.55	1.00	536717	0.009	0.026	0.014	20	1.857	0.538
121.00	121.50	0.50	536718	0.041	0.075	0.089	15	0.843	1.187
123.55	124.30	0.75	536719	0.081	0.150	0.197	15	0.761	1.313
176.22	176.72	0.50	536720	0.021	0.057	0.053	3	1.075	0.930
176.72	177.22	0.50	536721	0.012	0.031	0.031	1	1.000	1.000

**Hole No: LBN-2 Date: May 5-May 8, 1996 Grid: 0+51 S, 3+42 E**

**SUMMARY LITHO LOG****From To Lithological Unit**

0.00 3.50 Overburden  
 3.50 7.93 LTROC- 15% ol  
 7.93 16.60 LNOR- patches of net-bleb-mass po



**SUMMARY LITHO LOG LBN-2**

From	To	Lithological Unit
16.60	17.10	MS-NET 70% po, <1%cpy
17.10	17.60	LNOR
17.60	25.55	LANOR- patches mass-net po,cpy
25.55	31.76	LNOR-minor net-mass po,cpy
31.76	41.80	LANOR-patches of mass-net-diss po; cpy
41.80	46.09	LNOR
46.09	73.80	LANOR-patchy po,cpy
73.80	78.52	LANOR-patches of mass-net-diss po;cpy
78.52	81.59	LANOR-patches po, cpy
81.59	82.14	FAULT
82.14	102.37	LANOR-brown-beige alteration
102.37	103.00	Net-mass po, minor cpy; py
103.00	107.46	LANOR-patches of net-mass po, max 3%cpy
107.46	107.81	LNOR-20% opx, 15% mag
107.81	122.12	LANOR- patches po, cpy, py with po
122.12	150.00	MANOR-15%cpx,5%mag, anor alteration
150.00	167.70	ALTERED ANOR-calcite-chlorite alteration, minor po
167.70	173.43	LANOR-minor chlorite alteration
173.43	181.03	ANOR-3-5% opx, 3%mag
181.03	289.00	ANOR-brown altered feldspar, patchy 2-3%po, pyx patchy
289.00	290.00	EOH

**ASSAY LOG**

From	To	Width	Sample #	Co %	Cu %	Ni %	% Sulphide	Cu/Ni	Ni/Cu
9.50	10.50	1.00	536722	0.055	0.145	0.116	15	1.250	0.800
10.50	11.50	1.00	536723	0.039	0.162	0.081	15	2.000	0.500
11.50	12.50	1.00	536724	0.034	0.101	0.073	10	1.384	0.723
16.60	17.10	0.50	536725	0.111	0.203	0.258	75	0.787	1.271
17.10	17.80	0.70	536726	0.009	0.047	0.010	1	4.700	0.213
17.80	18.80	1.00	536727	0.038	0.133	0.076	10	1.750	0.571
18.80	20.00	1.20	536728	0.024	0.113	0.047	10	2.404	0.416
20.00	21.00	1.00	536729	0.084	0.380	0.190	20	2.000	0.500
21.00	22.00	1.00	536730	0.056	0.284	0.113	20	2.513	0.398
22.00	23.00	1.00	536731	0.065	0.247	0.129	20	1.915	0.522
23.00	24.00	1.00	536732	0.030	0.173	0.048	20	3.604	0.277
24.00	25.00	1.00	536733	0.023	0.070	0.032	10	2.188	0.457
25.00	26.00	1.00	536734	0.013	0.039	0.023	5	1.696	0.590
29.00	30.00	1.00	536735	0.010	0.030	0.016	2	1.875	0.533
30.00	31.00	1.00	536736	0.012	0.019	0.010	2	1.900	0.526
31.00	32.00	1.00	536737	0.019	0.057	0.025	3	2.280	0.439
32.00	32.90	0.90	536738	0.028	0.269	0.035	5	7.686	0.130
32.90	33.90	1.00	536739	0.113	0.383	0.227	80	1.687	0.593
33.90	34.90	1.00	536740	0.087	0.444	0.168	40	2.643	0.378
34.90	35.40	0.50	536741	0.110	0.418	0.226	80	1.850	0.541
35.40	36.40	1.00	536742	0.004	0.009	0.004	1	2.250	0.444
36.40	37.40	1.00	536743	0.007	0.019	0.008	1	2.375	0.421
37.40	38.40	1.00	536744	0.064	0.339	0.120	20	2.825	0.354
38.40	39.00	0.60	536745	0.011	0.047	0.012	1	3.917	0.255
39.00	40.00	1.00	536746	0.100	0.190	0.191	60	0.995	1.005
40.00	41.00	1.00	536747	0.030	0.071	0.049	10	1.449	0.690

From	To	Width	Sample #	Co %	Cu %	Ni %	% Sulphide	Cu/Ni	Ni/Cu
41.00	41.50	0.50	536748	0.032	0.087	0.057	5	1.526	0.655
49.88	50.88	1.00	536749	0.110	0.299	0.299	80	1.000	1.000
50.88	51.88	1.00	536750	0.106	0.154	0.289	85	0.533	1.877
51.88	53.00	1.12	536751	0.085	0.195	0.185	40	1.054	0.949
53.00	53.88	0.88	536752	0.006	0.008	0.004	1	2.000	0.500
53.88	54.88	1.00	536753	0.005	0.055	0.006	5	9.167	0.109
54.88	55.78	0.90	536754	0.019	0.075	0.030	10	2.500	0.400
55.78	56.78	1.00	536755	0.073	0.312	0.151	25	2.066	0.484
56.78	57.78	1.00	536756	0.096	0.154	0.202	20	0.762	1.312
57.78	58.78	1.00	536757	0.033	0.189	0.057	5	3.316	0.302
58.78	59.20	0.42	536758	0.092	0.404	0.230	80	1.757	0.569
69.30	70.50	1.20	536759	0.036	0.341	0.077	15	4.429	0.226
89.80	90.80	1.00	536760	0.015	0.041	0.036	5	1.139	0.878
91.56	92.00	0.44	536761	0.027	0.017	0.059	10	0.288	3.471
102.36	103.36	1.00	536762	0.049	0.269	0.139	30	1.935	0.517
103.36	104.36	1.00	536763	0.007	0.046	0.015	1	3.067	0.326
104.36	105.36	1.00	536764	0.032	0.073	0.068	10	1.074	0.932
105.36	106.36	1.00	536765	0.044	0.135	0.087	10	1.552	0.644
106.36	107.36	1.00	536766	0.049	0.299	0.125	30	2.392	0.418
107.36	108.36	1.00	536767	0.035	0.062	0.071	20	0.873	1.145
108.36	109.60	1.24	536768	0.083	0.198	0.228	30	0.868	1.152
109.60	110.60	1.00	536769	0.007	0.039	0.011	1	3.545	0.282
110.60	111.60	1.00	536770	0.023	0.118	0.045	5	2.622	0.381
120.47	121.47	1.00	536771	0.105	0.175	0.315	60	0.556	1.800
121.47	122.05	0.58	536772	0.081	0.145	0.233	60	0.622	1.607
154.00	155.00	1.00	536773	0.029	0.179	0.077	15	2.325	0.430
160.50	161.50	1.00	536774	0.003	0.007	0.005	3	1.400	0.714

Hole No: LBN-3      Date: May 12-15, 1996      Grid: 0+52 S, 3+42 E

#### SUMMARY LITHO LOG

From    To    Lithological Unit

0.00 4.50 Overburden  
4.50 4.95 ANOR-10%mag, tr po  
4.95 10.06 LTROC-10% mag, 3-10% ol, tr po  
10.06 12.97 ANOR-patchy po,cpy  
12.97 13.45 ANOR-10% opx  
13.45 21.80 MS 40% po, 2-3% cpy  
21.80 22.45 LNOR-3%ol, 10%mag, 7% c -v. c gr opx, patchy massive po, cpy  
22.45 38.95 LANOR-patchy po, cpy  
38.95 44.64 MS-po with plagioclase inclusions, then net-diss po  
44.64 47.25 LANOR-patchy po,cpy  
47.25 88.70 ANOR- patchy 3-15% pyx (opx), po-cpy  
88.70 89.30 FAULT/ALTERATION ZONE-diss py  
89.30 97.40 LANOR-patchy po,cpy  
97.40 100.70 LANOR-brown-white feldspar, greenish alteration, po  
100.70 134.28 LANOR-patchy mass-net-diss po,cpy  
134.28 147.86 MANOR-10-15%opx

**SUMMARY LITHO LOG LBN-3**

From	To	Lithological Unit
147.86	168.00	LANOR-patchy mass-net-diss po.cpy
168.00	170.88	ANOR-green alteration feldspar, diss-net po-py.cpy
170.88	187.00	LANOR-patchy po.cpy
187.00	202.08	LANOR-patchy po.cpy; calcite-chlorite veining
202.08	233.85	ANOR-7-10%opx, cal-chl alt, po.cpy
233.85	234.12	FAULT ZONE
234.12	248.44	ANOR-3-5%pyx +mag, chlorite alteration
248.44	249.00	EOH

**ASSAY LOG**

From	To	Width	Sample #	Co %	Cu %	Ni %	% Sulphide	Cu/Ni	Ni/Cu
10.80	11.80	1.00	536851	0.132	0.193	0.225	80	0.858	1.166
11.80	12.80	1.00	536852	0.068	0.228	0.120	30	1.900	0.526
12.80	13.80	1.00	536853	0.009	0.029	0.007	5	4.143	0.241
13.80	14.80	1.00	536854	0.012	0.008	0.009	1	0.889	1.125
14.80	15.30	0.50	536855	0.011	0.007	0.011	NIL	0.636	1.571
15.30	16.30	1.00	536856	0.017	0.031	0.025	NIL	1.240	0.806
16.30	17.30	1.00	536857	0.012	0.009	0.012	3	0.750	1.333
17.30	18.30	1.00	536858	0.038	0.448	0.059	20	7.593	0.132
18.30	18.68	0.38	536859	0.111	0.421	0.178	40	2.365	0.423
18.68	19.68	1.00	536860	0.010	0.013	0.014	NIL	0.929	1.077
19.68	20.68	1.00	536861	0.013	0.010	0.015	NIL	0.667	1.500
20.68	21.80	1.12	536862	0.053	0.110	0.085	30	1.294	0.773
21.80	22.45	0.65	536863	0.025	0.100	0.034	1	2.941	0.340
22.45	23.45	1.00	536864	0.085	0.211	0.150	40	1.407	0.711
23.45	24.45	1.00	536865	0.080	0.258	0.139	30	1.856	0.539
24.45	25.45	1.00	536866	0.011	0.030	0.012	NIL	2.500	0.400
25.45	26.45	1.00	536867	0.007	0.010	0.004	NIL	2.500	0.400
26.45	27.45	1.00	536868	0.075	0.119	0.099	15	1.20	0.832
27.45	28.45	1.00	536869	0.089	0.121	0.158	40	0.766	1.306
28.45	29.45	1.00	536870	0.014	0.045	0.021	NIL	2.14	0.467
29.45	30.45	1.00	536871	0.062	0.359	0.100	20	3.590	0.279
30.45	31.45	1.00	536872	0.024	0.079	0.038	NIL	2.07	0.481
37.40	38.40	1.00	536873	0.059	0.069	0.101	15	0.683	1.464
38.40	39.40	1.00	536874	0.086	0.099	0.149	40	0.664	1.505
39.40	40.40	1.00	536875	0.080	0.178	0.141	15	1.262	0.792
40.40	41.00	0.60	536876	0.074	0.181	0.119	20	1.52	0.657
46.90	47.25	0.35	536877	0.086	0.139	0.180	60	0.772	1.295
53.70	54.70	1.00	536878	0.067	0.309	0.110	20	2.809	0.356
54.70	55.70	1.00	536879	0.089	0.260	0.181	35	1.436	0.696
55.70	56.70	1.00	536880	0.017	0.031	0.022	5	1.409	0.710
56.70	57.50	0.80	536881	0.034	0.131	0.054	10	2.426	0.412
90.00	91.00	1.00	536882	0.049	0.109	0.079	15	1.380	0.725
106.30	107.30	1.00	536883	0.030	0.090	0.040	5	2.250	0.444
107.30	108.30	1.00	536884	0.025	0.039	0.031	2	1.258	0.790
108.30	109.30	1.00	536885	0.034	0.111	0.055	10	2.018	0.495
109.30	110.30	1.00	536886	0.018	0.027	0.023	3	1.174	0.852
110.30	111.30	1.00	536887	0.040	0.119	0.065	20	1.831	0.546
111.30	112.30	1.00	536888	0.046	0.140	0.080	15	1.750	0.571
112.30	113.30	1.00	536889	0.039	0.111	0.059	5	1.881	0.532

From	To	Width	Sample #	Co %	Cu %	Ni %	% Sulphide	Cu/Ni	Ni/Cu
113.30	114.30	1.00	536890	0.041	0.139	0.061	5	2.279	0.439
114.30	115.30	1.00	536891	0.006	0.010	0.010	5	1.000	1.000
115.30	116.30	1.00	536892	0.065	0.104	0.126	30	0.825	1.212
116.30	117.30	1.00	536893	0.056	0.139	0.119	20	1.168	0.856
117.30	118.30	1.00	536894	0.064	0.120	0.139	20	0.871	1.149
118.30	119.30	1.00	536895	0.006	0.010	0.007	1	1.429	0.700
119.30	120.30	1.00	536896	0.062	0.270	0.120	25	2.325	0.430
120.30	121.30	1.00	536897	0.048	0.060	0.089	20	0.764	1.309
121.30	122.30	1.00	536898	0.032	0.080	0.055	10	1.455	0.688
122.30	123.30	1.00	536899	0.048	0.149	0.091	15	1.637	0.611
123.30	124.30	1.00	536900	0.084	0.400	0.160	40	2.513	0.398
124.30	125.30	1.00	24051	0.033	0.168	0.052	10	3.231	0.310
125.30	126.30	1.00	24052	0.021	0.028	0.031	NIL	0.90	1.107
126.30	127.30	1.00	24053	0.020	0.169	0.026	NIL	6.50	0.154
127.30	128.30	1.00	24054	0.120	0.319	0.261	80	1.222	0.818
128.30	129.30	1.00	24055	0.105	0.251	0.229	60	1.096	0.912
129.30	130.30	1.00	24056	0.095	0.210	0.199	40	1.055	0.948
130.30	131.30	1.00	24057	0.074	0.331	0.150	20	2.207	0.453
131.30	132.30	1.00	24058	0.100	0.179	0.210	60	0.852	1.173
132.30	133.30	1.00	24059	0.015	0.018	0.014	NIL	1.28	0.778
133.30	134.30	1.00	24060	0.131	0.361	0.259	75	1.394	0.717
147.80	148.80	1.00	24061	0.083	0.244	0.165	40	1.479	0.676
148.80	149.80	1.00	24062	0.110	0.121	0.219	70	0.553	1.810
149.80	150.80	1.00	24063	0.101	0.159	0.191	40	0.832	1.201
150.80	151.80	1.00	24064	0.074	0.138	0.160	35	0.860	1.159
151.80	152.80	1.00	24065	0.099	0.198	0.197	60	1.005	0.995
152.80	153.80	1.00	24066	0.075	0.209	0.150	35	1.393	0.718
153.80	154.80	1.00	24067	0.109	0.298	0.220	70	1.355	0.738
154.80	155.60	0.80	24068	0.105	0.281	0.220	70	1.277	0.783
155.60	156.60	1.00	24069	0.016	0.048	0.019	NIL	2.520	0.396
156.60	157.60	1.00	24070	0.013	0.013	0.013	5	1.000	1.000
157.60	158.60	1.00	24071	0.039	0.057	0.080	5	0.713	1.404
158.60	159.60	1.00	24072	0.020	0.070	0.032	5	2.188	0.457
167.80	168.80	1.00	24073	0.035	0.129	0.060	15	2.150	0.465
168.80	169.80	1.00	24074	0.010	0.011	0.008	80	1.375	0.727
169.80	170.60	0.80	24075	0.119	0.064	0.258	80	0.248	4.031
176.80	177.80	1.00	24076	0.043	0.060	0.091	15	0.659	1.517
177.80	178.80	1.00	24077	0.084	0.119	0.160	40	0.744	1.345
178.80	179.80	1.00	24078	0.106	0.537	0.209	60	2.569	0.389
179.80	180.80	1.00	24079	0.119	0.230	0.210	75	1.095	0.913
180.80	181.80	1.00	24080	0.071	0.101	0.140	30	0.721	1.386
181.80	182.80	1.00	24081	0.007	0.010	0.007	NIL	1.429	0.700
182.80	183.80	1.00	24082	0.048	0.241	0.085	5	2.835	0.353
183.80	184.80	1.00	24083	0.036	0.091	0.063	15	1.444	0.692
184.80	185.80	1.00	24084	0.131	0.268	0.229	60	1.170	0.854
185.80	186.80	1.00	24085	0.073	0.639	0.140	20	4.564	0.219
186.80	187.80	1.00	24086	0.059	0.171	0.109	25	1.569	0.637
187.80	188.80	1.00	24087	0.110	0.179	0.202	70	0.886	1.128
188.80	189.80	1.00	24088	0.019	0.020	0.022	5	0.909	1.100
189.80	190.80	1.00	24089	0.126	0.458	0.211	70	2.171	0.461
190.80	191.80	1.00	24090	0.141	0.420	0.259	90	1.622	0.617

From	To	Width	Sample #	Co %	Cu %	Ni %	% Sulphide	Cu/Ni	Ni/Cu
191.80	192.80	1.00	24091	0.105	0.221	0.191	50	1.157	0.864
192.80	193.80	1.00	24092	0.022	0.089	0.030	NIL	2.967	0.337
193.80	194.80	1.00	24093	0.139	0.231	0.249	70	0.928	1.078

Hole No: LBN-4 Date: May 16-22, 1996

Grid: 1+00 S, 2+50E

#### SUMMARY LITHO LOG

From To Lithological Unit

0.00	3.62	Overburden
3.62	15.20	ANOR-7-5%opx, patches mass-net-diss po
15.20	50.57	LNOR-7-20%opx, 2%ol, pyx poor near po patches
50.57	56.18	LANOR-green beige alteration
56.18	64.20	MANOR-10%opx overall, 3% mag
64.20	115.60	LANOR-patches net-diss-mass po, <1%cpy
115.60	119.80	ALTERED LANOR-whitened/bleached feldspar
119.80	171.04	LANOR-patches po throughout
171.04	216.00	LANOR-po-cpy in patches + py
216.00	243.30	FAULT/ALTERATION ZONE in LANOR-po continued with py
243.30	245.15	LGAB dyke?- 15-20% cpx w. po
245.15	258.50	FAULT/ALTERATION ZONE in LANOR-po continued with py
258.50	261.71	Crumbled core, pink-green alteration with py, minor po,cpy
261.71	310.30	LANOR-patches po, minor cpy
310.30	311.80	ALTERED ANOR-chlorite alteration in pyx, py cubes
311.80	323.30	ANOR-continued patches po, minor cpy
323.30	326.00	LANOR-olive green alteration
326.00	390.46	LANOR-green+beige alteration, py, patches po,cpy
390.46	395.68	Massive po, cpy blebs-GONE TO ONTARIO
395.68	396.60	LANOR-patches po, cpy, py
396.60	401.60	LANOR-blue-green alteration, po-cpy-py
401.60	410.50	LANOR-brown-pink alteration, patches po-cpy
410.50	460.00	LANOR-blue-green alteration, patchy cpx (5%),po-cpy-py
460.00	461.00	EOH

#### ASSAY LOG

From	To	Width	Sample #	Co %	Cu %	Ni %	% Sulphide	Cu/Ni	Ni/Cu
6.20	7.20	1.00	27301	0.039	0.092	0.074	10.0	1.237	0.809
7.20	8.05	0.85	27302	0.052	0.089	0.119	20.0	0.748	1.337
10.90	11.90	1.00	27303	0.049	0.315	0.118	25.0	2.669	0.375
11.90	12.90	1.00	27304	0.053	0.209	0.125	10.0	1.672	0.598
12.90	13.90	1.00	27305	0.008	0.016	0.008	5.0	2.000	0.500
13.90	15.22	1.32	27306	0.020	0.080	0.032	3.0	2.500	0.400
15.22	16.22	1.00	27307	0.010	0.024	0.016	NIL	1.500	0.667
16.22	17.22	1.00	27308	0.061	0.157	0.147	20.0	1.068	0.936
17.22	18.22	1.00	27309	0.030	0.031	0.037	5.0	0.838	1.194
18.22	19.22	1.00	27310	0.012	0.011	0.012	NIL	0.917	1.091
19.22	20.22	1.00	27311	0.037	0.074	0.051	10.0	1.451	0.689
20.22	21.22	1.00	27312	0.028	0.060	0.037	1.0	1.622	0.617
21.22	22.22	1.00	27313	0.016	0.025	0.023	1.0	1.087	0.920

From	To	Width	Sample #	Co %	Cu %	Ni %	% Sulphide	Cu/Ni	Ni/Cu
22.22	23.22	1.00	27314	0.052	0.081	0.105	10.0	0.771	1.296
23.22	24.22	1.00	27315	0.014	0.025	0.026	1.0	0.962	1.040
24.22	25.22	1.00	27316	0.047	0.190	0.095	25.0	2.000	0.500
25.22	26.22	1.00	27317	0.019	0.033	0.036	2.0	0.917	1.091
31.45	32.45	1.00	27319	0.024	0.015	0.045	10.0	0.333	3.000
43.50	44.00	0.50	27318	0.018	0.037	0.040	15.0	0.925	1.081
66.85	67.85	1.00	27320	0.034	0.103	0.094	5.0	1.096	0.913
67.85	68.85	1.00	27321	0.027	0.074	0.053	10.0	1.396	0.716
68.85	69.35	0.50	27322	0.070	0.175	0.221	3.0	0.792	1.263
123.30	124.30	1.00	27323	0.055	0.159	0.104	10.0	1.529	0.654
124.30	125.30	1.00	27324	0.096	0.102	0.209	60.0	0.488	2.049
125.30	126.50	1.20	27325	0.078	0.369	0.164	40.0	2.250	0.444
126.50	127.50	1.00	27326	0.010	0.018	0.010	1.0	1.800	0.556
127.50	128.50	1.00	27327	0.031	0.137	0.044	1.0	3.114	0.321
128.50	129.50	1.00	27328	0.045	0.177	0.098	20.0	1.806	0.554
129.50	130.50	1.00	27329	0.098	0.186	0.230	60.0	0.809	1.237
130.50	131.50	1.00	27330	0.008	0.013	0.010	5.0	1.300	0.769
131.50	132.50	1.00	27331	0.059	0.128	0.118	40.0	1.085	0.922
136.50	137.00	0.50	27332	0.030	0.060	0.049	10.0	1.224	0.817
142.50	143.50	1.00	27333	0.047	0.160	0.066	10.0	2.424	0.413
143.50	144.50	1.00	27334	0.054	0.179	0.105	15.0	1.705	0.587
144.50	145.50	1.00	27335	0.092	0.119	0.208	40.0	0.572	1.748
145.50	146.50	1.00	27336	0.081	0.130	0.179	50.0	0.726	1.377
146.50	147.50	1.00	27337	0.050	0.139	0.109	20.0	1.275	0.784
147.50	148.50	1.00	27338	0.053	0.139	0.119	20.0	1.168	0.856
148.50	149.50	1.00	27339	0.094	0.366	0.262	50.0	1.397	0.716
149.50	150.50	1.00	27340	0.059	0.248	0.163	20.0	1.521	0.657
150.50	151.50	1.00	27341	0.007	0.013	0.010	1.0	1.300	0.769
151.50	152.50	1.00	27342	0.036	0.128	0.063	5.0	2.032	0.492
152.50	153.50	1.00	27343	0.020	0.049	0.028	3.0	1.750	0.571
153.50	154.50	1.00	27344	0.011	0.011	0.006	2.0	1.833	0.545
154.50	155.50	1.00	27345	0.022	0.037	0.027	5.0	1.370	0.730
164.00	165.00	1.00	27346	0.024	0.065	0.040	10.0	1.625	0.615
168.20	169.20	1.00	27347	0.026	0.051	0.043	10.0	1.186	0.843
169.20	170.20	1.00	27348	0.020	0.039	0.029	5.0	1.345	0.744
175.50	176.50	1.00	27349	0.026	0.169	0.061	20.0	2.770	0.361
224.30	225.30	1.00	27350	0.049	0.130	0.105	15.0	1.238	0.808
225.30	226.30	1.00	26181	0.016	0.101	0.044	10.0	2.295	0.436
226.30	227.30	1.00	26182	0.018	0.115	0.043	15.0	2.674	0.374
237.40	238.40	1.00	26183	0.009	0.066	0.026	10.0	2.538	0.394
238.40	239.40	1.00	26184	0.045	0.169	0.100	20.0	1.690	0.592
242.43	243.43	1.00	26185	0.023	0.045	0.053	15.0	0.849	1.178
243.43	244.43	1.00	26186	0.004	0.017	0.016	1.0	1.063	0.941
244.43	245.32	0.89	26187	0.016	0.075	0.040	10.0	1.875	0.533
249.00	250.00	1.00	26188	0.032	0.051	0.059	20.0	0.864	1.157
250.00	251.00	1.00	26189	0.030	0.081	0.059	10.0	1.373	0.728
261.10	262.10	1.00	26190	0.131	0.182	0.300	90.0	0.607	1.648
262.10	263.10	1.00	26191	0.092	0.248	0.251	65.0	0.988	1.012
263.10	264.10	1.00	26192	0.108	0.359	0.263	60.0	1.365	0.733
264.10	265.10	1.00	26193	0.068	0.361	0.160	30.0	2.256	0.443
265.10	266.10	1.00	26194	0.064	0.099	0.159	40.0	0.623	1.606

From	To	Width	Sample #	Co %	Cu %	Ni %	% Sulphide	Cu/Ni	Ni/Cu
266.10	267.10	1.00	26195	0.116	0.279	0.269	75.0	1.037	0.964
267.10	268.10	1.00	26196	0.097	0.301	0.250	80.0	1.204	0.831
268.10	269.10	1.00	26197	0.082	0.145	0.211	60.0	0.687	1.455
269.10	270.10	1.00	26198	0.001	0.010	0.003	NIL	3.333	0.300
270.10	271.10	1.00	26199	0.001	0.012	0.002	NIL	6.000	0.167
271.10	272.10	1.00	26200	0.001	0.010	0.003	NIL	3.333	0.300
272.10	273.10	1.00	25451	0.101	0.239	0.231	70.0	1.035	0.967
273.10	274.10	1.00	25452	0.091	0.611	0.199	70.0	3.070	0.326
274.10	275.10	1.00	25453	0.119	0.209	0.266	95.0	0.786	1.273
275.10	276.10	1.00	25454	0.082	0.311	0.202	70.0	1.540	0.650
276.10	277.10	1.00	25455	0.088	0.429	0.208	70.0	2.063	0.485
277.10	278.10	1.00	25456	0.004	0.013	0.004	NIL	3.250	0.308
278.10	279.10	1.00	25457	0.004	0.011	0.003	NIL	3.667	0.273
279.10	280.10	1.00	25458	0.072	0.129	0.169	40.0	0.763	1.310
280.10	281.10	1.00	25459	0.101	0.469	0.250	90.0	1.876	0.533
281.10	282.10	1.00	25460	0.054	0.508	0.119	15.0	4.269	0.234
282.10	283.10	1.00	25461	0.068	0.172	0.144	30.0	1.194	0.837
283.10	284.10	1.00	25462	0.080	0.361	0.178	50.0	2.028	0.493
284.10	285.10	1.00	25463	0.088	0.319	0.200	50.0	1.595	0.627
285.10	286.10	1.00	25464	0.086	0.172	0.202	50.0	0.851	1.174
286.10	287.10	1.00	25465	0.092	0.208	0.217	50.0	0.959	1.043
287.10	288.10	1.00	25466	0.093	0.421	0.265	40.0	1.589	0.629
288.10	289.10	1.00	25467	0.087	0.219	0.208	40.0	1.053	0.950
289.10	290.10	1.00	25468	0.041	0.308	0.090	30.0	3.422	0.292
290.10	291.10	1.00	25469	0.055	0.132	0.119	30.0	1.109	0.902
291.10	292.10	1.00	25470	0.093	0.231	0.211	30.0	1.095	0.913
292.10	293.10	1.00	25471	0.024	0.089	0.041	10.0	2.171	0.461
293.10	294.10	1.00	25472	0.008	0.028	0.015	NIL	1.867	0.536
294.10	295.10	1.00	25473	0.021	0.050	0.033	5.0	1.515	0.660
295.10	296.10	1.00	25474	0.016	0.034	0.020	5.0	1.700	0.588
296.10	297.10	1.00	25475	0.003	0.015	0.007	NIL	2.143	0.467
297.10	298.10	1.00	25476	0.003	0.014	0.006	NIL	2.333	0.429
298.10	299.10	1.00	25477	0.001	0.008	0.003	NIL	2.667	0.375
299.10	300.10	1.00	25478	0.045	0.209	0.109	10.0	1.917	0.522
300.10	301.10	1.00	25479	0.031	0.302	0.058	10.0	5.207	0.192
301.10	302.10	1.00	25480	0.115	0.239	0.272	75.0	0.879	1.138
302.10	303.10	1.00	25481	0.046	0.251	0.110	20.0	2.282	0.438
303.10	304.10	1.00	25482	0.001	0.010	0.004	NIL	2.500	0.400
304.10	305.10	1.00	25483	0.001	0.011	0.006	NIL	1.833	0.545
305.10	306.10	1.00	25484	0.079	0.259	0.172	50.0	1.506	0.664
306.10	307.10	1.00	25485	0.016	0.041	0.031	5.0	1.323	0.756
307.10	308.10	1.00	25486	0.072	0.221	0.149	30.0	1.483	0.674
308.10	309.10	1.00	25487	0.045	0.398	0.096	15.0	4.146	0.241
309.10	310.10	1.00	25488	0.091	0.161	0.201	50.0	0.801	1.248
310.10	311.10	1.00	25489	0.026	0.066	0.059	5.0	1.119	0.894
311.10	312.10	1.00	25490	0.041	0.119	0.085	20.0	1.400	0.714
312.10	313.10	1.00	25491	0.082	0.220	0.182	30.0	1.209	0.827
313.10	314.10	1.00	25492	0.090	0.151	0.209	40.0	0.722	1.384
314.10	315.10	1.00	25493	0.102	0.136	0.221	40.0	0.615	1.625
315.10	316.10	1.00	25494	0.041	0.278	0.079	NIL	3.519	0.284
316.10	317.10	1.00	25495	0.067	0.079	0.148	25.0	0.534	1.873

From	To	Width	Sample #	Co %	Cu %	Ni %	% Sulphide	Cu/Ni	Ni/Cu
317.10	318.10	1.00	25496	0.120	0.150	0.273	80.0	0.549	1.820
318.10	318.85	0.75	25497	0.130	0.192	0.295	90.0	0.651	1.536
318.85	319.85	1.00	25498	0.025	0.070	0.056	10.0	1.250	0.800
319.85	320.85	1.00	25499	0.001	0.007	0.002	NIL	3.500	0.286
320.85	321.85	1.00	25500	0.049	0.065	0.105	15.0	0.619	1.615
321.85	322.85	1.00	25901	0.047	0.169	0.114	20.0	1.482	0.675
322.85	323.35	0.50	25902	0.084	0.422	0.191	40.0	2.209	0.453
339.75	340.75	1.00	25903	0.099	0.255	0.205	50.0	1.244	0.804
364.75	365.25	0.50	25904	0.111	0.299	0.219	70.0	1.365	0.732
376.80	377.30	0.50	25905	0.053	0.206	0.114	50.0	1.807	0.553
378.60	379.60	1.00	25906	0.141	0.120	0.281	90.0	0.427	2.342
379.60	380.25	0.65	25907	0.130	0.178	0.246	90.0	0.724	1.382
381.30	381.80	0.50	25908	0.076	0.060	0.150	45.0	0.400	2.500
386.70	387.70	1.00	25909	0.129	0.649	0.250	80.0	2.596	0.385
387.70	388.70	1.00	25910	0.120	0.231	0.235	70.0	0.983	1.017
388.70	389.08	0.38	25911	0.131	0.170	0.272	80.0	0.625	1.600
389.08	389.90	0.82	25974	0.003	0.021	0.001	NIL	21.000	0.048
389.90	390.45	0.55	25701	0.004	0.015	0.005	NIL	3.042	0.329
390.45	391.35	0.90	25912	0.125	0.202	0.288	95.0	0.701	1.426
391.35	392.35	1.00	25913	0.135	0.250	0.299	95.0	0.836	1.196
392.35	393.35	1.00	25914	0.118	0.451	0.275	90.0	1.640	0.610
393.35	394.35	1.00	25915	0.118	0.640	0.276	85.0	2.319	0.431
394.35	395.45	1.10	25916	0.114	0.653	0.251	90.0	2.602	0.384
395.45	396.45	1.00	25917	0.003	0.034	0.005	5.0	6.800	0.147
396.45	397.45	1.00	25918	0.028	0.329	0.069	NIL	4.768	0.210
397.45	398.45	1.00	25919	0.030	0.181	0.075	5.0	2.413	0.414
398.45	399.45	1.00	25920	0.012	0.135	0.039	5.0	3.462	0.289
399.45	400.45	1.00	25921	0.015	0.045	0.024	NIL	1.875	0.533
400.45	401.40	0.95	25922	0.038	0.131	0.070	10.0	1.871	0.534
406.60	407.20	0.60	25923	0.109	0.459	0.251	90.0	1.829	0.547
407.20	408.20	1.00	25924	0.075	0.321	0.180	40.0	1.783	0.561
408.20	409.20	1.00	25925	0.057	0.179	0.125	30.0	1.432	0.698
409.20	410.20	1.00	25926	0.123	0.225	0.252	70.0	0.893	1.120

Hole No: LBN-5      Date: May 22-26, 1996      Grid: 1+00 S, 2+50 E

#### SUMMARY LITHO LOG

From To Lithological Unit

0.00 3.50 Overburden  
3.50 9.73 ANOR-max 10% pyx+mag, patchy po-cpy  
9.73 15.88 ANOR with LNOR layers (10% opx, 5-7% mag), po  
15.88 33.80 LANOR-5% cpx overall, <1%mag, minor patches po, cpy  
33.80 41.63 LNOR-15% opx, 2% ol, patchy po, cpy  
41.63 46.73 ANOR-blue feldspar, variable % pyx, mag, alteration, po-cpy  
46.73 47.06 PYROXENITE DYKE- maximum 50% c.gr cpx, 5% po, 1% py, tr cpy  
47.06 54.50 ANOR-variable % pyx, patchy po-cpy +/- py  
54.50 54.80 LNOR- 15% opx, 5% mag; salt and pepper texture  
54.80 70.38 ANOR-variable pyx (max 20% cpx), po-cpy patches  
70.38 70.84 LTROC- dull brown color, 7% ol, 2% opx?, 5% mag



# SUMMARY LITHO LOG LBN-5

## From To Lithological Unit

70.84	74.93	ANOR-salt and pepper cpx rich with po min
74.93	79.60	LNOR- max 20% cpx to opx, 5-10% mag, tr po
79.60	80.84	LANOR-3% cpx (but variable), po patches
80.84	81.46	Fe-DIO DYKE -10% mag, 10% opx/ol?
81.46	82.80	ANOR-variable pyx, patchy po-cpy continued
82.80	87.13	ANOR- very c gr opx, po, 1-2% ol
87.13	92.50	ANOR-minor alteration (qtz?)
92.50	93.50	LANOR-light green alteration with dark blue plg porphyry, po-cpy
93.50	141.00	ANOR-variable % pyx, tr ol?, po-cpy-py
141.00	156.37	LANOR- feldspar rich, brown-grey mortar texture, po-cpy
156.37	156.72	LTROC-10% ol, 3% mag
156.72	162.15	LANOR-minor po
162.15	166.20	LNOR-LANOR interbanding
166.20	193.64	LANOR-3-5% opx, patches po with py, mortar texture
193.64	194.96	LNOR-c.gr 10% opx, 3% mag, dull grey mineral (possibly leucoxene)
194.96	216.51	LANOR-patchy po-cpy, <5% mafics
216.51	218.35	LANOR-soft white alteration veins, chlorite alteration, py>po>cpy
218.35	220.80	ANOR-5% opx
220.80	223.00	LANOR-po patches
223.00	224.80	ANOR-5% opx with po-cpy rich veins
224.80	229.64	LANOR-light green groundmass, blue plg porphyry, po, cpy, py
229.64	230.80	ANOR - very c.gr 7% opx, 3% mag, tr green ol, brown glassy mineral?
230.80	274.80	LANOR-patches GP and po-cpy
274.80	276.80	LANOR-intense alteration, crumbled; calcite-chlorite alteration, py
276.80	278.10	LANOR-patches/bands po-cpy
278.10	278.50	LNOR?-20% opx-rich with weak foliation
278.50	284.65	LANOR- patches po-cpy, variable feldspar alteration
284.65	285.00	LNOR - m.gr 20% opx, 10% mag patches
285.00	334.00	LANOR- max 3% pyx, 2% mag, green feldspar alteration, po-cpy
334.00	335.00	EOH

## ASSAY LOG

From	To	Width	Sample #	Co %	Cu %	Ni %	% Sulphide	Cu/Ni	Ni/Cu
10.00	11.00	1.00	25927	0.034	0.073	0.063	5.0	1.159	0.863
11.00	12.00	1.00	25928	0.013	0.015	0.016	NIL	0.938	1.067
12.00	12.50	0.50	25929	0.064	0.191	0.123	20.0	1.553	0.644
15.36	15.96	0.60	25930	0.062	0.181	0.125	25.0	1.448	0.691
19.77	20.70	0.93	25931	0.031	0.075	0.048	5.0	1.563	0.640
36.10	37.10	1.00	25932	0.082	0.095	0.180	50.0	0.528	1.895
37.10	38.10	1.00	25933	0.078	0.232	0.171	15.0	1.357	0.737
38.10	38.80	0.70	25934	0.071	0.261	0.150	15.0	1.740	0.575
47.10	48.10	1.00	25935	0.075	0.115	0.150	10.0	0.767	1.304
48.10	49.38	1.28	25936	0.046	0.085	0.085	15.0	1.000	1.000
71.00	71.50	0.50	25937	0.028	0.038	0.043	10.0	0.884	1.132
83.00	84.00	1.00	25938	0.026	0.090	0.043	5.0	2.093	0.478
84.00	85.00	1.00	25939	0.092	0.212	0.232	60.0	0.914	1.094
85.00	86.00	1.00	25940	0.060	0.302	0.145	10.0	2.083	0.480
86.00	87.00	1.00	25941	0.054	0.070	0.100	15.0	0.700	1.429
87.00	88.00	1.00	25942	0.074	0.251	0.165	40.0	1.521	0.657
88.00	88.90	0.90	25943	0.070	0.151	0.165	30.0	0.915	1.093

From	To	Width	Sample #	Co %	Cu %	Ni %	% Sulphide	Cu/Ni	Ni/Cu
137.75	138.35	0.60	25944	0.101	0.260	0.265	80.0	0.981	1.019
138.35	139.10	0.75	25945	0.008	0.034	0.012	NIL	2.833	0.353
139.10	140.10	1.00	25946	0.030	0.355	0.065	NIL	5.462	0.183
140.10	140.60	0.50	25947	0.094	0.260	0.221	60.0	1.176	0.850
150.80	151.80	1.00	25948	0.067	0.123	0.131	20.0	0.939	1.065
151.80	152.80	1.00	25949	0.028	0.052	0.054	10.0	0.963	1.038
152.80	153.80	1.00	25950	0.052	0.043	0.105	15.0	0.410	2.442
153.80	154.80	1.00	25951	0.040	0.075	0.080	10.0	0.938	1.067
154.80	155.80	1.00	25952	0.021	0.041	0.038	10.0	1.079	0.927
155.80	156.80	1.00	25953	0.038	0.065	0.075	5.0	0.867	1.154
156.80	157.60	0.80	25954	0.080	0.140	0.155	20.0	0.903	1.107
186.50	187.55	1.05	29956	0.025	0.066	0.080	3.0	0.825	1.212
187.55	188.60	1.05	25955	0.046	0.105	0.045	5.0	2.333	0.429
195.90	197.00	1.10	25957	0.092	0.331	0.195	60.0	1.697	0.589
203.70	204.70	1.00	25958	0.105	0.080	0.260	90.0	0.308	3.250
204.70	205.70	1.00	25959	0.100	0.145	0.240	80.0	0.604	1.655
205.70	206.70	1.00	25960	0.078	0.115	0.165	30.0	0.697	1.435
226.20	227.20	1.00	25961	0.024	0.095	0.047	10.0	2.021	0.495
227.20	228.20	1.00	25962	0.037	0.105	0.080	5.0	1.313	0.762
228.20	229.20	1.00	25963	0.047	0.105	0.085	15.0	1.235	0.810
229.20	230.20	1.00	25964	0.027	0.060	0.048	5.0	1.250	0.800
230.20	231.20	1.00	25965	0.026	0.040	0.048	10.0	0.833	1.200
231.20	232.20	1.00	25966	0.050	0.131	0.090	15.0	1.456	0.687
250.30	251.30	1.00	25975	0.039	0.122	0.075	10.0	1.627	0.615
251.30	252.30	1.00	25976	0.046	0.170	0.085	15.0	2.000	0.500
252.30	253.20	0.90	25977	0.056	0.125	0.102	10.0	1.225	0.816
265.65	266.65	1.00	25978	0.081	0.175	0.165	35.0	1.061	0.943
266.65	267.65	1.00	25979	0.048	0.140	0.090	30.0	1.556	0.643
267.65	268.65	1.00	25980	0.030	0.126	0.052	10.0	2.423	0.413
268.65	269.65	1.00	25981	0.012	0.018	0.015	5.0	1.200	0.833
269.65	270.65	1.00	25982	0.008	0.017	0.008	NIL	2.125	0.471
270.65	271.65	1.00	25983	0.056	0.135	0.101	30.0	1.337	0.748
271.65	272.65	1.00	25984	0.067	0.151	0.120	25.0	1.258	0.795
272.65	273.50	0.85	25985	0.042	0.091	0.080	5.0	1.137	0.879
275.90	276.40	0.50	25986	0.041	0.100	0.071	10.0	1.408	0.710
276.40	277.40	1.00	25987	0.053	0.140	0.096	10.0	1.458	0.686
284.20	284.70	0.50	25988	0.047	0.115	0.111	60.0	1.036	0.965
285.90	286.90	1.00	25989	0.023	0.060	0.051	15.0	1.176	0.850
286.90	287.90	1.00	25990	0.031	0.265	0.062	5.0	4.274	0.234
287.90	288.90	1.00	25991	0.017	0.081	0.030	3.0	2.700	0.370
288.90	290.00	1.10	25992	0.016	0.038	0.031	2.0	1.226	0.816
321.50	322.50	1.00	25993	0.081	0.311	0.202	80.0	1.540	0.650

Hole No: LBN-6      Date: May 26-Jun 1, 1996      Grid: 1+00 S, 2+50 E

# SUMMARY LITHO LOG

From      To      Lithological Unit

0.00	2.00	Overburden
2.00	6.55	LNOR-10-15%opx, 1%cpx, tr diss po and mag
6.55	7.30	LNOR-40% po
7.30	8.00	LNOR
8.00	12.85	LANOR-5%cpx, 1% opx, patchy po-cpy
12.85	13.84	GAB-45%cpx, 1% diss po, tr diss mag
13.84	15.58	LGAB-<15% cpx, patches 45%cpx, 10%opx, po-cpy
15.58	17.55	LANOR-tr cpx, <3% mag overall, minor po vein
17.55	21.53	LNOR-15%opx, 1-5%mag, tr diss po
21.53	22.82	TROC-20%ol, 5%mag, 1%pyx; m.gr
22.82	35.18	LNOR/NOR-dominantly 30-40%opx, <1% mag, po-cpy
35.18	36.59	ANOR-patchy 5-10% opx, 5-20% cpx, 5-20% mag, po-cpy
36.59	37.06	LNOR DYKE- f-m gr lt grey, 15% opx, 25%mag
37.06	39.95	ANOR-variable % pyx
39.95	40.54	LGAB DYKE -15% c gr cpx, 5% opx
40.54	47.00	ANOR-variable % pyx, patchy po-cpy
47.00	53.26	LANOR-patchy 10-15% cpx, po-cpy patchy
53.26	53.95	MANOR-10%cpx, 5%opx, tr mag
53.95	58.19	LANOR-patchy cpx and sulphides
58.19	58.35	LNOR DYKE- m.gr 39% opx, tr diss po
58.35	60.90	ANOR-ranges from LGAB to LNOR locally, po-cpy
60.90	61.68	LGAB DYKE-m.gr 30% cpx, 10% mag
61.68	72.39	ANOR-ranges from LGAB to LNOR locally, po-cpy
72.39	73.08	LGAB- very c.gr 15% cpx, 5% opx
73.08	73.90	LNOR-c.gr grey, 20% opx, 2% cpx
73.90	93.63	LANOR-patches opx, cpx, mag, and po-cpy
93.63	94.20	LNOR-m.gr 40% opx, tr cpx
94.20	96.03	LANOR-patches opx,cpx,mag, and po-cpy
96.03	97.12	Diss po-rich (20%) band, 10% cpx
97.12	108.17	LANOR-patches opx, cpx, mag, and po-cpy
108.17	114.95	LNOR-very c.gr, grey-br, 30% then to 10%opx, po-cpy
114.95	207.21	LANOR-patchy opx, cpx, mag and minor po-cpy
207.21	229.00	FAULT ZONE in LANOR-localized faults, talc-chlorite alteration
229.00	253.86	LANOR-patchy po-cpy, mag; talc-carbonate veins
253.86	257.19	LANOR-patches K-feldspar rich veins
257.19	280.50	LANOR-pink alteration, local mass mag (85%), minor po, cpy
280.50	285.75	FAULT ZONE in LANOR-soft pink alteration
285.75	318.50	LANOR-patchy pyx, mag, talc filled faults
318.50	319.07	FAULT ZONE in LANOR
319.07	378.93	ANOR-pyx% inc, layers (max 50cm) opx and cpx rich
378.93	379.94	LNOR DYKE-20% opx, <1% diss mag, tr diss mag
379.94	387.67	ANOR-continued cpx and opx layers, tr diss po
387.67	402.24	LGAB-c.gr grey patchy (18%) cpx, 2% mag, tr po-cpy
402.24	405.16	LANOR-patchy mag, cpx, opx
405.16	405.70	Opx rich dyke; 15-30% opx with depth, max 30% mag center
405.70	409.72	LANOR-variable % pyx and mag
409.72	431.42	MANOR-10-15% c. gr pyx (dominantly opx)

**SUMMARY LITHO LOG LBN-6****From To Lithological Unit**

431.42	436.52	LNOR-15-20% c.gr patchy opx, tr diss po
436.52	459.25	ANOR-15% cpx, 1% opx, 1% mag
459.25	459.74	LNOR/FE DIO dyke-c.gr grey, 30% opx, 10% mag
459.74	464.57	LNOR- c.gr grey, 22% patchy opx, 3% cpx, <1% mag, tr po
464.57	479.88	LNOR- c.gr grey, 12% patchy opx, 2 % cpx, <1% mag, tr po
479.88	499.60	LANOR- patchy (3%) cpx, (<1%) opx, (3%) mag, tr po
499.60	505.38	ANOR- c.gr grey, 10% patchy opx, <1% cpx
505.38	512.93	LANOR-patchy minor (<5%) opx, cpx, mag, tr po
512.93	515.00	LGAB- c.gr grey, 15% cpx, 2% mag, tr diss po
515.00	523.00	LNOR- c.gr grey, 16% opx, 2% cpx, 2% mag, tr po
523.00	524.00	EOH

**ASSAY LOG** - Core was resampled in 1997 but data are not available for this study. The unavailable data are from minor small sulphide intersections, dominantly pyrrhotite (<10%).

From	To	Width	Sample #	Co %	Cu %	Ni %	% Sulphide	Cu/Ni	Ni/Cu
6.55	7.30	0.75	25994	0.062	0.176	0.147	40	1.197	0.835
8.00	8.85	0.85	25995	0.121	0.165	0.257	60	0.642	1.558

**Hole No:** LBN-7      **Date:** Jun 7-11, 1996

**Grid:** 3+75 S, 7+05 E

**SUMMARY LITHO LOG****From To Lithological Unit**

0.00	50.00	Overburden
50.00	86.41	LANOR-patches of opx (6%), cpx (<1%), mag (<1%), tr po
86.41	87.12	LANOR DYKE-plagioclase-rich (95%), 3% opx+cpx
87.12	131.00	LANOR-very lg plg porphyry, opx + cpx rich bands (few cm)
131.00	141.63	LANOR-same as above but with max 5% po
141.63	145.60	LANOR-green feldspar alteration, thin faults, 5% diss po
145.60	163.76	LANOR-very thin veinlets of opx, cpx, mag, K-feldspar, faults
163.76	173.10	ANOR-grey, c gr, 15% cpx, 3% mag, tr po
173.10	188.25	LANOR
188.25	198.00	LNOR-light grey, c gr-very c gr 35% opx, <1% mag, tr po
198.00	201.67	LANOR-blue, c gr, 2% cpx
201.67	204.84	ANOR-patches 15% total opx+cpx, minor mag
204.84	209.37	LANOR-max 10cm plg por, 2% cpx, <1% mag, tr po
209.37	244.93	ANOR-15% cpx+opx, c gr plg porphyry (1cm), 2% mag, tr po
244.93	246.75	LANOR-2% cpx, <1% mag
246.75	265.38	ANOR-5-10% cpx+opx, 3% mag, tr po
265.38	265.70	K-FELDSPAR-QUATZ vein (10cm) with top of vein cpx-rich zones
265.70	273.00	ANOR-with thin (few cm) K-feldspar veins, faults, chlorite alteration
273.00	289.20	FAULT ZONE-chlorite alteration, fractures, Kfsp-qtz veins in ANOR
289.20	313.03	LANOR-patches of <5% cpx, opx, mag, minor faults
313.03	316.11	LANOR-3% opx (max 2cm), <1% cpx
316.11	319.94	LANOR-patches of <5% opx, cpx, mag
319.94	325.71	ANOR-c gr plg porphyry (2cm), 5% opx, cpx, mag, opx (2cm)
325.71	343.32	LANOR-patchy opx, cpx, mag as before
343.32	364.27	LANOR-pink-white veinlets, plg alteration, minor faults
364.27	371.35	LANOR-grey, c gr, peppered >3% opx, <1% mag, tr po

**SUMMARY LITHO LOG LBN-7****From To Lithological Unit**

371.35	385.80	LANOR-grey, c gr, 3-5% m gr cpx+mag, tr po, fsp alteration
385.80	386.33	LANOR-feldspar alteration, chlorite alteration of pyx-rich veins
386.33	499.00	LANOR-light green alteration near pyx bands, pink-white alteration
499.00	500.00	EOH

**ASSAY LOG**

From	To	Width	Sample #	Co %	Cu %	Ni %	% Sulphide	Cu/Ni	Ni/Cu
135.82	137.00	1.18	25705	0.004	0.016	0.007	NIL	2.268	0.441
137.00	138.73	1.73	25706	0.003	0.017	0.011	NIL	1.585	0.631
138.73	140.43	1.70	25707	0.012	0.020	0.018	1	1.082	0.925
140.43	141.66	1.23	25708	0.004	0.012	0.007	NIL	1.731	0.578
141.66	143.00	1.34	25709	0.006	0.025	0.019	1	1.316	0.760
143.00	144.37	1.37	25710	0.013	0.041	0.040	2	1.022	0.978
144.37	145.78	1.41	25711	0.007	0.028	0.020	1	1.389	0.720
481.56	481.80	0.24	25712	0.005	0.010	0.006	NIL	1.531	0.653

**Hole No: LBN-8****Date: Aug 14-27,1996****Grid: L100 S TL1200 E****SUMMARY LITHO LOG****From To Lithological Unit**

0.00	75.28	Overburden
75.28	145.90	LANOR- c gr, 3-5% pyx, 2% mag, tr diss po-cpy
145.90	156.82	FAULT ZONE in LANOR-fractures/faults, Kfsp-qtz veins
156.82	188.15	LANOR-as before
188.15	193.27	LANOR-5-25% c gr opx, <1%mag, tr po
193.27	220.17	LANOR-c gr, 3-5% pyx, 1-2%mag, tr po, green alteration
220.17	222.00	LANOR-c gr 5-15% opx, tr mag, tr po
222.00	223.90	LANOR-c gr, green feldspar alteration, 1-3%cp, tr-<1%mag
223.90	227.56	LANOR-m-c gr,5-15%opx, tr mag, tr po
227.56	267.50	LANOR-c gr, 2%pyx, 1-3%mag
267.50	312.00	LANOR- as above with thin (2 cm max) qtz-biotite veins, py
312.00	313.63	FAULT ZONE in LANOR- Kfsp-qtz veins, fracture, gouge
313.63	344.88	LANOR-as before, green alteration
344.88	346.48	LANOR-1-5%pyx, 1-3%po, five 1-2 cm mag-rich veins
346.48	356.10	LGAB DYKE-grey-green, c-very c gr, 3-95%cp, 5-25%mag, po
356.10	363.36	LANOR-c gr, green alteration, <1-3%mag+pyx
363.36	457.85	LANOR-more green fsp+pyx alteration, mag rich bands with pyx
457.85	459.00	LANOR-ALTERATION ZONE-light green fsp alteration, 1%pyx+mag
459.00	469.33	LANOR-as before with green alteration, mag bands
469.33	470.00	FE DIO DYKE-c gr dark, 15%mag, 20%pyx, tr po
470.00	470.44	FE GAB DYKE- c gr dark, 15%mag, 20%cp
470.44	483.94	LANOR-as before with minor pink alteration in fault slips
483.94	487.00	FAULT ZONE in LANOR-pink alteration in fractures/slips
487.00	556.56	ANOR-feldspar alteration to green-brown, grade to 10%opx+mag
556.56	561.40	ANOR-feldspar alteration to pink-brown
561.40	563.42	ANOR- chlorite and pink alteration along slips, tr po
563.42	565.54	LANOR DYKE-c gr grey, 15-20% opx
565.54	581.48	LANOR-c gr, thin veins of chlorite-pink alteration, pyx-mag, pegmatitic

# SUMMARY LITHO LOG LBN-8

## From To Lithological Unit

581.48	583.08	LANOR-feldspar alteration to purplish-brown, tr po
583.08	599.72	ANOR-local patches 10-15%pyx, tr po, same veins above
599.72	601.20	ANOR-pink-purple feldspar alteration
601.20	602.00	ANOR-as before
602.00	627.05	LGAB-m-c gr grey, 10%cpv, 3-5%mag, tr po, peg veins
627.05	634.60	FAULT ZONE in LGAB-fractured+alteration, pegmatitic veins,1%mag
634.60	636.34	LGAB-as before
636.34	643.00	LANOR-BB,c gr patches 2%cpv,2%mag,tr po, feldspar alteration
643.00	644.00	LNOR DYKE?-18% c gr opx, 2% mag
644.00	644.53	MANOR-very c gr 15%cpv, 3% mag, tr po
644.53	648.51	LANOR-as before with thin cpv bands, green alteration slip
648.51	650.14	LNOR/MANOR- 10%opx, 15%mag?
650.14	652.60	LANOR-as before
652.60	654.00	MANOR-c gr grey, 7%opx, 10%mag
654.00	655.47	LANOR-as before with minor thin opx-mag rich band
655.47	655.90	LNOR DYKE-c gr dark grey, 25%opx, 15%mag
655.90	656.00	LANOR-as before
656.00	666.30	LGAB-m-c gr, light grey, 20%opx, 10%mag
666.30	697.84	ANOR-BB-c gr, 5-10% pyx+mag, 1% po, py, plg porphyry (3cm)
697.84	698.18	ALTERATION/FAULT ZONE in ANOR-fracture, chlorite alteration
698.18	698.95	ANOR- as before with minor fault/slips, chlorite alteration
698.95	715.83	MANOR-c gr,brown-grey, 10-15%opx, 3%mag, tr po, chlorite alteration
715.83	717.93	LNOR DYKE-f-m gr, 30%opx
717.93	727.95	MANOR-chlorite alteration with faults, thin pyx rich+poor bands
727.95	728.20	LANOR-c-very c gr, brown fsp alt, 5%mag+pyx patches
728.20	730.95	MANOR-15%opx, 3%mag, thin pyx poor bands, 4%po,cpy
730.95	731.30	LANOR-c gr, blue-brown, f gr green fsp alteration, patchy sulfides
731.30	733.78	LANOR-blue-brown fsp, 10%mag, 15% net po,<1%cpy, py
733.78	740.86	LANOR-c gr, brown fsp with fault alteration bands, py plating
740.86	741.54	LANOR-very c gr, brown fsp (5cm max), tr po
741.54	743.62	LANOR-very c gr dark blue-grey (5cm max),<1%po, tr cpy
743.62	753.06	LANOR-c gr,brown fsp with blue plg porphyry, calcite alteration, po,py
753.06	754.72	FAULT ZONE in LANOR-pale green,fractured, calcite, leucoxene,py
754.72	755.95	LANOR-c gr brown with green fsp, 2%po,<1%py,tr cpy
755.95	756.80	LANOR-25cm wide very c gr blue-gr fsp (GP) in BB,po,py
756.80	757.52	LANOR-c gr, po plating,chlorite with py, 3%cpv mag,15%po
757.52	758.37	LANOR-c gr brown fsp, 15%po,<1%cpy,15%mag, po plating
758.37	758.78	LANOR-ALTERED ZONE-bleached fsp,thin bands of py+chl,1%po
758.78	790.44	LANOR-c gr, brown porphyry fsp, chlorite alteration pyx,fault slip
790.44	794.85	LANOR-very c gr, blue-brown fsp,<1%po, tr mag
794.85	852.83	LANOR-as before with minor Kfsp-qtz bands, tr po
852.83	856.95	LANOR-very c gr, blue-brown fsp,with f gr brown ANOR
856.95	868.55	LANOR- with minor thin mag rich band
868.55	875.20	LANOR-with increasing c gr pyx (5%), minor patches mag-pyx
875.20	880.13	LANOR
880.13	907.68	LANOR-patches of c gr 3-7%cpv,<1%mag, tr po
907.68	998.81	LANOR-c gr brown alteration, patches of po, chlorite-calcite alteration
998.81	999.20	LANOR-c gr, brown-blue fsp, minor green alteration bands
999.20	1000.00	LANOR-v c gr blue (GP) fsp surrounded by brown fsp (BB)
1000.00	1037.00	LANOR-c gr blue fsp, minor brown alteration, plg porphyry (10cm)

**SUMMARY LITHO LOG LBN-8****From To Lithological Unit**

1037.00 1110.75 LANOR-c gr blue with light alteration, 3%mag,2%pyx, tr po, calcite-chlorite alteration  
 1110.75 1114.80 LANOR-fsp alteration due to thin pink-white calcite-chlorite veins  
 1114.80 1115.00 LANOR-c gr dark blue fsp surrounded by light brown-white  
 1115.00 1123.00 LANOR-c gr blue-brown, 3%mag+pyx, tr po  
 1123.00 1124.00 EOH

**ASSAY LOG**

From	To	Width	Sample #	Co %	Cu %	Ni %	% Sulphide	Cu/Ni	Ni/Cu
346.10	347.10	1.00	27351	0.010	0.012	0.002	1	6.000	0.167
347.10	348.10	1.00	27352	0.020	0.018	0.010	1	1.800	0.556
348.10	349.10	1.00	27353	0.009	0.011	0.050	1	0.220	4.545
349.10	350.10	1.00	27354	0.018	0.014	0.090	1	0.156	6.429
350.10	351.10	1.00	27355	0.016	0.010	0.090	1	0.111	9.000
351.10	352.10	1.00	27356	0.015	0.011	0.080	1	0.137	7.273
352.10	353.03	0.93	27357	0.011	0.009	0.010	1	0.900	1.111
353.03	354.03	1.00	27358	0.011	0.008	0.011	1	0.727	1.375
354.03	355.03	1.00	27359	0.012	0.008	0.010	1	0.825	1.212
355.03	355.78	0.75	27360	0.010	0.007	0.009	1	0.824	1.214
355.78	356.53	0.75	27361	0.013	0.010	0.011	1	0.917	1.090
729.26	730.28	1.02	1000	0.009	0.015	0.011	NIL	1.364	0.733
730.28	730.58	0.30	1001	0.012	0.040	0.064	5	0.625	1.600
730.58	730.95	0.37	1002	0.007	0.017	0.029	1	0.586	1.706
730.95	731.45	0.50	1003	0.004	0.008	0.011	1	0.727	1.375
731.45	732.30	0.85	1004	0.005	0.011	0.012	1	0.917	1.091
732.30	732.84	0.54	1005	0.010	0.036	0.055	5	0.655	1.528
732.84	733.52	0.68	1006	0.013	0.066	0.081	15	0.815	1.227
733.52	733.84	0.32	1007	0.042	0.159	0.290	35	0.548	1.824
733.84	734.94	1.10	1008	0.006	0.015	0.018	1	0.833	1.200
734.94	736.16	1.22	1009	0.005	0.010	0.003	1	3.333	0.300
736.16	736.31	0.15	1010	0.002	0.006	0.002	NIL	3.000	0.333
736.31	736.97	0.66	1011	0.005	0.011	0.003	NIL	3.667	0.273
736.97	737.61	0.64	1012	0.006	0.009	0.003	NIL	3.000	0.333
737.61	737.77	0.16	1013	0.006	0.008	0.002	NIL	4.000	0.250
737.77	738.42	0.65	1014	0.004	0.010	0.002	1	5.000	0.200
738.42	739.22	0.80	1015	0.005	0.009	0.004	1	2.250	0.444
739.22	739.95	0.73	1016	0.005	0.012	0.014	1	0.857	1.167
739.95	740.95	1.00	1017	0.005	0.009	0.007	NIL	1.286	0.778
740.95	741.70	0.75	1018	0.004	0.012	0.010	NIL	1.200	0.833
741.70	742.47	0.77	1019	0.004	0.008	0.007	NIL	1.143	0.875
742.47	743.27	0.80	1020	0.006	0.015	0.006	NIL	2.500	0.400
743.27	743.72	0.45	1021	0.008	0.053	0.060	10	0.883	1.132
743.72	744.47	0.75	1022	0.003	0.014	0.013	1	1.077	0.929
744.47	745.07	0.60	1023	0.004	0.015	0.014	1	1.071	0.933
745.07	745.97	0.90	1024	0.006	0.016	0.006	1	2.667	0.375
755.05	755.95	0.90	1025	0.009	0.021	0.025	3	0.840	1.190
755.95	756.80	0.85	1026	0.009	0.028	0.029	3	0.966	1.036
756.80	757.52	0.72	1027	0.030	0.088	0.157	15	0.561	1.784
757.52	758.00	0.48	1028	0.026	0.107	0.143	20	0.748	1.336

From	To	Width	Sample #	Co %	Cu %	Ni %	% Sulphide	Cu/Ni	Ni/Cu
758.00	758.37	0.37	1029	0.021	0.111	0.140	10	0.793	1.261
758.37	758.78	0.41	1030	0.006	0.133	0.049	1	2.714	0.368
758.78	759.30	0.52	1031	0.003	0.019	0.004	NIL	4.750	0.211
759.30	760.40	1.10	1032	0.008	0.015	0.002	NIL	7.500	0.133
763.50	764.00	0.50	1033	0.008	0.026	0.010	1	2.544	0.393
764.00	764.87	0.87	1034	0.007	0.018	0.004	1	4.450	0.225
764.87	765.87	1.00	1035	0.006	0.009	0.005	1	2.000	0.500
765.87	767.17	1.30	1036	0.006	0.015	0.006	1	2.508	0.399
786.90	787.15	0.25	1037	0.010	0.054	0.046	2	1.165	0.858
796.37	797.05	0.68	1038	0.009	0.052	0.070	1	0.743	1.346
797.05	797.98	0.93	1039	0.009	0.054	0.074	1	0.737	1.357
829.93	830.39	0.46	1040	0.013	0.075	0.056	3	1.349	0.741
916.32	916.52	0.20	1041	0.011	0.084	0.062	3	1.354	0.738
921.98	922.18	0.20	1042	0.020	0.068	0.095	5	0.717	1.394
923.09	923.40	0.31	1043	0.045	0.218	0.257	20	0.846	1.182
923.40	923.92	0.52	1044	0.010	0.025	0.027	10	0.930	1.075
923.92	924.12	0.20	1045	0.022	3.900	0.095	NIL	41.270	0.024
1123.14	1123.42	0.28	1046	0.006	0.023	0.014	NIL	1.642	0.609

Hole No: LBN-9    Date: Aug 29-Sep 5,1996    Grid: L2+95 S, 8+20 E

#### SUMMARY LITHO LOG

From    To    Lithological Unit

0.00 62.83 Overburden  
62.83 66.30 LANOR- c gr blue grey with plg porphyry, patches 3-5%mag+pyx  
66.30 67.18 LANOR-3% c gr pyx, <1%mag  
67.18 67.61 LANOR  
67.61 68.10 LANOR-very c gr blue-grey fsp, thin white fsp veins  
68.10 70.72 LANOR-with very thin cpx rich bands  
70.72 71.10 LANOR-very c gr blue fsp with white fsp veinlets  
71.10 83.60 LANOR-increasing to very c gr dark blue fsp,light green alteration,tr sul  
83.60 96.93 ANOR-increasing to 5-7%pyx+mag, less plg porphyry  
96.93 154.90 LANOR-very c gr,blue-grey, thin veins light fsp, green alteration  
154.90 155.06 LANOR-very c gr labradorite rich, blue-grey fsp (10cm max)  
155.06 157.18 LANOR  
157.18 158.59 LNOR DYKE-20%opx, 3%mag,<1%po, tr cpy  
158.59 162.32 LANOR-with several different cpx, opx, mag rich bands  
162.32 162.97 LGAB DYKE-30%mag, 20%cp, <50%plg, 2%po  
162.97 166.83 LANOR-opx and cpx bands with mag  
166.83 167.68 LNOR DYKE-15-20% opx  
167.68 170.03 LANOR-very c gr cpx (5%),1%mag, tr po  
170.03 175.05 LNOR-c gr, grey, 15-20% opx, <1%cp, mag, tr po  
175.05 217.55 LANOR-c gr,blue, light green alteration,<1%mag+cpx, mag veins  
217.55 218.18 ALTERED ZONE in LANOR-f gr light green fsp alteration, 1% mag  
218.18 219.95 LANOR  
219.95 220.67 LANOR-Kfsp-qtz dyke with hem+light green alteration, leucoxene,tr po  
220.67 299.00 LANOR-patches/thin bands of mag,pyx, minor po  
299.00 323.94 ANOR-increasing to foliated 15-20%opx, decreasing to 5%,greenish alteration  
323.94 324.35 ANOR-very c gr blue-grey fsp with beige fsp veinlets



**SUMMARY LITHO LOG LBN-9**

From	To	Lithological Unit
324.35	342.10	ANOR-overall c gr beige-green alteration, decreasing pyx+mag<10%
342.10	366.97	ANOR/MANOR-aligned 10-15%mag, 7-10%pyx, green alteration
366.97	367.59	LANOR-gradual decreasing to <3%pyx, <3%mag
367.59	368.00	LANOR with Kfsp-qtz-biotite dyke, <1%mag
368.00	399.25	ANOR-minor pegmatitic veins, thin po stringers, chlorite alteration
399.25	401.46	ANOR-3-5%cpv, 1%mag, chlorite alteration in fault slip
401.46	403.75	ANOR
403.75	404.00	ANOR with Kfsp-qtz-biotite dyke, pink-white alteration in ANOR
404.00	432.60	LANOR-labradorite-rich, 1-2%pyx+mag, tr po, chlorite alteration, pegmatitic vein
432.60	440.39	FAULT ZONE in LANOR-calcite-chlorite veins/faults, pink alteration
440.39	572.10	LANOR-c gr, blue-grey with green-pink alteration, <5%mag+pyx
572.10	572.73	LANOR-very c gr blue-grey fsp, minor calcite-chlorite alteration bands
572.73	584.21	LANOR-<1%po, 1%mag, <1%cpv, light green alteration
584.21	601.45	ANOR-c gr patchy 3-7%cpv+2%mag, <1%po
601.45	659.00	LANOR-c.gr blue-brown fsp, minor po, cpy, minor pegmatitic vein
659.00	662.00	ANOR-3-5% pyx
662.00	678.00	LANOR-with very thin dark green alteration band
678.00	680.00	ANOR-c gr grey, 3%pyx, 1%mag, tr diss po+cpy
680.00	694.00	ANOR-c gr grey, <2% mag+pyx, minor po-cpy
694.00	695.00	EOH

**ASSAY LOG**

From	To	Width	Sample #	Co %	Cu %	Ni %	% Sulphide	Cu/Ni	Ni/Cu
157.15	157.37	0.22	2001	0.010	0.031	0.017	1	1.824	0.548
157.37	158.00	0.63	2002	0.010	0.009	0.008	1	1.125	0.889
158.00	158.74	0.74	2003	0.007	0.011	0.007	0.5	1.571	0.636
158.74	159.16	0.42	2004	0.011	0.022	0.013	0.5	1.692	0.591
159.16	159.84	0.68	2005	0.008	0.007	0.005	0.5	1.400	0.714
159.84	160.14	0.30	2006	0.010	0.018	0.011	0.5	1.636	0.611
160.14	161.00	0.86	2007	0.007	0.005	0.060	0.5	0.083	12.000
161.00	161.93	0.93	2008	0.007	0.005	0.050	0.5	0.100	10.000
161.93	162.11	0.18	2009	0.010	0.017	0.014	0.5	1.214	0.824
162.11	162.71	0.60	2010	0.010	0.010	0.006	0.5	1.667	0.600
162.71	163.00	0.29	2011	0.012	0.020	0.020	0.5	1.000	1.000
163.00	164.00	1.00	2012	0.007	0.007	0.090	0.5	0.078	12.857
166.35	166.80	0.45	2013	0.006	0.003	0.070	0.5	0.043	23.333
166.88	167.00	0.12	2014	0.011	0.031	0.026	0.5	1.192	0.839
170.50	170.75	0.25	2015	0.011	0.030	0.022	0.5	1.364	0.733
265.77	266.00	0.23	2016	0.006	0.056	0.018	5	3.060	0.327
334.62	335.62	1.00	2017	0.005	0.009	0.007	0.5	1.257	0.796
335.62	336.65	1.03	2018	0.004	0.012	0.010	0.5	1.194	0.838
574.56	574.95	0.39	2019	0.005	0.009	0.006	0.5	1.467	0.682

Hole No: LBN-10      Date: Sep 15-27,1996      Grid: L2+00 S 8+92 E

# SUMMARY LITHO LOG

From To Lithological Unit

0.00	67.00	Overburden
67.00	71.22	LANOR-lg dark grey plg porphyry in buff plg matrix
71.22	76.40	ALTERATION in LANOR-fractures with f gr gr-green alteration; po, cpy
76.40	89.40	LANOR-buff plg matrix with <10%dk grey plg por (max 8 cm)
89.40	89.88	LANOR-as above w. 3% po
89.88	115.70	ANOR-<10%dk grey plg porphyry with grey-buff plg matrix, mag
115.70	115.97	ANOR-grey, equigranular fsp
115.97	118.15	ANOR-<10%dk grey plg porphyry with grey-buff plg matrix, mag
118.15	125.00	ANOR-as above with 0-5-3% po, tr cpy; mag
125.00	180.70	ANOR-buff grey fsp with 10% dk grey (max 7cm) plg porphyry, po
180.70	194.50	ALTERED ANOR-increasing blue-green alteration in matrix, mag vein
194.50	207.87	ANOR-5% dark grey plg porphyry in grey-buff m-c gr plg matrix
207.87	209.54	ANOR-c gr dark grey plg porphyry with few pegmatitic veins, fractured
209.54	235.15	ANOR-m gr, buff-grey with plg porphyry, minor blue-green alteration
235.15	237.40	ANOR-40% c gr dark grey plg porphyry, grey-buff matrix, altered, fractured
237.40	238.52	ANOR-m gr equigranular as before
238.52	238.85	ANOR-30% c gr, dark grey porphyry, fractured +altered matrix
238.85	255.97	ANOR-m gr buff-grey, 2cm dark grey plg porphyry; minor pyx, mag
255.97	256.16	ANOR-20% dark grey porphyry (2cm), blue-green altered matrix, fractured
256.16	264.60	ANOR-m gr with 5%dark grey porphyry (1cm), less altered as above
264.60	264.90	ANOR-20% dark grey porphyry in buff/grey matrix, blue-green alteration, fractured
264.90	317.88	ANOR-c gr, 10-15%dark grey porphyry, blue-green alteration, 1-2%cpv, mag
317.88	318.37	ANOR-c gr, blue-grey fsp, green alteration, 3%po, tr cpy, mag
318.37	330.96	LANOR-same as before with thin pegmatitic veins+alteration
330.96	333.74	LANOR-very c gr (3cm max) blue-grey porphyry
333.74	385.20	ANOR-increasing opx (5-7%), patchy 5-7%mag, pegmatitic veins, alteration, po
385.20	387.73	ANOR-as before with increasing fractured and slips, chlorite alteration
387.73	388.87	Kfsp-qtz dyke in ANOR, fractures/slips, green alteration, tr py
388.87	431.40	ANOR-gradual increase to 7-10% opx, 5%mag, chlorite alteration, pegmatitic vein
431.40	435.62	ANOR-decrease in pyx+mag (total <5%), minor light alteration
435.62	440.00	ANOR-chlorite+beige green alteration
440.00	461.86	ANOR-gradually less alteration to c gr dark blue plg
461.86	635.06	LANOR-gradual increase to light green alteration, chlorite alteration of pyx, tr sulfides
635.06	650.67	MANOR-c gr, blue-grey, 1-10%mag, 3-7%pyx, often as veins
650.67	651.32	ANOR-m gr 7%pyx, 5%mag
651.32	659.96	ANOR-<1%po, calcite/chlorite alteration veins
659.96	672.50	ANOR-5-7%pyx+mag, patchy green alteration, tr po, cpy, py
672.50	682.38	ANOR-c gr, 2%mag, 3-5%pyx, tr-<1%po
682.38	683.86	ANOR
683.86	721.25	MANOR-m-c gr, 15%opx, 3-5%mag, <1%po
721.25	725.33	LANOR-c gr, alteration brown-green fsp, 1-2cm chlorite, 3%pyx, 1%mag
725.33	726.94	ANOR-5%pyx, 1%mag
726.94	728.86	LANOR-white-green altered "bleached" fsp, 2%mag, 1%pyx
728.86	750.32	MANOR-c gr, 5-20%cpv, 3%mag, patches LANOR, tr po, chlorite alteration
750.32	753.25	ALTERED ZONE in ANOR-f gr, green alteration, very thin chlorite alteration vein
753.25	755.60	MANOR-as before
755.60	756.65	LANOR-blue-grey with green alteration
756.65	779.44	MANOR-as before

**SUMMARY LITHO LOG LBN-10**

From	To	Lithological Unit
779.44	795.69	LANOR-c gr, grey, m-c gr 3%pyx, 1%mag, <1%po, <1%cpy, alteration
795.69	795.99	LANOR-as before with 5%sul (po,cpy)
795.99	799.10	LANOR-as before, <1%sul
799.10	799.71	MANOR-m gr, 15%pyx, 2% diss po
799.71	807.94	LANOR-as before with <1% sul
807.94	814.70	ALTERED ZONE in LANOR-f gr, light green-grey, calcite, <1%pyx,py
814.70	823.22	LANOR-as before
823.22	825.48	LANOR-as before with chlorite-calcite alteration veins, fractures/gouge
825.48	841.84	LANOR-as before with thin po rich and mag rich veins
841.84	847.70	LANOR-3-5%pyx
847.70	848.00	LANOR-c gr, blue-grey (BB), 1%chlorite pyx, <1%mag, tr po
848.00	848.47	ALTERED ZONE in LANOR-chlorite-calcite (pink-green) soft alteration
848.47	856.00	LANOR-as above with no alteration
856.00	857.00	EOH

**ASSAY LOG**

From	To	Width	Sample #	Co %	Cu %	Ni %	% Sulphide	Cu/Ni	Ni/Cu
71.22	71.82	0.60	3000	0.007	0.027	0.029	1	0.938	1.066
71.82	72.60	0.78	3001	0.006	0.011	0.014	0.5	0.796	1.257
72.60	73.60	1.00	3002	0.008	0.016	0.019	0.5	0.800	1.250
73.60	74.26	0.66	3003	0.007	0.034	0.082	2	0.422	2.368
74.26	75.00	0.74	3004	0.009	0.026	0.044	1	0.591	1.691
75.00	76.00	1.00	3005	0.006	0.029	0.045	1	0.645	1.549
76.00	76.40	0.40	3006	0.004	0.017	0.026	1	0.654	1.530
76.40	76.80	0.40	3007	0.007	0.030	0.022	3	1.409	0.710
76.80	77.20	0.40	3008	0.008	0.046	0.056	0.5	0.813	1.231
77.20	77.60	0.40	3009	0.006	0.047	0.042	0.5	1.134	0.882
77.60	78.00	0.40	3010	0.009	0.066	0.067	0.5	0.987	1.014
78.00	78.40	0.40	3011	0.009	0.063	0.060	0.5	1.047	0.955
78.40	78.80	0.40	3012	0.011	0.084	0.071	0.5	1.18	0.845
78.80	79.20	0.40	3013	0.011	0.091	0.093	3	0.98	1.020
79.20	79.60	0.40	3014	0.009	0.084	0.077	2	1.098	0.911
79.60	80.00	0.40	3015	0.006	0.059	0.062	1	0.955	1.047
80.00	80.40	0.40	3016	0.010	0.024	0.009	3	2.693	0.371
80.40	80.80	0.40	3017	0.009	0.007	0.009	0.5	0.710	1.409
80.80	81.20	0.40	3018	0.006	0.008	0.007	1	1.014	0.987
81.20	81.60	0.40	3019	0.008	0.011	0.014	0.5	0.799	1.252
81.60	82.00	0.40	3020	0.006	0.010	0.011	0.5	0.833	1.200
82.00	82.40	0.40	3021	0.006	0.010	0.011	0.5	0.916	1.092
82.40	82.80	0.40	3022	0.004	0.006	0.009	0.5	0.663	1.509
82.80	83.20	0.40	3023	0.002	0.007	0.010	0.5	0.637	1.569
83.20	83.60	0.40	3024	0.002	0.007	0.009	0.5	0.776	1.288
83.60	84.00	0.40	3025	0.003	0.008	0.011	0.5	0.750	1.333
84.00	84.40	0.40	3026	0.002	0.008	0.009	0.5	0.798	1.253
84.40	84.80	0.40	3027	0.005	0.009	0.009	0.5	0.904	1.106
84.80	85.20	0.40	3028	0.013	0.042	0.043	0.5	0.977	1.024
85.20	85.60	0.40	3029	0.001	0.022	0.031	3	0.701	1.427
85.60	86.00	0.40	3030	0.014	0.031	0.069	5	0.446	2.241
86.00	86.40	0.40	3031	0.006	0.015	0.021	2	0.713	1.403
86.40	86.80	0.40	3032	0.005	0.016	0.015	5	1.061	0.943
86.80	87.20	0.40	3033	0.004	0.013	0.014	1	0.921	1.086
87.20	87.60	0.40	3034	0.006	0.017	0.021	2	0.820	1.219

From	To	Width	Sample #	Co %	Cu %	Ni %	% Sulphide	Cu/Ni	Ni/Cu
806.54	807.65	1.11	3035	0.005	0.010	0.008	0.5	1.250	0.800
807.65	807.93	0.28	3036	0.015	0.039	0.058	10	0.678	1.476
808.60	808.92	0.32	3037	0.007	0.020	0.029	1	0.713	1.402
818.28	818.98	0.70	3038	0.012	0.034	0.047	3	0.716	1.396
821.54	821.90	0.36	3039	0.015	0.053	0.060	2	0.877	1.140
832.78	833.00	0.22	3040	0.012	0.027	0.049	3	0.544	1.838
839.36	839.86	0.50	3041	0.007	0.022	0.016	0.5	1.358	0.736
841.30	841.55	0.25	3042	0.004	0.032	0.020	1	1.623	0.616

Hole No: LBN-11      Date: Sep 3-19,1997      Grid: 2+95 S, 8+20 E

#### SUMMARY LITHO LOG

From    To    Lithological Unit

0.00	67.84	Overburden
67.84	88.43	LANOR-c gr, blue-grey, green alteration fsp, <5%pyx, 1-3%mag
88.43	88.73	FE-DIO DYKE-m-c gr, dark grey, 20%pyx, 15%mag, ol? <1%, 1%po
88.73	94.80	LANOR-as above
94.80	140.00	ANOR-increasing pyx (7%), chlorite alteration, green fsp
140.00	167.65	LANOR-decreasing plg porphyry (<1%), mag+pyx(3%), green alteration
167.65	167.90	FE DIO DYKE-m gr equigranular, 25%mag, 20%pyx, 2%ol?
167.90	176.38	LANOR-as before
176.38	187.80	ANOR-5-7%opx with mag(0.5-1cm)
187.80	219.57	LANOR-minor po-cpy patches, chlorite fracture planes, pegmatitic vein
219.57	220.97	LANOR-very c gr mortar texture, brown fsp, 3%patchy c gr opx
220.97	272.00	LANOR-c gr, green fsp alteration, minor pyx+mag, tr po
272.00	292.70	LANOR-c gr, blue-grey, pegmatitic vein, <3%mag+pyx, decreasing green alteration
292.70	293.30	FRACTURED ZONE in LANOR-with chlorite alteration
293.30	294.25	LANOR-white+green(chlorite) alteration
294.25	294.90	LGAB-c gr, salt+pepper, 20%opx (max 2x4cm), chlorite alteration
294.90	298.00	LANOR-chlorite alteration
298.00	300.30	FAULT ZONE in LANOR-fractured, gouge, pegmatitic dyke
300.30	329.00	LANOR-3-5%mag+pyx, chlorite alteration, minor 1cm plg porphyry
329.00	341.54	LANOR-increasing pink alteration in fsp, thin mag rich veins
341.54	342.00	MANOR-very c gr anhedral opx, aligned
342.00	351.60	LANOR- as before
351.60	376.03	ANOR-c gr, green alteration, 2-7%pyx, 2-5%mag, py-po-mag bands
376.03	382.74	LANOR-pink-purple fsp alteration with dark purple plg porphyry, tr po
382.74	400.00	ANOR-as before
400.00	400.65	LANOR-very c gr, mortar texture, light grey-green alteration, 2%cgr opx
400.65	438.50	LANOR-c gr, grey-green alteration, patches 5%chlorite pyx+mag, po
438.50	438.83	ANOR-c gr 7%cp, <1%po, <1%py?
438.83	510.90	LANOR-c gr, dark blue plg porphyry, green alteration, <5%mag+pyx
510.90	512.66	LANOR-intense f gr green alteration, minor mag
512.66	517.92	LANOR-less green alteration
517.92	547.00	LANOR-soft pink-white alteration, cracked core
547.00	585.00	LANO -c gr, blue, mortar texture, <5%pyx+mag, tr po, thin alteration veins
585.00	595.40	LANOR-c gr, dark blue, mortar texture, patches of po, tr cpy
595.40	600.72	LANOR-as above but brown, beige-light green alteration bands
600.72	601.18	LGAB/LNOR-m gr, 15%pyx, <1%diss po
601.18	614.50	LANOR-blue, minor mag, diss po, cpy, py
614.50	615.95	LANOR-net-bleb po (1%), tr cpy, <<1%py

**SUMMARY LITHO LOG LBN-11**

From	To	Lithological Unit
615.95	616.84	LANOR-minor diss po
616.84	617.00	LANOR-semi-massive - bleb po (25%),<1%cpy
617.00	635.05	LANOR-patches-bands po from 2-20%,<1%cpy, py
635.05	635.90	LANOR-semimassive-bleb po (30%),1%cpy, 3%cpv, plg porphyry
635.90	636.13	LANOR-minor po (~1%)
636.13	639.30	LANOR-patches semi-mass-bleb po(15-60%),<1%cpy
639.30	651.83	LANOR-c gr, dark blue, minor green alteration, po-cpy continued
651.83	654.65	LANOR-c gr,brown, mortar texture, dark blue plg porphyry, tr po
654.65	655.32	LANOR-f gr, light green-white, bleb-diss po(15%),<1%py
655.32	656.00	LANOR-continued patches semi-mass-bleb-net po
656.00	657.00	LANOR-brown alteration with dark blue plg porphyry, po,py,cpy
657.00	659.00	LANOR-green alteration, po-cpy
659.00	661.00	LANOR-blue mortar texture, po-cpy
661.00	668.00	LANOR-brown, mortar texture, massive-semi-mass po, with cpy,py
668.00	672.06	LANOR-increasing light green alteration, decreasing po-cpy, white alteration veins
672.06	673.45	LANOR-85%mass po,<<1% cpy at lower contact
673.45	710.05	LANOR-brown, c gr, less alteration, small patches po,cpy,py?
710.05	710.88	MANOR-c gr, brown, 10%cumulate opx
710.88	716.84	LANOR-as before
716.84	722.73	ANOR-c gr, brown, 7%opx, tr-<1%py-po, minor chlorite alteration
722.73	728.17	LANOR-as before
728.17	730.50	LANOR-fractured, cracked
730.50	740.00	LANOR-brown, c gr continued with minor po-cpy-py, green alteration
740.00	741.00	LANOR-slight increasing blue, decreasing brown fsp
741.00	741.37	EOH

**ASSAY LOG**

From	To	Width	Sample #	Co %	Cu %	Ni %	% Sulphide	Cu/Ni	Ni/Cu
601.22	601.62	0.40	11051	0.002	0.005	0.004	1	1.250	0.800
608.55	608.70	0.15	11052	0.014	0.051	0.031	15	1.645	0.608
614.50	615.12	0.62	11053	0.003	0.010	0.006	1	1.667	0.600
615.12	615.49	0.37	11054	0.011	0.037	0.024	5	1.542	0.649
616.62	616.84	0.22	11055	0.005	0.014	0.010	2	1.400	0.714
616.84	617.00	0.16	11056	0.038	0.119	0.097	25	1.227	0.815
619.67	619.79	0.12	11057	0.009	0.023	0.022	30	1.045	0.957
620.00	620.10	0.10	11058	0.001	0.002	0.005	3	0.400	2.500
620.50	620.79	0.29	11059	0.001	0.002	0.003	1	0.667	1.500
624.42	624.60	0.18	11061	0.004	0.012	0.012	2	1.000	1.000
626.58	626.74	0.16	11062	0.003	0.008	0.006	2	1.333	0.750
627.35	627.85	0.50	11063	0.024	0.100	0.054	20	1.852	0.540
629.83	630.00	0.17	110631	0.004	0.013	0.004	1	3.250	0.308
630.88	631.08	0.20	11064	0.022	0.131	0.047	20	2.787	0.359
631.08	631.38	0.30	11064	0.067	0.190	0.162	60	1.173	0.853
631.38	632.00	0.62	11065	0.002	0.011	0.004	1	2.750	0.364
632.37	632.53	0.16	11067	0.014	0.056	0.030	7	1.867	0.536
635.05	635.50	0.45	11068	0.020	0.085	0.046	10	1.848	0.541
635.50	635.90	0.40	11069	0.043	0.154	0.102	30	1.510	0.662
635.90	636.90	1.00	11070	0.023	0.082	0.053	15	1.547	0.646
636.90	637.10	0.20	11071	0.050	0.145	0.124	25	1.169	0.855
637.10	638.00	0.90	11072	0.021	0.096	0.048	15	2.000	0.500
638.00	638.12	0.12	11073	0.022	0.065	0.048	10	1.354	0.738

From	To	Width	Sample #	Co %	Cu %	Ni %	% Sulphide	Cu/Ni	Ni/Cu
638.12	638.34	0.22	11074	0.017	0.075	0.038	15	1.974	0.507
638.34	638.54	0.20	11075	0.031	0.209	0.071	7	2.944	0.340
638.54	638.98	0.44	11076	0.066	0.197	0.175	25	1.126	0.888
638.98	639.28	0.30	11077	0.044	0.199	0.101	40	1.970	0.508
642.28	642.50	0.22	11078	0.054	0.148	0.135	40	1.096	0.912
642.50	643.10	0.60	11079	0.001	0.002	0.001	0.3	2.000	0.500
643.10	643.38	0.28	11080	0.004	0.014	0.009	7	1.556	0.643
643.38	643.90	0.52	11081	0.001	0.003	0.005	0.3	0.600	1.667
643.90	644.00	0.10	11082	0.056	0.236	0.145	50	1.628	0.614
644.00	644.50	0.50	11083	0.028	0.109	0.068	20	1.603	0.624
644.50	644.70	0.20	11084	0.018	0.069	0.044	10	1.568	0.638
644.70	645.20	0.50	11085	0.001	0.002	0.004	0.3	0.500	2.000
645.20	645.47	0.27	11086	0.011	0.060	0.024	5	2.500	0.400
645.47	646.00	0.53	11087	0.088	0.206	0.240	90	0.858	1.165
646.00	646.45	0.45	11088	0.096	0.065	0.280	90	0.232	4.308
646.45	646.70	0.25	11089	0.012	0.191	0.025	0.1	7.640	0.131
646.70	646.80	0.10	11090	0.004	0.282	0.007	2	40.286	0.025
646.80	647.23	0.43	11091	0.041	0.412	0.104	25	3.962	0.252
647.23	647.35	0.12	11092	0.075	0.600	0.198	70	3.033	0.330
647.35	647.47	0.12	11093	0.013	0.109	0.027	3	4.037	0.248
647.47	647.85	0.38	11094	0.001	0.004	0.001	0.1	4.000	0.250
647.85	648.00	0.15	11095	0.007	0.023	0.015	3	1.533	0.652
648.00	648.50	0.50	11096	0.001	0.004	0.003	1	1.333	0.750
648.50	649.05	0.55	11097	0.002	0.011	0.004	1	2.750	0.364
649.05	649.20	0.15	11098	0.016	0.068	0.039	3	1.744	0.574
649.20	649.60	0.40	11099	0.003	0.008	0.006	1	1.333	0.750
649.60	650.10	0.50	11100	0.003	0.008	0.007	0.3	1.143	0.875
650.10	650.38	0.28	11101	0.031	0.072	0.074	25	0.973	1.028
650.38	650.63	0.25	11102	0.001	0.002	0.003	0.1	0.667	1.500
650.63	650.98	0.35	11103	0.022	0.212	0.053	10	4.000	0.250
650.98	651.08	0.10	11104	0.002	0.007	0.006	0.3	1.167	0.857
651.08	651.24	0.16	11105	0.017	0.175	0.040	7	4.375	0.229
651.24	651.83	0.20	11106	0.054	0.147	0.129	45	1.140	0.878
652.70	652.83	0.13	11107	0.009	0.029	0.019	5	1.526	0.655
654.65	655.32	0.67	11108	0.017	0.070	0.041	15	1.707	0.586
655.32	655.48	0.16	11109	0.069	0.660	0.154	50	4.286	0.233
655.48	655.68	0.20	11110	0.004	0.034	0.009	2	3.778	0.265
655.68	655.88	0.20	11111	0.029	0.228	0.068	20	3.353	0.298
655.88	656.08	0.20	11112	0.051	0.570	0.118	35	4.831	0.207
656.08	656.23	0.15	11113	0.086	0.590	0.204	80	2.892	0.346
656.23	656.35	0.12	11114	0.017	0.060	0.040	3	1.500	0.667
656.35	656.80	0.45	11115	0.006	0.023	0.011	2	2.091	0.478
656.80	657.25	0.45	11116	0.029	0.079	0.068	30	1.162	0.861
657.25	657.55	0.30	11117	0.003	0.009	0.004	0.1	2.250	0.444
659.20	659.45	0.25	11118	0.018	0.037	0.041	15	0.902	1.108
661.17	661.65	0.48	11119	0.067	0.241	0.160	30	1.506	0.664
661.65	662.12	0.47	11120	0.001	0.004	0.001	0.1	4.000	0.250
662.12	662.47	0.35	11121	0.007	0.021	0.014	2	1.521	0.657
662.47	662.80	0.33	11122	0.052	0.249	0.133	35	1.872	0.534
662.80	663.70	0.90	11123	0.001	0.002	0.001	NIL	2.000	0.500
663.70	664.15	0.45	11124	0.010	0.041	0.022	5	1.864	0.537
664.15	664.33	0.18	11125	0.055	0.224	0.133	25	1.684	0.594
664.33	664.83	0.50	11126	0.077	0.540	0.184	75	2.935	0.341
664.83	664.95	0.12	11127	0.012	0.108	0.025	5	4.320	0.231

From	To	Width	Sample #	Co %	Cu %	Ni %	% Sulphide	Cu/Ni	Ni/Cu
664.95	665.35	0.40	11128	0.096	0.336	0.231	90	1.455	0.688
665.35	665.80	0.45	11129	0.111	0.296	0.275	95	1.076	0.929
665.80	666.53	0.73	11130	0.097	0.326	0.232	90	1.405	0.712
666.53	666.83	0.30	11131	0.004	0.012	0.007	0.1	1.714	0.583
666.83	667.20	0.37	11132	0.102	0.238	0.255	95	0.933	1.071
667.20	667.70	0.50	11133	0.005	0.121	0.011	0.1	11.000	0.091
667.70	667.85	0.15	11134	0.095	0.095	0.233	90	0.408	2.453
667.85	668.00	0.15	11135	0.001	0.002	0.002	NIL	1.000	1.000
668.00	668.15	0.15	11136	0.086	0.135	0.210	60	0.643	1.556
668.15	668.35	0.20	11137	0.017	0.064	0.038	7	1.684	0.594
668.35	669.18	0.83	11138	0.002	0.002	0.002	0.1	1.000	1.000
669.18	669.36	0.18	11139	0.011	0.024	0.019	2	1.263	0.792
672.60	673.05	0.45	11140	0.004	0.016	0.008	NIL	2.000	0.500
673.05	673.47	0.42	11141	0.099	0.104	0.250	85	0.416	2.404
673.47	674.00	0.53	11142	0.001	0.003	0.002	NIL	1.500	0.667
679.00	679.15	0.15	11143	0.034	0.097	0.103	15	0.942	1.062
679.15	679.65	0.50	11144	0.007	0.022	0.014	3	1.571	0.636
679.65	680.10	0.45	11145	0.005	0.014	0.012	0.1	1.167	0.857
688.86	689.04	0.18	11146	0.052	0.135	0.203	30	1.233	1.504
692.18	692.28	0.10	11147	0.014	0.053	0.043	15	NIL	0.811
722.00	722.46	0.46	11148	NA	NA	NA	0.5	NA	NA

Hole No: LBN-12      Date: Sep 21-Oct 02, 1997      GRID: 2+95 S, 8+20 E

#### SUMMARY LITHO LOG

From      To      Lithological Unit

0.00 65.15 Overburden  
65.15 83.00 LANOR-c gr, blue-grey, 1-2% pyx-mag, lg porphyry (max10cm)  
83.00 84.30 ANOR-c gr, 7-10%opx with few lg blue plg porphyry  
84.30 89.67 LANOR-c gr, 1-2%pyx+mag as before  
89.67 90.67 LANOR-very c gr blue porphyry (2-3cm)  
90.67 92.70 LANOR-c gr, 1-2%pyx-mag, very thin mag+pyx rich veins  
92.70 94.56 ANOR-c gr, 7-10%opx, few large plg porphyry  
94.56 105.47 LANOR-m-c gr, increasing to green alteration fsp, few plg porphyry  
105.47 110.13 LANOR-very c gr (GP), dark purple-brown plg porphyry, tr po  
110.13 130.27 LANOR-2-3%pyx, <1%mag, increasing light green alteration  
130.27 130.88 ANOR-coarser gr, tan 7%opx  
130.88 162.60 LANOR-m gr, light green alteration, dark blue plg porphyry, tr po  
162.60 166.88 ANOR-very c gr (max 5x2cm) 7%opx, light brown-pink-green alteration, tr py  
166.88 187.68 LANOR-increasing Kfsp-qtz pegmatitic veins, fracturing  
187.68 187.90 LANOR-very c gr, dark blue plg (GP)  
187.90 287.00 LANOR-mag 3%, max 5% opx, green fsp alteration, pegmatitic veins  
287.00 330.62 LANOR-dark blue, green fsp alteration, <1%mag, tr po, pegmatitic veins  
330.62 331.70 FAULT ZONE in LANOR-chlorite-pink-purple  
331.70 348.73 LANOR-5%pyx+mag, chlorite-talc veins, purple-green altered fsp  
348.73 396.00 LANOR-light blue-grey altered, minor mag+pyx (patchy to 7%), po  
396.00 398.95 LANOR-grade to c gr, dark blue with rare 1cm plg porphyry, pegmatitic veins  
398.95 399.28 LANOR-very c gr plg (GP)  
399.28 412.00 LANOR-tr diss po  
412.00 422.50 LANOR-blue mortar texture  
422.50 503.10 LANOR-green altered, dark blue mortar texture, plg porphyry, talc vein

**SUMMARY LITHO LOG LBN-12****From To Lithological Unit**

503.10	503.50	LANOR-light grey altered with pink-white alteration
503.50	534.55	LANOR-c gr, dark blue, pink alteration veins, green alteration
534.55	537.36	LANOR-light green alteration <0.5 cm blue plg porphyry
537.36	560.00	LANOR-with tr diss po
560.00	588.36	LANOR-increasing dark blue, mortar texture with minor green alteration
588.36	588.60	LANOR-light green alteration in blue ANOR, green alteration bands
588.60	630.00	LANOR-same dark blue mortar texture
630.00	654.00	LANOR-dark blue fsp, increasing white alteration, patchy 3-5%cpix+mag
654.00	689.45	LANOR-gradually to brown matrix, dark blue 0.5cm plg porphyry
689.45	756.00	LANOR-gradually to brown-blue fsp, increasing white alteration, 3-5%pyx+mag
756.00	757.00	EOH

**ASSAY LOG - assay data not available for this study**

From	To	Width	Sample #	Co %	Cu %	Ni %	% Sulphide	Cu/Ni	Ni/Cu
345.70	346.20	0.50	12100	N.A.	N.A.	N.A.	0.5	N.A.	N.A.
349.14	349.59	0.45	12101	N.A.	N.A.	N.A.	0.5	N.A.	N.A.
351.13	352.08	0.95	12102	N.A.	N.A.	N.A.	0.5	N.A.	N.A.
628.86	628.96	0.10	12103	N.A.	N.A.	N.A.	1.0	N.A.	N.A.
636.15	636.31	0.16	12104	N.A.	N.A.	N.A.	0.5	N.A.	N.A.
637.41	637.61	0.20	12105	N.A.	N.A.	N.A.	0.5	N.A.	N.A.
640.66	640.83	0.17	12106	N.A.	N.A.	N.A.	0.5	N.A.	N.A.
647.47	647.57	0.10	12107	N.A.	N.A.	N.A.	0.5	N.A.	N.A.
650.60	650.77	0.17	12108	N.A.	N.A.	N.A.	0.2	N.A.	N.A.
672.55	672.91	0.36	12109	N.A.	N.A.	N.A.	0.5	N.A.	N.A.
672.91	673.06	0.15	12110	N.A.	N.A.	N.A.	1.0	N.A.	N.A.
675.95	676.05	0.10	12111	N.A.	N.A.	N.A.	0.5	N.A.	N.A.
755.34	755.48	0.14	12112	N.A.	N.A.	N.A.	1.0	N.A.	N.A.



**Appendix A2.3 Additional assay results of selected samples from the Cirque property.**

**Selected core samples assayed by Chauncey Laboratories for Cartaway Resources in 1998.**

DDH: LBN-96-8

Sample	To	From	% Sulphide	% Co	%Cu	%Ni	Au (ppb)	Pd (ppb)	Pt (ppb)
27351	346.10	347.10	<1	0.01	0.01	0.00	35	<15	<30
27352	347.10	348.10	<1	0.02	0.02	0.01	10	<15	<30
27363	348.10	349.10	<1	0.01	0.01	0.01	24	<15	<30
27354	349.10	350.10	1	0.02	0.01	0.01	32	<15	<30
27355	350.10	351.10	<1	0.02	0.01	0.01	11	<15	<30
27356	351.10	352.10	5	0.02	0.01	0.01	15	<15	<30
27357	352.10	353.03	<1	0.01	0.01	0.01	13	<15	<30
27358	353.03	354.03	<1	0.01	0.01	0.01	10	<15	<30
27359	354.03	355.05	<1	0.01	0.01	0.01	11	<15	<30
27360	355.03	355.78	<1	0.01	0.01	0.01	10	<15	<30
27361	355.78	356.53	<1	0.01	0.01	0.01	16	<15	<30

DDH: LBN-98-1

Sample No.	536690	536691	536692	536693	536694	536695	536696	536697	536698	536699
Interval (m)	8.10-9.10	9.10-9.70	9.70-10.70	12.35-12.70	12.70-13.33	13.33-14.00	15.60-16.60	26.35-26.50	30.50-31.28	32.00-33.00
%Sulphur	2	60	1	5	1	5	10	30	5	10
Ag	<0.1	<0.1	<0.1	<0.1	<0.1	<0.1	<0.1	<0.1	<0.1	<0.1
Al	14.40%	7.80%	12.60%	13.50%	13.30%	12.70%	9.70%	9.50%	11.60%	9.90%
As	<10	<10	<10	<10	<10	<10	<10	<10	<10	<10
Bl	38	78	38	73	35	75	37	19	23	20
Ca	1.50%	0.60%	1.80%	1.10%	1.90%	1.30%	0.70%	0.60%	1.00%	0.90%
Cd	<10	<10	<10	<10	<10	<10	<10	<10	<10	<10
Co	56	1120	56	251	48	107	489	573	145	377
Cr	192	613	145	368	105	224	431	487	222	5059
Cu	221	2361	77	678	88	322	1369	2863	319	1091
Fe	4.80%	38.10%	2.90%	9.70%	1.90%	3.90%	19.60%	23.90%	4.80%	14.90%
Mg	0.70%	0.20%	0.50%	0.10%	0.20%	0.10%	0.20%	0.30%	0.10%	0.20%
Mn	356	171	290	145	171	167	166	191	174	198
Mo	<10	<10	<10	<10	<10	<10	<10	<10	<10	<10
Ni	154	2095	58	435	57	195	841	954	241	655
P	0.05%	0.10%	0.03%	0.05%	0.02%	0.02%	0.07%	0.05%	0.05%	0.04%
Pb	96	218	58	97	38	58	78	95	39	59
S	<10	0.10%	<10	0.06%	<10	0.60%	0.08%	0.06%	0.04%	0.03%
Sb	<10	<10	<10	<10	<10	<10	<10	<10	<10	<10
Sr	18	<10	23	10	28	12	<10	<10	<10	<10
Te	<10	<10	<10	<10	<10	<10	<10	<10	<10	<10
Th	<10	<10	<10	<10	<10	<10	<10	<10	<10	<10
U	<10	<10	<10	<10	<10	<10	<10	<10	<10	<10
V	<10	<10	<10	<10	<10	<10	<10	<10	<10	<10
W	<10	<10	<10	<10	<10	<10	<10	<10	<10	<10
Zn	48	88	43	57	36	19	59	95	58	49

DDH: LBN-96-1

Sample No.	536700	536701	536702	536703	536704	536705	536706	536707	536708	536709
Interval (m)	33.00-34.24	36.40-37.90	37.40-38.40	38.40-39.40	65.00-66.00	66.00-67.00	67.00-68.00	72.63-73.63	73.63-74.00	74.00-75.00
%Sulphur	10	75	5	5	5	10	10	10	10	5
Ag	<0.1	<0.1	<0.1	<0.1	<0.1	<0.1	<0.1	<0.1	<0.1	<0.1
Al	10.80%	4.70%	9.90%	13.90%	15.90%	15.80%	14.90%	15.70%	13.10%	16.40%
As	<10	<10	<10	<10	<10	<10	<10	<10	<10	<10
Bi	35	24	36	20	38	18	41	40	16	38
Ca	1.10%	0.30%	1.30%	1.10%	1.00%	1.70%	1.20%	1.40%	0.80%	1.40%
Cd	<10	<10	<10	<10	<10	<10	<10	<10	<10	<10
Co	363	1036	169	199	279	10	234	246	169	68
Cr	452	2633	338	329	398	159	346	354	301	133
Cu	648	2637	646	528	797	69	524	493	496	195
Fe	13.80%	89.50%	7.90%	8.50%	11.90%	1.90%	9.40%	9.80%	9.40%	2.40%
Mg	0.30%	0.09%	0.40%	0.20%	0.20%	0.50%	0.20%	0.30%	0.07%	0.10%
Mn	275	188	298	279	179	259	122	196	103	97
Mo	<10	<10	<10	<10	<10	<10	<10	<10	<10	<10
Ni	599	2637	348	367	558	90	449	491	403	155
P	0.08%	0.10%	0.05%	0.04%	0.07%	0.02%	0.05%	0.03%	0.05%	0.01%
Pb	50	75	39	28	69	29	37	48	56	35
S	0.05%	0.02%	0.02%	0.02%	0.03%	0.02%	0.04%	0.02%	0.03%	0.02%
Sb	<10	<10	<10	<10	<10	<10	<10	<10	<10	<10
Sr	12	<10	15	10	<10	23	10	15	<10	17
Ta	<10	<10	<10	<10	<10	<10	<10	<10	<10	<10
Th	<10	<10	<10	<10	<10	<10	<10	<10	<10	<10
U	<10	<10	<10	<10	<10	<10	<10	<10	<10	<10
V	<10	<10	<10	<10	<10	<10	<10	<10	<10	<10
W	<10	<10	<10	<10	<10	<10	<10	<10	<10	<10
Zn	57	85	56	59	100	81	47	69	47	48

DDH: LBN-98-1

Sample No.	536710	536711	536712	536713	536714	536715	536716	536717	536718	536719
Interval (m)	75.00-76.00	92.50-93.33	97.40-98.00	99.10-100.30	102.95-103.45	103.45-104.30	104.30-105.55	105.55-106.55	123.55-124.30	121.00-121.50
%Sulphur	10	15	20	60	60	2	20	2	15	15
Ag	<0.1	<0.1	<0.1	<0.1	<0.1	<0.1	<0.1	<0.1	<0.1	<0.1
Al	13.80%	13.80%	12.20%	6.50%	7.50%	15.70%	10.80%	18.80%	14.10%	13.40%
As	<10	<10	<10	<10	<10	<10	<10	<10	<10	<10
Bi	34	26	75	73	34	79	57	18	23	38
Ca	1.00%	1.30%	0.90%	0.40%	0.80%	2.40%	1.00%	1.80%	1.10%	1.50%
Cd	<10	<10	<10	<10	<10	<10	<10	<10	<10	<10
Co	131	540	656	1125	1032	58	688	93	413	811
Cr	243	501	544	629	469	167	452	150	310	395
Cu	356	1572	1313	2814	1310	78	3340	263	750	1501
Fe	5.20%	16.70%	22.50%	41.30%	33.80%	2.00%	24.60%	3.30%	13.30%	19.20%
Mg	0.10%	0.10%	0.20%	0.09%	0.10%	0.20%	0.10%	0.10%	0.30%	0.10%
Mn	113	157	188	159	131	167	196	169	188	122
Mo	<10	<10	<10	<10	<10	<10	<10	<10	<10	<10
Ni	281	1277	1595	3753	2908	49	1768	141	891	1970
P	0.01%	0.04%	0.05%	0.20%	0.10%	0.01%	0.10%	0.01%	0.01%	0.04%
Pb	66	59	28	94	131	86	108	38	56	73
S	0.07%	0.10%	0.03%	0.03%	0.03%	0.04%	0.02%	0.02%	0.20%	0.04%
Sb	<10	<10	<10	<10	<10	<10	<10	<10	<10	<10
Sr	<10	16	10	<10	<10	28	12	21	10	16
Te	<10	<10	<10	<10	<10	<10	<10	<10	<10	<10
Th	<10	<10	<10	<10	<10	<10	<10	<10	<10	<10
U	<10	<10	<10	<10	<10	<10	<10	<10	<10	<10
V	<10	<10	<10	<10	<10	<10	<10	<10	<10	<10
W	<10	<10	<10	<10	<10	<10	<10	<10	<10	<10
Zn	66	79	75	113	84	98	118	56	47	86

DDH: LBN-96-1

Sample No.	538720	538721
Interval (m)	176.22-178.72	176.72-177.22
%Sulphur	3	1
Ag	<0.1	<0.1
Al	19.00%	19.10%
As	<10	<10
Bi	27	24
Ca	2.10%	2.20%
Cd	<10	<10
Co	210	124
Cr	219	238
Cu	571	314
Fe	5.20%	4.80%
Mg	.020%	0.30%
Mn	152	287
Mo	<10	<10
Ni	533	305
P	0.01%	0.04%
Pb	38	19
S	0.06%	0.20%
Sb	<10	<10
Sr	19	25
Te	<10	<10
Th	<10	<10
U	<10	<10
V	<10	<10
W	<10	<10
Zn	77	95

Results are in ppm and %

DDH: LBN-96-1

Sample No. :

Lab. No. :	536697	536698	536699	536700	536701	536702	536703
Ag	<0.1	<0.1	<0.1	<0.1	<0.1	<0.1	<0.1
Al	9.50%	11.60%	9.90%	10.80%	4.70%	9.90%	13.90%
As	<10	<10	<10	<10	<10	<10	<10
Bi	19	23	20	35	24	36	20
Ca	0.60%	1.00%	0.90%	1.10%	0.30%	1.30%	1.10%
Cd	<10	<10	<10	<10	<10	<10	<10
Co	573	145	377	363	1036	169	199
Cr	487	222	5059	452	2633	338	329
Cu	2863	319	1091	648	2637	646	528
Fe	23.90%	4.80%	14.90%	13.80%	89.50%	7.90%	8.50%
Mg	0.30%	0.10%	0.20%	0.30%	0.08%	0.40%	0.20%
Mn	191	174	198	275	188	298	279
Mo	<10	<10	<10	<10	<10	<10	<10
Ni	954	241	655	599	2637	348	367
P	0.05%	0.05%	0.04%	0.08%	0.10%	0.05%	0.04%
Pb	95	39	59	50	75	39	28
S	0.06%	0.04%	0.03%	0.05%	0.02%	0.02%	0.02%
Sb	<10	<10	<10	<10	<10	<10	<10
Sr	<10	<10	<10	12	<10	15	10
Te	<10	<10	<10	<10	<10	<10	<10
Th	<10	<10	<10	<10	<10	<10	<10
U	<10	<10	<10	<10	<10	<10	<10
V	<10	<10	<10	<10	<10	<10	<10
W	<10	<10	<10	<10	<10	<10	<10
Zn	95	58	49	57	85	56	59

Results are in ppm and %.

**Assay results of sulphide-bearing grab samples (outcrop and talus) collected by Cartaway Resources in 1995 (from Cartaway Resources *inhouse* report; Beesley 1996). Samples were assayed by Chauncey Laboratories in Ontario.**

<b>Sample Number</b>	<b>Location + Description</b>	<b>% Ni</b>	<b>% Cu</b>	<b>% Co</b>	<b>Ni:Cu ratio</b>
CQL-2	Talus, massive sulphide	0.22	0.18	0.11	1:0.8
CQL-4	Talus, massive sulphide	0.20	0.23	0.1	1:1.15
CQL-8	Foot of cirque wall, S to SSW, talus, massive sulphide	0.34	0.35	0.09	1:1.03
CQL-9	Foot of cirque wall, NW, talus, massive sulphide	0.18	0.27	0.11	1:1.5
CQL-10	Foot of cirque wall, S to SSW, talus, massive sulphide	0.33	0.61	0.12	1:1.85
CQL-11	Foot of cirque wall, NW, talus, massive sulphide	0.22	0.27	0.09	1:1.23
CQL-12	Foot of cirque wall, S to SSW, talus, massive sulphide	0.36	0.15	0.11	1:1.42
CQL-14	Foot of cirque wall, S to SSW, talus, massive sulphide	0.13	0.32	0.06	1:2.46
CQL-15	South end of cirque wall, talus, massive sulphide	0.20	0.24	0.08	1:1.20
CQL-16	South end of cirque wall, talus, massive sulphide	0.25	0.12	0.09	1:0.48
CQL-17	South end of cirque wall, talus, massive sulphide	0.24	0.28	0.08	1:1.17
CQL-18	South end of cirque wall, talus, massive sulphide	0.24	0.24	0.09	1:1
CQL-50	Anorthosite	0.04	0.03	0.01	1:0.75
CQL-5401	Troctolite	0.006	0.01	0.01	1:1.67
CQL-5402	Anorthosite, rusty	0.01	0.04	0.01	1:4
CQL-5403	Anorthosite, 2% pyrrhotite	0.03	0.05	0.01	1:1.67
CQL-5404	Dunite ?	0.005	0.006	0.008	1:1.20
CQL-5405	Massive sulphide	0.20	0.4	0.09	1:2
CQL-5406	Troctolite, magnetite band	0.01	0.01	0.01	1:1
CQL-5407	Troctolite	0.006	0.006	0.009	1:1
CQL-5408	Anorthosite with orthopyroxene-rich bands	0.01	0.01	0.006	1:1

Assay results of sulphide-bearing grab samples (outcrop and talus) from the Cirque property. Samples were assayed at the Earth Sciences Department, Memorial University of Newfoundland. The symbol \* denotes those samples assayed by Chauncey Laboratories in Ontario for Cartaway Resources.

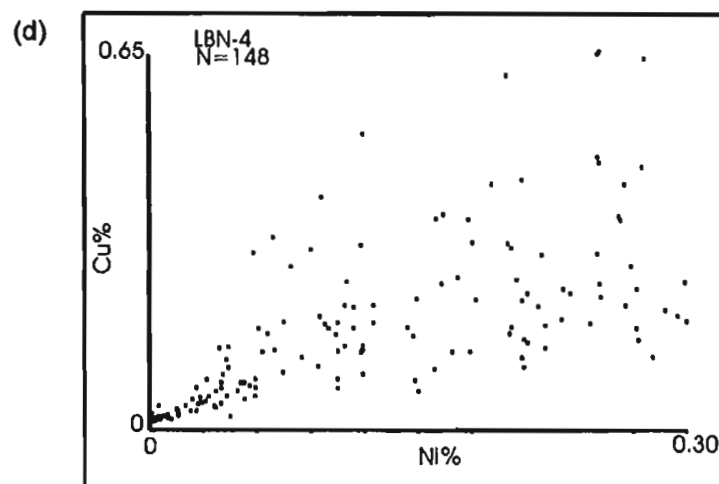
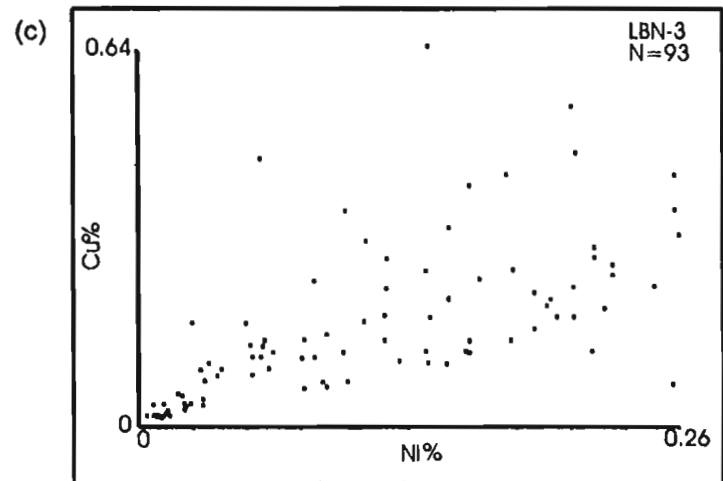
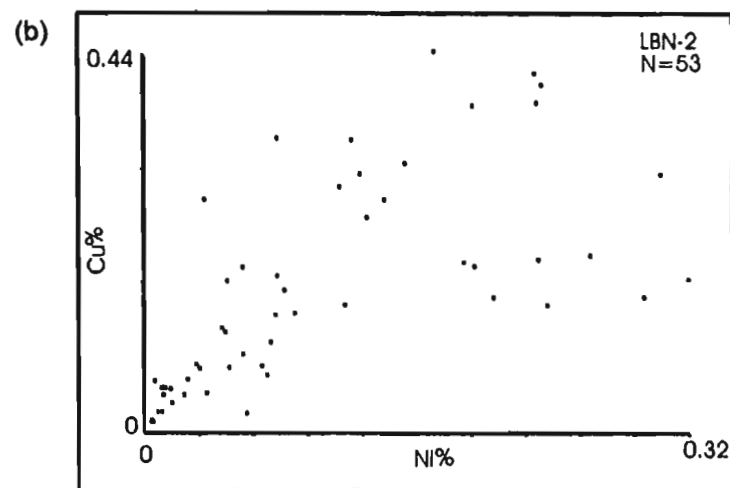
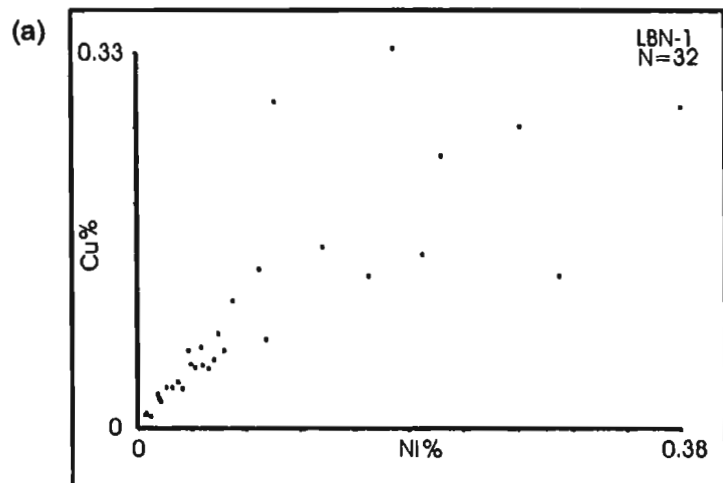
Sample Number	Location + Description	%Ni	%Cu	%Co	Ni:Cu Ratio
LD-96-10	O/c in south arm, green altered An, <1% po, cpy	0.07	0.05	-	1:0.71
LD-96-10*	O/c in south arm, green altered An, <1% po, cpy	0.10	0.06	0.02	1:0.60
LD-96-11*	O/c in south arm, green altered An, <1% po, cpy	0.17	0.12	0.02	1:0.74
LD-96-12	O/c in south arm, rusty An, po, cpy	0.24	0.12	-	1:0.50
LD-96-12*	O/c in south arm, rusty An, po, cpy	0.24	0.16	0.04	1:0.69
LD-96-13*	O/c in south arm, rusty An, po, cpy	0.16	0.10	0.03	1:0.63
LD-96-14*	O/c in south arm, rusty An, po, cpy	0.16	0.10	0.03	1:0.66
LD-96-15*	O/c in south arm, rusty An, po, cpy	0.13	0.09	0.02	1:0.73
LD-96-16*	O/c in south arm, rusty An, po, cpy	0.14	0.13	0.03	1:0.90
LD-96-17*	O/c in south arm, rusty An, po, cpy	0.10	0.09	0.02	1:0.95
LD-96-18*	O/c in south arm, rusty An, po, cpy	0.18	0.09	0.03	1:0.49
LD-96-27	O/c in south arm, near CQL-12, gossanous An, po	0.59	0.13	-	1:0.22
LD-96-29	O/c in south arm, near CQL-12, gossanous An, po	0.42	0.23	-	1:0.55
LD-96-30	O/c in south arm, rusty An, mass po with cpy	0.01	0.06	-	1:6
LD-96-31	O/c in south arm, rusty altered An, mass po	0.07	0.03	-	1:0.43
LD-96-45	Boulder east of Knob Hill, rusty Ferrodiorite	0.21	0.11	-	1:52
LD-96-87	S arm, Gossan#2, talus, purple stained An	0.01	0.05	-	1:5
LD-96-88	S arm, Gossan#2, talus, purple stained An	0.03	0.06	-	1:2
LD-96-90	S arm, Gossan#2, talus, purple stained An	0.40	0.14	-	1:35
LD-96-96	Back wall, Gossan#1, talus, rusty, gossan An	0.08	0.47	-	1:5.88
LD-96-97	Back wall, Gossan#1, talus, rusty, gossan An	0.02	0.12	-	1:600
LD-96-98	Back wall, Gossan#1, talus, rusty, gossan An	0.04	0.12	-	1:3
LD-96-99	Back wall, Gossan#1, talus, rusty, gossan An	0.26	0.28	-	1:1.08
LD-96-101	S arm, Gossan#2, talus, rusty bands in An	0.13	0.49	-	1:3.77
LD-96-105	S arm, Gossan#2, gossanous, altered An with mass po	0.22	0.51	-	1:2.32

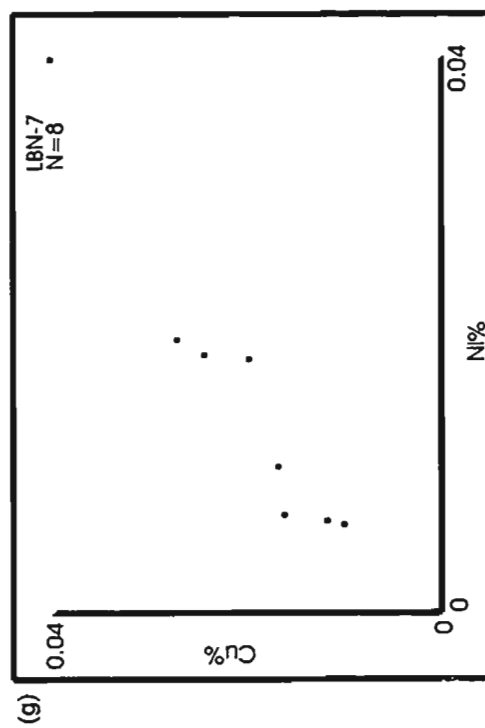
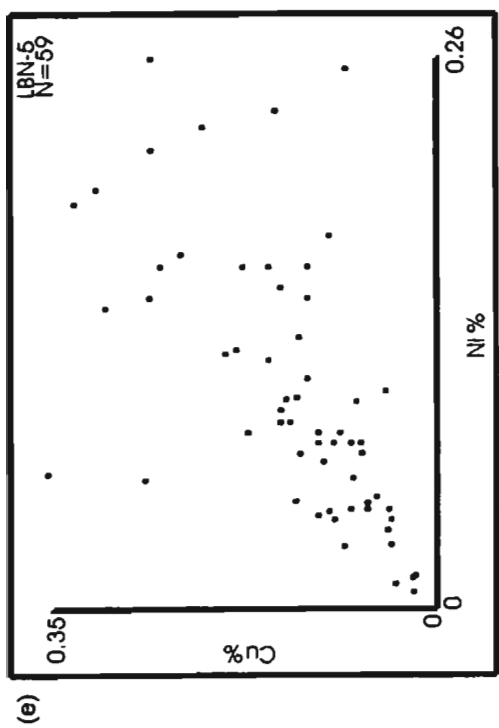
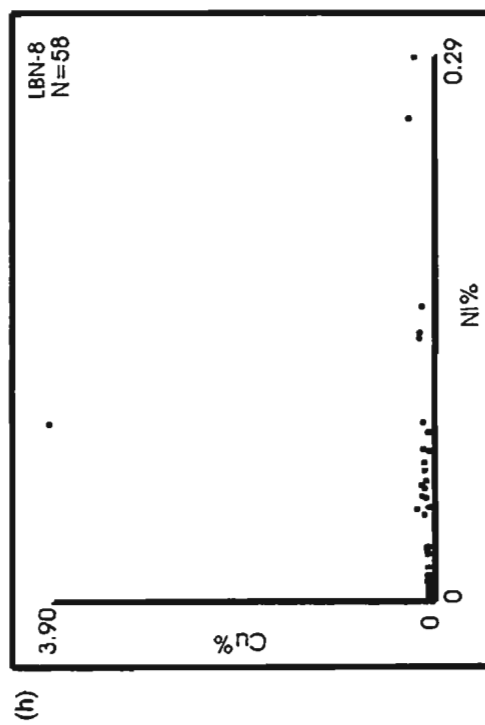
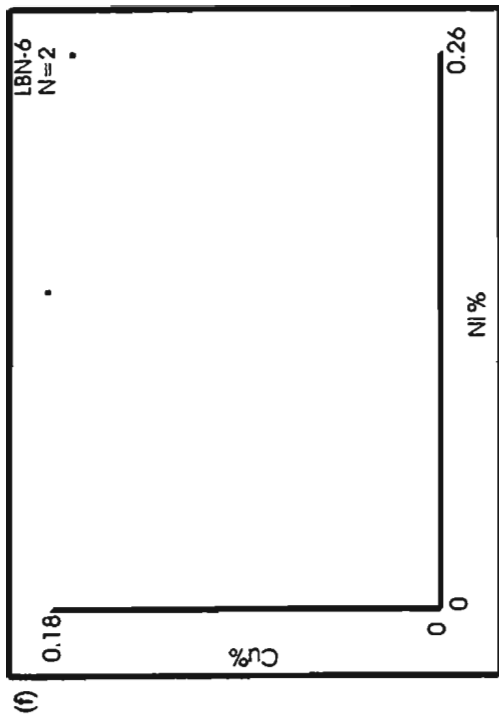


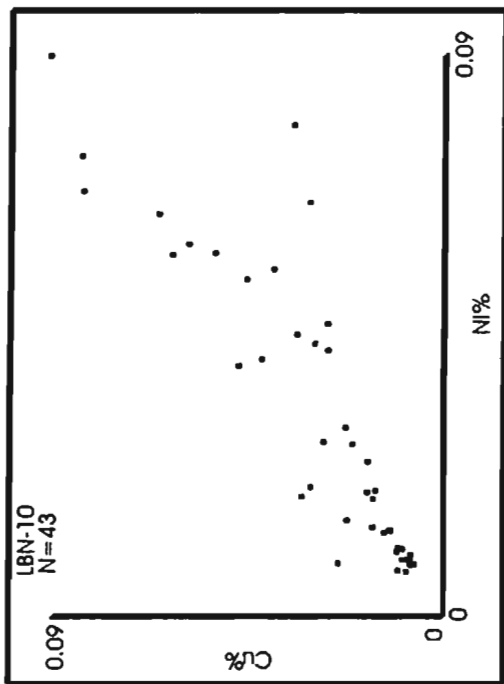
Sample Number	Location + Description	%Ni	%Cu	%Co	Ni:Cu Ratio
LD-96-111	Back wall, below Bleached An, rusty An, 15%po	0.01	0.02	-	1:2
LD-96-113	Back wall, below Bleached An, po-rich An	0.04	0.05	-	1:1.25
LD-96-114	Most E point of N arm, rusty An/Leucogabbro	0.0003	0.001	-	1:0.33
LD-96-156	Top of Cirque (~835m),N corner, rusty An	0.00	0.002	-	-
LD-96-164	Top of Cirque (~890m),to W, rusty altered An	0.02	0.03	-	1:1.5
LD-96-167	Top of Cirque (~969m),to W, An with po, tr cpy	0	0.0001	-	-
LD-96-170	Gossan at top centre Cirque, mass coarse-grained po	0.32	0.10	-	1:0.31
LD-96-170 <sup>2</sup>	Same location as above, ~915m	0.25	0.36	-	1:1.44
LD-96-171	Near above location, coarse grained mass po in An	0.003	0.02	-	1:6.67

Legend: An = anorthosite, po = pyrrhotite, cpy = chalcopyrite, mass = massive, tr = trace, o/c = outcrop

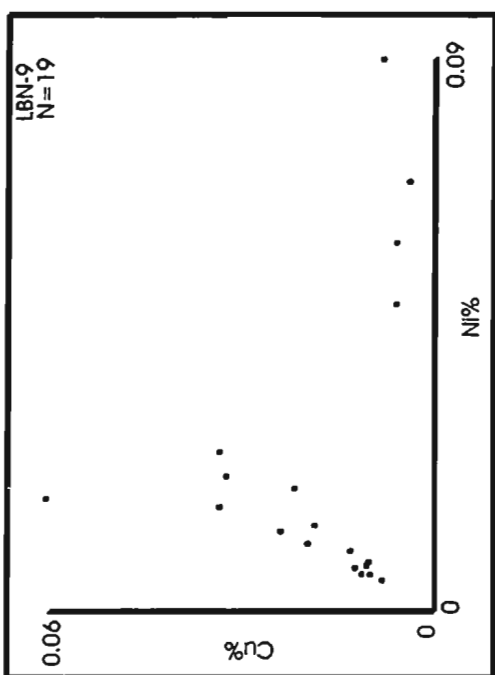
Appendix A2.4.1 Scatter plots of Cu % versus Ni % from drill holes LBN-1 to 11 from the Cirque grid. Data from LBN-12 are not available for this study.



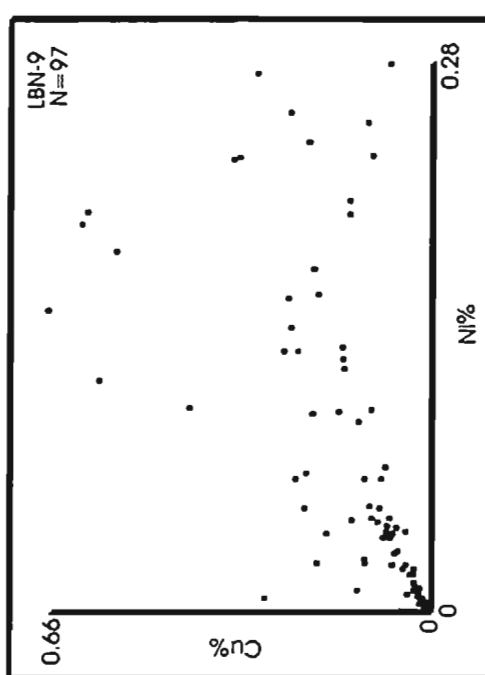




(j)

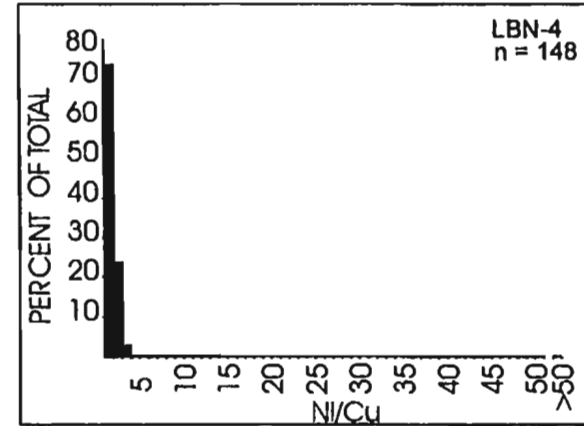
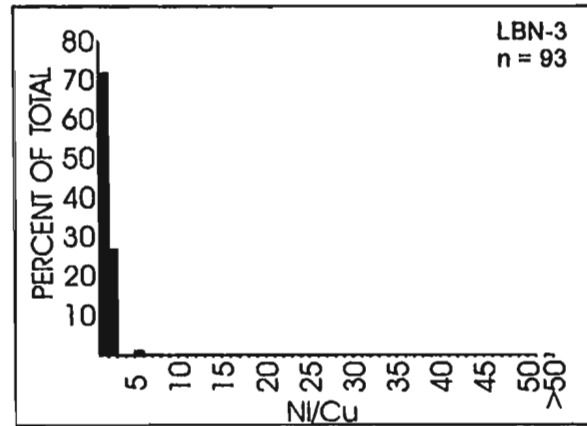
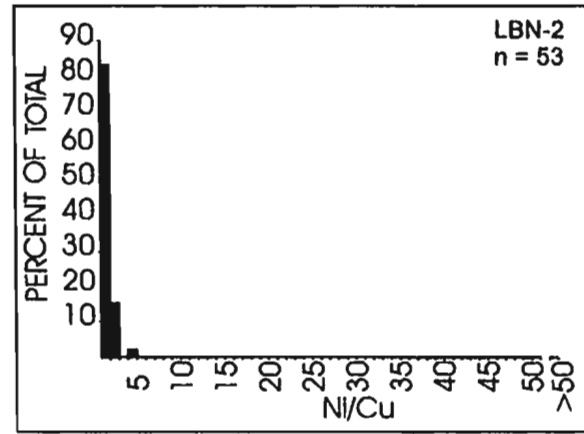
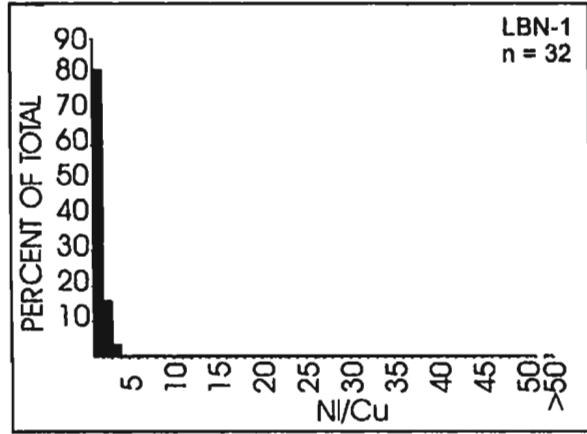


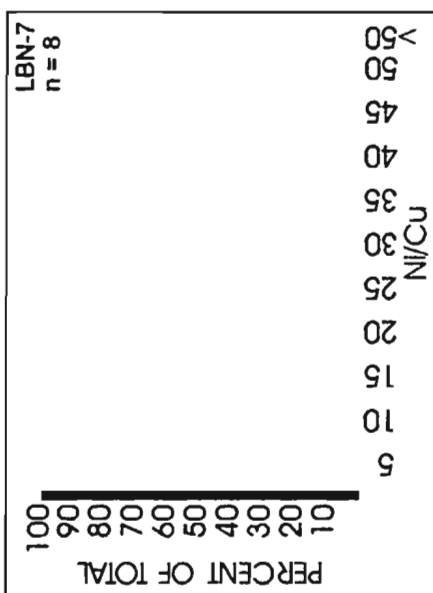
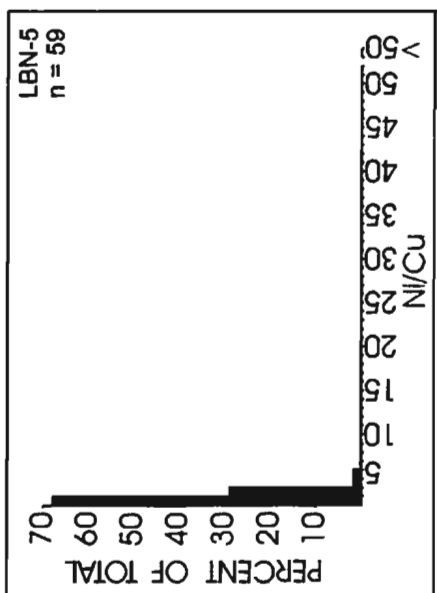
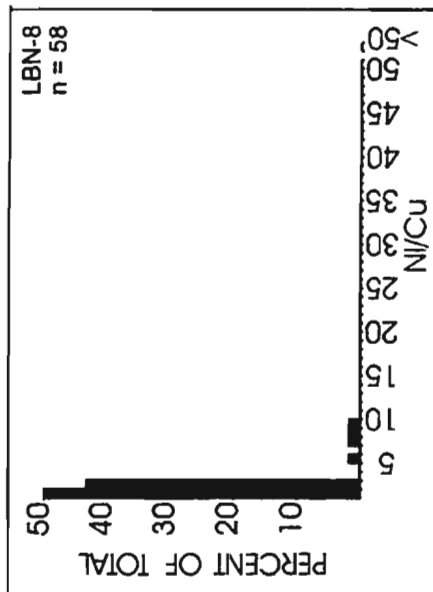
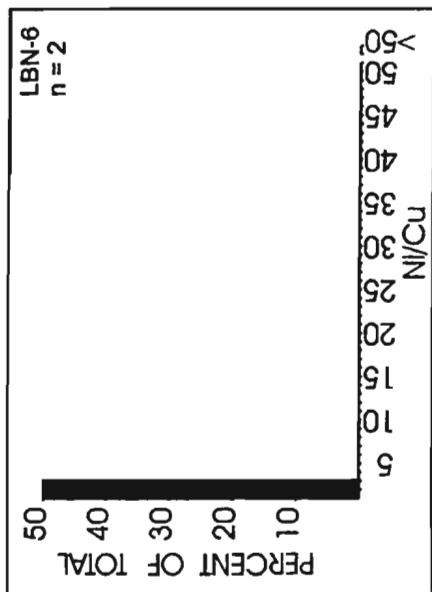
(i)

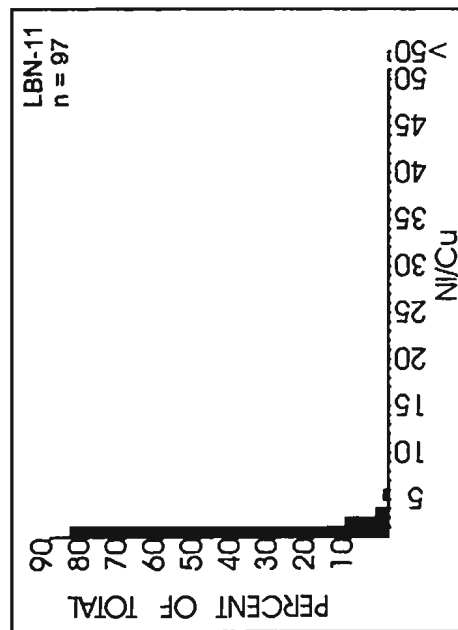
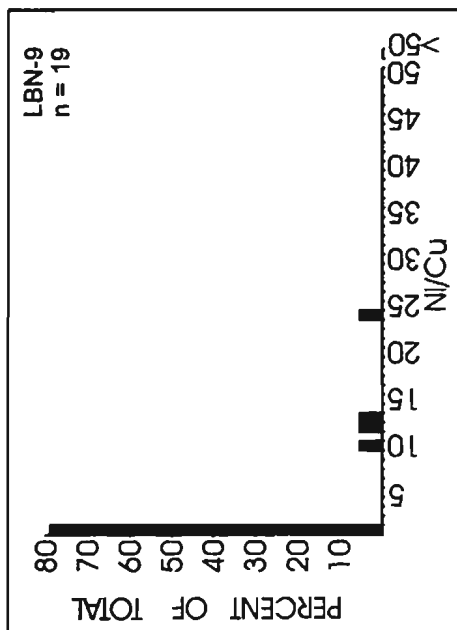
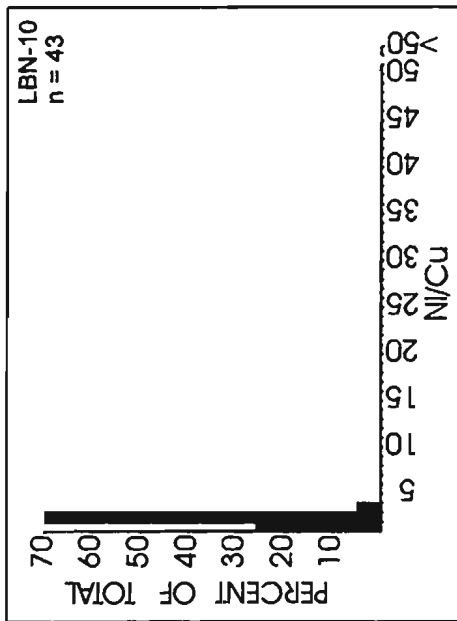


(k)

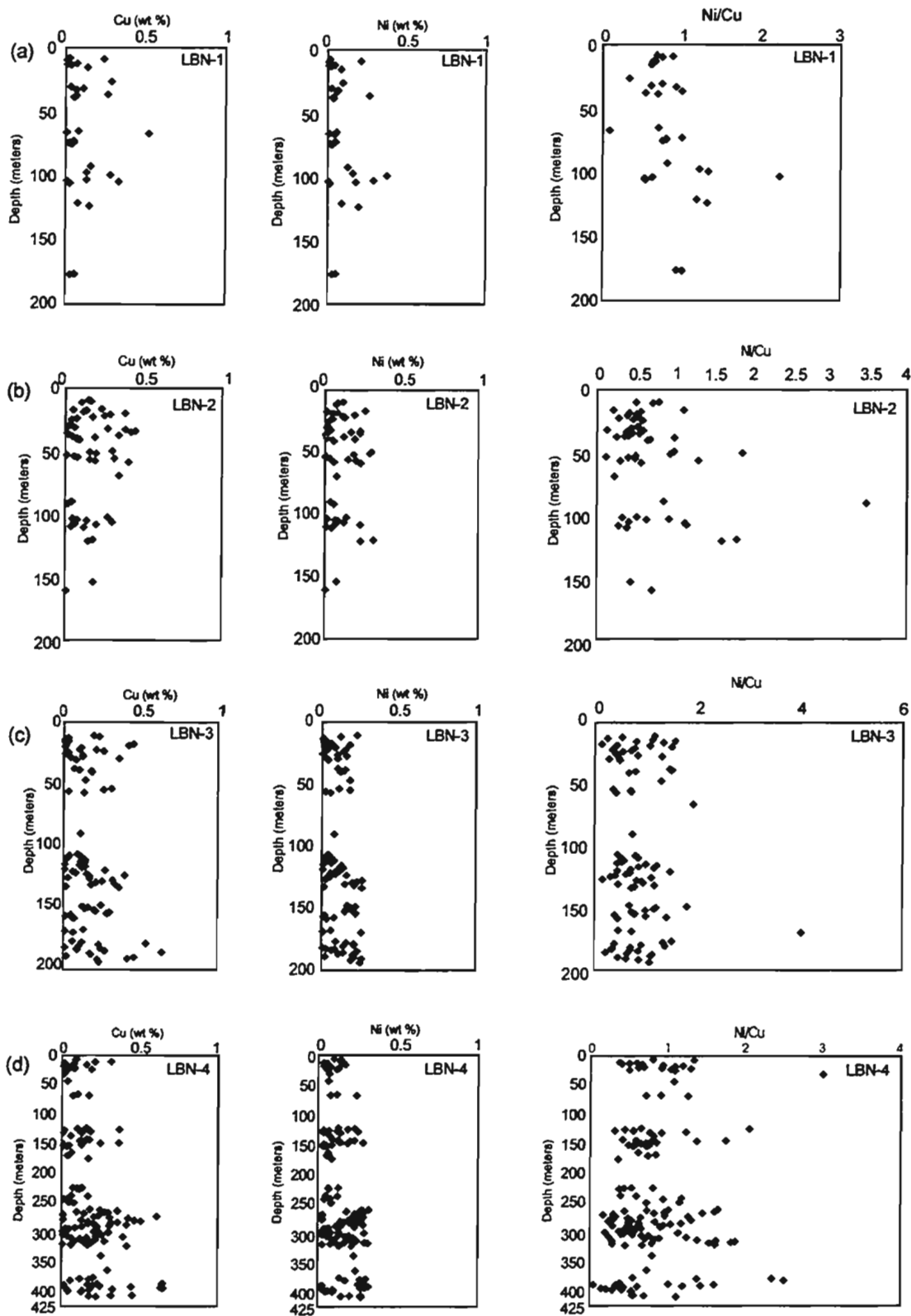
Appendix A2.4.2 Histogram plots of Ni/Cu for assays from drill hole LBN-1 to 11 on the Cirque grid. Data for LBN-12 are not available for this study.



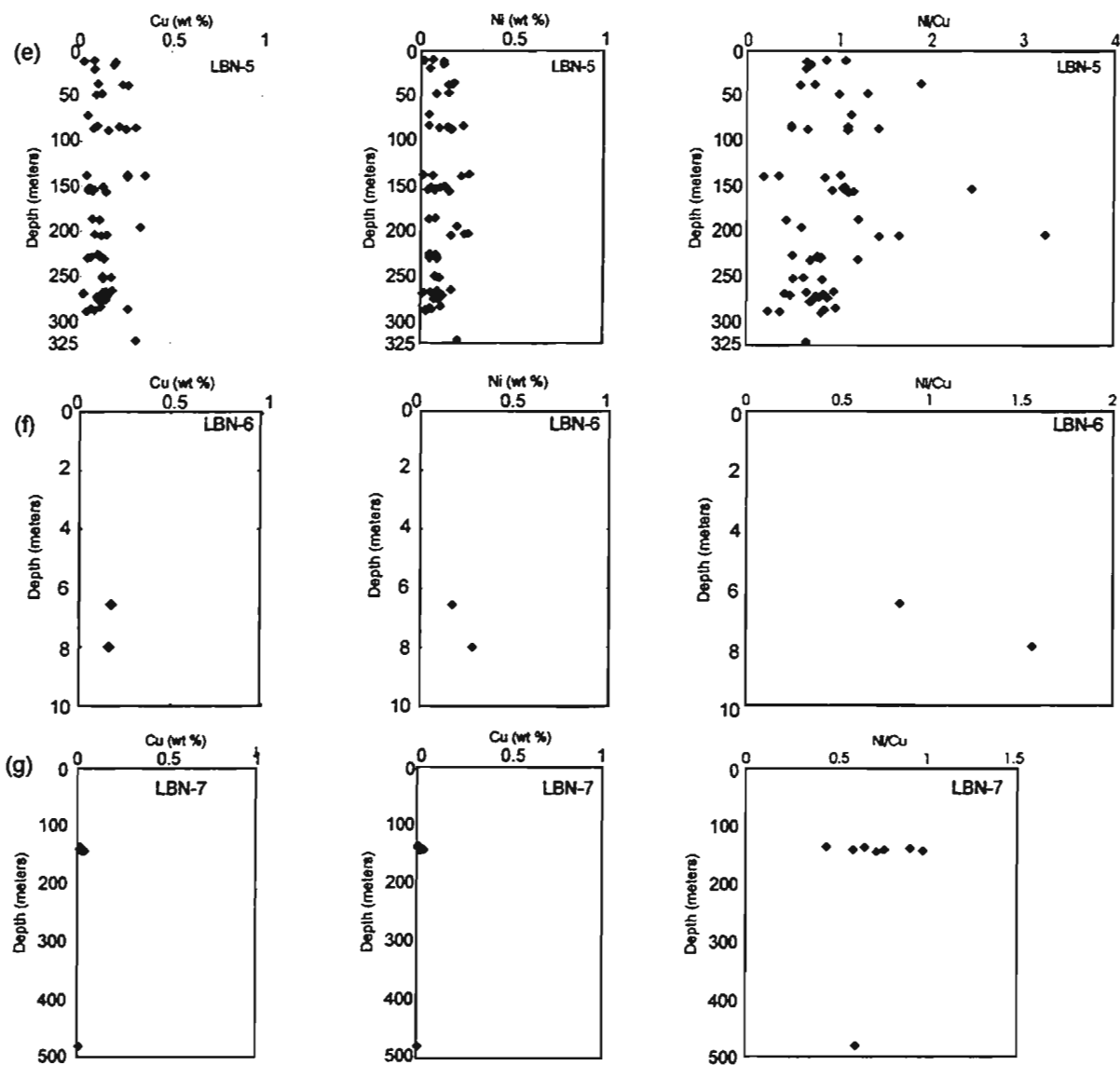


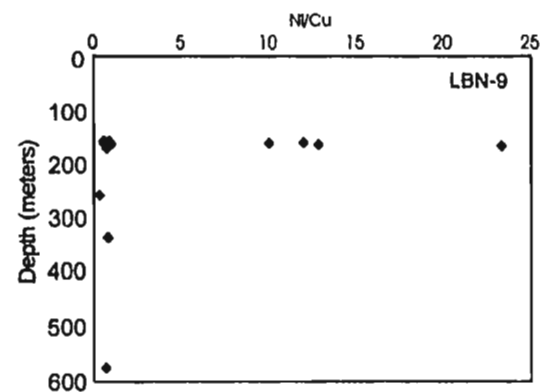
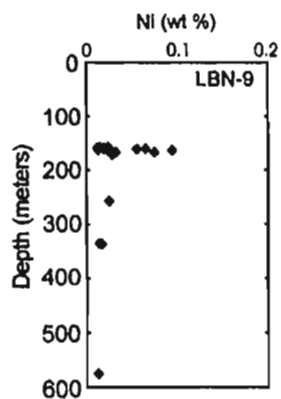
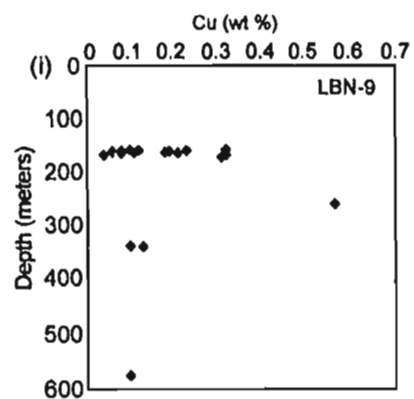
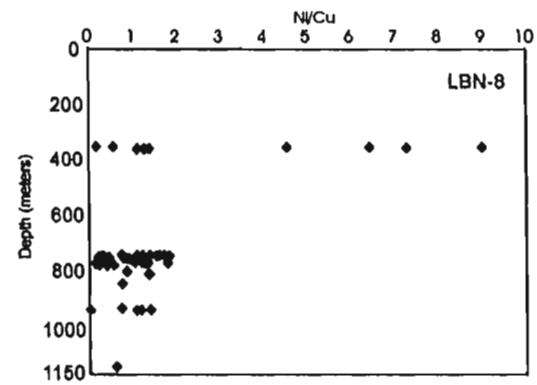
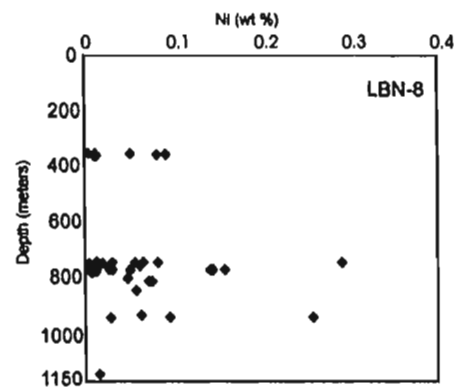
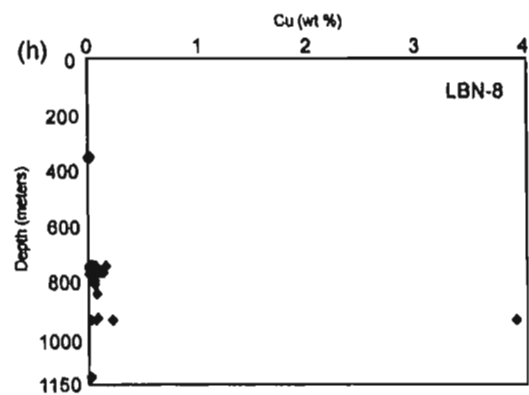


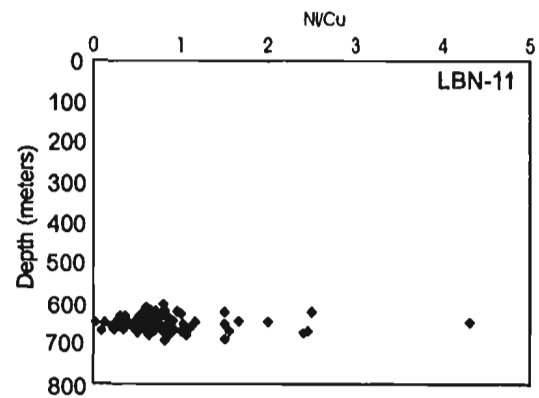
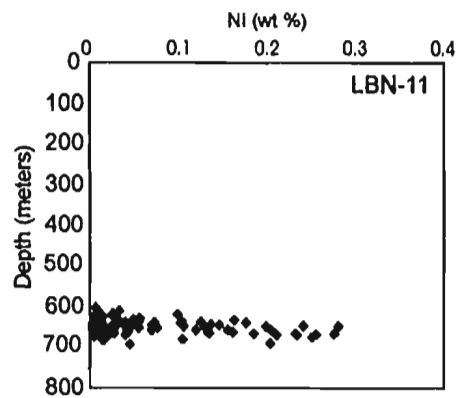
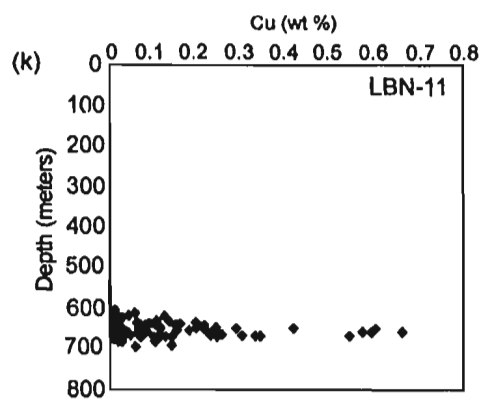
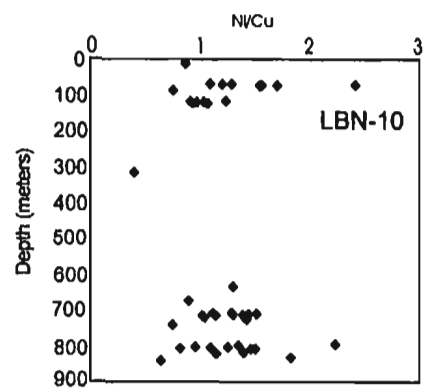
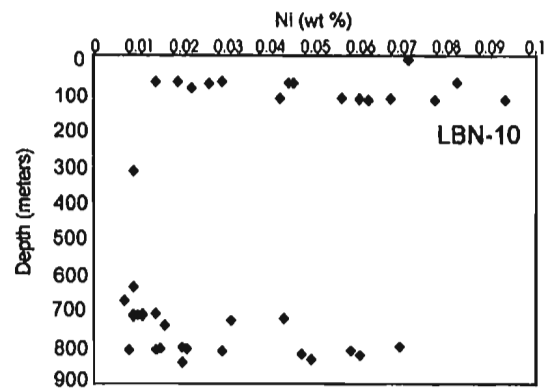
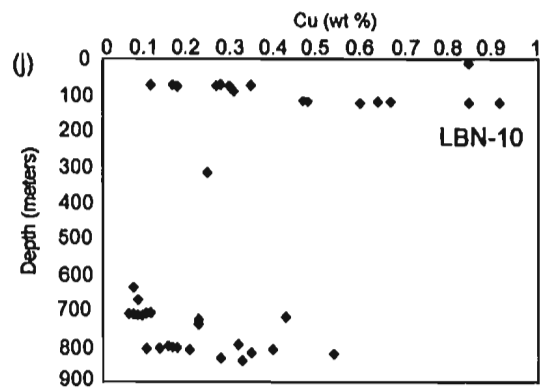
Appendix A2.4.3 Downhole cross sections of mineralized intersections from drill holes LBN-1 to LBN-11 (a to k) on the Cirque property. Data from LBN-12 are not available. Plots show depth versus Cu wt%, Ni wt%, and Ni/Cu.











### Appendix 3.1 Microprobe data - Table of endmember fractions

#### Atomic percent of pyroxene

Sample	LD-96-91	LD-96-91	LD-96-37	LD-96-37	LD-96-5b	LD-96-120	LD-96-120	LD-96-120	LD-96-120
Stage point	1pyx91	2pyx91	1pyx37	1pyx37(2)	1pyx5b	1pyx120	2pyx120	3pyx120	6pyx120
Rock type	pyx	pyx	anor	anor	Fe-pyx	Fe-pyx	Fe-pyx	Fe-pyx	Fe-pyx
Mg	5.00	7.47	10.16	10.81	5.04	9.85	5.65	7.08	5.38
Fe	4.34	3.10	9.27	8.78	6.56	7.16	5.60	11.77	5.68
Ca	2.99	8.96	0.45	0.33	4.75	2.84	8.70	1.01	8.57
EN	40.58	38.27	51.12	54.26	30.82	49.61	28.32	35.65	27.40
FS	35.18	15.85	46.63	44.09	40.15	36.07	28.06	59.27	28.96
WO	24.24	45.88	2.25	1.65	29.04	14.32	43.61	5.08	43.65
Total	100.00	100.00	100.00	100.00	100.00	100.00	100.00	100.00	100.00
Mg#	53.56	70.71	52.30	55.17	43.43	57.91	50.23	37.56	48.62

Endmember percentage calculations from Deer, Howie, and Zussman (1992)

Mg endmember : Enstatite, En = 100 Mg / (Mg + Fe + Ca)

Fe endmember : Ferrosillite, Fs = 100 Fe / (Mg + Fe + Ca)

Ca endmember : Wollastonite, Wo = 100 Ca / (Mg + Fe + Ca)

#### Atomic percent of plagioclase feldspar

Sample	LBN-96-2	LBN-96-3	LBN-96-4	LD-96-37	LD-96-37	LD-96-5b
Stage point	200PL+	1plg338	1plg413a	1plg37	2plg37	1plg5b
Rock type	l.troc	anor	l.nor-gab	anor	anor	Fe-pyx
Ca	4.56	3.72	3.653	3.34	2.92	BD
Na	3.04	3.45	3.888	3.53	2.38	0.29
AN	60.04	51.91	48.44	48.60	55.09	NA
AB	39.96	48.09	51.56	51.4	44.91	NA
Total	100	100	100	100	100	

Endmember percentage calculations from Deer, Howie, and Zussman (1992)

Ca endmember : Anorthite, An : 100 Ca / (Ca + Na)

Na endmember : Albite, Ab : 100 Na / (Ca + Na)

l.troc = leucotroctolite, anor = anorthosite, Fe-dior = ferrodiorite, pyx = pyroxenite, Fe-pyx = ferropyxenite

l.nor-gab = leuconorite/leucogabbro, BD = below detection, NA = not available

Magnesian number, Mg# = 100 Mg / (Mg + Fe)

Appendix A3.2 Sulphide-bearing rocks (core and outcrop; variable abundances of sulphides) assayed at Memorial University.

Sample	Source	Description	S %	Sulphide content %	Total FeO wt%	Ni ppm	Cu ppm	Ni %	Ni* %	Cu %	Cu* %	(Ni/Cu)*
536787	LBN-2, 26.0m	An, 5% diss, bleb po	1.09	3.13	6.95	55.14	244.02	0.01	0.18	0.02	0.78	0.23
536795	LBN-2, 46.2m	An, 5% diss po	1.16	3.33	3.53	58.23	299.28	0.01	0.18	0.03	0.90	0.19
536956	LBN-2, 49.53m	An, 15% net-diss po	4.99	14.24	10.76	288.61	571.05	0.03	0.20	0.06	0.40	0.51
536798	LBN-2, 59.20m	An, 10% net-diss po	1.07	3.05	3.14	43.37	144.37	0.00	0.14	0.01	0.47	0.30
536799	LBN-2, 60.2m	An, 2% net-diss po	0.69	1.98	2.89	27.34	103.86	0.00	0.14	0.01	0.52	0.26
536800	LBN-2, 61.2m	An, 10% net-diss po	2.81	8.03	6.10	136.24	390.22	0.01	0.17	0.04	0.49	0.35
536951	LBN-2, 62.2m	An, 15% net-diss po	2.86	8.18	6.19	145.85	309.74	0.01	0.18	0.03	0.38	0.47
536954	LBN-2, 65.2m	An, trace diss po	0.12	0.35	1.45	5.55	54.03	0.00	0.16	0.01	1.56	0.10
536957	LBN-2, 67.2m	An, 2% diss po	0.55	1.57	2.29	50.55	103.46	0.01	0.32	0.01	0.66	0.49
536958	LBN-2, 68.2m	An, 1% diss po	0.15	0.44	1.76	0.73	63.59	0.00	0.02	0.01	1.44	0.01
536959	LBN-2, 70.50m	An, 1% diss po	0.44	1.25	2.32	16.29	111.49	0.00	0.13	0.01	0.89	0.15
536960	LBN-2, 71.50m	An, 2% diss po	0.32	0.92	1.86	7.73	71.26	0.00	0.08	0.01	0.78	0.11
536964	LBN-2, 75.60m	An, 1% diss po	0.26	0.76	2.63	102.86	118.40	0.01	1.36	0.01	1.57	0.87
24059	LBN-3, 132.3m	An, <1% diss po, cpy	0.48	1.38	2.53	14.37	107.06	0.00	0.10	0.01	0.77	0.13
24060	LBN-3, 133.3m	An, 75% MS po, 6% cpy	29.62	84.62	42.11	2809.54	4740.57	0.28	0.33	0.47	0.56	0.59
24061	LBN-3, 147.8m	An, 40%, Semi-MS po, cpy	17.03	48.67	28.44	1413.76	3408.09	0.14	0.29	0.34	0.70	0.41
24062	LBN-3, 148.8m	An, 70% MS-net po, cpy	5.89	16.82	11.62	341.40	1370.97	0.03	0.20	0.14	0.82	0.25
24063	LBN-3, 149.8m	An, 40% MS-net po, cpy	19.29	55.11	33.16	1826.97	2446.52	0.18	0.33	0.24	0.44	0.75
24064	LBN-3, 150.8m	An, 35% Semi-MS po, cpy	12.65	36.15	25.76	1124.40	1859.88	0.11	0.31	0.19	0.51	0.60
24065	LBN-3, 151.8m	An, 60% MS po	17.36	49.59	35.09	1962.22	3594.85	0.20	0.40	0.36	0.72	0.55
24066	LBN-3, 152.8m	An, 35% Semi-MS po, cpy	14.46	41.31	25.67	1156.43	2490.82	0.12	0.28	0.25	0.60	0.46
24069	LBN-3, 155.6m	An, <1% diss po	1.19	3.39	3.87	52.34	325.93	0.01	0.15	0.03	0.96	0.16
24071	LBN-3, 157.6m	An, 5% diss, bleb po	6.68	19.09	13.22	395.89	484.25	0.04	0.21	0.05	0.25	0.82
24072	LBN-3, 158.6m	An, 5% MS-net po band	2.74	7.83	6.66	125.68	199.44	0.01	0.16	0.02	0.25	0.63
24073	LBN-3, 167.8m	An, 15% po, cpy	19.40	55.44	33.98	1831.75	6176.54	0.18	0.33	0.62	1.11	0.30
24074	LBN-3, 168.8m	An, 80% diss, net po, py	0.29	0.82	2.62	0.00	52.79	0.00	0.00	0.01	0.65	0.00
24076	LBN-3, 176.8m	An, 15% diss po	7.58	21.66	14.01	468.66	562.66	0.05	0.22	0.06	0.26	0.83
24077	LBN-3, 177.8m	An, 40% Semi-MS, bleb po	24.95	71.29	39.48	2478.79	2341.19	0.25	0.35	0.23	0.33	1.06
24078	LBN-3, 178.8m	An, 60% MS, bleb-net po cpy	13.66	39.03	26.36	1232.03	1623.29	0.12	0.32	0.16	0.42	0.76
24080	LBN-3, 180.8m	An, 30% Semi-MS, net po	13.67	39.06	22.57	1014.41	1157.98	0.10	0.26	0.12	0.30	0.88
24081	LBN-3, 181.8m	An, <1% diss po	0.24	0.68	2.61	0.17	58.45	0.00	0.00	0.01	0.85	0.00
24082	LBN-3, 182.8m	An, 5% bleb po, cpy, py	9.03	25.79	15.89	582.80	2298.48	0.06	0.23	0.23	0.89	0.25
24083	LBN-3, 183.8m	An, 15% bleb po, cpy	6.35	18.13	13.20	401.03	833.67	0.04	0.22	0.08	0.46	0.48
24084	LBN-3, 184.8m	An, 60% MS-net po, cpy	20.21	57.75	40.14	2365.48	3658.85	0.24	0.41	0.37	0.63	0.65

Sample	Source	Description	S %	Sulphide content %	Total FeO wt%	Ni ppm	Cu ppm	Ni %	Ni* %	Cu %	Cu* %	(Ni/Cu)*
24086	LBN-3, 186.8m	An, 25% Semi-MS po, cpy	8.60	24.56	21.99	800.67	1686.95	0.08	0.33	0.17	0.69	0.47
24088	LBN-3, 188.8m	An, 5% diss, bleb po	1.71	4.89	5.18	65.68	157.48	0.01	0.13	0.02	0.32	0.42
24091	LBN-3, 191.8m	An, 50% MS, net-bleb po	17.26	49.32	3227.96	1657.07	2669.54	0.17	0.34	0.27	0.54	0.62
25901	LBN-4, 321.85m	An, 20% Semi-MS po, cpy	12.64	36.11	20.74	827.29	2176.57	0.08	0.23	0.22	0.60	0.38
25902	LBN-4, 322.85m	An, 40% Semi-MS po, cpy	7.71	22.02	13.63	472.31	805.26	0.05	0.21	0.08	0.37	0.59
25903	LBN-4, 339.75m	An, 50% MS po, trace cpy	21.53	61.52	34.14	2040.62	3349.65	0.20	0.33	0.33	0.54	0.61
25904	LBN-4, 364.75m	An, 70% MS po, cpy, py	22.13	63.24	36.16	2148.13	4360.88	0.21	0.34	0.44	0.69	0.49
25905	LBN-4, 376.80m	An, 50% MS-net po	12.48	35.66	20.47	825.55	2022.27	0.08	0.23	0.20	0.57	0.41
25907	LBN-4, 379.60m	An, 90% MS-net po, cpy	29.26	83.61	40.35	2682.82	2536.40	0.27	0.32	0.25	0.30	1.06
25908	LBN-4, 381.30m	An, 45% Semi-MS po	16.00	45.73	25.56	1269.41	793.42	0.13	0.28	0.08	0.17	1.60
25908**	LBN-4, 381.30m	An, 45% Semi-MS po	16.47	47.05	25.67	1309.36	755.68	0.13	0.28	0.08	0.16	1.73
25919	LBN-4, 397.45m	An, 5% bleb-diss po, cpy, py	5.21	14.88	9.85	268.61	1389.08	0.03	0.18	0.14	0.93	0.19
25921	LBN-4, 399.45m	An, <1% net po	1.98	5.66	4.89	79.11	228.72	0.01	0.14	0.02	0.40	0.35
25921**	LBN-4, 399.45m	An, <1% net po	1.95	5.58	4.92	77.60	234.49	0.01	0.14	0.02	0.42	0.33
25922	LBN-4, 400.45m	An, 10% net po, trace cpy	6.94	19.83	12.84	368.69	1075.09	0.04	0.19	0.11	0.54	0.34
25923	LBN-4, 406.60m	An, 90% MS, net po, cpy	21.69	61.97	35.69	2113.42	6053.56	0.21	0.34	0.61	0.98	0.35
25924	LBN-4, 407.20m	An, 40% Semi-MS po, cpy	16.54	47.27	27.64	1309.04	3310.76	0.13	0.28	0.33	0.70	0.40
25927	LBN-5, 10.0m	LNor-An, 90% MS po, cpy	4.31	12.32	9.15	225.61	473.98	0.02	0.18	0.05	0.38	0.48
25928	LBN-5, 11.0m	LNor-An, <1% diss po	0.31	0.89	5.18	18.06	81.65	0.00	0.20	0.01	0.91	0.22
25929	LBN-5, 12.0m	LNor-An, 20% net-diss po, cpy	11.41	32.59	19.99	854.31	1952.99	0.09	0.26	0.20	0.60	0.44
25930	LBN-5, 15.36m	LNor-An, 25% net-diss po, cpy	11.30	32.27	22.52	887.25	1916.64	0.09	0.27	0.19	0.59	0.46
25931	LBN-5, 19.70m	An, 5% net po, cpy	3.29	9.41	7.31	171.52	566.94	0.02	0.18	0.06	0.60	0.30
25932	LBN-5, 36.10m	An, 50% MS-net po, cpy	17.42	49.76	27.11	1509.35	1265.39	0.15	0.30	0.13	0.25	1.19
25933	LBN-5, 37.10m	An, 15% net po, cpy	16.00	45.70	25.49	1307.91	2330.17	0.13	0.29	0.23	0.51	0.56
25935	LBN-5, 47.10m	An, 10% net po, cpy	12.56	35.88	22.26	1026.22	1088.31	0.10	0.29	0.11	0.30	0.94
25937	LBN-5, 71.0m	An, 10% net, bleb po, cpy	2.76	7.87	6.04	137.94	200.72	0.01	0.18	0.02	0.25	0.69
25938	LBN-5, 83.0m	An, 5% bleb po, trace cpy	2.66	7.60	12.33	166.75	642.01	0.02	0.22	0.06	0.84	0.26
25939	LBN-5, 84.0m	An, 60% MS po, trace cpy	22.77	65.04	34.69	2272.81	2797.77	0.23	0.35	0.28	0.43	0.81
25940	LBN-5, 85.0m	An, 10% bleb po, trace cpy	14.25	40.71	22.93	1078.25	3177.60	0.11	0.26	0.32	0.78	0.34
25941	LBN-5, 86.0m	An, 15% bleb po, trace cpy	8.59	24.55	15.13	580.39	778.68	0.06	0.24	0.08	0.32	0.75
25942	LBN-5, 87.0m	An, 40% Semi-MS po, cpy	15.33	43.79	25.88	1205.92	2457.76	0.12	0.28	0.25	0.56	0.49
25943	LBN-5, 88.0m	An, 30% Semi-MS po, cpy	15.74	44.97	25.44	1271.69	1583.00	0.13	0.28	0.16	0.35	0.80
25944	LBN-5, 137.75m	An, 80% MS po, <1% cpy	25.73	73.51	38.32	2683.12	3877.24	0.27	0.37	0.39	0.53	0.69
25945	LBN-5, 138.35m	An, <1% diss po	0.70	1.99	3.36	17.59	168.91	0.00	0.09	0.02	0.85	0.10
25946	LBN-5, 139.10m	An, <1% diss po	5.17	14.78	9.56	271.56	958.28	0.03	0.18	0.10	0.65	0.28
25947	LBN-5, 140.10m	LGab-An, 60% MS-net po, cpy	16.84	48.12	33.33	1977.56	3103.22	0.20	0.41	0.31	0.64	0.64
25948	LBN-5, 150.80m	An, 20% net-bleb po, trace cpy	11.95	34.14	19.50	980.71	1251.22	0.10	0.29	0.13	0.37	0.78

Sample	Source	Description	S %	Sulphide content %	Total FeO wt%	Ni ppm	Cu ppm	Ni %	Ni* %	Cu %	Cu* %	(Ni/Cu)*
25949	LBN-5, 151.80m	An, 10% net po, trace cpy	4.13	11.81	8.09	237.35	382.89	0.02	0.20	0.04	0.32	0.62
25950	LBN-5, 152.80m	An, 15% net po, trace cpy	9.52	27.19	15.70	714.51	400.90	0.07	0.26	0.04	0.15	1.78
25951	LBN-5, 153.80m	An, 10% net po, trace cpy	7.16	20.46	12.26	500.69	529.51	0.05	0.24	0.05	0.26	0.95
25952	LBN-5, 154.80m	An, 10% net po, trace cpy	2.66	7.59	5.76	129.28	221.23	0.01	0.17	0.02	0.29	0.58
25953	LBN-5, 155.80m	An, 5% net po, trace cpy	6.44	18.40	12.36	435.63	419.78	0.04	0.24	0.04	0.23	1.04
25954	LBN-5, 156.80m	An, 20% net-bleb po, trace cpy	13.76	39.33	22.02	1197.14	1383.16	0.12	0.30	0.14	0.35	0.87
25955	LBN-5, 187.55m	An, <5% net po, trace cpy	20.17	57.62	30.45	1704.56	5076.28	0.17	0.30	0.51	0.88	0.34
25956	LBN-5, 186.50m	An, 5% diss po	2.87	8.21	6.09	138.61	398.17	0.01	0.17	0.04	0.49	0.35
25957	LBN-5, 195.90m	An, 60% MS po, 1% cpy	21.50	61.44	32.33	1945.58	3834.88	0.19	0.32	0.38	0.62	0.51
25958	LBN-5, 203.70m	An, 90% MS po, <1% cpy	28.62	81.76	41.59	3038.00	1222.70	0.30	0.37	0.12	0.15	2.48
25959	LBN-5, 204.70m	An, 80% MS po, <1% cpy	27.32	78.06	38.85	2723.74	2065.25	0.27	0.35	0.21	0.26	1.32
25960	LBN-5, 205.70m	An, 30% Semi-MS po, cpy	17.15	49.01	26.23	1376.17	1238.59	0.14	0.28	0.12	0.25	1.11
25961	LBN-5, 226.20m	An, 10% net-bleb po, cpy	3.51	10.04	7.72	178.66	632.98	0.02	0.18	0.06	0.63	0.28
LD-96-10	outcrop	<1% diss po, trace cpy, An	2.47	7.04	5.36	740.42	492.45	0.07	1.05	0.05	0.70	1.50
LD-96-12	outcrop	<1% diss po, trace cpy, An	7.86	22.46	12.63	2420.03	1162.35	0.24	1.08	0.12	0.52	2.08
LD-96-15	outcrop	Rusty An, po, cpy	4.32	12.34	8.27	1066.07	1428.31	0.11	0.86	0.14	1.16	0.75
LD-96-27	outcrop	MS po in An	33.65	96.14	40.55	5934.07	1275.15	0.59	0.62	0.13	0.13	4.65
LD-96-29	outcrop	MS po in An	31.94	91.27	45.30	4186.78	2295.33	0.42	0.46	0.23	0.25	1.82
LD-96-30	outcrop	An, MS po, <1% cpy	2.41	6.89	5.49	149.35	627.40	0.01	0.22	0.06	0.91	0.24
LD-96-31	outcrop	An, MS po	12.07	34.48	17.07	654.75	310.27	0.07	0.19	0.03	0.09	2.11
LD-96-45	outcrop	Ferrodiorite, diss po	3.07	8.77	12.54	2088.52	1071.02	0.21	2.38	0.11	1.22	1.95
LD-96-46	outcrop	Ferrodiorite, diss po	0.71	2.02	23.69	0.00	56.19	0.00	0.00	0.01	0.28	0.00
LD-96-48	outcrop	Ferrodiorite, diss po	0.63	1.79	24.46	0.00	58.80	0.00	0.00	0.01	0.33	0.00
LD-96-61	outcrop	Rusty weathered An	0.55	1.56	4.62	145.54	200.33	0.01	0.93	0.02	1.28	0.73
LD-96-87	talus	MS po, An	1.69	4.83	3.79	97.14	456.69	0.01	0.20	0.05	0.95	0.21
LD-96-88	talus	Rusty weathered An, MS po	4.56	13.03	8.24	284.70	630.92	0.03	0.22	0.06	0.48	0.45
LD-96-90	talus	Rusty weathered An, MS po	34.53	98.65	45.39	3980.27	13687.11	0.40	0.40	1.37	1.39	0.29
LD-96-91	talus	Pyroxenite, trace diss po	1.48	4.22	13.74	52.24	115.58	0.01	0.12	0.01	0.27	0.45
LD-96-96	talus	MS po, An	15.86	45.30	24.18	818.21	4722.15	0.08	0.18	0.47	1.04	0.17
LD-96-97	talus	MS po in An	3.71	10.59	7.22	238.48	1237.41	0.02	0.23	0.12	1.17	0.19
LD-96-98	talus	Rusty stained An	8.91	25.46	13.09	396.36	1195.80	0.04	0.16	0.12	0.47	0.33
LD-96-99	talus	MS po, An	33.35	95.27	43.39	2589.92	2787.65	0.26	0.27	0.28	0.29	0.93
LD-96-101	talus	An with sulphide bands	16.08	45.93	24.36	1258.62	4949.28	0.13	0.27	0.49	1.08	0.25
LD-96-102	talus	Rusty An	0.31	0.89	2.54	0.00	45.94	0.00	0.00	0.00	0.52	0.00

Sample	Source	Description	S %	Sulphide content %	Total FeO wt%	Ni ppm	Cu ppm	Ni %	Ni* %	Cu %	Cu* %	(Ni/Cu)*
LD-96-105	outcrop	Altered An, rusty weathering	20.90	59.71	30.18	2205.71	5149.56	0.22	0.37	0.51	0.86	0.43
LD-96-111	outcrop	Thin rusty bands in An	2.59	7.41	5.47	137.85	195.20	0.01	0.19	0.02	0.26	0.71
LD-96-113	outcrop	Rusty sulphide bands in An	3.81	10.89	7.67	363.79	510.55	0.04	0.33	0.05	0.47	0.71
LD-96-125	outcrop	Ferrodiorite, diss po	0.20	0.57	19.99	0.00	38.86	0.00	0.00	0.00	0.68	0.00
LD-96-150	outcrop	Rusty An, MS po	12.75	36.44	18.96	623.77	458.25	0.06	0.17	0.05	0.13	1.36
LD-96-153	outcrop	Rusty An, <1% diss po	1.72	4.92	5.41	32.83	273.42	0.00	0.07	0.03	0.56	0.12
LD-96-156	outcrop	Altered An, <1% diss po	0.13	0.38	2.39	0.00	15.12	0.00	0.00	0.00	0.40	0.00
LD-96-157	outcrop	Rusty An	0.20	0.56	2.15	0.00	19.99	0.00	0.00	0.00	0.36	0.00
LD-96-164	outcrop	LGab-An, <1% po	1.07	3.07	3.86	245.52	295.00	0.02	0.80	0.03	0.96	0.83
LD-96-170	outcrop	Rusty An, MS po	32.24	92.13	44.91	3166.20	976.74	0.32	0.34	0.10	0.11	3.24
LD-96-170(2)	outcrop	MS po in An	27.73	79.23	38.08	2518.58	3555.20	0.25	0.32	0.36	0.45	0.71
LD-96-171	outcrop	Rusty An, MS po	0.82	2.34	3.33	33.92	186.42	0.00	0.14	0.02	0.80	0.18
LD-96-180	Subcrop	Leucogabbro	2.00	5.71	12.62	86.75	186.90	0.01	0.15	0.02	0.33	0.46
BW01	rubble	Hilltop, ferrodiorite, diss po	3.72	10.64	40.62	873.06	2394.52	0.09	0.82	0.24	2.25	0.36
BW02	rubble	Hilltop, anorthosite, diss po	0.18	0.51	1.25	11.62	16.00	0.00	0.23	0.00	0.32	0.73

An = Anorthosite, LNor = Leuconorite, LGab = Leucogabbro

MS = massive sulphide, diss = disseminated, po = pyrrhotite, cpy = chalcopyrite, py = pyrite

\* recalculated to 100% sulphides, \*\* duplicate sample



### Appendix A3.3 Major and trace element geochemistry from XRF analyses of the Cirque rocks.

Sample	Sample description	[Mg]	SiO <sub>2</sub>	TiO <sub>2</sub>	Al <sub>2</sub> O <sub>3</sub>	Fe <sub>2</sub> O <sub>3</sub>	FeO	MnO	MgO
			wt%	wt%	wt%	wt%	wt%	wt%	wt%
LD-96-48	Ferrodiorite, outcrop	10.22	38.68	3.65	12.49	4.31	21.97	0.29	1.65
LD-96-69	Ferrodiorite, outcrop	31.17	45.76	4.54	15.69	2.51	12.82	0.22	3.83
LD-96-46	Ferrodiorite, outcrop	10.98	37.00	5.29	10.13	4.45	22.68	0.31	1.85
LD-96-82	Ferrodiorite, outcrop	30.22	44.92	4.45	15.07	2.62	13.37	0.23	3.82
LD-96-75	Ferrodiorite, outcrop	31.67	44.78	4.83	14.93	2.62	13.36	0.22	4.09
LD-96-47	Ferrodiorite, outcrop	26.21	47.61	3.11	16.54	2.68	13.68	0.24	3.21
LD-96-83	Ferrodiorite, outcrop	24.61	29.70	8.83	2.29	6.03	30.73	0.46	6.62
LD-96-125	Ferrodiorite, outcrop	16.33	44.35	4.28	13.79	3.34	17.01	0.25	2.19
536775	Leucotroctolite, LBN-2 (3.43m)	53.08	48.09	0.41	22.57	1.55	7.91	0.12	5.91
536776	Leucotroctolite, LBN-2 (4.43m)	51.83	49.47	0.70	24.63	1.10	5.63	0.09	4.00
536778	Leucotroctolite, LBN-2 (6.43m)	53.00	49.16	0.89	24.67	1.08	5.52	0.09	4.11
536779	Leuconorite, LBN-2 (7.43m)	54.45	48.64	0.91	23.67	1.25	6.35	0.10	5.01
536787	Leuconorite, LBN-2 (26.00m)	46.17	50.37	0.72	23.21	1.28	6.51	0.10	3.68
536788	Leuconorite, LBN-2 (27.00m)	52.55	48.13	1.63	20.76	1.71	8.73	0.15	6.38
536789	Leuconorite, LBN-2 (28.00m)	52.40	49.42	1.29	22.54	1.36	6.92	0.12	5.03
536795	Anorthosite, LBN-2 (46.20m)	16.32	53.31	0.12	27.28	0.61	3.10	0.03	0.40
536952	Anorthosite, LBN-2 (63.20m)	26.64	53.98	0.08	27.03	0.23	1.19	1.79	0.29
536953	Anorthosite, LBN-2 (64.20m)	25.32	55.21	0.09	27.26	0.24	1.22	0.02	0.27
536954	Anorthosite, LBN-2 (65.20m)	19.08	55.10	0.09	27.33	0.26	1.34	0.02	0.21
536955	Anorthosite, LBN-2 (66.20m)	18.98	54.91	0.09	27.48	0.25	1.28	0.02	0.20
536957	Anorthosite, LBN-2 (67.20m)	11.73	53.59	0.08	26.75	0.41	2.07	1.61	0.18
536958	Anorthosite, LBN-2 (69.30m)	19.94	54.96	0.09	27.35	0.32	1.61	0.02	0.26
536959	Anorthosite, LBN-2 (70.50m)	12.41	54.33	0.10	27.38	0.42	2.15	0.02	0.20
536960	Anorthosite, LBN-2 (71.50m)	15.91	54.73	0.00	27.34	0.34	1.73	0.02	0.22
536961	Anorthosite, LBN-2 (72.50m)	30.52	55.10	0.09	27.21	0.26	1.32	0.02	0.38
536964	Anorthosite, LBN-2 (75.60m)	51.05	55.03	0.01	25.47	0.49	2.48	0.03	1.71
536965	Anorthosite, LBN-2 (76.60m)	58.33	54.85	0.42	25.56	0.41	2.09	0.03	1.93
536799	Anorthosite, LBN-2 (60.20m)	16.19	53.85	0.11	27.28	0.52	2.64	0.03	0.34
536952	Anorthosite, LBN-2 (63.20m)	26.64	54.95	0.09	27.52	0.24	1.21	0.02	0.29
536957	Anorthosite, LBN-2 (67.20m)	11.73	57.50	0.08	28.70	0.44	2.22	0.02	0.19
24059	Anorthosite, LBN-3 (132.30m)	51.29	53.73	0.10	26.60	0.47	2.39	0.06	1.66
24069	Anorthosite, LBN-3 (155.60m)	22.70	52.88	0.08	27.13	0.72	3.65	0.04	0.71
24071	Anorthosite, LBN-3 (157.60m)	3.48	45.74	0.13	23.60	2.64	13.44	0.04	0.32
24072	Anorthosite, LBN-3 (158.60m)	17.51	51.11	0.11	25.51	1.27	6.47	0.04	0.91
24081	Anorthosite, LBN-3 (181.80m)	30.71	52.80	0.10	28.16	0.48	2.43	0.04	0.71
24088	Anorthosite, LBN-3 (188.80m)	24.40	52.18	0.10	25.91	1.00	5.11	0.05	1.09
25919	Anorthosite, LBN-4 (398.45m)	1.16	49.37	0.09	24.02	1.97	10.02	0.04	0.08
25921	Anorthosite, LBN-4 (399.45m)	5.08	52.75	0.10	25.91	0.96	4.90	0.04	0.17
25921*	Anorthosite, LBN-4 (399.45m)	4.92	52.70	0.09	26.07	0.96	4.90	0.04	0.17
25931	Anorthosite, LBN-5 (19.70m)	11.58	50.46	0.12	24.70	1.46	7.44	0.04	0.64
25938	Anorthosite, LBN-5 (83.00m)	35.01	45.34	2.70	20.21	2.43	12.38	0.14	4.40
25945	Anorthosite, LBN-5 (138.35m)	10.61	53.58	0.10	26.65	0.67	3.40	0.03	0.27
25953	Anorthosite, LBN-5 (155.80m)	9.67	46.77	0.20	22.27	2.59	13.20	0.04	0.93
25956	Anorthosite, LBN-5 (187.55m)	2.26	51.64	0.09	25.52	1.21	6.16	0.02	0.09

Sample	CaO wt%	Na2O wt%	K2O wt%	P2O5 wt%	Cr ppm	Ni ppm	Sc ppm	V ppm	Cu ppm	Pb ppm	Zn ppm
LD-96-48	10.43	2.37	0.56	3.59	0.00	0.00	54.36	103.46	62.14	12.00	218.39
LD-96-69	9.38	3.20	0.29	1.75	60.44	6.26	36.48	350.03	34.69	9.94	102.12
LD-96-46	12.03	1.81	0.37	4.10	0.00	0.00	69.64	136.24	63.29	9.02	211.61
LD-96-82	9.91	3.12	0.32	2.18	39.06	24.27	37.80	323.38	47.45	3.92	140.99
LD-96-75	9.76	3.10	0.23	2.07	46.02	12.18	37.76	330.93	39.27	7.81	129.64
LD-96-47	8.72	3.04	0.33	0.83	39.79	0.00	44.11	206.59	32.20	7.95	135.48
LD-96-83	12.23	0.35	0.01	2.74	33.40	0.00	90.98	253.76	27.18	15.10	388.81
LD-96-125	9.81	2.61	0.42	1.95	0.23	0.00	56.77	188.39	38.89	7.84	170.63
536775	9.61	3.34	0.42	0.08	41.01	60.87	10.76	42.49	43.77	4.74	20.44
536776	10.28	3.65	0.39	0.07	34.50	34.58	4.69	33.12	35.62	2.82	0.00
536778	10.20	3.78	0.39	0.10	35.75	36.21	6.53	38.39	37.98	4.23	3.31
536779	9.91	3.63	0.41	0.12	33.44	64.15	9.93	45.06	43.83	4.56	11.83
536787	9.80	3.82	0.46	0.05	65.01	60.75	16.31	53.66	268.84	4.41	12.08
536788	8.96	3.09	0.37	0.07	99.90	40.31	16.49	97.91	47.46	3.90	32.77
536789	9.33	3.44	0.45	0.11	89.57	28.88	5.73	83.99	45.48	2.84	21.45
536795	9.81	4.79	0.52	0.03	23.10	60.25	2.23	3.20	309.65	1.98	0.00
536952	9.62	5.23	0.54	0.02	19.18	0.00	6.56	1.38	54.05	4.28	0.00
536953	9.80	5.35	0.53	0.02	18.40	0.00	3.73	1.32	52.84	0.00	0.00
536954	9.85	5.27	0.52	0.02	16.37	6.03	5.78	2.47	58.73	1.18	0.00
536955	9.88	5.35	0.51	0.02	29.82	2.33	1.91	6.45	59.37	4.18	0.00
536957	9.58	5.21	0.51	0.02	21.96	53.69	0.23	5.26	109.88	4.31	0.00
536958	9.56	5.21	0.59	0.02	17.56	0.79	2.32	0.00	68.39	8.15	0.00
536959	10.12	4.75	0.52	0.02	23.62	17.76	3.03	0.22	121.55	6.69	0.00
536960	10.02	5.05	0.54	0.02	25.45	8.46	7.66	2.63	77.92	5.10	0.00
536961	9.68	5.26	0.67	0.02	15.76	3.73	3.72	0.12	67.54	5.16	0.00
536964	9.33	4.83	0.61	0.02	39.90	114.15	2.12	24.73	131.39	2.45	0.00
536965	9.07	5.01	0.61	0.02	26.61	25.21	9.75	22.42	62.93	2.63	0.00
536799	10.03	4.66	0.52	0.02	16.20	29.41	4.14	3.93	111.74	6.13	0.00
536952	9.79	5.33	0.55	0.02	19.52	0.00	6.68	1.41	55.03	4.35	0.00
536957	10.28	0.00	0.55	0.02	23.57	57.61	0.25	5.65	117.90	4.62	0.00
24059	9.85	4.67	0.47	0.02	44.61	15.95	11.96	10.56	118.80	2.84	0.00
24069	9.26	4.45	1.05	0.01	23.29	58.12	8.07	8.94	361.89	3.59	0.00
24071	10.34	3.41	0.31	0.02	42.22	473.81	11.00	15.59	579.55	9.87	0.00
24072	9.76	4.24	0.57	0.02	41.76	143.48	12.70	12.31	227.67	8.27	0.00
24081	10.02	4.00	1.24	0.01	20.21	0.18	10.04	5.14	64.09	6.45	0.00
24088	9.42	3.87	1.25	0.01	50.89	76.30	8.44	7.35	182.96	7.35	0.00
25919	9.92	4.02	0.46	0.02	29.34	321.61	0.00	11.67	1663.16	26.13	54.05
25921	10.32	4.33	0.50	0.02	21.59	93.20	0.00	3.46	269.45	14.44	4.54
25921*	10.20	4.36	0.49	0.02	36.67	90.97	0.00	3.33	274.88	12.62	0.60
25931	10.82	3.88	0.42	0.02	46.30	205.63	6.02	23.35	679.68	12.55	13.19
25938	8.86	2.94	0.45	0.14	110.32	197.02	19.78	157.55	758.55	9.98	72.90
25945	10.53	4.32	0.44	0.02	41.74	20.94	6.05	7.12	201.16	3.06	0.00
25953	9.86	3.72	0.38	0.04	33.03	547.27	6.83	9.32	527.37	9.44	0.00
25956	10.61	4.20	0.44	0.02	18.16	165.10	4.81	0.00	474.28	10.99	0.00

Sample	S	As	Rb	Ba	Sr	Ga	Nb	Zr	Y	Th	U	Ce	Cl
	ppm	ppm	ppm	ppm	ppm	ppm	ppm	ppm	ppm	ppm	ppm	ppm	ppm
LD-96-48	6611.99	0.00	1.46	423.63	399.82	31.39	6.52	37.84	60.37	0.00	0.00	122.60	133.06
LD-96-69	177.22	4.06	0.00	407.91	611.75	21.40	9.86	0.00	19.41	0.00	0.00	28.03	43.75
LD-96-46	7946.43	7.91	1.76	354.57	350.86	25.78	9.71	50.09	75.07	0.00	0.00	138.42	116.83
LD-96-82	483.59	2.36	0.00	484.27	640.42	24.03	9.60	0.73	26.74	0.00	0.00	52.79	47.72
LD-96-75	330.65	0.00	0.00	372.82	600.11	24.43	10.64	2.62	25.26	0.25	0.00	21.40	34.68
LD-96-47	249.47	0.00	0.00	341.30	384.49	26.97	13.41	44.77	31.36	1.40	0.00	33.36	43.68
LD-96-83	130.06	3.14	0.00	0.00	42.20	18.23	16.66	6418.61	73.95	0.00	3.99	50.76	86.31
LD-96-125	2001.46	0.00	0.00	352.28	350.44	25.78	16.40	54.33	47.62	0.00	1.49	64.32	62.98
536775	817.84	0.00	1.52	312.02	820.18	22.81	0.97	16.38	3.81	0.64	0.72	1.15	161.18
536776	399.04	1.33	1.59	339.73	889.50	24.14	1.44	26.08	2.38	0.00	0.68	0.00	101.55
536778	325.51	0.00	2.03	353.39	838.80	22.26	1.90	24.23	4.22	1.53	0.00	0.00	96.49
536779	625.57	0.18	1.87	320.97	827.94	23.49	2.13	25.90	5.21	0.00	0.00	0.00	121.97
536787	12056.57	4.69	1.69	392.21	885.14	25.70	0.90	2.91	3.44	1.59	0.00	0.00	60.78
536788	422.40	0.00	0.92	413.82	715.94	24.76	2.79	9.65	2.81	0.00	0.42	0.00	71.31
536789	617.38	0.00	2.06	427.04	810.58	23.43	2.27	13.94	3.45	0.26	0.00	0.08	77.79
536795	12044.23	0.00	1.48	431.37	985.38	26.81	0.78	0.00	0.00	0.33	1.34	21.54	35.86
536952	557.21	3.88	1.14	465.74	1074.70	27.83	0.09	0.00	0.00	0.00	0.00	3.54	192.69
536953	370.69	0.00	0.89	491.35	1102.81	28.86	0.24	0.00	0.00	0.00	0.00	4.17	161.74
536954	1318.13	0.00	1.14	518.16	1097.49	28.12	0.16	0.00	0.00	0.00	0.00	0.00	166.02
536955	662.10	0.00	1.25	453.61	1115.76	28.14	0.00	0.00	0.00	0.00	0.00	2.59	179.58
536957	5850.39	4.07	1.09	447.88	1071.39	27.56	0.39	0.00	0.00	0.00	0.00	10.49	214.19
536958	1660.64	0.00	1.64	458.33	1069.34	29.30	0.37	0.00	0.00	0.00	0.00	2.71	209.16
536959	4772.16	0.00	1.55	440.96	1066.85	28.97	0.58	0.00	0.00	0.00	0.00	0.00	94.22
536960	3512.86	0.00	1.96	436.75	1090.37	29.67	0.00	0.00	0.00	0.00	0.00	0.00	168.09
536961	935.83	2.62	2.74	502.76	1141.26	29.19	0.00	0.00	0.00	0.07	0.00	15.73	217.71
536964	2932.62	0.00	1.26	563.56	965.46	29.38	0.43	0.00	0.00	0.00	0.00	0.00	134.78
536965	775.16	6.54	2.06	523.39	979.95	28.29	0.25	0.00	0.00	0.12	0.00	0.00	130.86
536799	7461.53	0.00	1.37	462.12	1002.13	25.13	0.18	0.00	0.04	0.34	0.00	0.00	66.67
536952	567.26	3.95	1.16	474.14	1094.09	28.33	0.09	0.00	0.00	0.00	0.00	3.61	196.16
536957	6277.37	4.36	1.17	480.57	1149.58	29.57	0.42	0.00	0.00	0.00	0.00	11.26	229.82
24059	5373.86	0.58	1.81	536.49	1144.25	25.94	0.11	0.00	0.00	0.38	0.00	0.00	92.68
24069	13185.08	4.40	4.49	479.37	1066.43	29.41	0.00	0.00	0.00	0.33	0.00	0.00	97.84
24071	79967.72	6.40	0.22	227.75	755.38	22.81	1.94	0.00	0.33	0.00	0.00	0.00	63.81
24072	31268.07	1.75	2.67	385.24	978.54	28.02	0.55	0.00	0.00	0.08	0.00	0.00	96.82
24081	2627.48	4.53	6.43	468.16	1239.01	27.24	0.13	0.00	0.00	0.00	0.00	0.00	134.92
24088	19871.09	11.94	4.80	450.67	1001.91	27.05	0.33	0.00	0.00	0.00	0.00	0.00	127.65
25919	62352.87	0.00	0.62	403.54	1082.22	31.24	0.19	0.00	0.00	0.06	0.00	18.46	93.09
25921	23327.31	3.72	1.12	478.71	1123.84	31.88	0.00	0.00	0.00	0.00	0.00	29.40	196.81
25921*	22910.58	0.00	1.07	481.45	1110.67	29.98	0.00	0.00	0.00	0.72	0.00	0.00	113.64
25931	39468.10	2.82	1.11	369.43	944.80	23.92	0.17	0.00	0.00	0.00	0.00	5.69	109.71
25938	31442.54	0.00	2.87	442.00	767.56	28.41	4.05	125.76	6.60	0.00	0.00	0.00	89.02
25945	8291.97	2.86	0.84	440.31	1038.61	22.29	0.30	0.00	0.00	1.65	0.00	0.00	85.87
25953	80912.06	16.89	1.38	363.86	1092.36	32.91	0.77	0.00	0.35	0.00	0.00	7.13	105.91
25956	34210.96	0.00	1.66	420.09	1182.99	33.09	0.00	0.00	0.00	0.80	1.26	8.30	253.14

Sample	Sample description	[Mg]	SiO2 wt%	TiO2 wt%	Al2O3 wt%	Fe2O3 wt%	FeO wt%	MnO wt%	MgO wt%
LD-96-7A	Bleached anorthosite, outcrop	41.40	54.96	0.23	28.05	0.21	1.05	0.02	0.49
LD-96-24A	Bleached anorthosite, outcrop	38.37	55.19	0.37	27.49	0.24	1.20	0.02	0.49
LD-96-34A	Bleached anorthosite, outcrop	72.43	54.20	0.14	27.97	0.18	0.91	0.02	1.58
LD-96-109	Bleached anorthosite, outcrop	40.08	53.30	0.07	29.10	0.21	1.05	0.01	0.47
LD-96-111	Anorthosite with sulphides, outcrop	5.92	50.66	0.08	27.46	1.02	5.22	0.01	0.22
LD-96-156	Anorthosite, outcrop	16.11	53.97	0.08	28.23	0.43	2.19	0.03	0.28
LD-96-102	Anorthosite, talus	16.38	53.86	0.09	27.57	0.49	2.51	0.01	0.32
LD-96-10	Anorthosite with <1% po, outcrop	5.47	50.97	0.09	27.23	1.01	5.17	0.01	0.20
LD-96-3	Anorthosite, outcrop	56.33	54.60	0.45	25.57	0.41	2.08	0.03	1.77
LD-96-61	Anorthosite, outcrop	24.92	54.41	0.43	24.58	0.86	4.37	0.02	0.96
LD-96-153	Anorthosite, outcrop	3.92	52.33	0.09	26.18	1.05	5.35	0.01	0.14
LD-96-157	Anorthosite, outcrop	31.75	54.82	0.09	27.23	0.39	2.01	0.01	0.62
LD-96-92	Anorthosite, outcrop	48.87	55.07	0.46	26.93	0.23	1.16	0.02	0.73
LD-96-159	Anorthosite, outcrop	48.41	52.62	0.24	19.82	1.55	7.88	0.21	4.88
LD-96-114	Pyroxene-rich anorthosite, outcrop	18.94	51.10	4.02	19.01	1.95	9.94	0.12	1.53
LD-96-77	Altered anorthosite, outcrop	49.02	55.56	0.29	25.90	0.35	1.78	0.03	1.13
LD-96-115	Anorthosite/Leucogabbro, outcrop	24.30	45.55	4.55	11.91	3.35	17.09	0.35	3.62
LD-96-91	Pyroxenite, talus	64.83	50.31	0.87	1.69	2.37	12.09	0.29	14.71
LD-96-117	Pyroxenite, outcrop	30.61	44.42	0.59	0.85	5.95	30.35	0.98	8.84
BW02	Anorthosite, Noranda	30.97	52.34	0.07	29.51	0.23	1.19	0.01	0.35

Sample	CaO wt%	Na2O wt%	K2O wt%	P2O5 wt%	Cr ppm	Ni ppm	Sc ppm	V ppm	Cu ppm	Pb ppm	Zn ppm
LD-96-7A	9.28	5.08	0.59	0.04	0.00	0.00	3.35	10.22	6.05	0.43	0.00
LD-96-24A	9.52	4.95	0.52	0.01	0.14	8.34	4.81	14.55	3.15	3.35	0.00
LD-96-34A	9.36	4.96	0.64	0.03	0.00	0.00	0.47	4.12	12.60	2.74	0.00
LD-96-109	11.17	4.23	0.39	0.01	16.73	8.45	15.00	0.00	23.64	3.39	0.00
LD-96-111	11.10	3.84	0.37	0.01	4.70	154.91	4.66	7.64	219.35	2.81	0.00
LD-96-156	9.94	4.32	0.51	0.02	0.00	0.00	6.64	0.00	16.37	1.81	0.00
LD-96-102	10.23	4.41	0.48	0.02	5.53	0.00	4.10	0.98	53.48	5.01	0.00
LD-96-10	10.84	4.01	0.45	0.02	9.16	841.52	10.87	0.00	559.69	4.96	0.00
LD-96-3	9.37	4.79	0.84	0.09	4.18	0.00	9.00	38.58	5.31	4.72	0.00
LD-96-61	8.65	4.80	0.75	0.18	18.44	161.89	8.09	31.99	222.83	5.79	0.00
LD-96-153	10.46	3.98	0.39	0.02	16.08	38.19	11.83	4.82	318.06	8.03	0.00
LD-96-157	9.62	4.69	0.52	0.01	0.00	0.00	1.84	6.09	21.99	3.72	0.00
LD-96-92	9.21	5.46	0.64	0.10	0.67	0.00	7.11	20.99	6.22	5.75	0.00
LD-96-159	9.04	3.33	0.41	0.02	74.61	0.11	20.71	43.22	7.88	0.00	44.60
LD-96-114	5.73	4.89	1.26	0.46	18.60	2.82	14.41	187.61	14.62	3.49	151.52
LD-96-77	8.84	5.36	0.66	0.10	5.08	0.00	7.22	20.78	3.56	2.91	0.00
LD-96-115	8.71	3.25	0.44	1.18	20.00	0.00	49.87	148.74	5.07	6.17	223.48
LD-96-91	17.40	0.26	0.01	0.01	464.86	54.07	118.63	230.81	119.64	6.12	35.51
LD-96-117	7.80	0.17	0.01	0.05	16.00	0.00	103.00	64.00	21.00	12.00	444.00
BW02	11.96	3.97	0.36	0.01	12.82	13.08	9.73	0.00	18.00	3.78	0.00

Sample	S ppm	As ppm	Rb ppm	Ba ppm	Sr ppm	Ga ppm	Nb ppm	Zr ppm	Y ppm	Th ppm	U ppm	Ce ppm	Cl ppm
LD-96-7A	121.78	12.54	1.47	518.45	887.44	23.67	1.15	0.00	1.01	0.35	0.00	4.74	45.32
LD-96-24A	380.39	5.53	0.00	646.39	959.58	25.80	0.60	0.00	0.00	0.00	0.00	6.20	91.98
LD-96-34A	293.10	4.07	1.46	547.65	916.04	22.60	0.40	0.00	0.89	0.00	0.00	3.25	109.71
LD-96-109	1027.22	2.33	0.78	389.90	1228.99	27.71	0.00	0.00	0.00	0.00	0.00	26.12	105.83
LD-96-111	29160.49	9.81	0.56	356.28	1244.84	29.28	0.47	0.00	0.00	0.32	0.00	0.00	58.74
LD-96-156	1429.67	11.50	1.43	397.95	1076.43	25.31	0.11	0.00	0.00	0.00	0.00	0.00	63.94
LD-96-102	3611.03	5.64	0.69	591.84	1183.35	30.55	0.00	0.00	0.00	0.00	0.00	0.00	75.78
LD-96-10	28022.97	11.31	0.90	492.47	1378.76	26.95	0.29	0.00	0.00	0.00	0.00	13.77	35.73
LD-96-3	293.43	6.94	2.51	671.57	899.93	25.53	1.00	0.00	3.30	0.00	0.00	44.43	77.06
LD-96-61	6079.00	0.00	0.96	737.40	866.95	25.23	2.21	0.52	3.17	0.00	0.00	25.03	58.02
LD-96-153	20018.25	3.63	0.58	407.62	1097.56	26.85	0.00	0.00	0.00	2.00	0.00	10.29	87.01
LD-96-157	2145.62	6.48	1.09	621.40	1078.11	26.59	0.48	0.00	0.00	0.00	0.00	2.05	47.23
LD-96-92	238.86	4.49	0.99	631.41	891.89	24.23	1.56	0.00	0.82	0.00	0.00	6.94	120.11
LD-96-159	318.83	0.00	0.51	468.72	812.08	26.05	0.00	0.00	4.19	0.00	0.00	29.01	79.99
LD-96-114	205.55	0.00	0.00	2409.87	839.33	32.58	4.65	0.00	7.30	0.00	1.94	12.15	52.42
LD-96-77	145.28	0.80	2.19	676.97	968.79	25.96	1.06	1.99	3.13	0.76	1.59	21.28	46.30
LD-96-115	75.36	0.00	0.00	535.42	361.10	17.80	1.79	168.24	18.06	2.28	1.31	4.97	36.94
LD-96-91	15280.38	0.61	0.00	0.00	31.28	4.15	1.23	22.12	15.56	0.44	0.00	0.00	30.73
LD-96-117	524.53	3.31	0.00	6.00	8.00	1.00	0.90	24.00	22.00	0.00	0.88	33.02	28.26
BW02	1989.52	1.21	1.26	433.50	1250.34	30.02	0.00	0.00	0.00	0.00	0.00	16.17	52.41

Appendix A3.4 Trace element geochemistry (ICP-MS analyses) of samples from the Cirque and neighbouring properties.

Sample Name	Rock Type	Pb ppm	Bi ppm	Mo ppm	Rb ppm	Cs ppm	Ba ppm	Sr ppm	Tl ppm	Li ppm	Ta ppm
LD-96-7A	Bleached anorthosite, outcrop	2.38	0.00	0.18	1.47	0.00	539.30	887.44	0.00	5.89	1.97
LD-96-109	Bleached anorthosite, outcrop	3.04	0.02	0.07	0.78	0.01	338.84	1228.99	0.02	6.30	0.94
538958	Anorthosite, 1% po, LBN-2 (89.3m)	6.05	0.01	0.00	1.64	0.01	422.02	1089.34	0.00	4.63	0.03
LD-96-10	Anorthosite with <1% diss po, outcrop	2.94	0.03	0.14	0.90	0.01	485.48	1378.78	0.02	7.41	0.85
LD-96-161	Anorthosite/leucogabbro, outcrop	1.19	0.00	0.01	0.91	0.00	356.80	769.44	0.01	5.32	2.39
536788	Leuconorite, LBN-2 (27.0m)	2.17	0.00	0.00	0.92	0.01	380.02	715.94	0.00	2.02	0.18
25928	Leuconorite, LBN-5 (11.0m)	7.78	0.01	1.40	1.77	0.01	412.12	953.99	0.00	3.34	0.05
536775	Leucotroctolite, LBN-2 (3.43m)	3.22	0.00	0.00	1.52	0.00	285.84	820.18	0.00	5.31	0.11
536776	Leucotroctolite, LBN-2 (4.43m)	2.16	0.01	0.00	1.59	0.00	342.88	889.50	0.00	4.17	0.12
536778	Leucotroctolite, LBN-2 (6.43m)	2.02	0.01	1.23	2.03	0.00	315.17	838.80	0.02	3.29	0.13
LD-96-48	Ferrodiorite, outcrop	1.44	0.01	0.00	1.46	0.02	343.53	399.82	0.00	2.43	2.39
LD-96-83	Ferrodiorite, outcrop	0.61	0.01	2.01	0.00	0.00	5.59	42.20	0.00	0.98	0.63
LD-96-125	Ferrodiorite, outcrop	1.85	0.01	2.38	0.00	0.01	341.67	350.44	0.08	1.84	2.03
LD-96-91	Pyroxenite, talus	0.17	0.01	0.00	0.00	0.00	1.42	31.28	0.00	3.97	0.52
LD-96-117	Pyroxenite, outcrop	0.64	0.01	0.52	0.34	0.00	11.27	12.26	0.00	2.82	0.77
25908	Anorthosite, 45% po, LBN-4 (381.3m)	385.59	0.06	6.83	1.17	0.01	294.51	884.87	0.02	4.34	0.02
25933	Anorthosite, 15% po, LBN-5 (37.1m)	5.67	0.02	2.35	1.97	0.00	267.86	888.10	0.00	3.38	0.02
LD-96-31	Massive po, outcrop, Gossan #2	2.67	0.02	0.68	1.07	0.00	367.44	1096.27	0.02	6.51	0.49
LD-96-171	Massive po, outcrop, Gossan #1	5.10	0.03	0.16	2.27	0.02	499.64	1052.73	0.04	9.10	1.28
CANST	Massive po with cpy, Can. States Res.	0.70	0.03	1.32	0.00	0.00	10.32	0.00	0.00	0.15	0.17
BW02	Anorthosite, Noranda	2.90	0.04	0.10	1.26	0.03	369.79	1250.34	0.04	6.68	0.90
BW01	Ferrodiorite, Noranda	0.98	0.01	3.91	1.22	0.00	149.94	327.88	0.03	0.46	1.15

CANST = Canadian States Resources, Licence # 1514M; major element data (XRF) are not available (NA).

BW01 and BW02 = Noranda, Licence #915M ("Hilltop" property)

Those samples analysed using both XRF and ICP-MS, the following element concentrations from XRF have been used: Rb, Sr, Y, Zr, Nb, [Mg] and total FeO values are calculated using Newpet software.

Appendix A3.4 Trace element data from ICP-MS analyses.

Sample Name	Nb ppm	Hf ppm	Zr ppm	Y ppm	Th ppm	U ppm	La ppm	Ce ppm	Pr ppm	Nd ppm	Sm ppm
LD-96-7A	1.2	0.57	9.97	1.01	0.07	0.01	6.15	10.83	1.19	4.20	0.69
LD-96-109	0.2	0.09	1.20	0.41	0.03	0.02	4.28	6.22	0.62	1.76	0.24
536958	0.4	0.21	3.62	0.52	0.04	0.00	4.68	7.25	0.73	2.08	0.24
LD-96-10	0.3	0.13	3.45	0.77	0.08	0.01	7.23	10.97	1.05	3.22	0.39
LD-96-161	5.0	1.22	25.35	0.33	0.04	0.01	3.53	6.21	0.72	2.46	0.39
536788	2.8	0.87	9.65	2.81	0.16	0.03	6.45	11.95	1.35	4.84	0.87
25928	0.1	0.69	12.12	0.71	0.09	0.02	6.36	11.22	1.32	4.64	0.69
536775	1.0	0.99	16.38	3.81	0.19	0.02	7.31	15.07	1.79	7.07	1.27
536776	1.4	0.43	26.08	2.38	0.07	0.01	6.17	11.87	1.48	5.20	0.97
536778	1.9	0.83	24.23	4.22	0.08	0.02	6.32	12.53	1.58	6.44	1.24
LD-96-48	6.5	1.54	37.84	60.37	0.65	0.10	39.36	94.27	13.57	59.26	13.54
LD-96-83	16.7	2.76	6418.61	73.95	0.15	0.12	17.01	55.05	11.33	62.46	16.55
LD-96-125	16.4	1.90	54.33	47.62	0.28	0.06	26.47	60.51	9.05	39.81	9.35
LD-96-91	1.2	0.86	22.12	15.56	0.06	0.02	3.31	11.99	2.33	11.77	3.47
LD-96-117	1.4	2.16	38.40	34.39	0.04	0.00	1.45	6.06	1.48	10.35	4.09
25908	1.2	0.12	6.47	0.69	0.09	0.02	3.68	6.13	0.61	1.93	0.28
25933	2.1	0.42	8.54	1.45	0.12	0.04	3.07	5.36	0.59	2.16	0.39
LD-96-31	0.1	0.05	2.41	0.37	0.01	0.01	4.19	6.85	0.63	1.93	0.26
LD-96-171	0.5	0.24	4.69	0.00	0.08	0.03	5.39	8.47	0.91	2.98	0.45
CANST	0.0	0.13	0.00	0.00	0.19	0.03	0.79	1.54	0.19	0.61	0.12
BW02	0.3	0.18	3.14	0.41	0.08	0.04	7.88	11.62	1.10	3.30	0.34
BW01	19.9	1.80	48.45	10.94	0.08	0.02	4.44	11.77	1.83	8.09	1.91



Appendix A3.4 Trace element data from ICP-MS analyses.

Sample Name	Eu	Gd	Tb	Dy	Ho	Er	Tm	Yb	Lu
	ppm	ppm	ppm	ppm	ppm	ppm	ppm	ppm	ppm
LD-96-7A	1.20	0.56	0.07	0.40	0.07	0.22	0.03	0.12	0.02
LD-96-109	1.10	0.13	0.02	0.07	0.01	0.06	0.02	0.04	0.00
536958	1.25	0.18	0.02	0.10	0.02	0.05	0.01	0.03	0.00
LD-96-10	1.11	0.20	0.03	0.18	0.02	0.05	0.02	0.04	0.00
LD-96-161	1.15	0.39	0.06	0.38	0.08	0.24	0.04	0.29	0.05
536788	1.19	0.80	0.12	0.72	0.14	0.43	0.07	0.40	0.06
25928	1.55	0.69	0.08	0.46	0.09	0.25	0.04	0.23	0.04
536775	1.35	1.04	0.16	1.03	0.19	0.61	0.09	0.58	0.10
536776	1.46	0.82	0.10	0.70	0.12	0.31	0.06	0.29	0.05
536778	1.41	1.14	0.17	1.03	0.18	0.48	0.07	0.45	0.08
LD-96-48	2.95	14.34	1.96	11.25	2.16	5.46	0.70	3.98	0.59
LD-96-83	1.23	17.40	2.21	12.67	2.47	6.37	0.81	4.81	0.84
LD-96-125	2.40	10.37	1.50	9.01	1.79	4.69	0.67	4.05	0.66
LD-96-91	1.00	3.74	0.56	3.42	0.65	1.71	0.22	1.34	0.20
LD-96-117	0.99	5.66	1.02	6.87	1.48	4.15	0.61	4.47	0.84
25908	0.97	0.11	0.02	0.10	0.02	0.06	0.03	0.04	0.01
25933	0.83	0.38	0.04	0.24	0.06	0.14	0.03	0.08	0.01
LD-96-31	1.06	0.14	0.01	0.06	0.01	0.04	0.02	0.02	0.01
LD-96-171	1.53	0.23	0.04	0.18	0.03	0.10	0.04	0.05	0.00
CANST	0.02	0.08	0.01	0.05	0.01	0.04	0.01	0.03	0.00
BW02	0.97	0.18	0.02	0.09	0.02	0.06	0.03	0.03	0.00
BW01	0.79	2.14	0.30	1.75	0.34	0.78	0.10	0.64	0.10

Appendix A3.5.1 Electron microprobe analytical results: Sulphide-bearing core and outcrop samples - Cirque grid

Mineral analysed: pyrrhotite

Sample	Rock Type	Source	Ni %	Fe %	S %	Co %	Cu %	Se %	Total %	Se/Sx10E6
200S	LTroc with diss po	LBN-2, 6.00m	0.04	63.90	37.61	0.00	0.10	0.00	101.54	0.00
201	MS po	LBN-2, 9.40m	0.27	60.82	39.77	0.08	0.11	0.00	101.04	0.00
304BS	LTroc with diss po	LBN-3, 10.35m	0.14	61.17	40.80	0.15	0.17	0.01	102.43	188.71
304BS	LTroc with diss po	LBN-3, 10.35m	0.17	61.01	40.98	0.14	0.11	0.00	102.29	0.00
304BS	LTroc with diss po	LBN-3, 10.35m	0.14	60.30	40.75	0.15	0.08	0.00	101.34	0.00
316A	LGab with bleb po-cpy	LBN-3, 18.02m	0.30	60.32	40.84	0.20	0.15	0.00	101.66	0.00
316A	LGab with bleb po-cpy	LBN-3, 18.02m	0.30	60.38	40.63	0.14	0.05	0.00	101.45	86.14
316A	LGab with bleb po-cpy	LBN-3, 18.02m	0.23	60.45	40.88	0.08	0.05	0.00	101.64	9.79
406	An with 5% diss po	LBN-4, 12.63m	0.24	60.33	40.34	0.09	0.07	0.00	100.99	14.87
406	An with 5% diss po	LBN-4, 12.63m	0.21	59.93	40.15	0.10	0.06	0.00	100.38	0.00
406	An with 5% diss po	LBN-4, 12.63m	0.24	60.47	40.50	0.09	0.06	0.00	101.31	103.69
406	An with 5% diss po	LBN-4, 12.63m	0.24	60.00	40.39	0.11	0.00	0.00	100.74	2.48
406	An with 5% diss po	LBN-4, 12.63m	0.22	59.93	40.15	0.07	0.03	0.00	100.37	0.00
406	An with 5% diss po	LBN-4, 12.63m	0.24	60.64	40.60	0.09	0.13	0.00	101.57	0.00
406	An with 5% diss po	LBN-4, 12.63m	0.21	60.36	40.55	0.09	0.11	0.01	101.2	150.42
406	An with 5% diss po	LBN-4, 12.63m	0.22	60.86	40.34	0.11	0.17	0.00	101.71	0.00
406	An with 5% diss po	LBN-4, 12.63m	0.24	60.47	40.51	0.10	0.08	0.00	101.32	0.00
443a	MS po	LBN-4, 146.56m	0.31	61.99	40.29	0.13	0.16	0.01	102.72	148.90
443a	MS po	LBN-4, 146.56m	0.30	61.15	39.81	0.08	0.11	0.01	101.45	183.38
452c	Bleb-pseudo net po, LAn	LBN-4, 183.93m	0.32	60.40	40.15	0.11	0.06	0.01	100.98	236.62
452c	Bleb-pseudo net po, LAn	LBN-4, 183.93m	0.32	46.86	54.83	0.09	0.14	0.00	102.09	0.00
452c	Bleb-pseudo net po, LAn	LBN-4, 183.93m	0.32	60.56	40.59	0.09	0.14	0.00	101.56	0.00
452c	Bleb-pseudo net po, LAn	LBN-4, 183.93m	0.34	60.32	40.43	0.15	0.03	0.00	101.23	0.00
452c	Bleb-pseudo net po, LAn	LBN-4, 183.93m	0.35	60.16	40.48	0.12	0.20	0.00	101.31	0.00
492b	Altered LAn with py	LBN-4, 328.50m	0.61	60.38	40.50	0.10	0.08	0.00	101.59	79.01
492b	Altered LAn with py	LBN-4, 328.50m	0.74	60.46	40.59	0.06	0.22	0.00	102.05	0.00
492b	Altered LAn with py	LBN-4, 328.50m	0.32	60.55	40.51	0.08	0.13	0.01	101.46	165.37
492b	Altered LAn with py	LBN-4, 328.50m	0.36	60.03	40.29	0.08	0.27	0.00	101.04	0.00
492b	Altered LAn with py	LBN-4, 328.50m	0.39	60.19	40.51	0.08	0.14	0.00	101.16	51.84
492b	Altered LAn with py	LBN-4, 328.50m	0.40	60.22	40.48	0.08	0.04	0.01	101.18	326.12
157	Mag and po-rich An	LBN-8, 157.70m	0.43	61.44	40.13	0.04	0.02	0.00	102.04	0.00
157	Mag and po-rich An	LBN-8, 157.70m	0.42	61.71	40.15	0.04	0.22	0.00	102.53	77.22
157	Mag and po-rich An	LBN-8, 157.70m	0.41	61.67	40.21	0.03	0.06	0.01	102.32	174.07
157	Mag and po-rich An	LBN-8, 157.70m	0.44	61.18	40.13	0.02	0.08	0.01	101.75	149.50
157	Mag and po-rich An	LBN-8, 157.70m	0.37	61.31	40.12	0.04	0.11	0.00	101.83	44.86
157	Mag and po-rich An	LBN-8, 157.70m	0.31	61.30	40.22	0.01	0.04	0.00	101.83	49.73
91	Pyroxenite	Talus	0.21	60.85	40.99	0.15	0.08	0.01	102.19	243.98
91	Pyroxenite	Talus	0.21	61.00	40.85	0.14	0.17	0.00	102.37	48.96
91	Pyroxenite	Talus	0.20	60.80	40.93	0.15	0.20	0.00	102.27	0.00
91	Pyroxenite	Talus	0.20	61.44	41.02	0.16	0.13	0.01	102.82	190.15
91	Pyroxenite	Talus	0.19	61.04	41.13	0.17	0.15	0.02	102.55	452.23
91	Pyroxenite	Talus	0.19	60.46	40.76	0.15	0.17	0.00	101.73	0.00
91	Pyroxenite	Talus	0.38	61.12	41.02	0.03	0.02	0.01	102.56	124.32
113	LAn with diss po	Outcrop	0.44	60.89	40.05	0.07	0.00	0.00	101.44	27.47
113	LAn with diss po	Outcrop	0.22	59.94	40.52	0.06	0.14	0.00	100.73	0.00
113	LAn with diss po	Outcrop	1.78	45.03	53.42	0.46	0.01	0.01	100.69	175.96
113	LAn with diss po	Outcrop	0.38	60.83	39.90	0.03	0.15	0.00	101.14	22.56
113	LAn with diss po	Outcrop	0.16	60.53	40.80	0.07	0.12	0.01	101.56	193.62
113	LAn with diss po	Outcrop	0.36	61.15	40.09	0.06	0.10	0.00	101.66	0.00
113	LAn with diss po	Outcrop	0.21	60.11	40.23	0.03	0.00	0.00	100.57	0.00
113	LAn with diss po	Outcrop	0.20	61.08	40.55	0.08	0.17	0.01	102.07	221.94
113	LAn with diss po	Outcrop	0.21	60.66	40.48	0.06	0.09	0.00	101.41	0.00
113	LAn with diss po	Outcrop	0.34	60.41	40.56	0.08	0.12	0.01	101.4	150.39

Average, n=52

0.31994 60.20 40.93 0.10 0.11 0.00 101.59 77.25

Electron microprobe analytical results: Sulphide samples - Cirque grid

Mineral analysed: chalcopyrite

Sample	Rock Type	Source	Ni %	Fe %	S %	Co %	Cu %	Se %	Total %	Se/Sx10E8
201	MS po	LBN-2, 9.40m	0.00	30.88	35.35	0.01	32.69	0.01	98.94	189.54
316A	LGab with bleb po-cpy	LBN-3, 18.02m	0.00	30.62	35.71	0.00	32.63	0.00	98.97	103.61
316A	LGab with bleb po-cpy	LBN-3, 18.02m	0.00	30.79	35.72	0.00	32.97	0.01	99.47	282.77
406	An with 5% diss po	LBN-4, 12.63m	0.01	30.95	35.59	0.01	32.79	0.01	99.33	272.58
406	An with 5% diss po	LBN-4, 12.63m	0.01	31.15	35.60	0.00	33.00	0.00	99.76	0.00
406	An with 5% diss po	LBN-4, 12.63m	0.01	31.50	35.48	0.01	32.34	0.00	99.32	0.00
406	An with 5% diss po	LBN-4, 12.63m	0.00	31.13	35.58	0.00	33.02	0.00	99.73	0.00
452c	Bleb-pseudo net po in LAn	LBN-4, 183.93m	0.01	31.02	35.57	0.03	32.65	0.01	99.26	278.35
452c	Bleb-pseudo net po in LAn	LBN-4, 183.93m	0.00	30.81	35.60	0.00	32.76	0.00	99.17	0.00
492b	Altered An with py	LBN-4, 328.50m	0.01	30.38	35.54	0.00	32.63	0.00	98.55	0.00
492b	Altered An with py	LBN-4, 328.50m	0.02	30.77	35.51	0.00	32.74	0.00	99.02	0.00
492b	Altered An with py	LBN-4, 328.50m	0.00	30.37	35.25	0.02	32.28	0.01	97.91	292.20
492b	Altered An with py	LBN-4, 328.50m	0.00	31.18	35.46	0.03	32.77	0.00	99.43	59.23
157	Mag and po-rich An	LBN-8, 157.70m	0.02	31.05	35.58	0.00	32.92	0.00	99.57	137.72
157	Mag and po-rich An	LBN-8, 157.70m	0.00	31.11	35.89	0.02	33.31	0.00	100.31	0.00
157	Mag and po-rich An	LBN-8, 157.70m	0.03	31.05	35.84	0.02	33.08	0.01	100.02	332.04
157	Mag and po-rich An	LBN-8, 157.70m	0.04	31.02	35.71	0.00	33.13	0.01	99.89	140.02
91	Pyroxenite	Talus	0.01	31.20	35.06	0.02	32.22	0.00	98.5	0.00
91	Pyroxenite	Talus	0.01	31.61	36.85	0.01	32.57	0.00	101.03	0.00
91	Pyroxenite	Talus	0.00	31.59	35.68	0.00	32.86	0.00	100.13	128.93
113	LAn with diss po	Outcrop	0.02	30.98	35.48	0.00	32.75	0.01	99.22	202.91
113	LAn with diss po	Outcrop	0.00	31.22	35.52	0.01	32.99	0.00	99.73	22.53
113	LAn with diss po	Outcrop	0.08	31.18	35.70	0.07	32.95	0.00	99.98	0.00
113	LAn with diss po	Outcrop	0.03	31.00	35.54	0.02	32.66	0.00	99.25	75.97
113	LAn with diss po	Outcrop	0.00	31.52	35.46	0.00	32.48	0.01	99.46	163.55
Average, n=25			0.01	31.04	35.61	0.01	32.77	0.00	99.44	107.28

**Mineral analyzed: pentlandite**

Sample	Rock Type	Source	Ni %	Fe %	S %	Co %	Cu %	Se %	Total %	Se/Sx10E8
443a	MS po	LBN-4, 146.56m	24.46	22.15	34.56	21.14	0.00	0.00	102.32	141.76
443a	MS po	LBN-4, 146.56m	24.64	21.21	33.80	21.89	0.03	0.00	101.54	62.13
157	Mag and po-rich An	LBN-8, 157.70m	32.14	29.30	33.99	6.34	0.05	0.00	101.77	0.00
157	Mag and po-rich An	LBN-8, 157.70m	32.83	28.97	34.08	5.73	0.11	0.00	101.61	38.15
157	Mag and po-rich An	LBN-8, 157.70m	32.50	28.57	34.20	5.85	0.03	0.00	101.12	90.64
157	Mag and po-rich An	LBN-8, 157.70m	32.20	28.43	34.33	6.34	0.20	0.00	101.5	78.64
113	LAn with diss po	Outcrop	30.41	25.78	34.00	11.64	0.25	0.01	102.07	150.02
113	LAn with diss po	Outcrop	26.17	28.49	34.43	11.21	1.25	0.01	101.56	284.64

Average, n=8

29.42 26.61 34.17 11.27 0.24 0.00 101.69 105.75

**Mineral analyzed: pyrite**

Sample	Rock Type	Source	Ni %	Fe %	S %	Co %	Cu %	Se %	Total %	Se/Sx10E8
452c	Bleb-pseudo net po in LAn	LBN-4, 183.93m	0.32	46.74	54.98	0.08	0.07	0.01	102.13	101.85
452c	Bleb-pseudo net po in LAn	LBN-4, 183.93m	0.06	45.22	53.45	0.28	0.14	0.01	99	97.29
492b	Altered An with py	LBN-4, 328.50m	0.01	47.28	55.33	0.01	0.05	0.00	102.61	23.49
492b	Altered An with py	LBN-4, 328.50m	0.01	45.78	52.36	0.01	0.02	0.01	98.14	166.17
492b	Altered An with py	LBN-4, 328.50m	0.06	47.04	55.12	0.04	0.09	0.00	102.26	0.00

Average, n=5

0.09 46.41 54.25 0.08 0.08 0.00 100.83 77.76

**Appendix A3.5.2 Electron microprobe analytical results: Sulphide-bearing samples from properties throughout the NPS.**

**Mineral analysed: pyrrhotite**

Sample	Location	Rock Type	Ni %	Fe %	S %	Co %	Cu %	Se %	Total %	Se/Sx10E6
BW01B	Hill Top	Ferro-diss po	0.24	61.66	38.75	0.01	0.14	0.00	100.65	103.23
BW01B	Hill Top	Ferro-diss po	0.22	61.00	38.75	0.03	0.00	0.00	100.00	59.36
BW01B	Hill Top	Ferro-diss po	0.23	61.16	39.55	0.01	0.13	0.00	100.94	78.39
BW01B	Hill Top	Ferro-diss po	0.23	60.93	38.78	0.02	0.12	0.00	99.96	0.00
BW01B	Hill Top	Ferro-diss po	0.22	61.37	38.69	0.01	0.07	0.00	100.28	0.00
BW01B	Hill Top	Ferro-diss po	0.23	60.82	38.74	0.00	0.16	0.01	99.95	224.60
BW01B	Hill Top	Ferro-diss po	0.23	60.69	38.86	0.02	0.13	0.00	99.79	95.22
BW01B	Hill Top	Ferro-diss po	0.23	60.83	38.56	0.01	0.00	0.00	99.61	0.00
BW01B	Hill Top	Ferro-diss po	0.20	60.47	38.70	0.04	0.06	0.00	99.41	95.60
average, n=9			0.22	60.99	38.82	0.02	0.09	0.00	100.07	72.93
CANST	Lic #1514M	MS	0.27	61.21	41.08	0.02	0.07	0.01	102.58	155.79
CANST	Lic #1514M	MS	0.23	60.84	41.19	0.02	0.24	0.00	102.53	21.85
CANST	Lic #1514M	MS	0.31	61.28	41.16	0.02	0.04	0.00	102.77	65.60
average, n=3			0.27	61.11	41.15	0.02	0.12	0.00	102.63	81.08
okg	OKG	MS	0.52	61.24	40.08	0.02	0.12	0.00	101.87	44.91
okg	OKG	MS	0.54	61.30	40.30	0.03	0.15	0.01	102.16	136.49
okg	OKG	MS	0.40	61.67	40.30	0.02	0.17	0.00	102.56	0.00
okg	OKG	MS	0.55	61.18	40.11	0.02	0.07	0.01	101.86	152.08
average, n=4			0.50	61.35	40.20	0.02	0.13	0.00	102.11	83.37
jhc41	Nain Hill	MS	0.31	62.50	40.16	0.02	0.15	0.01	102.99	136.96
jhc41	Nain Hill	MS	0.08	64.02	37.54	0.00	0.10	0.00	101.65	0.00
jhc41	Nain Hill	MS	0.22	62.17	39.88	0.01	0.19	0.00	102.47	0.00
jhc41	Nain Hill	MS	0.20	63.64	39.15	0.01	0.11	0.00	102.99	48.53
jhc41	Nain Hill	MS	0.40	64.31	37.61	0.09	0.06	0.00	102.40	0.00
jhc41	Nain Hill	MS	0.30	62.11	39.87	0.02	0.17	0.01	102.44	130.43
jhc41	Nain Hill	MS	0.29	62.29	39.79	0.01	0.03	0.00	102.37	90.47
average, n=7			0.26	63.01	39.14	0.02	0.12	0.00	102.47	58.06
W96-23	Voisey's Bay	MS	0.14	60.90	38.57	0.00	0.10	0.01	99.60	137.41
W96-23	Voisey's Bay	MS	0.07	62.70	37.30	0.00	0.02	0.00	100.08	109.91
W96-23	Voisey's Bay	MS	0.26	61.04	38.89	0.00	0.08	0.00	100.19	69.43
W96-23	Voisey's Bay	MS	0.01	63.34	36.88	0.00	0.06	0.01	100.22	246.73
average, n=4			0.12	61.99	37.91	0.00	0.06	0.01	100.02	140.87
LP-96-40	Voisey's Bay	MS	0.41	60.81	38.87	0.00	0.17	0.00	100.26	59.17
LP-96-40	Voisey's Bay	MS	0.44	60.54	39.15	0.00	0.14	0.00	100.13	48.53
LP-96-40	Voisey's Bay	MS	0.34	60.39	38.84	0.00	0.39	0.00	99.96	113.29
LP-96-40	Voisey's Bay	MS	0.37	60.96	38.99	0.00	0.11	0.00	100.32	66.68
average, n=4			0.39	60.68	38.96	0.00	0.20	0.00	100.17	71.92
RS25	S. V. B. P.	MS	0.61	60.22	38.80	0.00	0.08	0.01	99.63	239.68
RS25	S. V. B. P.	MS	0.58	59.90	38.84	0.03	0.12	0.00	99.35	105.56
average, n=2			0.59	60.06	38.82	0.02	0.10	0.01	99.49	172.62

Hill Top : Noranda; Lic #1514M : Canadian States Resources; OKG : Castle Rock  
Nain Hill : NDT Ventures; Voisey's Bay: Voisey's Bay Nickel Ltd.  
S.V.B.P or South Voisey's Bay Project : Donner Minerals

**Mineral analysed: chalcopyrite**

Sample	Location	Rock Type	Ni %	Fe %	S %	Co %	Cu %	Se %	Total %	Se/Sx10E6
BW01B	Hilltop	Ferro-diss po	0.02	30.52	34.58	0.00	33.19	0.01	98.31	159.07
BW01B	Hilltop	Ferro-diss po	0.00	30.25	34.55	0.00	32.56	0.02	97.38	451.52
BW01B	Hilltop	Ferro-diss po	0.01	30.91	34.98	0.00	33.10	0.00	98.99	0.00
average, n=3			0.01	30.56	34.70	0.00	32.95	0.01	98.23	203.53
CANST	Lic #1514M	MS	0.02	31.27	36.00	0.01	33.75	0.00	101.04	0.00
CANST	Lic #1514M	MS	0.01	31.40	35.92	0.00	33.54	0.00	100.86	0.00
CANST	Lic #1514M	MS	0.01	31.39	36.08	0.00	33.60	0.00	101.08	0.00
CANST	Lic #1514M	MS	0.01	31.35	35.99	0.00	33.59	0.00	100.95	27.79
average, n=4			0.01	31.35	36.00	0.00	33.62	0.00	100.98	6.95
jhc41	Nain Hill	MS	0.07	31.25	35.82	0.01	33.11	0.01	100.25	298.71
jhc41	Nain Hill	MS	0.20	31.53	35.76	0.07	32.73	0.00	100.30	0.00
jhc41	Nain Hill	MS	0.07	39.28	36.02	0.04	25.55	0.00	100.95	0.00
jhc41	Nain Hill	MS	0.07	31.23	35.57	0.00	32.76	0.01	99.63	340.20
average, n=4			0.10	33.32	35.79	0.03	31.04	0.01	100.28	159.73
W96-23	Voisey's Bay	MS	0.00	30.98	34.95	0.01	33.31	0.01	99.24	303.28
W96-23	Voisey's Bay	MS	0.00	30.55	34.89	0.00	33.12	0.01	98.56	260.83
W96-23	Voisey's Bay	MS	0.00	30.86	35.03	0.00	33.31	0.01	99.20	194.12
W96-23	Voisey's Bay	MS	0.01	30.56	34.61	0.00	33.09	0.01	98.26	210.94
W96-23	Voisey's Bay	MS	0.01	30.88	34.89	0.00	33.02	0.01	98.80	300.98
W96-23	Voisey's Bay	MS	0.02	41.21	35.31	0.02	22.73	0.01	99.29	266.24
average, n=6			0.01	32.51	34.94	0.01	31.43	0.01	98.89	256.07
LP-96-40	Voisey's Bay	MS	0.01	30.54	34.75	0.00	32.95	0.01	98.24	256.11
LP-96-40	Voisey's Bay	MS	0.04	30.66	34.46	0.00	32.80	0.01	97.96	200.21
LP-96-40	Voisey's Bay	MS	0.03	30.92	34.79	0.00	33.06	0.00	98.80	0.00
LP-96-40	Voisey's Bay	MS	0.05	30.87	34.76	0.00	33.30	0.01	98.98	247.41
average, n=4			0.03	30.75	34.69	0.00	33.03	0.01	98.50	175.93
RS25	S. V. B. P.	MS	0.00	31.50	34.67	0.01	33.12	0.00	99.28	121.16
RS25	S. V. B. P.	MS	0.00	30.72	34.75	0.02	33.27	0.00	98.75	0.00
RS25	S. V. B. P.	MS	0.02	30.91	34.82	0.00	32.61	0.00	98.35	0.00
RS25	S. V. B. P.	MS	0.00	30.72	34.68	0.00	33.02	0.00	98.42	92.27
RS25	S. V. B. P.	MS	0.01	30.65	34.24	0.00	32.99	0.00	97.88	0.00
average, n=5			0.01	30.90	34.63	0.00	33.00	0.00	98.54	42.69

**Mineral analysed: pentlandite**

Sample	Location	Rock Type	Ni %	Fe %	S %	Co %	Cu %	Se %	Total %	Se/Sx10E6
jhc41	Nain Hill	MS	30.99	31.64	34.44	4.66	0.02	0.01	101.74	357.12
okg	OKG	MS	30.11	32.18	35.42	3.99	0.08	0.00	101.70	0.00
okg	OKG	MS	33.03	29.36	34.25	4.92	0.07	0.00	101.55	35.04
average, n=2			31.57	30.77	34.84	4.45	0.07	0.00	101.63	17.52
CANST	Lic #1514M	MS	34.15	29.71	34.51	3.75	0.18	0.00	102.13	0.00
CANST	Lic #1514M	MS	33.96	30.11	34.45	3.44	0.12	0.00	101.97	136.42
CANST	Lic #1514M	MS	25.72	30.35	35.17	2.14	8.71	0.00	102.08	14.22
CANST	Lic #1514M	MS	33.67	30.50	34.70	3.17	0.14	0.00	102.05	77.81
average, n=4			31.88	30.17	34.71	3.13	2.29	0.00	102.06	57.11
W96-23	Voisey's Bay	MS	30.85	34.57	33.34	1.07	0.02	0.01	99.82	149.97
W96-23	Voisey's Bay	MS	30.78	34.73	33.38	1.06	0.09	0.02	99.97	497.26
W96-23	Voisey's Bay	MS	30.80	34.33	33.42	1.14	0.12	0.01	99.69	203.48
W96-23	Voisey's Bay	MS	31.13	34.24	33.44	1.25	0.08	0.01	100.06	167.47
W96-23	Voisey's Bay	MS	32.42	33.22	33.31	1.28	0.00	0.02	100.25	468.26
W96-23	Voisey's Bay	MS	30.81	34.27	33.19	1.27	0.11	0.02	99.56	457.95
average, n=6			31.13	34.22	33.35	1.18	0.07	0.01	99.89	324.06
LP-96-40	Voisey's Bay	MS	33.77	30.13	33.24	2.43	0.15	0.00	99.57	0.00
LP-96-40	Voisey's Bay	MS	33.65	30.49	33.35	2.45	0.06	0.01	99.95	221.89
LP-96-40	Voisey's Bay	MS	33.75	30.55	33.40	2.38	0.15	0.01	100.08	398.26
LP-96-40	Voisey's Bay	MS	33.59	30.23	33.19	2.34	0.01	0.01	99.35	171.72
average, n=4			33.69	30.35	33.30	2.40	0.09	0.01	99.74	197.97

**Appendix A3.6 PGE-Au-Ni-Cu data for semi-massive to massive sulphide outcrop and core samples from the Cirque. Two samples are ferrodiorite (Fe-diorite) with disseminated sulphides. CANST is a massive sulphide sample from the Canadian States Resources property, Licence #1514M. All data are given in ppb.**

<b>Sample</b>	<b>LD-46</b>	<b>LD-83</b>	<b>LD-29</b>	<b>LD-96</b>	<b>LD-99</b>	<b>LD-101</b>	<b>LD-170(2)</b>
<b>Description</b>	<b>Fe-diorite</b>	<b>Fe-diorite</b>	<b>MS</b>	<b>MS</b>	<b>MS</b>	<b>Po bands</b>	<b>MS</b>
<b>Source</b>	<b>Outcrop</b>	<b>Outcrop</b>	<b>Outcrop</b>	<b>Talus</b>	<b>Talus</b>	<b>Talus</b>	<b>Outcrop</b>
Ni	4450.00	5250.00	2641400.00	32700.00	57900.00	34450.00	102450.00
Cu	10600.00	1575.00	1374650.00	2364500.00	1649850.00	2138100.00	1450400.00
Ru	1.80	2.00	9.10	4.20	7.30	7.10	10.30
Rh	0.10	0.70	9.20	7.90	8.40	24.50	32.80
Pd	0.10	0.40	5.20	65.80	63.50	51.30	50.50
Re	0.10	1.40	3.90	0.20	bdl	0.60	0.30
Os	0.80	3.00	6.30	0.50	0.40	0.20	0.30
Ir	bdl	0.60	0.30	1.10	3.00	1.20	0.40
Pt	0.20	2.50	6.50	1.30	3.20	47.40	13.60
Au	0.90	2.60	7.00	23.50	1.30	18.50	5.80
Ni/Cu	0.42	3.33	1.92	0.01	0.04	0.02	0.07
Ni/Pd	44500.00	11666.67	512893.19	496.96	911.09	672.20	2026.71
Cu/Pd	106000.00	3500.00	266922.31	35934.65	25961.45	41719.02	28692.38
Pd/Ir	na	0.78	14.71	59.82	21.36	42.71	126.38
<b>Sample</b>	<b>24061</b>	<b>24065</b>	<b>25902</b>	<b>25907</b>	<b>25965</b>	<b>21102</b>	<b>CANST</b>
<b>Description</b>	<b>Semi-MS</b>	<b>MS</b>	<b>Semi-MS</b>	<b>MS</b>	<b>Net-bleb</b>	<b>MS</b>	<b>MS</b>
<b>Source</b>	<b>LBN-3</b>	<b>LBN-3</b>	<b>LBN-4</b>	<b>LBN-4</b>	<b>LBN-5</b>	<b>LBN-11</b>	<b>Core</b>
Ni	137867.00	109400.00	7700.00	1090600.00	6150.00	675950.00	477825.00
Cu	217700.00	43750.00	51450.00	176300.00	23800.00	2509250.00	2203075.00
Ru	5.50	7.40	9.20	3.50	0.90	16.50	18.50
Rh	14.40	18.80	13.30	19.80	2.50	44.40	34.50
Pd	34.20	40.60	27.40	46.90	5.30	69.90	38.80
Re	2.90	2.30	24.40	6.30	0.70	2.30	3.60
Os	0.50	2.50	7.60	2.30	0.40	8.60	0.90
Ir	1.30	4.00	3.10	bdl	0.10	0.60	2.50
Pt	8.10	2.30	6.30	16.10	2.30	4.60	27.00
Au	2.30	97.30	35.30	19.70	1.70	28.20	15.10
Ni/Cu	0.63	2.50	0.15	6.19	0.26	0.27	0.22
Ni/Pd	4031.19	2694.58	281.02	23253.73	1171.43	9663.33	12323.02
Cu/Pd	6365.50	1077.59	1877.74	3759.06	4533.33	35872.05	56816.89
Pd/Ir	27.00	10.15	8.84	na	105.00	127.18	15.36

Sulphides are pyrrhotite with minor chalcopyrite.  
bdl = below detection limit; na = not available



**Appendix A3.7 Sulphur isotope data for samples from the Cirque property.  
One sample (CANST) is from Licence #1514M (Canadian States Resources).**

Sample	Type	Mineral	$\delta_{34S}^{CDT}$
LD-29	massive, outcrop	po	2.79
LD-86	massive, talus	cpy	2.89
LD-86	massive, talus	po	2.83
LD-86	massive, talus	po (dup)	2.86
LD-97	massive, talus	po	2.9
LD-97	massive, talus	po (dup)	2.83
LD-99	massive, talus	cpy	3.01
LD-99	massive, talus	po	2.73
20375 (LBN-3)	massive, core	po	3.05
20375 dup	massive, core	cpy	2.69
20470 (LBN-4)	massive, core	po	2.6
20470 dup	massive, core	cpy	2.54
20011(LBN-11)	massive, core	po	2.77
CANST	massive, core	cpy	2.49
CANST	massive, core	po	2.3
NBS-123		standard	17.05
MUN-PY		standard	1.67

dup = duplicate sample





